

TRUCK EMERGENCY-BRAKING IMPULSE EFFECT MOORED FERRY

by

Xuelei Feng¹, W.V. Reenen¹, T. Hope¹, Mark Willbourn²

ABSTRACT

Heavy trucks may exert significant impulse loads on the moored ferry due to sudden braking when trucks move from linkspan to ferry deck. Its effect on motions of the moored ferry is studied in this paper to examine the ferry operations during loading and unloading processes involving the safety of vehicles and passengers.

The ferry crossing Thames river is moored by intelligent Docklocking System® (iDL), which is an innovative automated mooring system replacing the use of ferry thrusters. The feasibility and potential of this iDL system to minimize the horizontal movements of the moored ferry are presented in this paper based on numerical simulations of dynamic mooring analysis (DMA) in time domain.

The truck impulse model is linked with a multi-body system including numerical models of the ferry and the jetties. Wind, current and wash wave are also considered, together with the impulse load of the truck to represent a combination of possible loads. This paper first gives a systematic procedure to evaluate truck impulse effect on a moored ferry and then presents motion responses of the ferry when moored by the iDL system.

INTRODUCTION

Ferry mooring

Ferries are conventionally moored along berths using thrusters or mooring ropes. To minimize fuel consumption or to increase safety of personnel involving in moorings and reduce mooring time, the *intelligent* Docklocking System® (iDL) can effectively replace thrusters or mooring ropes for mooring purposes. Thus, to meet London's Low Emission Zone standards and to minimize safety risks, the iDL system will be delivered in 2018 for the mooring of Woolwich Ferries in London, where existing Woolwich ferries (**Figure 1**) will be replaced with hybrid diesel-electric ferries (**Figure 2**) and Woolwich terminals are also replaced with floating pontoons anchored by fixed piles[1].

The safety involving the mooring of the ferries has two noticeable aspects:

- The holding capacity of the mooring system shall be greater than the design environmental loads.
- The movements of the moored ferry shall be within the allowable limits of linkspan.

Truck emergency braking

Heavy-weighted trucks or trailers, when loading on/off the ferry, should be checked carefully in terms of speed limit and maximum weight. A critical scenario is the emergency braking of the truck, which has not been fully studied in terms of its influence on ferry movements, though LR *Rules and Regulations for the Classification of Linkspans, June 2016* has dictated as following:

¹ Mampaey Offshore Industries, B.V., the Netherlands, x.feng@mampaey.com

² Briggs Marine, Burntisland, UK

To allow for the possibility of emergency braking or skidding incidents, a horizontal load of $0,2 \times$ vehicle weight is to be considered in conjunction with the vertical vehicle loadings.

This statement indicates a deceleration rate of 0.2g during emergency braking. Beyond that, two aspects related to emergency braking are also worth noting: 1) the influence of truck emergency braking on the ferry's motion is not known quantitatively; 2) the potential damage is also unclear if the horizontal load exceeds the specified value in the LR rules above.

Although the vehicle speed limit is often marked on the ground of the linkspan before any vehicle drives onto the ferry, to what extent this speed limit is observed is hard to measure as the human factor is involved. Even with strictly observed speed limit, the emergency braking of the truck with exceedingly heavy weight might still be hazardous.



Figure 1: Existing Woolwich Ferry Terminal



Figure 2: New Woolwich Ferry

This paper gives a quantitative study of the ferry movement due to the emergency braking of heavy trucks when the ferry is moored with an automated mooring system (iDL) during realistic environmental conditions (wind, current and wave etc.).

First, the focus is to establish a numerical model of the physical mechanism of the truck emergency braking. For the floating ferry and pontoon jetties, a multibody model is built for hydrodynamic analysis in frequency domain to obtain the required hydrodynamic coefficients. Mooring systems, including iDLs and fenders, are also included in the time domain analysis, taking into account the non-linearities of the mooring systems.

With a complete numerical model as described above, a parametric study is carried out to investigate the influence of varied impulse loads on the ferry movements due to emergency braking. Next, the relationship between ferry oscillatory movements and fender damping is found. This enhances the understanding the effect of truck braking and some preliminary conclusions are drawn regarding the safety of roll-on/off operations.

NUMERICAL MODEL

The objective of a numerical model is to simulate the physical behavior of the complete system involving the ferry, mooring equipment (iDL) and the truck under environmental conditions. The overview of the numerical model is shown in **Figure 3**.

Two inputs for the numerical model are environment conditions and truck impulse. For the environment conditions, they are in line with the site conditions at Woolwich. The truck impulse model is the critical part of the whole simulation to determine the motion response of the ferry.

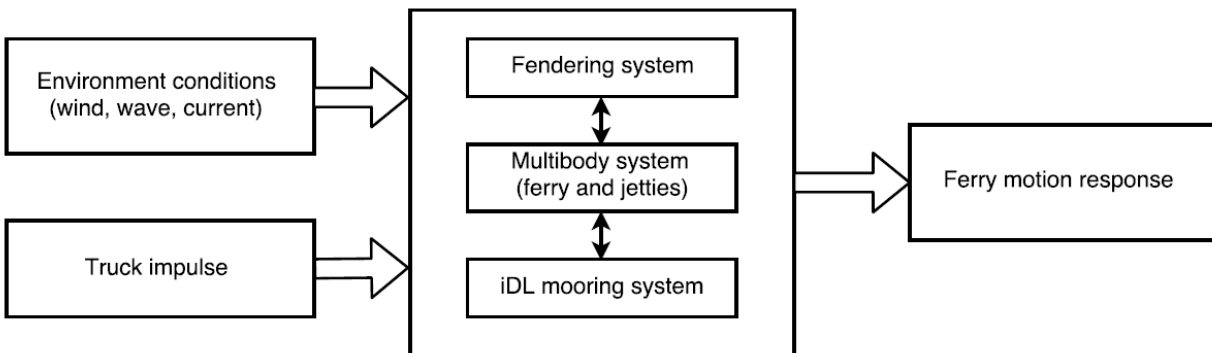


Figure 3: Overview of the numerical model

Environment conditions

The Woolwich berths are located along the inland river, Thames River. Water depth at berthing locations are taken as 10.5 meters corresponding to the highest tide. The wind wave and swell are considered negligible compared to the wash wave generated by passing vessels. Wash wave is assumed to be a regular wave with the height of **0.4 meters** and the period is **3 seconds**. Other input environmental conditions include wind and current. Wind speed is **20 knots** based on 30 seconds gust in transverse direction of the ferry. Current speed is **3 knots** in longitudinal direction.

Multi-floating body

The numerical model includes three floating bodies: two pontoon jetties and the ferry (**Figure 4** and **Figure 5**). The floating pontoons are relatively fixed by piles driven into the riverbed, which allows for free heave movement but very limited horizontal movements for the pontoons. The ferry is a 6-DOF floating body which is moored only by iDLs and fenders.

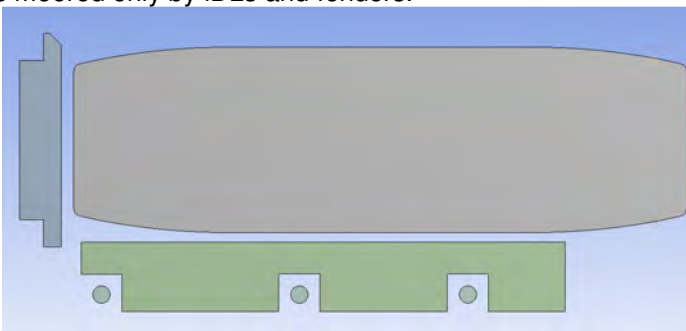


Figure 4: Multi-floating Body (top view)

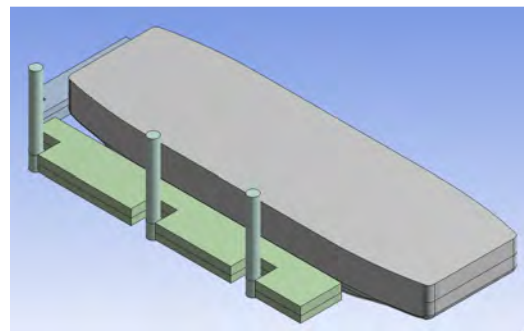


Figure 5: Multi-floating Body (iso view)

External lids are added between pontoons and ferry to suppress the unrealistic standing waves in the gap. Internal lids are also added to remove the irregular frequencies.

In the diffraction model, the pontoons and piles are assumed motionless; this means the diffraction or the shielding effects of the pontoons are considered but the radiation force caused by pontoons is neglected.

Truck impulse model

Despite no directly available element in AQWA to model truck braking process, it can be simulated as the external impulse force connected to AQWA. This impulse force signal is estimated based on the braking deceleration, initial speed, duration of brake etc.

The maximum truck speed before braking is adopted as **10 mph** in this paper based on the speed limit currently marked on the connecting bridge to linkspan of Woolwich ferry berths.

To generate an impulse force signal, three values should first be determined for the signal: shape, magnitude and duration. For the shape of the signal, the rectangle function is assumed to simplify the analysis. Physically, this means braking force will be constant over the course of braking. The magnitude of the signal is the value of the braking force calculated by truck weight multiplying deceleration rate. The duration of the impulse signal is determined based on initial speed and deceleration rate.

Fendering system

The fenders installed on the bow pontoon and the side pontoon are specified as TTV 800 and TTV 600 type respectively. The fender locations on the pontoons are shown in **Figure 8**. To model the load deformation curve of the fenders, a fifth order polynomial function is used:

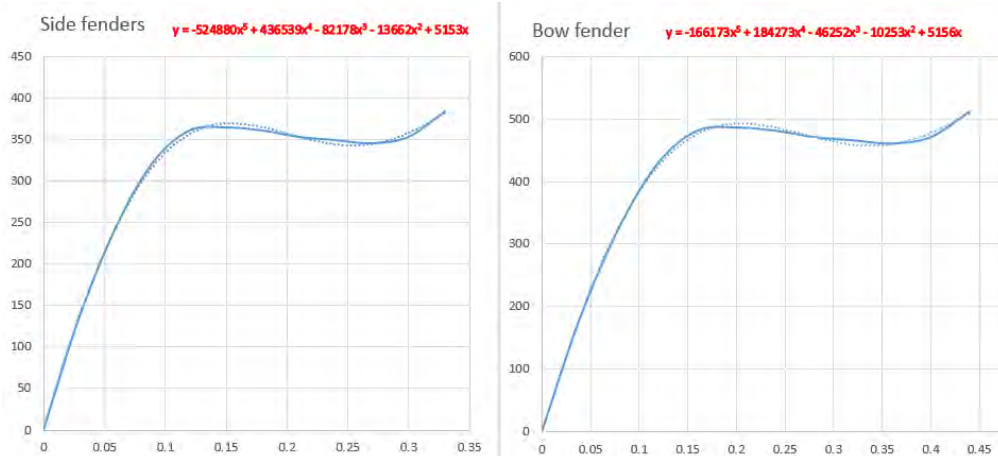


Figure 6: Load Deformation Curve for Bow and Side Fenders

The solid blue curve is the fender compression curve from the manufacturer and the blue dotted curve is the fitted curve by fifth order polynomial. Fender friction coefficient in the DMA analysis is taken as 0.1 in a conservative manner for the selected case, as the manufacturer has specified a value of 0.2; fender damping is not specified and this topic will be discussed later in the results section.

Automated mooring system (iDL)

The iDL is an automated mooring system based on magnets translated by hydraulic cylinders. It is a complicated system that restricts surge and sway movements, but allows for the heave, roll and pitch

movements of the vessel. This movement of the vessel needs to be restricted to keep linkspans on the vessel and allow for a safe passage of vehicles.

Two iDL units are placed on the side pontoon symmetrically w.r.t the CoG of the vessel (**Figure 7** and **Figure 8**). iDL units are integrated into the numerical model based on its force and displacement characteristics as well as its control system. Due to confidentiality, the exact details cannot be disclosed in this paper.

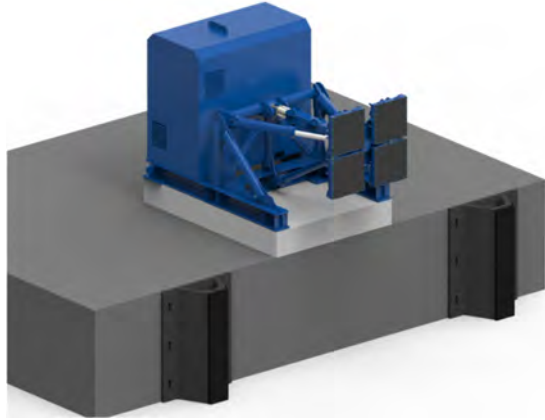


Figure 7: intelligent Docklocking System® (iDL)

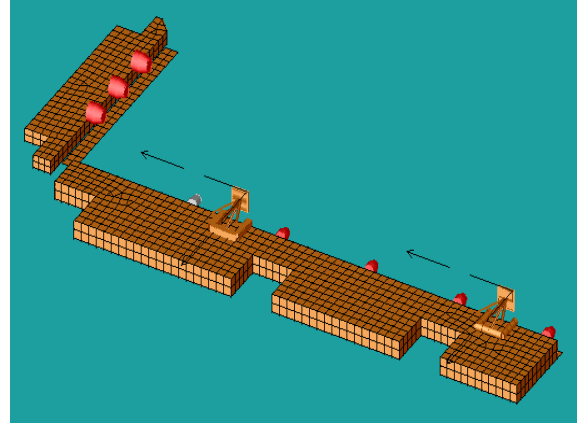


Figure 8: Two iDLs Mounted on the Side Pontoon With Fenders Installed (red).

THEORY

With all the elements defined in the numerical model, the 6-DOF movements of the ferry subjected to truck impulse loads as well as environmental factors will be evaluated in time domain. The motions in time domain are solved in AQWA based on Cummins[2] EoM (Equation of Motions):

$$(m + A_{\infty})\ddot{X} + c\dot{X} + kX + \int_0^t R(t - \tau)\dot{X}(\tau)d\tau = F(t) \quad (1)$$

where external m is the ferry mass matrix and A_{∞} is the added mass at infinite frequency, c is the linear damping matrix due to radiation and k is the total stiffness matrix; R is the impulse response function which can be integrated to represent 'memory' effect. Also noted that $F(t)$ is the time-varying external force including Froude-Krylov force, diffraction force, drift force, viscous damping force and other user-defined external force etc. Hence, the truck impulse force is input into AQWA as the user-defined external force which is a rectangular pulse function of duration T based on the Dirac Delta function:

$$\delta_T(t) = \begin{cases} 0 & \text{for } t \leq T_1 \\ \frac{a}{(T_2 - T_1)} & \text{for } T_1 < t \leq T_2 \\ 0 & \text{for } t > T_2 \end{cases}$$

where a is the magnitude of impulse momentum.

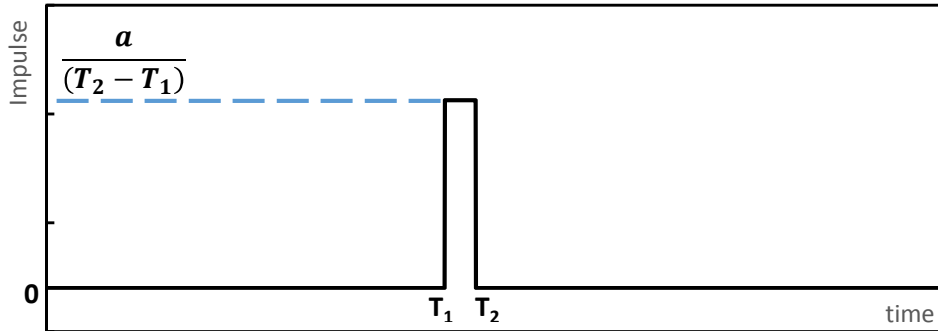


Figure 9: Rectangular Pulse Function

By solving time domain equations, the velocity of the ferry can be obtained such that the energy balance equation is established between the truck impulse-kinetic energy, the ferry kinematic energy and other damping dissipated energy:

$$E_{truck} = E_{fender} + E_{damping} \quad (2)$$

where the truck kinetic energy E_{truck} due to impulse is defined as:

$$E_{truck} = \frac{1}{2} m_{truck} v_{initial}^2 \quad (3)$$

Here the dissipated damping energy is only vaguely defined as the sources of the damping force can be varied: linear radiation damping, viscous damping and material damping etc.

RESULTS & ANALYSIS

Base case

The base case is presented here to give an overview of the response of the entire system subject to environmental conditions and truck impulse load. Input environmental conditions are based on the table 1.

The truck impulse deceleration is taken as 0.2g m/s² in the longitudinal direction (surge) based on LR rules. The input truck weight is 44 tons, giving an impulse load of 86.3 kN. The impulse starts from 101s and ends at 103.3s, within the total 200 seconds of time series record.

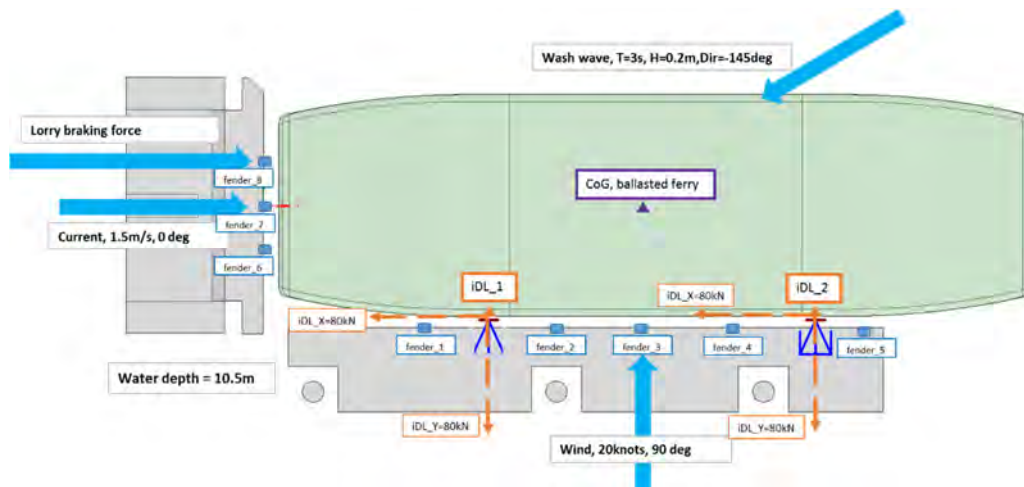


Figure 10: Directions of Environmental and Truck Braking Loads

As shown in **Figure 11**, iDLs could effectively keep the ferry in position with minimized ferry responses. The ferry dynamic surge movement due to wash wave is within ± 5 mm range. When subjected to impulse load due to truck (**Figure 12**), the surge movement spikes to $[\pm 15\text{mm}, -10\text{mm}]$ range, but still within a very acceptable limit for safe ferry operations for vehicles and passengers.

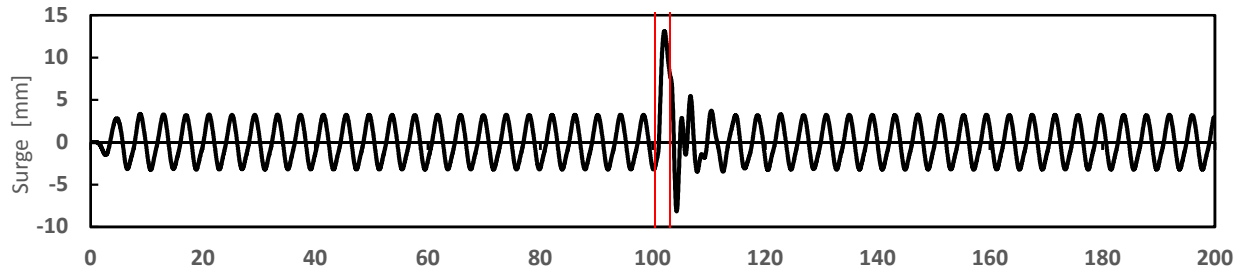


Figure 11: surge movement of the ferry

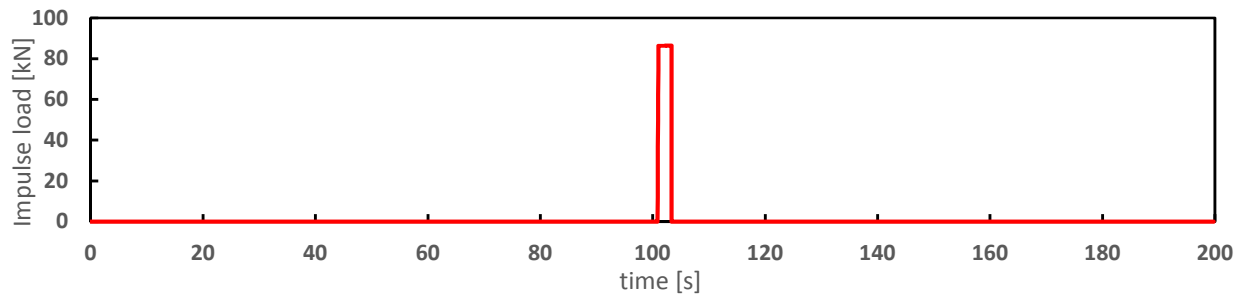


Figure 12: impulse signal due to truck emergent brake

Varying truck impulse

The influence on ferry surge motions due to varying decelerations of truck brake impulse from 0.1g to 0.4g is studied here based on equation of motions in time domain. In line with base case, for each deceleration, the impulse starts from 101 second and the impulse load is constant over the impulse duration. The impulse duration is determined by the initial truck kinetic energy and deceleration rate.

The impulse signals are illustrated in **Figure 13**, where the area under each truck impulse signal from 0.1g to 0.4g has the same value, as the area represents the total impulse kinetic energy, which is constant as the initial speed of the truck is defined as 10 mph for all cases.

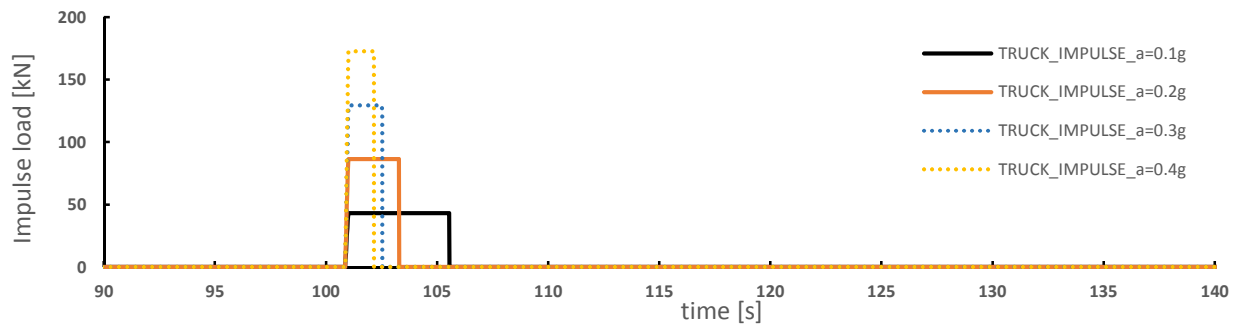


Figure 13: Varied Truck Impulse Rates

The influence of varying truck impulse on ferry surge motions is illustrated in **Figure 14**. Two patterns can be distinguished from it: the dotted lines show large oscillatory surge movements pattern lasting more than 10 seconds, whereas solid lines last only 5 seconds with surge movements less than 10 mm.

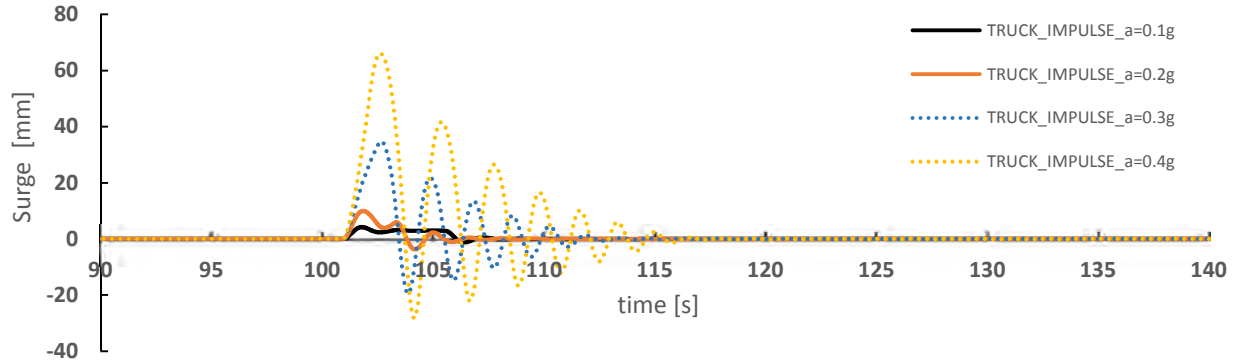


Figure 14: Surge Movement of the Ferry with Varied Truck Impulse Rates

To analyze the behaviour of the ferry under sharp impulse load in details, with the case for truck impulse of 0.4g, this large oscillatory surge movement pattern can be further divided into 3 stages based on kinematics as shown in **Table 1** and **Figure 15**.

| Stage | Stage 1, S1 | Stage 2, S2 | Stage 3, S3 |
|--------------------|-----------------------------|-----------------------------|------------------------------|
| Duration | Equal to impulse duration | Dependent on iDL force | Dependent on damping |
| Characteristics | Impulse load due to truck | iDL holding vessel back | iDL and fender force exerted |
| Ferry movement | Started to move | Movement reaching peak | Oscillatory movement |
| Ferry velocity | Increased from zero to peak | Decreased from peak to zero | Oscillatory velocity |
| Ferry acceleration | Accelerated | Decelerated | Accelerated and decelerated |

Table 1: Three Stages of Ferry Responses due to Truck Impulse

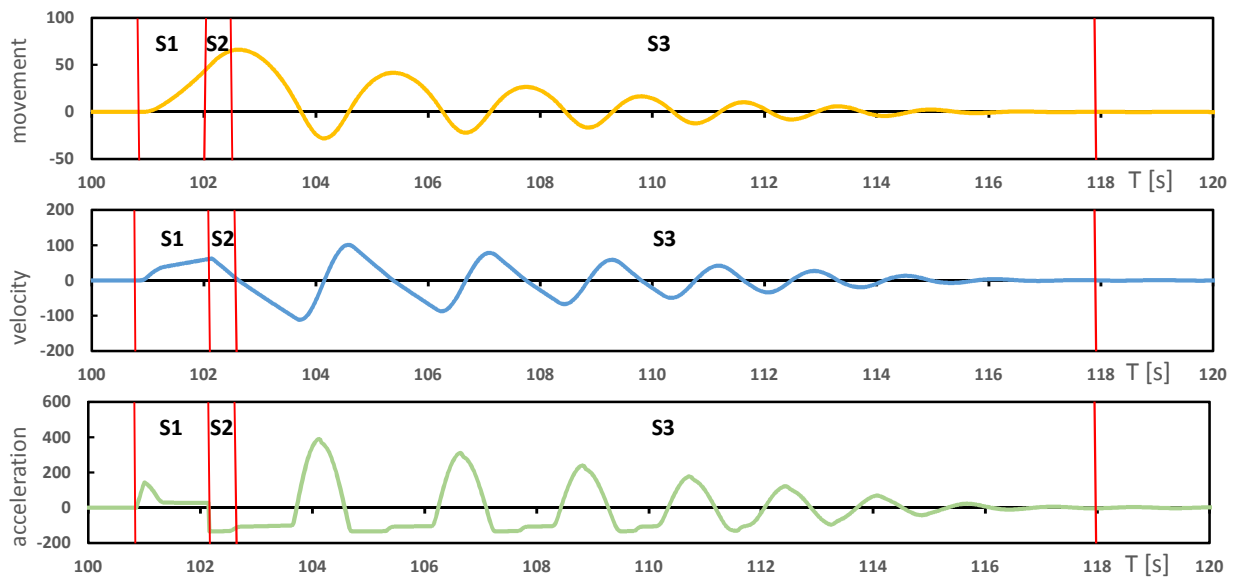


Figure 15: Movement [mm], Velocity [mm/s] and Acceleration [mm/s²] of Ferry due to Truck Impulse of 0.4g

Varying fender damping

Stage 3 is the oscillatory stage where damping plays a pivotal role in ferry response. In previous sections where the fender damping is assumed zero, the decay rates of oscillatory ferry movements are determined by hydrodynamic damping, whose values have been widely studied elsewhere.

Therefore, the focus here is on fender damping due to hysteresis[3], despite it being ignored in most motion analysis (**Figure 16**). The fender hysteresis is the phenomenon that over a full cycle of compression and decompression, part of the absorbed energy is dissipated in the recoil cycle (**Figure 17**).

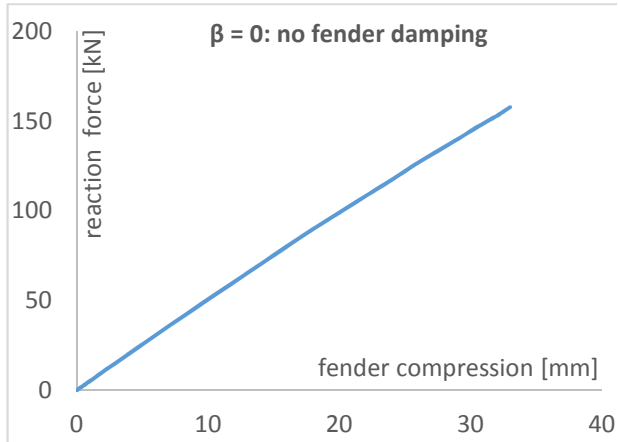


Figure 16: Fender load-deformation curve

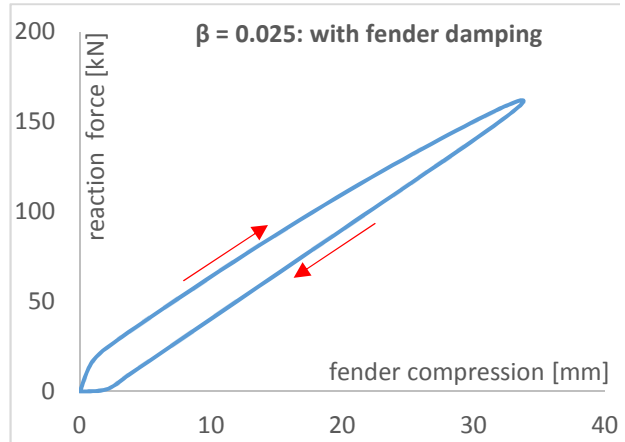


Figure 17: Fender load-deformation curve

By varying fender damping coefficient, its influence on ferry movement is investigated. As shown in **Figure 18**, with increased fender damping, both the amplitudes and cycles of oscillation of ferry surge response are reduced. Furthermore, the first peak is not so much influenced by fender damping coefficients as the subsequent peaks.

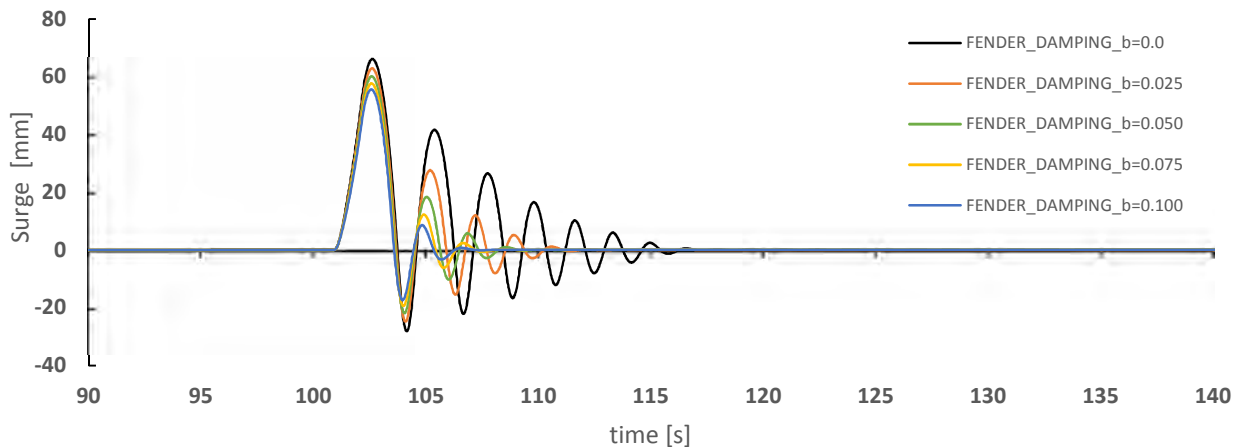


Figure 18: Influence of Fender Damping on Surge Movement of Ferry due to Truck Impulse of 0.4g

CONCLUSION

This paper describes a systematic numerical model encompassing the key elements to simulate the process of truck emergency braking. The focus was to investigate the influence of truck impulse on the motions of the ferry moored by iDL and fenders. Summarizing the results, several conclusions are made:

1. The automated mooring system, iDL, can effectively keep the ferry in position safely under the truck impulse force and environmental conditions specified in this paper.
2. The response of the ferry under pure truck impulse can be divided into 3 stages; the first stage reaches the highest velocity of the ferry, second stage with the peak movement and third stage with oscillatory decay response lasting much longer than the duration of impulse load.
3. By varying truck brake impulse from 0.1g to 0.4g and keeping the same amount of input kinetic energy, it is found that with sharp impulse (e.g., 0.4g), the response of the ferry will be much increased compared to mild impulse. Moreover, the duration of the decaying oscillation due to sharp impulse is also longer than that of mild impulse.
4. For the third stage with long oscillatory decay response due to sharp impulse, the significance of fender damping caused by hysteresis is reflected on the reduced amplitudes and cycles of the ferry movements. Thus, the fender damping will help reduce the oscillatory movement of the ferry.

Based on the numerical model established in this paper, further work should be continued. Field measurements are necessary to verify and fine-tune the numerical model. Obtaining practical fender hysteresis damping coefficient is an often-overlooked effort but worth doing as it could effectively dampen ferry movement due to impact. Also, the practical kinetic energy of the ferry due to truck impulse will be further reduced based on eccentricity factor, softness factor and berth configuration factor.

REFERENCE

- [1] "Woolwich Ferry upgrade - Transport for London." [Online]. Available: <https://tfl.gov.uk/travel-information/improvements-and-projects/woolwich-ferry-upgrade>.
- [2] W. E. CUMMINS, "THE IMPULSE RESPONSE FUNCTION AND SHIP MOTIONS." 1962.
- [3] PIANC MarCom WG33, "Guidelines for the Design of Fenders Systems: 2002," *Pianc*, 2002.

Automating Mooring for Increased Safety and Security

by

Mike Howie,

Sales Director, MoorMaster,

Cavotec

mike.howie@cavotec.com

INTRODUCTION

Mooring vessels using ropes or cables is one of the very few operations undertaken on a ship and in the port that has not significantly changed for centuries. While minor improvements have been made it remains a very dangerous operation that results in an unacceptable number injuries and fatalities every year. Furthermore, it also presents a significant risk to the vessels themselves as, while it has been studied and monitored, conventional mooring has no situational awareness to provide warnings should a hazardous situation arise. Automated mooring systems remove all risk to personnel and reduce the risk to the vessel to almost nothing by removing the personnel from the risky tasks and providing full situational awareness of mooring and environmental status.

TIME FOR CHANGE

Many aspects of port operations, have been improved by automation in recent years. These improvements have increased the throughput of port and visibility of operations. However, in most ports mooring continues to be a manual time consuming and dangerous task. Indeed mooring and the required line handling is one of the few tasks left in modern industry that regularly exposes staff to life threatening risks on a daily basis. Furthermore, conventional mooring provides no feedback to the port or vessel regarding mooring performance or integrity.

Automated mooring system that do not employ ropes are able to eradicate the risks associated with line handling for all staff on board and land side. There are no handling injuries and snap back risks making mooring significantly safer for personnel and reducing lost time due to injuries to nothing.

Furthermore these systems are able to monitor environmental conditions and mooring performance with a high level of precision and provide real time detailed feedback on mooring performance and integrity. Data stored over time can be used to compare to current conditions to predict potential upcoming events and provide advance warning to the port and vessel. Also stored data can be examined and stored in much the same way as Voyage Data Recording (VDR).

This paper and presentation will examine the pros and cons of automated mooring implementation and provide real world examples. Three ports and one canal system will be presented.

PORT HEDLAND, WA

Port Hedland has been able to secure cape size bulk carriers on a berth originally only intended, and long enough, for panamax vessels. This has enabled the port to realise a large increase in through put due to increased vessel size and speed of mooring while reducing risk to personnel. What was originally intended as a 6-7mtpa facility regularly exceeds 20mtpa.

Additionally, as the berth is very close to the busy port entrance the system has removed the effects of passing vessels at the berth and thus the removal of the risk to the moored vessel and personnel of parted lines.

During construction of the berth major savings were also realised as the mooring dolphins that are traditionally used in this location to allow for the large tidal variations were not required. However, the cost of the automated mooring system and its installation did add some cost, however, this was significantly less than the amount saved due to the elimination of the dolphins.



Cavotec MoorMaster™ MM200C¹⁷ system installed in Port Hedland

PORT OF SALALAH, OMAN

The port of Salalah experiences a long wave during the Khareef (monsoon) season that can cause the vessels to surge back and forth in the berth. The surge often times resulted in ceasing of cargo operations and parted lines and the associated risks to port staff and the vessel. The automated mooring system has reduced vessel surge to insignificant amounts removing all the risks associated with it.

Furthermore the port can be kept fully informed of the longwave condition and how the mooring system is coping with it. This situational awareness was also employed by the port to monitor the conditions and provide early warning of issues for the berth that still used traditional moorings in the port.

As with all installations of automated mooring the drawbacks are cost and space taken on the berth by the system itself.

The port has taken staff safety to a new level with the vessels now being moored by staff that are not on the berth at all. Mooring is now undertaken from the port control offices using cameras to provide vision on the berth.



Cavotec MoorMaster™ MM400E¹⁵ system installed in the Port of Salah



Automated mooring situational awareness

PORT OF NGQURA, SOUTH AFRICA

Similarly to the Port of Salalah the Port of Ngqura experiences vessel surge as a result of long wave. This combined with significant and steady winds resulted in significant risks to both staff and vessels while in the port. Again these effects have been completely removed through the implementation of automated mooring resulting in safe and secure vessels while along side and a safer work environment for the staff.

The ability of the system to monitor wave and wind activity also enables the port to forecast events that may present a danger to the vessel or personnel on the shore or ship.



Cavotec MoorMaster™ MM200C17 system installed in the Port of Ngqura

ST LAWRENCE SEAWAY, CANADA

Finally we look at the St Lawrence Seaway, the river and lock system connecting the Atlantic Ocean with the Great Lakes of North America.

Mooring vessels in these locks exposed staff to significant risks from falling and parting ropes as a result of gear failure.

Additionally at low water level the mooring lines were extremely ineffective at preventing surge in the vessel and thus the risk to vessel or lock at this point of the lockage was very hazardous. Managing these risks was a major part of the operation of the locks. After the implementation of automated mooring not only are the risks to the vessel and staff reduced to almost nothing the locks can now be transited faster and the operation implemented remotely.

Furthermore the automated mooring system has been used to arrest the motion of a vessel with failed propulsion as it entered the locks. This prevent damage to the lock gates and the vessel and significant disruption to the operation of the seaway syste.

Mooring in the locks is now managed from remote control rooms in some cases many kilometres from the locks themselves.

Due to the restricted vessel space in the locks the costs of installation of the system were significant in this case. However disruption to canal operations was avoided by completing this work during the winter when the Seaway is closed due to ice.



Cavotec MoorMaster™ MM400L²² system installed in the St Lawrence Seaway, Canada



Lockside operation of the Cavotec MoorMaster™ MM400L²² system installed in the St Lawrence Seaway, Canada

CONCLUSION

It is an unavoidable fact that conventional mooring presents a danger to staff both on board the vessel and shore side. Furthermore it is unpredictable and performance is difficult to monitor accurately. Automated mooring removes all of the risks and presents a real opportunity for operators to improve their safety records.

CONSTRUCTING MODERN PORTS WITHOUT STEPPING ON WATER

by

Sabino, Leandro Mendes¹ and Filho, Rubens da Costa Sabino²

ABSTRACT

When the decision for the construction of a new port is taken, investors and operators look for a modern and economic engineering solution and a tight schedule for construction and starting of operations.

Engineering solutions for mostly ports structures involves the installation of piles supporting concrete or steel superstructures. In the case of Piers and Jetties an approach trestle is required to reach adequate water depths, and in some cases, pass along shallow or mangrove areas inaccessible or avoided for floating equipment.

For these situations, the strong integration between the structural design and the construction methodology is a key factor for the execution of the works. The cantitravel method which is a system that allows the work to progress regardless of the environmental conditions without stepping in water also means less impact on the environment.

This paper approaches 20 modern port installations worldwide designed and constructed with innovative construction solutions for achieving low costs, low risk, reduced construction time and reduced downtime due to adverse environmental conditions.

1. INTRODUCTION

When the decision for the construction of a new port is taken, investors and operators look for a modern and economic engineering solution and a tight schedule for construction and starting of operations.

Engineering solutions for mostly ports structures involves the installation of piles supporting concrete or steel superstructures. In the case of Piers and Jetties an approach trestle is required to reach adequate water depths, and in some cases, pass along shallow or mangrove areas inaccessible or avoided for floating equipment.

For these situations, the strong integration between the structural design and the construction methodology is a key factor for the execution of the works. The cantitravel method which is a system that allows the work to progress regardless of the environmental conditions without stepping in water also means less impact on the environment.

This paper approaches 20 modern port installations worldwide designed and constructed with innovative construction solutions for achieving low costs, low risk, reduced construction time and reduced downtime due to adverse environmental conditions.

These 20 ports were successfully constructed in Brazil (8), Peru (6), Cuba (1), Dominican Republic (1), Equator (1), Algeria (1) and Republic of Djibouti (2).

¹ Leandro Mendes Sabino, EXE ENGENHARIA LTD, leandro@exeengenharia.com, Brazil

² Rubens da Costa Sabino Filho, EXE ENGENHARIA LTD, rubens@exeengenharia.com, Brazil

2. PORTS AND TERMINALS

2.1. 2001: Belmonte Terminal- Veracel Celulose S.A – Brazil

2.1.1. Brief Description of the Terminal

- Timber loading terminal
- Platform: 136 x 30m, 7 mooring / berthing dolphins and Trestle: 382m long / Breakwater: 320m long
- Barges up to 5.000 DWT



Figure 1: Belmonte terminal – Veracel, Brazil

2.1.2. Why the cantitravel construction method was selected

- Open sea exposed location subject to waves, current and wind action
- Environmental restrictions avoided the construction of temporary jetties in the coast to support the construction activities
- Very shallow water along the coastline

2.1.3. Structure Conception x construction methodology

A technical evaluation of three different spans (8,0 m 10,0 m and 12,0 m) has been performed to define the best regarding the structures and the construction methodology, resulting in the selection of a 10, 0 m typical span.

The structure comprises precast RF concrete elements with minor in situ concrete, supported on steel pipe piles with a RF concrete plug in the top.



Figure 2: Cantitravel - Belmonte terminal – Veracel, Brazil

2.1.4. Key Figures

- 25 m of structure and foundations / week, achieving a production of 1 span/14 h.

2.2. 2002: Pier III- Iron ore Export Terminal – Vale – Brazil

2.2.1. Brief Description of the Terminal

- Causeway: 250m and Trestle: 132 x 10.10m

- Platforms: 24 x 30.10m; 35.6 x 33m and Loading Pier: 364 x 18.75m
- Vessels: 364.767 DWT / 75.000 DWT
- Tide variation: 7.0 m
- Currents: 6 Knots



Figure 3: Pier III, VALE, Brazil

2.2.2. Why the cantitravel construction method was selected

- Extreme tidal conditions with tide variations up to 7.0 m originating currents up to 6 knots.
- Floating equipment and self-elevating platform not suitable for local conditions;
- Accident with a self-elevating platform at the site before the cantitravel method was adopted where applicable;



Figure 4: Pier III, Brazil

2.2.3. Structure Conception x construction methodology

The premise of using a single cantitravel starting from the shore line and proceeding along the trestle and the loading pier was a key factor to define the spans, pile arrangement, structure conception, and weight of the structure elements and equipment to be handled by the cantitravel crane.

Thus, the span of the access bridge and the loading pier were defined at 12 meters and 9 meters respectively.

In the layout there is a 100.95 degrees deflection between the trestle and the loading pier.

Along the trestle the cantitravel advanced in the position in which it would be used in the construction of the loading pier so that its displacement along the same was possible by means of jacking and relocation of its wheels.

The pile guides and templates as well as the cantitravel travelling girders used along the trestle have been reused along the pier after quick adaptations.

All piles were drilled in the rock.

2.2.4. Key Figures

- Trestle: 24 m (2spans) /week

- Loading Pier: 22,5 m (2,5 spans/ week)

2.3. 2004: Liquid Bulk Terminal Doraleh – Djibouti

2.3.1. Brief Description of the Terminal

- Flammable Bulk Liquid Import Terminal
- Causeway: 1,060 m long;
- Foundations with steel pipe piles, steel decks and precast slabs;
- Trestle / pipe racks: 197.5 m long and loading platforms: 15 x 71.25 and 15 m x 56 m;
- Connection between the two Loading Platforms: 14 x 75 m;
- 4 Mooring dolphins.
- Vessels: Main berth 30.000 to 80.000 DWT and secondary berth 5.000 to 30.000 DWT
- Tide variation: 2.9m
- Current velocity: 1 knot

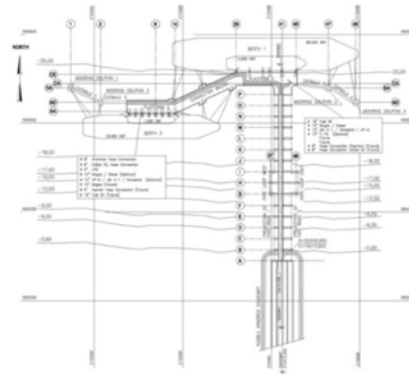


Figure 5: Liquid Bulk Terminal Doraleh – Djibouti

2.3.2. Why the cantitravel construction method was selected

- Substantial reduction of possible delays due to weather conditions, tidal variation, wind, currents and waves;
- Access for men and supplies from behind through the already finished permanent structure;
- Jetty and trestle structures designed mostly with steel structures, reducing cycle time for the cantitravel construction method.

2.3.3. Structure Conception x construction methodology

The 1060 meters long causeway at the beginning of the access to the pier was located at shallow waters close to the shoreline. The trestle is 197.50 meters long, consisting of fifteen 12.50 meters spans. Both platforms consists of 7.5 meters longitudinal spans.

The jetty and the trestle structures were designed mostly with steel structures for the traveler construction method.

The rubble armored causeway replaced part of the steel trestle and allowed the anticipation of the activities on site while the erection of the Cantitravel was underway.

The Cantitravel was used for the construction of the trestle and the berthing structures. For the execution of the mooring dolphins and catwalks, floating equipment was selected.

The Cantitravel was designed to have its wheels relocated due to direction changes along its path.



Figure 6: Liquid Bulk Terminal Doraleh – Djibouti- Cantitravel

2.3.4. Key Figures

- Steel structures fabricated and pre-assemble in Brazil and shipped to the site.
- Construction and installation in Djibouti in 6 months.

2.4. 2005: Areia Branca Offshore Export Salt Terminal Expansion– Brazil

2.4.1. Brief Description of the Terminal

The cantitravel has been used in the construction of the expansion of the storage area of the terminal. The original characteristics of the terminal are:

- Artificial island 10 miles offshore, built with steel circular sheet piles cells filled with dredged sand
- Storage area 100 x 200 m
- Conveyor trestle: 500 m
- 3 mooring / berthing dolphins plus 2 additional new ones and 3 mooring buoys
- Vessels: up to 75,000 DWT
- Barge unloading wharf 200 x 12 m

The cantitravel was used for the expansion of the storage area by 100 x 100 m and the expansion of the barge unloading wharf. The perimeter of the expansion area comprises a sheet pile double wall cofferdam filled with dredged sand. The storage area was also filled with dredged sand



Figure 7: Areia Branca Offshore Export Salt Terminal Expansion– Brazil

2.4.2. Why the cantitravel construction method was selected

- Very exposed location with rough sea conditions
- Use of floating equipment not feasible

2.4.3. Structure Conception x construction methodology

- Vertical steel pipe pile were intercalated along each cofferdam wall to allow the progress of the cantitravel.



Figure 8: Structure Conception x construction methodology

2.4.4. Key Figures

- The average progress of the cantitravel was 15m/week double wall cofferdam

2.5. 2006: Cais 4 – Container Berth Terminal- Suape – Brazil

2.5.1. Brief Description of the Terminal

- Wharf: 600m long x 24m wide;
- Container Carriers: up to 75.000 DWT;
- Tide variation: 2,50m



Figure 9: Cais 4- Suape- Brazil

2.5.2. Why the cantitravel construction method was selected

- Logistics Convenience;
- Local experience;
- Construction speed / Schedule Constraints

2.5.3. Structure Conception x construction methodology

The use of cantitravel makes construction easy due to the high downtime resulting from local currents, waves and winds.

The wharf consists of concrete piles spaced every 4m, supporting a superstructure of precast elements with cast in place concrete.

The wharf construction was divided into two spreads. The first was performed by the Cantitravel and a main crawler crane to execute the activities of pile driving. The secondary spread performed the activities of precast assembly, concreting and rock layer construction with a secondary crawler crane.



Figure 10: Cais 4- Suape- Brazil

2.5.4. Key Figures

- The average progress of the cantitravel was 25 m/week along the wharf

2.6. 2006: Container Terminal - Doraleh - Djibouti

2.6.1. Brief Description of the Terminal

- Vessels: up to 180,000DWT, 12,500 TEU's;
- Yard: 480 x 1050m / Trestle: 2,080 x 36.50m / Wharf: 1050m long;
- Tidal variation: 2.7m



Figure 11: Container Terminal - Doraleh - Djibouti

2.6.2. Why the cantitravel construction method was selected

- Construction activities independent of weather conditions, tidal variation, wind, currents and waves.

2.6.3. Structure Conception x construction methodology

The wharf spans were defined in order to obtain the most effective arrangement to withstand the construction and operational loads. The longitudinal axes were spaced each 6m along the wharf.

The foundation was composed by steel pipe piles with concrete filling at the top. The superstructure consisted of reinforced concrete with 4 longitudinal beams, part in precast concrete and part in cast-in-place concrete connected by T precast elements.

The progress of the wharf construction was based in two main spreads:

- Spread 1: Is the advanced spread performed by the Cantitravel and the main crawler crane, regarding the activities of pile driving;
- Spread 2: Is the secondary construction front following the Cantitravel performed by a secondary crawler crane, regarding the activities of precast assembly and concreting.

The method using two spreads advancing independently permitted to speed up the cycle of activities and the total time of construction works.

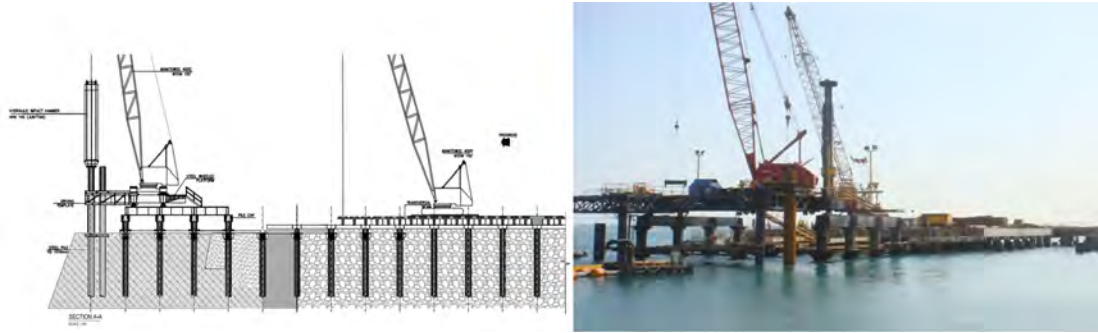


Figure 12: Container Terminal - Doraleh - Djibouti

2.6.4. Key Figures

- The average progress of the cantitravel was 18 m/week along the wharf

2.7. 2007: LNG Melchorita – Peru

2.7.1. Brief Description of the Terminal

- LNG Export Terminal;
- Breakwater: 760m pre-cast concrete blocks / Trestle: 1,350m long;
- 10 Mooring and Breasting Dolphins;
- 120m access bridge to the RLOF (Rock Load Out Facility)
- Utility Dock and Loading Platform: 31.95m wide and 54m long;
- Vessels: tankers up 165,000 m³ of capacity;
- Waves: Hs= 4.2m.



Figure 13: LNG Melchorita – Peru

2.7.2. Why the cantitravel construction method was selected for the construction of the Trestle and the RLOF

- Exposed location to rough seas and wave breaking zone turning unfeasible the use of floating equipment, barges and jack up barges.

2.7.3. Structure Conception x construction methodology

Driven steel pipe piles were used all along the trestle and loading platform. The roadway comprises pre-cast concrete slabs supported by steel decks

Additionally, to the trestle and the platform the use of the cantitravel allowed to build a temporary trestle used to transport and launch majority of rocks for the breakwater, resulting in significant savings.

Also, in this project, with a longitudinal span of 18m, a heavy crane was necessary. Due to the weight of piles and steel structure, all the structure was designed specially to accommodate such operational conditions. Seismic and wave attack have been considered during detail design of the cantitravel.



Figure 14: LNG Melchorita – Peru

2.7.4. Key Figures

- The average progress of the cantitravel was 30 m/week along the trestle;

2.8. 2007: Rock Load Out Facility - RLOF - Melchorita Peru

2.8.1. Brief Description of the Terminal

This work is part of the LNG Melchorita Project, previously described.

The rock load out facility (RLOF), constituted of a quay protected by a breakwater, allowed during construction the load of materials on the split barge used for the construction of the rubble mound breakwater (760m long). After completion of the Marine Works, the RLOF remained as a permanent berth facility to accommodate up to 4 tug boats, a pilot vessel and line boats.

A 250m structure was built to access the rock load out facility. This structure is connected to a rock loading platform 242m long.

- Breakwater: 242.35m long / Trestle: 104.55m long and pier: 141.7m long
- Split barges for the construction of the rubble mound breakwater
- Waves: $H_s = 4.2\text{m}$

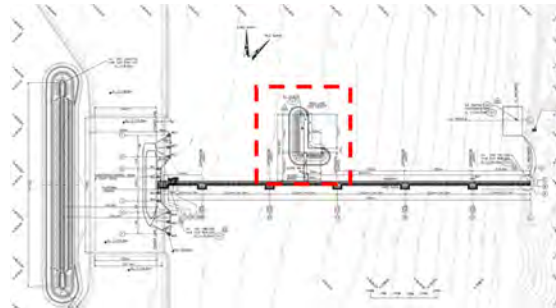


Figure 14: Rock Load Out Facility - RLOF - Melchorita Peru

2.8.2. Why the cantitravel construction method was selected

- Due to the same reasons mentioned for the main structure. As this structure is located 700m from shoreline, the swell is even a worse problem for floating equipment;
- Reducing downtime due to action of waves and breaking zone.

2.8.3. Structure Conception x construction methodology

The concept of the structure is very like the main trestle. Steel pipe piles, steel structure with a pre-cast concrete roadway.

The pier spans of 13m were defined in order to obtain the most effective arrangement to withstand the construction and operational loads.

Due to the inclination of the RLOF, a safety control system was installed in order to guarantee a regular and safe displacement of the RLOF Cantitravel, mainly seawards.

All piles were driven with the Cantitravel system.



Figure 15: Rock Load Out Facility - RLOF - Melchorita Peru

2.9. 2009: Container Terminal - Callao – Peru

2.9.1. Brief Description of the Terminal

- Entrance yard: 400 x 150m / Container yard: 650 x 225m / Wharf: 650 x 36m;
- Vessels: ULCS up to 130,000DWT;
- Embankment.



Figure 16: Container Terminal - Callao – Peru

2.9.2. Why the cantitravel construction method was selected

- Optimizing cycle of activities and reducing total construction time;
- The terminal was to be built in a very confined area with restricted room to barges maneuvering and anchoring. The anchors would interfere with the normal operation of the existing port;
- The cantitravel system has proven in Peru to be an efficient and reliable method for quay construction.

2.9.3. Structure Conception x construction methodology

The piles were steel pipe piles with concrete filling on the top.

The superstructure is pre-cast concrete elements dome shape. This superstructure is a very innovative design eliminating formwork on site.

The wharf spans of 6m were defined to withstand mainly the operational and seismic loads.

The wharf construction was divided into two spreads. The Spread 1 was performed by the Cantitravel and a main crawler crane to execute the activities of pile driving. The Spread 2 performed the activities of precast assembly, concreting and rock layer construction with a secondary crawler crane.

The method using two spreads advancing independently permitted to speed up the cycle of activities and the total time of construction works.



Figure 17: Container Terminal - Callao – Peru

2.9.4. Key Figures

- The average progress of the cantitravel was 18 m/week along the wharf

2.10. 2009: ARZEW Fertilizer Export terminal – Algeria

2.10.1. Brief Description of the Terminal

This work comprised the detailing of Cantitravel system, in order to attend the construction methods of the Access Trestle and Loading Platform as part of the marine structures of the Algeria/Oman Fertilizer Project.

- Bulk Urea and Liquid Ammonia Export Terminal;
- Trestle: 1,200m long and Loading Platform: 260 x 62m;
- Mooring dolphins;
- Vessels: up to 60.000 DWT;
- Steel wheeled platform: 22.10 x 36.60 m;
- Capacity (Crane of 300 tons and Spans up to 20m)
- Waves: $H_s = 4.16$ m for a return period of 1 year.

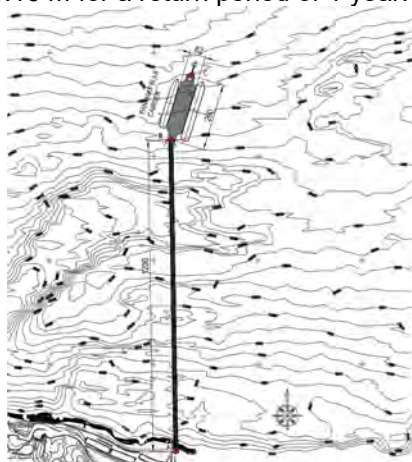


Figure 18: ARZEW Fertilizer Export terminal – Algeria

2.10.2. Why the cantitravel construction method was selected

- Local meteocean severe conditions and unprotected area did not allow the use of floating equipment;
- Heavy equipment for pile driving and assembly structure was required and not available in the region. The equipment to be used on barges would be significantly bigger.

2.10.3. Structure Conception x construction methodology

All structures designed for Trestle construction were adapted to perform also the construction of the Loading Platform.

The Trestle structure was composed of 60 spans 20m long and the platform of 27 axes with variable spans (11.5m and 9m long spans). Foundation is 60" diameter steel pipe piles. Superstructure is formed by steel beams and girders, welded and flanged.

The structure was designed to support a 300 tones crawler crane and all the equipment required for construction activities. The design allowed the crane tracks to be parallel to the trestle axis to increase the load chart capacity for lifting piles and precast slabs up on the trestle.



Figure 19: ARZEW Fertilizer Export terminal – Algeria

2.10.4. Key Figures

Not disclosed.

2.11. 2010: Phosphate Export Terminal - BAYOVAR – PERU

2.11.1. Brief Description of the Terminal

- Trestle: 250m long and Wharf: 250m long;
- Vessels: up to 75,000 DWT;
- Tide variation: 2.14m;
- Waves: $H_s = 4\text{m}$.



Figure 19: Phosphate Export Terminal - Bayovar – Peru

2.11.2. Why the cantitravel construction method was selected

- Unprotected construction area opened to the Pacific Ocean increases considerable the downtime using floating equipment. Rocky bottom profile also makes difficult to operate both barges and jack up barges.
- The height of the structure at the abutment also contributed for the cantitravel method option.

- The use of drilled shafts in the execution of the foundation required a fixed platform to guarantee safe operations.

2.11.3. Structure Conception x construction methodology

The structures of the trestle and platform were constructed in two spreads, Spread 1 and Spread 2. The Spread 1 consisted of a crawler crane on the steel wheeled platform to perform the activities of pile driving. The Spread 2 included a static platform with a secondary crawler crane to perform the activities of precast assembly and concreting.

The static platform was composed of two separated parts located in two spans for its movement. The displacement was performed by the crane to lift and transfer one part towards forward or backward.

The trestle was designed to withstand a 10m span and the wharf was designed with a longitudinal axis each 6.67m. For that, it was possible to develop a solution with a cantitravel that could advance and drive two axes of piles at a time on the wharf construction sequence, reducing the time of the cycle of activities.

The foundations were composed by steel casing allowing the drilling and concrete of the drilled shaft.

The superstructure was a mix of pre-cast and cast in place reinforced concrete.



Figure 20: Phosphate Export Terminal - BAYOVAR – PERU

2.11.4. Key Figures

- Trestle 15 m/week
- Pier 14 m/week

2.12. 2010: Embraport Container (3 Cantitravelers) – Brazil

2.12.1. Brief Description of the Terminal

- Wharf: 660 x 110m;
- Container yard on piles / Container yard on landfill;
- Vessels: up to 120,000 DWT.



Figure 21: Embraport Container– Brazil

2.12.2. Why the cantitravel construction method was selected

- Due to the width of the structure, the use of three cantitravelers speed up the total construction time.

2.12.3. Structure Conception x construction methodology

The wharf was divided into 4 longitudinal segments, with a total length of 660m, consisting of precast and in-situ concrete superstructure supported by concrete piles with 90cm of diameter. The 660m long corresponds to the 1^a Phase of the Terminal, already built. The second phase foresees an extension of 440m, totalizing 1,100m long.

The piles are spaced longitudinally every 3.75m in the axis "A" and every 7.5m for the other axes ("B", "C" and "D").

The construction methods included the use of three cranes on three cantitravelers, working simultaneously to lift and drive the concrete piles of their axes. The precast assembly was performed by a gantry crane, independently of the cantitravelers spread.

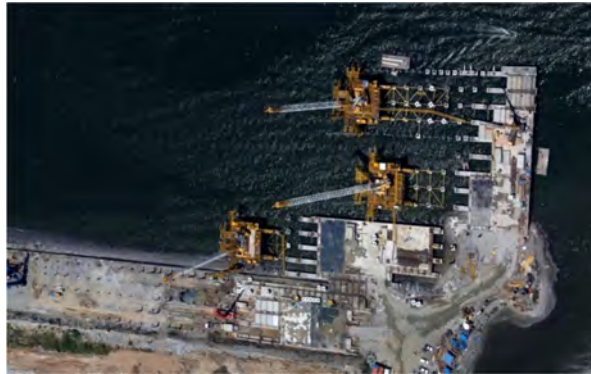


Figure 21: Embraport Container– Brazil

2.12.4. Key Figures

- Wharf 15 m/week/ cantitravel

2.13. 2012: Pier IV – Iron ore Export Terminal- São Luis – Brazil

2.13.1. Brief Description of the Terminal

- Vessels: up to 400.000 DWT;
- Tide variation: 7m;
- Current velocity: 6 knots



Figure 22: Pier IV – São Luis – Brazil

2.13.2. Why the cantitravel construction method was selected

- The structures at this project were initially being built using a jack up barge;
- The conditions at the site do not recommend the use of floating equipment. The currents are very high (up to 6 knots) and tide variation of 7m makes the maneuvering and handing of floating equipment extremely. Not without reason

the jack barge operating at the project has collapsed, turned down and was completely lost.

- At this time, a cantitravel system was quickly mobilized and finished the remaining structures.

2.13.3. Structure Conception x construction methodology

The foundations were composed by steel casing allowing the drilling and concrete of the drilled shaft.

The superstructure is a mix of pre-cast and cast in place reinforced concrete.

The Cantitravel was designed to execute the structures for the Accesses to Pivot 1 and 2 and the platforms of Pivot 1 and 2. The longitudinal spans were 11.30m/15.50m.

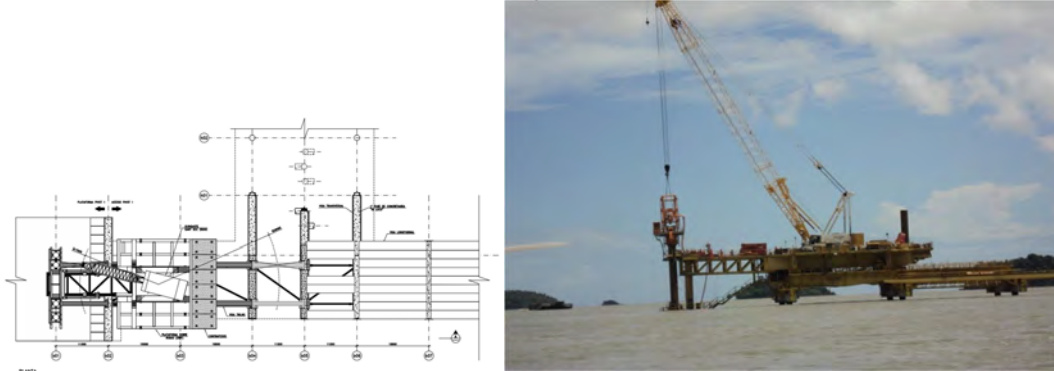


Figure 23: Pier IV – São Luis – Brazil

2.13.4. Key Figures

Not disclosed.

2.14. 2012: Matarani Export Bulk Terminal– Peru

2.14.1. Brief Description of the Terminal

- Trestle: 171m long / Pier: 261m x 21.4m;
- Vessels: up to 50.000 DWT;
- Waves: Hs= 2.84m.



Figure 24: Matarani Export Bulk Terminal– Peru

2.14.2. Why the cantitravel construction method was selected

- The wave conditions, the rock bottom profile and logistics aspects prevent the use of floating equipment;
- Severe wave climate would cause high operation construction downtime. There was no anchoring system allowing safe operation for barges;

- The use of drilled shafts in the execution of the foundation required a fixed platform to guarantee safe operations.

2.14.3. Structure Conception x construction methodology

The foundation is drilled shafts using steel casings. It consists of a system of concrete piles cased with steel pipes, distributed longitudinally every 7.5m and drilled in rock.

The superstructure is composed by pre-cast elements connected by cast in place concrete. The trestle had a slope of 3%, starting at the level +10,60m to the level +7,00m in accordance with the pier elevation.

The cantitravel system was used as support to all construction activities, including pre-cast element and concrete pouring. The crane used in the cantitravel had capacity of 250t, and performed all the activities in only one Spread, such as driving and drilling the piles, lifting and assembly the precast elements.

The cantitravel was designed to have its wheels relocated due to the direction change along its path.

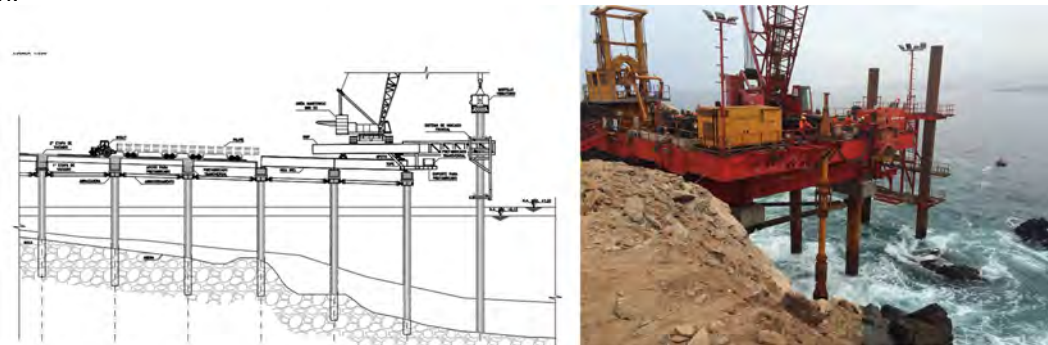


Figure 25: Matarani Export Bulk Terminal– Peru

2.14.4. Key Figures

Not disclosed.

2.15. 2012: Minerals Export Terminal - Callao, Peru

2.15.1. Brief Description of the Terminal

- Trestle: 315m long / Pier: 220m x 21.25m;
- Vessels: up to 60.000 DWT.

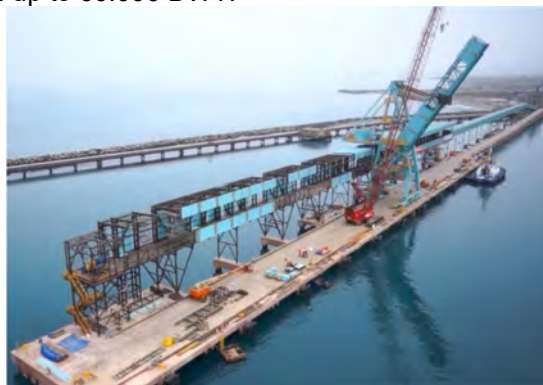


Figure 25: Minerals Export Terminal - Callao, Peru

2.15.2. Why the cantitravel construction method was selected

Similarly, to the Callao Container Terminal, this terminal was built in a very confined area with restricted room to barges maneuvering and anchoring.

2.15.3. Structure Conception x construction methodology

The piles were steel pipe piles with concrete filling on the top. The piles were spaced longitudinally each 10m at the trestle and every 9m at the pier.

The superstructure was pre-cast concrete elements as well as cast in place concrete for connecting the structures.

The pier and the trestle were located continuously, with no deflection between them, and not requiring cantitravel turning.

The construction activities were divided into two Spreads. The Spread 1 was performed by the Cantitravel and the main crawler crane, regarding the activities of pile driving. The Spread 2 was the secondary construction front following the Cantitravel and performed by a secondary crawler crane, regarding the activities of precast assembly and concreting. Both cranes had a capacity of 250t.



Figure 26: Minerals Export Terminal - Callao, Peru

2.15.4. Key Figures

- 25m/week

2.16. 2012: Mariel Container terminal - Cuba

2.16.1. Brief Description of the Terminal

- Wharf: 702m x 37m and Dike;
- Container storage area: 281.115 m²;
- Vessels: up to 200.000 DWT.



Figure 27: Mariel Container terminal - Cuba

2.16.2. Why the cantitravel construction method was selected

- Optimizing cycle of activities and reducing total construction time;
- This project was similar to the Callao Container Terminal, which used successfully the construction method with Cantitravel.

2.16.3. Structure Conception x construction methodology

The wharf consists of a reinforced concrete platform supported by steel pipe piles with concrete filling at the top. The piles are spaced in the longitudinal direction each 7.62m.

The superstructure is composed by a mix of precast type “Domus” and in-situ concrete.

The wharf construction was divided in two spreads. The Spread 1 was performed by the Cantitravel and a main crawler crane to execute the activities of pile driving. The Spread 2 performed the activities of precast assembly, concreting and rock layer construction with a secondary crawler crane.

The method using two spreads advancing independently permitted to speed up the cycle of activities and the total time of construction works.



Figure 28: Mariel Container terminal - Cuba

2.16.4. Key Figures

- 18m/week

2.17. 2016: Import Coal Terminal - Punta Catalina – Dominican Republic

2.17.1. Brief Description of the Terminal

- Trestle: 1300m long / Pier: 335m x 27m;
- Vessels: up to 80.000 DWT;
- Breakwaters;
- Outfall and Intake structures;
- Shore protection;
- Hurricane waves: H=11.5m.



Figure 29: Import Coal Terminal - Punta Catalina – Dominican Republic

2.17.2. Why the cantitravel construction method was selected

- Exposed location to severe wave conditions turn into unfeasible the use of floating equipment, barges and jack up barges

2.17.3. Structure Conception x construction methodology

The trestle connects the structure of the pier to the continent and is divided into 7 segments. The deck of the trestle is at variable elevations, with an increasing slope towards the sea of 0,254%. In the longitudinal direction, the axes are spaced every 12 m.

The pier is divided into two segments. The mainly deck of pier is at elevation of +10.5 m. Fenders and bollards are located on both sides of the pier, connected by a concrete beam placed at the level +7.00 for berthing and mooring of vessels. The piles are spaced longitudinally every 8.7m.

All the piles are steel pipes with concrete filling at the top, and battered 1:10 in the transverse direction only at the trestle. The piles support the precast elements and in situ concrete.

The pier and the trestle were located continuously, with no deflection between them, and not requiring cantitravel turning.

The construction activities were divided into two Spreads. The Spread 1 was performed by the Cantitravel and the main crawler crane, regarding the activities of pile driving. The Spread 2 was the secondary construction front following the Cantitravel and performed by a secondary crawler crane, regarding the activities of precast assembly and concreting.



Figure 30: Import Coal Terminal - Punta Catalina – Dominican Republic

2.17.4. Key Figures

- Trestle: 30m/week
- Pier: 15m/week

2.18. 2018: Posorja Multi-Purpose Terminal – Ecuador

2.18.1. Brief Description of the Terminal(Under Construction)

- Wharf: 200m x 36.43m / Dike / Container yard;
- Vessels: up to 157.000 DWT;
- Tide variation: 3.6m

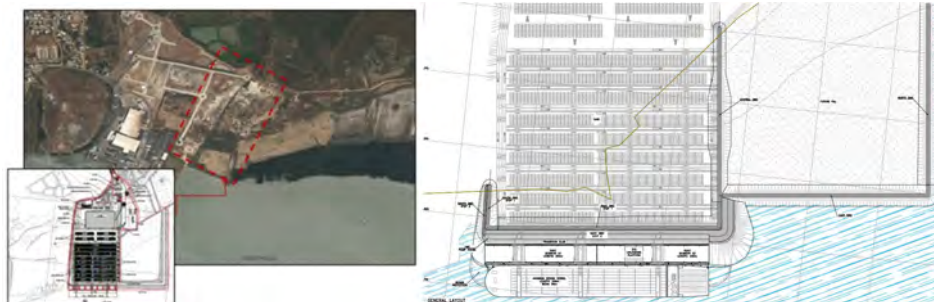


Figure 31: Posorja Multi-Purpose Terminal – Ecuador

2.18.2. Why the cantitravel construction method was selected

- The use of the cantitravel system for the client became very familiar and due to previous experiences the Client considered the construction preferential method.
- Also, the location of the berth related to the access channel to the inner port associated to unfavorable environmental conditions made the cantitravel system a more feasible method.

2.18.3. Structure Conception x construction methodology

The quay of the Posorja Multi-purpose terminal is divided into two segments of 200m each. Under the quay, the dike is sloped, creating different effective lengths for the piles of different axes. All piles are vertical, made of steel pipe piles filled with reinforced concrete, spaced longitudinally every 6.30m.

The piles are drilled shafts into the claystone and sandstone.

Superstructure are domes form pre-cast elements with a cast in place cover slab. This scheme has been proven an efficient and durable structure under hard seismic conditions.

The structure is being constructed using the cantitraveler method, through two construction spreads. The activities of pile driving and drilling are being performed by the main spread, composed by a crawler crane at a steel wheeled platform. The activities of precast assembly and in situ concreting are being performed by a secondary spread, with a crawler crane in the retroarea.

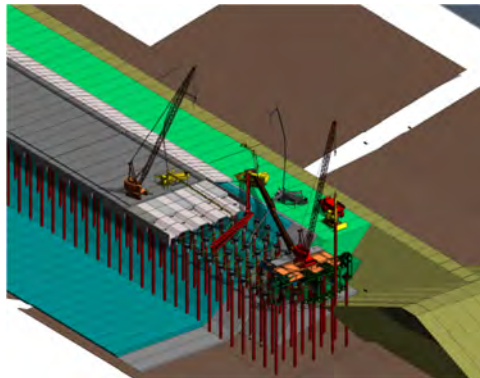


Figure 32: Posorja Multi-Purpose Terminal – Ecuador

2.18.4. Key Figures

- Expected: 15m/week

3. COPYRIGHT

Papers accepted become the copyright of PIANC. The proceedings should be referenced and have ISBN code (to be provided by PIANC HQ).

References

Sabino, L.S., Tepedino M., Hueb M. & Filho R.C.S. (2006). Offshore Bulk Terminals in Developing Countries – Innovative Techniques For Construction, 31st PIANC Congress, Portugal.

BOLLARD LOADS ON NEW PORT INFRASTRUCTURE, PORT OF ROTTERDAM AUTHORITY POLICY

E.J. Broos¹, W. Hoebee², B.R.J. van Scherpenzeel², J.J. Burgers¹, L. Schweter³, A. van Deyzen⁴

ABSTRACT

Mooring of vessels is very important for safe and efficient cargo handling of ships in ports, just as safe infrastructure is important. Civil Engineers and Mariners used to have a different approach for the same problem: what should be the safe working load (SWL) of a bollard. Mariners use the Minimum Breaking Load (MBL) of their mooring lines to determine the desired Safe Working Load (SWL) of the bollard, civil engineers commonly use design tables from international standards or guidelines with a relation between displacement of the vessel and bollard loads. There is a big gap between these two approaches, especially concerning the mooring of large container vessels.

Both disciplines meet each other in dynamic mooring analysis (DMA); a computer calculation that calculates the vessel motions and resulting maximum loads on the mooring point resulting from wind, wave (sea, swell), current and passing vessel forces acting on the moored vessel. As a DMA is a rather complex calculation, a DMA is not carried out for every project and usually not in a preliminary design stage.

This position paper describes a design approach for bollard loads that is understandable and acceptable for all involved disciplines and that is used by the Port of Rotterdam Authority for new builds.

¹ Port of Rotterdam Authority, Port Development, PO Box 6622, 3002 AP Rotterdam, The Netherlands, Phone +31 10 252 1010, Mail: EJ.Broos@portofrotterdam.com & TU Delft, Department of Ports and Waterways

² Port of Rotterdam Authority, Harbor Master Division, PO Box 6622, 3002 AP Rotterdam, The Netherlands, Phone +31 10 252 1010, Mail: w.hoebee@portofrotterdam.com

³ Arcadis Nederland B.V, P.O. Box 137, 8000 AC Zwolle, The Netherlands, Phone +31 88 426 1440, Mail: lutz.schweter@arcadis.com

⁴ Royal Haskoning DHV, PO Box 8520, 3009 AM Rotterdam, Phone +31 88-348 9481, Mail: alex.van.deyzen@rhdhv.com

1. CURRENT CIVIL ENGINEERING DESIGN PRACTICE

Designers of port infrastructure commonly use design tables from international standards or guidelines, for instance Table 1, that can be found in the German EAU 2012 as 'Tabelle E 12-1. Festlegung der Pollerzuglasten für Seeschiffe'. Or similar table 2, that can be found as table 5 from the BS 6349-4:2014.

Table 1. Relation between Displacement and Bollard Loads (EAU)

| Wasserverdrängung [t] | Pollerzuglast [kN] ⁵ |
|-----------------------|---------------------------------|
| bis 10,000 | 300 |
| bis 20,000 | 600 |
| bis 50,000 | 800 |
| bis 100,000 | 1.000 |
| bis 200,000 | 2.000 |
| bis 250,000 | 2.500 |
| > 250,000 | > 2.500 |

Table 2: Mooring point loads for general cargo vessels and bulk carriers (BS6349-4)

| Vessel displacement T | Mooring point load t |
|---|-------------------------|
| 20 000 up to and including 50 000 | 80 |
| Above 50 000 up to and including 100 000 | 100 |
| Above 100 000 up to and including 200 000 | 150 |
| Above 200 000 | ≥200 |

NOTE Storm bollards may be used in the mooring pattern. These are typically >250 t in capacity.

Although not many incidents are known originating from applying these tables⁶, the approach is not always logical. Typical displacements of a Very Large Crude Carrier (VLCC) and a Very Large Ore Carrier (VLOC) are between 300,000 and 400,000 ton whilst a typical Ultra Large Container Ship (ULCS) is between 150,000 and 200,000 ton. Tables 1&2 suggest that the bollards loads are higher for a VLCC or VLOC than for a ULCS. This might be true if these vessels are subject to current loads as a VLCC has a larger draft than a ULCS resulting in more drag in the same current. In many ports however, current loads are relatively low and wind loads may be high to very high for the ULCS due to the large lateral wind area. The pictures in figure 1 show it clearly.

⁵ EAU recommends increasing the bollard loads with a factor 1.25 for vessels > 50,000 ton at berths with strong currents.

⁶ In Rotterdam two bollards are torn from a quay wall, both with human error as main cause. One bollard was overloaded with eight lines, the other with a steep line and with lacking winch supervision. In Antwerp also two cases are reported,



Figure 1. ULCS (CSCL Globe, Albanpix.com) and VLOC (Vale Rio de Janeiro) mooring (PoR)

A second, and perhaps better method is a calculation by hand of the static wind and current loads on a moored ship, for instance using the EAU 2012, British Standard 6349 or guidelines like the OCIMF (Oil Companies International Marine Forum) Mooring Equipment Guidelines (MEG3). Mooring loads derived from a static analysis are only reliable for sheltered locations. PoR recommends using these analyses only to cross check other calculations.

The third method to determine mooring loads is the computer based dynamic mooring analysis (DMA). DMA is a complex computer analysis done by specialists. A DMA is, time consuming, but faster and less expensive than physical model testing. A DMA is the most realistic way to calculate expected mooring loads (under the assumption that the DMA software has been properly validated). A DMA is recommended for the following scenarios:

- Waves are not negligible (sea (<12 s), swell (10-30 s) or infra-gravity waves (30-500 s));
- Passing vessels effects;
- Strong currents (> 3 kn), eddies/unsteady current, rapidly changing speed and direction;
- Strong winds (> 40 kn), unsteady winds, squalls;
- Investigation of sudden line failures (accident analysis);
- A combination of above mentioned items.

Note that for civil engineers it is desired that the ship breaks loose before the bollard or quay wall gets damaged. So all the loads mentioned/ determined in this paper are mooring point loads, not line loads.

2. THE CLASSICAL NAUTICAL APPROACH

Mariners aware of the importance of safe mooring will often have an (international) accepted guideline like the OCIMF MEG3 in mind (it is planned that MEG3 will be replaced with the MEG4 in 2018). The basis is the mooring system. The system contains three main elements: the mooring line, the mooring winch and the bollard.

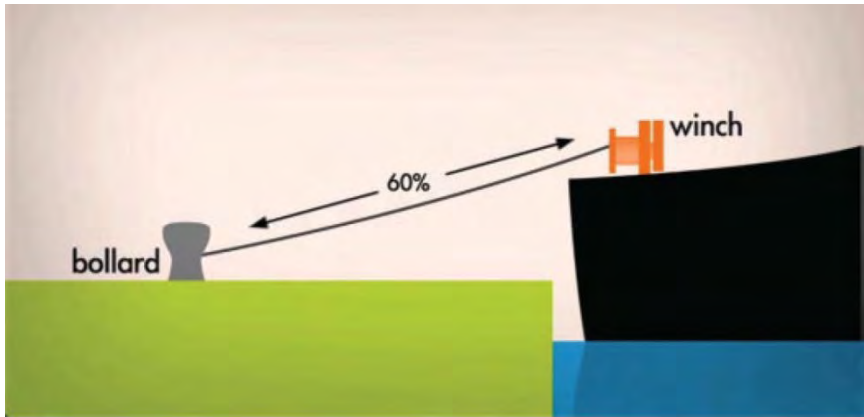


Figure 2. Mooring system (Handbook Quay Walls fig: 5.7)

The key property of a mooring line is the Minimum Breaking Load (MBL) and its Minimum Working Load (Safe Working Load of a mooring line). The MWL is between 50% and 60% of the MBL depending on the exact material properties of the used line. The MBL is a certified value.

A ship is classified with an 'Equipment Number' a parameter related mainly to the frontal surface area to determine the anchoring equipment. The Equipment Number is also used to determine the minimum number and the MBL of the mooring lines on board a ship.

The winch holds the mooring line. It has an 'auto tension' function and a brake function. Auto tension is used under moderate conditions. If the wind strengthens, winches are placed on their brake which increases their applied holding capacity. If a winch in brake mode is overloaded it starts to render. The winch is supposed to render at maximum 60% of the MBL; this is the Maximum Holding Capacity (MHC) of a winch. Remarkably, the MHC is NOT a certified value.

Therefore the failure mechanism is that first the winch should render, then the mooring line should break, then the bollard should fail and finally the quay wall is allowed to fail. Therefore to the "mariner's" opinion the SWL of the bollard should be higher than the sum of the MBLs of the mooring lines secured to that bollard. It is noted that the SWL of a bollard is a certified and representative value. Failure of supporting infrastructure is not considered to be part of the system, although on a dolphin it can be a (not recommended) strategy.

3. THE CLASH BETWEEN THE CIVIL AND THE NAUTICAL APPROACH

At this point the nautical and civil engineering approaches clash as it is common practice to have three or four mooring lines per bollard. Almost all ULCSSs are equipped with mooring lines with a MBL of 130 ton. If three lines are used on one bollard, that would require a bollard with a SWL of 3900 kN.

Bollards that strong are not available on the market and certainly not installed on most quay walls world wide. Therefore a bollard with a $SWL \geq N \times MBL$ (N = number of lines on bollard) is not feasible.

4. HOW THE MOORING SYSTEM REALLY WORKS

Under normal conditions a ship is moored with winches on auto tension, if allowed by the Port Authority. Auto tension function results in relatively low holding forces, typical maximum reported forces are 30 tons for the largest vessels. If conditions worsen, winches are set to brake mode. Under heavy storm conditions a single winch can be overloaded. In that situation 1) the winch renders little and loads are redistributed or 2) the winch continues rendering and a second and third winch are

overloaded and also start rendering. At this point tugs are already needed, otherwise the ship breaks loose. Rendering should occur at maximum 60% of the MBL.

It is therefore reasoned that the maximum loads on mooring point should not be linked to a vessel's displacement, but to the MBL of the lines aboard.

5. TRANSLATING LINE FORCES TO CIVIL ENGINEERING BOLLARD LOADS

In the EU, a civil engineer designs the bollard foundation according to Eurocode. Eurocode doesn't describe anything about mooring of ships; however it states that all constructions have to withstand the following limit states:

- SLS (Serviceability Limit State)
SLS is the maximum expected load during operational conditions. Under SLS conditions the construction behaves normally.
- ULS (Ultimate Limit State)
ULS is a combination of factored loads and factored resistances resulting in the required safety level according to Eurocode 2. Loads are raised with a partial load factor (1.5) and ground parameters are reduced with material factors.
- ALS (Accidental Limit State)
ALS is a geotechnical limit state with all factors back to 1.

As switching from auto tension to brake mode is common practice, the situation of winches in brake mode must be considered the SLS for a bollard. The Port of Rotterdam Authority doesn't send vessels to sea under storm conditions. Therefore, the shore side mooring system should survive a ship with all winches rendering. This winch rendering should be taken as the design value for a bollard. The winch will render at the Maximum Holding Capacity (MHC) of the winch. The MHC varies between 50% and 60% of the MBL of the mooring lines. So tension will never be larger than the MHC. Thus the representative load (F_{rep}) on a bollard is 60% MBL per line:

$$\text{SLS: } F_{rep} = N \times 0.6 \times \text{MBL} \quad (1)$$

The ULS is a combination of factored loads and factored resistances resulting in the required safety level according to Eurocode 2. Loads are raised with a partial load factor (1.5) and ground parameters are reduced with partial material factors. The design value of the bollard load will be:

$$\text{ULS: } F_d = 1.5 \times F_{rep} = N \times 0.6 \times \text{MBL} = 0.9 \times N \times \text{MBL} \quad (2)$$

The ALS or the human factor: If the winch is in brake mode, the following situations can occur:

- Due to poor maintenance of winches, the brake is fully blocked and the winch will not render;
- There is poor communication between ship and shore and/ or;
- There is no winch supervision.

Under these conditions, the tension in the shortest mooring line will rise up to MBL once e.g. the tide is rising/falling or the vessel is being (un-)loaded. Either this line (and the bollard) survives this overload or the line breaks and the tension in the next line will rise towards MBL and breaks as well. At this point the ship will start moving and the entire mooring system will fail and the ship breaks loose.

If one winch suffers from poor maintenance, it can be argued that the other winches are poorly maintained as well. The same is valid for bad communication and poor winch supervision. So the question is: can two or more lines on the same bollard reach the MBL simultaneously?



Figure 3. Parallel mooring lines in Rotterdam (photo Marco Alpha Fotografie)

Simultaneously reaching the MBL of more than one line requires that these lines have the exact same properties (e.g.: material, diameter, length, angle and initial tension). This is not impossible as all mooring lines aboard generally have the same properties and lines very often run parallel per two. However, due to small differences in e.g. angles or different winch positions on deck, different fairleads or chocks, it will be very difficult to reach this situation. It is therefore physically almost impossible that two lines at the same bollard reach the MBL at the same time.

Therefore even if human and material failure is complete, maximum two mooring lines at one bollard will reach MBL at once.

In Eurocode, the ALS is a geotechnical limit state for which all factors are reduced back to 1. In this situation all the winches fail and they do not render at 60% MBL. Nobody monitors the winches. Two lines have exactly the same properties and other lines on the same bollard have less tension; arbitrarily assumed to be max 60% of the MBL. The accidental limit state will therefore be:

$$\text{ALS: } F_{\text{acc}} = 2 \times \text{MBL} + (N-2) \times 0.6 \times \text{MBL} \quad (3)$$

The three limit states are summarized in Table 3 and the consequences for 2, 3 and 4 lines per bollard are indicated.

Table 3. Limit states for bollards

| | Formula | 2 lines | 3 lines | 4 lines |
|-----|--|---------|---------|---------|
| SLS | $N \times 0.6 \times \text{MBL}$ | 1.2 MBL | 1.8 MBL | 2.4 MBL |
| ULS | $1.5 \times N \times 0.6 \times \text{MBL}$ | 1.8 MBL | 2.7 MBL | 3.6 MBL |
| ALS | $2 \times \text{MBL} + (N-2) \times 0.6 \times \text{MBL}$ | 2 MBL | 2.6 MBL | 3.2 MBL |

As the Port of Rotterdam Authority allows three mooring lines on one bollard, this means that the ULS is the governing limit state, especially because the ALS uses no factors on the material properties whilst ULS does. The SWL of a bollard should (at least) equal the load in the SLS. However, this Table 3 is still quite rough and can be nuanced as a few things are ignored.

The following MBLs are suggested be used for container vessels in Port of Rotterdam Authority projects:

Table 4. MBLs and bollards for container vessels

| Vessels | DWT (scantling [t]) | LOA [m] | Beam [m] | Scantling Draft [m] | MBL | Bollard load |
|--------------|---------------------|-----------|---------------|---------------------|---------|--------------|
| Coaster | 6,200 - 15,000 | 107 - 150 | 17.20 - 23.00 | 7.70 - 9.10 | 50 ton | 900 kN |
| Feeder | 17,700 - 38,500 | 160 - 222 | 25.00 - 30.00 | 9.50 - 12.00 | 50 ton | 900 kN |
| Panamax | 38,500 - 66,000 | 211 - 294 | 32.20 | 12.00 - 13.50 | 64 ton | 1152 kN |
| Post-Panamax | 70,000 - 118,000 | 263 - 334 | 40.00 - 45.60 | 14.00 - 14.50 | 83 ton | 1494 kN |
| New-Panamax | 143,000 - 157,000 | 366 | 48.40 | 15.00 - 16.50 | 130 ton | 2340 kN |
| ULCS | 171,000 - 195,000t | 397 - 430 | 56.40 - 59.00 | 16.00 | 130 ton | 2340 kN |

6. NUANCES TO THE N x MBL APPROACH

The approach looking at the winches and mooring lines is still a simplification of the actual situation. The following aspects are ignored and will affect the actual bollard loads. If stated with a [-] this aspect will reduce the load. If indicated with a [+] this aspect will increase the load on a bollard.

[-] Stretching of mooring lines

Long lines will not transfer all the loads directly to the bollard, but will stretch and dampen the peak load that occurred. Steel wires and Dyneema lines are not elastic, but will always have a synthetic (e.g. polypropylene or nylon) tail of typically 11 m long. This tail is elastic and will dampen the peak loads.

[-] Dynamic Mooring Analysis (DMA)

A DMA results in more realistic bollard loads. A DMA is typically carried out assuming fixed winches and unbreakable lines. So the mooring loads can rise to infinity in the model. In the analyses of the results all situations with line loads higher than the MWL or winch loads above 0,6 x MBL are considered to be system failures. These scenarios will not be allowed and result in a certain window where a vessel should leave the berth or other measures have to be taken (e.g. tug support), the “limiting conditions”. Although a solution, tug support is not recommended as a standard scenario in big ports. If the situation is critical, tugs should be available for emergency work and not be used to support insufficient mooring configurations, that can only be done in dedicated situations.

A DMA is currently still a complex calculation that requires a significant amount of work for one berth. This makes that DMAs are not made on a daily base for average ships/berths. PoR makes DMA’s for irregular cases, either very large vessels or untypical situations (e.g. side-by-side mooring at busy fairways like the Calandkanaal in Rotterdam) or to investigate innovative mooring systems like the ShoreTension. The Rotterdam Harbormaster, being responsible for port safety, is mostly the driving force behind such case studies.

[-] Rendering winches

Actually a vessel with all winches rendering should not be considered as a SLS scenario. It should be threatened as an ALS scenario; it is a very undesired scenario. However, to be able to use the rendering winch and not a blocked winch as the design criterion, this will require certified winches. This is NOT the case; the Port of Rotterdam Authority is working on this subject with the IACS (International Association of Classification Societies) and IHMA/EHMC (International Harbour Master’s Organization/ European Harbour Master Committee). Results on this aspect will take a very long time.

[-] Bending of mooring lines in the fairlead

Bends in the mooring line will reduce the tension on the bollard as a part of the tension is transferred at each bend. On a vessel there is at least one force transfer point, the fairlead where the line leaves the ship, often a second one is found in a roller at deck as can be seen in Figure 4. Therefore a

fairlead should actually be considered as an additional element in a mooring system next to the bollard, line and winch.



Figure 4. Mooring lines at forecastle deck in Rotterdam (photo Port of Rotterdam)

Note: The Boatmen in Rotterdam, who developed the hydraulic mooring support Shore-Tension, report that lines often break below the MBL. This can be explained by normal wear and tear, but this may also be caused by these additional force transfers. As the mooring lines, although kept on or below their SWL, broke so often that Shore-Tension nowadays only applies their own dyneema lines with the Shore-Tension system.

[-] Load factor of 1.5 between SLS and ULS

As the proposed philosophy is quite conservative, the factor of 1.5 in the Eurocode to determine the ULS load is quite (or perhaps too) high. In the past this factor was according to the EAU 2004 and older versions 1.3 (and 1.5 for the bollard anchors). The EAU 2012 uses 1.5 as well for both the bollards and the anchors. As stated earlier the BS6349 1:2 still uses 1.3 despite Eurocode. More statistic research in actual bollard loads can either change the SLS or the ULS values. This research could be a combination of DMAs and field measurements.

[-] The spatial dimensions of a bollard and the angles of the mooring lines on a bollard

Although considered to be a point, the bollard is actually a solid structure with relatively large dimensions. This whole theory determines a horizontal point load on bollard foundations, perpendicular to the fender line of a berth. This is a simplification of the worst case and input for the quay wall or dolphin design.

In practice, line forces act on the bollard and these result in shear forces and bending moments within the bollard that are transferred to the foundation. Secondly, the lines almost always have (different) horizontal and vertical angles. These angles result in smaller resultant stresses in the bollard and certainly lower forces on the bollard foundation.

The effect can be adequately calculated, however in Rotterdam this will be reserved only for re-validating existing bollards if they don't meet the simplified theory as described in this paper.

In such a case, the approach (in Rotterdam) would be a DMA and use the output of the DMA as input for the PoR internal bollard calculation sheet, and if any doubt still is present, a FEM calculation of the bollard. This will result in a governing scenario for safe mooring of a specific ship at a specific existing berth.

[+] Development in winch & line capacity

The described approach in this paper is based on winches and mooring lines capacity. There is obviously a chance that mooring lines and or winches will increase in capacity. If that would happen, theoretic bollard loads will increase. It is interesting so see that although container vessels have grown dramatically in size, mooring lines did not. The main solution is to increase the amount of lines and winches.

Increasing of the MBL will challenge many ports around the world. Berths often cannot be adapted on this point, either due to a lack of space for additional bollards or a lack of horizontal capacity in the structure itself. And if the berth is adapted, this is generally done by applying larger distances between moored vessels; this reduces quay capacity and might still result in unfavorable mooring configurations. So increasing MBL will generally create a false safety for ship owners or less optimal berth utilization on terminals. Secondly, the strength of winch decks is limited, the equipment number is currently the design base for these decks and thus for ship classification. Thirdly, a short inventory with mooring line producers and IACS teaches that 130 ton MBL is a maximum that is ordered for vessels at present. Stronger lines are available, but are only used for offshore activities and some ULCs. Therefore, values like the MBL values in Table 4 are considered to be realistic for the purpose of designing safe bollards. In Rotterdam a larger version of Table 4 is used for design of new infrastructure. Specific ships that deviate from this table are ignored for new building situations.

[+/-/?] Equipment number as basis for MBL

Currently the equipment number of a ship is used to determine the minimum required MBL of vessels. In practice much higher MBL's are used by ship owners (source: IACS). It makes sense to use mainly the lateral surface of a vessel to determine the minimal MBL instead of the frontal surface, as is done with the equipment number. Using the lateral surface should result in a higher minimal required MBL, closer to daily practice.

[+] Ships without winches

The entire theory is based on vessels with winches. However some ships pay out additional lines and belay them on the gypsy head or bollard because the amount of winches is too low. In that case there is no MHC and it is easier to reach the MBL in an extreme scenario (e.g. due to human failure).

7. QUICK RELEASE HOOKS

For the foundation of a QRH unit the same approach as for a bollard can be used. However there is one additional requirement that should be taken into account: The SWL of an individual hook should at least equal the MBL of the applied line, as it is never certain which line will be failing first. The mooring point load then becomes: $SLS: F_{rep} = N \times 0.6 \times SWL_{hook}$. It may be that two lines are used on the same hook; although this is not recommended it is regularly seen in practice. In such cases the hook can be approached as a bollard, meaning that the SWL of the hook should be $\geq 2 \times 0.6 \times MBL$. But this situation requires an expansion of the mooring facilities such that one line per hook can be used. QRHs can generally be found on liquid bulk terminals, a breaking bollard is obviously very dangerous to humans present, but a breaking QRH can increase this risk due to the cargo handled as one spark can result in a massive blast.

An additional advantage of QRHs is that they can be monitored, in terms of line loads during the entire time of the mooring. With that knowledge for each hook - the terminal operator can easily verify that conditions are within the allowable operational limits, and record values. If there is an incident, the history can be reviewed. With bollards this can't be done easily, it is only possible to install gauges on the mooring line, which is time consuming. There is a challenge here for the market.

8. COMPARING THE NEW POR POLICY WITH INTERNATIONAL RECOMMENDATIONS

The Port of Rotterdam Authority is not the only party in the world concerned about determining safe bollard loads. As stated, for bollards often only tables like Table 1 & 2 are used. For quick release hooks there are more guidelines.

MOTEMS recommends a mooring point load of $F_d = 1.2 \times MBL (1 + (N-1) \times 0.75)$ and only one line should be placed on each hook.

The latest guideline on this point is the PIANC MarCom report 153 “Recommendations For The Design And Assessment Of Marine Oil And Petrochemical Terminals”. This report recommends: $F_d = SWL (1 + 0.6 \times (n-1))$ for US terminals where SWL is de SWL of an individual hook in a multiple hook unit. MarCom report 153 follows BS6349 1:2 for the EU. BS6349 1:2 states in table H.2: for three lines on one mooring point: $F_d = 1.3 \times F_{rep} = 1.3 \times 3 \times 0.6 \times MBL = 2.34 MBL$, this deviates from the BS 6349-4. Most relevant seems to be the BS6349 1:2, where the same conclusion is drawn, only the factor to obtain the ULS value differs. 1.3 is not in line with Eurocode and also not in line with EAU 2012. It is in line with the outdated EAU 2004. A comparative overview is presented in table 5.

Table 5. Comparing various approaches for mooring foundations design loads

| 3 lines, MBL 1,300 kN | F_{rep} (SLS) | F_d (ULS) |
|------------------------------|------------------------------|---|
| PoR | 1.8 MBL = 2,340 kN | F _d = 1.5 x F _{rep} = 2.7 MBL = 3,510 kN |
| EAU (<200,000 ton) | 2,000 kN | F _d = 1.5 x F _{rep} = 3,000 kN |
| BS 6349-4 (<200,000 ton) | 1,500 kN | F _d = 1,4 x F _{rep} = 2,100 kN |
| PIANC US terminals | - | F _{za} = SWL _{hook} (1+ 0.6 x (N-1)) ≥ 2.2 MBL ≥ 2,860 kN |
| PIANC EU terminals | 1.8 MBL | F _d = 1.3 x F _{rep} = 2.3 MBL = 3,042 kN |
| MOTEMS | - | F _d = 1.2 x MBL (1+ (N-1) x 0.75) = 3.0 MBL = 3,900 kN |

It should be noted that limit state design is not used in the US and not in the same way in the UK. It can be concluded that the new approach results in heavier bollards than previously designed, but that the bollards are in line with other international recommendations valid for quick release hooks. This new design approach does not disqualify existing bollards, but points out that for mooring large vessels on old quay walls, often a more detailed study, like a DMA, essential is to guarantee safe mooring.

It should also noted that EAU recommends to apply a heavier bollard as soon as the DWT develops over 200.000 ton (F_{rep} 2,500 kN, F_d 3,750 kN) . The November 2017 announced CMA CGM carriers with a capacity of 23,500 TEU will have more displacement, but PoR assumes they still will have lines with a MBL of 1300 kN.

It is important to realize that PIANC, but also OCIMF refer to locally available standards to determine mooring point loads, just as described in this paper.

9. DIFFERENCE BETWEEN QUAY WALL AND DOLPHINS

The impact of a heavier bollard in the design of a quay wall is negligible. This is however NOT the case for a mooring dolphin where mooring loads are often governing for design (a breasting dolphin also has to withstand fender loads of the mooring vessel). Therefore, it is recommended to use the simplified approach only in the preliminary design and execute a DMA in the final design stage to obtain a more specified design. For a dolphin it might also be acceptable to have buckling in the pile as third failure mechanism before the bollard or QRH collapses. PoR however does not accept

buckling to be the third failure mechanism, is results in expensive damage and a long down time period for the entire berth. .

10. ROTTERDAM STANDARD BOLLARD

Rotterdam modified its existing standard bollards. In the past PoR used at some container terminals central break bolts in the bollards, but mostly breaking welds. Due to bad experience on a test bank, PoR stopped with breaking bolts. From 2015 PoR decided that buckling of the base plate should occur before failure of the anchors. This change mainly influenced the dimensions of the weld between the casted bollard and the rolled base plate, as it is no longer a breaking weld, it became much stronger. The plates at the end of the anchor that transfer the load into the concrete are designed with a safety factor of 1.75 instead of 1.5 to guarantee that the anchor itself will fail before the concrete will fail.

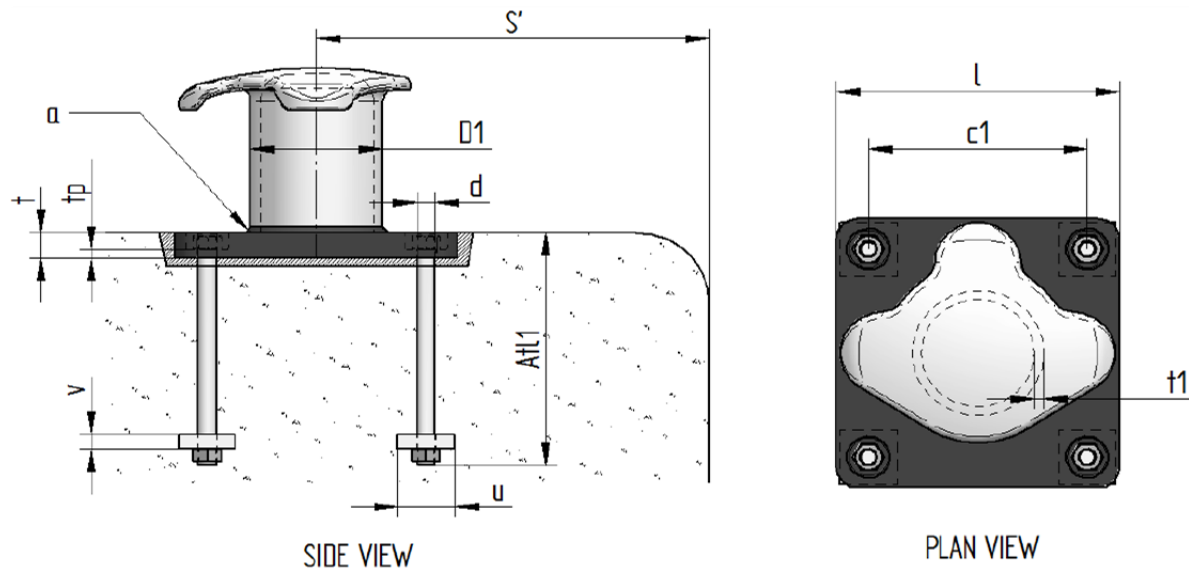


Figure 5. Standard bollard Rotterdam

Furthermore, PoR decided to go back from six types of bollards (SWL: 600, 800, 1000, 1500, 1750 & 2400 kN) to four. A 600 kN bollard for barges, a 1000 and 1500 kN bollard for sea going vessels and a 2400 kN bollard for the large vessels, especially ULCS. This makes the port more flexible to use and optimizes management of the assets. This SWL is permanently indicated on top of the bollard as can be seen in Figure 6. The supporting infrastructure is obviously designed with the SWL of the bollard as representative load in the SLS and not with the applied MBLs.



Figure 6. Standard 2400 kN bollard Rotterdam

11. CONCLUSIONS

Safe mooring equipment and its foundations for new infrastructure in Rotterdam should be designed for human failure based on the MBL and number of the applied mooring lines. The direct relation between displacement and expected maximum bollard loads, as used in the past, is not accurate.

Using the method as described in this paper the civil and nautical approaches to determine bollard loads match. It is advised to use the following table for the bollard design:

| | Formula | 2 lines | 3 lines | 4 lines |
|-----|--|---------|---------|---------|
| SLS | $N \times 0,6 \times \text{MBL}$ | 1.2 MBL | 1.8 MBL | 2.4 MBL |
| ULS | $1.5 \times N \times 0.6 \times \text{MBL}$ | 1.8 MBL | 2.7 MBL | 3.6 MBL |
| ALS | $2 \text{ MBL} + (N-2) \times 0.6 \times \text{MBL}$ | 2 MBL | 2.6 MBL | 3.2 MBL |

This still is a conservative approach, but it guarantees safe mooring points ashore. Nuances can be made, but these nuances require more research and probably make it more difficult for all parties to understand whether it is safe or not to moor their vessel at fewer bollards. For existing infrastructure a more complex method of DMA and FEM can prove the safety of a moored vessel.

The Port of Rotterdam Authority wants to gain more insight in actual bollard loads by doing more DMAs and do as much field measurements as possible.

However, to create a really good and 100% safe mooring arrangement, mooring winches should be part of the certification of a ship.

12. ACKNOWLEDGEMENTS

The authors wish to thank PIANC WG 153, especially Martin Eskian, PIANC WG 186, IACS and the 'Arbeitsausschuss Ufereinfassungen' for the cooperation and the good discussions.

REFERENCES

BS 6349-4:2014, Maritime works. Code of practice for design of fendering and mooring systems. 30 June 2014, ISBN: 978-0-580-66969- 9

BS 6349-1-2:2016, "Maritime Works. General Code of Practice for Assessment of Actions", June 2016.

California Building Standards Commission (2013). California Building Code, Title 24, Part 2, Chapter 31F, Marine Oil Terminal Engineering and Maintenance Standards (MOTEMS).

Empfehlungen des Arbeitsausschusses "Ufereinfassungen" Häfen und Wasserstraßen EAU 2012 , November 2012, ISBN: 978-3-433-01848-4

Gijt, J.G. de, Broeken, M.L. (2013). Quay Walls – Second edition 2013, C211E, ISBN 978-1-138-00023-0

OCIMF Mooring Equipment Guidelines (MEG3), October 2008, ISBN 13: 978-1-905331-32-1 (9781905331321)

PIANC MarCom report 153 "Recommendations For The Design And Assessment Of Marine Oil And Petrochemical Terminals", 2016.

www.shoretension.com

The safe use of cylindrical fenders on LNG, Oil and Container Terminals

E.J. Broos¹, M.P.M. Rhijnsburger², A. W. Vredeveltdt², W. Hoebee³,

ABSTRACT

The PIANC 'Guidelines for the design of fender systems' MarCom report of WG 33 – 2002 specifies allowable maximum hull pressures for various vessels. Fender manufactures provide maximum hull pressures resulting from their fenders. The stated maximum hull pressures of cylindrical fenders exceed the recommended values by PIANC 2002 for gas carriers, oil tankers and container vessels. However, cylindrical fenders are in use for over 25 years in North West Europe on major container terminals without any complaints by masters, ship owners, pilots or any other stake holder.

In the Hamburg – Le Havre range only the Port of Rotterdam Authority had, mid eighties, these fenders (Delta Terminal) checked against the old fender guidelines. After PIANC 2002 release all new projects are equipped with panels with cone fenders or similar.

The maintenance department of the Port of Rotterdam has fairly bad experience with panel fenders as recently applied at the new container terminals and has quite positive experience with the 'old' cylindrical fenders.

The positive user experience with cylinders and the negative maintenance experience with panels lead to plans with cylindrical fenders on an LNG berth and on six oil berths. The actual ship-fender interaction was investigated by FEM calculations as these cylindrical fenders do not match PIANC 2002 recommendations. The outcome of these FEM calculations is that cylindrical fenders can safely be used for both LNG carriers and oil tankers.

This paper explains these FEM calculations and the old calculations for the Delta Terminal and shows that cylindrical fenders can be used safely on liquid bulk terminals and gives a perspective for container terminals. The authors recommend that table 4.4.1 in PIANC 2002 will be updated.

¹ Port of Rotterdam Authority, Port Development, PO Box 6622, 3002 AP Rotterdam, The Netherlands, Phone +31 10 252 1010, Mail: EJ.Broos@portofrotterdam.com & TU Delft, Department of Ports and Waterways

² TNO Technical Sciences, P.O. Box 49, 2600 AA Delft The Netherlands, Phone +31 (0)88 866 14 66, Mail: marnix.rhijnsburger@tno.nl

³ Port of Rotterdam Authority, Harbor Master Division, PO Box 6622, 3002 AP Rotterdam, The Netherlands, Phone +31 10 252 1010, Mail: w.hoebee@portofrotterdam.com

1. DESIGN AND USE OF FENDER TYPES ON QUAY WALLS IN ROTTERDAM

In the far past vessels were moored against wooden beams. Small rubber rolls were installed between the masonry and the wooden beam when some energy absorption was desired. Up to today dry bulk and break bulk vessels in Rotterdam are moored on either a wooden fender system, or a HDPE system, both fully rigid without energy absorption. These vessels don't need an energy absorbing fender system (Broos, 2013).

In the mid 80's Rotterdam started the development of Europe's largest container terminal, the ECT Delta Terminal. This modern container terminal then was fitted out with cylindrical fenders. The usability of these fenders was proven by intensive calculations by Lloyds in 1989.

In 2005 Rotterdam started with the construction of the Euromax container terminal, which was outfitted with cone fenders with large panels. Quay walls of the same design with similar fenders were built at Maasvlakte 2 for the container terminals RWG and APM. See figure 1.



Figure 1: Overview Maasvlakte 1 and 2 with container terminals (photo PoR GIS database)

1.1 Use of cylindrical fenders in North West Europe.

Cylindrical fenders are also widely used in the surrounding ports in North West Europe. Sometimes combined with floating foam fenders (the German Swim Fenders), often just with cylinders. Today these fenders are still in use to the satisfaction of the Port Authorities, the pilots, the ship owners and the Terminals. New projects however are often equipped with panel fenders.



Figure 2: Cylindrical fenders at Delta Terminal Rotterdam (photo PoR)

1.2 New container terminals and cone fenders with panel

The massive step in cone fender systems with large panels in Rotterdam comes from Euromax container terminal. For which a 1900 m deep sea quay wall was constructed between 2005 and 2007 on the most northern part of Maasvlakte 1. The choice for using fender panels was clearly derived from the hull pressure criterion stated in PIANC 2002. During the construction of Maasvlakte 2, 2.2 km of the same cross section, with the same fender system has been built for both RWG and APM container Terminals.

Although these quay walls are primarily designed for deep sea, there is a clear mixed use of the facilities by barges, short sea and deep sea vessels. As a result of the use by barges, 30% of the fender panels are equipped with ladders in or on the panel.



Figure 3: Damaged fender panels at Euromax Container Terminal Rotterdam (Photos PoR)

1.3 Maintenance of fenders

The asset management department of port of Rotterdam experiences differences between the fender systems. At the Delta terminal there is hardly any damage to the cylindrical fenders. Once in a while a fender is heavenly hit, the chain breaks and the rubber cylinder sinks directly in front of the quay wall. A diver is send down, the cylinder is hoisted to the surface and with a new shackle the fender is reinstalled. The cost of the entire operation is below 5,000 Euro without downtime at the terminal. Recently, after 25 years of operation, at the end of their technical life time, the chains and bars of the cylinders are replaced; the rubber cylinders are still in good condition and were completely maintained.

At the panel fenders a few damages occur very often:

- Damage to the PE sheets covering the panel. The sheets on the sides of the panel are so often damaged that these sheets are not be replaced any more. Figure 3;
- Damage to the steel of the fender panel, mainly due to bow contact by barges or feeders;
- Corrosion of the panel, leading to leakage;
- Damage to the platform that connects the in panel ladders with the quay front, mainly caused by mooring lines;
- Damage to the ladders on the side of the panel;
- Rupture of rubber cylinder by shear force, average 2 per year in Rotterdam;
- Breaking chains, mainly by ropes or by ship contact;
- Loss of tension in the chains, reason unknown but a lack of action will damage primarily the rubber and the walk platform towards the shore.

For most of the repairs, it is necessary to remove the panel from the quay wall, bring in a spare panel. There is downtime at the terminal and the costs of a repair action are on average between 50,000 and 70,000 Euro.

The amount of damages to cylinders is significantly lower than damage to fender panels. Over the last ten years less than 5% of the cylinders were teared off and are brought back. Only at Euromax 70% of the panels has been removed, repaired and installed back to the quay.

1.4 Experience of Pilots with the different fender systems

The pilots don't experience real differences during berthing operations. The only aspect mentioned by pilots is, when mooring tankers, with the steel lines connected but slack so the lines are under water, the spring lines can get stuck under the cylinders when heaved. If such happens, the line has to be released; that requires quick release hooks for steel spring lines.

1.5 Experience on container terminals with the two fender systems

When a vessel is moored alongside a quay wall there is a different behavior between rubber cylinders and HDPE panels. Between the rubber cylinders and the concrete quay wall, as well as between the ship hull and the fender, there is friction. When properly moored this friction dampens the surge motions of a vessel. The HDPE sheets on the panels with cone fenders generate hardly any friction. Especially with passing vessels it is easier to reduce ship movements with cylindrical fenders (statement Rotterdam Boatmen - KRVE). Less surge motion at container terminals means a more efficient loading or unloading operation.

In Rotterdam often ShoreTension® is used to improve the mooring of Ultra Large Container Ships. At terminals with cylindrical fenders the pair of ShoreTensions is applied to the breasting lines, pulling the vessel a little into the rubber, reducing both surge and sway (figure 4). At terminals with fender panels, a pair of ShoreTensions is applied on the spring lines to reduce surge motion. Sway motions are not dampened in this way, but hinder by sway for operations is only limited.



Figure 4: Shore tension applied at Delta Terminal (Photo PoR-Erik Broos)

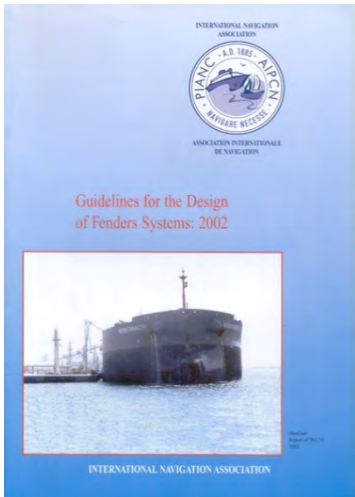
Most terminal operators only work with one fender system, so up to now this difference has never been an issue in project development. But from an operational point of view cylinders are recommended.

2. THE DEVELOPMENT OF THE SMALL SCALE LNG TERMINAL IN ROTTERDAM

As LNG is demanded in smaller volumes, both for small ports, power plants and especially for bunkering sea going vessels, the Port of Rotterdam developed a small scale facility together with Gate Terminal. This was a quay wall in a separate basin, the Yukonhaven (Broos, 2016). Oil bunkering in Rotterdam is always executed with barges and such is also foreseen for LNG in the future. So this Small scale facility will receive a mixture of barges and small sea going vessels (LOA up to 160 m in phase 1 and 210 in phase 2). Design according to SIGTTO standards will result in the need for energy absorbing fenders. Being the home base for bunker barges, there will be a lot of inland vessels to the quay as well. This, in combination with the experiences on the container terminals lead to a design with cylindrical fenders.

2.1 The issue: cylinders do not match PIANC recommend hull pressures

When designing cylindrical fenders one specific aspect arose. The cylinders will result in a hull pressure more than twice as high as the PIANC Guidelines for the design of fender systems 2002 (PIANC 2002) recommends in table 4.4.1



| Type of vessel | Hull Pressure kN/m ² |
|---|------------------------------------|
| Container vessels 1st and 2nd generation | <400 |
| 3rd generation (Panamax) | <300 |
| 4th generation | <250 |
| 5th and 6th generation (Superpost Panamax) | <200 |
| General cargo vessels | |
| =/ < 20.000 DWT | 400-700 |
| > 20.000 DWT 40 | <400 |
| Oil tankers | |
| =/ < 60.000 DWT | <300 |
| > 60.000 DWT | <350 |
| VLCC | 150-200 |
| Gas carriers (LNG /LPG) | <200 |
| Bulk carriers | <200 |
| SWATH | } |
| RO-RO vessels | } these vessels are usually belted |
| Passenger Vessels | } |

Figure 5: PIANC 2002 table 4.4.1 Hull Pressure Guide

Hull pressure resulting from cylindrical fenders will be around 400 to 500 kN/m². However, looking to the table only 200 kN/m² is allowed for gas carriers. So there is a mismatch, looking further into the table, there is also a mismatch between large container vessels and cylindrical fenders. However no ship owner or terminal ever complained about the cylindrical fenders damaging the vessel in the last 25 years in Rotterdam, nor in the surrounding large ports. This increased confidence about the use of cylindrical fenders, but also started a tough discussion with the launching customer of the Gate Small Scale Terminal about the fender design, stating that it is not an industry standard and therefore unacceptable. At this point TNO was contracted to examine the real impact of cylindrical fenders on LNG carriers.

The PIANC 2002 table 4.4.1 is also present in the British Standard (BS 6349-4:2014, paragraph 4.6.2 table 3). Where PIANC is still a recommendation, the British Standard is a design code.

2.2 The FEM analyses executed for Small Scale LNG

The analyses done by TNO started with a desk design of the weakest ship web frame section of the weakest possible vessel that could come into contact with the fenders (see figure 6). The ship side plating is modelled using Mild Steel properties for the upper strake (yield stress 235 MPa, tensile strength 400 MPa and 'minimum fracture strain 22%) and AH 32 for the remainder (yield stress 315 MPa, tensile strength 440 MPa and 'minimum fracture strain 22%), as per Lloyd's Register material specification. This is therefore a conservative design.

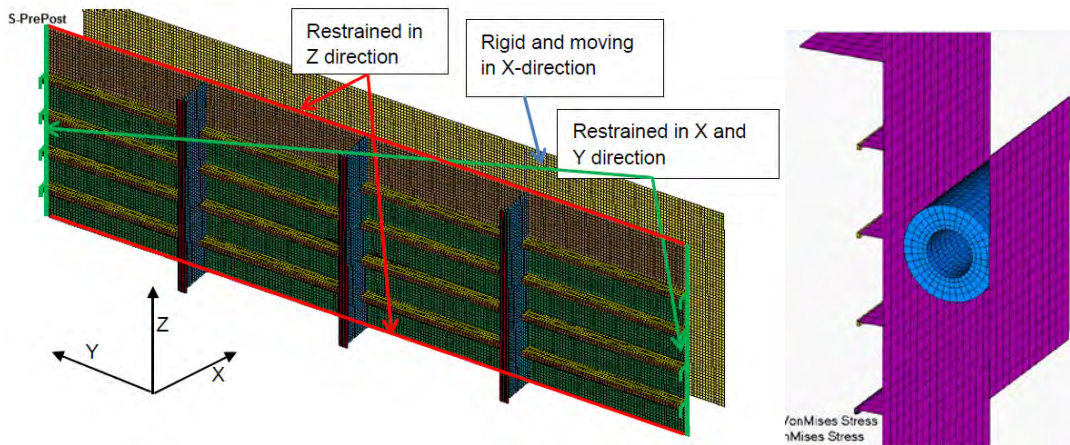


Figure 6: design hull section FE model, original case: no constraints in x-direction on web frames

The design of the fenders was determined by the engineering consultant from the Port of Rotterdam Authority. The physical behavior of the cylindrical fenders was modelled according to lower bound data provided by supplier ,Shibata (2017), see figure 7.

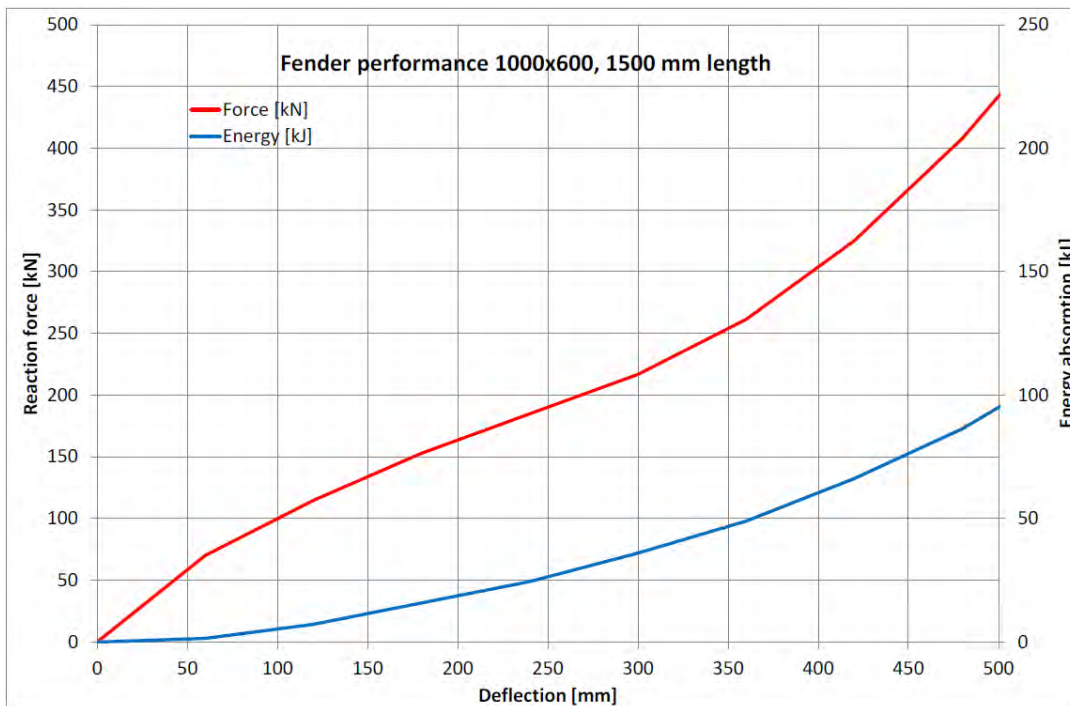


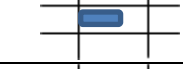


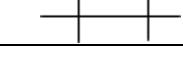


Figure 7: Energy-Displacement diagram 1000 x 600 fender, 1500 mm length, according to supplier catalogue

Then the ship hull section was impacted at all possible positions by the cylindrical fender with various cylinders. The criteria for stating the limit deformation on the fenders is based on the allowable stress level in the side structure. This is chosen such that the Von Mises stress shall not exceed 90% of yield stress. The operations for which the analyses are performed are normal operating conditions, hence plasticity shall not be accepted. From the deformation of the fender, the absorbed energy can be retrieved. This shall be compared with the energy absorption requirement from the berthing analysis.

Table 1: Overview of results of series without constraint of web frame in x-direction. Results shown where ship side structure reaches 90% yield stress criterion

| Case | Impact location | Compression [m] | Energy [kJ] | Reaction Force [kN] | Local Y stress [MPa]* |
|------|---|-----------------|-------------|---------------------|-----------------------|
| I |  | 0.41 | 47 | 250 | 272 |
| II |  | 0.44 | 55 | 265 | 281 |
| III |  | 0.44 | 55 | 270 | 282 (near web frame) |
| IV |  | 0.34 | 32 | 185 | 283 |
| V |  | 0.35 | 34 | 200 | 282 (@ 1/3 of long'l) |
| VI |  | 0.33 | 30 | 180 | 282 (near web frame) |

A secondary outcome was that the stiff cylinders, with a resulting hull pressure of 700 kN/m² will give damage to the ship hull. The stiffness of a cylindrical fender is determined by the ratio between inner and outer diameter. It was concluded that only the 'soft' cylinders can be used safely. For Gate terminal that means 1000-600 mm cylinders are good but 1000-500 mm cylinders are not good under all conditions.

The outcome of the study was to the full satisfaction of Gate Terminal, Shell the client behind Gate and PoR. The cylindrical fenders are installed and the terminal is in operation since September 2016. See figure 8.



Figure 8: Gate Jetty 3, the Small Scale facility (Photo Paul Martens).

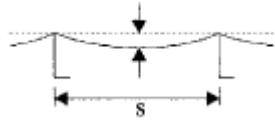
3. THE OIL TERMINAL (HES HARTEL TANK TERMINAL)

Knowing the outcome of the LNG Study for Gate Terminal, PoR decided to design the new HES Hartel Tank Terminal also with cylindrical fenders at the quay wall. This terminal will give berth to the entire vessel range from VLCC down to 70m 'long' coasters. Again TNO was asked to calculate if cylindrical fenders could be used safely.

Again FEM models were made, in this case for VLCC, Aframax and Handymax type of vessels. The other vessels in between are judged on basis of expert judgement, as there is not a large difference in the construction of the various class tankers.

This time the vessels were judged against the clear damage criterion. Guidelines for a damage criterion can be found in IACS (2013), the Recommendation No. 47 Shipbuilding and Repair Quality Standard - Rev.7 June 2013 of the International Association of Classification Societies. Chapter 6 in this document addresses fabrication and fairness of plating between frames (Table 6.10). The table shows that 5 mm permanent deformation of the shell plate is allowable for fore and aft parts of the structure (see Table 2 below). This criterion is used as damage limit.

Table 2: Damage criterion for fairness of plating between frames (from Table 6.10 [X]).

| Item | | Standard | Limit | Remarks |
|-------------|-------------------|----------|-------|--|
| Shell plate | Fore and Aft part | 5 mm | 8 mm |  |

This study determined the fender impact on the vessel following the PoR design berthing velocities derived from Roubos 2017 & 2018. After that, the berthing velocity was determined at which the IACS damage criterion was reached. The outcome of this study is summarized in table 3, the used fenders are D= 1400 mm, d = 800 mm and L= 2200 mm.

Table 3: Standard sea going tanker berthing dynamic results.

| Ship type | Normal berthing Impact speed PoR [m/s] | Maximum fender deformation [mm] | Maximum fender force [kN] | IACS 5 mm damage impact speed [m/s] | Maximum fender deformation [mm] | Maximum fender force [kN] |
|-----------|--|---------------------------------|---------------------------|-------------------------------------|---------------------------------|---------------------------|
| Coaster | 0.15 | 90 | 254 | 0.27 | 180 | 346 |
| Handysize | 0.15 | 173 | 340 | 0.27 | 366 | 529 |
| Handymax | 0.12 | 188 | 354 | 0.18 | 316 | 468 |
| Panamax | 0.12 | 214 | 376 | 0.18 | 359 | 520 |
| Aframax | 0.10 | 256 | 414 | 0.15 | 426 | 608 |
| Suezmax | 0.10 | 341 | 498 | 0.13 | 469 | 669 |
| VLCC | 0.08 | 388 | 556 | 0.10 | 504 | 724 |

This study again proved that cylindrical fenders can be beneficially used at oil terminals for the entire range of vessels under “Port of Rotterdam conditions”, which means sheltered conditions, deployment of sufficient tugs and experienced pilots. Secondly one has to consider the fact that the berthing velocities are determined on jetty and dolphin structures. At a quay wall there is also a water cushion that reduces the berthing velocity. Thirdly at a quay wall multiple fenders absorb the berthing energy and there is a low angle at the moment of impact (Roubos 2017 & 2018).

Hull pressures on oil tankers

The maximum occurring hull pressures can easily be calculated. The compression of the fenders is known, the contact surface with quay wall and vessel is known. This results with the data from table 3 in table 4. Again for the HHTT fenders (D= 1400 mm, d = 800 mm and L= 2200 mm).

Table 4: hull pressures by cylindrical fender during berthing

| Ship type | Design Impact speed PoR [m/s] | Maximum fender deformation [mm] | Contact height [mm] | Pressure [kPa] | IACS 5mm damage impact speed [m/s] | Maximum fender deformation [mm] | Contact height [mm] | Pressure [kPa] |
|-----------|-------------------------------|---------------------------------|---------------------|----------------|------------------------------------|---------------------------------|---------------------|----------------|
| Coaster | 0,15 | 90 | 141 | 817 | 0,27 | 180 | 283 | 556 |
| Handysize | 0,15 | 173 | 272 | 569 | 0,27 | 366 | 575 | 418 |
| Handymax | 0,12 | 188 | 295 | 545 | 0,18 | 316 | 496 | 429 |
| Panamax | 0,12 | 214 | 336 | 508 | 0,18 | 359 | 564 | 419 |
| Aframax | 0,10 | 256 | 402 | 468 | 0,15 | 426 | 669 | 413 |
| Suezmax | 0,10 | 341 | 536 | 423 | 0,13 | 469 | 737 | 413 |
| VLCC | 0,08 | 388 | 609 | 415 | 0,10 | 504 | 792 | 416 |

As clearly can be seen from table 4 that berthing velocities that result in no damage to the vessel, actually result in higher pressure on the ship hull than the critical berthing velocities. The lighter the ship, the larger this difference is. This is because the cylindrical fender reacts more stiff when hardly compressed. This clearly indicates that using hull pressure as a design criterion for cylindrical fenders is not the right approach. The Port of Rotterdam impact speeds result in a safe berthing with hull pressures way above the recommended values in PIANC 2002 table 4.4.1. and with no damage to the ships. There is however at this moment not a simple replacement available for this table.

The majority of the load on the hull is taken by the web frames and stiffeners, only a small percentage (roughly 5%) is taken by the hull membrane. The worst case is a cylindrical fender directly on one stiffener, not as might be expected in the middle of the frame on only the hull plate.

Therefore we can conclude also that if a panel fender is properly designed, and significant larger than the spacing between the stiffeners, the load will be entirely taken by the stiffeners (and the web frames). This makes hull pressure an irrelevant criterion for panel fenders as well.

4. PERSPECTIVE FOR CONTAINER VESSELS

The last standing question is obviously what to do with the container vessels. In the 80's Lloyds proved the safe use of cylindrical fenders on the large ships at that time. Lloyds actually checked a 280 m long 4000 TEU vessel for use on super cone panel fenders and the use with cylindrical fenders. This study concluded that cylinders could perfectly well be used without harming the vessels. As an outcome the Delta Terminal was equipped with cylindrical fenders 1400-800 mm. As stated, these fenders are in use to the satisfaction of almost all stakeholders. Only barge shippers don't like the cylinders because they can't reach the quay top easily. Therefore PoR designed a special ladder on small buckling fenders, see figure 9. In this way also the stepping criterion stated by the ADN (2008) can be met.

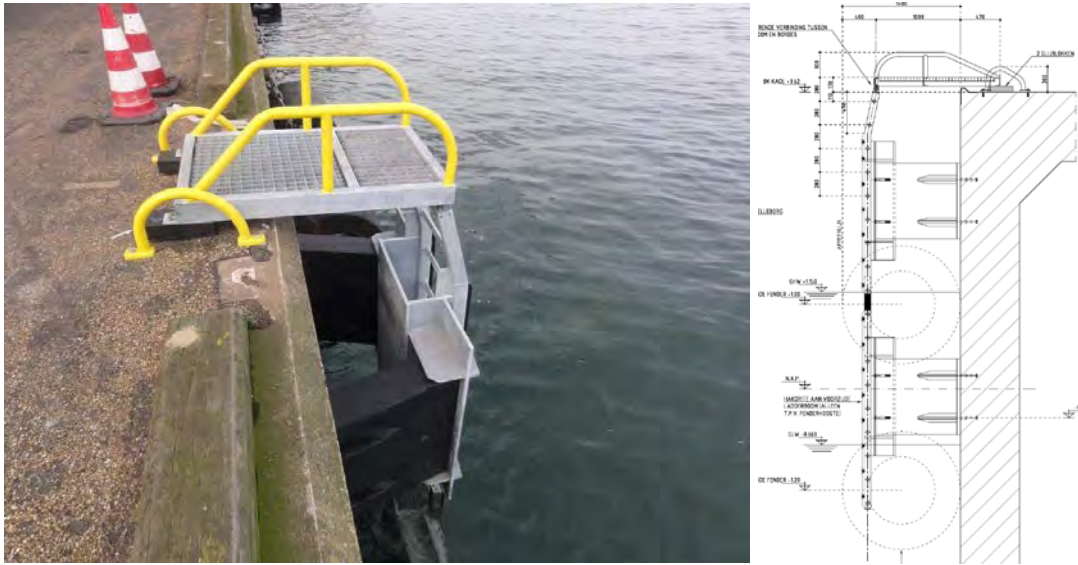


Figure 9: barge ladder between cylindrical fenders to provide barge access (photo PoR)

To verify that cylindrical fenders indeed can be safely used for the entire range of container vessels (as experienced in Rotterdam) further FEM calculations are currently being executed. The preliminary findings will be published separately as they are expected April 2018. On the conference there will be a preview on the outcome.

5. CONCLUSIONS & RECOMMENDATIONS

Cylindrical fenders can be used to berth and moor liquid bulk tankers ranging from small oil tanker towards large LNG carriers or VLCC.

It is expected that in the near future additional FEM calculations will confirm daily practice that all container vessels can berth safely on cylindrical fenders. For smaller vessels it has been proven in the 80's

As dry bulk and break bulk vessels can moor safely on rigid wooden fenders, they can also moor on cylindrical fenders.

The occurring hull pressures when using cylindrical fenders, are much higher than recommended by PIANC 2002 and the BS-6349-4. This study indicates that these hull pressures are however of no risk to the vessels. Therefore it is recommended to replace these tables into a more suitable criterion. The best way to replace these tables should be subject to further study in which the Port of Rotterdam Authority wants to participate.

6. REFERENCES

ADN (2008) : Accord européen relatif au transport international des marchandises Dangereuses par voies de Navigation intérieures. A European Agreement concerning the International Carriage of Dangerous Goods by Inland Waterways . By: United Nations Economic Commission for Europe (UNECE) and the Central Commission for the Navigation of the Rhine (CCNR). Into force by 29 February 2008.

Broos, E.J., Schaik, C van & Huitema, S, (2013) Innovative Rigid Concrete Fender System Reduces Life Cycle Costs., ASCE COPRI Ports '13 conference Seattle, august 25-28 2013

Broos, E.J, Hoebee, W., Peeperkorn, M.G.C.M. & Sibbes, R. (2016), The small scale LNG facility Rotterdam, ASCE COPRI Ports '16 conference New Orleans, 12-15 June 2016

IACS (2013) International Association of Classification Societies LTD, Recommendation No. 47 Shipbuilding and Repair Quality Standard - Rev.7 June 2013,
http://iacs.org.uk/document/public/Publications/Guidelines_and_recommendations/PDF/REC_47_pdf193.pdf

Lloyd's Register of Shipping (1989), Strength of side shell structure to resist quayside fender loads, Class Computational Services Group, Report no. CSD 89/24, SEPT 1989, CONFIDENTIAL

PAINC (2002), Guidelines for the Design of Fender Systems: 2002, report of working group 33 of the Maritime Navigation Commission, Brussels 2002

Roubos, A.A., Groenewegen, L., & Peters, D.J. (2017). Berthing velocity of large seagoing vessels in the port of Rotterdam. *Marines Structures*. 51. pp. 202-219

Roubos, A.A., Peters, D.J., Groenewegen, L. & Steenbergen, R.D.J.M. (2018). Partial safety factors for berthing velocity and loads on marine structures. *Marines Structures*. 58. pp.73-91

Roubos , A.A., Groenewegen, L., Ollero, J., Hein, C. & Wal, E. vd. (2018), Design values for berthing velocity of large Seagoing vessels, PIANC World Congress Panama 2018.

Shibata (2017), Product Information Cylindrical Fenders, http://shibata-fender.team/files/content/products/Cylindrical_Fenders/Product_Information_Cylindrical_Fenders.pdf, 2017

The British Standards Institution (2014), BS 6349-4:2014, Maritime works – Part 4: Code of practice for design of fendering and mooring systems, June 2014, ISBN 978 0 580 66969 9

www.shoretension.com

BIM APPLICATION IN PIER CONSTRUCTION

by

Tetsushi Noguchi¹, Hitoshi Ishida², Tsuyoshi Kotoura³ and Satoshi Katsuta⁴

ABSTRACT

This paper presents the results of applying Building Information Modeling/Management (BIM) in the port facilities construction work in Japan. In this Pier construction work, BIM was applied for the verification of Pile foundation, interference check between the structural elements and safe operation of crane ships. Even though the application of BIM had issues like securing 3-D Operators, it was found that the 3-D information can be efficiently utilized in all the phases of construction, even in port facilities construction work.

1. INTRODUCTION

BIM is used in the construction of 3D model to adjust the 3D positions of the material and is being utilized as a database for design, construction planning and maintenance by recording the construction procedure and member specifications.

Initially it was mainly used for the construction of building structures. In recent times the application of BIM to civil engineering structures has begun to get progressed to be utilized in structures such as roads, bridges and tunnels. However BIM has never been applied to port facilities in Japan. This paper presents the result of applying BIM in the construction work of Liquefied Natural Gas receiving pier.

2. SUMMARY OF CONSTRUCTION AND PURPOSE OF BIM APPLICATION

Pier construction is in the northeastern part of Japan, Soma port in Fukushima prefecture. In order to overcome the energy depletion immediately after the Great East Japan earthquake 2011, it was necessary to secure diverse energy sources. The petroleum resources company has pushed forward the pier mooring the imported ship by advancing the import of Liquefied Natural Gas in about 2 years. The aerial view of the receiving pier is shown in **Figure 1**.



Figure 1: Aerial view of the receiving pier

¹ Penta-Ocean Construction Co.,Ltd., tetsushi.noguchi@mail.penta-ocean.co.jp, Japan

² Penta-Ocean Construction Co.,Ltd., hitoshi.ishida@mail.penta-ocean.co.jp, Japan

³ Penta-Ocean Construction Co.,Ltd., tsuyoshi.kotoura@mail.penta-ocean.co.jp, Japan

⁴ Penta-Ocean Construction Co.,Ltd., satoshi.katsuta@mail.penta-ocean.co.jp, Japan

During initial stage of construction, there were few concerns such as, the abundant rise and fall in bearing layer under the seabed as shown in **Figure 2**, that drives the foundation pier, the facilities making up the pier were close to each other and the equipment installation of the platform was complicated.

In this pier construction, we aimed at achieving the following three by applying BIM.

1. To confirm and predict whether the pile foundation certainly attains the bearing layer.
2. To confirm that the structures do not interfere with each other before construction and to explain the workaround measures to the workers in advance.
3. To calculate the vessel position where the pier could be constructed safely and to decide appropriate anchor placement position in advance.

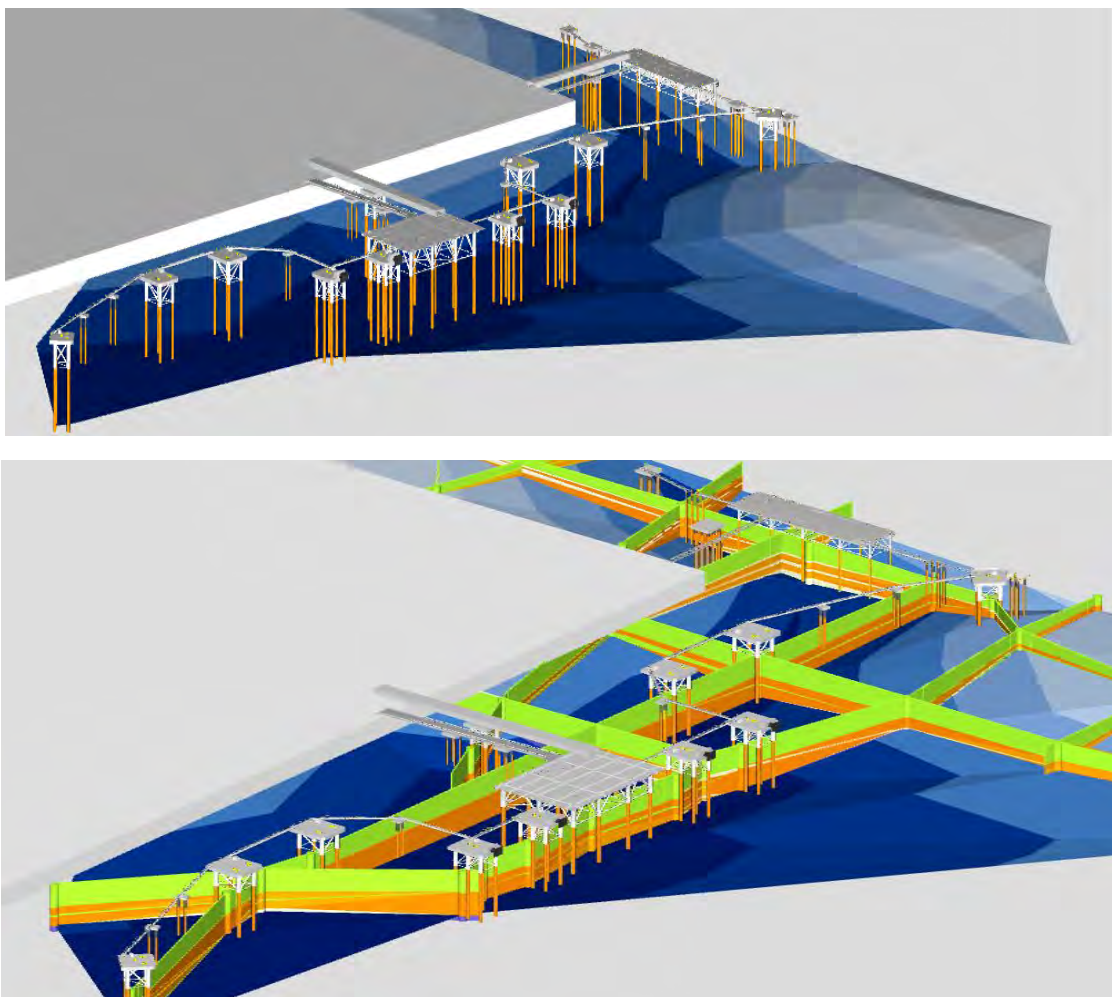


Figure 2: Bearing layer under the seabed

Key words: BIM, bearing layer, interference, safety operation

3. PROBLEMS AND MEASURES

By applying BIM in this construction work, we achieved the objectives by overcoming the problems/issues by the following procedures.

3.1 Bearing Layer

At first the depth of the bearing layer is represented by the 3D model from the boring data as shown in **Figure 3**.

After that each time a pile is driven, the electric resistance value of the piling installation is measured as shown in **Figure 4** and the height of the bearing layer of the 3D data is corrected sequentially. As a result of repeating this work and completely ascertaining the correct bearing layer height, we realized the necessary embedded depth is required for all piles.

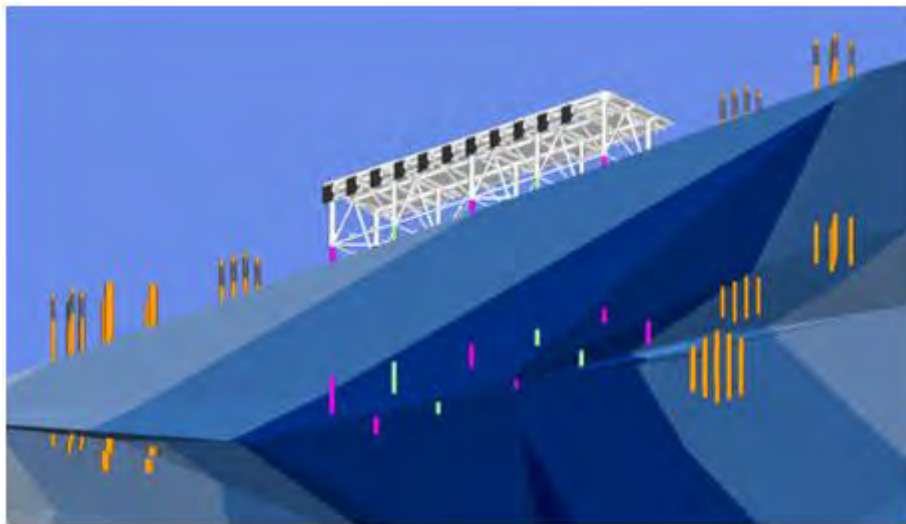


Figure 3: 3D Model of the seabed bearing substrate/layer

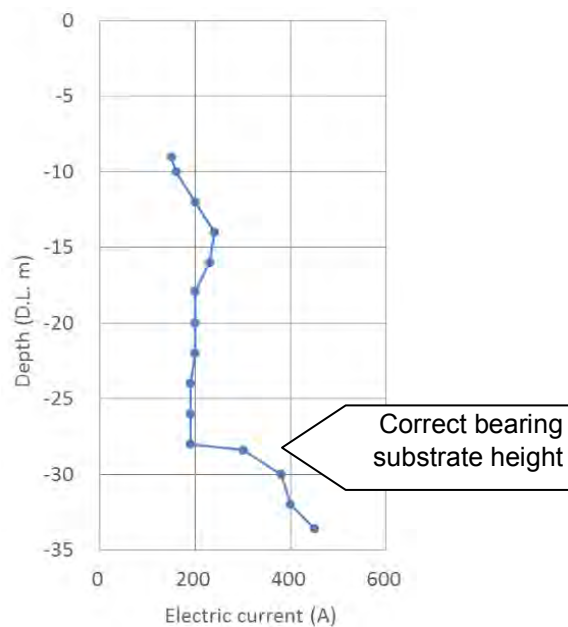


Figure 4: Current resistance value during pile driving

3.2 Interference Check

By inserting a jacket model into the reproduced pile shaped model, we confirmed that there was no interference with the data. In addition a surveillance camera was installed inside jacket sheath pipe as shown in **Figure 5**, to properly guide the jacket to the pile position.

A drone equipped with the digital camera flew and captured the shape of the wave dissipating concrete blocks under the bridge position as shown in **Figure 6** and **Figure 7**. By superimposing the model of the bridge on this, interfered blocks were identified and removed.



Figure 5: Jacket Induction with the help of surveillance camera

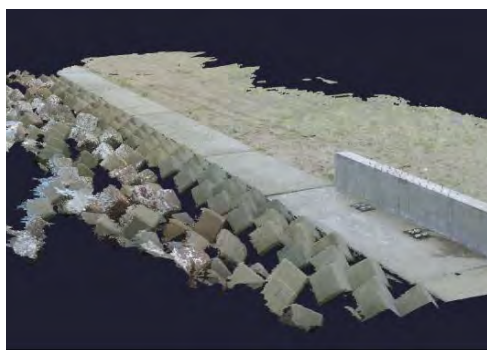


Figure 6: Digital camera image of wave dissipating concrete blocks

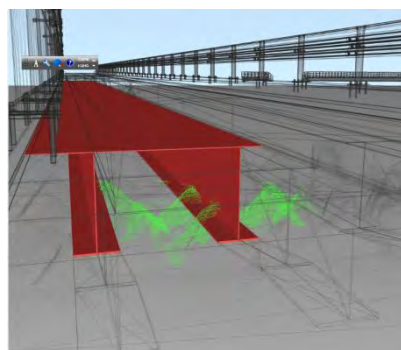


Figure 7: Interference of the wave dissipating concrete blocks and the bridge girder

As shown in **Figure 8**, the slab concrete reinforcing bars of the pier platform were reproduced on the model and the embedded metal fittings of the equipment were superimposed on this and confirmed that both did not interfere. In case of interfering, we moved the rebar before attaching the anchor. Showing these work procedures in a 3D model enabled the workers to have a deep understanding of the construction procedures.

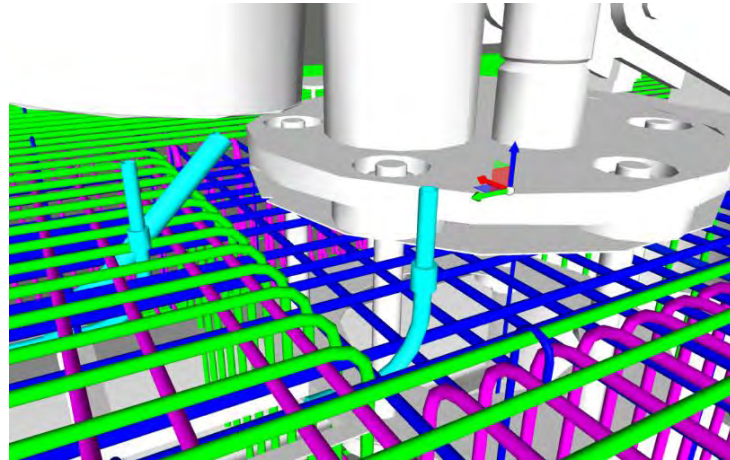


Figure 8: 3D Model of reinforcing bars of Slab concrete

3.3 Safe Operation of Crane Ship

According to the work process, the vessel position during construction is reproduced on the model and the anchor position was reproduced at the same time as shown in **Figure 9**. We confirmed that the crane ship can enter the installation position while hanging the jacket and the anchor of the work vessel can be placed in the required position beforehand. We also explained it to the vessel operator by an illustration. Through this series of procedures, the construction was implemented safely and smoothly.

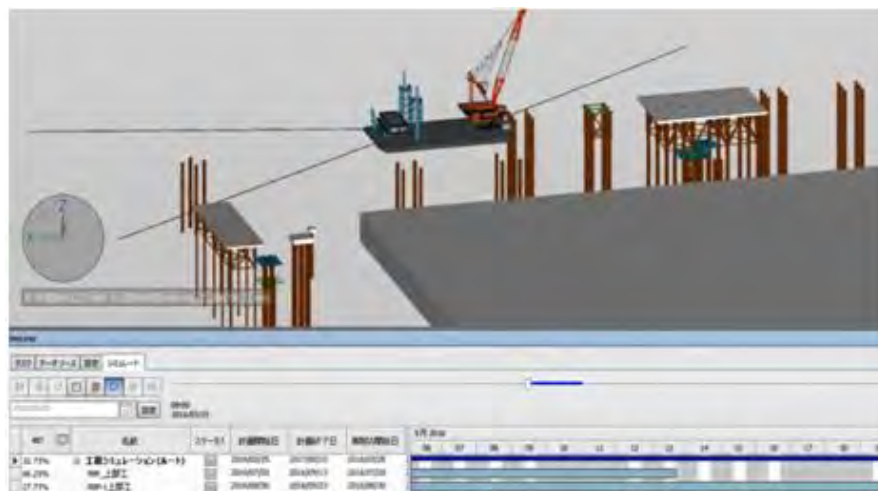


Figure 9: Positioning and anchoring of the crane ship

4. CONCLUSION

As described above, the BIM plan that includes the electric resistance value of the pile, monitoring with built-in camera, shape conformation by aerial photography and so on, were carried out concurrently and as a result the construction was done with high accuracy. In addition, even the complex events can be easily understood by the 3D model combining the BIM model and field verification results. Thus, it is very effective in giving work instructions to the operator.

On the other hand, it is also a fact that the data input into BIM needs time and experience. In case of civil engineering work, it is necessary to combine the construction ground data and the surrounding landscape data with the structure model, and the number of software to be handled becomes more. As a result, it takes time to learn the program operation. And since the number of operator expertise in BIM operations are still few in Japan, it is mandatory to train within the company for the time-being. While consensus on the application of BIM is progressing within the construction industry, securing human resource is an urgent issue.

WEB BASED OPERATIONAL SYSTEM FOR OPTIMIZING SHIP TRAFFIC IN DEPTH CONSTRAINED PORTS

by

*Simon B. Mortensen¹, Franz Thomsen¹, Alex Harkin¹, Senthil Kumar Shanmugasundaram¹,
Claus Simonsen² and Robert Nave³*

ABSTRACT

Low freight rates and high competition in the shipping and maritime industry has driven a strong demand towards optimizing the supply chain and establishing better utilization of increasingly larger vessels entering the world fleet. The dynamic complexity of physical port constraints and their effect on cargo traffic is usually well understood and appreciated in the port planning phase, but seldom incorporated in much detail into subsequent operational traffic management systems. In most ports, the timely flow of cargo depends on efficient collaboration and information sharing between the shipping companies, port authority and terminal operators. Yet at present, most of these entities use operational planning systems that do not interface with each other and seldom accounts directly for any physical constraints effecting operations. Usually separate systems are used for dealing with operational dynamic constraints such as under keel clearance (UKC), and many ports still to this day rely on static guidelines for such factors as high winds, passing vessel distances and safe mooring.

In this paper, we will introduce a new generation of physics-based port traffic management systems that utilise a cloud-based web platform to provide an integrated service that offers interactive operational user-interfaces to all important supply chain stakeholders. The backend of the systems includes a realistic representation of physics based operability constraints with an accuracy converging on the capabilities previously only found in full mission bridge 3D ship simulators.

The system is called Nonlinear Channel Optimization Simulator (NCOS) ONLINE and was developed by DHI Water & Environment, in collaboration with Port of Brisbane Pty Ltd (PBPL) and FORCE TECHNOLOGY. NCOS ONLINE has been operational 24/7 at Port of Brisbane since 1 August 2017. Based on the first six months of operations, the percentage of deep drafted bulk carriers above 13.5 m draft had increased by 43%, while deep drafted container vessels above 13.0 m had increased 167%. In December 2017 the system supported the safe passage of the 9,500TEU *Susan Maersk* (at the time, the largest container vessel ever to visit Australia) and in January 2018, the Port surpassed its record for deepest drafted container (13.9 m), which was 0.5 m deeper than the largest vessel the previous year. Without the need for additional dredging of the approach channel.

These results stand as a good example of how utilizing an online physics based traffic management system can significantly increase port capacity to accommodate larger and deeper drafted vessels compared to historical systems, resulting in large savings in capital dredging and reduced in environmental impacts.

1. INTRODUCTION

Low freight rates and high competition in the shipping and maritime industry has driven a strong demand towards optimizing the supply chain and establish better utilization of increasingly larger vessels entering the world fleet.

Both trends are currently increasing pressures on many ports and terminal operators to accommodate tighter transit schedules, reduce delays and accommodate larger and deeper drafted vessels. For more

¹ DHI Water & Environment, Australia, sbm@dhigroup.com

² FORCE Technology, Denmark

³ Port of Brisbane Pty Ltd, Australia

than a decade, full mission bridge 3D ship simulators have been an essential tool in identifying and solving capacity constraints through the shipping channel, turning basin and at berth. To this day high-end simulators such as SIMFLEX4 by FORCE TECHNOLOGY has provided the most realistic representation of vessel response physics in port, while also allowing for assessment of the influence of the human factor. As a result, ship simulators provides a critical role in strategic port design and expansion projects.

The dynamic couple of physical port constraints and their effect on cargo traffic is usually well understood and appreciated in the port planning feasibility phase, but seldom incorporated in much detail into subsequent operational traffic management systems. In most ports, the timely flow of cargo depends on efficient collaboration and information sharing between the shipping companies, port authority and terminal operators as illustrated in Figure 1. Yet at present, most of these entities use operational planning systems that do not interface with each other and seldom accounts directly for any physical constraints affecting operations. Typically separate systems are used for dealing with operational dynamic constraints such as under keel clearance (UKC), and many ports often rely on static guidelines for such factors as high winds, air gap space, passing vessel distances and safe mooring.

In this paper we will introduce a new generation of physics-based port traffic management systems that utilise a cloud-based web platform to provide an integrated service that offers interactive operational user-interfaces to all important supply chain stakeholders, while including a realistic representation of physics based operability constraints with an accuracy converging on the capabilities previously only found in full bridge 3D ship simulators.



Figure 1: Timely flow of cargo depends on efficient collaboration and information sharing between the shipping companies, port authority and terminal operators

2. A NEW GENERATION OF PORT TRAFFIC MANAGEMENT SYSTEMS

NCOS ONLINE belongs to a new generation of physics based port traffic management systems that utilise a cloud based web platform to provide an integrated service that offers interactive operational user-interfaces to all important supply chain stakeholders.

NCOS ONLINE incorporates the powerful vessel response engine NCOS (Mortensen et al 2016 and Harkin et al 2018, including detailed system description and full scale validation) which is capable of resolving the detailed response of each unique vessel entering a port with the same level of accuracy as a 3D full bridge simulator. 7-day forecasts of wind, waves and hydrodynamics (2D/3D current and water level) for the entire port domain are provided by MIKE Powered by DHI industry standard computational MIKE 21/3 models issued up to 4 times daily. In combination, the traffic management system is implicitly capable of taking into account any relevant vessel constraint such as UKC, manoeuvrability or berth configuration that may constrict the movement of vessels through the channel or operability at berth.

The Figure 1 illustrates how the timely flow of cargo through a port relies on the coordinated actions of several key stakeholders on a day to day basis. As a result, NCOS ONLINE has been designed to support multiple user groups each with their own unique access levels and tailored dashboards such as for Shipping Operators, Port Owners, Port Traffic Control, Terminal Operators and Pilots. As an example, shipping operators have the capacity to submit inbound vessels directly through their individual user profile and request preferred berth times. Port traffic control is provided the graphical overview (Figure 2) of available transit windows for each individual vessel 7 days into the future and from which transit times can be locked in and shared with pilots, tug masters and terminal operators.

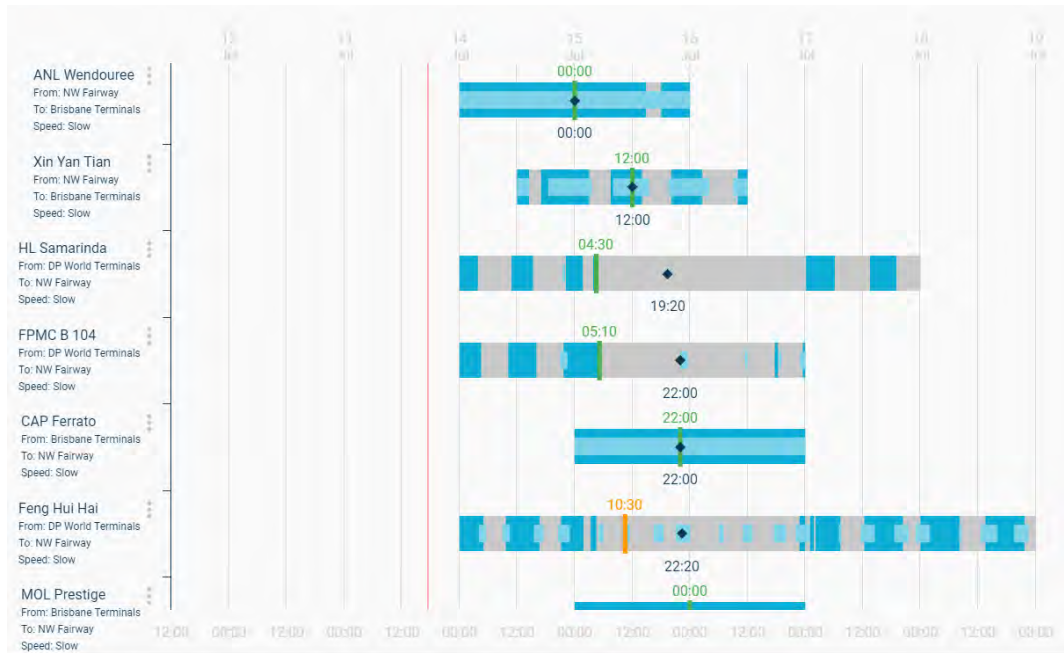


Figure 2 : Port Traffic in NCOS ONLINE is executed through a graphical interface showing all available transit windows (in dark blue).

As soon as a transit is locked, the scheduled transit becomes accessible to the Pilot, who gets notified of the roster update and is then able to inspect the specifics of his transit such as the UKC profile, his speed profile, vessel response and weather conditions (Figure 3). Harbour Masters oversee the entire process through their own dashboards and have exclusive access rights to increase the conservatism of various safety parameters in the system if unusual circumstances dictate this type of action.

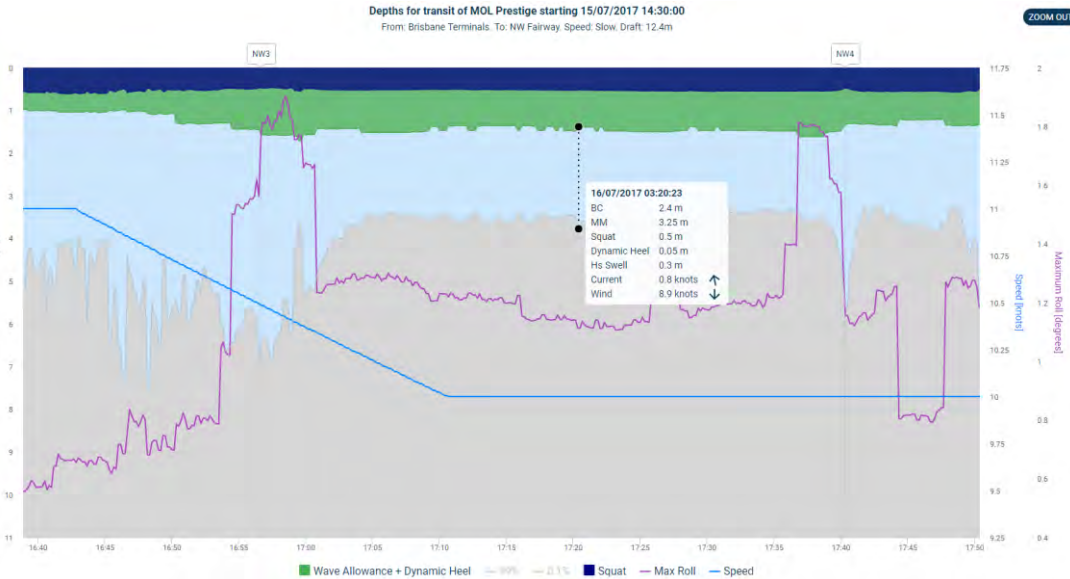


Figure 3 : As soon as a vessel transit is designated, the Pilot has access to a range of detailed decision support information.

As a general feature, the system provides a series of map view type dashboards that provides Port Owners and Authorities an overview of live and forecast marine weather conditions through the entire port domain (Figure 4).

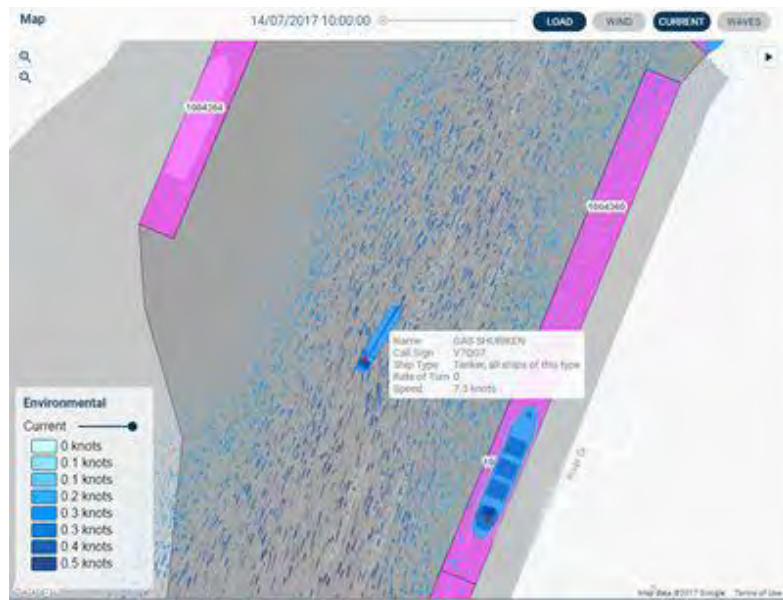


Figure 4 : Map view of NCOS ONLINE showing a moored Bulk Carrier and enroute Tanker inside the Port of Brisbane. The blue streamlines illustrate live predicted current speeds.

After the NCOS ONLINE system was installed for one of Australia's largest container ports it was found that not only did the system allow for a more precise prediction of day to day channel capacity, in many cases the system allowed for larger and deeper drafted vessels than the Ports previous system. Importantly, due to the capability for all key stakeholders and operators to visualize, share and query information provided by the system, it provided an improved trust platform for all port stakeholders and the subsequent confidence to follow recommendations even during challenging circumstances.

3. INCREASING LARGE VESSEL TRAFFIC FOR PORT OF BRISBANE

The Port of Brisbane (PoB) is one of Australia's fastest growing container ports and Queensland's largest general cargo port. Port of Brisbane Pty Ltd (PBPL) is responsible for the maintenance and development of the port facilities as well as maintaining navigable access to the port for commercial shipping. Day to day operational management of vessel traffic is handled by Marine Safety Queensland (MSQ), who also provides the Harbourmaster responsible for the safe operation of ships in the Port. Brisbane Marine Pilots (BMP) is the private corporation responsible providing piloting services to all commercial ships entering the shipping channel. Port of Brisbane's main navigational channel is 90km long and extends from the Pacific Ocean, through Moreton Bay, and into the entrance of the Brisbane River. The minimum maintained depth is 15 m LAT in the outer channel and 14 m LAT in the approach channel and container berths. Inbound and outbound vessels are subjected to significant temporal and spatial variability in tidal levels, currents, waves and winds as they pass through the channel and navigate through several narrow channel sections and confined bends.

When PBPL found it necessary to accommodate larger 8,500 TEU container vessels, it carried out a strategic capacity study for its shipping channel, (Mortensen et al 2016). The study concluded that subject to careful dynamic utilization of favourable tides and weather conditions, 8,500 TEU containers could access the port during most weather conditions without the need for capital dredging.



Figure 5 : The Port of Brisbane (PoB) is one of Australia's fastest growing container ports and Queensland's largest general cargo port. Port of Brisbane Pty Ltd (PBPL) is responsible for the maintenance and development of the port facilities as well as maintaining navigable access to the port for commercial shipping

In order to provide day-to-day operational support, DHI Water & Environment developed NCOS ONLINE, in collaboration with PBPL and FORCE TECHNOLOGY. NCOS ONLINE was adopted by PBPL and has been used to safely plan the transit of deep drafted inbound and outbound vessels at the Port of Brisbane since August 1 2017.

After its implementation, recorded feedback from VTS and Pilots is that the system provided a user-friendly platform for providing dynamic decision support in planning deep drafted vessel transits and that predicted vessel response agreed well with live observations.

In December 2017 the system supported the safe passage of the 9,500TEU *Susan Maersk*, the largest container vessel ever to visit Australia. In January 2018, the Port surpassed its record for deepest drafted container (13.9 m), which was 0.5 m deeper than the largest vessel the previous year.

As shown in Figure 6 after the first 8 months of operations, the percentage of deep drafted bulk carriers above 14.0 m draft had increased by 300%, while deep drafted containers above 13.0 m had increased by 233%.

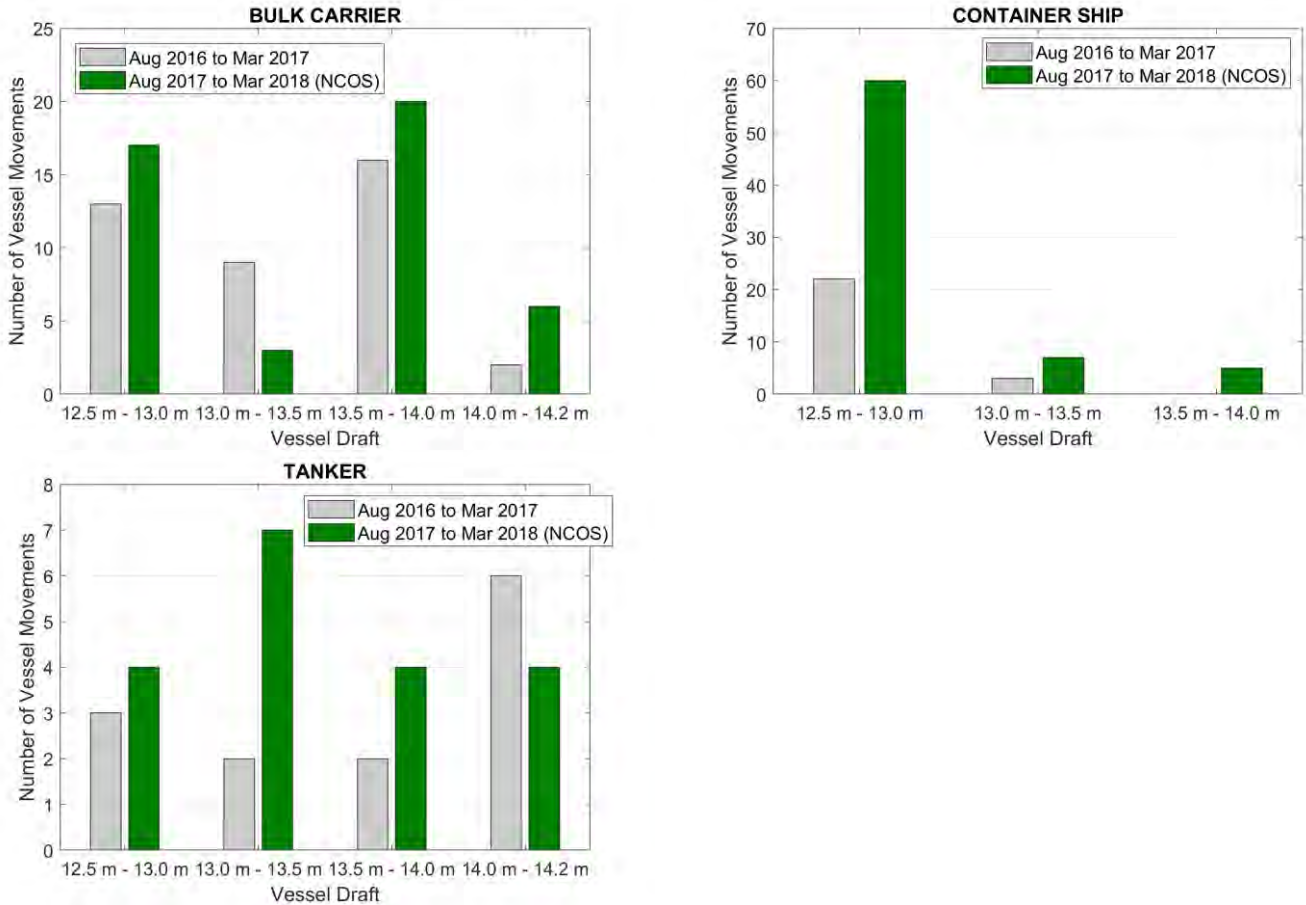


Figure 6 : Comparison between number of vessel movements in Port of Brisbane 2016/2017 versus 2017/2018 for bulk carriers, container vessels and tankers.

4. SUMMARY

The results presented above confirms that utilizing an online physics based traffic management system can significantly increase port capacity to accommodate larger and deeper drafted vessels compared to its historical systems and resulting in large savings in capital dredging and reductions in environmental impacts. In addition, the system's capacity to incorporate the operational user group requirements of multiple operators, regulators and asset owners provides a flexible platform for a more effective and user-friendly management tool for optimizing constrained port traffic flow both now and in the future.

5. REFERENCES

Harkin A, Harkin J, Suhr J, Mortensen S.B, Tree M, Hibberd, W (2018) Validation of a 3D underkeel clearance model with full scale measurements, 34th PIANC World Congress, Panama City, Panama.

Mortensen S.B, Jensen B.T, Nave R. (2016) A Nonlinear Channel Optimization Simulation Framework for Port of Brisbane Australia, PIANC COPEDEC Conference Proceedings, Rio de Janeiro, Brazil.

VALIDATION OF A 3D UNDERKEEL CLEARANCE MODEL WITH FULL SCALE MEASUREMENTS

Alex Harkin¹, Jarrod Harkin,² Jacob Suhr², Marcus Tree², Will Hibberd²,
Simon Mortensen²

ABSTRACT

The continuing growth of commercial vessel sizes is putting increasing pressure on the world's port authorities to adopt effective expansion strategies to ensure that their asset is able to meet growing capacity demands. Channel capacity expansion projects usually involve the consideration of extensive dredging which introduces considerable constraints with respect to cost and environmental impacts. Depth constrained ports require accurate under keel clearance (UKC) monitoring in order to safely and economically operate. Inaccurate determination of UKC can lead to excessive port design and dredging cost or even unsafe operations leading to vessel grounding.

This paper presents the full scale validation of an improved integrated approach for optimizing shipping channel capacity utilizing DHI's new state-of-the-art 3D under keel clearance (UKC) model Nonlinear Channel Optimization Simulator (NCOS). The aim of this validation exercise is to demonstrate the accuracy envelope of a 3D method for UKC prediction through various approaches for treatment of key input forcing parameters, wave frequency response, dynamic heel and squat. Measurements used for validation consisted of high resolution time series of UKC, roll, pitch and heave obtained during vessel inbound and outbound transits through the Port of Brisbane. Vessels included a mix of large bulk carriers and container vessels.

NCOS belongs to a new breed of UKC models that converge towards the same level of sophistication and realism as Full Bridge Simulators. The NCOS model uses the numerical 3D vessel frequency engine in the Full Bridge Simulator *SIMFLEX4* by FORCE TECHNOLOGY for predicting wave-induced UKC allowance, which greatly improves the potential for using it in close integration with detailed maneuverability studies. The model uses a 2nd Order 3D panel method for evaluating vessel frequency response incorporating implicitly the effect of vessel forward speed and varying water depths. Adopting a Rayleigh distributed sea state; the probabilistic vessel execution is evaluated in each time step for various return periods. To ensure accurate predictions of UKC, NCOS relies on temporally and spatially varying environmental inputs such as wind, wave and hydrodynamic data to serve as forcing inputs to the model

Serving as the bases for this validation are full scale measurements taken during vessel transits through the Port of Brisbane. Differential Global Positioning Systems (DGPS) were located at the bow and on both the port and starboard bridge wings of the vessels to measure trajectory and the vertical position at each location. From these measurements roll, pitch, heave and total vertical excursion of the vessels throughout the transits were calculated.

With regards to calculating UKC wave allowance, the 3D vessel frequency response engine in NCOS supports wave forcing from a full directional wave spectrum, which provides the most accurate prediction. However due to the increased computational and storage overheads associated with the full integration in an operational framework, a simplified approach using synthetic JONSWAP spectra from integral wave parameters has also been investigated and benchmarked in this paper.

¹ DHI Water & Environment, Australia, alha@dhigroup.com

² DHI Water & Environment, Australia

In addition most ports have long term trust relationship with the use of empirical squat formulae presented in PIANC WG 121-2014 when estimating basic UKC, which raises a demand for assessing how these can be incorporated into a sophisticated 3D UKC framework. As a result we assess the performance impacts of incorporating an array of well-known squat formulations and we also investigate the effect of representing waves using either synthetic wave spectra from integral parameters to using full directional spectra as modelled by a spectral wave model.

The comparison includes timeseries of roll, pitch, heave, squat and total minimum vessel vertical excursion above the seabed (UKC). Comparisons to date show that NCOS has very accurately reproduced the measurements numerically which gives confidence that it can be used by ports to achieve target levels of channel operability, while potentially reducing required dredge volumes significantly compared to conventional estimates.

1 INTRODUCTION

The continuing growth of commercial vessel sizes is putting increasing pressure on the world's port authorities to adopt effective expansion strategies to ensure that their asset is able to meet growing capacity demands. Channel capacity expansion projects usually involve the consideration of extensive dredging which introduces considerable constraints with respect to cost and environmental impacts (Mortensen, 2017). Depth constrained ports require accurate under keel clearance (UKC) monitoring in order to safely and economically operate. Inaccurate determination of UKC can lead to excessive port design and dredging cost or even unsafe operations leading to vessel grounding.

This paper presents the full scale validation of an improved integrated approach for optimizing shipping channel capacity utilizing DHI's new state-of-the-art 3D under keel clearance (UKC) model Nonlinear Channel Optimization Simulator (NCOS). The aim of this validation exercise is to demonstrate the accuracy envelope of a 3D method for UKC prediction through various approaches for treatment of key input forcing parameters, wave frequency response, dynamic heel and squat. Measurements used for validation consisted of high resolution time series of UKC, roll, pitch and heave obtained during vessel inbound and outbound transits through the Port of Brisbane. Vessels included a mix of large bulk carriers and container vessels.

Serving as the bases for this validation are measurements taken during vessel transits through the Port of Brisbane. Measurements of the vessels roll, pitch, heave and total vertical excursion have been produced for 10 inbound and outbound transits. The vessels included in this paper are a mix of four large bulk carriers and container vessels. These measurements will enable the validation of the NCOS calculations including wave response, wind and turning heel and squat.

2 NOMENCLATURE

| | |
|--|---|
| B: Vessel beam | RAO: Response amplitude operator |
| C: Restoring Force | SWD: Still water depth |
| C_θ : Rudder angle coefficient | l_R : Turning heel moment arm |
| d: Vessel motion point | $T^{(2)}$: Set down due to second order drift forces |
| ∇ : Ship volume displacement | T_{heel} : Set-down due to wind and turning heel |
| $F^{(2)}$: Second order force/moments | T: Vessel draft |
| F_k : Bilge keel factor | T_p : Peak wave period |
| GM: Metacentric height | $T_{p,cor}$: Peak wave period correction factor |
| H_s : Significant wave height | T_{squat} : Set-down due to squat |

$H_{s,cor}$: Significant wave height correction factor
 M_w : Wind heel moment
 MWD : Mean wave direction
 η : Timestep and vessel position
 R_c : Turing radius

θ : Wave direction
 ϕ : Heel angle
 U_c : Vessel speed relative to water
 ω : Wave frequency
 x : Ship motion

3 MEASUREMENT CAMPAIGN

Serving as the bases for this validation are measurements taken during vessel transits through the Port of Brisbane. Differential Global Positioning Systems (DGPS) were located at the bow (**Figure 1**) and on both the port and starboard bridge wings (**Figure 2**) of the vessels to measure trajectory and the vertical position at each location. An XSens Inertial Measurement Unit (IMU) was also used to measure the vessel roll and pitch as contingency in the event that any of the DGPS units did not work correctly. From these measurements roll, pitch, heave and total vertical excursion of the vessels throughout the transits were calculated.

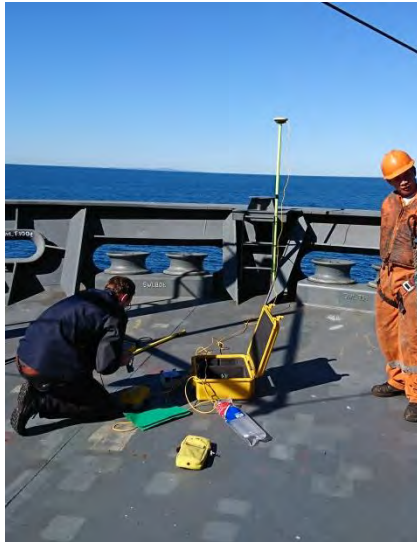


Figure 1: DGPS Setup on Bow



Figure 2: DGPS Setup on Starboard Bridge Wing

Table 1 describes the vessel transits included in the validation.

| Vessel Name | Vessel Class | Draft (m) | LOA (m) | LPP (m) | Beam (m) | Transit Start Date and Time | Direction of Travel |
|-------------|--------------|-----------|---------|---------|----------|-----------------------------|---------------------|
| B2 | Bulk Carrier | 13.50 | 253.50 | 249.20 | 43.00 | 15/06/2017 - 11:30 | Outbound |
| B3 | Bulk Carrier | 13.53 | 253.50 | 249.20 | 43.00 | 30/07/2017 - 13:30 | Outbound |
| C1 | Container | 12.10 | 294.10 | 282.20 | 32.20 | 11/07/2017 - 16:30 | Inbound |
| C2 | Container | 12.68 | 255.00 | 244.00 | 37.30 | 24/07/2017 - 00:30 | Inbound |

Table 1: Description of Vessels included in the Measurement Campaign

4 NUMERICAL MODELLING METHODOLOGY

4.1 Vessel Wave Response

NCOS belongs to a new breed of UKC models that converge towards the same level of sophistication and realism as Full Bridge Simulators. The NCOS model uses the numerical 3D engine, SOMEGA, which is used in the Full Bridge Simulator *SIMFLEX4* by FORCE TECHNOLOGY for calculating wave response, which greatly improves the potential for using it in close integration with detailed maneuverability studies. The model uses a 2nd Order 3D panel method for evaluating vessel frequency response incorporating implicitly the effect of vessel forward speed and varying water depths. Adopting a Rayleigh distributed sea state; a probabilistic vessel approach is evaluated in each time step for various return periods.

NCOS is directly integrated with SOMEGA and the MIKE 21 Spectral Wave model (MIKE21 SW) enabling the accurate prediction of spatially and temporally varying wave response through a channel. SOMEGA provides the frequency domain wave response in the form of motion response amplitude operators (RAOs) and MIKE21 SW provides the wave conditions. Based on the inputs from SOMEGA and MIKE21 SW, NCOS computes the full linear motion RAOs of responses to unit wave amplitude along with 2nd order vertical motions ($T^{(2)}$).

The spectral form of the 1st order motions of a user-specified number of motion points (d) on the vessel in a specific sea state is calculated from the motion RAO for the specified point and the sea spectrum as shown in (1).

$$S_d(\omega) = RAO_d^2(\omega) \cdot S_\eta(\omega) \quad (1)$$

Where RAO_d is the RAO calculated by SOMEGA translated to each motion point on the vessel d , S_η is the wave spectra at each timestep and vessel position η and S_d is the resulting motion response spectra at each motion point d . The motion points are selected such that at any time one of the motion points will be the deepest point of the vessel.

In order to provide a robust solution NCOS allows for live wave data assimilation which enables manipulation of the wave spectra to more accurately match measured data when available. Separate wave height and wave period correction factors are used for the sea and swell wave components. This paper will investigate two alternative implementations for calculating the fully directional spectra S_η .

1. Implementation 1 involves extracting sea and swell integral wave components H_s , T_p and MWD from the MIKE21 SW model and synthetically generating fully directional spectra based on a JONSWAP spectrum in conjunction with user defined wave spreading and wave correction factors. In this implementation the wave correction factors for both sea and swell are applied as shown in (2) to (5).

$$H_s(Sea) = H_s(Sea) * H_{s,cor}(Sea) \quad (2)$$

$$H_s(Swell) = H_s(Swell) * H_{s,cor}(Swell) \quad (3)$$

$$T_p(Sea) = T_p(Sea) + T_{p,cor}(Sea) \quad (4)$$

$$T_p(Swell) = T_p(Swell) + T_{p,cor}(Swell) \quad (5)$$

2. Implementation 2 involves extracting the fully directional spectra directly from the MIKE21 SW

model. In this implementation the wave correction factors are applied as shown in (6) and (7). Where n is the number of discrete peaks in the measured wave spectrum.

$$S_{\eta} = \sum_{p=1}^n S_{\eta}(T_p(p)) * H_{s,cor}(p) \quad (6)$$

$$S_{\eta} = \sum_{p=1}^n S_{\eta}(T_p(p) + T_{p,cor}(p)) \quad (7)$$

Implementation 1 is expected to provide a more conservative calculation of the vessel motions since the wave energy will be more concentrated at the peak periods and mean wave directions. Implementation 2 is expected to be more accurate since it better describes the wave energy distribution. We compare both approaches herein, noting that despite being more conservative, implementation 1 allows for easier data assimilation of the SW results with measured wave conditions.

Once the motion spectra is determined NCOS then calculates the significant motions (9) and maximum motions (10) at each timestep.

$$m_n = \int_0^{\infty} \omega^n S_d(\omega) d\omega \quad (8)$$

$$x_{sig} = 2 * \sqrt{m_0} \quad (9)$$

$$x_{max} = \sqrt{2 * m_0 * \ln\left(\frac{D}{2 * \pi * \alpha} \sqrt{\frac{m_2}{m_0}}\right)} \quad (10)$$

Where D is the time duration where the spectra moments remain essentially constant and α is a small number which represents the likelihood that the maximum design motion will be exceeded. The results in this paper are based on an α value of 0.01 as recommended by (Lewandowski, 2014).

The 2nd order set down, $T^{(2)}$, is calculated from (11) to (13) where $F^{(2)}$ is the second order force/moments extracted from SOMEQA, θ is the wave direction and C is the restoring force.

$$S_{F^{(2)}}(\omega, \theta) = F^{(2)}(\omega, \theta) \cdot S_{\eta}(\omega, \theta) \quad (11)$$

$$x^{(2)}(\theta) = \frac{\int S_{F^{(2)}}(\omega, \theta) d\omega}{C} \quad (12)$$

$$T_d^{(2)}(\omega, \theta) = x_{heave}^{(2)}(\theta) + x_{roll}^{(2)}(\theta) * d_y + x_{pitch}^{(2)}(\theta) * d_x \quad (13)$$

This paper will compare the measured wave induced motions with the significant wave induced motions calculated by NCOS.

4.2 MIKE21 SW Model and Correction Factors

For this validation a MIKE21 SW model was produced for the Port of Brisbane. The MIKE21 SW model has been setup to generate a 2D unstructured data file containing sea and swell integral wave parameters to be used with wave response implementation 1. For wave response implementation 2 the MIKE21 SW model was setup to produce 40 fully direction spectra timeseries along the Port of Brisbane shipping channel. The locations of these 40 directional spectra are displayed in **Figure 3**.

For validation purposes the MIKE21 SW model outputs timeseries of sea and swell integral wave parameters at the location of multiple wave buoys (see locations in **Figure 4**) along the Port of Brisbane shipping channel.

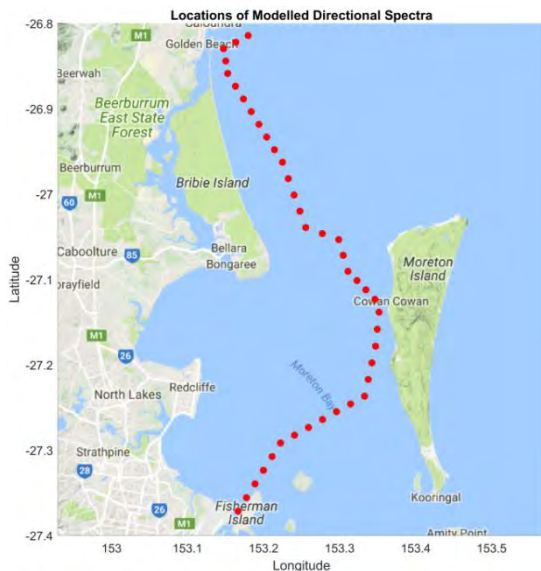


Figure 3: Port of Brisbane Directional Spectra Locations

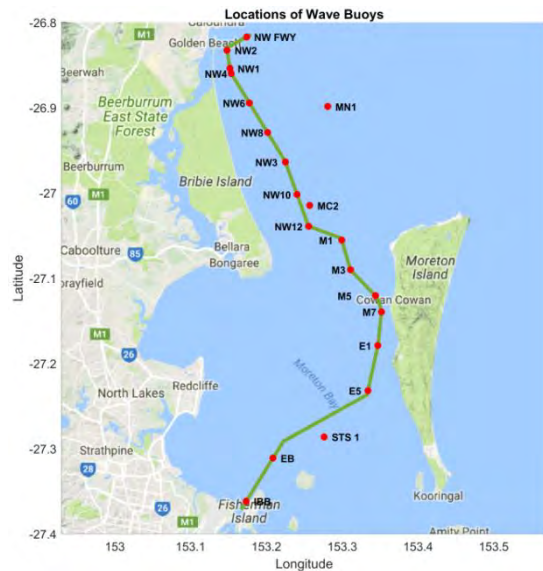


Figure 4: Wave Buoys Locations

The MIKE 21 SW results have been compared to the measured data at wave buoys MC2, NW3, MN1 and NW4 in order to generate correction factors for each transit. Significant wave height correction factors were calculated by dividing the measured wave height by the modelled wave height at a distinct time step. Similarly, the peak wave period correction factors were calculated by subtracting the modelled period from the measured period. Correction factors were calculated separately for each wave buoy. The calculations were made at half hour intervals for two hours leading up to each transit and then these values were averaged giving an average correction factor for each wave buoy. The most conservative correction factor was then selected for use in the NCOS model. The correction factors are displayed in Table 2.

| Vessel Name | Correction Factors | | | |
|-------------|--------------------------------------|------------------------------------|------------------------------|----------------------------|
| | Significant Wave Height (Swell) [()] | Significant Wave Height (Sea) [()] | Peak Wave Period (Swell) [s] | Peak Wave Period (Sea) [s] |
| B2 | 0.902 | 0.973 | 0.231 | 3.687 |
| B3 | 0.624 | 1.216 | 1.360 | 0.526 |

| | | | | |
|-----------|-------|-------|-------|-------|
| C1 | 0.892 | 1.106 | 3.297 | 0.877 |
| C2 | 0.971 | 2.121 | 1.939 | 0.367 |

Table 2 Wave Correction Factors

4.3 Dynamic Heel

As well as wave induced motions NCOS includes dynamic heel. Heel is a ships non-wave induced roll motion and is caused by wind and turning. The wind and turning heel are calculated based on the guidelines provided in (PIANC, 2014) as detailed in (14) to (17).

$$\phi_w = \frac{M_w}{g\rho\nabla GM} \quad (14)$$

$$\phi_R = C_\phi \frac{\iota_R U_c^2}{gR_c GM} \quad (15)$$

$$\phi_{WR} = \phi_w + \phi_R \quad (16)$$

$$T_{heel} = F_k \left(\frac{B}{2} \sin \phi_{WR} \right) \quad (17)$$

The wind forcing in NCOS comes from The Bureau of Meteorology and rudder angles through the Port of Brisbane are based on observations made through the measurement campaign.

4.4 Squat

Squat is a steady downward displacement consisting of a translation (sinkage) and rotation (trim) due to the flow of water past the moving hull (PIANC, 2014). **Figure 5** visualizes this phenomenon.

Squat=Sinkage+Trim



Figure 5: Ship Squat (PIANC, 2014)

NCOS is directly integrated with the MIKE 21 Hydrodynamic Model (MIKE21 HD) which provides the current speed and direction enabling the accurate calculation of the transiting vessels speed relative to water and consequently squat. NCOS utilizes well known empirical squat formulae including Millward (Millward, 1990), Yoshimura (Ohtsu K, 2006), Barrass (Barrass, 1979) and Huuska (Huuska, 1976).

The most important factors influencing ship squat are the speed through water, the block coefficient and the blockage factor. Ship squat is approximately proportional to the square of the ship speed, and generally squat is not significant for speeds less than 6 knots. The squat of a ship also depends on the block coefficients where ships with larger block coefficients have more squat compared to more

slender vessels. Squat is generally directly proportional to the block coefficient. In shallow or restricted channels the non-dimensional blockage factor, the ratio of ship area to channel area, can lead to large increases in squat. Factors influencing the blockage factor include water depth, channel width, channel height and channel slope.

Channel parameters water depth, channel width, channel height and channel slope are generated by details bathymetry data through the Port of Brisbane.

This paper will evaluate the accuracy of each squat formula through comparisons with the measured results and ultimately develop a set of equations for utilizing a combination of each squat formula.

4.5 Governing Equations

Once the wave induced vessel motions (m_0 and $T^{(2)}$), squat (T_{squat}) and heel (T_{heel}) have been evaluated the grounding probability can be calculated. The residual depth Z , calculated in (18), defines the wave-induced depth threshold of the transit vessel.

$$Z = SWD + Tide - (T + T_{squat} + T_{heel} + T^{(2)}) - \Delta Z \quad (18)$$

Where *Tide* is produced by a MIKE21 HD model and ΔZ is the minimum allowable water depth under the vessel after all other effects have been taken into account. $Q(Z)$, calculated in (19), is the grounding probability in each timestep.

$$Q(Z) = 1 - \left[1 - e^{\left(-1/2 \frac{Z^2}{m_0}\right)} \right]^n \quad (19)$$

Where n is the number of waves passing the ship in the timestep.

Using (18) and (19) NCOS is capable of calculating the ships total vertical excursion based on a given exceedance probability and iteratively shifting a virtual sea floor by altering ΔZ . Keel levels calculated in this paper are based on an exceedance probability of 1% and a 20min wave ensemble.

P_{tot} , calculated in (20), is the integrated grounding probability for the whole transit based on the product of the grounding probability at each timestep $t1 - tn$.

$$P_{tot} = 1 - (1 - Q_{t1})(1 - Q_{t2}) \dots (1 - Q_{tn}) \quad (20)$$

5 RESULTS

5.1 Wave Response Comparison and Validation

This section aims to directly investigate the validity of wave response implementation 1 and wave response implementation 2. In order to do this analysis, the measured vessel motion data has been high pass filtered to remove any motions with a period greater than 60s. This was done to attempt to remove roll motions induced by wind and turning and pitch and heave motions induced by squat so only motions that are purely wave induced are considered. Next, the significant motions were calculated. This was done by finding the mean of the highest one third of the vessel motions using a wave ensemble of 20 minutes at each timestep. This section of the paper will display comparative plots for the roll, pitch and heave motions for each transit. All motion plots in the following sections will include the measured motion after filtering, the significant measured motion and the significant motion

calculated from the two NCOS models as well as time stamps of when each wave buoy (Figure 4) was passed.

One of the DGPS instruments located on the bridge of vessel B2 failed during its transit. As a result, the backup xsens device was used to measure the roll of the vessel in order to calculate the heave at the vessel center of gravity. The xsens device has a margin of error of 0.2 degrees. Since the beam of the ship is 43m, translating this error to the centre of the ship results in a vertical excursion error of up to 0.075m. This margin of error will be acceptable for calculating roll and pitch. However, heave will not be calculated with sufficient accuracy, so transit B2 will be left out of the heave calculations. For transits C1, C2 and B3 all three DGPS instruments performed successfully.

5.1.1 Roll

Figure 6 and Figure 7 show that the calculated wave-induced significant roll of the bulk carriers was well represented by both wave response implementations with implementation 2 being the most accurate. This included the relatively calm inner components of the transit, moving to the more exposed regions in the latter half of the outbound transits.

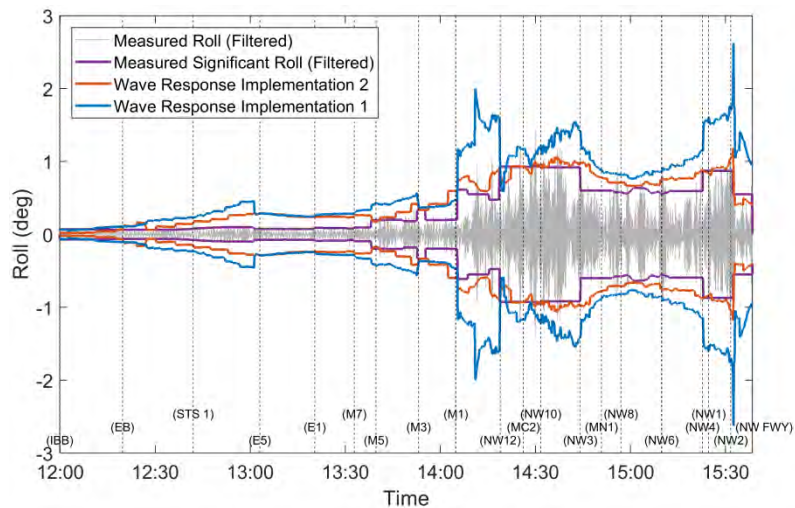


Figure 6: B2 Filtered Roll Validation (Bulk Carrier, Outbound)

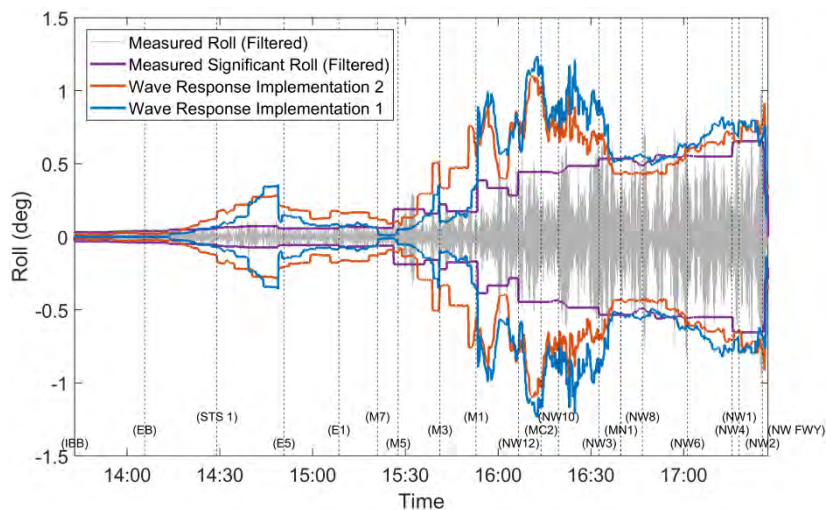


Figure 7: B3 Filtered Roll Validation (Bulk Carrier, Outbound)

For the container vessels the high pass filtering was not able to remove the noticeable roll generated

by frequent rudder corrections through the transit and largely exceeded the wave induced roll motions. As a result the comparison for both the high pass filtered roll and total roll have been presented for these two ships. **Figure 9** and **Figure 11** present the total roll which shows that the character of the container roll response differs from that of the bulk carriers and is far more affected by wind and turning/rudder corrections. **Figure 8** and **Figure 10** show that the magnitude of the high pass filtered container measured roll is largely consistent along the length of the as opposed to being proportional to the large difference in wave conditions through the channel. **Figure 12** and **Figure 13** show that both the sea and swell significant wave height was largest offshore and reduced as ship C2 approached the port and that the peak wave periods remained constant. We thus expect the wave induced roll response will be decreasing along the transit, but this not being the case for measured roll confirms the expectation that the prominent roll motion is not wave induced for these two cases.

Residual turning and rudder correction response can be seen in the high pass filtered container measured roll signal after corners as the ship stabilizes. This gives an indication that the container vessels respond with the same roll period to wind and turning agitation as they do to wave forcing and the high pass filtering cannot remove the wind and turning induced roll. Importantly for roll motion, containers have a high centre of gravity and large windage area when compared to bulk carriers. As a result, their response to turning and wind is much greater and this response has not been fully removed by the high pass filter.

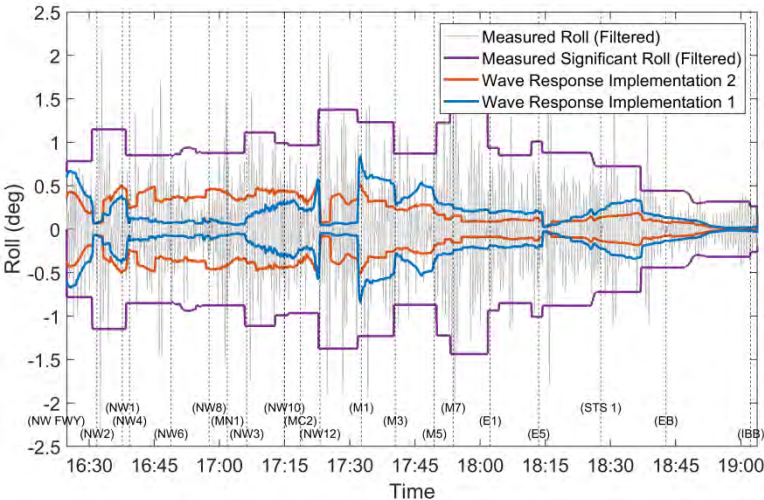


Figure 8: C1 Filtered Roll Validation (Container Vessel, Inbound)

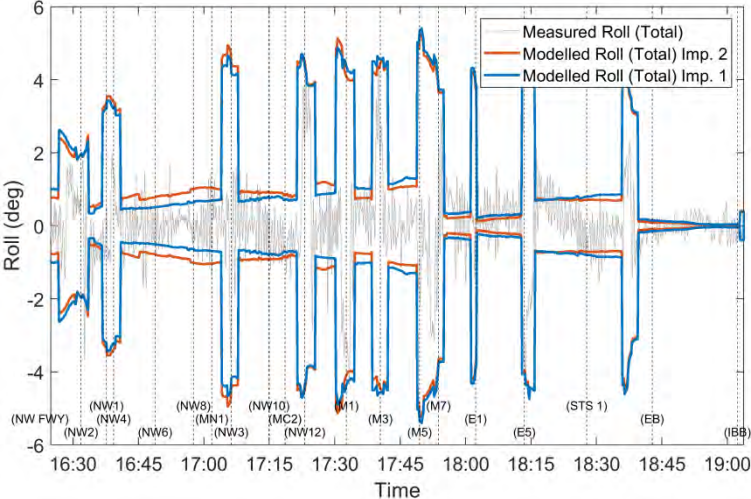


Figure 9: C1 Non-filtered Roll Validation incl. effects of wind and turning (Container Vessel, Inbound)

Inbound)

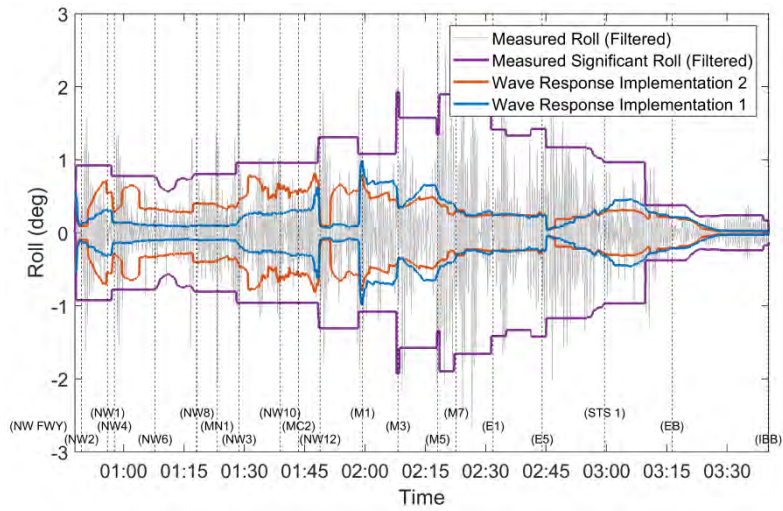


Figure 10: C2 Filtered Roll Validation (Container Vessel Inbound)

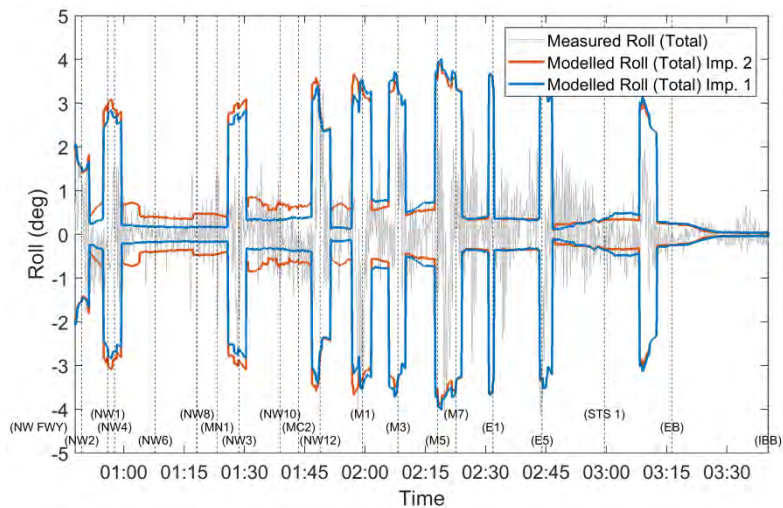


Figure 11: C2 Non-filtered Roll Validation incl. effects of wind and turning (Container Vessel Inbound)

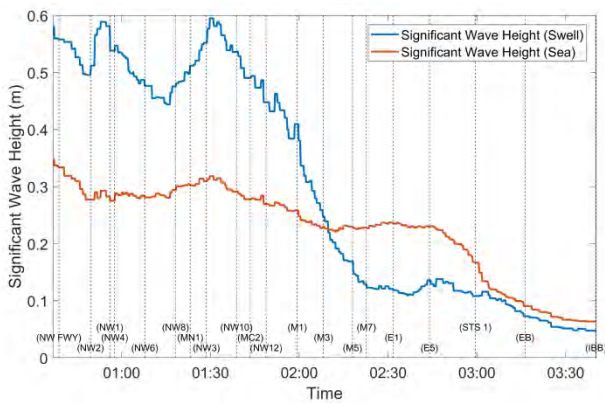


Figure 12: C2 Sea and Swell Significant Wave Height

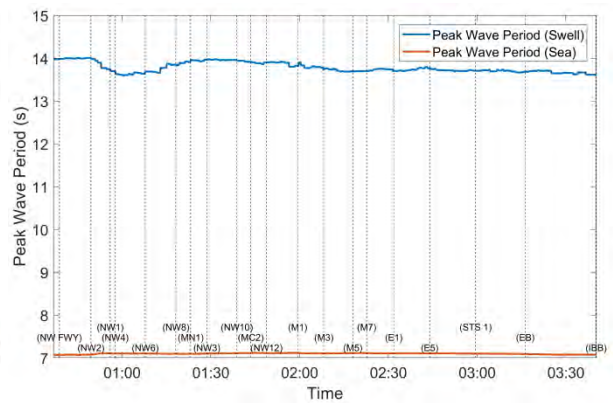


Figure 13: C2 Sea and Swell Peak Wave Period

The root-mean-square (RMS) error, average absolute error and maximum absolute error have been calculated for the roll of the above transits over their entire domain and are displayed below in **Table 3**. Because the wave induced roll motion cannot be extracted from the measured roll data for the container vessels, and this investigation involves comparing purely wave induced motions, the two containers were not included in these error calculations.

| Vessel | RMS Error (deg) | | Mean Absolute Error (deg) | | Max Absolute Error (deg) | |
|----------------|-----------------|---------|---------------------------|--------|--------------------------|--------|
| | Imp. 1 | Imp. 2 | Imp. 1 | Imp. 2 | Imp. 1 | Imp. 2 |
| B2 | 0.3814 | 0.1493 | 0.2919 | 0.121 | 2.0724 | 0.631 |
| B3 | 0.2204 | 0.1932 | 0.1372 | 0.1366 | 0.7905 | 0.6522 |
| Average | 0.3009 | 0.17125 | 0.21455 | 0.1288 | 1.43145 | 0.6416 |

Table 3: RMS and Mean/Max Absolute Error of Wave Induced Roll

From the figures, it can be seen that wave response implementation 2 provides a more accurate fit to the measured roll data than wave response implementation 1. The quantifiable data displayed in **Table 3** supports this observation with the wave response implementation 2 demonstrating close to an average decrease of 50 percent in all errors from the wave response implementation 1. This indicates that forcing NCOS with the fully directional wave spectra is recommended to most accurately represent the wave induced roll motions.

5.1.2 Pitch

Figure 14 to **Figure 17** show that the squat motion experienced during each transit has successfully been filtered from the measurements leaving just the wave induced pitch motion. These figures and **Table 4** all show that both wave response implementation 1 and 2 have accurately reproduced the measured wave induced pitch response. As with roll, wave response implementation 2 has provided a more accurate result than wave response implementation 1.

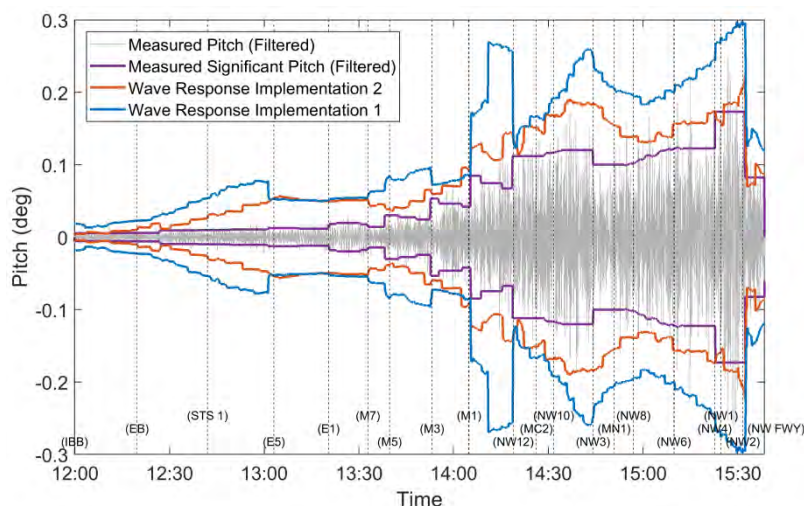


Figure 14: B2 Pitch Validation

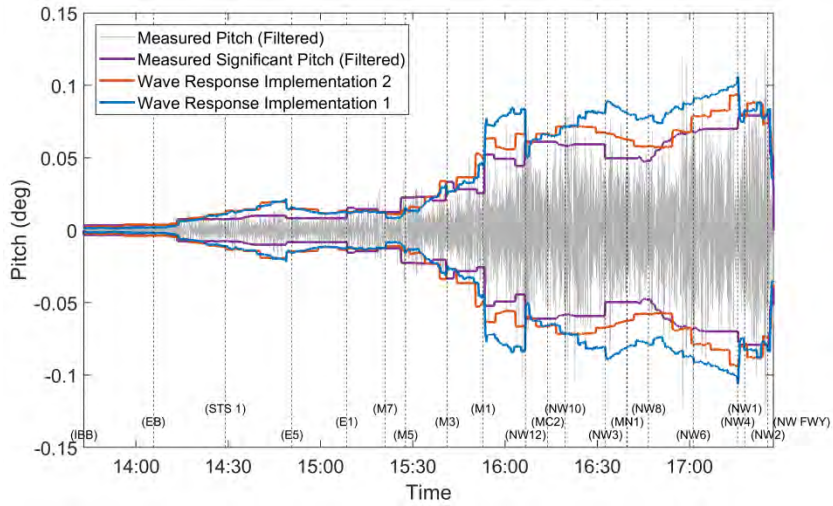


Figure 15: B3 Pitch Validation

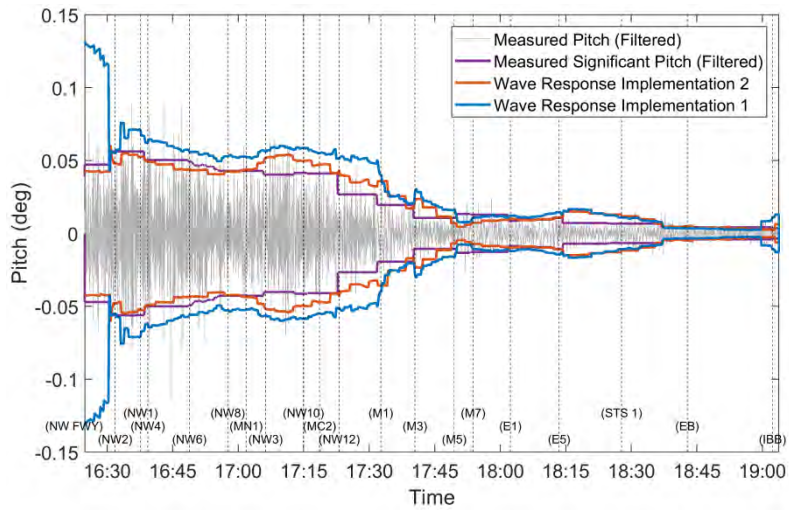


Figure 16: C1 Pitch Validation

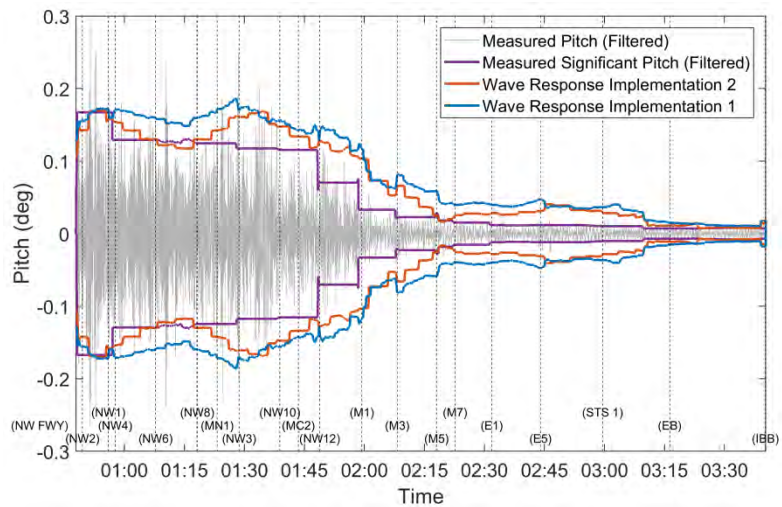


Figure 17: C2 Pitch Validation

| Vessel | RMS Error (deg) | | Mean Absolute Error (deg) | | Max Absolute Error (deg) | |
|----------------|-----------------|--------|---------------------------|--------|--------------------------|--------|
| | Imp. 1 | Imp. 2 | Imp. 1 | Imp. 2 | Imp. 1 | Imp. 2 |
| B2 | 0.0756 | 0.0345 | 0.0632 | 0.0288 | 0.2138 | 0.1414 |
| B3 | 0.0152 | 0.0085 | 0.0108 | 0.0064 | 0.0397 | 0.0274 |
| C1 | 0.0179 | 0.006 | 0.0106 | 0.0045 | 0.0851 | 0.0165 |
| C2 | 0.0342 | 0.0244 | 0.0293 | 0.0185 | 0.0917 | 0.0734 |
| Average | 0.0357 | 0.0184 | 0.0285 | 0.0146 | 0.1076 | 0.0647 |

Table 4: RMS and Mean/Max Absolute Error of Wave Induced Pitch

Table 4 shows that wave response implementation 2 demonstrates close to an average decrease of 50 percent in all errors from the wave response implementation 1. This indicates that forcing NCOS with the fully directional wave spectra is recommended to most accurately represent the wave induced pitch motions.

5.1.3 Heave

Figure 18 to **Figure 20** again show that the squat motion experienced during each transit has successfully been filtered from the measurements leaving just the wave induced heave motion. These figures and **Table 5** show that both wave response implementation 1 and 2 have accurately reproduced the measured wave induced heave response for transits B3, C1 and C2. Again, wave response implementation 2 has provided a more accurate result than wave response implementation 1.

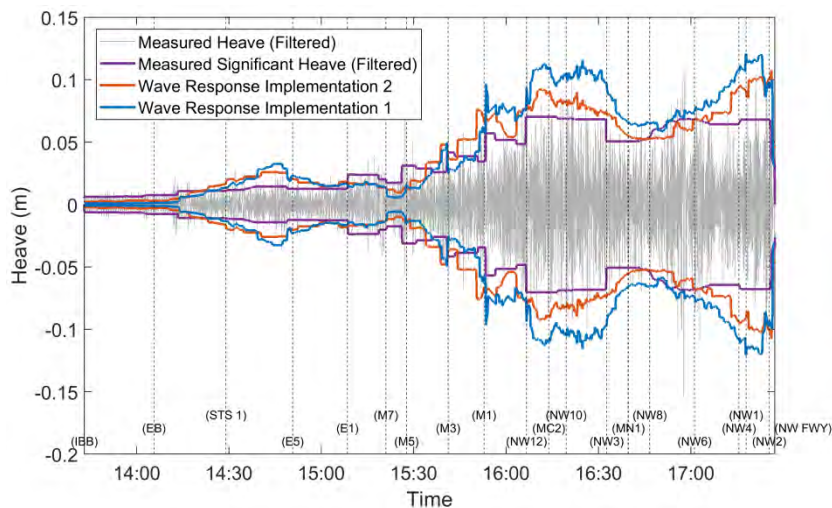


Figure 18: B3 Heave Validation

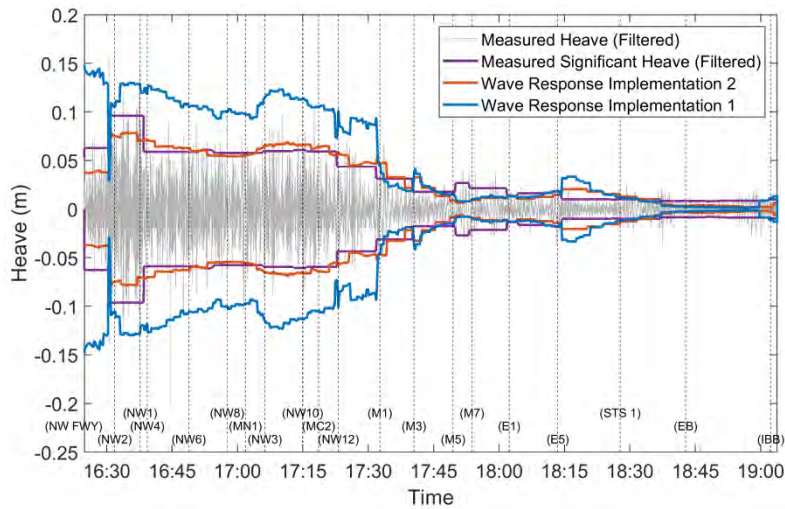


Figure 19: C1 Heave Validation

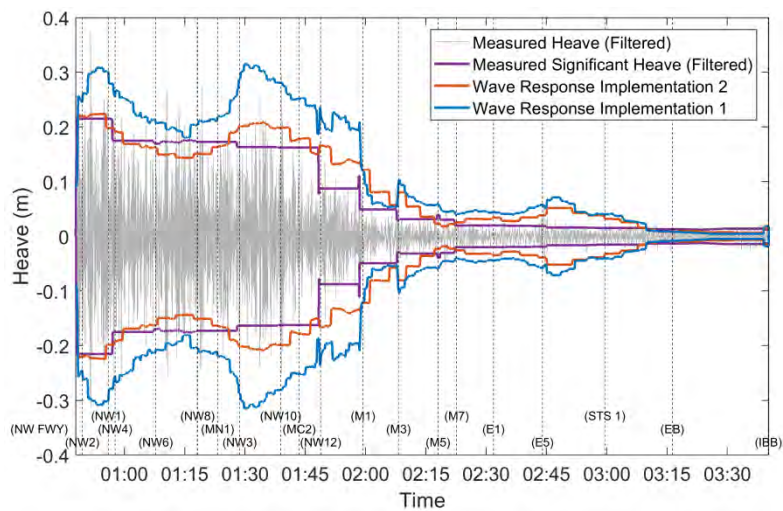


Figure 20: C2 Heave Validation

| Vessel | RMS Error (m) | | Mean Absolute Error (m) | | Max Absolute Error (m) | |
|----------------|---------------|--------|-------------------------|--------|------------------------|--------|
| | Imp. 1 | Imp. 2 | Imp. 1 | Imp. 2 | Imp. 1 | Imp. 2 |
| B3 | 0.0197 | 0.0127 | 0.0148 | 0.0096 | 0.0638 | 0.072 |
| C1 | 0.0333 | 0.0098 | 0.0244 | 0.0074 | 0.0871 | 0.0594 |
| C2 | 0.0602 | 0.0262 | 0.0449 | 0.0198 | 0.1607 | 0.115 |
| Average | 0.0377 | 0.0162 | 0.0280 | 0.0123 | 0.1039 | 0.0821 |

Table 5: RMS and Mean/Max Absolute Error of Wave Induced Heave

Table 5 shows that wave response implementation 2 demonstrates close to an average decrease of 50 percent in the RMS and mean absolute errors with similar maximum absolute errors from the wave response implementation 1. This indicates that forcing NCOS with the fully directional wave spectra is recommended to most accurately represent the wave induced heave motions.

Overall, both wave response implementation 1 and 2 are capable of accurately reproducing the measured results with wave response implementation 2 providing the most accuracy.

5.2 Squat Comparison and Validation

NCOS utilizes well known empirical squat formulae Millward (Millward, 1990), Yoshimura (Ohtsu K, 2006), Barrass (Barrass, 1979) and Huuska (Huuska, 1976). Each formula is most suitable under different vessel and channel specific parameters. As a result, NCOS utilizes a combination of these squat formulae simply choosing which formula to use based on the corresponding vessel and channel specific parameters in order to provide the most accurate result while still being conservative.

The development of the combined squat implementation resulted in selection criteria for choosing between squat formulae. The best squat formula is considered to be the one which gives a value closest to the measured squat while still being conservative. Once the best squat formula for each timestep of each measured transit was found, ranges of block coefficient, vessel speed (relative to water) and blockage factor were assigned to each squat formula. Equations representing these ranges are displayed in **Table 6** and **Table 7**.

| Selection Criteria | | |
|--------------------|--------------------------|----------------|
| Speed Interval | Blockage Factor Interval | Combined Squat |
| ≥ 18 knts | < 0.05 | Huuska |
| ≥ 18 knts | ≥ 0.05 | Yoshimura |
| 14 knts - 18 knts | > 0.05 | Huuska |
| 15 knts - 17 knts | 0.04 - 0.05 | Yoshimura |
| 17 knts - 18 knts | ≤ 0.05 | Barrass |
| 14 knts - 17 knts | ≤ 0.04 | Barrass |
| 8 knts - 17 knts | > 0.1 | Millward |
| 4 knts - 8 knts | > 0.09 | Millward |
| 10 knts - 14 knts | 0.08 - 0.1 | Huuska |
| 8 knts - 10 knts | 0.08 - 0.1 | Barrass |
| 8 knts - 14 knts | ≤ 0.08 | Barrass |
| 4 knts - 8 knts | ≤ 0.09 | Barrass |
| ≤ 4 knts | | Millward |

Table 6: Best Fitting Squat Formula Ranges for Ships with Block Coefficient < 0.75

| Selection Criteria | | |
|--------------------|--------------------------|----------------|
| Speed Interval | Blockage Factor Interval | Combined Squat |
| | ≤ 0.075 | Millward |
| > 10 knts | 0.075 - 0.1 | Huuska |
| 4 knts - 10 knts | 0.075 - 0.12 | Barrass |
| 4 knts - 10 knts | 0.12 - 0.18 | Huuska |
| ≥ 10 knts | 0.1 - 0.18 | Barrass |
| > 4 knts | ≥ 0.18 knts | Millward |
| ≤ 4 knts | ≥ 0.075 knts | Yoshimura |
| 7.4 knts - 8 knts | 0.138 - 0.16 | Yoshimura |
| 7.4 knts - 8 knts | 0.12 - 0.138 | Huuska |
| 7.4 knts - 8 knts | 0.16 - 0.18 | Huuska |
| 4 knts - 7.6 knts | 0.12 - 0.18 | Huuska |
| 8 knts - 10 knts | 0.12 - 0.18 | Huuska |

Table 7: Best Fitting Squat Formula Ranges for Ships with Block Coefficient ≥ 0.75



Figure 21: Squat Comparison and Validation Legend

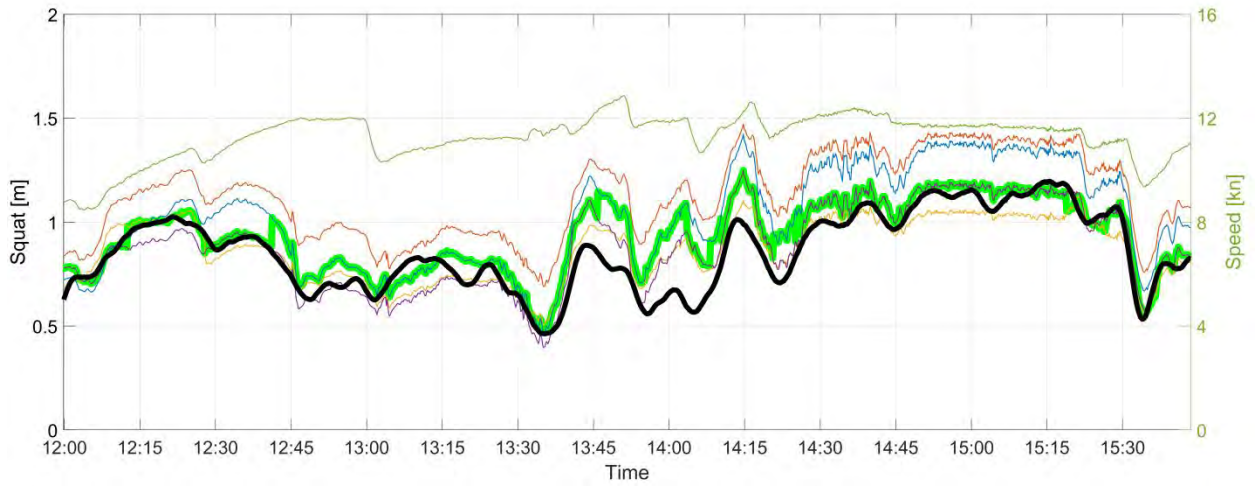


Figure 22: B2 Squat Comparison

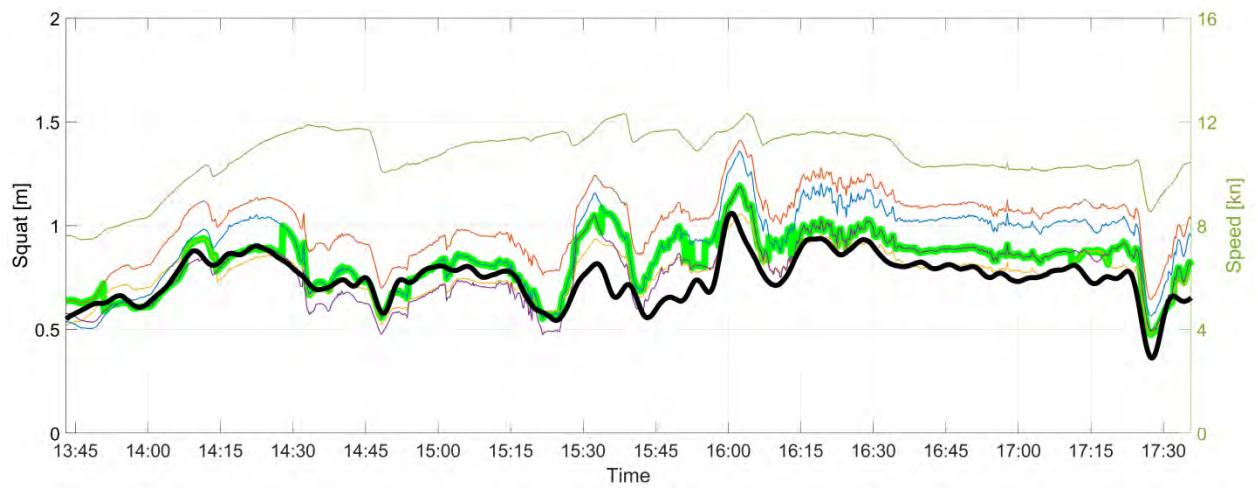


Figure 23: B3 Squat Comparison

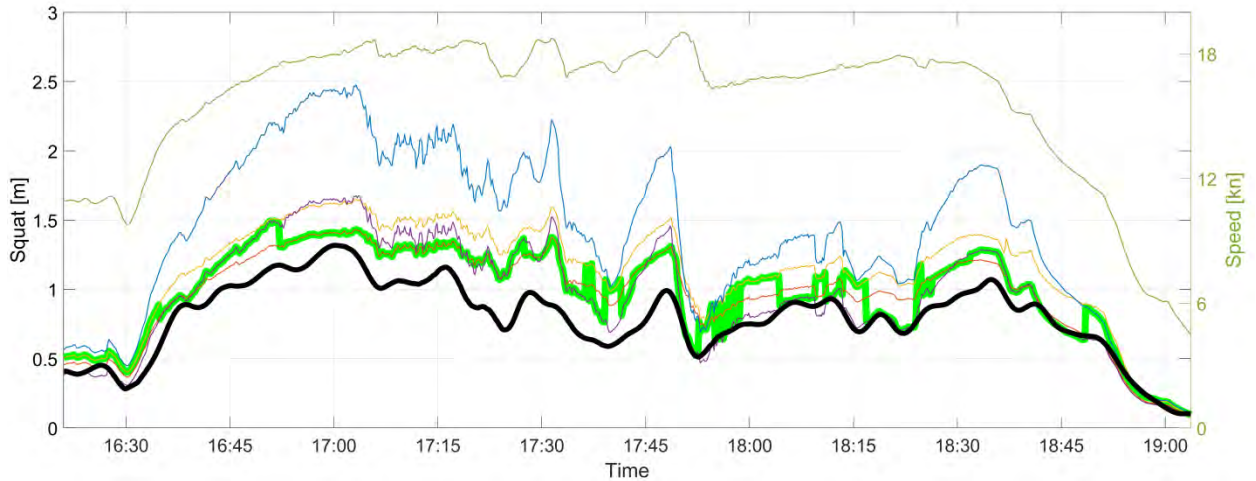


Figure 24: C1 Squat Comparison

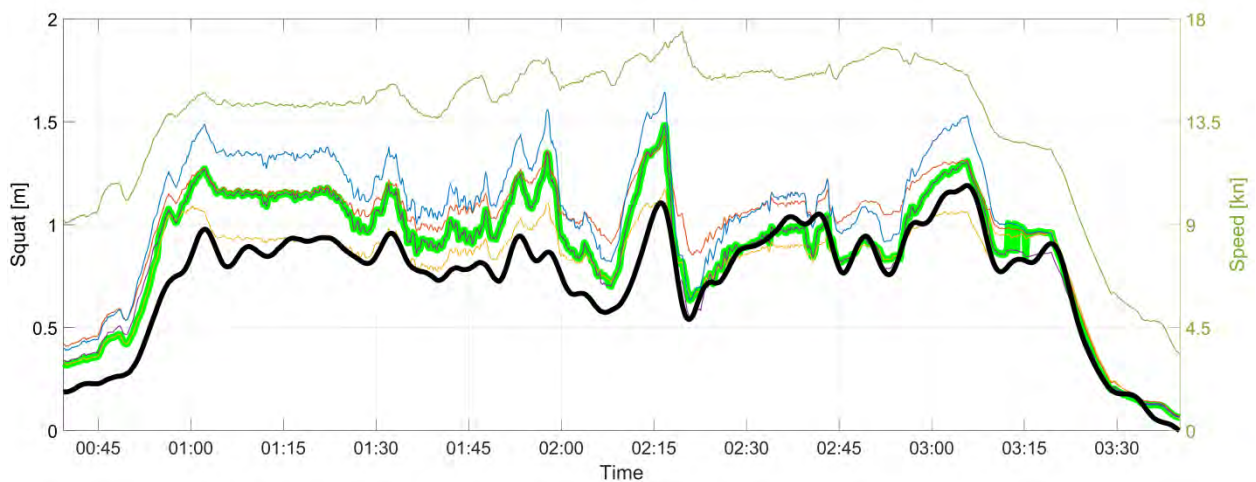


Figure 25: C2 Squat Comparison

Figure 22 to Figure 25 show that the squat formulae behave differently for bulk carrier and container ships. Container ships are more slender and typically have block coefficient values in the range from 0.54 to 0.71, where bulk carriers typically have block coefficient values greater than 0.8 to 0.85. In general, a bulkier ship will have comparatively more squat than a more slender container ship for the same speed (PIANC, 2014). Through the Port of Brisbane container ships travel much faster than bulk carriers. As a result the various squat formulae will relate to these two vessel types differently.

Figure 22 and Figure 23 show that the Barrass and Huuska squat formulae provide adequate results for the bulk carrier squat, while Yoshimura and Millward are more conservative. **Figure 24 and Figure 25** show that Barrass, Huuska and Yoshimura provide adequate results for the container squat, while Millward is again more conservative.

5.3 UKC Validation

The total vertical excursion was calculated for each transit and compared to the measurements. Wave response implementation 2 and the combined squat implementation have been applied for calculating the wave induced vessel motions and squat. In order to provide both likely and conservative results, the total vertical excursion is calculated based on two depth exceedance probabilities 1% and 75%.

- Measured Vertical Excursion
- Modelled Vertical Excursion 75% Depth Exceedance
- Modelled Vertical Excursion 1% Depth Exceedance
- Depth

Figure 26: UKC Validation Legend

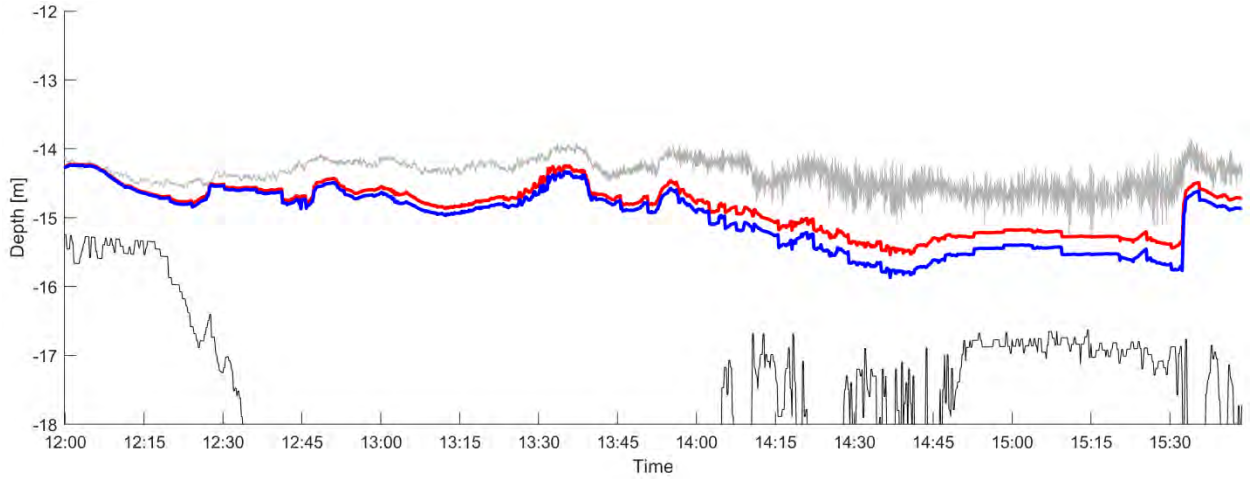


Figure 27: B2 UKC Validation

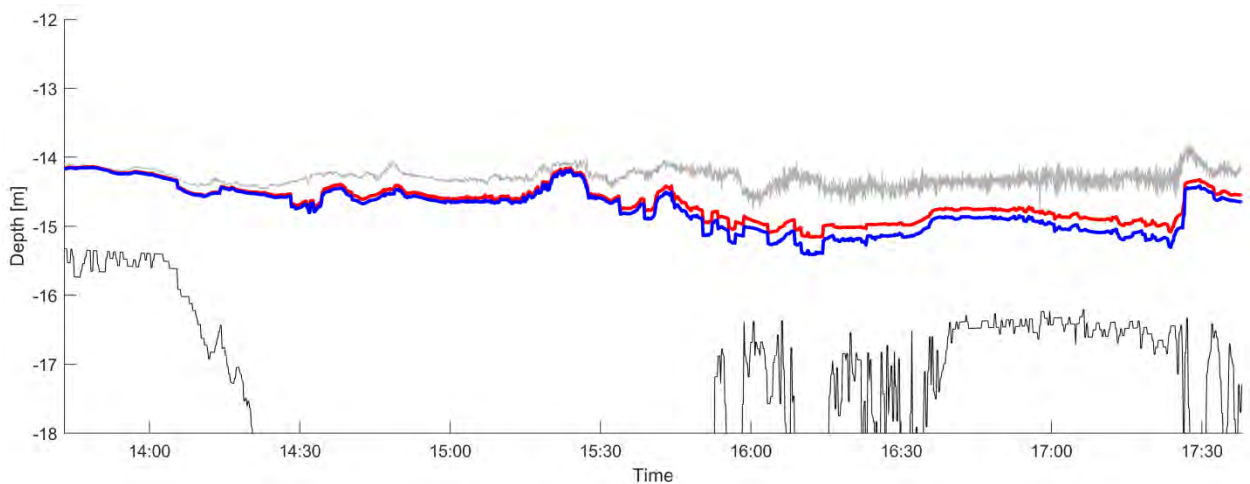


Figure 28: B3 UKC Validation

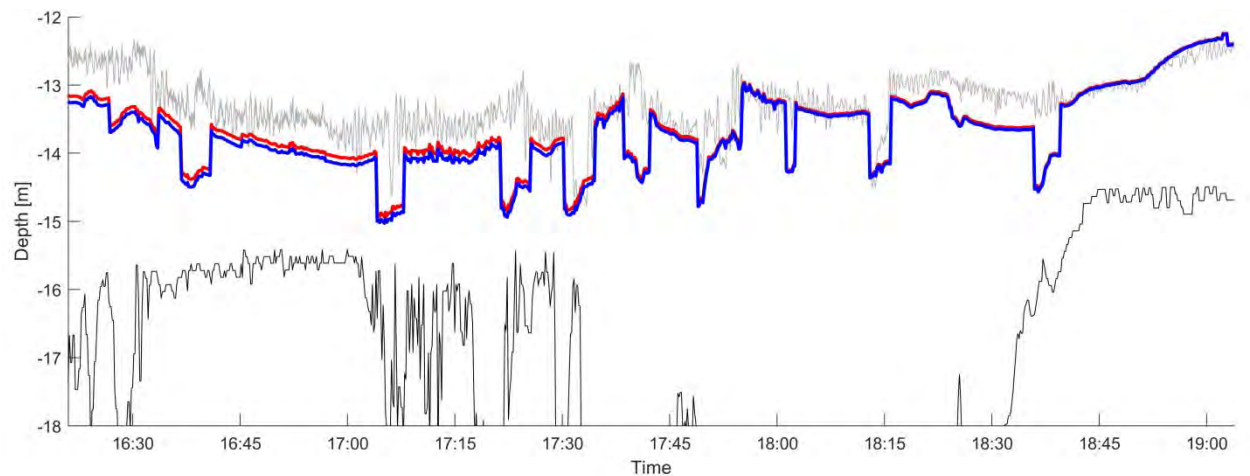


Figure 29: C1 UKC Validation

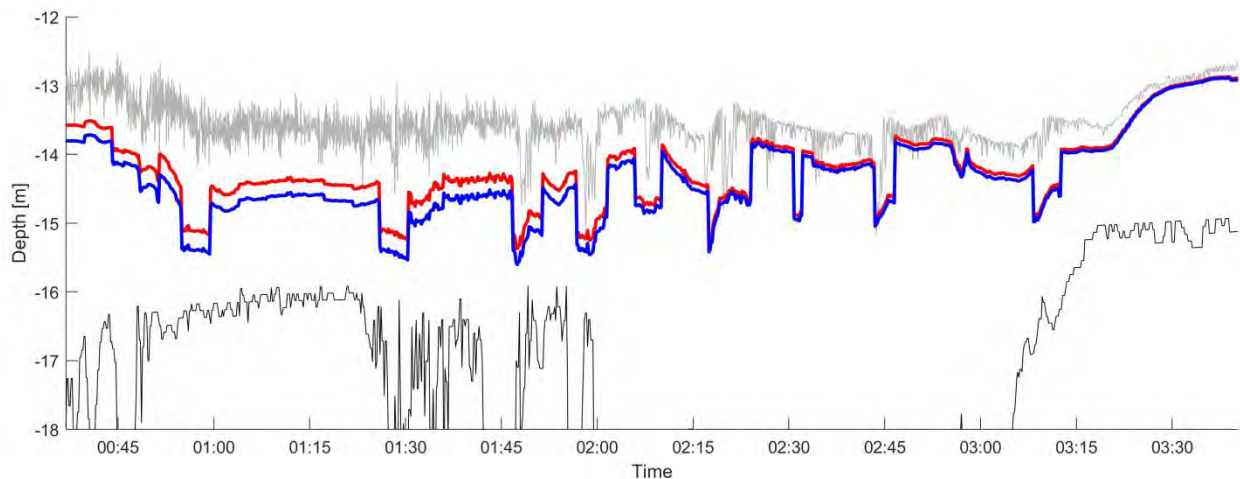


Figure 30: C2 UKC Validation

Figure 27 to Figure 30 show that NCOS has been able to accurately reproduce the measured total vertical excursion.

6 SUMMARY

In order to validate DHI's new UKC model NCOS, model results have been compared to the measurements taken during four transits through the Port of Brisbane. The comparison includes timeseries of roll, pitch, heave, squat and total vertical excursion. Two wave response implementations have been tested which resulted in the finding that it is recommended to force NCOS with a fully directional wave spectra then with separated sea and swell integral wave components. Four empirical squat formulae have been compared. This comparison demonstrated that all squat formulas performed well with varies levels of conservatism and each formula being suitable under different vessel and channel specific parameters which resulted in the generation of a combined squat implementation which provides very accurate squat predictions while still being conservative. Direct comparison between measured and modelled UKC was excellent and demonstrated a high level of accuracy in capturing various drivers conservatively without being overly conservative.

7 REFERENCES

- Barrass, C. B. (1979). Phenomena of Ship Squat. *Int Shipbuild Prog*, 26(294), (pp. 44-47).
- Huuska, O. (1976). On the Evaluation of Underkeel Clearances in Finnish Waterways. Helsinki: Helsinki University of Technology.
- Lewandowski, E. M. (2014). *The Dynamics of Marine Craft*. Arlington: World Scientific Publishing.
- Millward, A. (1990). A Preliminary Design Method for the Prediction of Squat in Shallow-Water. (pp. 10-19). *Marine Technology and SNAME News*.
- Mortensen, S. (2017). *An Improved Integrated Approach for Optimizing Shipping Channel Capacity for Australian Ports*. Cairns: Coasts & Ports 2017 Conference.
- Ohtsu K, Y. Y. (2006). Design Standards for Fairway in Next Generation. Asia Navigation Conference 2006, No. 26.
- PIANC. (2014). *Harbour Approach Channels Design Guidelines*. Brussels.

COMPARISON OF VALIDATION STUDIES OF WAVE-PENETRATION MODELS USING OPEN BENCHMARK DATASETS OF DELTARES

by

*P. (Pepijn) P.D. van der Ven¹, S. (Bas) P. Reijmerink¹, A. (Arne) J. van der Hout¹
and M. (Martijn) P.C. de Jong^{1,2}*

ABSTRACT

This paper presents a collection of open benchmark datasets. These datasets are made available by Deltares for numerical model validation studies, including port applications such as wave penetration models and tools for computing wave forces exerted on moored ships. The paper summarises the contents and characteristics of each available dataset. Furthermore, the paper makes a comparison of different validation studies that have used specific parts of these datasets to this date. This comparison is made to illustrate the possibilities of using these datasets, but it also highlights remaining questions and challenges related to numerical model validation. Researchers, engineers and advisors working on related topics are encouraged to contact Deltares to explore cooperation possibilities using these benchmark datasets.

1. INTRODUCTION

Downtime in ports is often dominated by the local nearshore wave climates and the resulting wave penetration into port basins. Geometry complexities and specific bathymetric influences, such as the effect of entrance channels, will complicate the description of wave penetration into ports and may make verifying wave conditions in relation to expected port downtime far from trivial (De Jong *et al.*, 2016, PIANC COPEDEC).

Wave conditions inside ports can be determined during the port design process with physical scale model tests or with numerical tools. Scale model tests can be considered the most complete way of design verification prior to construction. However, particularly in early stages of design numerical methods are generally preferred. Several types of numerical wave models are available, including spectral models, mild-slope models, Boussinesq-type models and (multi-layer) flow models adapted to represent also short waves. These different types of numerical wave models all have their own specific advantages and drawbacks. And although the fundamentals of such wave models have generally been validated in detail, validation of the performance of these numerical models for representing wave penetration into ports has often been rather limited. One of the main reasons for this is that datasets for validation are quite scarce. As a result, downtime estimates based on the outcomes of insufficiently validated numerical models may be inaccurate and unreliable.

Field measurement datasets for model validation are often limited in duration, cannot describe future situations, will typically not cover extreme conditions and may include only a few observation locations. To complement and extend such data, over the past decades Deltares has performed several elaborate physical scale model tests on wave penetration in different port layouts, under a wide range of controlled wave conditions and always including several measurement locations. These test series ranged from specific existing (or planned) port layouts to more schematic situations. The former were aimed at verifying the performance of specific port extension plans, whereas the latter were intended to highlight and record specific aspects of the wave penetration process. Some of the test series from the latter collection have been especially designed to serve as (schematised) validation material for numerical wave penetration models. Having these different datasets available has allowed Deltares to validate its numerical wave penetration tools in detail and it has given us detailed insights into the capabilities and limitations of different types of numerical wave penetration models (see e.g. De Jong *et al.*, 2016).

Deltares wants to make a part of its archived wave penetration datasets available to interested parties, so that they can use them in their research initiatives on numerical model validation in consultation with Deltares. It is our intention to maximize the usefulness of these datasets by sharing them with

¹ Deltares, PO Box 177, 2600 MH Delft, The Netherlands

² Communicating author, tel. +31 88 335 8596, martijn.dejong@deltares.nl

others and by jointly working on the validation and development of numerical wave models and on related computational tools for ports, such as calculating wave forces exerted on moored ships.

Even though already quite some studies by others and by Deltares have used the datasets presented in this paper, these data still form a valuable collection for future work. This is because parts of the presented datasets have not yet been exploited in model validation studies, and because so far only a limited set of specific models (model types) has been considered. Furthermore, parts of the validation outcomes obtained so far have been inconclusive and still require further analyses, as will be illustrated in sections further below.

The present paper summarises the contents and characteristics of the three available datasets by Deltares (Section 2). The largest part of this paper (Sections 3 to 5) consists of a comparison of a selection of the different validation studies that have used specific parts of the datasets to this date. Those earlier studies typically focussed on validating a specific numerical model, using a selection of data from the available test series. This paper presents for the first time an inter-comparison and an overarching analysis of those different results obtained based on these measurements by Deltares. This comparison is made to illustrate the potential use of these datasets, but it also highlights remaining questions and challenges related to validating numerical methods. The comparison focusses on two of the three presented datasets, since only a few studies have used the third dataset to this date and because a separate publication is foreseen on those tests. The paper ends with conclusions on the presented datasets and on the comparison of earlier studies using those data (Section 6).

Both the description of the available datasets and the comparison of earlier validation studies are meant to serve as a starting point for further cooperation with interested parties.

2. AVAILABLE OPEN DATASETS BY DELTARES

2.1 Overview of available open datasets

Table 1 gives a summary of the datasets that Deltares intends to make available to parties interested in a joint research effort on the validation of numerical methods. The available datasets include one full port layout, a schematic port layout with a captive ship (to enable the measurement of wave forces acting on the ship) and a series of schematic port layouts of increasing complexity. In the following sections the contents of each of these datasets is described in more detail. In the future we plan to extend the collection of datasets with other port situations.

Table 1: overview of available datasets

| Number | Short name/reference | Compact description |
|--------|---|---|
| 1 | schematic rectangular port layout with a captive ship | A large dataset of different wave conditions with a captive ship in open water and inside a schematic port layout. Conditions considered involve high waves as well, to allow the assessment of non-linear wave phenomena. |
| 2 | full port layout | This is a dataset that includes only wave parameters (H_s , T_p). However, it is useful dataset since it describes an existing port layout, a wide range of wave conditions and different construction phases of the port layout. |
| 3 | series of different schematic port layouts | This is a dataset generated specifically for wave model validation purposes and includes a systematic variation of geometry and wave conditions (regular, irregular, long/short-crested). The starting point was deliberately very simple, i.e. a rectangular basin, and complexity was added in the course of the measurement campaign (side basin, breakwater). |

2.2 Dataset 1 – Captive ship in rectangular basin

An extensive measurement campaign was undertaken in 2003 in the large directional wave basin at Deltares (back then Deltares was named WL | Delft Hydraulics). The main situation measured consisted of a vessel moored in a schematic harbour basin (Figure 1 and Figure 2).

A scale of 1:100 was used for the measurements, leaving ample space in the basin (40x40 m)³ for rubble mound slopes along all the outer vertical walls of the basin (Figure 1) to ensure sufficient damping of wave energy and avoiding as much as possible any spurious waves in the scale model.

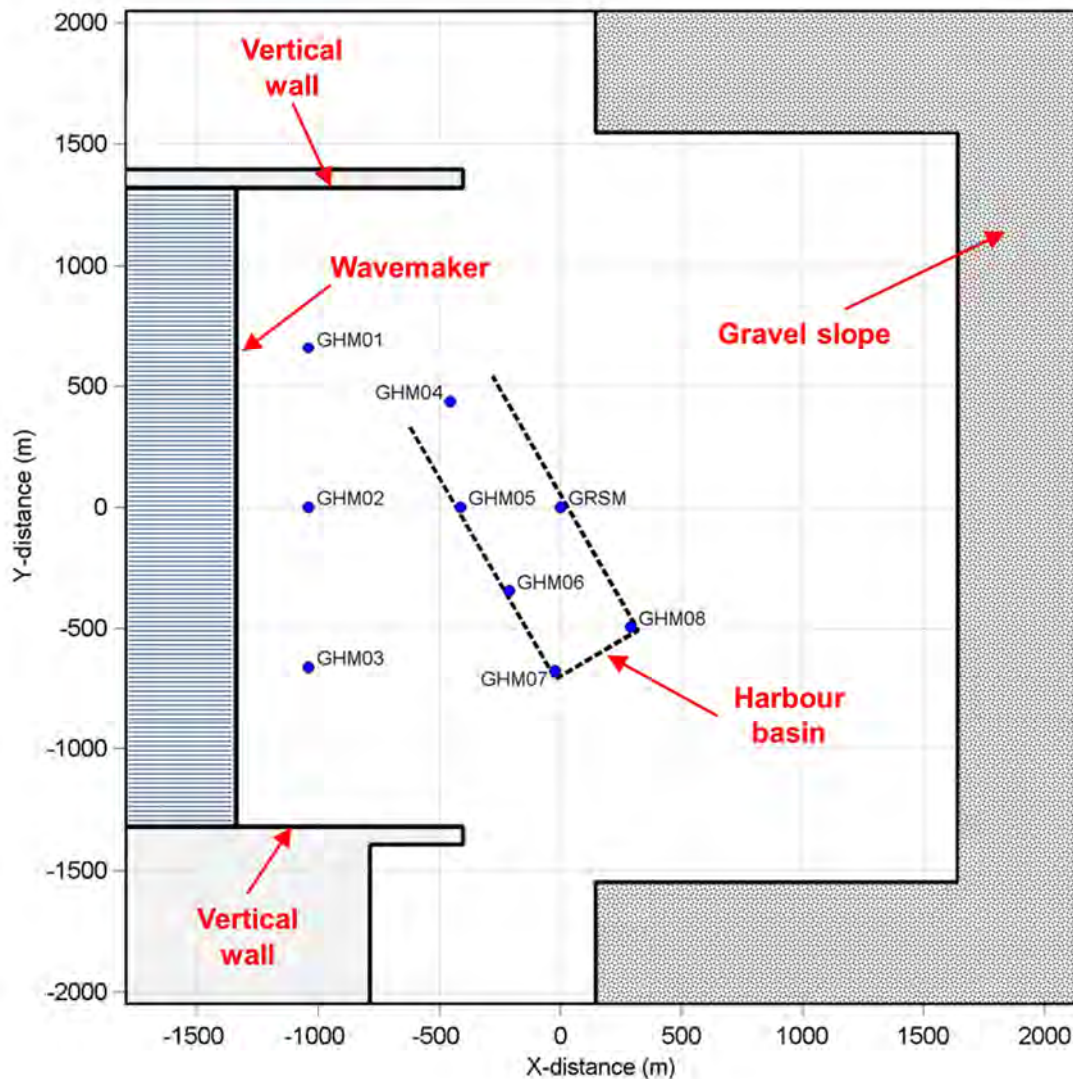


Figure 1: schematic plan view of the measurement setup of Dataset 1.

The following series of tests were performed for Dataset 1:

- Wave measurements in open water
- Measurements of wave-induced forces and moments on a vessel in open water
 - Regular and irregular wave conditions
 - Passing-ship events (focussing on secondary waves generated by the wave maker)
- Wave measurements including a schematic port basin
- Measurements of wave-induced forces and moments on a vessel in a schematic basin

A part of the test series included a 1:100 scale model of a containership (length: 255 m, width: 32 m, further details available). The ship was held captive in a rigid force measurement frame (Figure 3), allowing measurement of wave forces exerted on the ship. Situations without the vessel present were considered to measure the undisturbed incoming wave conditions. These were compared to measurements of the same wave conditions with the vessel present to assess the influence of diffraction of waves around the vessel.

³ Since then this directional wave basin has been upgraded to outer dimensions of 50x50m and a new directional wave maker has been inserted of 40m length with state-of-the-art active reflection compensation.



Figure 2: overview photo of a moored ship in a schematic representation of a harbour basin in the large directional wave basin of Deltares (the photo shows only a part of the basin).

The measurement campaign also included test series in open water that were intended for developing and verifying wave directionality analysis methods. The measurement locations used for this purpose included five wave probes distributed evenly on a circle, resulting in a pentagon shape. The applied radius of the circle was 75 m (prototype scale). A wave height probe was placed at the centre of the pentagon to obtain the wave signal at that location for comparison.

JONSWAP wave spectra from multiple main directions were generated, with different wave parameters. The generated waves included second-order wave forcing. The following wave parameters (prototype scale) have been used:

- T_p : 7, 10 and 15 s;
- H_s : 0.5 and 1.5 m;
- direction relative to wave board (α): 60, 90 and 120°;
- unidirectional waves;
- directional spreading (ψ): \cos^2 and \cos^4 .



Figure 3: detail of moored ship held captive in the scale model (open water reference tests).

Additional test series were performed of schematic passing-ship events (wakes/secondary waves). These test series included the vessel measurement setup in open water (Figure 3). The passing-ship effects were mimicked by serial movements of the individual panels of the wave maker (vessel speeds of 12 m/s and 21 m/s, i.e. a subcritical and a supercritical vessel speed, respectively). Even though the wave maker can only make a rather crude approximation of a passing-vessel event (e.g. the panels in the shallow-water wave basin move the entire water column, whereas in reality the vessel would only occupy the upper part), these situations do provide interesting validation material.

All conditions included a water depth of 20 m and each measured irregular wave condition lasted 1800 s (prototype scale) or longer to obtain statistically representative results.

2.3 Dataset 2 – Complete port layout

The second dataset consists of scale model tests for the Port of Limassol. The city of Limassol is located along the south coast of the Mediterranean island of Cyprus, see Figure 4 for a situation sketch. Around 1990, Deltares (back then called WL | Delft Hydraulics) carried out these physical model experiments⁴ to advise on the best approach for a planned port extension.



Figure 4: location and present layout of the port of Limassol, Cyprus.

Physical model experiments were carried out on a scale of 1:100 for three main directions of wave incidence, i.e. 80°, 100° and 130°N. Breakwaters were constructed in the physical scale model using rubble mound. The considered wave conditions (Table 2) included long-crested and short-crested conditions ($m = 2$, $\sigma = 31.5^\circ$). In total 46 scenarios were measured. Wave heights were measured at up to 28 positions, including a number of locations outside the port for wave calibration purposes. Recorded wave data were filtered for the high-frequency part of the spectrum (0.05-0.5 Hz) and the low-frequency part (<0.05 Hz). Significant wave heights were recorded for both frequency ranges separately. Due to data storage limitations at that time, full time series were not archived and only processed wave parameter values were stored.

Table 2: wave conditions considered in Dataset 2.

| Wave direction | Type of wave field | Operational | | Extreme (once per year) | |
|----------------|------------------------|-------------|-----------|-------------------------|-----------|
| | | H_s (m) | T_p (s) | H_s (m) | T_p (s) |
| 80°N | Short and long-crested | 1.75 | 6.0 | 2.50 | 7.00 |
| 100°N | Short and long-crested | 1.75 | 6.0 | 2.50 | 7.00 |
| 130°N | Short-crested | 1.75 | 6.0 | 4.00 | 9.00 |

In total four layouts were considered (Figure 5), including the – back then – existing situation ('Hm0') for reference. Layouts were tested with and without vessels at the berths. The former were aimed at measuring the influence of local wave conditions on the moored ships, whereas the latter focussed only on wave penetration in the overall port layout.

Following the work by Deltares (WL | Delft Hydraulics) the port selected the western basin and the elongated breakwater to be constructed, which remains the existing situation to date.

2.4 Dataset 3 – Series of schematic port layouts

Dataset 3 consists of a dedicated measurement campaign that was performed to generate validation cases for different wave penetration software (Van der Ven, 2016). Three schematic port layouts (Table 3) were considered in the extended directional wave basin of Deltares (Delta Basin), which presently has outer dimensions of 50x50 m. This basin includes a 40 m wide wave maker. These tests were performed at scale 1:45. The port layouts considered were deliberately quite schematic, partly because that would provide the most straightforward validation situations and results, but also partly because of research budget restrictions. A total of 86 wave conditions were measured, including monochromatic waves, bi-chromatic waves and full wave spectra (JONSWAP). The test programme

⁴ The tests for Dataset 2 were performed in a predecessor of the basin used for Dataset 1 (Figure 1). The tests facility used for Dataset 2 included a wave maker of 25.6 m length.

included a wide range of incoming wave heights (0.5 m to 9.5 m) and wave periods (4.5 s to 17 s), aimed at generating a dataset that would have a wide applicability (mild and severe wave conditions). Measurements included 22 wave height probes (estimated accuracy 0.5%) and five directional wave height probes (estimate accuracy 1%). These probes were positioned in front of and inside the schematic port basin geometry. The coordinates of the measurement locations are described in Van der Ven (2016).

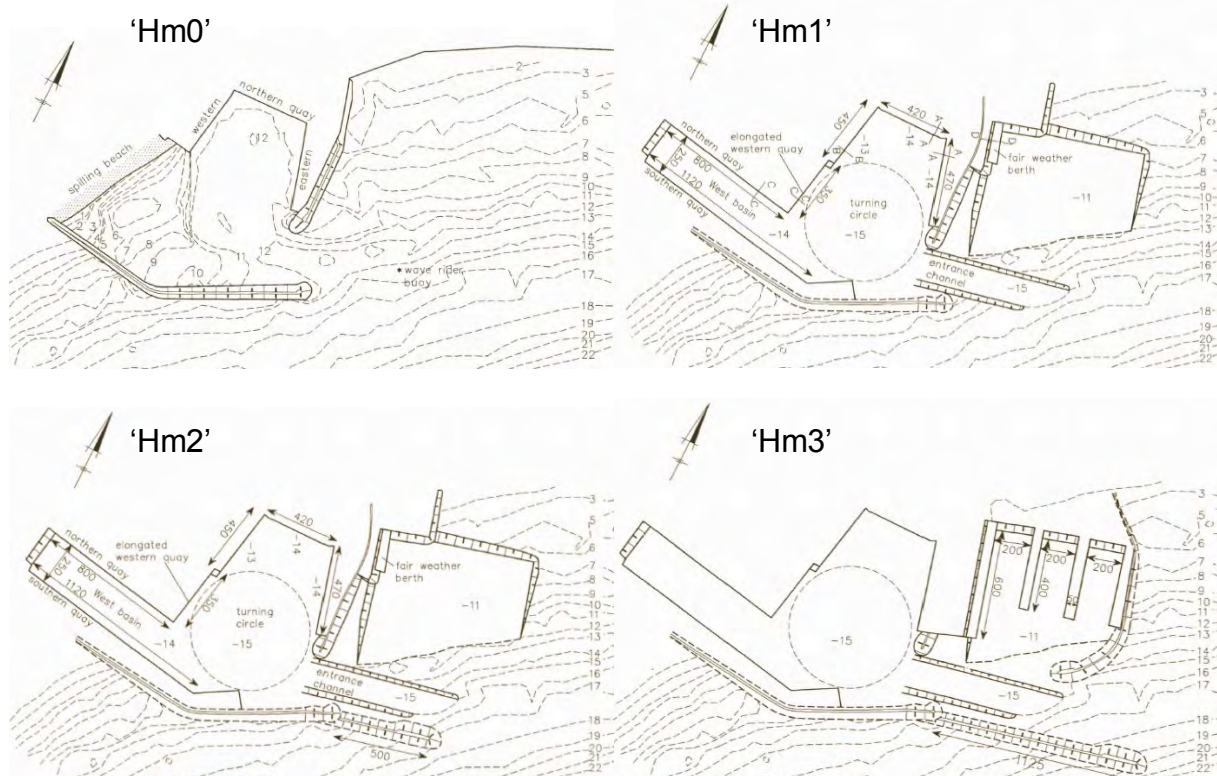


Figure 5: layouts considered in the physical scale model tests for the port of Limassol (Dataset 2).

Table 3: the three layouts considered for Dataset 3

| | Layout 1 | Layout 2 | Layout 3 |
|---------------------------------|------------------------------------|---|---|
| | | | |
| Governing wave processes | Reflection Harbour oscillations | Reflection Diffraction Harbour oscillations | Reflection Diffraction Refraction over the breakwater slope Transmission Harbour oscillations |
| Eigenmodes | Trivial | Less trivial | Several, increased complexity |

The measurements started with a plain basin layout and additional complexity – a side basin and a breakwater – was added in two steps (Table 3). As an example, Figure 6 shows the most complex layout that was included in the final part of the test series.



Figure 6: photograph of the most complex model setup considered in Dataset 3 (Layout 3).

3. COMPARISON OF VALIDATION STUDIES USING DATASET 1

Dataset 1 has been used by De Jong *et al.* (2005), Van der Molen (2006), Dobrochinski (2014), Rijnsdorp (2016) and Wong (2016). Below we describe a selection of these studies as examples of how the information included in this dataset has been used to this date.

De Jong *et al.* (2005) used Dataset 1 to extend and illustrate the application of a phase resolving wave splitting method (Directional Phase Resolving Analysis, DPRA, originally introduced in Janssen *et al.*, 2001). Methods that allow to split a number of local surface-elevation time series (measured or computed) in separate wave components are very useful for (moored) vessel applications in and around ports, since the motion response of a vessel in complex wave conditions depends not only on the local wave height and wave frequency, but also on the wave phases and directions of the multiple wave components typically present at such locations. De Jong *et al.* (2005) considered a selection of wave height measurements from a circular array (a pentagon, hence 5 different time series). In the considered method, the full directionally spread wave system in the basin is mimicked using a small set of discrete directions. The splitting method determines a representative wave spectrum in each of these pre-selected discrete wave directions. The outcomes of the method showed that the wave signal at the centre of the pentagon could be forecasted with rather high accuracy using only three main wave directions to mimic the full directionally spread wave field (e.g. for $T_p = 15$ s, $\alpha = 90^\circ$, $H_s = 1.5$ m and $\psi = \cos^4$, correlation coefficient 0.91, time series not reproduced here).

The wave signals in the three main directions were converted to wave forces exerted on a moored vessel in open water by applying linear response amplitude operators (RAOs). The force contributions from each of the main directions were then summed to represent the influence of the full directionally spread wave system. Even though only three main directions were used to mimic the effect of directional spreading in the wave field, the accuracy of the calculated forces improved significantly compared to assuming only one main wave direction (Table 4). In the latter case the measured signal is assumed to correspond to unidirectional waves propagating in the main direction of the generated wave field, thereby neglecting the influence of directional spreading. Although relatively crude, similar methods are still frequently used in nautical / vessel motion applications.

The time series of wave forces and moments determined with the phase resolving splitting method (Figure 7) show a good correspondence with the measured forces on the ship. The accuracy found may well be within practically acceptable limits. An exception is found for roll (see also Table 4). Already during first interpretations of the measurements this was attributed to a side effect of the method that was used to derive this parameter from the signals of the force probes included in the scale model set-up: the value for roll needed to be calculated by determining the difference between two signals with relatively high values; a relatively small measurement error in one of the probes therefore could have easily resulted in a relatively large error in the value for roll.

Table 4: correlation coefficient between calculated and measured forces and moments (from De Jong *et al.*, 2005).

| method \ parameter | F _x surge | F _y sway | F _z heave | M _x roll | M _y pitch | M _z yaw |
|---|-------------------------|------------------------|-------------------------|------------------------|-------------------------|-----------------------|
| Measured wave signal, no directional spreading included | 0.77 | 0.71 | 0.73 | 0.36 | 0.74 | 0.73 |
| Directional spreading approximated by 3 wave directions | 0.94 | 0.96 | 0.96 | 0.64 | 0.93 | 0.90 |

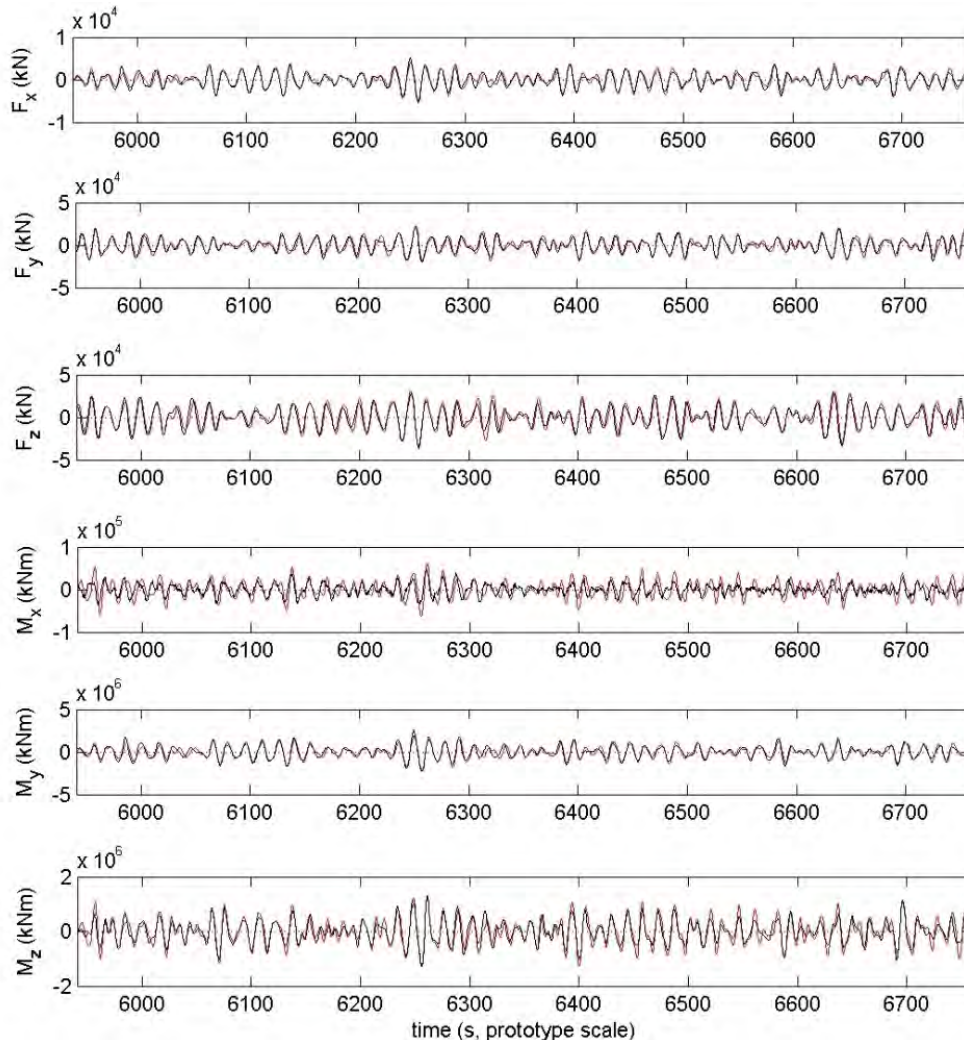


Figure 7: measured (black) and computed (red) forces and moments on the studied ship (top to bottom: surge, sway, heave, roll, pitch and yaw) (from De Jong *et al.*, 2005)

Van der Molen (2006), amongst other analyses not considered here for brevity, used parts of Dataset 1 to validate an approach for calculating the wave-induced forces on the captive vessel. He describes a similar comparison as shown in Figure 7, but now based on measured wave conditions close to the wave maker translated to the location of the ship in open water using linear wave theory.

He combined the outcome of that method with a strip theory approach to compute the corresponding wave forces on the captive vessel. The results that he presents for $H_s = 6$ m, $T_p = 15$ s (Figure 8) show quite a good agreement with the measured time series, albeit with the same issues for the roll component, as explained above.

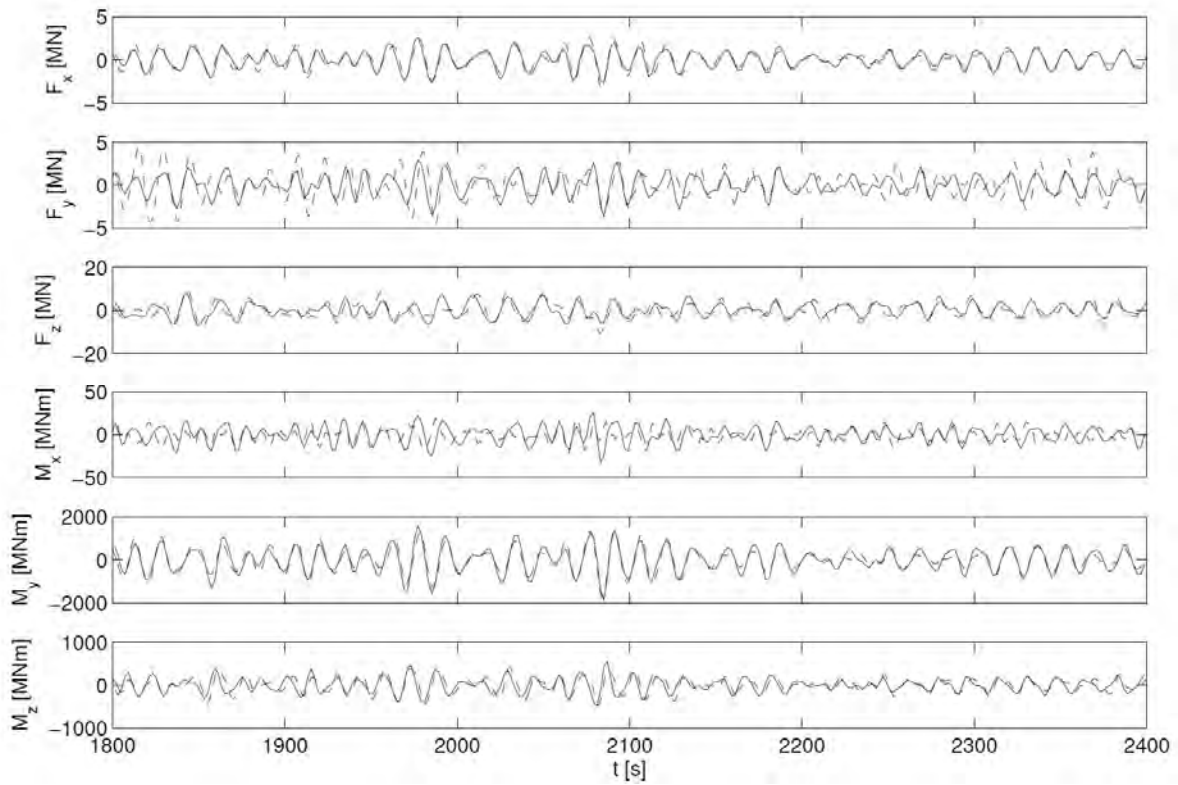


Figure 8: comparison of wave forces in open water; $H_s = 1.5$ m, $T_p = 15$ s, 210° relative to ship; -- measurements, — strip theory (from Van der Molen, 2006).

More recently, Dobrochinski (2014) used the numerical model SWASH to reproduce a selection of the measurements included in Database 1. SWASH (an acronym of Simulating WAVes till SHore) is a non-hydrostatic wave-flow model that is used in multiple vertical layers (Zijlema *et al.*, 2011). For computing forces and moments on the captive vessel the SWASH wave model was coupled by Dobrochinski to a boundary-integral diffraction model, originally developed and applied by Van der Molen (2006). Dobrochinski (2014) analysed primary waves (sea and swell) and infragravity waves from the SWASH model using two or three vertical computational layers. After calibration of the numerical wave model, the spectral results for a selection of tests in open water (not reproduced here) showed that the numerical wave model was capable of simulating the correct spectral shape of the primary waves at the considered measurement locations. Also the measured and computed spectra of forces and moments on the ship in open water showed a rather good agreement.

Condition C3 from Dobrochinski (2014), i.e. $H_s = 6$ m, $T_p = 15$ s, \cos^4 directional spreading, main direction 30° and including the schematic port basin, is used here to illustrate the main findings from that work. Figure 9, from Dobrochinski (2014), depicts the computed results for this condition. The dashed line in the right panel of Figure 9 indicates the extent of a damping slope that was placed in the scale model alongside the outer wall of the schematic port basin to reduce wave reflections of this part of the port layout directly facing the wave maker (see also Figure 2).

Dobrochinski (2014) describes comparisons of measured and computed total wave heights and low-frequency wave heights ($T > 33$ s). The average difference found is around 6% for the total significant wave height and around 12% for the low-frequency wave heights, with only a few marked outliers at specific locations. The wave spectra for this condition (Figure 10) show quite a good agreement between the computation and the measurements, including the peaks measured in the low-frequency spectrum. These results indicate that the numerical model is capable of capturing (parts of) the complex processes governing high-frequency and low-frequency wave generation and propagation. A

fair agreement was also found by Dobrochinski for the resulting computed forces and moments acting on the vessel moored inside the schematic port basin (not reproduced here).

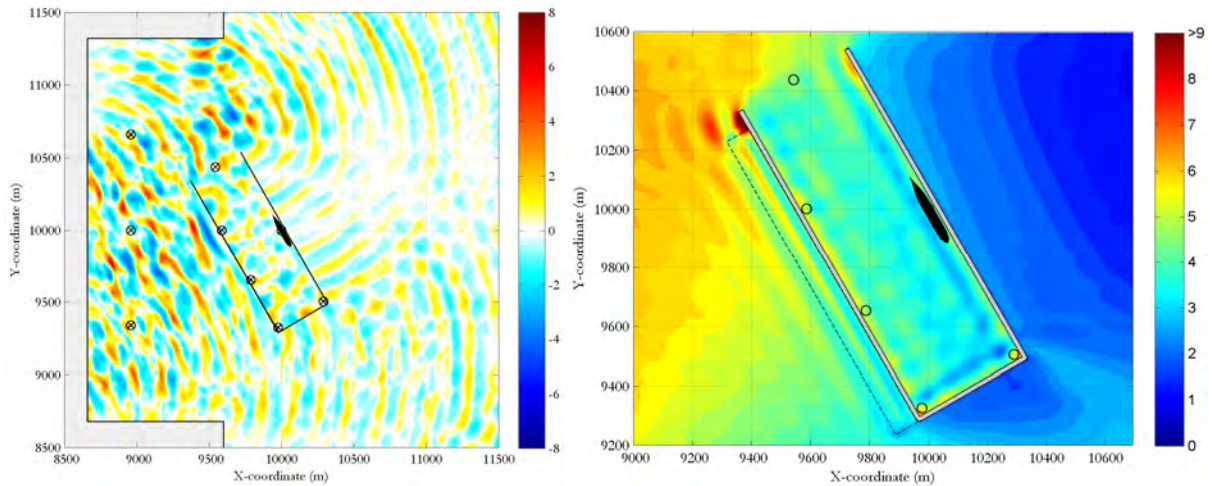


Figure 9: left panel: snap shot of the computed surface elevation inside the scale model basin; right panel: significant wave height inside and around the schematic harbour basin. $H_s = 6$ m, $T_p = 15$ s, \cos^4 directional spreading, main direction 30° (from Dobrochinski, 2014).

Dobrochinski (2014) finds that quite a high bottom friction had to be applied in the SWASH model for the situations including the schematic port basin (the ‘C’ series in his report, including cases with $H_s = 3$ m and $H_s = 6$ m) to match the primary and low-frequency wave heights. He ascribes this to scale effects in the laboratory measurements. This is striking, since other studies using the same data or datasets from the same or a similar basin at the same model scale (some examples are discussed further below) did not report this effect at all. Therefore, bottom friction may not be the ultimate explanation of the discrepancies found. Other possible causes for the apparent overestimation of the wave heights in the (uncalibrated) numerical model could be specific choices in numerical model settings and schematisations.

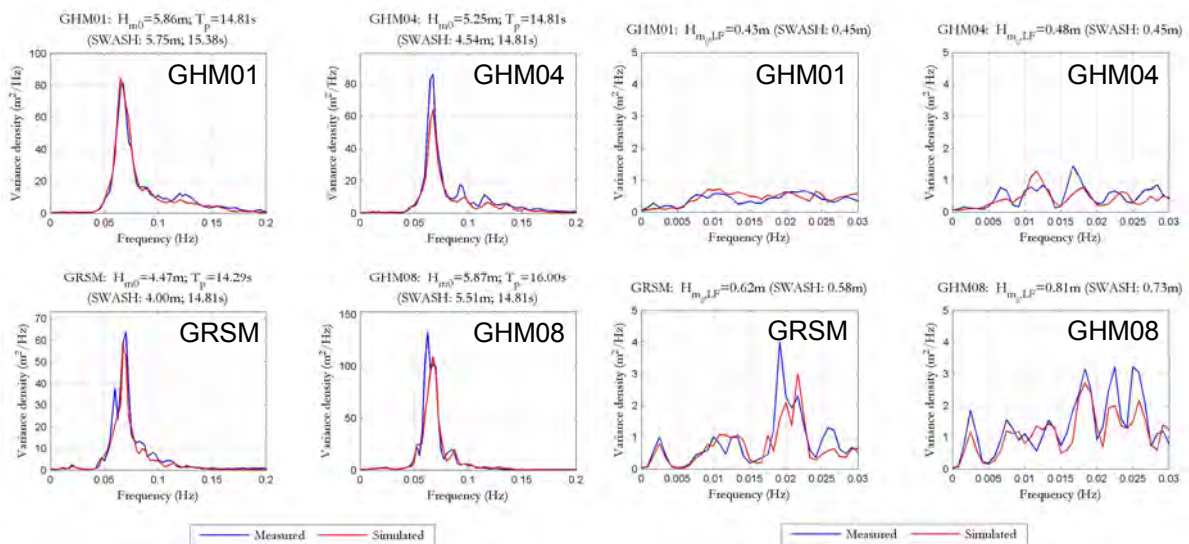


Figure 10: wave spectra of measured and computed wave conditions for Case C3. Left set of four panels: total frequency range; right set of four panels: low-frequency range (from Dobrochinski, 2014). See Figure 1 for the numbered locations.

Also Rijnsdorp (2016)⁵ considered a selection of conditions from Database 1 in the model SWASH, including situations with and without the schematic port basin (up to and including $H_s = 3$ m). He applied the default (low) bottom friction value and does not report a systematic overestimation of wave heights in the SWASH computations compared to the measured conditions. We hypothesise that a possible explanation for this may be the use of a different computational scheme in the numerical model than was used by Dobrochinski (2014). Regardless, even though Rijnsdorp only considered the schematic port basin layout for the lower of the wave heights considered by Dobrochinski (i.e. a smaller importance of non-linear influences), this could very well indicate that scale effects related to bottom friction were not the main reason for the wave height discrepancies found in Dobrochinski (2014). As discussed above, the detailed causes of those discrepancies still need to be identified.

Before describing his validation results, Rijnsdorp (2016) first states that relatively large measurement errors are to be expected with the approach taken in tests of Dataset 1 for measuring wave-induced forces on the captive vessel, particularly in the measured moments. Building on that premise, he then ascribes the discrepancies between measured values and results from his computations, both for open water situations and with the schematic port basin, mostly to those hypothesised inaccuracies in the scale model measurements. Figure 11 shows an example of his results for the situation with the schematic port basin, $H_s = 3$ m, $T_p = 10$ s, \cos^2 directional spreading.

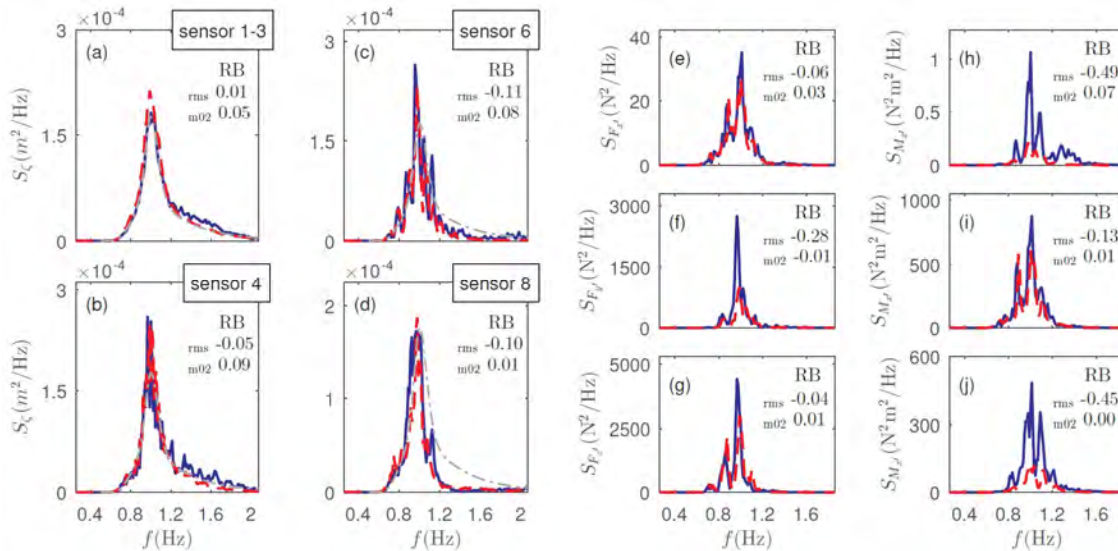


Figure 11: Predicted (red line) and observed (blue line) spectra of the surface elevation S_z (a), and the forces S_F (b-d) and moments S_M acting on the ship (e-g) for a condition with the schematic port basin (from Rijnsdorp, 2016). See Figure 1 for the location numbers.

This general expectation of a limited accuracy of the force probe measurements is contradicted by the findings from both De Jong *et al.* (2005) and from Van der Molen (2006), described above, which showed quite a good agreement between computed and measured times series of the three forces and of the pitch and yaw moments (Figure 7 and Figure 8). The good agreement reported in those studies, based on two different computational methods, indicates that fundamentally the measurements of those degrees of freedom – i.e. aside from the known issues for the roll measurement – did not particularly suffer from low accuracy as a result of the scale model setup. This means that the cause of the discrepancies identified in Rijnsdorp (2016) for degrees of freedom other than roll should be sought in other (numerical) modelling aspects, either in the description of the wave conditions in SWASH, in the approach used for representing the vessel inside the computational domain or in his method for deriving the resulting wave forces and moments acting on the vessel. Those alternate possible causes are only briefly considered in Rijnsdorp (2016), mentioning the possible influence of leaving out the bulbous bow in the representation of the vessel in the numerical wave model and the coarse vertical resolution applied in the SWASH schematisation.

⁵ We cite here the PhD Thesis of Rijnsdorp. These same results have also been published as part of: Rijnsdorp, D.P. and M. Zijlema (2016): Simulating waves and their interactions with a restrained ship using a non-hydrostatic wave-flow model, *Coastal Engineering*, 114, 119–136.

4. COMPARISON OF VALIDATION STUDIES USING DATASET 2

Three studies have so far considered (parts of) Dataset 2. Here we use one specific wave condition and layout to illustrate typical results, which has been considered in all three studies. It involves Layout Hm1 (top right panel in Figure 5), which resembles the present situation, aside from the lacking extension of the main breakwater. The selected wave condition has an incident wave direction of 80°N and is represented with a JONSWAP spectrum with a peak period of $T_p = 7$ s, a peak enhancement factor of $\gamma = 3.3$, a significant wave height of $H_s = 2.5$ m and a directional spreading of $\sigma = 31.5^\circ$.

Reijmerink (2012) modelled the port layout in the numerical wave models SWAN (Booij *et al.*, 1999) and PHAROS (Berkhoff, 1972, 1976, De Jong and Borsboom, 2012a,b). In absence of full modelling of diffraction, SWAN is generally known to have limited applicability inside small and confined port layouts, even more so in case of longer incident wave periods. Nevertheless, the spectral wave model SWAN was considered by Reijmerink (2012) as a reference and to assess up to which point (possibly conservative) SWAN results (not reproduced here) may still be acceptable in practice. The mild-slope model PHAROS of Deltares includes full modelling of diffraction and therefore was expected to provide more accurate descriptions of wave penetration. The mild-slope formulation results in a practical and computationally efficient numerical wave model, which in essence is a linear modelling approach but PHAROS includes parameterised descriptions representing the effects of wave breaking and of bed friction that can optionally be activated. Wave conditions relevant for wave penetration computations, often focussed on operational wave conditions, will typically correspond to quite low resulting wave heights inside port basins, supporting the use of a linear wave model. Directional spreading and frequency spreading can be represented efficiently in this model by a weighted sum of separately computed wave components that together make up the full wave spectrum.

The reflection values in the model schematisation applied in Reijmerink (2012) were taken from earlier references cited in his report, without further optimisations or calibrations. Incoming wave boundary conditions were prescribed as-is, i.e. without any tuning, calibration or amplifications.

Figure 12 depicts the results from PHAROS for the selected wave condition. The coloured circles in the panels of this figure indicate the measured values at each probe location using the same colour scale as applied for plotting the numerical results in that panel. A matching colour inside and around each circle therefore indicates a good match between measured and calculated results.

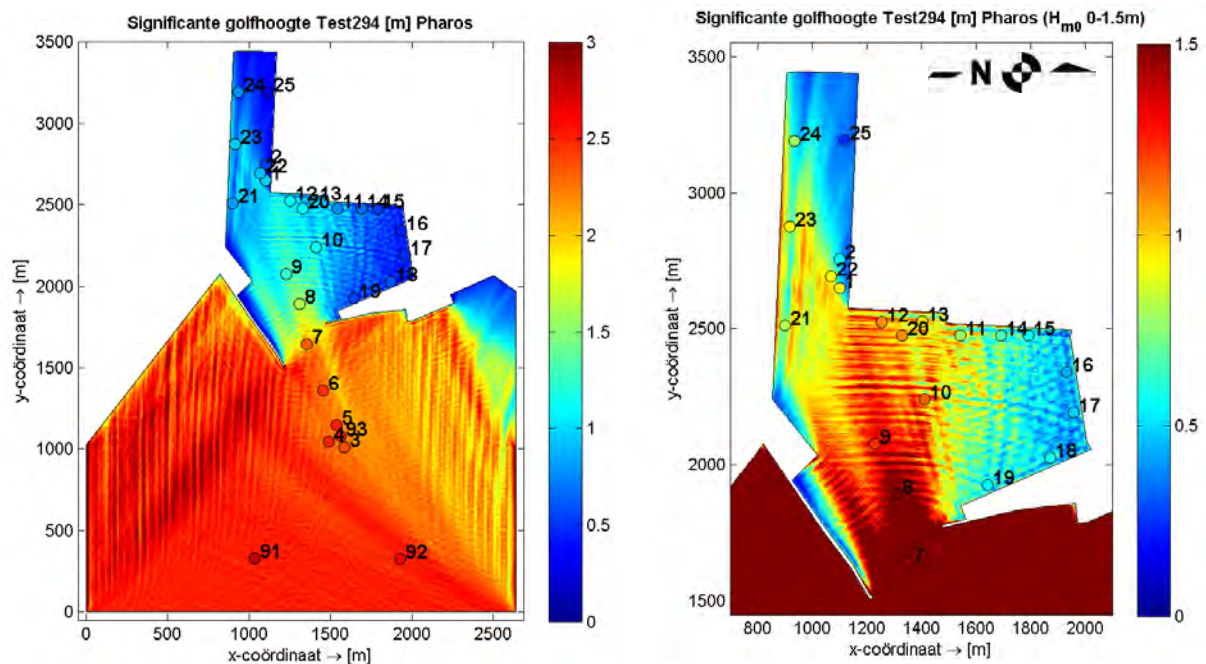


Figure 12: results from the PHAROS model for Limassol (from Reijmerink, 2012). Left panel: overview of the computational area; right panel: same results, now for a zoom of the port area. Note the difference in colour scale between both panels.

The figure shows that the agreement between measured and computed values is rather good. Detailed analyses of the computed results described in Reijmerink (2012) indicate that at most locations the calculated wave heights for this condition (averaged within a circle with a diameter of the wave length around the main location to account for the rather outspoken standing wave height pattern in the numerical wave model⁶) are typically accurate within about 5-10%, although a few specific locations showed higher relative deviations. Larger relative deviations were found typically for locations furthest into the port layout, i.e. in case of low absolute wave heights.

Van Vledder and Zijlema (2014) considered the same wave condition and layout in the numerical wave model SWASH. Contrary to other studies using this test case (Reijmerink, 2012 and Adytia, 2014, considered below), they specified only one reflection characteristic along the breakwater and quay walls in the harbour. However, apparently this has not decisively influenced the computational results. This is striking, since wave heights inside port basins often depend strongly on such reflection values. Why it does not prove critical in their computations is not discussed by Van Vledder and Zijlema. We hypothesise that it may be related to the specific shape of the port and that the uniform settings at least describe with sufficient accuracy the quay sections within the port that dominate local reflection.

The computations in SWASH by Van Vledder and Zijlema (2014) included the default value for bottom friction. They report that the incoming boundary conditions in the SWASH model had to be tuned using the output locations closest to the wave maker to obtain suitable results inside the computational domain. From this calibration it followed that the SWASH model *underestimated* the incoming wave conditions at the model boundary and the model had to be forced with a wave height of around 2.9 m, i.e. about 15% enhancement of the actual value (Figure 13), to achieve comparable wave heights at the observation locations within the computational domain. This observed model characteristic is striking, since the computations in SWASH by Dobrochinski (2014), using Dataset 1, indicated that SWASH apparently *overestimated* the measured wave heights for those conditions, which was (likely unfoundedly) compensated in the computations by Dobrochinski (2014) by using an amplified bottom friction in the SWASH model.

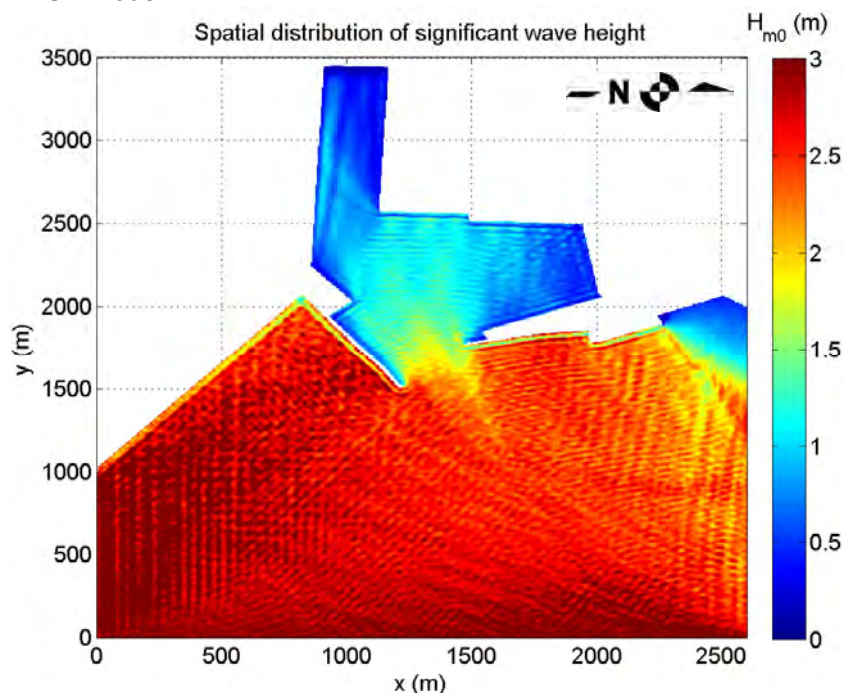


Figure 13: results from the SWASH model for the considered wave condition at the Port of Limassol (from Van Vledder and Zijlema, 2014). Note the unequal scales of the axes, resulting in a horizontally stretched plot of the layout.

⁶ Since the work by Reijmerink (2012), Deltares has developed an efficient and accurate wave splitting method specifically aimed at analysing output of phase resolving wave models such as mild-slope models, see De Jong and Borsboom (2012a,b). This tool is presently part of the PHAROS software package. Applying this post-processing tool removes the requirement of spatially averaging computed wave heights.

Adytia (2014) modelled the same layout and wave condition in an Optimised Variational Boussinesq-type wave Model (OVBM). In that paper he states that this numerical model is a relatively efficient version of a Boussinesq-type model that includes less complex derivative terms than many other Boussinesq-type wave models. The output of the non-linear OVBM is expressed in Adytia (2014) as the linear fraction (percentage) of the incoming wave height. Figure 14 shows the results for the main wave condition considered from Dataset 2. Adytia (2014) reports that typical deviations between computed and measured values at the observation locations are within 5-10%. This would certainly be within a practically suitable accuracy.

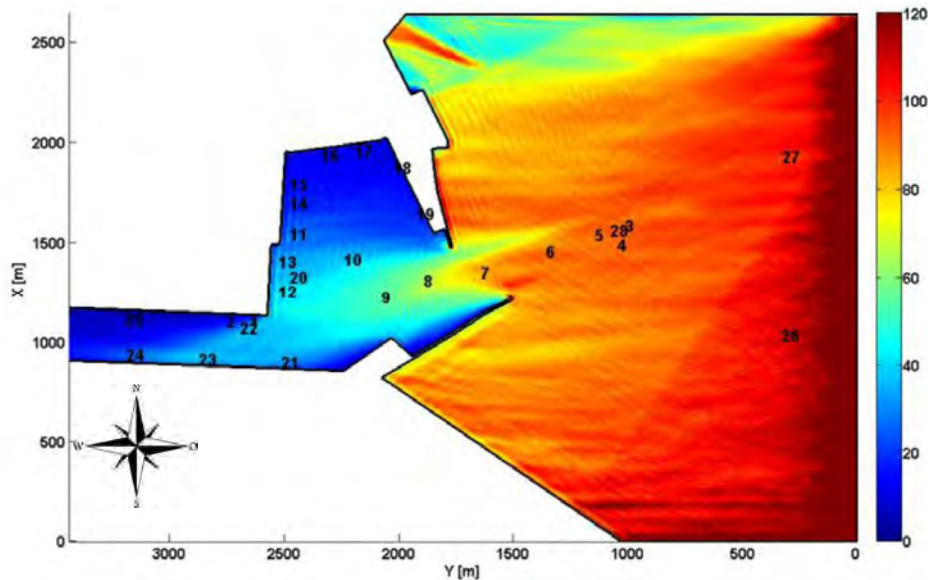


Figure 14: results from the OVBM wave model for Limassol (from Adytia, 2014). Wave heights are expressed as percentage of the incoming wave height.

Adytia describes how the dispersive properties of the Boussinesq-type model (i.e. the description of the phase speeds of waves of different period) were optimised for this particular targeted wave condition prior to making the calculation. A wave generation region of 4 wave lengths (increasing in strength from the boundary inward from 0 to 1, i.e. up the full incoming wave height) was included in the modelled domain of the considered case. How generic these settings and modelling choices will be is not reported in Adytia (2014).

Furthermore, as is also briefly noted by Vledder and Zijlema (2014), the wave height at the incoming boundary of the modelled domain in the OVBM appears to include a similar enhancement (of over 20%, Figure 14) as Vledder and Zijlema (2014) reported to be required for the SWASH model (15%). Such an enhancement was apparently required to achieve the reported computed values at the measurement locations inside the computational domain. The detailed causes of this numerical model behaviour are not analysed in the cited papers. We hypothesise that it may be related to model formulation-specific aspects such as numerical damping caused by the applied calculation schemes, but this remains to be verified.

Both Vledder and Zijlema (2014) and Adytia (2014) do not consider how the observed characteristics of their numerical wave models will influence the practical use of those models, including cases where no measurements will be available for detailed model optimisation and boundary condition calibrations, and when results are typically required to be provided quickly and indisputably (e.g. for consultancy).

5. COMPARISON OF VALIDATION STUDIES USING DATASET 3

The application of Dataset 3 is only briefly considered here, since only a very limited part of this dataset has been considered so far and because a separate publication is foreseen on this test series.

So far this dataset has been considered in a number of master studies at Delft University of Technology (Van Mierlo 2014, Monteban, 2016 and Wong, 2016). They all used the same selection of wave conditions from Dataset 3 to validate and compare different numerical wave models (PHAROS, TRITON, SWASH and Mike21 BW). Overall, their findings seem to confirm general conclusions from earlier studies cited above: wave penetration can typically be modelled with a practical accuracy, whereas long waves and resonant modes are generally computed with less accuracy. Remaining attention points mentioned in these MSc reports include: requirements for data analysis methods (e.g. spectral resolutions), reflection settings in the numerical models, stability of the numerical models (most notably related to the use of SWASH and Mike21 BW) and practical aspects related to performing physical scale model tests. This shows that there is still ample work to be done on validating and improving numerical wave penetration models to enable application of such models in daily practice.

6. CONCLUSIONS

This paper introduces a collection of benchmark datasets by Deltares that is made available for validation of numerical wave penetration models and related tools such as methods for calculating wave-induced forces on moored vessels. Since datasets for validation of such numerical methods are quite scarce we have already received and honoured several requests for use of these datasets. This paper gives a summary of the typical findings from a selection of those studies and for the first time provides an inter-comparison and an overarching analysis of those different results.

Even though already several studies have used the presented datasets, these data still form a valuable collection for future work. This is because several parts of the available datasets have not yet been exploited in model validation studies, and because so far only a few specific models (model types) have been considered. Furthermore, parts of the validation outcomes obtained so far have been inconclusive and still require further analyses for reaching complete and definitive conclusions. In addition, in the future we expect to expand the open data collection by adding other physical scale model projects by Deltares.

Overseeing the discussed selection of publications that used the open datasets by Deltares to this date, we conclude that identifying the causes of differences between computed and measured values is often not straightforward. Hypothesised causes in one study may be refuted (implicitly) in others. This shows that there is still quite some work to be done in this field and that cooperation between different organisations will remain essential to reach proper conclusions. Therefore, researchers and advisors working on related topics are encouraged to contact Deltares to explore cooperation possibilities. Together we will continue to show the large added value that physical scale model tests provide in engineering, consultancy and research, including calibration and validation of numerical methods.

ACKNOWLEDGEMENTS

The authors acknowledge O.M. Weiler as developer/originator and project manager of the physical scale model tests performed in 2003 (Dataset 1). His foresight on preparing and generating that large and still very relevant dataset has proven invaluable. We thank the authors that have used the described datasets to this date for their interest in these data and their willingness to confront their numerical model results with these measurements. M.J.A. Borsboom is acknowledged for commenting on an earlier draft of this paper. His suggestions on document structure that were processed for this final paper version are much appreciated.

REFERENCES

- Adytia, D. (2014), Simulations of Short-crested Harbor Waves with Variational Boussinesq Modelling. Proc. 24th Int. Ocean and Polar Engineering Conference. ISOPE-I-14-451.
- Berkhoff, J.C.W. (1972), Computation of combined refraction-diffraction, *13th Int. Conf. Coastal Eng.*, pp. 471-490.
- Berkhoff, J.C.W. (1976), Mathematical models for simple harmonic linear water waves, wave diffraction and refraction, Delft Hydraulics Publication No. 163.

- Booij, N., R.C. Ris, and L.H. Holthuijsen (1999), A third-generation wave model for coastal regions, Part I, Model description and validation, *J. Geoph. Res.*, 104(C4), 7649-7666.
- De Jong, M.P.C., O.M. Weiler, M.J.A. Borsboom and A.R. van Dongeren (2005), A phase-resolving analysis technique for short-crested wave fields, Paper presented at the 5th International Symposium on Ocean Wave Measurement and Analysis, WAVES 2005, held in Madrid, Spain, 3-7 July 2005. - Paper number: 026.
- De Jong, M.P.C. and M.J.A. Borsboom (2012a), A practical post-processing method to derive design wave parameters from wave model results, *PIANC-COPEDEC VIII*, February 2012, Chennai, India, pp. 345-356 (ISBN : 978-93-80689-06-7).
- De Jong, M.P.C. and M.J.A. Borsboom (2012b), A practical post-processing method to obtain wave parameters from phase-resolving wave model results, *International Journal of Ocean and Climate Systems*, **Vol.3**, Number 4, December 2012, pp. 203-216, ISSN 1759-3131
- De Jong, M.P.C., S.P. Reijmerink, A. Capel and A.J. van der Hout (2016), Combining numerical wave models for efficient design of port layouts and entrance channels, *PIANC-COPEDEC IX*, Rio de Janeiro, Brazil.
- Dobrochinski, J.P.H. (2014), A combination of SWASH and Harberth to compute wave forces on moored ships, MSc Thesis, Delft University of Technology (repository.tudelft.nl).
- Janssen, T.T., A.R. Van Dongeren and C. Kuijper (2001), Phase Resolving Analysis of Multidirectional Wave Measurements. *Proc. Waves 2001*, San Francisco, CA, U.S.A., 377-386.
- Monteban, D. (2016), Numerical modelling of wave agitation in ports and access channels - A comparison study between SWASH and MIKE 21bw, MSc Thesis, Delft University of Technology (repository.tudelft.nl).
- Reijmerink, S.P. (2012), Wave boundary conditions inside ports – application limits of numerical models (in Dutch), MSc Thesis, Delft University of Technology (repository.tudelft.nl).
- Rijnsdorp, D.P. (2016), Modelling waves and their impact on moored ships, PhD Thesis, Delft University of Technology (repository.tudelft.nl).
- Van der Molen, W. (2006), Behaviour of Moored Ships in Harbours, PhD Thesis, Delft University of Technology, ISBN-10: 90-9021264-7, ISBN-13: 978-90-9021264-7 (repository.tudelft.nl).
- Van der Ven, P.P.D. (2016), Benchmark tests of wave penetration in harbours - Measurement report, Deltares Technical Report, reference 1209490-000-HYE-0001.
- Van Mierlo, F.A.J.M. (2014), Numerical modelling of wave penetration in ports, MSc Thesis, Delft University of Technology (repository.tudelft.nl).
- Van Vledder, G.Ph. and M. Zijlema (2014), Non-hydrostatic wave modelling in partly sheltered areas, *Proceedings of 34th Conference on Coastal Engineering*, Seoul, Korea, 2014, Editor: Patrick Lynett, ISBN: 978-0-9896611-2-6.
- Wong (2016), Wave hydrodynamics in ports - Numerical model assessment of XBeach, MSc Thesis, Delft University of Technology (repository.tudelft.nl).
- Zijlema, M.; Stelling, G.; Smit, P., (2011). SWASH: An operational public domain code for simulating wave fields and rapidly varied flows in coastal waters. *Coastal Eng.* 58, 992-1012, doi:10.1016/j.coastaleng.2011.05.015.

SHUNT-E
Autonomous zero emission shunting processes in port and hinterland railway operations
by

Dr. Iven Krämer¹

ABSTRACT

Hinterland connectivity is one of the most competitive distinguishing factors for today's sea- and dry ports. Therefore innovations with a clear focus on autonomous and emission free port operations are crucial to safeguard a prosperous future of global ports. Significant steps for this are the optimization and gradually atomization of rail operational processes on the last mile including necessary modern and transparent IT systems and to design autonomous shunting processes. Together with partners ISL (Institute of Shipping Economics and Logistics Bremen), BIBA (Bremen Institute for Production and Logistics) and IVE (Institute for Transport, Railway Construction and Operation in Brunswick) in connection with associated business partners the project "*Shunt-E 4.0 - Autonomous zero emission shunting processes in port and hinterland railway operations.*" has been applied for at the German Federal Ministry of Transportation in the funding initiative IHATEC (Innovated Harbour Technologies) – and had won a grant to perform the proposed work. The practical research program is conducted together with Bremen's port railway which is regarding to the modal share of rail hinterland transport the leading European port railway system. This article highlights the overall objectives ambitions and expected outcomes of this project.

1. TODAY'S PORT RAILWAY PROCESSES

The railway operation in port areas in Europe is characterized by split-up responsibilities, a high number of players and a lack of comprehensive planning and optimization of all relevant processes. Still innovative technologies and business processes are useful to achieve key steps on the way to overall optimization. A substantial part of the European rail freight transport has its origin or its destination in an inland or sea port. Considering the railway system, ports play a more important role for urgently needed innovations than the pure interfaces between sea and land transport. Especially ports with their own railway system have a greater responsibility in this matter.



Shunting Locomotives within the Port of Bremerhaven

¹ Free Hanseatic City and Ports of Bremen (Germany), Head of Port Economy and Shipping,
iven.kraemer@wah.bremen.de

Port railway operations today are comparably complex processes. The general container train process which involves different partners like railway undertakings, shunting operators, infrastructure providers, energy providers, terminals operators, port management organizations etc. is on the example of a typical European railway system (Bremen's port railway) divided in various steps as follows:

- Train arrival with separation of the electrical main-line locomotive in the port area
- Transport of train section or wagons with shunting locomotives (diesel) towards forwarding groups and later on to the terminals
- control and supervision works by terminal operators on the train and on the cargo (i.e. seal-check), unlocking of containers
- Unloading and loading processes by terminal operators
- Transport of train section or wagons with shunting locomotives towards forwarding groups
- Brake tests, checking procedures by railway operators
- Train departure

As a consequence of these steps the first cargo movements can and do only start hours after train arrival in the port area. A comparable long procedure is (still) needed after completion of train loading process. Trains with import goods need to have specific brake tests and load control works with following shunting processes. Just by these rules they remain in the port area for an average of two hours before they can start towards the national and European hinterland destinations. As a result port railway operation today is much more complex and thus disadvantaged compared to truck and barge processes. The reasons are mainly self-made rules and regulations by the industry sector. In intermodal transport on European level it would be possible to improve productivity by at least 20 percent alone by optimizing the railway operation on the last mile.

2. **EXAMPLE: PORT RAILWAY OPERATION IN BREMERHAVEN**

The port railway network in Bremerhaven (Figure 1) is non-discriminatory accessible and part of the public infrastructure company "*Bremische Hafeneisenbahn*" who belongs to the Free Hanseatic City of Bremen which takes care of its infrastructure with related operational and technical service providers. Currently the tracks are regularly used by more than 30 European railway companies with 60 more having license agreements. These companies connect the ports of Bremen with national and international hinterland traffic.

Several competing shunting companies take the task of transporting the trains and wagons within the harbour area – which are usually loaded with vehicles or containers in Bremerhaven – from the starting rails to the receiving terminals and vice versa. They carry out the tasks on behalf of the corresponding railway company which in return make sure to provide the electrical operated mainline locomotives including their destined train drivers for entering and leaving the port area right on time.

Currently there are 13 shunting locomotives of different type and age – all Diesel operated- being active 360 days a year in a 24/7 system. To operate a shunting locomotive a train driver and a shunting worker is needed. Shift planning for them is done by the on-site managing clerk of the respective railway company. The actual driving and shunting operation is based on the regulations of Bremen Port Railway. Their managing staff organizes the track use and their dispatcher at the signal box sets and authorizes the driving route. The handling companies set with their loading and unloading processes the pulse for the train movements. In Bremerhaven, loading and unloading containers as well as automobiles follow slot times specified beforehand. The processes also take into account the load levels of the specific wagons to avoid idle and waiting times.

There is no direct contractual relationship between the terminals, the port train operator and the shunting companies so that communication and coordination between the involved parties is of major importance.

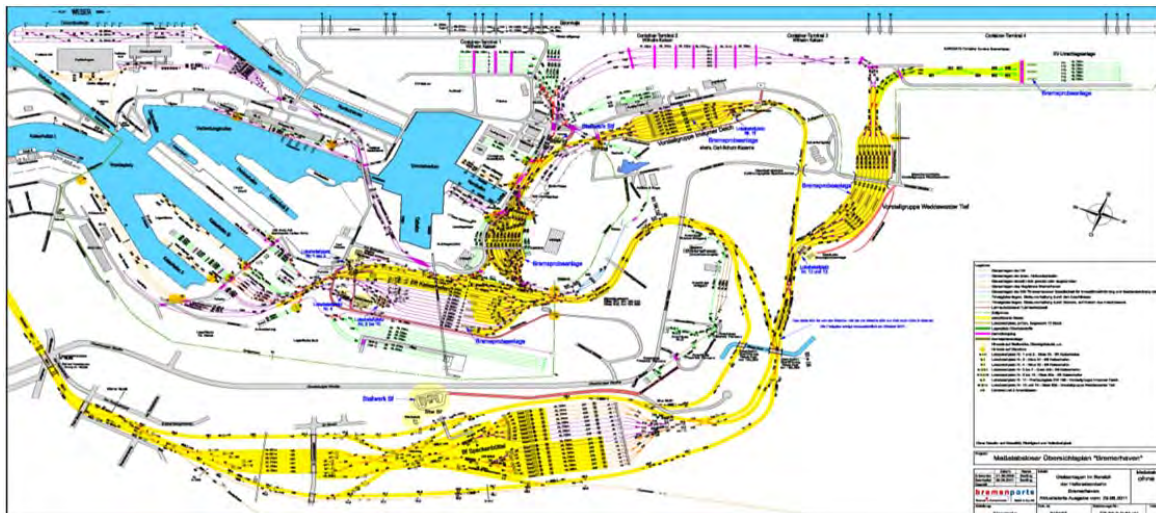


Figure 1: Port Railway Network within the Port of Bremerhaven (electrified tracks are marked in yellow)

All together Bremen's Port Railway system has been developed over more than 150 years always being an integral part of the overall port system and development strategy. As a result the port of Bremerhaven today has a leading railway modal share in container hinterland transportation of about 50 percent (Figure 2)

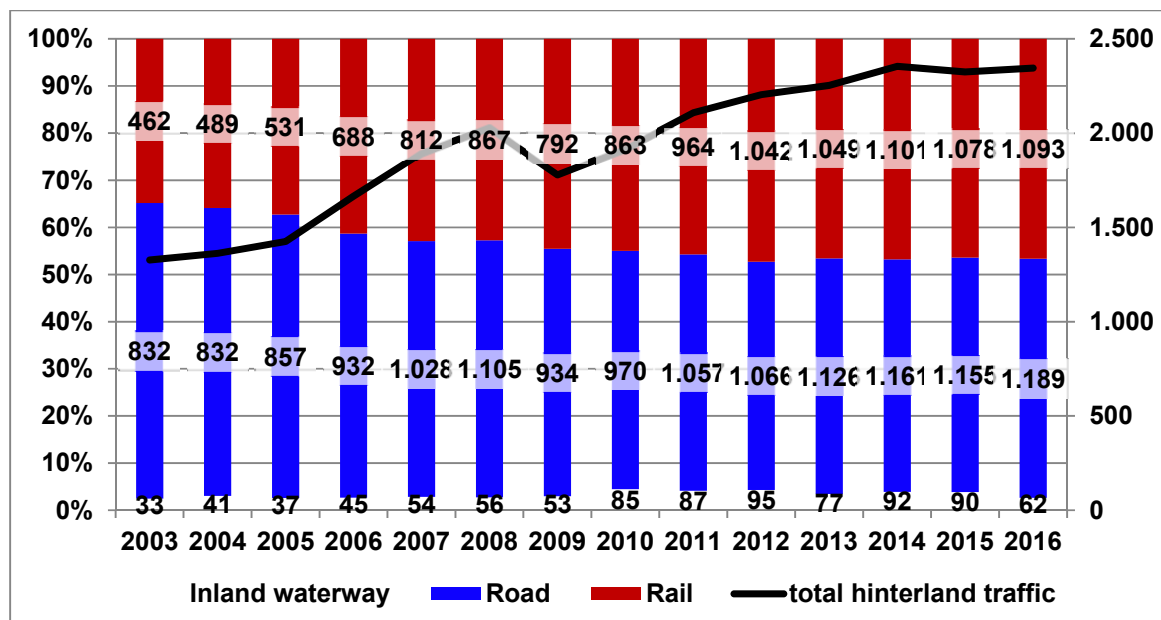


Figure 2: Modal split development in Container Hinterland Transport in Bremerhaven in TEU

In terms of the automobiles transported from the German and European factories to the port the rail share is even higher with almost 90 percent.

3. NEED FOR ACTION MORE THAN OBVIOUS

Innovations in cargo rail sector are rare, even if good ideas do exist. Many previous projects on automatization and process optimization failed or were stopped by various reasons. In fact technical solutions like automatic clutches, automatic brake tests, remote train control systems, automatic load controls, obstacle detection and many more rail related optimization measures are technically feasible and were successfully tested in the past. But, they didn't make it to the broader market.

As a consequence rail transport of goods until today is in most regions of the world very traditional and old-fashioned. Especially in comparison to truck transport the rail sector is falling back. Ongoing innovative projects like truck-Platooning or autonomous trucks endanger the system advantage of rail and thus the transport-political perspective of rail transport. If global ports want to improve railway transport they strongly need innovative port railway systems and processes.

4. PROJECT SETUP

On Bremen's port railway today various competing companies offer shunting services to the railway operators within Bremerhaven port area. It's their task to move the train sections and wagons between the forwarding groups and the terminals. The main-line transport to and from the national and European hinterland is conducted by currently about 80 different companies (Railway undertakings). These companies also take care that enough train drivers are in place at the time when they are needed for the port leave. The railway undertakings are the purchasers of shunting services.

With the support of Germany's Ministry of Transportation Bremen's port railway has been selected as a test bed for autonomous emission free shunting processes as an example for general port railway systems. Scientific partners in the project "*Shunt-E 4.0 - Autonomous zero emission shunting processes in port and hinterland railway operations*" are:

- ISL (Institute of Shipping Economics and Logistics), Bremen,
- BIBA (Bremen Institute for Production and Logistics) and
- IVE (Institute for Transport, Railway Construction and Operation) in Brunswick.

Besides these scientists there are several supporters and partners from the ports and logistics sector directly involved in the project. These are:

- Eurogate (Container terminal operator),
- BLG Logistics Group (Automobile terminal operator as well as railway undertaking)
- DB Cargo (railway undertaking as well as port shunting operator)
- Elbe Weser Verkehrsbetriebe - evb (railway undertaking as well as port shunting operator)
- Verband deutscher Verkehrsunternehmen VDV (Association of German Transport Companies).

5. PROJECT OBJECTIVES

The aim of a totally autonomous shunting operation can and will be reached only with intermediate process automatization steps. The expected effects of autonomous emission free shunting operations to date are the following:

- Simplification of operational rail processes
- Avoidance of empty-locomotive-drives
- Reduction of the overall shunting stock (Savings of about 30 percent are expected)
- Avoidance of communication-interfaces
- Optimization of infrastructure use with savings on future investments
- Reduction of operational efforts and costs (on the locomotive and in the offices) through reduction of personnel
- Safety-Improvements
- Disruptions reduction in port railway operations

Compared to the actual system with manned shunting locomotives (most of them many decades old and running on diesel) and dispatchers within the train control centres *Shunt-E* will be able to operate on her own. To do so *Shunt-E* will continuously check and monitor its current position and status, she will know about and plan all upcoming transfer orders and she will via IT interfaces have access to all necessary information from terminal operators (time slots, loading and unloading status, customs declaration, dangerous cargo...) port officials and railway undertakings (planned as well as real arrival and departure times, train and cargo status, availability of train drivers...). Building on these information *Shunt-E* will be able to plan and conduct optimal transfer procedures which leads to an optimised infrastructure utilisation. *Shunt-E* will be able to operate 24/7 with no delays due to shift changes, staff meetings etc. And finally *Shunt-E* will be operated either electrically or on fuel cells which makes the whole shunting process or the last mile in intermodal transport emission free.

The research work done with this project will identify the necessary technical, organisational as well as legal measures to improve the overall performance of rail transport in port hinterland transport. It is expected that a minimum of two hours can be saved for every single train in long-haul port services. Furthermore the costs for operational personnel on board of the shunting locomotives as well as in related offices can be drastically reduced, so that autonomous shunting locomotives will be in service in various ports of the world at least from 2030 onwards. It is not yet clear if Bremerhaven with its traditionally grown port infrastructure will be the right place for a *Shunt-E* implementation or if instead an "easier" port system like green field projects might be better testbeds.

6. RELEVANCE FOR THE GLOBAL PORT COMMUNITY

Shunt-E 4.0 - Autonomous zero emission shunting processes in port and hinterland railway operations is of high relevance to the global port community as it combines the necessary innovation approach for future port development with a sustainable greenports strategy.

ACKNOWLEDGEMENTS

On behalf of the Ports of Bremen the author would like to thank all companies and institutions involved for their support, funding and hospitality. Special thanks to the German Federal Ministry of Transportation that set up a supporting programme for innovation in Port Technology (IHATEC) and thus made the whole idea going forward. Further thanks go to the scientific partners ISL (Institute of Shipping Economics and Logistics Bremen), BIBA (Bremen Institute for Production and Logistics) and IVE (Institute for Transport, Railway Construction and Operation in Brunswick). And finally many thanks to the associated business partners Eurogate, BLG Logistics, DB Cargo, evb and VDV. The port administration of Bremen expresses their appreciation of the partnership with all the companies and institutions involved.

CONSTRUCTION AND OPERATION OF A WORK VESSEL LOCATION AND NAVIGATION INFORMATION SYSTEM FOR FISHING PORT CONSTRUCTION

by

Shimpei Nagano¹, Masaaki Wada²(Ph.D.), Shuichi Tanaka³, Masayuki Fudo⁴ and Akira Nagano⁵(Ph.D.)

ABSTRACT

When Tsunami and typhoon attack ports, a large amount of drifts materials and debris appears and fills in basin of port and waterway. The first work to do is open the waterway buried with debris and drifts by work vessels. Work vessels are dredger and crane vessels. After then, cargo ships carry relief goods to the port. The work vessels carry out recovery work for the destroyed port facilities. In large-scale disaster ex. East Japan great earthquake disaster, the work vessels at the disaster area are destroyed, therefore work vessels must be dispatched from the other areas.

In order to promptly dispatch work vessels, the following three conditions are necessary. (1) to catch the location of work vessels, (2) to determine the necessary work vessels and (3) to rapid navigation to the damaged ports under the weather conditions. We construct a system that accumulates the location information sequentially and displays the current locations and navigation history information of each work vessels. In addition, the work vessels location and navigation information are accompanied with the weather condition information at the current location and the destination. In order to verify the effectiveness of this system with weather condition information, we installed GPS and transmitters in 35 work vessels in the Nagasaki prefecture waters area.

1. INTRODUCTION

In East Japan great earthquake disaster 3.11st.2011, the work vessels at the disaster area are destroyed, therefore work vessels must be dispatched from the other areas to open waterways of many destroyed ports. At first, it is necessary to get information what kind of work vessels are where. After deciding which vessels to send to which ports, It took nine days to dispatch work vessels to destroyed ports from another area. Even at fishing ports, It took 41 days to dispatch work vessels.

We should have dispatched these work vessels more quickly. Therefore, the location information of work vessels are acquired by GPS(Global Positioning System) and the location information are transmitted in real time via the Internet. We construct a system that accumulates the location information sequentially and displays the current locations and navigation history information of each work vessels. In addition, the work vessels location and navigation information are accompanied with the weather condition information on the wind direction, wind speed, wave height and wave direction at the current location and the destination. Therefore, it is a system that can ensure the safety of the action of the work vessels at the time of a disaster.

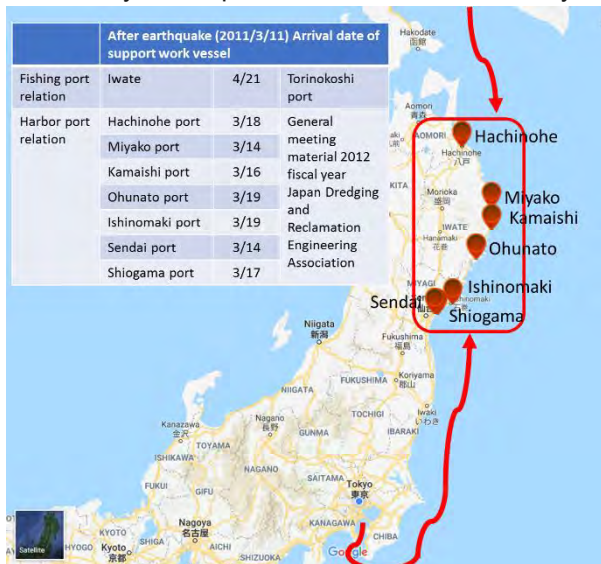


Figure 1: Work Vessels from Non Affected Area

¹ The Graduate School of Future University Hakodate, Japan. g3216002@fun.ac.jp

² Future University Hakodate Professor, Japan

³ Nagasaki Port Construction Association, Japan

⁴ Construction Division Fisheries Infrastructure Department Fisheries Agency, MAFF, Japan

⁵ All Japan Fishing Port Construction Association, Japan

In order to verify the effectiveness of this system with weather condition information, we installed GPS and transmitters in 35 work vessels in the Nagasaki prefecture waters area. After that, the system has been put to practical use.

2. FLOW OF RESEARCH

This research is conducted as shown Fig.2.

The research consists of three parts. The first part is the construction of following each systems, location and navigation information system of the work vessels, weather condition information system, and a system for searching and browsing those synchronized two systems. The second part is to implement the equipment that transmits the location information of the work vessels. Then we obtain and input the weather information of the sea area and synchronize with the location information of the work vessel. The third part is the construction of a search and browsing system to grasp the movement of a specific work vessels.

In this pater, We implement GPS and transmitter at 35 work vessels in Nagasaki prefecture sea area and grasp the weather information. We operate this system and verified its usefulness.

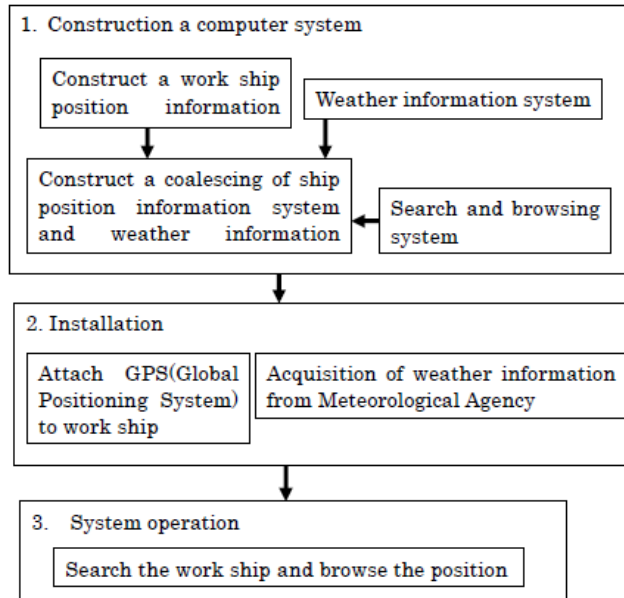


Figure 2: The Flow of The Research

3. CONSTRUCTION OF COMPUTER SYSTEM

(1) construction of work vessels location information system

At first, We construct the system to transmitter the work vessels location to cloud server. Second, the application of monitor screen is constructed in order to view the work vessels location. As the result, viewer ex. civil officer in charge of disaster restoration search and browse the work vessels location information.

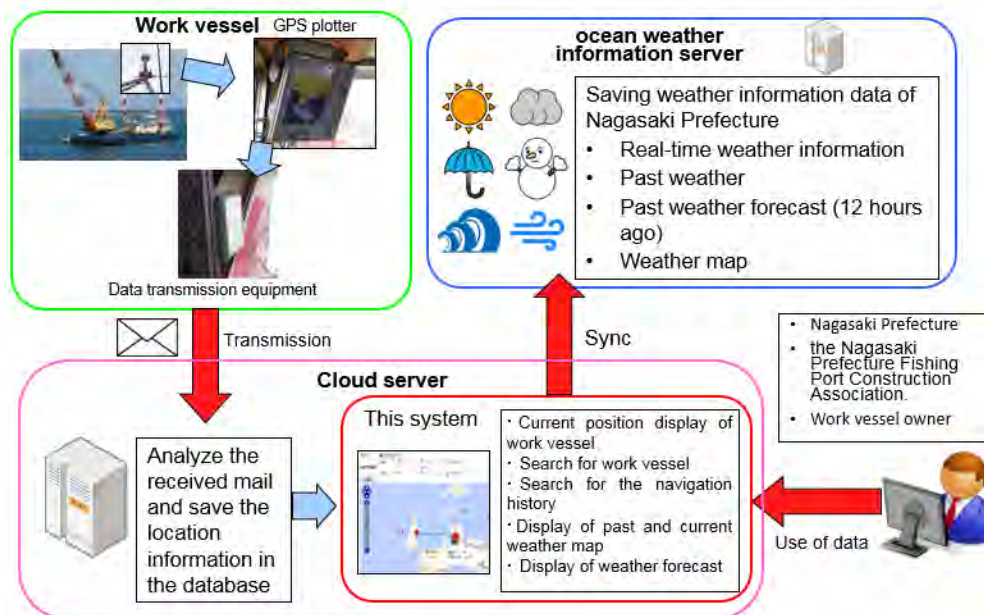


Figure 3: Work Vessels Location Information system

(2) construction of weather information system synchronizing location system of work vessels

The application is constructed to indicate weather information of Meteorological Agency synchronizing with location of work vessels. This application covers in range where work vessels navigate sea area, Nagasaki prefecture.

4. INSTALLATION OF GPS AND TRANSMITTER OF WORK VESSELS LOCATION INFORMATION

We installed GPS antennas and plotters and transmitters via the Internet on 35 work vessels in the Nagasaki prefecture waters area. The location information is acquired by the GPS antenna and the transmitter of the NMEA0183 standard is used. Work vessels speed and location information are accumulated in the cloud server. The transmitter is a 3G communication module. It transmit location information of the work vessels to cloud server every 5 minutes on the Internet.

There is an AIS (Automatic Identification System) system that identifies the position of a vessels. But the GPS and 3G-transmission method is adopted for comparison of expenses and convenience for system program. The all coastal area of Japan (coastal area 22.2 km) is a communicable area of 3G-transmission.

| | AIS | AIS (ClassB) | 3G communication machine |
|--|--|---|---|
| Data transmission method | VHF radio wave | | 3G communication (same as mobile phone) |
| Accumulation of data | Not accumulated (It can not be confirmed whether the receiving station has received the radio waves.) | | When 3G communication is out of range, data is accumulated and transmitted collectively when entering the area. |
| Open scope | All the world (anyone can set up reception stations) | | Specific person |
| Vulnerability | Security hole report that can tamper with information on ship, etc. Reported | | Same as mail service of used mobile carriers (docomo, au, SOFTBANK etc) |
| Size (mm) Horizontal * Width * High | 420*250*85 | 1/2 - 1/4 of AIS | 130*90*35 |
| Price | \$1,500 | \$1,000~\$3,000 GPS antenna required If you want to monitor output on board, you need a GPS plotter separately (There is also a monitor function if it is an expensive item) | \$1,500 GPS antenna required If you want to monitor output on board, you need a GPS plotter separately |
| Communication cost | Free | | \$120/Year |
| Remarks | GPS antenna \$200~\$300 GPS plotter \$1,200~\$3,500 | | |

Table 1: The comparison 3G-transmission method with AIS

In this system, when outside the 3G communication range of the outside seas and the shelter of the mountains, data is accumulated in the transmitter, and within the communication range, the accumulated data is transmitted to the server. From the accumulated data, the navigation route history of the work vessel is displayed on the map (Fig.4).

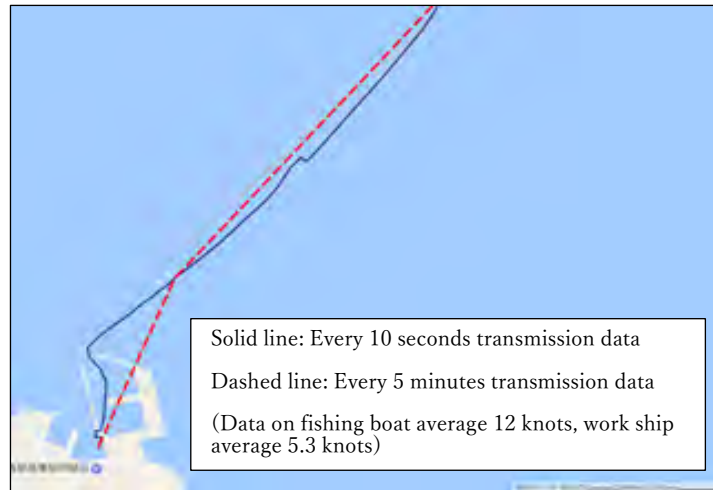


Figure 4: Navigation Route History of The Work Vessel

5. OPERATION OF SYSTEM

(1) work vessel location information system

Currently, the Nagasaki Harbor Fishing Port Construction Association manages the location navigation information system of 35 work vessels. Therefore, it is possible to dispatch some work vessels early when a disaster occurs. In order to carry out the restoration work of the harbor, they have established a system that can dispatch work ships efficiently.

The basic screen on the monitor of this system is shown in Fig.5.

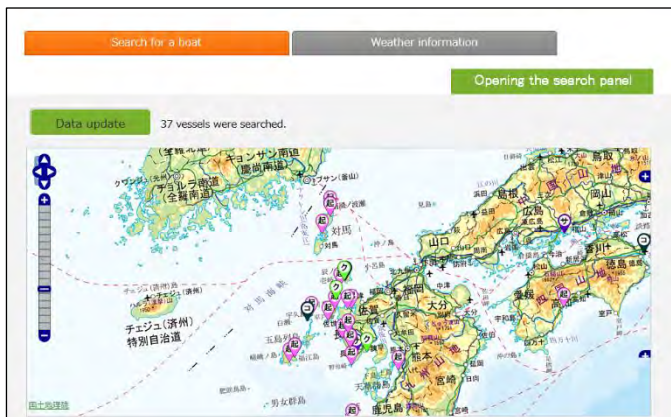


Figure 5: Location of Work Vessels



Figure 6: Details Information of Work Vessels

On this monitor, the position of the work vessel is indicated by the icon. Icons are displayed separately by the type of work vessels, hoist vessels and dredger vessels, etc.. As clicking the icon of the work vessel, the type and ability of the work vessel are displayed in detail (Fig.6). As clicking the character of root, the route history of the work vessel is displayed. When weather character is clicked, weather information on the position of the work vessel is displayed.

(2) weather information system

The basic screen of weather conditions necessary for the operation of the work vessels is displayed on the monitor as shown in Fig.7. In Nagasaki prefecture area, forecast of rainfall amount, wind data and wave data are displayed. Clicking on one point in the sea area, Forecast of the rainfall amount, the wind data and the wave data are displayed with numerical value and graph (Fig.8). Based on these information, it is possible to decide the navigation of the work vessels.

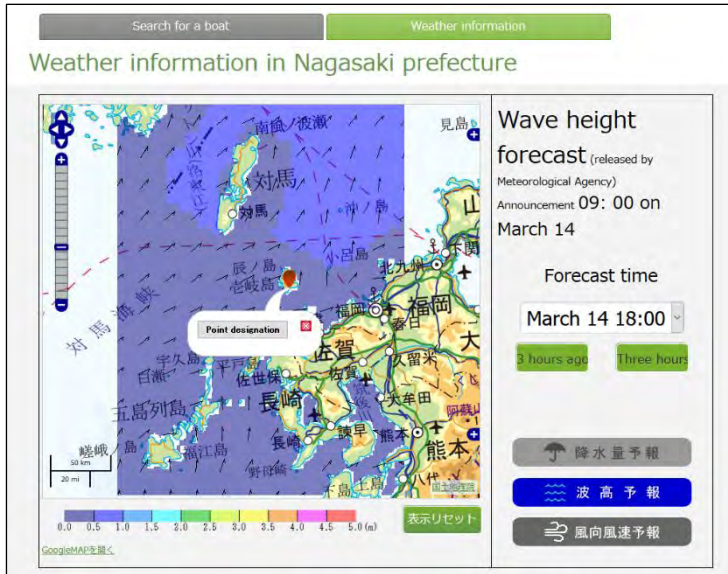


Figure 7: Weather Information Map

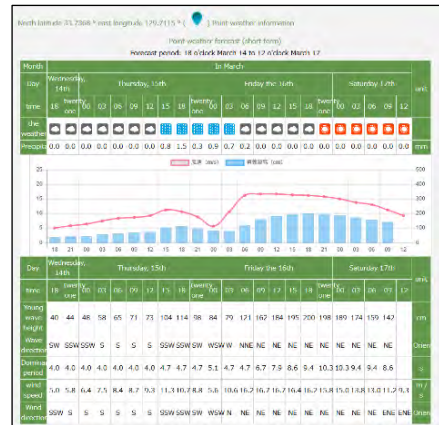


Figure 8: Numerical Weather Information

(3) coalescing of work vessels location and weather information system

Fig. 9 shows the monitor screen combining the navigation history of the work vessel and weather information. When the departure time and the arrival time of the work vessel are entered, the navigational trajectory during that time is displayed. And weather information of departure time and arrival time is displayed. This fig.9 is used as a document certifying that navigation was safe and appropriate. Current weather information and weather forecasts of the destination should be acquired, the current and predicted weather information can be obtained by clicking the destination as shown in Fig.7 & Fig.8



Figure 9: Navigation History and Weather Information

6. CONCLUSION

Construction of the work vessel location and navigation information system with weather information for port restore and construction port quickly. The Nagasaki Harbor Fishing Port Construction Association manages the location navigation information system of 35 work vessels. The Nagasaki Harbor Fishing Port Construction Association can dispatch the necessary work vessels to restore and construct port quickly. In order to take measures to large-scale disasters throughout Japan, it is necessary to participate in this system on not only 35 working vessels in Nagasaki prefecture's area but also working vessels in all over Japan.

References

Shimpei NAGANO, Masaaki WADA(Dr.), Shuichi TANAKA, Minoru NAKATA, Kouki ABE, Masayuki TAHARA and Akira NAGANO(Dr.). CONSTRUCTION AND OPERATION OF INFORMATION SYSTEM FOR POSITION AND NAVIGATION OF WORK SHIP. Journal of JSCE B3(Marine development),Vol 73(2017) No.2 I_977-I_982(in Japanese with English abstract)

SPECTRAL MODELING OF WAVE PROPAGATION IN COASTAL AREAS WITH A HARBOR NAVIGATION CHANNEL

by

B.J.O. Eikema¹, Y. Attema¹, H. Talstra¹, A.J. Bliet^{1,2}, L. de Wit¹ and D.W. Dusseljee³

ABSTRACT

This study presents a comparison of numerical model results and laboratory experiments of wave propagation in a coastal area with a harbor navigation channel. The results of wave models SWASH, SWAN and HARES are compared with physical model results in order to investigate the performance of these models. It turns out that HARES, a 2D parallel spectral wave model based on the Mild-Slope Equation with non-linear damping, yields the most accurate results and a computational time that is only a small fraction of the time needed by SWASH. It appears that the large computational effort and resolution required by full 3D time-dependent wave models like SWASH may prevent them from exploiting their full potential accuracy, even though they contain all relevant physics for wave propagation. Furthermore, the phase-resolving wave modeling approach used by both HARES and SWASH yields more accurate results than the phase-averaged approach used by SWAN when channel reflection and diffraction effects are involved, which can be important in the vicinity of harbor navigation channels. HARES combines the advantages of a stationary and two-dimensional calculation (enabling sufficient model resolution at low cost) with a phase-resolving modeling approach. This underlines the ongoing applicability of mild-slope wave models like HARES in practice and makes them a preferable tool for the design of harbor layouts.

1. INTRODUCTION

The numerical wave model HARES is a stationary phase-resolving 2D model based on the Mild-Slope Equation. Since the first introduction of the modeling concept by Berkhoff (1972), the development of mild-slope-type wave models has become widespread. HARES is often used in practice for the modeling of wave penetration into harbor areas. Similar models are e.g. PHAROS (Hurdle et al., 1989), TELEMAC ARTEMIS and MIKE21 EMS. In recent years, 3D non-hydrostatic wave models like SWASH (Zijlema et al., 2011) have been introduced and increasingly used. Conceptually such full 3D models can yield more accurate results than 2D mild-slope models, because they take into account non-linear wave propagation effects like Stokes waves and cnoidal waves; yet, some downsides are the large amount of computational time needed and possible difficulties to obtain stable results in practice. Another type of wave model, often used for computing wave conditions outside a harbor, is a phase-averaged spectral wave-energy model like SWAN (Booij et al., 1999). This model is often applied in near-shore areas, but is less suitable for wave penetration in regions where diffraction and reflection play an important role.

In 2014 a comparison was made between a SWASH and SWAN wave model and 3D laboratory experiments of a harbor navigation channel area (Dusseljee et al., 2014). Recently, Svašek Hydraulics has remodeled these laboratory experiments using the mild-slope model HARES. This paper presents the HARES results and the comparison with the physical and other numerical model results.

The paper has two main objectives:

1. Comparison of HARES results with experimental results in order to investigate model accuracy;
2. Comparison of HARES results with SWAN and SWASH results to assess the performance of the mild-slope model HARES compared to wave models of quite different characters.

2. PHYSICAL MODEL

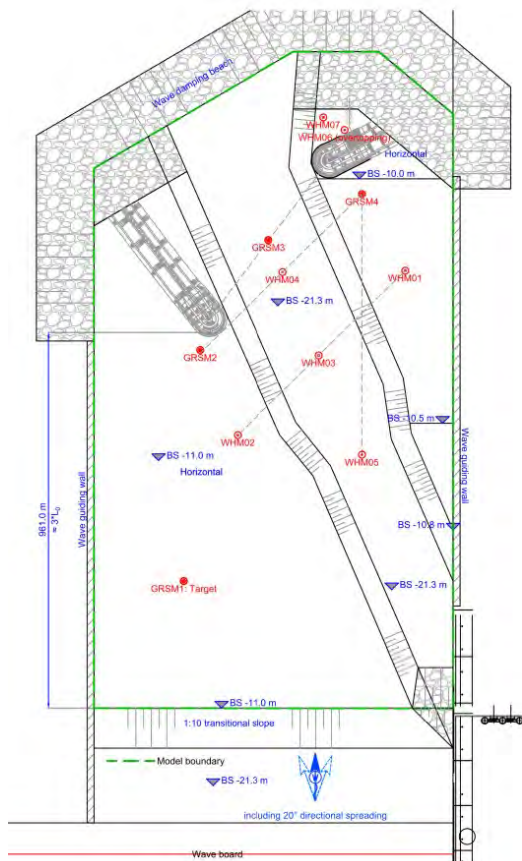
The physical model setup of a harbor navigation channel region is described in Dusseljee et al. (2014) and Riezebos (2014). This section gives a brief summary of the model setup. At prototype scale, the 3D laboratory experiment represents an existing navigation channel towards a harbor, with a 15 km

¹ Svašek Hydraulics - coastal, harbor and river engineering consultants, the Netherlands, eikema@svasek.com

² Presenting author, bliet@svasek.com

³ Witteveen+Bos Consulting Engineers, the Netherlands, daniel.dusseljee@witteveenbos.com

long straight access channel; see Fig. 1 for the experimental set-up of the harbor entrance. Waves are generated on deep water, at a water depth of -21.3 m, which is also the water depth of the access channel. A gentle transition slope (1:10) guides the waves towards the actual foreshore of the harbor. The side slopes of the access channel are designed with a 1:5 slope. The width of the channel at the bottom level is 250 m near the harbor entrance (in between the two breakwaters) and 170 m further offshore.



Entrance channel



Western breakwater

Figure 1: Set up of physical model in basin (Riezebos, 2014).

Physical scale-model tests were performed in a 3D wave basin of Deltares in the Netherlands, equipped with a multi-directional wave generator, able to generate short-crested random waves. The wave generators are equipped with active wave absorption in order to prevent the re-reflection of waves (generated by structures and bathymetry in the basin) upon the wave paddles.

The physical model is Froude-scaled at scale 1:60, implying that gravity-based wave processes are included correctly as compared with prototype conditions. The applied orientation of the incident waves is 0° (normal to the wave paddles) for all tests. The waves approach the access channel with an incident angle of 23° . At the basin end a wave-damping beach is installed to dissipate outgoing wave energy. A normally-distributed directional spreading (with 20° standard deviation) is applied.

Wave conditions are measured at several locations, as indicated in Fig. 1. The open circles are standard resistant-type wave gauges (WHM). The closed circles are directional wave gauges (GRSM).

Two distinguished wave scenarios are presented, with relatively small wave angles between the incident wave direction and channel axis. A single-peaked wind-sea wave spectrum (case C1) and a double-peaked spectrum including both local wind conditions and swell (case C2) are applied (see Fig. 2). In both the numerical and physical models, wave boundaries are applied as 2D wave spectra with a directional wave spreading of 20° . The water level for both conditions is CD+0.8 m.

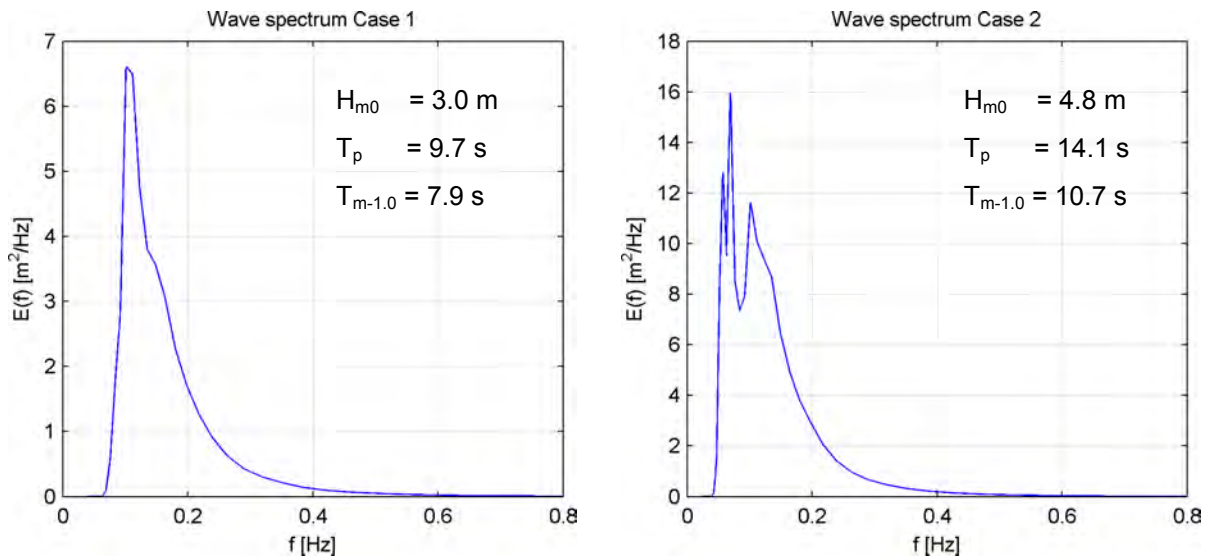


Figure 2: Imposed wave spectra for case C1 (left) and C2 (right).

3. HARES NUMERICAL MODEL

3.1 Introduction

The focus of this paper is on wave modeling using HARES; results of SWASH and SWAN model simulations have been taken from Dusseljee et al. (2014) for comparison. In this section, first a general description of the mild-slope wave model HARES is given; subsequently, the present numerical model set-up is presented. Finally, numerical model results as well as a comparison with experiments and other models will be given.

3.2 Description of the mild-slope wave model HARES

The Finite Element model HARES (“*HARbor RESonance*”) has been developed in-house by Svašek Hydraulics. HARES is a one- or two-dimensional parallel model based on the Mild-Slope Equation (Berkhoff, 1972), with non-linear damping terms incorporated, which can be applied to simulate the propagation and possible resonance of waves in coastal zones and harbor areas. It is especially useful in harbor and breakwater optimization studies and for determining the natural frequencies of a harbor basin. The Mild-Slope Equation is a practical example of a Helmholtz problem, in which the complex amplitude of a harmonic wave component is computed in the model domain; within the field of Helmholtz-type problems, the Mild-Slope Equation is characterized by the relative dominance of damping/dissipation and spatial variation of bathymetry (and hence wave celerity).

Within HARES the Mild-Slope Equation has been discretized using the Continuous Galerkin approach, employing an unstructured triangular flexible mesh of linear finite elements (yielding a second-order accurate discretization in space). This enables the user to fit boundaries accurately into the model area and increase resolution in the region of interest in a flexible way, without the need for nesting of grids. The Finite Element discretization gives rise to global systems of linear equations, which are solved on a parallel cluster. HARES employs a rather efficient form of parallelism.

Model input includes incoming wave characteristics (e.g. wave height/period and wave direction), domain bathymetry, water level, reflection and transmission coefficients for hydraulic structures and other physical borders.

HARES includes the following model features:

- One- or two-dimensional wave propagation over topography;
- Diffraction around obstacles;
- Refraction and shoaling;
- Wave damping due to bottom friction and wave breaking (depth- or steepness-induced);
- Reflection at boundaries (full or partial);
- Combined (full or partial) reflection and (full or partial) transmission at internal boundaries (e.g. breakwaters);
- Uniform incident wave at seaward boundaries;

- Monochromatic versus spectral computations (frequency spreading and directional spreading);
- Consistent spectral treatment of damping terms (optional);
- Solving systems in parallel using a direct solver (MUMPS) or iterative solver (BiCGSTAB);
- Very fast solution algorithm for spectral computations thanks to efficient reuse of matrices.

The software package HARES has been developed by Svašek Hydraulics for several decades. The scientific basis of the Mild-Slope Equation as implemented in HARES has been given in many text books, e.g. Dingemans (1997); a lot of numerical pioneering work on Finite Elements within Svašek Hydraulics has been performed by Labeur, which have been reported in his PhD thesis (2009). Among the more recent improvements and extensions to the model are the full parallelization of HARES (2014-2015), the incorporation of combined reflection-transmission boundaries along breakwaters (2017) with a very user-friendly user interface, and the addition of a consistent and accurate spectral treatment of bottom friction and wave breaking based on the entire wave spectrum (2017), inspired after the spectral wave model SWAN. A speedup of the model of over a factor 10 has been reached thanks to efficient matrix reuse (2017).

3.3 Model setup

Wave conditions

The wave conditions for case C1 and C2 are discretized by dividing the 2D wave spectra into a large number of frequencies with a 0.01 Hz interval, see Fig. 3. This results in 28 frequency bins for C1 and 30 frequency bins for C2.

The red lines represent the frequencies that are modeled in HARES, including a line precisely at the peak frequency. For each frequency bin the amount of wave energy is determined. The maximum frequency in this case is set to is 0.33 Hz, which corresponds to a wave period of 3.0 seconds. This cut-off frequency results from a trade-off between two practical considerations: on the one hand a 3.0 s wave can still be resolved on the present computational grid, on the other hand more than 95% of the total spectral energy is resolved by the discretized frequencies. Moreover, all energy in the tail of the spectrum ($f > 0.33$ Hz) is assigned to the last frequency bin.

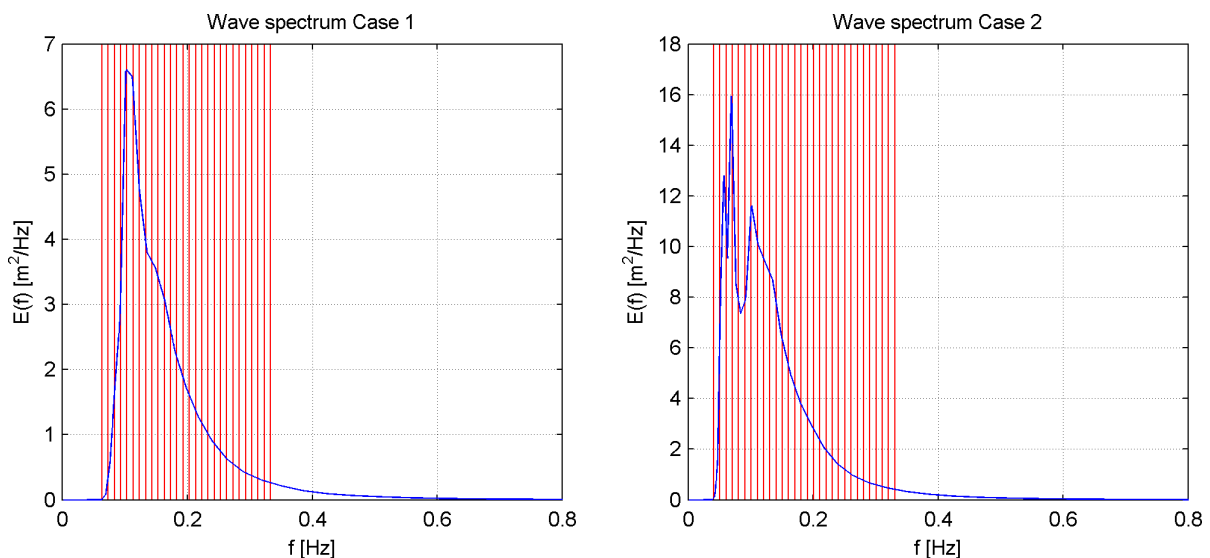


Figure 3: Discretization of 2D wave spectrum for case C1 (left) and C2 (right).

For each frequency a directional wave spreading is applied with a standard deviation of 20° . This directional spreading is schematized by distributing the wave energy over a main wave direction and wave directions up to 45° at both sides of the main wave direction, with an interval of 5° . The total wave energy is 100%. Fig. 4 depicts the distribution of the wave energy, normalized by the peak value, over the 19 discrete wave directions for a single frequency.

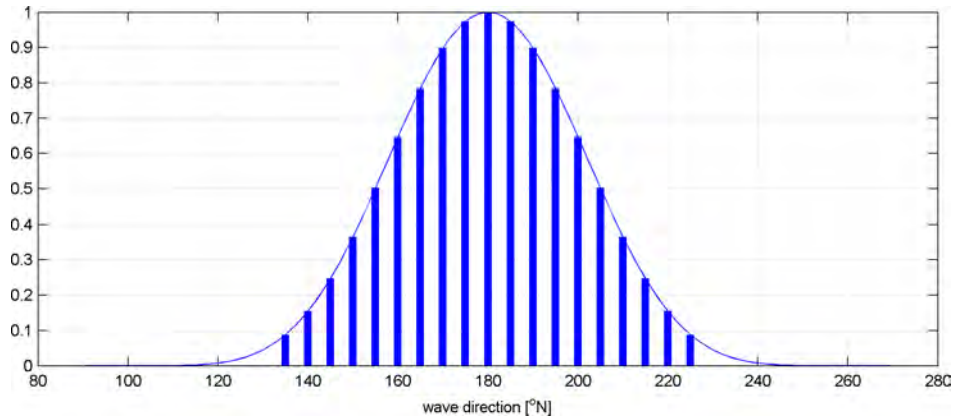


Figure 4: Directional spreading for case C1 and C2.

The above results in a total of 532 individual wave components for case C1 (28 frequency bins times 19 directions) and 570 wave components for case C2 (30 frequency bins times 19 directions). As described in Section 3.2, HARES applies this set of wave components on behalf of a consistent spectral treatment of bottom friction and wave breaking based on the entire wave spectrum, inspired after the model SWAN. Hence, the above set of wave components is considered as a single wave spectrum by HARES.

Model domain and bathymetry

The computational domain and bathymetry used within HARES are based on the corresponding SWASH input files (Dusseljee D.W., et al., 2014). For the HARES bathymetry the SWASH bathymetry and structure height are combined. The resulting HARES bathymetry is depicted in Fig. 5.

The flexible mesh of the computational domain consists of 1.06 million triangular elements with a size of approximately 1.5 meters on average. For both cases a water level of CD+0.8 m is used, in accordance with SWASH input files.

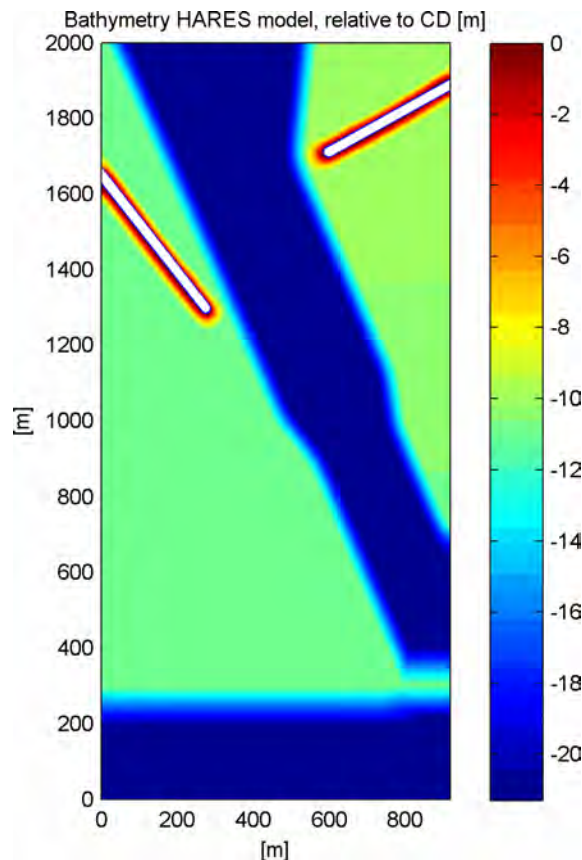


Figure 5: Model domain and applied bathymetry.

For the breakwaters a reflection coefficient of 0.53 for case C1 and 0.55 for case C2 is applied, in accordance with Riezebos (2014). The vertical basin walls have a reflection coefficient of 1.0 and the wave-damping beach has a reflection coefficient of 0.0. Besides these reflection coefficients, domain bathymetry and spectral wave components, only a few model settings are required: a wave bottom friction parameter $C_f = 0.001$ (suitable for the present concrete-wall laboratory set-up) and two wave breaking criteria, i.e. a maximum wave height (relative to water depth) of 0.88 and a maximum wave steepness of 0.14. Hence, the number of settings to “tune” the model are rather limited.

3.4 Results and discussion

In this section, HARES results for both scenarios are presented and compared with results by the physical model and the numerical models SWASH and SWAN.

The presence of an approach channel can change local wave conditions considerably. When travelling waves approach the channel under an angle larger than the critical angle (to the channel-normal axis), they are fully reflected at the downward channel slope (total reflection). When the wave direction angle compared to the channel-normal axis is smaller than the critical angle, waves may (partially) cross the channel. This phenomenon is described in literature, e.g. Zwamborn and Grieve (1974).

In cases C1 and C2, most of the waves in the spectrum have an approach angle beyond the critical angle, resulting in a considerable concentration of wave energy at the left side of the approach channel. Fig. 6 shows spatial distributions of the significant wave height H_{m0} as computed with SWASH, SWAN and HARES for both cases.

Table 1 summarizes (for each output location) the results (H_{m0}) of the physical model (PHM) and the SWASH, SWAN and HARES wave models for case C1. Results for case C2 are given in Table 2. The columns with SWASH, SWAN and HARES results also show the relative difference (in percentages) with the measured wave heights in the physical model.

From Fig. 6 it is notable that, generally, the HARES results contain more wave energy on both sides of the navigation channel (compared to SWASH and SWAN) as well as inside the navigation channel and the harbor basin itself. Especially the wave reflection pattern along the right side of the channel (on the seaward side of the eastern breakwater) is noteworthy. As can be seen from physical model results at the points GRSM4 and WHM01 within Table 1 and 2, this energy content crossing the navigation channel as computed by HARES is in accordance with the physical model experiments.

For case C1 the HARES model gives significantly better results than the SWASH and SWAN model. The over-all average absolute error (based on the absolute value of all error percentages) for HARES is only 3%, for SWASH and SWAN these are 24% and 18% respectively. Moreover, the SWASH and SWAN results are all (systematic) underestimations of experimental results, whereas the HARES results give both small under- and overestimations. The computational time on a 16-core cluster-computer for HARES was only 21 minutes, which is 0.7% of the SWASH computation (48 hours and 20 minutes).

| Location | PHM | SWASH | | SWAN | | HARES | |
|------------------------|--------------|---------------|--------|--------------|--------|--------------|-------|
| | H_{m0} [m] | H_{m0} [m] | diff | H_{m0} [m] | diff | H_{m0} [m] | diff |
| GRSM1 | 3.03 | 2.51 | (-17%) | 2.82 | (-7%) | 3.04 | (0%) |
| GRSM2 | 3.63 | 3.14 | (-13%) | 3.36 | (-7%) | 3.67 | (1%) |
| GRSM3 | 2.36 | 1.80 | (-24%) | 2.06 | (-13%) | 2.53 | (7%) |
| GRSM4 | 2.50 | 1.85 | (-26%) | 1.64 | (-34%) | 2.64 | (6%) |
| WHM01 | 2.81 | 2.07 | (-26%) | 1.60 | (-43%) | 2.88 | (2%) |
| WHM02 | 3.55 | 3.25 | (-8%) | 3.30 | (-7%) | 3.64 | (3%) |
| WHM03 | 2.77 | 1.93 | (-30%) | 2.15 | (-22%) | 2.65 | (-4%) |
| WHM04 | 2.60 | 1.88 | (-28%) | 2.11 | (-19%) | 2.62 | (1%) |
| WHM05 | 2.73 | 1.85 | (-32%) | 2.10 | (-23%) | 2.61 | (-4%) |
| WHM07 | 1.30 | 0.89 | (-32%) | 1.33 | (2%) | 1.22 | (-6%) |
| Average absolute error | | 24% | | 18% | | 3% | |
| Computational time | | 48 hrs 20 min | | 17 min | | 21 min | |

Table 1: Results for case C1, significant wave height H_{m0} [m].

For case C2 the HARES model yields better results as well. The average absolute error for HARES is 10%, for SWASH and SWAN these are 15% and 20% respectively (with systematic underestimation). Again, the computational time needed by HARES is only a fraction of the time needed by SWASH. Computational times needed by HARES and SWAN have equal order of magnitude for both cases.

| Location | PHM H_{m0} [m] | SWASH | | SWAN | | HARES | |
|------------------------|---------------------|---------------|--------|--------------|--------|--------------|--------|
| | | H_{m0} [m] | diff | H_{m0} [m] | diff | H_{m0} [m] | diff |
| GRSM1 | 4.80 | 4.37 | (-9%) | 4.64 | (-3%) | 4.84 | (1%) |
| GRSM2 | 5.33 | 5.26 | (-1%) | 5.42 | (2%) | 5.61 | (5%) |
| GRSM3 | 3.56 | 2.96 | (-17%) | 2.93 | (-18%) | 3.43 | (-4%) |
| GRSM4 | 4.31 | 3.82 | (-11%) | 2.37 | (-45%) | 3.87 | (-10%) |
| WHM01 | 4.36 | 3.42 | (-22%) | 2.42 | (-44%) | 4.21 | (-3%) |
| WHM02 | 5.36 | 5.26 | (-2%) | 5.44 | (2%) | 5.76 | (7%) |
| WHM03 | 4.42 | 3.40 | (-23%) | 3.16 | (-29%) | 3.81 | (-14%) |
| WHM04 | 3.98 | 3.14 | (-21%) | 3.07 | (-23%) | 3.56 | (-11%) |
| WHM05 | 4.66 | 3.47 | (-26%) | 3.03 | (-35%) | 3.54 | (-24%) |
| WHM07 | 2.11 | 1.69 | (-20%) | 2.07 | (-2%) | 1.63 | (-23%) |
| Average absolute error | | 15% | | 20% | | 10% | |
| Computational time | | 49 hrs 20 min | | 14 min | | 26 min | |

Table 2: Results for case C2, significant wave height H_{m0} [m].

Finally a comparison of the modeled and measured wave spectra at the wave gauges is depicted in Fig. 7 (for case C1) and Fig. 8 (for case C2). These wave spectra show that for almost all locations the HARES spectrum comes closest to the measurement. The SWASH and SWAN results mostly show significantly lower energy densities compared to measurements, especially for case C1. For case C2 the differences are less pronounced, yet HARES results still come closest to the experimental data. Applying wave damping (due to bottom friction and wave breaking) on the full spectrum in HARES is an important improvement, as previous tests (not shown in this paper) with damping applied at individual wave bins only, instead at the total wave spectrum, gave less accurate results.

As pointed out previously by Dusseljee et al. (2014) the high-frequency waves as computed by SWASH ($f > 0.13$ Hz) show significant damping, which has been attributed to a relatively low spatial resolution of the SWASH model (i.e. a grid size of 3.0m, equal to SWAN). This results in an inaccurate reproduction of the high-frequency part of the spectrum; indeed, as can be seen from Fig. 7 and 8, wave energy is lacking in the right-hand-side part of most spectra. Sensitivity simulations performed by Dusseljee et al. (2014) indicate that a considerable improvement of SWASH results might be expected if the horizontal resolution is enhanced to 0.5 m and the vertical resolution to 3 layers (instead of the present 2 layers). Yet, such simulations were considered quite unfeasible due to constraints regarding computational time, even though the present computational effort ratio between SWAN/HARES and SWASH is about 1% already (as pointed out by Tables 1 and 2).

These considerations tend to the conclusion that the 3D time-dependent model SWASH, although it contains all relevant physics for spectral wave propagation, is generally outperformed by time-independent and spectra-based models like SWAN and HARES, which prevents it from exploiting its full potential accuracy. This implies that 2D spectral wave models form a more practical tool for use in real-life cases where relatively wide wave spectra are involved.

From Fig. 6 it can be observed as well that the significant wave height results for SWAN are more smooth than those for HARES and SWASH; this is due to the fact that SWAN is a phase-averaged wave model, whereas SWASH and HARES are intrinsically phase-resolving. From Table 1 and 2 it can be noted that (for both scenarios) SWAN performs relatively well along the wave-ward side of the channel, where the measurement locations GRSM2 and WHM02 are situated. A substantial part of the incoming multi-directional wave spectrum travels at angles where waves (theoretically) do not cross the navigation channel, which causes wave energy to pile up against the western slope of the channel, giving rise in turn to breaking waves and a “sharp edge” of wave energy. As observed by Dusseljee et al. (2014), wave heights along the lee-ward side of the channel are significantly underpredicted by SWAN compared to measurements and also to SWASH results (see locations GRSM4 and WHM01 in Table 1 and 2), which may be caused by inaccuracies regarding the effects of channel reflection and

diffraction within SWAN (due to its phase-averaged modeling approach). Apparently, the use of a phase-resolving modeling approach may be advantageous when waves cross a navigation channel under a certain angle: both HARES and SWASH give better significant wave height results than SWAN along the lee-ward side of the channel (even though high-frequency waves in SWASH are known to show too much damping).

In view of the above observations, we may state that mild-slope models to a certain extent combines “the best of both worlds” conceptually. On the one hand, the 2D time-independent spectral approach which is characteristic for mild-slope models provides them with an efficiency advantage above full 3D time-dependent models, which include all relevant physics but whose resolution requirements cause them to be outperformed. On the other hand, the mild-slope approach still remains a phase-resolving approach which includes phase-related wave phenomena like diffraction accurately, which can give an advantage (for geometries like the present one) above the phase-averaged approach employed by spectral wave-energy models. Both advantages can be observed from the comparison between SWASH, SWAN and HARES as depicted in Figures 6-8 and Tables 1-2.

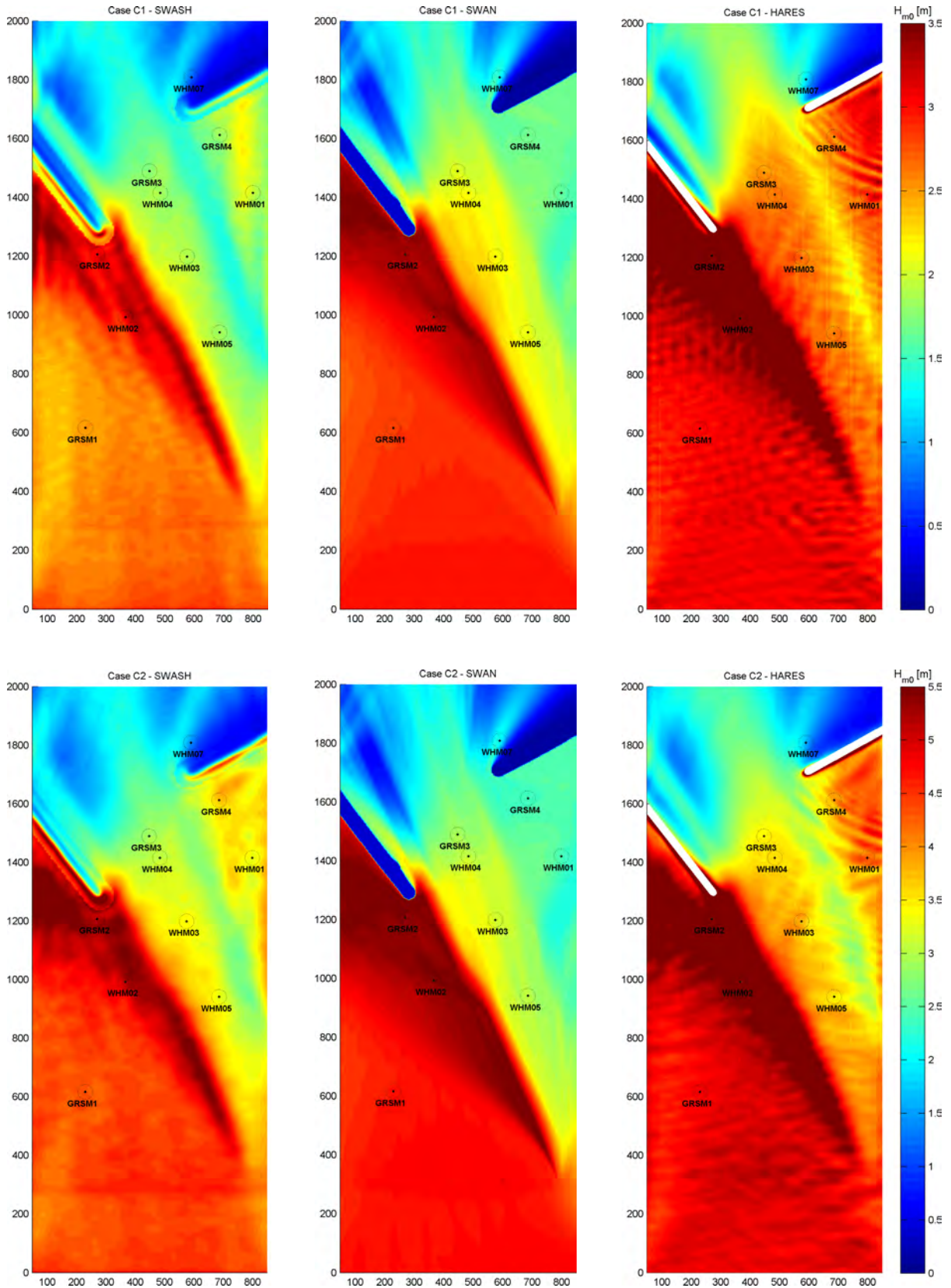


Figure 6: Spatially varying significant wave height H_{m0} [m], as computed by SWASH (left), SWAN (middle) and HARES (right). Top: scenario C1. Bottom: scenario C2.

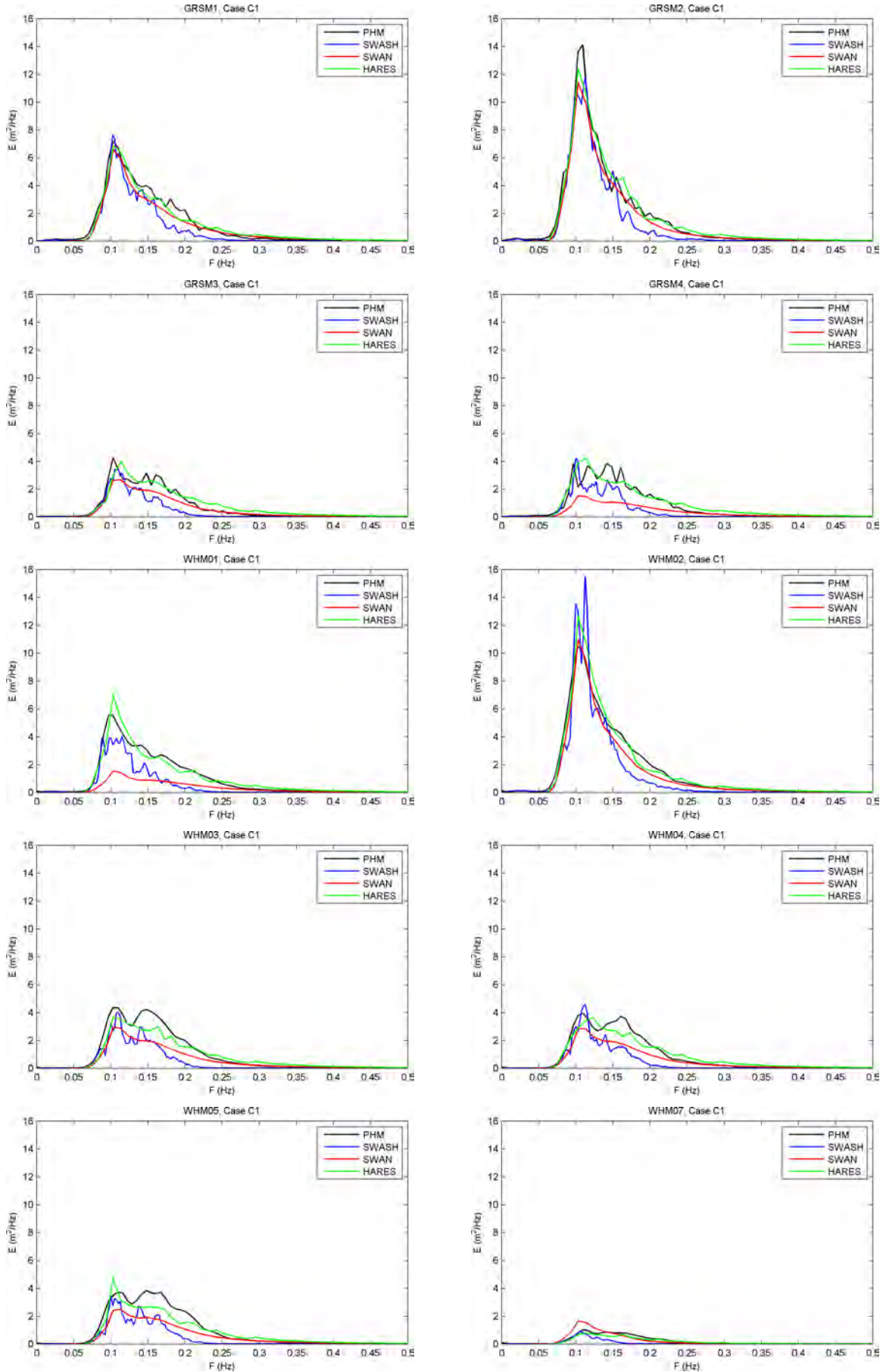


Figure 7: Frequency wave spectra at the wave gauges for all models for case C1. (Black: physical model, blue: SWASH, red: SWAN and green: HARES).

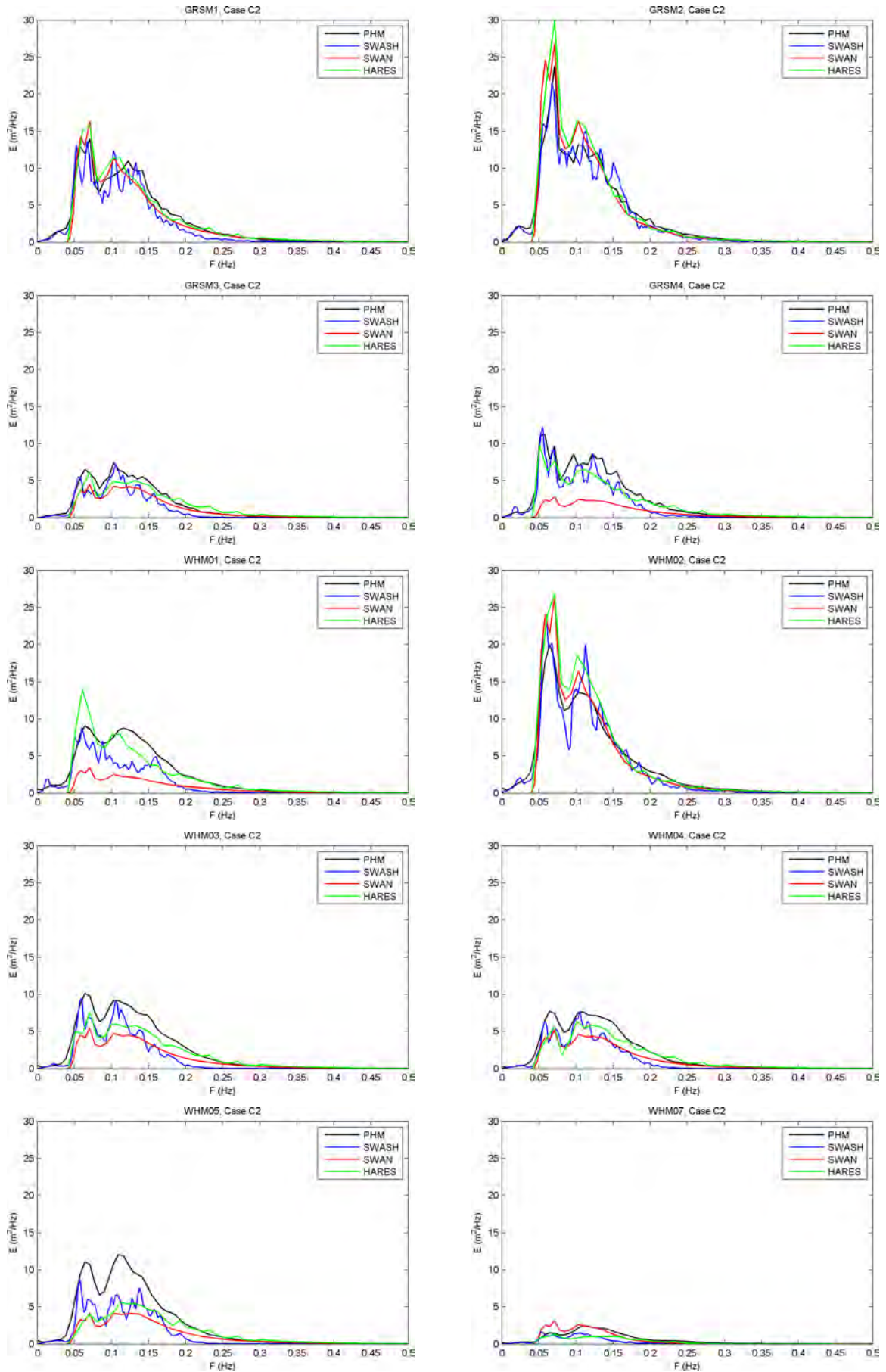


Figure 8: Frequency wave spectra at the wave gauges for all models for case C2. (Black: physical model, blue: SWASH, red: SWAN and green: HARES).

4. EXAMPLE: WAVE TRANSMISSION ALONG BREAKWATERS

The latest improvements of the HARES numerical wave model include the addition of a consistent and accurate spectral treatment of bottom friction and wave breaking, based on the entire wave spectrum, and the incorporation of combined reflection-transmission boundaries along breakwaters. The case of the approach channel discussed above showed the positive effect of spectral damping treatment. As for the combined reflection-transmission boundaries, an example will be presented in this section.

To this end a small real-life harbor is considered (using a fictitious but realistic bathymetry), see Fig 9. The harbor is protected by two breakwaters, a large one and a smaller one. In this case a very high water level is applied, resulting in a wave transmission coefficient of 50% for both breakwaters. Furthermore, realistic reflection coefficients are used for all other model boundaries.

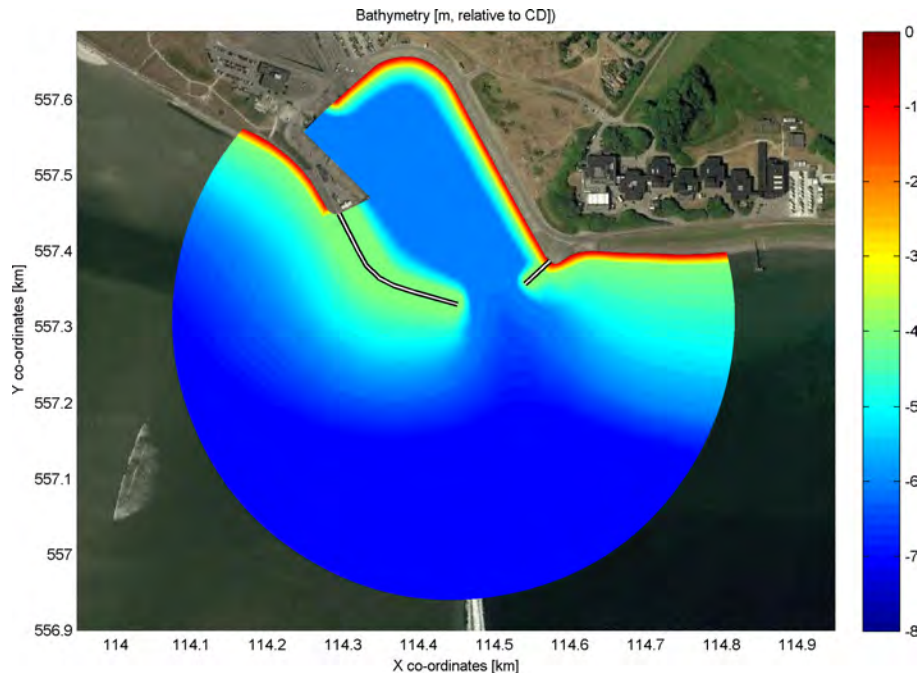


Figure 9: Model domain and applied bathymetry for transmission example.

In order to present the influence of wave transmission, two cases are modeled: a case with no transmission and 30% partial reflection of the breakwaters and a case with both transmission (50%) and partial reflection (30%) along both breakwaters. The wave condition imposed is $T_p = 6.0$ s, $H_{m0} = 1.0$ m and a wave direction of 240° N. Again, this wave condition is subdivided into a large number of frequencies and directions.

Model results are given in Fig. 10 for the case without transmission (top panel) and for the case with 50% transmission (center panel). The differences in wave height for both cases are presented in the bottom panel of Fig. 10. In a circular area inside the harbor, the average wave height is computed and plotted in the figures as well.

The wave height behind the main breakwater increases with almost 0.50 m (which is 50% of the 1.0 m offshore wave height) due to transmission; hence, the wave transmission process over and through the breakwater is modeled adequately. Some processes like diffraction and refraction, however, hinder a fully quantitative 1-to-1 comparison of the wave transmission effects.

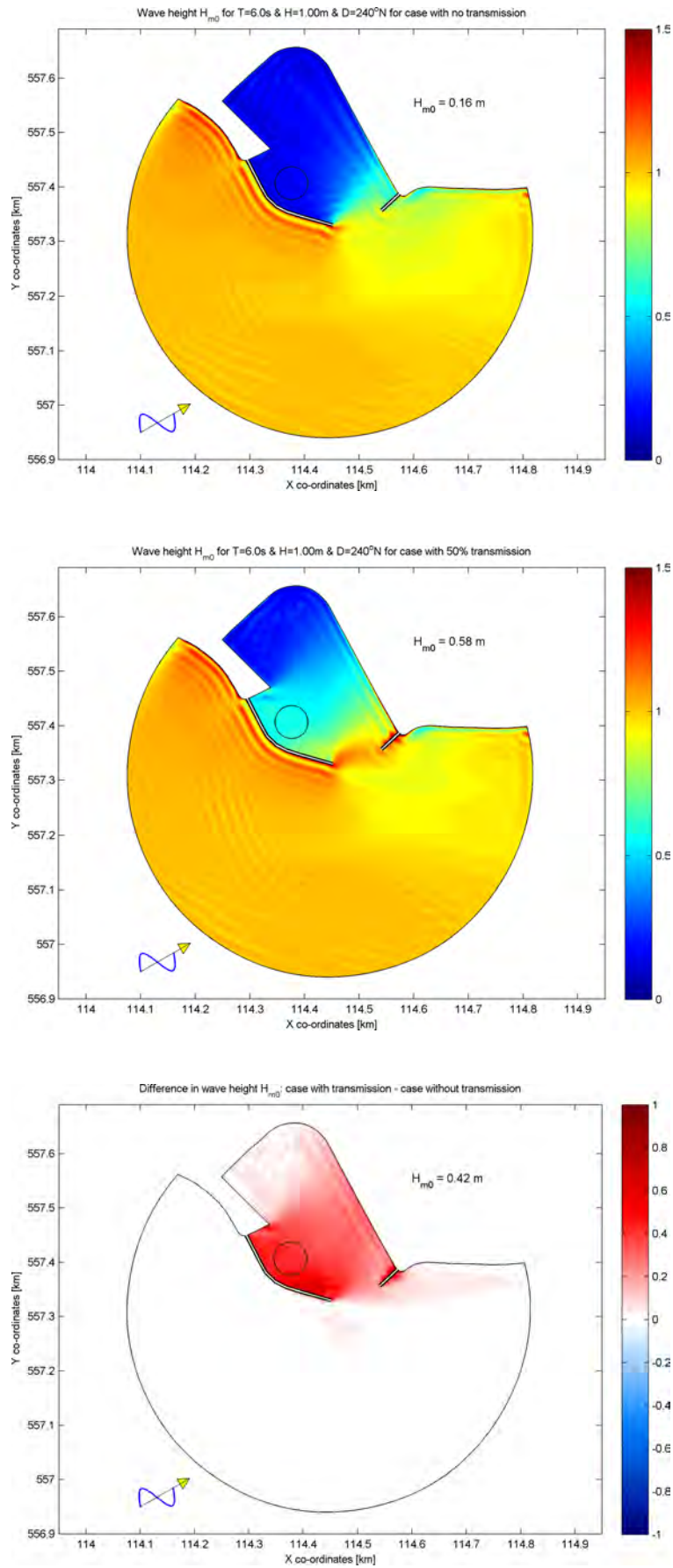


Figure 10: Spatially varying significant wave height H_{m0} [m] for case without transmission (top), case with 50% transmission (center) and difference in wave height between both cases (bottom).

5. CONCLUSION

Wave propagation throughout a coastal area with a harbor entrance navigation channel has been investigated using a physical scale experiment and three numerical models of very different character. For 10 different output locations, significant wave heights and wave energy density spectra computed by the numerical mild-slope model HARES have been compared to experimental data and results by the numerical models SWASH and SWAN.

From this comparison it is concluded that, for the investigated cases, the mild-slope model HARES gives significantly more accurate results than SWASH and SWAN, without significant tuning of default model input coefficients. Furthermore, the computational time needed by HARES is less than 1% of that needed by SWASH, whereas the computational speeds of HARES and SWAN are comparable.

It appears that the strict resolution requirements by full 3D time-dependent models like SWASH (which include all relevant physics) make it virtually unfeasible to perform spectral wave computations at reasonable computational cost without causing the high-frequency waves to dampen out too fast. On the other hand, it has been shown that a phase-averaged modeling approach (as employed by spectral wave-energy models like SWAN) may cause inaccuracies regarding channel reflection and diffraction effects, which are important in the present case of a harbor with navigation channel. Because 2D spectral mild-slope models like HARES are both time-independent and phase-resolving (instead of phase-averaged), whereas the correct spectral treatment of damping terms is maintained, we may state that they combine "the best of both worlds" from a conceptual point of view.

An additional case of a harbor with breakwater crests just above the water level shows that HARES is able to model partial wave transmission over and through breakwaters in a realistic manner.

These results underline the ongoing applicability and convenience of mild-slope-type numerical wave models for harbor design purposes (or other situations where multiple variants have to be investigated and computational time is limited), despite the fact that the mild-slope modeling concept is relatively old compared to more recent scientific developments like phase-averaged spectral wave-energy models (SWAN) or fully 3D non-hydrostatic models (SWASH).

We conclude that wave models based on the Mild-Slope Equation, in combination with efficient computational procedures for a fast and accurate spectral treatment of bottom friction and wave breaking based on the entire wave spectrum, are quite competitive to numerical models that are conceptually more sophisticated. In practice, mild-slope models like HARES remain a preferable tool for the design of harbor layouts.

References

- Berkhoff, J.C.W. (1972). Computation of combined refraction-diffraction. Proc. 13th Int. Conf. Coastal Engineering, pp. 471-490.
- Booij, N., Ris, R.C. and Holthuijsen, L.H. (1999): A third-generation wave model for coastal regions, Part I, Model description and validation. J. Geophys. Res., 104(C4), 7649–7666.
- Dingemans, M.W. (1997). Water wave propagation over uneven bottoms. Part 1 – Linear wave propagation. World Scientific, Singapore.
- Dusseljee, D.W., Klopman, G., Van Vledder, G. Ph. and Riezebos, H.J. (2014). Impact of harbor navigational channels on waves: a numerical modeling guideline. Coastal Engineering 2014.
- Hurdle, D.P., Kostense, J.K. and Van den Bosch, P. (1989). Mild-slope model for the behaviour in and around harbours and coastal structures in areas of variable depth and flow conditions. Proc. 2nd Int. Syp. Water Modelling and Measurement.
- Labeur, R.J. (2009). Finite element modelling of transport and non-hydrostatic flow in environmental fluid mechanics. Ph.D. thesis, Delft University of Technology, Delft, 2009.
- Riezebos, H.J. (2014). Validation of SWASH for wave-channel interactions. Additional thesis, Delft University of Technology, Delft. 12 March 2014.
- Zijlema, M., Stelling, G. and Smit, P. (2011). SWASH: An operational public domain code for simulating wave fields and rapidly varied flows in coastal waters, Coastal Engineering 58(10), 992–1012.
- Zwamborn, J.A., and Grieve, G. (1974). Wave attenuation and concentration associated with harbours approach channels, Proc. 14th Int. Conf. Coastal Eng., Copenhagen, June 24–28, Denmark, 2068–2085.

KEYWORDS: Ports, wave modeling, harbor tranquility, navigation channel, HARES

AI PORT INITIATIVES

- POSSIBLE MODERNIZATION OF PORT OPERATION AND MANAGEMENT THROUGH CUTTING EDGE ICTs -
by

Kenji Ono¹, Masayuki Tanemura² and Yasuhiro Akakura³

ABSTRACT

Improving port productivity may be currently one of the most common and prioritized agendas for international container terminal operators. This paper highlights and discusses possible application of modern information and communication technology (ICT) such as the internet of things (IoT), big data and artificial intelligence (AI) to the container port operation and management. An importance of creating a port big data based on the daily operations for fostering AI, as an artificial port manager, is concluded. Difficulties and issues of port communities to invite and include the AI into their daily operations and business practice are also addressed.

1. INTRODUCTION

Port productivity may be one of the key issues for the global container terminal operators, which are competing each other for surviving in the global and regional container trade market. This situation is more and more accelerated by reflecting recent changes in business environment at ports, which are strongly requested by clients to be a more efficient logistics service provider among the global supply chain networks. There is no doubt that the modern world economy fully depends on the global production network and sophisticated supply chain management. Nowadays, materials, parts and components for automotive assembly lines, for example, are gathered across oceans in a regular basis, hence ports, as essential connecting nodes of waterborne and land surface transportation networks, are one of key players of global production activities. In this context, commitment to the extremely sophisticated but complicated and fragile supply chain management requires the port community more time and cost consciousness, with resulting in introduction of recent cutting-edge information and communication technology (ICT) for improving port operation efficiency and productivity. The global port operators are now facing the client's strong requests to renovate their business practice for providing more quality logistics services with less port charges.

2. APPLICATION OF THE RECENT CUTTING-EDGE ICTS

2.1 Automatization of container port operations

In 2005, Tobishima Container Terminal of Nagoya Port, Japan, commenced its operation, which involves automated guided vehicles (AGV) and remote controlled rubber mounted yard gantry cranes. Toyota Motor Company's car assembly line technology was applied to the terminal operation system. This was the first challenge to a mechanization and automatization of container terminal in Japan. In those days, there were only few terminals which adopted such a cutting-edge ICT for container terminals, among which the port of Rotterdam was also another icon of automatized container port.

More than ten years later, an automatization of container terminal operation has become a main stream of global mega-container ports. Table 1 highlights global top ten ports and their introduction of

¹ Executive vice president, Kobe-Osaka International Port Corporation, k-ono@hanshinport.co.jp

² Senior coordination officer for international affairs, Ports and Harbor Bureau, Ministry of Land, Infrastructure, Transport and Tourism (MLIT), Japan

³ Head, Port Systems Division, National Institute of Land and Infrastructure Management, MLIT

PIANC-World Congress Panama City, Panama 2018

automation technologies into container terminal operation. Among the top twenty container hub ports, fifteen have had or will soon have at least partially automatized one or more terminals.

| Rank | Ports | Container Throughput ('000 TEU) | Automatized terminal operation |
|------|-------------------|---------------------------------|--------------------------------|
| 1 | Shanghai | 36,540 | Yes |
| 2 | Singapore | 30,920 | Yes |
| 3 | Shenzhen | 24,200 | No |
| 4 | Ningbo - Zhoushan | 20,620 | No |
| 5 | HongKong | 20,110 | Yes |
| 6 | Busan | 19,450 | Yes |
| 7 | Qingdao | 17,510 | Yes |
| 8 | Canton | 16,970 | No |
| 9 | Dubai | 15,590 | Yes |
| 10 | Tianjin | 14,100 | Yes |
| 11 | Rotterdam | 12,240 | Yes |
| 12 | Port Klang | 11,890 | No |
| 13 | Kaohsiung | 10,260 | Yes |
| 14 | Antwerp | 9,650 | Yes |
| 15 | Dalian | 9,450 | No |
| 16 | Xiamen | 9,180 | Yes |
| 17 | Tanjung Pelepas | 9,100 | Yes |
| 18 | Hamburg | 8,850 | Yes |
| 19 | Los Angeles | 8,160 | Yes |
| 20 | Long Beach | 7,190 | Yes |

Notes: i Container throughputs are statistics in 2015.

ii "Yes" means automatized terminal operation has been introduced or to be introduced soon in some of terminals of the port.

Data: Ports and harbor Bureau, Ministry of Land, Infrastructure, Transport and Tourism, Japan

Table 1: Introduction of automatized terminal operation in the global top 20 ports

2.2 Recent challenges for ICT application at ports

In 2011, the government of Germany launched a new ICT policy, Industry 4.0, which aims at introducing automation and data exchange in manufacturing technologies. It focuses on digitization and interconnection of industries, value chains and business models, which are all likely depend on the recent development of ICTs including cyber-physical systems, Internet of things (IoT), cloud computing and cognitive computing. (EU, 2017) An artificial intelligence (AI) based on deep learning programming, accurate sensor technology and big data is also rapidly attracting a big attention of the world business community. In line with these recent trends, the global port community is gradually going to step in the more ICT based and client oriented port operation and management.

An example of the ICT driven operation and management in the port sub-sector may be the smart-PORT logistics (SPL) concept initiated by the port of Hamburg, Germany, which includes IT based traffic management system and real time information transmission on the port traffic and infrastructure situation along with the demand-oriented networking via a central public cloud. While the services have

been just started after several years pilot phase, the SPL is considered a pioneer to pave the way of dramatically changing the future port operation scene.

It has become a common business environment for shipping lines, terminal operators, shipping agencies, forwarders and other port service entities to be connect each other for providing more efficient and speedy port logistics services and trade processing. Challenges were mainly undertaken by shipping lines, among which Nippon Yusen Co. Ltd., for example, has initiated to build up new ship operation and management information system by connecting ship navigation and landside arrangement information through IoT technique. These challenges strongly request port administration offices, terminal operators and other port logistics service providers to prepare integrated and seamless data and information exchange and processing system for more smoothly sharing shipside information among port business colony with less cost and time consuming manners.

Considering the above mentioned global trend of creating more smart and competitive port operation and management, the government of Japan have decided to launch, as a part of its recent port policy reforms, a new ICT based port concept, namely "AI terminal initiatives", for improving port operation productivity and port traffic traceability through employing AI for port terminal operation system configuration. The new terminal system is expected to enable AI independently to operate container yard cranes for minimizing crane movements. AI controlled terminal operation system is also expected to manage container dray traffic at port for realizing quick container check-in and release.

3. POSSIBLE ICT-DRIVEN PORT MANAGEMENT AND OPERATION

3.1 Port traffic and big data generation

Daily operations of port terminals involve a variety of administration, management and business oriented information in association with ship accommodation, trade processing, cargo handling, storage and delivery, taxation, quarantine clearance, port facility management, border control and cargo dray. The information is essential for daily port logistics activities, therefore, are generated day and night at port, and transmitted from/to port. Figure 1 schematically illustrates, by showing an example of container importation, the system of port logistics administration and business flow, which generates a variety of related data and information.

When container ship arrives at port, the ship and maritime information are transmitted to the port authority, CIQ offices, container terminal operator and marine service providers by ship itself or through shipping agent for their processing ship arrival and departure, customs clearance, quarantine inspection, and other commodity importation and delivery related procedures. In modern ports, shipping lines, port authority and terminal operators are generally equipped information and data processing systems for implementing these procedures. These systems are, however, not necessary well linked each other. Some of data and information are automatically duplicated and transmitted, but many are still to be manually fed and transmitted among these systems for storing and processing. Furthermore, the parties involved are not always cooperative to mutually being connected, because of their own tradition, practices and business secret. As such, there are long continued many difficulties to develop a common architecture to share business data and information among the port business colony.

On the other hand, modern container terminals are mostly under tough port competition, therefore, the terminal operators are normally keen on improving terminal competitiveness including berth window efficiency, and terminal yard and dray productivities. Reducing terminal lead time and check-in gate waiting time is also big concerns extended by consignees. Border control for preventing terrorism and intrusion of alien species is among basic requirements in the modern port terminals.

The above mentioned policy agenda for creating more effective, efficient and secured terminal may be common issues in modern ports, thus needs to be addressed accordingly. In this context, building

properly designed data and information exchange and processing platform is considered of a great importance for all port terminals to survive the global container port competitions.

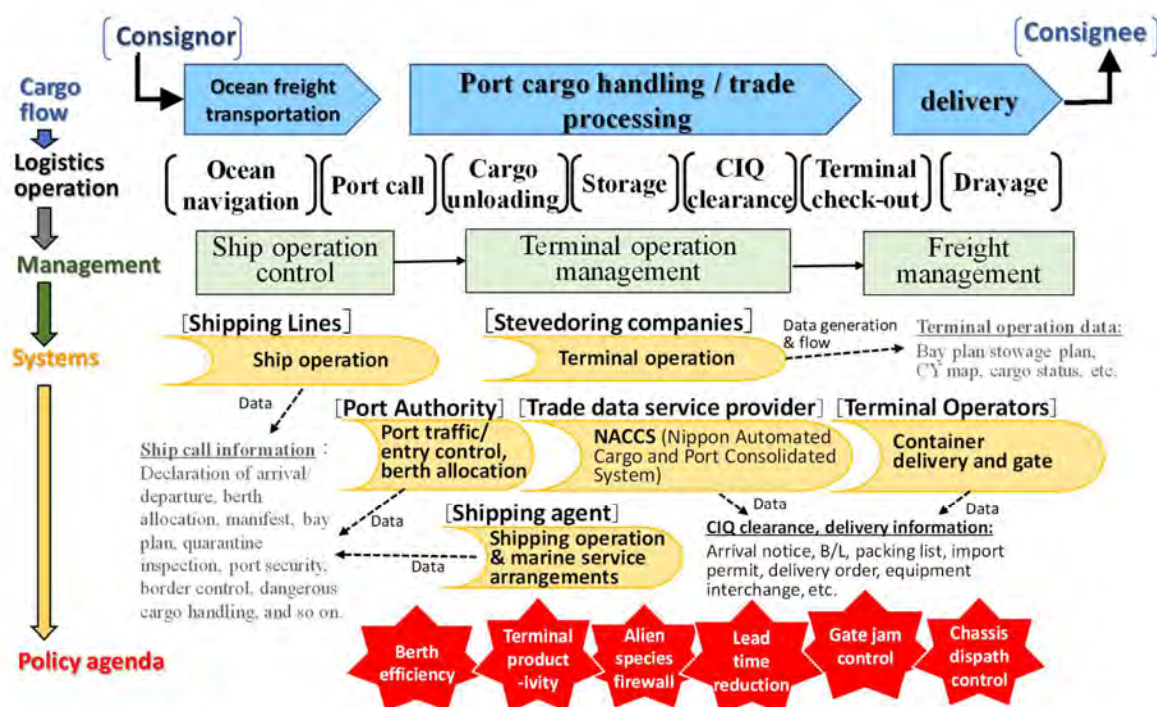


Figure 1: Typical port procedures, and involved data and information processing (An example of import containers)

3.2 Possible solutions for the port policy issues by adopting cutting-edge ICTs

Among key elements for building the data and information exchange and processing platform as referred in Section 3.1, big data is rapidly attracting an attention of port and shipping sub-sector community. Big data is defined as data set with a size beyond the ability of commonly used software tools to capture, curate, manage, and process within a tolerable elapsed time. (Snijders et al., 2012) An appearance of AI supported by deep learning programming has dramatically increased a significance of big data. Now big data is strongly believed to have an unlimited potential as a gold mine of AI driven economic and social developments.

Introducing IoT techniques into container terminal operations enables port terminal operators and other port related entities to collect, process and store a bulky digitalized data from daily terminal operations on 24 hours and 365 days per year basis without no terminal staff intervention. Rapidly improving sensor technologies, in combination with IoT, are another development for creating port big data in an effective and efficient manner.

Artificial Intelligence (AI) is also expected to become a newly emerging player of port operation and management. AI will learn port operation skills and practices by analyzing the big data. Deep learning is a recently highlighted programming technique for realizing more efficient and effective AI controlled operation and management capacity, which will assist the terminal staff in all over daily operations and management works. For example, AI will provide terminal planners with an indicative optimum solution and best practices including best stowage and yard plans for assisting prompt decision making based

on the past experiences included in the big data. It may enable terminal operators to undertake quick control and processing of container cargo traffic in the fully automatized container terminal yard.

Table 2 identifies possible innovations in the area of port operation by mobilizing cutting-edge ICT. Targeted terminal operation innovations and results of ICT applications are discussed and summarized. Challenges currently being and to be undertaken by the Japanese ports are also shown on the table.

As a sensor technology for generating port big data, image analysis techniques, global positioning system (GPS) and automatic identification system of ships (AIS) are identified as well as traditional electric and mechanical sensor systems. Progress in these sensor technology is considered an epoch making event for facilitating recently observed rapid development of port business data digitalization.

| Cutting edge ICT | | Terminal operation Innovation | ICT Applications | Current challenges |
|--|----------------|---|--|--|
| Sensor tech-nology | Image analysis | Digitalizing all data and information generated by movements of things and persons within terminals. | <ul style="list-style-type: none"> • Generating cargo status digital data based on motion picture and still image of the yard operation scene. • Identification of freak incident in container yard through monitoring camera. • Monitoring gate check-in queue | <ul style="list-style-type: none"> ➢ Automatic detection of container and vehicle identification numbers. ➢ Automatic container damage check. |
| | GPS /AIS | | <ul style="list-style-type: none"> • Monitoring port traffic, ship arrivals, berth window situation, location and traffic lines of cranes and yard chesses . | <ul style="list-style-type: none"> ➢ Berth window control based on AIS data. |
| | Others | | <ul style="list-style-type: none"> • Detecting alien species in container. (odor sensor, thermal sensor, etc.) | N.A |
| IoT | | Automatically collecting, storing and shearing digital data of generated, input or transferred in terminals without any manual control. (Port Big Data) | <ul style="list-style-type: none"> • Creating Port Big Data by automatically collecting: i) ship data, terminal operation data, trade data and CIQ clearance data, and ii) digital data and image data generated by sensors equipped in terminal. | <ul style="list-style-type: none"> ➢ Quay crane data collection through IoT for mobilizing to undertake facility maintenance and life cycle management. ➢ Delivery of check-in waiting time and cargo clearance information. |
| AI | | Implementing highly complex analysis and decision making based on the port Big Data. | <ul style="list-style-type: none"> • Automatically applying CIQ clearances, documenting delivery order, and informing cargo status at port. • Assisting in: i) controlling cranes, ii) preparing optimal stowage and bay plans, and iii) managing berth window. • Controlling automatic operation of yard cranes, including safety management. • Predicting container release time and check-in waiting times. | <ul style="list-style-type: none"> ➢ AI driven yard crane semi-automatic remote control operation. ➢ Preparation of optimal stowage plan for minimizing container yard marshalling works. |
| Automatic Vehicle operation technique. | | Undersupply of port workers incl. crane operator and truck driver. | <ul style="list-style-type: none"> • Vehicle platooning for container delivery. | N.A |

Table 2: Possible innovations of port operation by mobilizing cutting-edge ICTs

3.3 Examples of big data application at port: AIS data

As stated in this paper, generating big data is probably one of the most important elements of AI controlled port operation and management. Then, what does the big data in ports look like? The authors consider that AIS (Automated Identification System) may provide one of most up-dated examples of viable big data application in the area of port and navigation canal planning, design, operation and management, thus demonstrate it in this section.

AIS is an automatic tracking system used on ships. AIS was initially introduced to improve navigation safety, and to increase search and rescue capacity for ships. AIS integrates a standardized VHF transceiver with a GPS positioning system, with other electronic navigation sensors such as a gyrocompass or rate of turn indicator. AIS equipped ships can be tracked by AIS base stations located along coast lines or, when out of range of terrestrial networks, through satellites. The International Maritime Organization's International Convention for the Safety of Life at Sea (IMO SOLAS Convention) requires AIS to be equipped for international navigation ships with 300 or more gross tonnage, and all passenger ships regardless of the size.

While AIS information including unique identification, position, course, and speed of ships originally intends to assist the watch standing officers in avoiding ship collision, it is recently found useful for maritime authorities and port operators to track and monitor ship movements, and to identify suspicious ships.

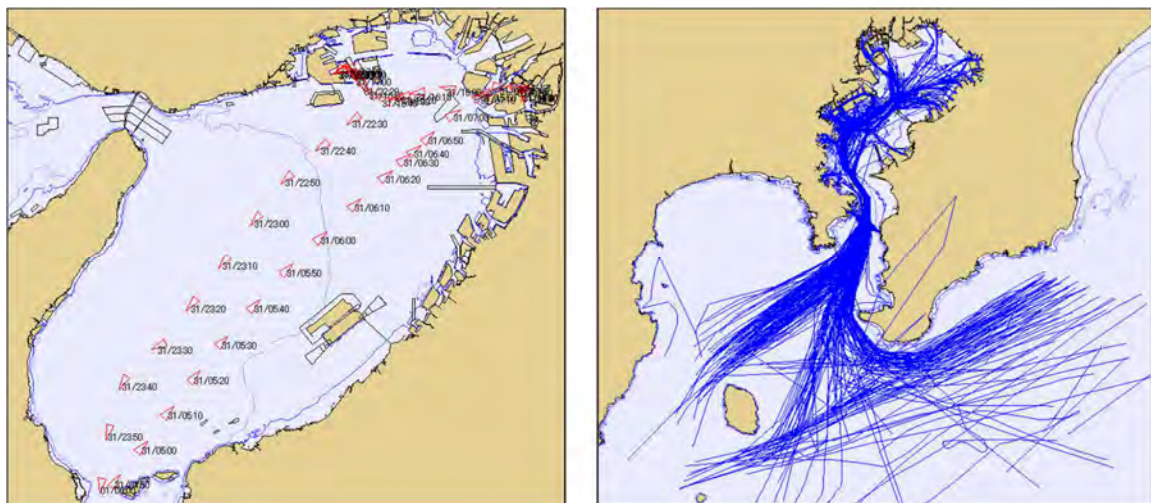


Figure 2: Track chart created based on AIS data

A figure in the left-hand side shows a ship track which entered ports of Osaka and Kobe. At 4: 50 in the early morning, the ship passed the mouth of Osaka bay and it arrived at offshore Osaka port at 7:00. In the afternoon of the day, the ship transferred to the port of Kobe and departed the port at 22:00 at night. By superimposing these track charts of ships, the right figure visualizes navigation situation in Tokyo Bay, where intensive traffic control is essential for ship security and navigation safety, and maintaining port logistics capability. (Takahashi et al., 2007)

Figure 3 demonstrates possible visualization of ship turnaround and berthing at Hirara ports, Okinawa, Japan. The figure provides information of detailed ship movement in the port waters therefore, port engineers, for instance, can easily identify an actually used water area by the ship.

In the quay side, AIS based data identifies an exact location of GPS antenna which shows location of ship berthing. As such, AIS-based big data is currently being expected to assist in more detailed and

sophisticated planning and designing works. AIS data also enables us to visualize an actual berth window situation as a chart shown in Figure 4.

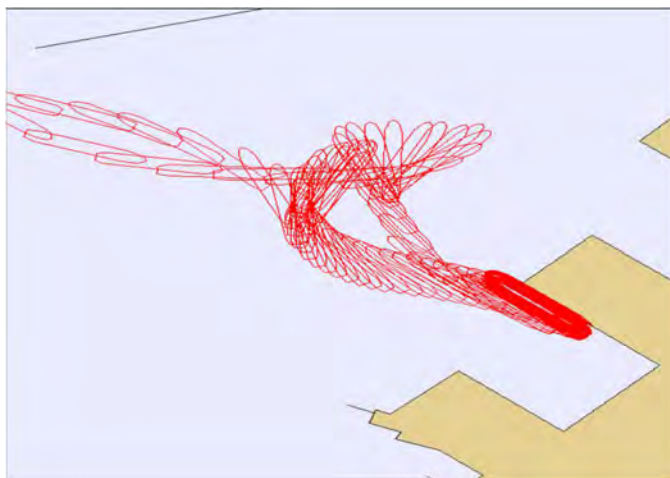
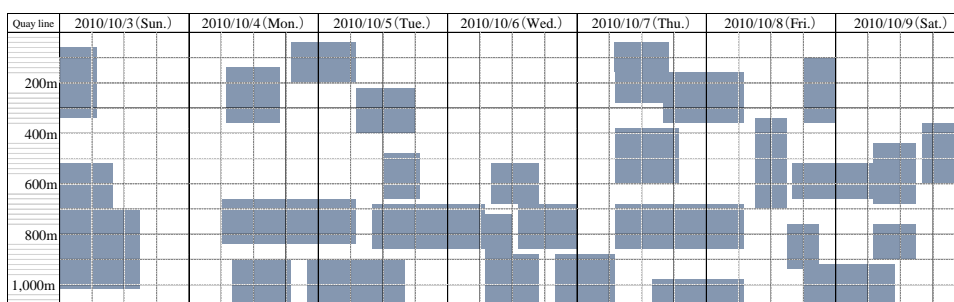
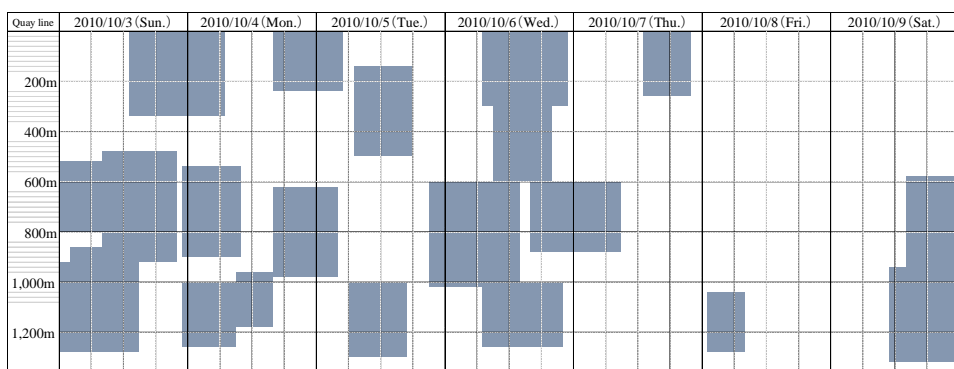


Figure 3: Visualization of ship turnaround and berthing

Figure 4 visualizes berth windows of Dream Island International Container Terminal (DICT), Osaka, Japan and Kwai Chung CT 8 (CT8), Hong Kong, China. Terrestrial AIS data of one week period from 3th to 9th October 2010 was used by Akakura et al. (2012) for preparing the berth window charts. DICT has a quay length of 1,100 meters and annual throughput of about 2 million TEUs, and CT 8; 1380 meters and 4 million TEUs.



Dream Island International Container Terminal, Osaka, Japan (Oct. 3-9, 2010)



Kwai Chung CT 8, Hong Kong, China (Oct. 3-9, 2010)

Figure 4: Berth window charts drawn based on AIS data

Berth window chart looks like a table with time line in the horizontal axis and occupied quay line in the vertical axis. Occupied berth window is defined as product of occupied quay length and occupied time period by ships, which is shown in the chart in figure 4 as light gray areas. It is noted that DICT has a space for accommodating more ships on Wednesday, and CT8; from Thursday afternoon to Saturday morning. Controlling berth windows may be one of the most important operations for the port terminals to increase in berth utilization, therefore, to obtain more incomes. Visualizing berth window charts may become a powerful tool for terminal operators to improve berth widow productivity.

4. AI PORT CHALLENGES

4.1 Possible system configuration

As discussed in Section 3.2, the ICT based management and operation system at ports are considered notably promising to provide with attractive solutions for the currently requested port policy agenda. There are many possibilities to dramatically increase terminal operation efficiency and competitiveness, contribute to the global logistics innovation, and improve business profitability and working environment at ports. AI will play a key role for the overall port operation and management through accurate and tireless data processing and analysis, self-sustained judgments and recommendations, and appropriate communications. Figure 5 illustrates a schematic view of AI-led terminal operation and management system.

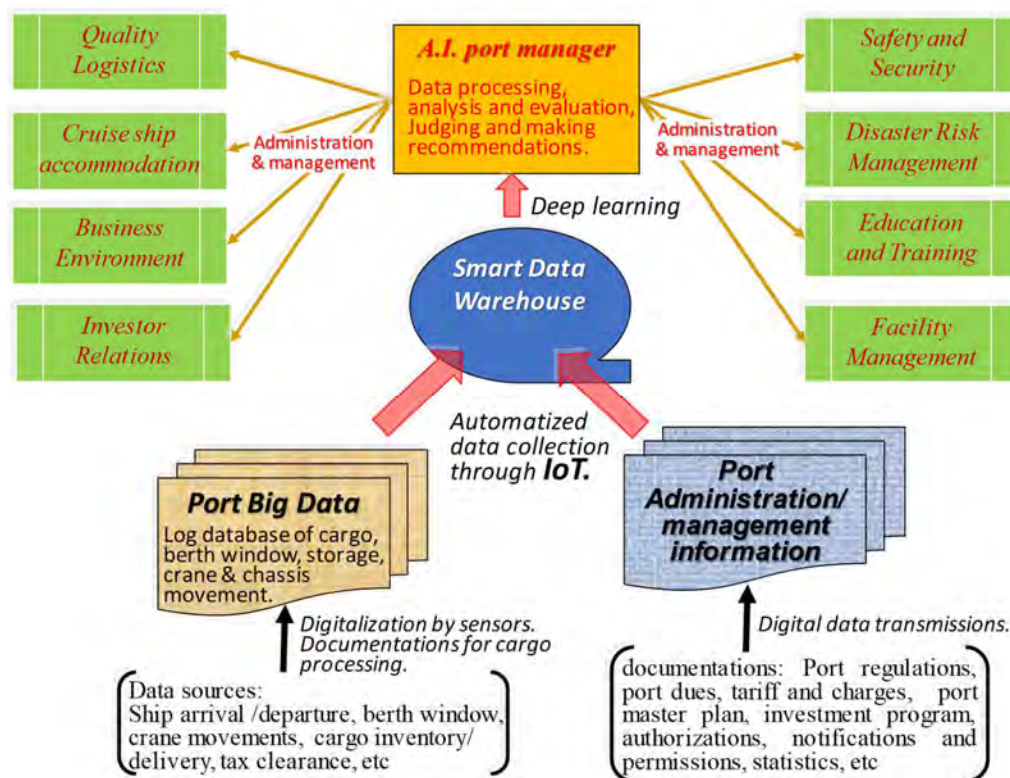


Figure 5: Basic configuration of AI-led port system

For cultivating terminal operation and management AI by mobilizing deep learning programming technique, big data creation is an essential and vital challenges.

As discussed in Section 3.1, possible sources of port big data should be a daily port operations and management procedures such as ship operation, port traffic control, terminal operation, cargo storage/delivery, and check-in/out gate control. From these procedures and operations, a bulky data is generated in terms of arrived ship specifications, arrival and departure details, berth window situation, quay and yard crane movements, cargo location and inventory, consignee/consigner information, delivery time and final destination, tax clearance status, quarantine inspection, safety, security and environment protection information, and any other notifications, authorizations and permissions. Some of these data and information are transmitted from outside port, and others are directly typed in or digitalized through sensors embedded in the terminal facilities and equipment. Smart data warehouse have a function of collecting and storing these data and information in a fully digitalized form. As such, properly employing IoT coupled with sensor technologies will be a key skill for automatically digitalize, glean, process and store the bulky port operation related information, which is generated from daily port activities in 24 hours and 365 days basis.

Another important information sources for AI as a port manager may be port statistics and administration and management related documentations which include rules and regulations, port dues, tariff and charges, port master plan and investment program, and authorizations, notifications and permissions of port traffic. Availability of these information directly affect to the quality of port business practice and environment, thus, profitability of the port. In this context, the information must be also digitalized and stored in the data warehouse for contribution of AI to support port administration, operations and businesses.

4.2 Challenges

The above mentioned AI led port operations and management are still on the way of technical development and institutional arrangement.

Major challenges however may include: i) smooth introduction of the newest sensor technologies for efficiently and effectively collecting all terminal operation related information as digitalized data, ii) materializing an accurate big data transmission between on-site sensors and the terminal control host computer through IoT channels, iii) developing man-machine interface for assisting operator's prompt decision making, iv) renovating current terminal operating system by employing AI based architecture, and v) introducing appropriate countermeasures against computer virus and hacking. A variety of deep learning software including many open software is currently available. Mobilizing these existing software resources may save the project time and cost, and enable to input more human and financial resources for developing AI loaded terminal operation system. Most advanced sensor technologies such as image processing techniques also may contribute, as eyes of AI, to the system development.

Legal and social aspects of current port systems will be also requested to make necessary adjustment for adopting these ICT-led port operation and management reforms. Particular issues to be address may include: i) increase in a vulnerability of port logistics in association with employing highly sophisticated ICT for port operation and management system, ii) ambiguity of legal responsibility for the third party liability at the AI controlled port, and iii) infringement of information ownership in association with creating big data. AI port manager may have a big operation and management capability much beyond human capacity, but is not the Omnipotent. Once AI port manager lose its function due to natural or human made disasters, it may not easy humanly to recover it. When AI port manager make a misjudgment or has a serious malfunction resulting in causing damages or violating rights of the third party, who supposedly will take a responsibility for it?

It must be carefully consider and discuss how is the best course to invite AI into our ports as a good partner. The port community are not always welcome to build a robot port. What needed in a practical viewpoint may be how to create a well-designed human-AI collaborative system for making our port operation and management smart. AI controlled terminal may be a common business interest of the port community and also a common challenge, therefore to be discussed globally. Some of the cutting edge technologies are just waiting for the application at ports.

5. CONCLUSIONS

This paper was prepared for inviting an attention of conference attendees to the recently developed cutting-edge ICT, in particular artificial intelligence (AI), Internet of things (IoT) and big data at ports, in the context of possible application to the port operation and management.

Considering continuously intensifying international port competition and recent diversification of port uses, global mainstream ports have started their consideration of further involvement of cutting-edge ICT into the port operation and management. Remarkable development of sensor technologies, coupled with IoT, has been enabling us to create a big data at port, which may lead to employment of AI at port. Actually some of global ports have already been tackling to introduce AI, IoT and big data into their ports. On the other hand, inviting cutting-edge ICT to the ports may raise many issues and new challenges from technological, legal and social aspects. In this context, starting discussion about this emerging agenda, and sharing data and information among PIANC community will surely benefit not only the conference attendees but also the whole member port community as well. The authors are pleased to have this opportunity of 34th PIANC world Conference to raise this hot topic for our PIANC colleagues.

References

Akakura, Y.; Andou, K. (2012). Analysis of berth occupancy rate of world container terminals by the development of berth window with using AIS data. *Journal of Japan Society of Civil Engineers B3 (Ocean Engineering)*. Vol.68, No.2, 1_1175-1180, 2012 (*in Japanese*)

EC (2017). Digital Transmission monitor, Germany: Industrie 4.0, Directorate-General Internal Market, Industry, Entrepreneurship and SMEs. European Commission. January 2017.

Snijders, C.; Matzat, U.; Reips, U. (2012). 'Big Data': Big gaps of knowledge in the field of Internet, *International Journal of Internet Science*, 2012, 7(1), 1–5.

Takahashi, H.; Goto, K. (2007). Study on inflection to the port and harbour development by AIS data. Technical Note of National Institute for Land and Infrastructure Management. No. 420 (*in Japanese*)

EXPERIMENTAL STUDY OF TSUNAMI-INDUCED FORCES ON ONSHORE SEAWALLS

by

Naoki Furuichi¹, Y. Ohmura², H. Yagi³, A. Nakayama⁴, M. Yoneyama⁵, H. Kato⁶, and A. Kado⁷

ABSTRACT

Several “onshore” seawalls, built behind the fishing ports to protect villages, collapsed because of the tsunami that immediately followed the Great East Japan Earthquake on March 11, 2011. As seawalls collapsed frequently regardless of the scouring due to tsunami overflow, we reconsidered the methods of calculating tsunami-induced hydrodynamic forces. In this study, we conducted hydraulic model experiments to evaluate tsunami-induced forces acting on onshore seawalls under non-overflow and overflow conditions. On the basis of the obtained results, we proposed formulae to calculate the tsunami-induced forces under the non-overflow condition using 1) the hydrostatic pressure relation and a correction factor of 1.1, and 2) using a quadratic function of the Froude number. Under the overflow condition, we proposed a calculation formula using the inundation depths in front of and behind the seawalls.

1. INTRODUCTION

The Great East Japan Earthquake (magnitude 9.0) and the resulting tsunami on March 11, 2011 caused serious damage to the fishing ports and villages of Japan. It is believed that the external forces that acted on the fishing port facilities far surpassed the conventional design requirements.

Field surveys, conducted after the earthquake, reported that several “onshore” seawalls, built behind the fishing ports to protect the villages, collapsed because of the tsunami (**Figures 1 and 2** show the examples of disaster areas and seawalls). Although the major reason for the collapse was scouring due to tsunami overflow, seawalls collapsing without any scouring were also frequently reported. On the other hand, in the conventional design methods, tsunami-induced forces are often calculated based on the hydrostatic pressure profile corresponding to the inundation depth of a tsunami (e.g., Japan Society of Civil Engineers 2004). In other words, partly because the period of a tsunami is significantly greater than that of wind waves, the conventional methods only considered the water level effect, but seldom considered the effect of dynamic pressure (movement of water).

Although recent studies have examined the wave forces acting on breakwaters, onshore structures, and bridge superstructures (Tanimoto et al. 1984, Asakura et al. 2000, 2002, Nakamura et al. 2016) and the characteristics of tsunami’s inundation after the earthquake (Adriano et al. 2016), the effects of the slope of the bottom topography, the slope of the seawall structure, and the distance of the structure from the shoreline were not fully understood. Furthermore, few studies have investigated the wave-force characteristics of onshore structures under tsunami overflow conditions; in particular, the characteristics of wave forces acting on the landward side of a seawall are poorly understood. Hence, we modified the methods of calculating the tsunami-induced forces acting on seawalls.

1 National Research Institute of Fisheries Engineering, Japan Fisheries Research and Education Agency, Japan, furu1naoki@affrc.go.jp

2 National Research Institute of Fisheries Engineering, Japan Fisheries Research and Education Agency, Japan

3 National Defense Academy, Japan

4 National Research Institute of Fisheries Engineering, Japan Fisheries Research and Education Agency, Japan. Currently, Alpha Hydraulic Engineering Consultants, Co. LTD, Japan

5 Reconstruction Agency, Japan

6 The Japanese Institute of Fisheries Infrastructure and Communities, Japan

7 International Meteorological & Oceanographic Consultants Co. Ltd., Japan



Figure 1: (a) A cross-sectional view of tsunami-affected seawall, (b) Example of seawall position (black-colored line). The red-colored line indicates the position of tsunami-affected seawall whose construction is similar to (a), and (c) Aerial photograph of the red-colored box area in (b). The arrow indicates a tsunami-affected area. (From the website of National Research Institute of Fisheries Engineering, Japan)



Figure 2: Images of tsunami-affected seawalls confirmed in the red-colored box area in Figure 1(b). (From the website of National Research Institute of Fisheries Engineering, Japan)

Recently, we conducted hydraulic model experiments to evaluate the tsunami-induced forces acting on onshore seawalls by changing the conditions of the slope of the bottom topography, the slope of the seawall structure, and the distance of the seawall from the shoreline (Ohmura et al. 2014, 2015). Based on the results obtained, we explored the methods of calculating the wave forces under non-overflow and overflow conditions with special attention on comparing the measured wave pressure to that predicted using the hydrostatic pressure relation. In this paper, we introduce the main results of the previous papers.

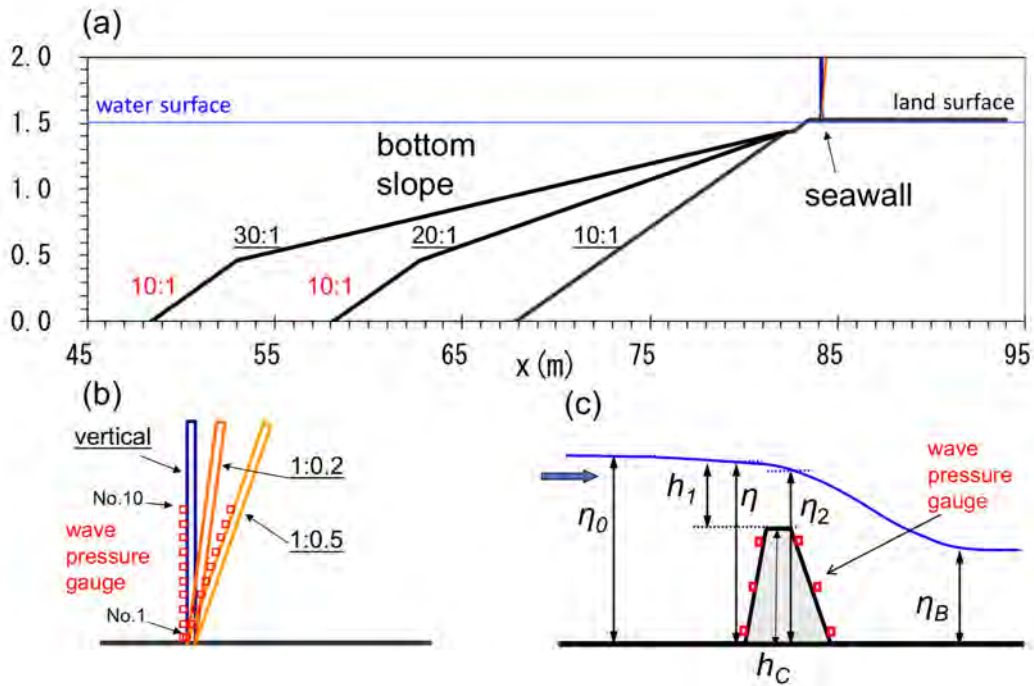


Figure 3: (a) Sketch of wave flume layout, (b) Position of wave pressure gauge for the non-overflow cases, and (c) Position of wave pressure gauge for the overflow cases.

2. HYDRAULIC MODEL EXPERIMENTS

Figure 3 and Tables 1 and 2 summarize the overview of the present experiment. The experiments were performed in a wave flume (100 m in length, 2 m in height, and 1 m in width) on a scale of 1/81. Beginning at the wavemaker, the bathymetry consisted of a 47–68 m flat-ocean bottom section, a 17–38 m slope section, and a 15-m flat-land surface section. We installed three types of bottom slopes with ratios of 30:1, 20:1, and 10:1. The seawall was positioned at the point where the distance from the shoreline (x) is in the range of 0–150 m (unless otherwise stated, the experimental parameters mentioned herein are described according to the corresponding local scale). The seawall height was set such that it satisfactorily exceeded the tsunami inundation depth for the non-overflow conditions (Figure 3(b)). Moreover, it was set in the range of 4.6–8.3 m for the overflow conditions (Figure 3(c)). The shoreward slopes of the seawall were set to 1:0 (vertical), 1:0.2, and 1:0.5, whereas the landward slope was set to 1:0.5.

| (a) Non-overflow condition | | | (b) Overflow condition | | | |
|----------------------------|---------------------------------------|-------------------------------------|------------------------|---------------------------------------|------------------------------|-------------------------------------|
| Bottom slope | Distance from shoreline (local scale) | Shoreward slope of seawall | Bottom slope | Distance from shoreline (local scale) | Seawall height (local scale) | Shoreward slope of seawall |
| (s_B) | (x) | (s_W) | (s_B) | (x) | (h_c) | (s_W) |
| 30:1 20:1 10:1 | 0 m | vertical (1:0) 1:0.2 1:0.5 | 30:1 20:1 10:1 | 0 m | 4.6 m | vertical (1:0) 1:0.2 1:0.5 |
| | 25 m | | | 6.4 m | | |
| | 50 m | | | 8.3 m | | |
| | 75 m | | | | | |
| | 100 m | | | | | |
| | 150 m | | | | | |

Table 1: Experimental conditions of present study. The values for the distance from the shore line (x) and the seawall height (h_c) are described according to the corresponding local scale.

| No. | Offshore wave height | Wave period ($T/2$) |
|-----|----------------------|----------------------------|
| 1 | 8.1 cm (6.6 m) | 12.5 s (half period 113 s) |
| 2 | 6.7 cm (5.4 m) | 15.0 s (half period 135 s) |
| 3 | 5.0 cm (4.1 m) | 20.0 s (half period 180 s) |

Table 2: Experimental parameters of incident waves. The values based on the corresponding local scale are shown in brackets.

Using forward paddle movement, the tsunami was modeled as an idealized solitary wave with half-periods of 113, 135, and 180 s, corresponding to offshore wave heights of 6.6, 5.4, and 4.1 m, respectively (**Table 2**). In addition, we performed experiments considering the tsunami inundation without the seawall model. The local free surface elevation was measured using wave height gauges with a sampling interval of 50 Hz at locations including the offshore of the shoreline, mid-point between the shoreline and the seawalls, and just in front of the seawall for non-overflow cases. For the overflow cases, the height behind the seawalls was also measured (e.g., η_B in **Figure 3(c)**). The pressure was measured using 6 to 10 wave pressure gauges with a sampling interval of 1000 Hz at different locations on the seawalls (**Figures 3(b) and (c)**). For the wave pressure, we used 10-Hz moving averaged data in later analyses.

3. RESULTS AND DISCUSSIONS

3.1 Overview of freely propagating tsunami flow

Prior to discussing the wave pressure acting on the seawalls, we first examined the characteristics of freely propagating tsunami flow (e.g., see the dashed line in **Figure 4(a)**) reproduced by conducting non-seawall experiments. **Figures 5(a) and (b)** show the distributions of the maximum inundation depth of the freely propagating tsunami (η_{max}) at each point and of the near-bed horizontal velocity (U) measured 0.01 m above the land surface (laboratory scale) when η_{max} was measured.

Figure 5(a) shows that the inundation depth (η_{max}) reached up to ~ 8.1 m at shoreline ($x = 0$). Along with an increase in the distance from the shoreline (x), a decrease in η_{max} and an increase in U were confirmed. Consequently, the Froude number (Fr) calculated using

$$Fr = \frac{U}{\sqrt{g\eta_{max}}} \quad (1)$$

(where g is the acceleration due to gravity) also increased with the increase in the distance from the shoreline (**Figure 5(c)**). Note that the horizontal axis in **Figure 5(c)** indicates the ratio of x to the offshore wave length (L), which is determined as follows.

$$L = \sqrt{gh} \times T \quad (2)$$

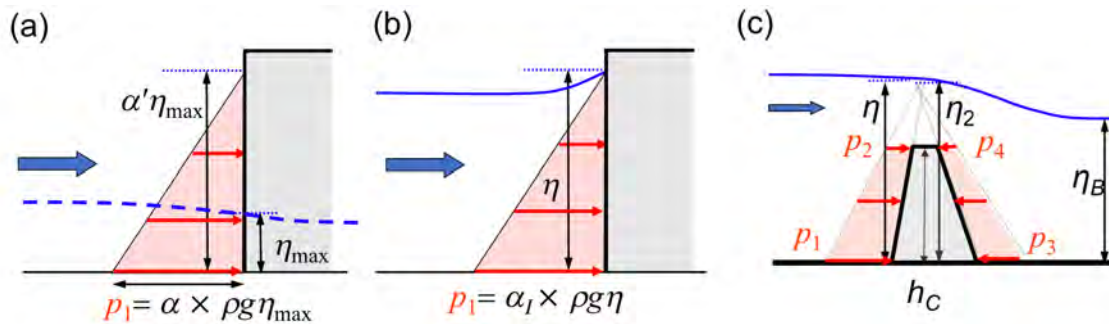


Figure 4: (a) Schematic view of tsunami-induced forces under non-overflow conditions where η_{max} is referred, (b) non-overflow conditions where η is referred, and (c) overflow conditions. The present study assumed that the wave pressure increases linearly in the downward direction.

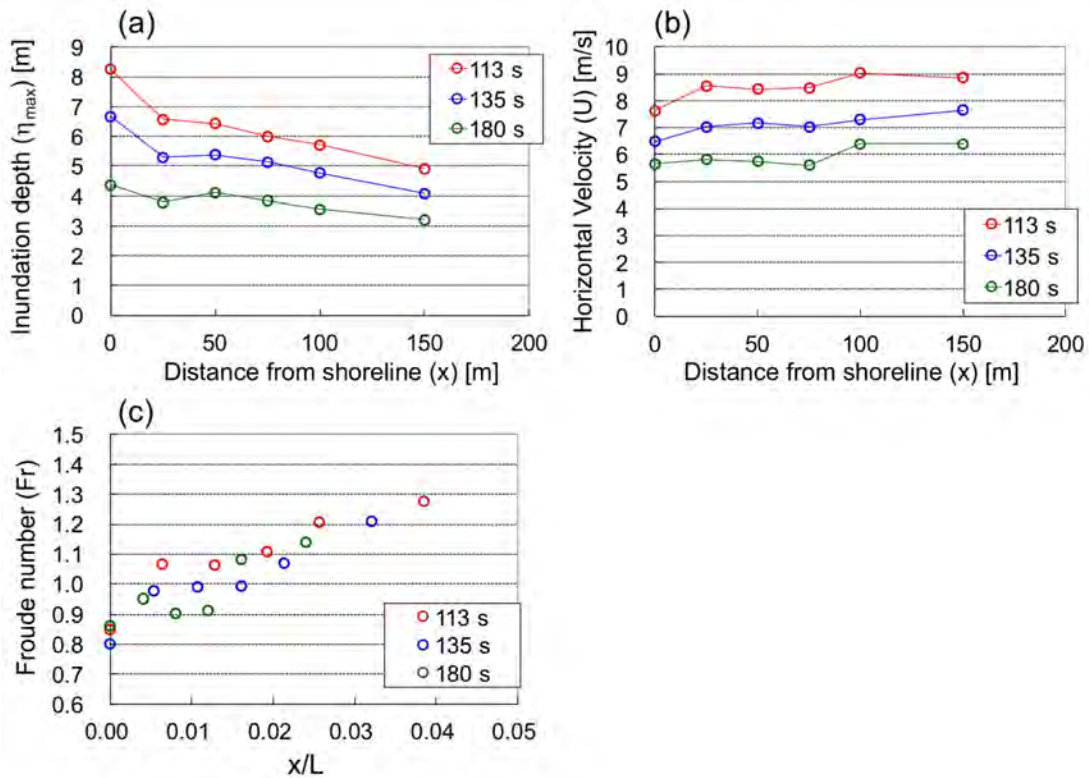


Figure 5: (a) Distribution of η_{max} , (b) horizontal velocity (U), and (c) corresponding Froude number (Fr). The red, blue, and green colors denote wave periods of 113 s, 135 s, and 180 s, respectively.

where h (≈ 121 m; local scale) is the offshore water depth. The ranges of x/L and Fr in the present experiment were $0 < x/L < 0.04$ and $0.8 < Fr < 1.3$, respectively.

3.2 Non-overflow cases

3.2.1 Results

Figure 6 shows a laboratory image for the non-overflow cases as well as the time series of the wave pressure and inundation depth in front of the seawall (η , see Figure 4(b)). As indicated by the red arrow

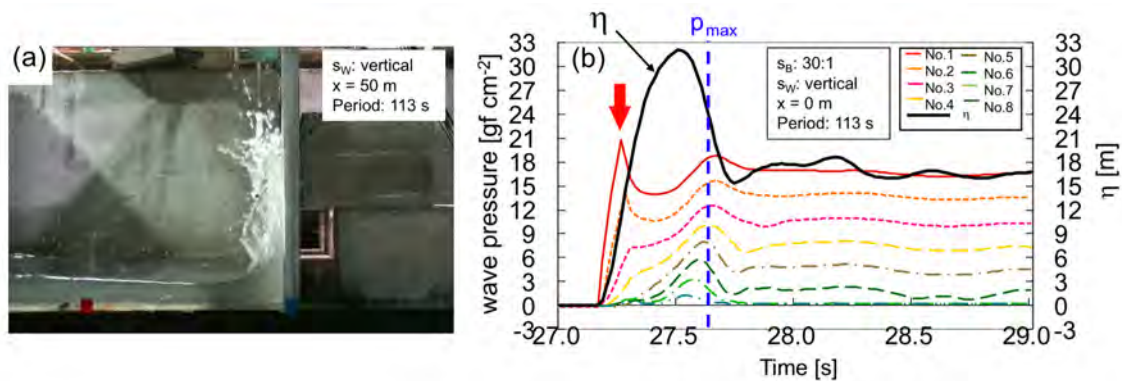


Figure 6: (a) Laboratory image of non-overflow tsunami action, and (b) Sample time series of wave pressure and inundation depth (η). The vertical blue line indicates the time when p_{max} is measured.

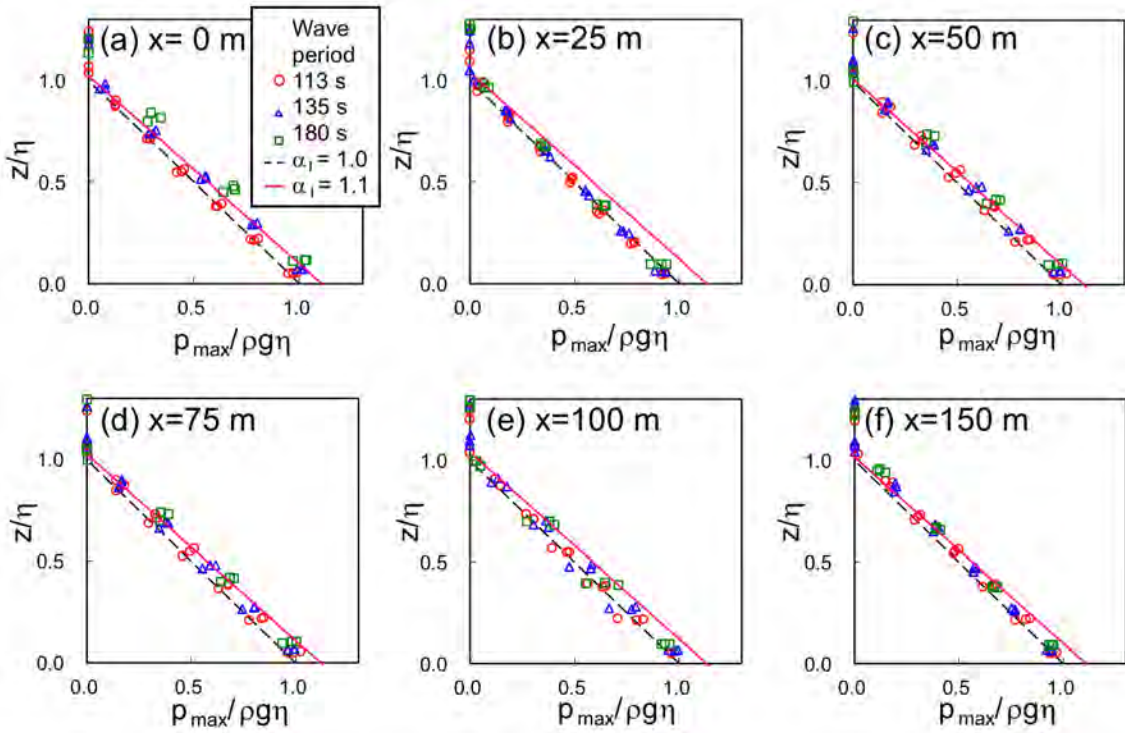


Figure 7: Comparison of vertical profiles of $p_{max}/\rho g \eta$ (symbols) classified in terms of the distance from the shoreline (x) (a to f) and the wave period (red, blue, and green symbols); and those of the corresponding hydrostatic pressure ($p_{max} = \alpha \times \rho g \eta$). The red and black lines represent $\alpha = 1.1$ and $\alpha = 1.0$, respectively.

in Figure 6(b), a local maximum of the wave pressure is confirmed in the case with a wave period of 113 s before η becomes maximum (black line in Figure 6(b)). On the other hand, the maximum vertically integrated wave pressure (i.e., the wave force) is measured after η becomes maximum (vertical blue line). In this study, we analyzed the experimental results by focusing on the vertical profiles of the “maximum” wave pressure (p_{max}) when the corresponding wave force was maximum.

Figures 7 and 8 show the vertical profiles of the normalized wave pressure $p_{max}/\rho g \eta$ (where ρ is the density of water, and η is the value when p_{max} was measured). We found that $p_{max}/\rho g \eta$ was not

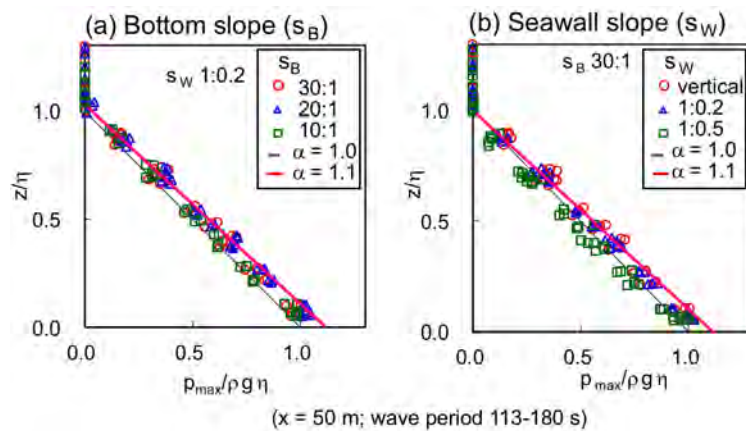


Figure 8: Comparison of vertical profiles of $p_{max}/\rho g \eta$ (symbols) classified in terms of (a) bottom slope s_B , and (b) s_W ; and those of the corresponding hydrostatic pressure ($p_{max} = \alpha \times \rho g \eta$) (lines). The red and black lines represent $\alpha = 1.1$ and $\alpha = 1.0$, respectively.

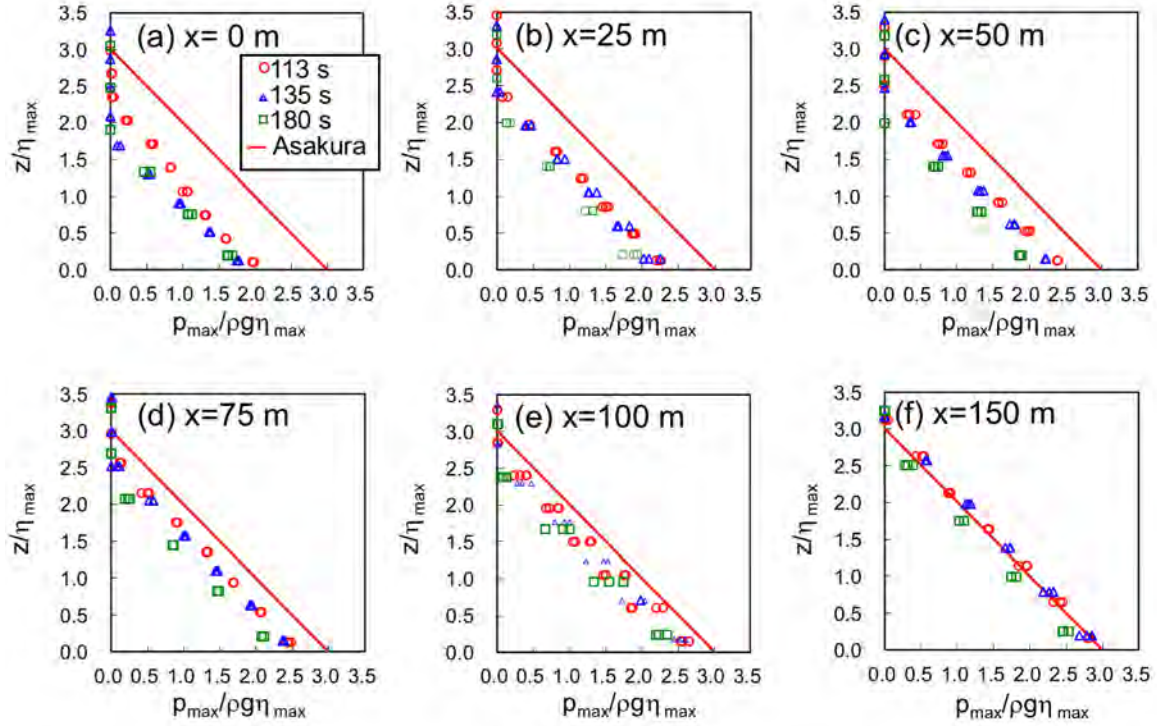


Figure 9: Comparison of vertical profiles of $p_{max}/\rho g \eta_{max}$ (red, blue, and green symbols) and those predicted by Asakura et al. (2000) (red line) classified in terms of the distance from the shoreline (x).

remarkably affected by the change in the slope of the bottom topography (s_B), the slope of the seawall (s_W), the period of the incident wave (T), or the distance of the seawall from the shoreline (x). Moreover, the value of $p_{max}/\rho g \eta_{max}$ increased roughly linearly in the downward direction, along with the red and black lines indicating the hydrostatic pressure relation. The ratio of $p_{max}/\rho g \eta_{max}$ to the normalized hydrostatic pressure z/η (where z is the height from the land surface) was largely in the range of 1.0–1.1.

As previous studies investigated the wave-force characteristics using η_{max} , (Tanimoto 1984, Asakura et al. 2000), we examined the vertical profile of $p_{max}/\rho g \eta_{max}$ (**Figure 9**), where η_{max} is the value when p_{max} was measured. The figure shows that $p_{max}/\rho g \eta_{max}$ increases with an increase in the distance from the shoreline (x), reaching the values proposed by Asakura et al. (2000) (red line in **Figure 9**).

$$p_{max} = \rho g (3 \times \eta_{max} - z) \quad (3)$$

As shown in **Figures 9(a)–(f)** and **Figures 10(a) and (b)**, the values of $p_{max}/\rho g \eta_{max}$ are not significantly affected by the changes in the wave period, bottom slope, or seawall slope. As indicated by previous studies on onshore structures (e.g., Afmad et al. 2009) and from **Figure 5(b)**, it is believed that the increase in p_{max} with the increase in the distance from the shoreline (x) is due to the change in the Froude number (Fr).

To evaluate the relationship between Fr and increase in p_{max} , we introduced a correction factor (α_{E1}) defined as follows.

$$\alpha_{E1} = 1 + \overline{\frac{p_{max}}{\rho g \eta_{max}} - \left(1 - \frac{z}{\eta_{max}}\right)} \quad (4)$$

where the overbar denotes the arithmetic mean for heights (z) $< \sim 15$ m (local scale) in each vertical profile, and the second term in the right-hand side indicates the difference in the measured normalized pressure at each point from the value predicted using the hydrostatic pressure relation.

Figure 10(c) shows the comparisons of Fr and α_{E1} for the non-overflow cases. Although the present results roughly agree with the linear relation proposed by Sakakiyama (2012) (blue line in **Figure 10(c)**), i.e.,

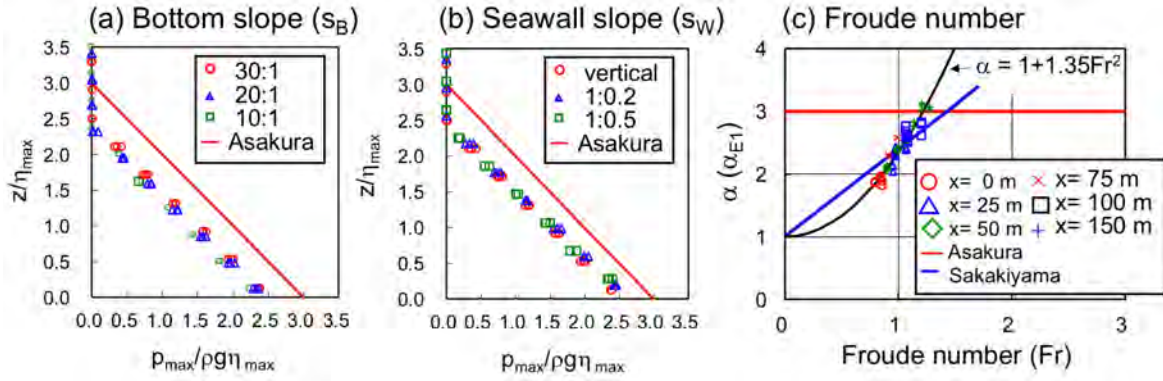


Figure 10: (a, b) Comparison of vertical profiles of $p_{max}/\rho g \eta_{max}$ classified in terms of (a) bottom slope (s_B), (b) seawall slope (s_W), and (c) Ratio of $p_{max}/\rho g \eta_{max}$ to z/η_{max} (α) as a function of the Froude number (Fr). The brown and blue lines indicate those predicted by Asakura et al. (2000) and Sakakiyama (2012), respectively.

$$\alpha = 1 + 1.4Fr, \quad (5)$$

we found that the results agree better with a quadratic relation (cf. Matsutomi et al. 2013) (black line in Figure 10(c)), i.e.,

$$\alpha = 1 + 1.35Fr^2 \quad (6)$$

in terms of the root-mean-square error.

3.2.2 Proposed formula

On the basis of the results obtained, we proposed formulae to calculate the tsunami-induced forces under the non-overflow condition to be used in the facility design, as shown below.

First, when the inundation depth in front of the seawall (η) is known, the pressure near the land surface (p_1 , Figure 4(b)) can be calculated as follows.

$$p_1 = \alpha_1 \times \rho g \eta, \quad \alpha_1 = 1.1 \quad (7)$$

It should be noted that we assumed that the wave pressure increases linearly in the downward direction. Furthermore, when the inundation depth of the freely propagating tsunami (η_{max}) and the corresponding Froude number (Fr) are known, the pressure (p_1) and the operative inundation depth ($\alpha' \eta_{max}$) (Figure 4(a)) can be calculated as follows.

$$p_1 = \alpha \times \rho g \eta_{max}, \quad \alpha' = \max(3, \alpha) \quad (8)$$

where α can be determined using (6). Note that we proposed the value of α' as the value that is greater between 3 and α in order to evaluate it as a safe-side value. It should also be noted that the present experiment covered only for $0.8 < Fr < 1.3$ (Figure 5(c)). However, considering the fact that Sakakiyama (2012) confirmed the available range of the proposed relation (4) for $0 < Fr < 2$, we assumed that (8) can be used when $0 < Fr < 1.5$. If Fr is unknown, the pressure (p_1) and the operative inundation depth ($\alpha' \eta_{max}$) can be calculated based on the study conducted by Tanimoto et al. (1984), i.e., using η_{max} at the shoreline ($x = 0$), with $\alpha = 2.2$, and $\alpha' = 3$.

3.3 Overflow cases

3.3.1 Results

Figure 11 shows the laboratory images for the overflow cases, where t is the time after the tsunami generation (laboratory scale). After the tip of the tsunami flow reached the front of the seawall, the flow rose significantly and subsequently splashed down behind the seawall. The tsunami-induced force, defined as the difference in the vertically integrated wave pressures between the front and rear of the seawall, became maximum after the water level increased (Figure 11(b), $t = 29.2$ s panel).

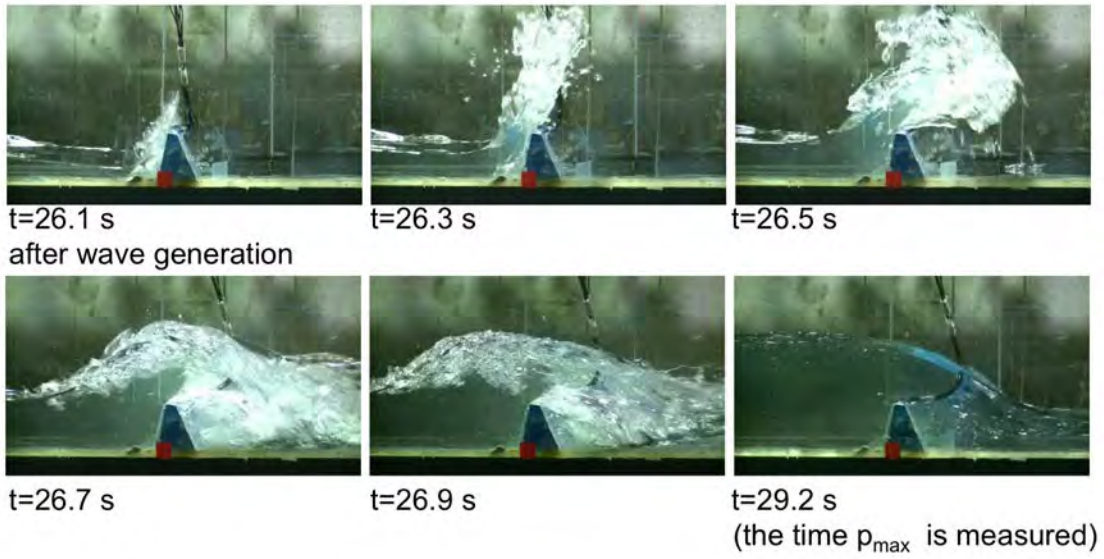


Figure 11: Laboratory images of overflow tsunami action (t indicates the time after wave generation).

Figure 12 compares the vertical profiles of $p_{max}/\rho g\eta$ on the shoreward side of the seawall, classified in terms of the slope of the bottom topography (s_B), distance from the shoreline (x), and the slope of the shoreward seawall (s_W), with those predicted by the hydrostatic pressure relation ($p_{max} = \alpha \times \rho g\eta$ with $\alpha = 1.0, 1.1, \text{ and } 1.2$). We found that $p_{max}/\rho g\eta$ was not considerably affected by the changes in the parameters, and the ratio of $p_{max}/\rho g\eta$ to the hydrostatic pressure was in the range of 1.0–1.2.

Figure 13(a) shows a scatterplot of h_d/η with respect to the correction factor (α_{E2}), defined in a manner similar to α_{E1} (4) as follows.

$$\alpha_{E2} = 1 + \frac{\overline{p_{max}}}{\rho g\eta} - \left(1 - \frac{z}{\eta}\right) \quad (9)$$

where the overbar denotes the arithmetic mean of the data at the three points on the shoreward slope (**Figure 3(c)**). As the magnitude of the overflow decreases (i.e., as h_d/η approached 1), α_{E2} approaches a value in the range of 1.0–1.1. This agreed with the results obtained under the non-overflow cases ((7), **Figure 7**).

However, it should be noted that the numerical simulation of tsunami inundation used for the facility design (in Japan) sometimes cannot efficiently reproduce the water-level variation just in front of the seawall, because of its coarse spatial resolution (e.g., 5 m). Hence, we examined the relationship between the inundation depth ~ 20 m shoreward of the seawall (η_0) (see **Figure 3(c)**) and the shoreward wave pressure. **Figure 13(b)** shows a scatterplot of h_d/η_0 with respect to the correction factor (α_{E3}) defined using η_0 in a manner similar to (9). In this case, the correction factor was ~ 1.1 at maximum, which agreed with the results obtained under the non-overflow cases. From the scatterplot of the magnitude of overflow (h_d/η) with respect to the ratio η_0/η (**Figure 13(c)**), the two water levels tended to be largely the same (i.e., $\eta_0 \sim \eta$), as h_d/η approaches 1 but significantly different ($\eta_0 > \eta$) when $h_d/\eta < 1$, which is consistent with the difference between **Figures 13(a)** and **(b)**.

Finally, we examined the relationship between the landward wave pressure and the water level just behind the seawall (η_2 , **Figure 3(c)**). Taking into account the possibility that the tsunami simulation used for the facility design cannot efficiently reproduce the corresponding water-level variation, the value of η_2 is determined from η using the Homma's formula, which was originally proposed for low overflow condition ($\eta_2 = 0.45h_1 + h_C$; see **Figure 3(c)**) (Homma 1940). **Figure 14(a)** shows a scatterplot of h_d/η_2 with respect to the correction factor (α_{E4}) (α_{E4} is defined in a manner similar to (9) using η_2). The correction factor for the landward wave pressure exceeded 0.4 for the high overflow cases ($h_d/\eta_2 < 0.8$), whereas it approached 0 for the low overflow cases ($0.8 < h_d/\eta_2 < 1$).

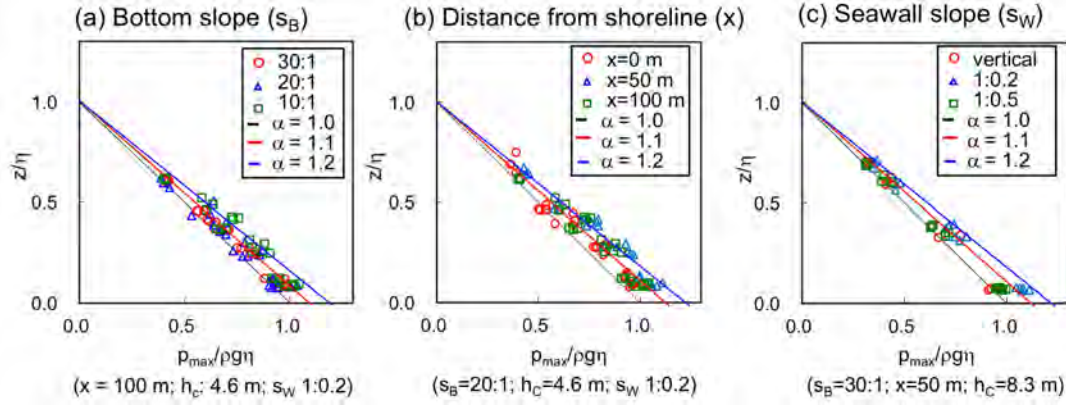


Figure 12: Comparison of vertical profiles of the shoreward $p_{max}/\rho g \eta$ classified in terms of (a) bottom slope, (b) distance from the shoreline, and (c) seawall slope; and those of the corresponding hydrostatic pressure ($p_{max} = \alpha \times \rho g \eta$). The blue, red, and black lines represent $\alpha = 1.2$, $\alpha = 1.1$ and $\alpha = 1.0$, respectively.

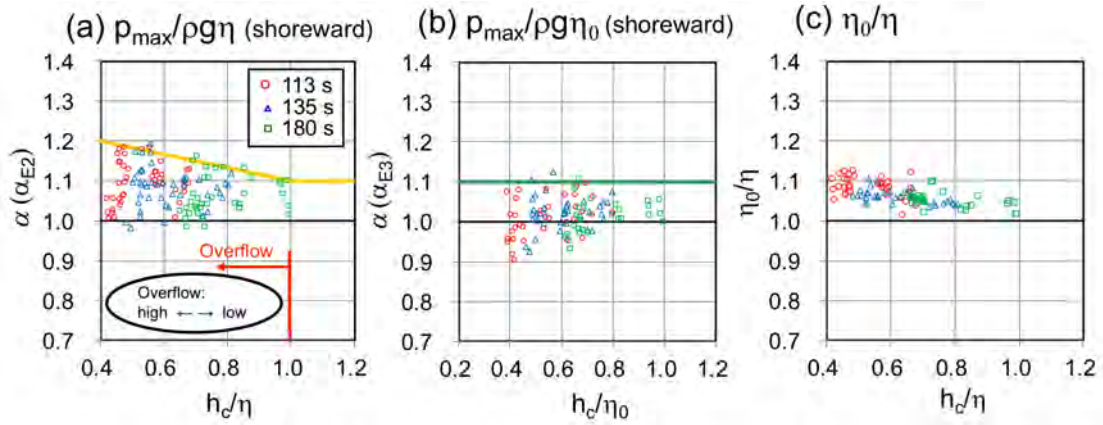


Figure 13: Scatterplots of (a) h_c/η versus α_{E2} , (b) h_c/η_0 versus α_{E3} , and (c) h_c/η versus η_0/η for shoreward slope.

Because the estimation of η_2 likely includes an uncertainty, particularly under high overflow conditions, we examined the vertical profiles of $p_{max}/\rho g \eta_B$, where η_B is the water level at $\sim 10 \text{ m}$ landward of the seawall (Figure 3(c)). The value of $p_{max}/\rho g \eta_B$ tend to be greater than 0.4 times that calculated using the hydrostatic pressure relation (i.e., $p_{max}/\rho g \eta_B = 0.4 \times (\eta_B - z)$; yellow line in Figure 14 (b)) for the large wave pressure depths ($z/\eta_B < \sim 0.3$).

3.3.2 Proposed formula

On the basis of the results obtained, we proposed formulae to calculate the tsunami-induced forces under the overflow condition to be used in the facility design, as shown below.

For the shoreward side of the seawall, the wave pressure (p_1 and p_2 in Figure 4(c)) is calculated using the inundation heights just in front of or somewhat shoreward of the seawall ($\eta_X = \eta_0$ or η) and the correction factor (α_i) such that

$$p_1 = \alpha_1 \times \rho g \eta_X, \quad p_2 = p_1 (\eta_X - h_c)/\eta_X. \quad (10)$$

The correction factor (α_i) is determined as follows.

$$\alpha_1 = 1.1 \quad (11)$$

when η_0 is known (see green line in Figure 13(b)). Alternatively, it can be calculated as follows.

$$\alpha_1 = -0.17 \times h_c/\eta + 1.27 \quad (12)$$

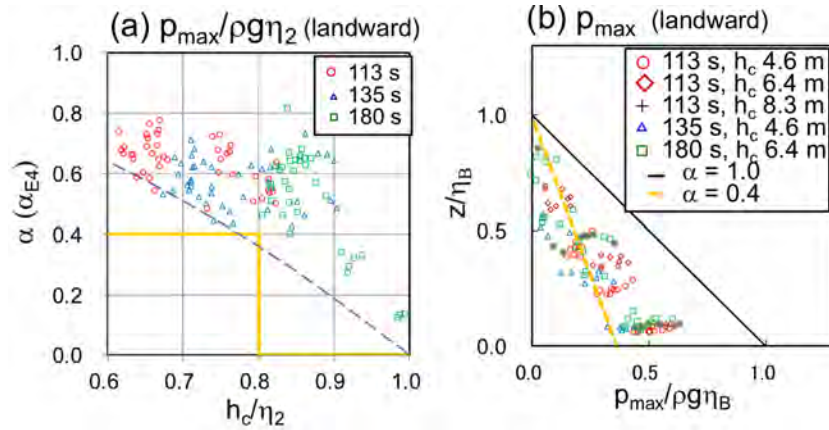


Figure 14: Scatterplots of (a) h_c/η_2 versus α_{E4} , and (b) $p_{max}/\rho g \eta_B$ versus z/η_B for landward slope.

when η is known (see yellow line in **Figure 13(a)**).

For the landward side of the seawall, the wave pressure (p_3 and p_4 in **Figure 4(c)**) is calculated using the inundation depths landward or just behind the seawall ($\eta_Y = \eta_B$ or η_2) and the correction factor (α_{IB}) such that

$$p_3 = \alpha_{IB} \times \rho g \eta_Y, \quad p_4 = p_1 (\eta_Y - h_{CB}^*) / \eta_Y, \quad h_{CB}^* = \min(h_C, \eta_Y). \quad (13)$$

The correction factor (α_{IB}) is determined as follows.

$$\begin{aligned} \alpha_{IB} &= 0.4 & (h_C/\eta_Y < 0.8) \\ \alpha_{IB} &= 0 & (h_C/\eta_Y > 0.8) \end{aligned} \quad (14)$$

(see the yellow line in **Figure 14(a)**). The experiment results show that the correction factor (α_{E4}) decreases gradually as h_c/η_2 approaches unity (cf., dashed line in **Figure 14(a)**). However, although a detailed analysis is skipped, a numerical study reported that the value of α_{E4} fluctuated considerably and frequently approached 0 when $h_c/\eta_2 > 0.8$. Therefore, from a safety viewpoint, we consider that (14) is more appropriate at this point in time.

4. CONCLUSION

On the basis of the results of hydraulic model experiments, we explored the methods of calculating the tsunami-induced hydrodynamic forces under non-overflow and overflow conditions to be used in the facility design. Special attention was paid to modifications by incorporating a correction factor in the hydrostatic pressure relation.

Under the non-overflow condition, the tsunami-induced force acting on the seawall were appropriately evaluated using (1) the hydrostatic pressure relation and a correction factor of 1.1, and (2) a quadratic function of the Froude number (Fr). Furthermore, under the overflow condition, the forces were appropriately evaluated using the function of the inundation depths in front of and behind the seawalls. **Figure 15** shows the proposed formulae and a related flow diagram.

The conventional design methods for calculating tsunami-induced forces (in Japan) seldom considered the effects of dynamic pressure, the behavior under overflow conditions, nor the wave forces acting on the landward side of the seawalls. The present findings (e.g., **Figure 15**) were mentioned in the tentative design guideline for onshore seawalls, published by the Fisheries Agency and the Ministry of Land, Infrastructure, Transport, and Tourism in Japan (November, 2015; see http://www.jfa.maff.go.jp/j/gyoko_gyozyo/g_hourei/pdf/20151214.pdf (in Japanese)). We hope that the results of this study will

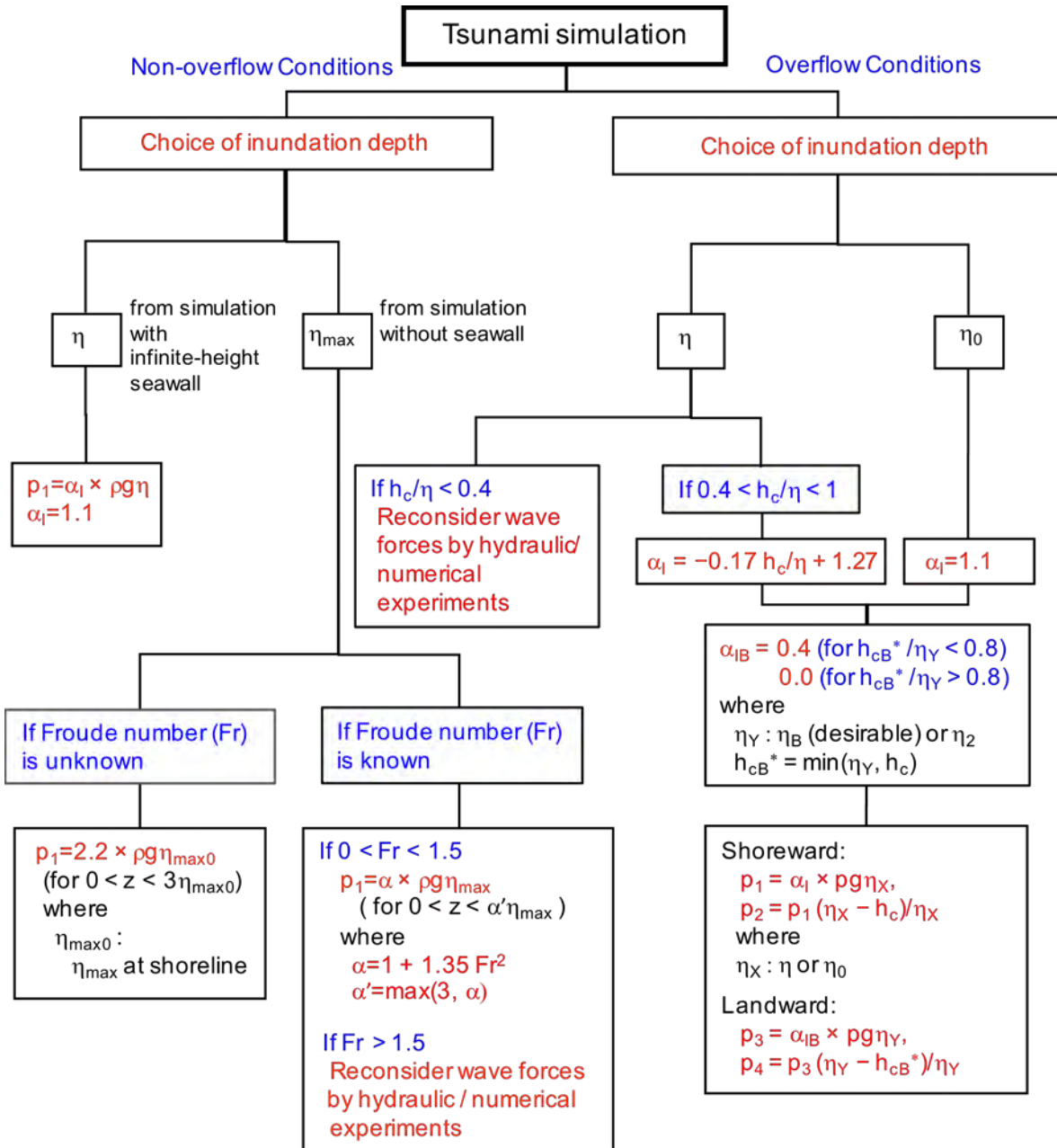


Figure 15: Flow diagram for calculating tsunami-induced forces. For definition of parameters, see Figures 3(c) and 4.

provide useful information in promoting disaster prevention and mitigation measures that will be effective against tsunamis.

Nevertheless, several issues need to be considered in future researches. For example, the present study investigated the tsunami-induced forces acting on seawalls only in the horizontal direction. However, the vertical forces, not only the buoyancy force but also the uplift pressure, might affect the stability of the structures. Furthermore, the present hydraulic experiment covered a limited range of parameters ($0.8 < Fr < 1.3$, and the ratio of the seawall height (h_c) to the inundation depth (i.e., η_0) was greater than 0.4; see **Figures 10 and 13**). Therefore, additional investigation is particularly required for tsunami cases when $Fr > 1.5$ or when $h_c < 0.4\eta_0$, if the corresponding wave pressure needed to be calculated (**Figure 15**) (in the present study, e.g., such a wave pressure might have been confirmed wherein the distance from the shoreline is greater than 150 m; see **Figure 5(c)**, or when $\eta_0 > 11.5$ m and/or $h_c < 4.6$ m). For the cases that surpass the design specification, studies on structural modifications, e.g., delaying the collapse due to tsunami are required. Further studies employing

additional hydraulic experiments as well as numerical simulations at appropriate scales need to be conducted to address these issues.

Acknowledgments

Report on the tsunami-affected areas such as **Figures 1 and 2** due to the Great East Japan Earthquake can be referred to at the website of National Research Institute of Fisheries Engineering, Japan Fisheries Research and Education Agency, Japan (http://nrife.fra.affrc.go.jp/topics/touhoku-taiheiyoujishin_hisaijyoukyou/gyokoutyousahoukoku.pdf (in Japanese)).

References

- Adriano, B., Hayashi, S., Gokon, H., Mas, E., Koshimura, S. (2016). Understanding the Extreme Tsunami Inundation in Onagawa Town by the 2011 Tohoku Earthquake, Its Effects in Urban Structures and Coastal Facilities, *Coast. Eng. J.*, 58(4), 1640013, doi:10.1142/S0578563416400131.
- Afmad, F., Shigihara, Y., Fujima, K., & Mizutani, N. (2009). A Study on Estimation of Tsunami Force Acting on Structures, *J.JSCE (Ser.B2, Coastal Engineering)*, 65(1), 321-I_325 (in Japanese with an English abstract).
- Asakura, R., Iwase, K., Ikeya, T., Takao, M., Kanto, T., Fujii, N., & Ohmori, M (2000). Experimental Study on Wave Force by Tsunami Overflowing Seawalls, *Proc. Coastal Engineering, JSCE*, 47, 911-915 (in Japanese with an English abstract).
- Asakura, R., Iwase, K., Ikeya, T., Takao, M., Kanto, T., Fujii, N., & Ohmori, M (2002). The Tsunami Wave Force Acting on Land Structures, *Proc. 28th ICCE*, pp.1191-1202.
- Homma, H. (1940). Coefficient of flow volume on low overflow weir., *Civ. Eng. JSCE*, 26 (6), 635-645 (in Japanese).
- Japan Society of Civil Engineers (2004). *Design Manual for Coastal Facilities 2000*, 577 p. ISBN 4810604748.
- Matsutomi, H., Kettoku, G., & Saitoh, M. (2013). Experiments on Tsunami Fluid Force Acting on a Reinforced Concrete Building with Aperture, *J.JSCE (Ser.B2, Coastal Engineering)*, 69(2), 326-I_330 (in Japanese with an English abstract).
- Nakamura, T., Sawa, Y., & Mizutani, N. (2016). Study of the Evaluation of Temporal Change in Horizontal and Vertical Tsunami Forces Acting on a Bridge Superstructure, *Coast. Eng. J.*, 58(4), 1640020, doi:10.1142/S0578563416400209.
- Ohmura, Y., Yagi, H., Nakayama, A., Mori, K., Kawano, D., Kato, H., Kado, A., & Namekawa, J. (2014). Experimental Study on Tsunami Induced Forces on Breast Type Seawalls Under Non-Overflow Condition, *J.JSCE (Ser.B2, Coastal Engineering)*, 70(2), I_881-I_885 (in Japanese with an English abstract).
- Ohmura, Y., Yagi, H., Nakayama, Yoneyama, M., Narita, T., Kato, H., Kado, A., & Namekawa, J. (2015). Experimental Study on Tsunami Induced Forces on Breast Type Seawalls, *J.JSCE (Ser.B2, Coastal Engineering)*, 71(2), I_991-I_996 (in Japanese with an English abstract).
- Sakakiyama, T (2012). Tsunami Inundation Flow and Tsunami Pressure on Structures, *J.JSCE (Ser.B2, Coastal Engineering)*, 68(2), I_771-I_775 (in Japanese with an English abstract).
- Tanimoto, K., Tsuruya, K., & Nakano, S. (1984). Study on Tsunami-Force and Disaster Cause of Landfill Seawall due to the tsunami by the 1983 Sea of Japan earthquake, *Proc. Coastal Engineering, JSCE*, 31, 257-261 (in Japanese).

PHYSICAL MODELING SUPPORTING DESIGN AND CONSTRUCTION OF LOW CRESTED BREAKWATER FOR THE AYIA NAPA MARINA, CYPRUS

M. WESSON¹, M. PROVAN², J. COX³, P. KNOX⁴

1 SmithGroupJJR, Madison, USA, Mauricio.Wesson@SmithgroupJJR.com

2 Ocean Coastal and River Engineering, National Research Council, Canada, Mitchel.Provan@nrc.ca

3 SmithGroupJJR, Madison, USA

4 Ocean Coastal and River Engineering, National Research Council, Canada

ABSTRACT

SmithGroupJJR undertook the design a new marina and accompanying land development at Ayia Napa, Cyprus. The marina features a 600-slip mega-yacht harbour framed by a large shoreline protection scheme comprised of wave absorbing block walls, revetments, breakwaters, and pocket beaches. Significant upland development, including two, 25-story towers and residential villas are also included in the design, with some of the new development near the sheltering breakwater. An innovative one-kilometer long, low-crested breakwater with tetrapod armor and a wide rock berm was designed to protect the harbor and land development. One of the primary design goals was maintaining a crest height low enough to provide the villa owners and marina users with unobstructed views of the sea. Therefore, a key element in the design was to limit the amount of wave overtopping that could pass over the low crested structure and potentially threaten the villas, yachts, cars and people on the lee side of the breakwater. The maximum overtopping flow rate was of interest rather than the mean time-averaged flowrate, since the maximum flow rate is more closely linked to risks to people and property.

A physical model study of a revised breakwater design was carried out at the National Research Council of Canada (NRC). A two-dimensional physical model of an idealized foreshore at the project site was constructed at a geometric scale of 1:42.2 in a 63m long by 1.22m wide wave flume. Scale models of two breakwater cross-sections (one in shallow water, the other in deeper water), due to the variable bathymetry, were constructed and exposed to scaled reproductions of the design-wave conditions forecast for the site. The physical model provided a good simulation of the important hydrodynamic processes influencing the stability and overtopping of the tetrapod armor layer, including nearshore wave transformation, wave breaking, wave run-up, and interstitial flows through the armor and filter layers.

The Ayia Napa breakwater is currently under construction, with approximately 50% of the breakwater constructed to date and completion expected by April 2019. Breakwater construction has been closely supervised, assuring that it meets the conditions specified by the design and observed in the physical model. The innovative double berm, low crested design approach of the Ayia Napa Marina breakwater provides a casebook example of how to achieve a harmonic, high-performance breakwater integrated with its landscape and environmental context, as well as highlighting the value of using a physical model to deal with design changes that arise during construction.

1 INTRODUCTION

The Ayia Napa Marina breakwater was designed based on calculations and physical model tests carried out in March 2015 at Wallingford, England (Boshek 2015). Flume physical model tests at scale 1:45.1 were done to define a stable breakwater cross-section consisting of 8 m³ Tetrapod armor units as armor layer, with a 10.2 m wide berm, and a 7.8 m-high crown wall, which produced the desired overtopping rate. The cross-section design was confirmed in a 3D physical model test, where head and toe instability were observed. The cross-section was adapted implementing a trenched toe solution with larger 10 m³ tetrapod units at the head of the breakwater.

The master plan of the marina was further developed, locating villas within the marina, its commercial areas, and two residential towers. The height of the crown wall, 7.8 m above the low-water tide level, became a problem obstructing the views of the marina and the villas. Once construction began in October 2016, the owner requested the analysis of a possible alternative that would reduce the height of the breakwater to improve the views from the residential villas and the marina. SmithGroupJJR developed

two possible solutions to reduce the height of the crown wall while maintaining the design overtopping rate: a submerged reef in front of the breakwater, or a wide-berm breakwater. The wide-berm breakwater was selected as the most feasible solution based on the environmental and permitting conditions of the project.

A key design goal for the breakwater was to maintain a crest height low enough to provide the landside villa owners and marina users with unobstructed views of the ocean. Therefore, it was important to limit the amount of wave overtopping that could pass over the structure and pose a threat to the villas, yachts, cars and people on the lee side of the breakwater. The maximum-overtopping flow rate rather than the mean time-averaged flow rate was utilized as a critical design criterion, since it is more closely linked to the risks posed to people and property.

The first step in designing the new low-crested breakwater cross-section was to use the Neural Network Overtopping design tool from TU Delft to estimate the berm width and structure geometry. The berm stone sizes were determined based on the work completed by Van Gent (2013). The newly proposed low-crested breakwater cross-section consists of two layers of 8 m³ tetrapod armor units placed on a structured grid with a front slope of 1:1.33. The crest of the breakwater extends to an elevation of +4.6 m above the design waterline and a 20.5 m wide berm, 10 meters of a Tetrapod Berm and 10.5 meters of a 4-ton rock berm, backed by a crown wall at the same +4.6 m elevation (see Figure 1).

Due to construction issues while trying to excavate a toe trench in calcarenite bottom, the feasibility of eliminating the toe trench was also investigated in the physical model. Given the various water depths where the breakwater's toe trench would be located and recognizing the reduction in wave forces with increasing water depth, a shallow-water portion and a deep-water portion of the breakwater were physically modeled with alternative solutions to the toe trenching. The need to secure the toe of the breakwater was verified by the physical model.

In order to investigate these two proposed design changes—lowering the crown wall height and removing the toe trench—physical model tests at a scale of 1:42.2 were carried out at the Ocean, Coastal and River Engineering Research Centre of the National Research Council of Canada. The performance of the breakwater's cross-sections was assessed by observing the stability of the armor units and amount of overtopping during exposure to a series of irregular wave conditions and elevated water levels representing design storms. The effects of different widths of the top “berm” on structural stability and overtopping rates was explored using a double-berm-width tray system to optimize use of the laboratory time. Each test series generated much information with respect to the interaction of the extreme design waves with the foreshore and the breakwater (wave breaking, run-up, and overtopping), and the response of the breakwater to this forcing (stability of the armor and the resulting overtopping discharges). This physical modeling was crucial in refining and confirming the proposed design changes developed to accommodate the site conditions encountered during construction of the breakwater. The efficiency of the model study led to reduced downtime in the field while these design sections were verified and optimized.

Several large storms have been encountered to date during construction, which have allowed for verifying the design parameters as observed in the physical model tests. A wave gauge was installed at the project site in a location corresponding to the location of the wave paddle in the physical model. Overtopping rates have been measured, the behaviour of the trenched tetrapods have been documented, and the observed performance of the portions of the breakwater built thus far are in agreement with the physical model results and design expectations.

2 PROPOSED DESIGN OPTIMIZATIONS

2.1 Design Conditions

The site's deep-water wave and wind conditions were obtained from Mediterranean hindcasts and reported in the SmithgroupJJR 2013 Wave Conditions Report. The analysis showed the occurrence of waves from different directions ranging from east to west with 100-year-return-period significant wave heights of up to 7.2 m. The wave conditions for the deep-water conditions are summarized in

Table 1.

Table 1: Deepwater Design Wave Conditions

| Offshore Wave | 1-year | | 10-year | | 25-year | | 50-year | | 100-year | |
|---------------|--------|-------|---------|-------|---------|-------|---------|-------|----------|-------|
| | Hs(m) | Tp(s) | Hs(m) | Tp(s) | Hs(m) | Tp(s) | Hs(m) | Tp(s) | Hs(m) | Tp(s) |
| West | 3.5 | 8.4 | 4.9 | 9.4 | 5.5 | 9.7 | 6.0 | 10.0 | 6.5 | 10.3 |
| WSW | 4.5 | 9.1 | 5.9 | 10.0 | 6.4 | 10.2 | 6.8 | 10.5 | 7.2 | 10.7 |
| SW | 3.4 | 8.3 | 4.5 | 9.1 | 4.9 | 9.4 | 5.2 | 9.6 | 5.5 | 9.7 |
| SSW | 2.2 | 7.2 | 3.8 | 8.6 | 4.4 | 9.0 | 4.9 | 9.4 | 5.3 | 9.6 |
| South | 1.2 | 5.9 | 2.0 | 7.0 | 2.4 | 7.4 | 2.6 | 7.6 | 2.8 | 7.8 |
| SSE | 1.0 | 5.5 | 1.7 | 6.6 | 2.0 | 7.0 | 2.2 | 7.2 | 2.4 | 7.4 |
| SE | 1.0 | 5.5 | 2.1 | 7.1 | 2.5 | 7.5 | 2.8 | 7.8 | 3.1 | 8.1 |
| ESE | 0.8 | 5.1 | 1.3 | 6.0 | 1.5 | 6.3 | 1.7 | 6.6 | 1.8 | 6.7 |
| East | 1.0 | 5.5 | 1.5 | 6.3 | 1.6 | 6.5 | 1.8 | 6.7 | 1.9 | 6.8 |

The deep-water wave conditions were numerically modeled to the project site using state-of-the-art, steady state spectral model SWAN. The physical model boundary conditions were developed based on the transformed wave heights obtained from the spectral model results. Wave conditions in the physical model were measured at six specific locations using capacitance wave probes, including one probe at the -20m depth contour. The waves used in the physical model were calibrated by adjusting the command signals used to drive the wave generator so that the wave conditions measured at the -20 m depth contour were in agreement with target-wave conditions derived from numerical wave modelling completed by SmithGroupJJR. The target wave conditions for each design storm at the 20 m water depth contour are shown in Table 2. The other five wave gauges were placed at specific depths along the model's bathymetry, including one gauge placed near the toe of the breakwater structure.

Table 2. Specified wave conditions at -20m contour.

| Return Period | H _s (m) | T _p (s) | SWL (m CD) |
|---------------|--------------------|--------------------|------------|
| 1 | 2.58 | 8.3 | 0.91 |
| 10 | 3.56 | 8.8 | 0.91 |
| 50 | 4.51 | 9.7 | 0.91 |
| 100 | 4.85 | 9.9 | 0.91 |
| 20% | 5.82 | 10.8 | 0.91 |

2.2 Marina Layout Design

Conceptual design for the basin and breakwater at the Ayia Napa Marina was first evaluated and refined by a series of 2D flume and 3D basin physical model tests at the Laboratories of HR Wallingford, in England. In addition to the physical modeling, numerical modeling was performed at the same time by SmithGroupJJR. The testing addressed; the sizing and stability of the breakwater and the armor units, wave penetration and berthing tranquility in the basin, wave overtopping of the breakwater, wave absorption and reflection damping methods within the basin, and water quality and circulation in the marina.

Due to the observed results of the 3D physical model, additional numerical modeling was conducted to address structural changes to the design of the basin, which either corrected unexpected deficiencies or in some cases further enhanced performance. The original basin plan remains essentially as envisioned in both size and configuration, with minor changes undertaken to assure safety and performance of the facility.

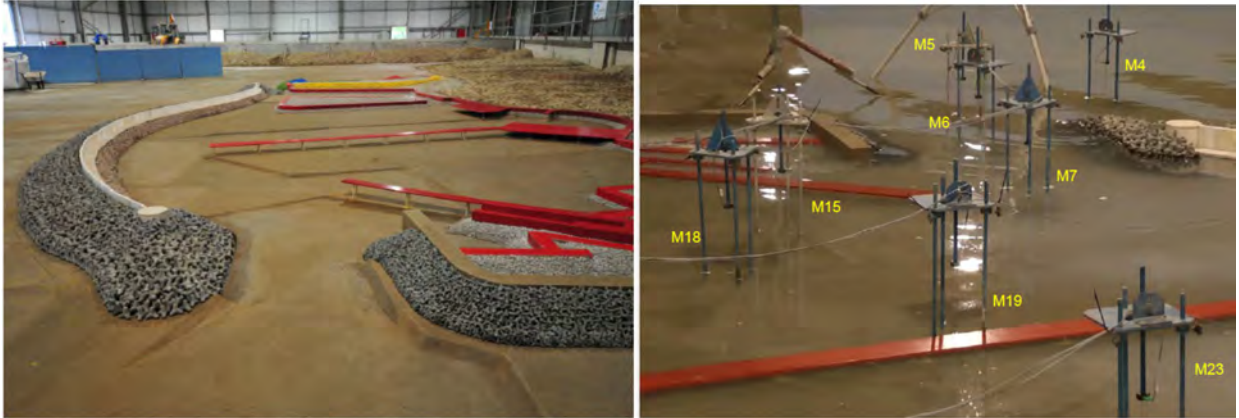


Figure 1. 3D physical model conducted by HR Wallingford for the Marina layout design.

The numerical model NOWT-PARI (Hiraishi 2002), developed by the Port and Airport Research Institute of Japan, was utilized to numerically transform the extreme wave events for modeling the design changes. The events modeled in the 3D physical laboratory were used to calibrate and validate the numerical model. NOWT-PARI is a state-of-the-art, completely non-linear, Boussinesq-type wave transformation model that calculates the water-surface elevation for every time-step instance; this model also considers partial wave absorption-reflection, wave diffraction, wave shoaling and refraction, and wave breaking and nonlinear interactions. The first stage of the numerical modeling study was to reproduce the observed results in the 3D physical model for validation purposes. The same wave input conditions used in the physical model were also used in the numerical model by implemented an irregular, directional wave maker located at the south boundary of the model. The numerical model was set up using a 4 by 4 m regular grid with a partial reflection coefficient of 0.5 applied to the structures. The partial reflection coefficient was then calibrated to reproduce, as closely as possible, the wave conditions as measured in the physical model tests. A reflection coefficient of 0.3 was specified at the beach areas, and sponge energy-absorbing boundaries were implemented at the lateral extents of the numerical model domain. The model time-step calculation was set to 1/600 of the peak spectral period. The resulting numerical model was run for each extreme event for the same duration as the physical model. The numerical model results are shown in figure 2.

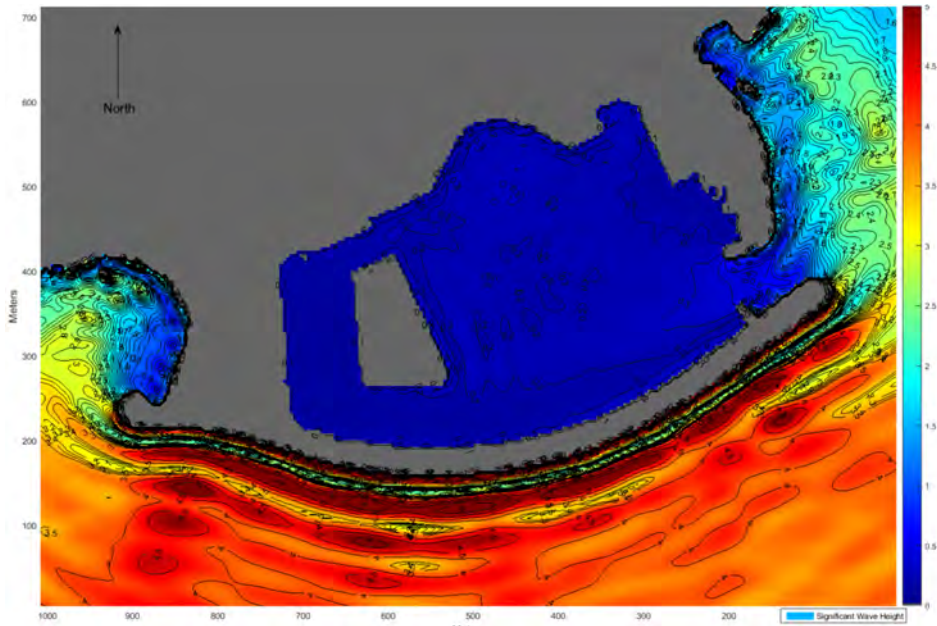


Figure 2. Validated Numerical Model of the Marina Layout

The wave-calmness conditions within the basin of the revised marina layout were obtained and verified with the calibrated and validated state of the numerical model. The resulting layout changes included a geometrical modification to the south breakwater, a revised curvature of the eastern breakwater, modified island location, and complete closure of the west circulation channel, which will affect how waves enter and behave within the marina basin. The final modified marina layout is shown in Figure 3.

The results from the numerical model showed that deep-water waves approaching from the SSW direction produced the largest wave agitation in the basin. The SSW waves had the largest wave heights and periods closest to the project site and presented the largest amount of wave energy in the basin; these results were similar to what was found in the physical model study. To minimize the wave energy entering the basin, a special wave-energy-absorbing block wall was created and implemented throughout the basin perimeter.

The resulting wave agitation in the basin was compared to the tranquility criteria to determine if the basin would comply with the climate targets. The critical wave gauging locations, where the wave climate criteria were compared with the modeled waves, were located on the slips closest to the marina entrance.



Figure 3. Final Marina Layout Design

2.3 Breakwater Cross Section Design

The preliminary design of the breakwater was tested in a physical model conducted at HR Wallingford (Boshek 2015). A detailed analysis on the overtopping rates produced by Accropode armor and Tetrapod armor units was undertaken. The tests revealed that 19.2-ton Tetrapod armor units provided smaller overtopping rates compared to the Accropode units. The conditions at the site present variable water depths ranging from 4.5m to 12m with a sharp slope between the 8m and 5m contours. This condition creates plunging waves which break on the breakwater slope, significantly increasing the overtopping rates. Due to these breaking conditions, smaller waves were observed to ride up the filter layer through the pores in the armor units. While not visible, this same process occurred for larger waves, which suggests that runup height, and therefore overtopping, was much larger in one-layer systems. This

finding is also consistent with the predictions of overtopping behavior for different armor types by Cox and Clifford (2014), who developed a means to correlate overtopping volumes to wave transmission; they found that tetrapod armoring produced the least overtopping compared to single layer elements or even rock armor for the same overall breakwater cross-section. Based on the results of both tests and the perceived changes that would be required to effectively reduce the overtopping, the breakwater cross-section was designed with a double-layer of 19.2-ton Tetrapod armor units and a crest height of 7.8 m above the low water level.

The Tetrapod placement specified for the breakwater was based on a recommended pattern by FUDO TETRA, reproduced in figure 4. This placement pattern provides increased interlocking between the units, which adds an increased amount of stability to the weight of the armor units. Placing Tetrapods in this specific pattern required extra attention by the contractor compared to the traditional random Tetrapod placement.

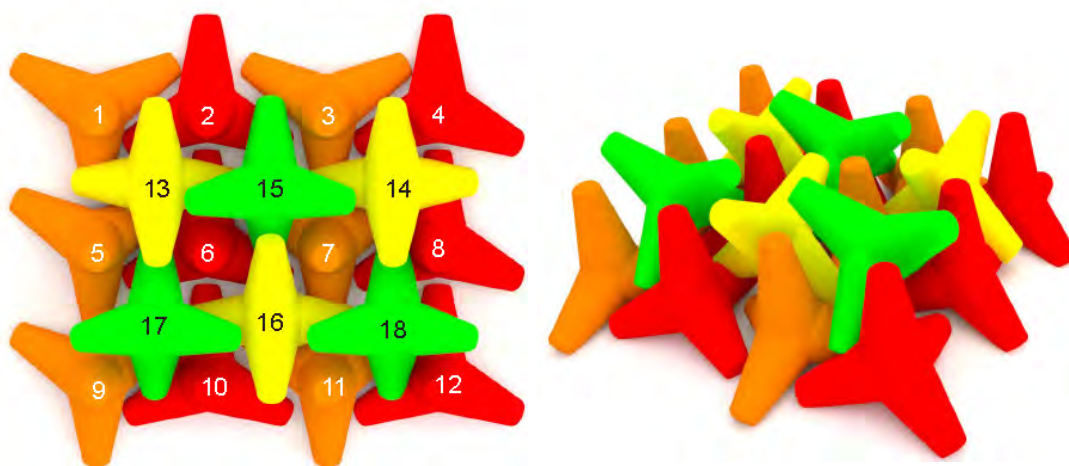


Figure 4. Tetrapod Placement Pattern

Two issues with the breakwater cross-section were observed during the 3D Physical model tests. The first issue was observed at the shallow sections of the breakwater (sections where the water depth is less than 7 m) where the breaking waves created a down rush causing the toe Tetrapods to slide seaward. This issue was not observed in the deeper water sections of the breakwater where the wave drawdown was not as severe. The second issue was poor interlocking of Tetrapods at the head of the breakwater. The original design specified 19.2-ton Tetrapods at the head of the breakwater, and these units were pulled out of position during the model tests. Furthermore, green-water overtopping was observed at some sections of the breakwater due to three-dimensional wave propagation effects due to the shape and variable bathymetry; as a result, any intent to reduce the crown height of the breakwater was abandoned.

The toe sliding had not been observed in the first 2D flume cross section tests, as the breakwater section modeled at HR Wallingford was chosen where the highest waves were observed, in the deeper water section. The issue only became apparent during the 3D physical model tests, where down rush from breaking waves at the shallower portion caused sliding of the Tetrapods. The toe sliding was corrected by introducing a toe trench that can contain the two toe Tetrapod units. The instability of the Tetrapods in the head of the breakwater was corrected by increasing the size of the Tetrapods to 10 m³, or 24 tons. The crown height of the breakwater remained at 7.8 m above the water level.

Construction of Ayia Napa Marina started in September 2016. During the initial stages of construction, the excavation of the toe trench proved to be a difficult task due to the nature of the soil and the method used. The crown height of the breakwater also obstructed the views from marina, villas and commercial

areas. SmithgroupJJR was asked to analyze the possibility of reducing the crown height of the breakwater.

SmithGroupJJR developed two alternative designs to reduce the height. The first alternative created a wider breakwater with a berm to reduce wave overtopping. The second alternative created an offshore, semi-submersed reef to cause wave breaking that would reduce the wave energy at the breakwater. Due to navigation, environmental, and permitting concerns, the submerged reef alternative was abandoned. The wide berm alternative was preliminary designed and a second physical model was carried out at the National Research Council of Canada, NRC.

Based on the results of the initial 2D and 3D physical models conducted by HR Wallingford, calculations were carried out to determine a revised breakwater cross-section including a wide berm. Ideally, a wide berm with a lower crest height would provide the same overtopping rates as the initial design with the higher crest. A target breakwater crown-wall elevation of +5.5m from the low tide water level was selected and overtopping for different berm widths was estimated, the low crested breakwater cross section tested in the physical model is shown in figure 5.

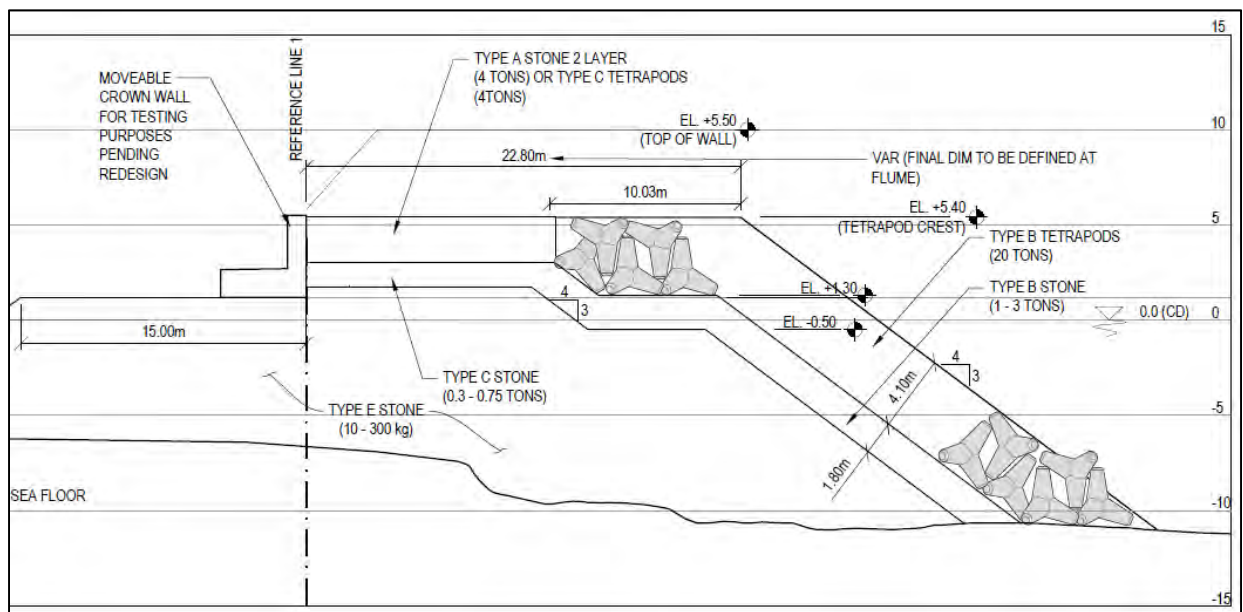


Figure 5. Preliminary Wide Berm Low Crest Breakwater Cross Section

The specific berm-type breakwater section selected for design is unprecedented and out of the range of validity for most commonly used design equations. Thus, a Neural Network method was used to estimate an initial cross-section for the revised breakwater. Even with this method, mathematical uncertainty about the results was significant, making physical model tests required for designing the breakwater. The estimation of mean overtopping was done using the Neural Network software developed by WL | Delft Hydraulics. The Neural Network predictions were only used as first estimates of mean overtopping discharges.

The initial results of the Neural Network software indicated that a 25 m wide berm with Tetrapods on the slope and stone on the inner berm area would produce a lower overtopping discharge than the original 7.8m high cross section. The calculated overtopping discharge rate for the original cross section was estimated at 1.64 l/s/m, while the 25 m berm was estimated to be 1.09 l/s/m. This indicated that a berm width of 25 m should produce similar amounts of overtopping compared to the +7.8m crest height of the previous designed cross-section. However, the 95% confidence-level calculation still showed a slightly higher overtopping rate. The 95% overtopping for the existing 7.8 m crest elevation was 5.31 l/s/m, and for a 5.5m crest elevation with a 25 m berm was 6.45 l/s/m. It was expected that higher individual waves might produce higher individual overtopping rates.

Van Gent's (2013) method to determine the stability of rubble mound breakwaters with a berm was applied to estimate the size of stone required in the horizontal berm behind the Tetrapods, shown in

figure 5. This is a horizontal berm located at the crown of the breakwater, where the usual stability equations are inapplicable; the stones must withstand the force of jets of water from breaking waves. The calculation indicated that the size of the berm stone can be reduced by a factor of 3.9 to the equivalent required stone on the slope. Considering that the Ayia Napa berm is out of the validity range stated in Van Gent (2013), an additional safety factor was applied and 4-ton stones were selected. Given the horizontal placement, where interlocking can't be taken into account, they can be substituted with 4-ton armor units (horizontal placement).

3 PHYSICAL MODEL TO SUPPORT BREAKWATER CROSS-SECTION DESIGN CHANGES

Additional physical model tests were commissioned at the National Research Center of Canada to finalize the design changes to the breakwater cross section in November 2016, while the construction of the marina proceeded by creating the access to the breakwater. The available time to finalize the design changes was short as the Contractor progressed and therefore an expedited physical modelling study was undertaken.

3.1 TESTING PROGRAM AND RESULTS

The principal objective of the physical model study was to assess the performance of breakwater toe stability and overtopping in extreme conditions associated with storms of varying return periods. Breakwater performance was primarily assessed by observing the stability of the armor units and the amount of overtopping for various crest widths and corresponding crown wall positions. The overtopping criterion that was applied to this study is as follows:

- 1:100 year mean discharge < 0.1 L/s/m
- 20% overload storm mean discharge < 1.0 L/s/m

In addition to the mean discharge criteria, a maximum single overtopping event of 5000 L/m was also imposed to examine the breakwater performance.

Two simple, accurate and reliable overtopping measurement systems were developed for use in the model. The overtopping system consisted of a water storage reservoir, a capacitance wave gauge to measure the level of the water in the reservoir and a tray that collects all of the overtopped water over a portion of the breakwater cross-section and carries it into the water storage reservoir. The reservoirs were placed on the leeside of the model breakwater and ballast to prevent them from moving. The collection trays were placed immediately behind (and slightly below) the crown wall to capture all overtopping along the width of the conveyance trays. This system is able to capture single overtopping events, which was of importance to the testing program as the maximum overtopping flowrate was used as a critical design criterion compared to the mean time-average flowrate.

A photographic damage analysis system comprising of two remotely-operated digital cameras was used in this study to monitor the movement of armor units on the surface of the breakwater. The two cameras were securely mounted above the flume and aimed to view the seaward breakwater slope and the breakwater crest. Since each camera remained fixed throughout a test series, the movement of armor units could be detected by comparing photographs taken at different times. In addition, a video camera with remote pan, tilt and zoom capabilities was installed outside the flume (looking through the flume's glass viewing windows towards the model breakwater) and was used to digitally record all tests.

3.2 Shallow Water Cross-Section

The shallow breakwater cross-section, shown in figure 6, was tested first. The first tested design features two layers of 20-ton Tetrapod units and a single row of 25-ton Tetrapods at the toe of the breakwater. The initial breakwater design called for a toe trench to be constructed in which the Tetrapods along the toe would be placed. However, during early stages of constructing the breakwater, the hard rock experienced at the site led to difficulties in excavating the trench. One of the driving forces of the physical modelling studies was to investigate the possibility of eliminating the toe trench and instead use larger

Tetrapod units to secure the toe. The crest height of the breakwater was +5.4 m, the height of the crown wall was +5.5 m, and the toe of the breakwater was located near the -6 m depth contour. The design and a photo of the final constructed shallow water cross-section breakwater are shown in **Figure**. The pink Tetrapods represent the 25-ton toe armor units.

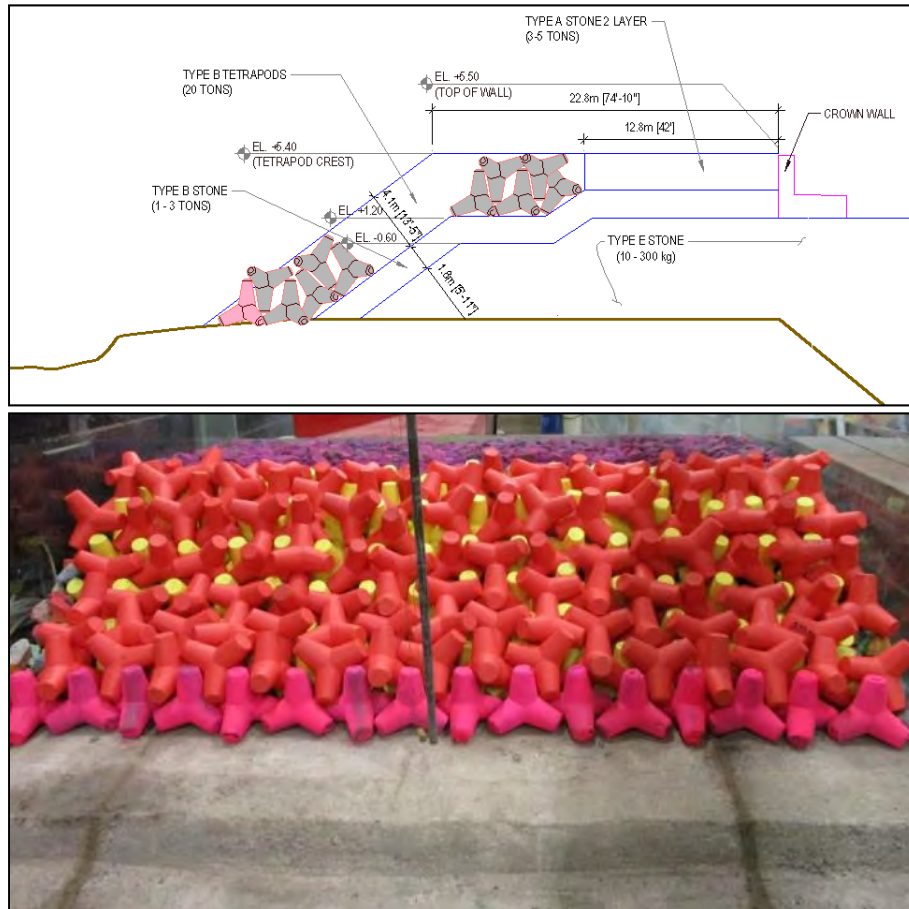


Figure 6. Top – shallow water cross-section design; bottom - constructed shallow-water cross-section.

3.2.1 Toe Stability

The breakwater was exposed to the 1-year and 10-year return period wave conditions shown in table 2. During the course of the 1-year storm, the toe units near the center of the structure shifted seaward, likely caused by drawdown from the larger waves dragging the toe units. After the 3-hour storm duration, the toe row of Tetrapods appeared to have moved approximately 2.1m (0.05m model scale) seaward in the center of the structure. The breakwater was then subjected to the 10 year storm during which the toe shifted even further seaward and caused the armor units on the slope of the breakwater to slump (see Figure 6) and a Tetrapod unit was plucked from the second layer on the toe and was deposited offshore of the breakwater. The amount of armor unit displacement was considered a structure failure and therefore the structure was not tested any further.

The breakwater was rebuilt using larger 30-ton Tetrapod units for the toe to try and increase the toe stability. The larger 30-ton toe units appeared to have been more stable under the 1-year return period storm compared to the previously tested 25-ton units, showing no movement during the storm. Seaward movement of the toe was observed during the 10-year storm. The rundown from a large wave initially pulled two to three of the toe units seaward and subsequent large events caused further displacement of the toe. After the 10-year storm, there were a total of four toe units that were displaced approximately

0.5m seaward. This toe displacement caused a slight slumping of the second layer armor units, directly above the displaced toe units. The 50-year storm caused further displacement of the toe; the toe units that moved seaward during the 10-year storm were dragged even further offshore (resulting in a total displacement of approximately 1m). The maximum wave rundown on the face of the structure would almost fully expose the toe units during large wave events. This rundown appeared to exert a large slope-normal force on the toe units, causing the large 30-ton units to be displaced seaward, which in-turn caused additional slumping of the Tetrapods on the slope of the breakwater particularly in the first two to three rows. The 100-year storm caused a failure of the breakwater section with the toe being displaced approximately 3.8m offshore. The increased toe displacement furthered the slumping of the armor units on the slope of the breakwater. The slumping was significant enough to open gaps through the armor, which exposed some of the filter layer stone. The structure was not tested for the overload case as failure had already been deemed to have occurred under the 100-year storm.



Figure 6 – Displaced toe and slumping of breakwater armor.

Based on these initial tests it was concluded that the toe trench which was initially part of the prototype design was required for a stable breakwater cross-section. The amount of force exerted on the breakwater toe from the drawdown of the waves would require an impractically large Tetrapod size without a toe trench to key in that unit. A section of the model bathymetry was removed and a trench section was re-cast in concrete at the correct elevation. A small portion of the trench, which represents an approximately 6m wide section, was not cast in concrete and was backfilled with small stone (see Figure 7). This was done in order to simulate a potential construction method that would be used in the prototype; if the toe trench is dug too deep the trench will need to be backfilled with stone to the proper elevation. The purpose of including a small section of exposed stone in the model was to investigate if the backfilled trench stone may be pulled out and through the toe armor units. After constructing the toe trench, the shallow water breakwater section was reconstructed using 20-ton Tetrapod units (the same size units used in the armor layer) placed in the trench. It was found that the toe trench greatly increased the stability of the armor layer. No movement of the toe was observed during or after the 50 year, 100 year or the 20% overload storm. In addition, the backfill stone in the trench remained stable throughout all tests.

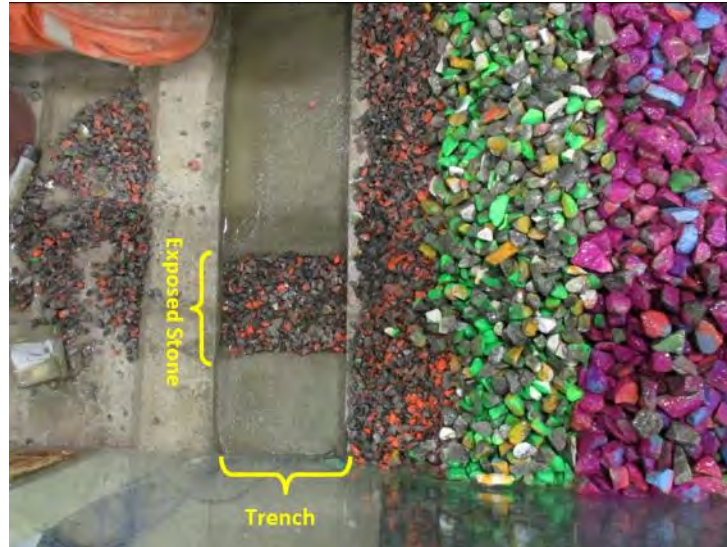


Figure 7. 1m deep toe trench with exposed backfill stone.

3.2.2 Armor Unit Stability

The only significant armor unit movements observed during the shallow water tests was slumping of the armor layer due to the offshore shifting of the toe units. During the testing of the cross-section with the toe trench, no significant movement of the Tetrapods was observed. Since the cross-section was located in relatively shallow waters, the larger waves would break offshore, reducing the amount of wave energy that the structure was exposed to. The specified armor unit placement pattern seemed to perform well under all wave conditions up to and including the 20% overload scenario.

3.2.3 Overtopping

There was limited overtopping of the crown wall observed during the shallow water cross-section tests. This was likely due to the fact that the larger waves would break in the deeper waters offshore, limiting the amount of wave energy that reached the breakwater. The three largest storm events, the 50-year, 100-year and overload scenario all produced only a fine spray over the crown wall and onto the collection tray, however there was not enough water to provide any measurable overtopping. A number of large waves during the overload scenario produced green water landing approximately 10.5m onto the breakwater crest, which fell short of the crown wall which was located 12.8m landward of the offshore crest line.

3.3 Deep Water Cross-Section

The deep-water cross-section has a similar profile as the shallow-water section except that the toe of the breakwater was in deeper water, near the -10m contour (opposed to the shallow-water section where the toe was near the -6m contour) and the toe was not recessed into a 1m deep trench. The deep-water section design also featured two layers of 20-ton Tetrapod units installed following the same ordered placement pattern presented in figure 4. The crest height and height of the crown wall both remained the same at +5.4m and +5.5m, respectively. Figure 8 presents both the design drawing and the final constructed structure for the deep-water cross-section.

The focus of the deep-water cross-section was to try and optimize the crown wall location by reducing the breakwater crest width while at the same time ensuring the overtopping amounts remained within the design limits. The stability of both the toe units and the armor layer were observed during testing. The crest of the deep water cross-section was split into two halves in order to efficiently test two different crown wall offsets simultaneously. A rectangular piece of sheet metal was placed between the two different crown wall offsets to ensure that no cross-over splashing would interfere with the measurement of the individual overtopping rates.

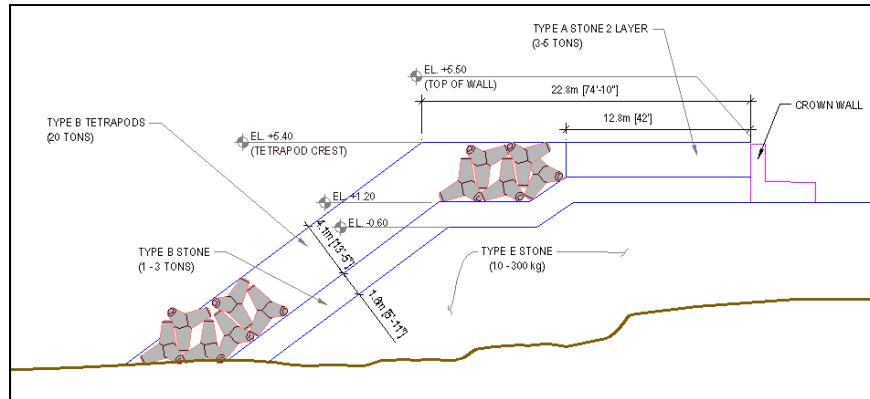


Figure 8. Top – deep water cross-section design; bottom - constructed deep water cross-section breakwater.

3.4 Toe Stability

The deep-water cross-section was constructed with 20-ton Tetrapod units both on the face and at the toe of the structure. The deeper waters at the toe of the structure reduced the drawdown forces acting on the toe and the toe units remained stable during all tested storms, including the 20% overload scenario.

3.4.1 Armor Unit Stability

The deep-water cross-section remained stable throughout the entire testing series, which included 17 different storm segments ranging from the 10-year return period storm to multiple overload storms. Since the main focus of the testing for this section was to examine the overtopping for different crest widths and crown wall locations, the crown wall was moved and the structure was exposed to multiple severe storms without rebuilding the structure. Small movements (shifting in place) of approximately half of the Tetrapod units was observed during the 100-year return period and the overload storms, particularly the Tetrapods located along the SWL. There was no significant movement, rotation, or displacement of any of the Tetrapod units.

3.4.2 Overtopping

Overtopping measurements were taken for a total of five crown wall positions which resulted in testing five breakwater crest widths; 3.5m, 6.5m, 8.2m, 10.5m and 12.8m. Both the average overtopping discharge and single overtopping events were measured and Equation 6.13 of the Eurotop guidelines was applied as a scale and model effect correction factor (Eurotop, 2016) to all recorded overtopping discharges.

The 3.5m crest width produced significant amounts of overtopping during the 100-year storm and the overload scenario (see Figure 9), with single overtopping events in the overload scenario reaching 24000 L/m. This level of overtopping could potentially cause significant damage or sinking of larger yachts in the marina on the leeside of the breakwater (Eurotop, 2016). The average overtopping discharge was 12.18 L/s/m during the overload storm, well above the 1.0 L/s/m criterion set by SGJJR. As the crown wall was moved further from the front slope of the breakwater, thereby creating an increasing crest width, the overtopping discharges and maximum single events decreased, as expected. After completing the testing of the five crest widths, the optimum crest width was found to be 10.5m. Placing the crown wall 10.5m back from the breakwater offshore crest line produced overtopping discharges of 0.05 L/s/m and 0.62 L/s/m for the 100-year return period storm and the overload scenario, respectively. The maximum event recorded during the 100-year storm was 110 L/m, and 2000 L/m for the overload scenario.



Figure 9. Overtopping of the 3.5m crest width.

Finally, due to the possible problems with the supply of sufficient amount of 4-ton armor stones, a 4.8 ton concrete armor unit was used to replace the stones in the berm to revise the overtopping. Two layers of small 4.8-ton Core-loc units were installed on the breakwater crest, replacing the 4-ton rock. The design of the prototype breakwater structure included smaller 4-ton Tetrapod units on the crest of the structure. However, due to the expedited nature of the physical model, there was not enough time to procure smaller Tetrapod units. Since the stability of the Tetrapods on the crest was previously tested by others and deemed stable, similarly sized rock was used on the breakwater crest for modelling purposes. Using rock on the crest may decrease the friction and size of the voids when compared to using Tetrapods, potentially causing larger overtopping rates compared to what may be observed when using Tetrapods. Therefore, 4.8-ton Core-loc units were installed on the breakwater crest (Figure 10) to investigate the difference between using rock and using armor units on the crest with regards to overtopping. Overtopping tests were repeated for the 10.5m and 12.8m crest widths.



Figure 10. Overhead view of the breakwater crest with a 12.8m crest width and a Core-loc armor layer.

In general, using Core-loc units for the armor crest layer appeared to reduce the amount of overtopping for both the tested 100-year and overload storms. This can be attributed to the increase in roughness and porosity on the breakwater crest provided by the armor units. Table 3 summarizes overtopping results for the 12.8m crest width exposed to the overload storm for both the 4-ton rock and the 4.8-ton Core-loc armor layers used on the breakwater crest.

Table 3. Overtopping summary for 12.8m crest width exposed to overload storm.

| Crest Armor Layer | Total Overtopping Volume (L/m) | Overtopping Discharge (L/s/m) | Maximum Event (L/m) |
|-------------------|--------------------------------|-------------------------------|---------------------|
| 4-ton rock | 9659 | 0.89 | 1700 |
| 4.8-ton Core-loc | 5761 | 0.55 | 1500 |

The overtopping results for all the different breakwater cross sections tested are shown in table 3. To determine the allowable overtopping discharges the consequences of the overtopping must be identified. Considering that there are permanently occupied structures behind the breakwater, overtopping at the Ayia Napa Marina can cause a hazard, injury or death to people behind the defense. Overtopping can cause damage to the comfort station, service docks and beach club, and it can cause damage to the small and medium sized boats moored behind the structure. The characteristics of the observed jets showed that when heavy green water went over the crown wall a large amount of water plunged into the parking and roadway increasing the speed of the flow, furthermore the crown wall obstructs visibility of the incoming water jet, providing no warning to the event. Based on the considerations above a level of protection of less than 0.1 l/s/m is required for the 100-year return period. Considering the dramatic change in overtopping rate in a couple of meters along the berm, and the existence of the building elements behind the breakwater the overtopping rate for the overload condition not to exceed 1 l/s/m.

Based on these provisions, the inner rock berm width is set to 10.5m for the final design. The obtained mean discharge rates and maximum water volume for an individual wave for each tested cross section for the different return periods is shown in table 3. The total berm width in these tables include the 10m of Tetrapods the additional tested rock berm. For a rock berm of less than 10m, total berm width 20 meter, there is a sharp increase in the maximum individual volume of water during the test. The reason for this sharp increase is due to green water overtopping. The green water overtopping on top of the wall and into the road way is considered very dangerous as the people will not see the water and it can create a thick

sheet of water that would have the potential to displace persons and heavy objects into the Marina Basin. The design avoids such events for 100 year return periods. Figure 12 exhibits the reduction in overtopping rates when the additional rock berm width is increased.

Table 4: Individual and Maximum Overtopping Discharges for variable Berm Widths

| Cross Section Condition | TEST | ROCK BERM (m) | 10yr | | 50yr | | 100yr | | 1.2x100yr | |
|-------------------------|------|---------------|----------|--------|----------|--------|----------|--------|-----------|--------|
| | | | Q(l/s/m) | V(l/m) | Q(l/s/m) | V(l/m) | Q(l/s/m) | V(l/m) | Q(l/s/m) | V(l/m) |
| DEEPWATER | A | 12.8 | 0 | 0 | 0 | 0 | 0.007 | NA | 0.005 | NA |
| DEEPWATER | B | 8.2 | 0 | 0 | 0.1 | NA | 0.2 | 200 | 2.9 | 8000 |
| DEEPWATER | B | 8.2 | x | x | x | x | x | x | 1.95 | 7600 |
| DEEPWATER | C | 6.5 | x | x | x | x | x | x | 1.47 | 7400 |
| DEEPWATER | D | 3.5 | x | x | 0.04 | NA | 0.54 | 3550 | 12.18 | 24000 |
| SHALLOW WATER | C | 6.5 | x | x | 0.05 | 200 | 0.08 | 270 | 2.12 | 7000 |
| SHALLOW WATER | B | 8.2 | x | x | 0.01 | 90 | 0.07 | 280 | 2.36 | 9700 |
| DEEPWATER | A | 12.8 | x | x | x | x | 0 | NA | 0.17 | 1000 |
| DEEPWATER | E | 10.5 | x | x | x | x | 0 | NA | 0.23 | 1000 |
| SHALLOW WATER | A_s | 12.8 | x | x | 0 | NA | 0.05 | 250 | 0.89 | 1700 |
| SHALLOW WATER | E_s | 10.5 | x | x | 0 | NA | 0.03 | 70 | 0.7 | 2200 |
| SHALLOW WATER Corelock | A_s | 12.8 | x | x | x | x | 0.03 | NA | 0.55 | 1500 |
| SHALLOW WATER Corelock | E_s | 10.5 | x | x | x | x | 0.05 | 110 | 0.62 | 2000 |

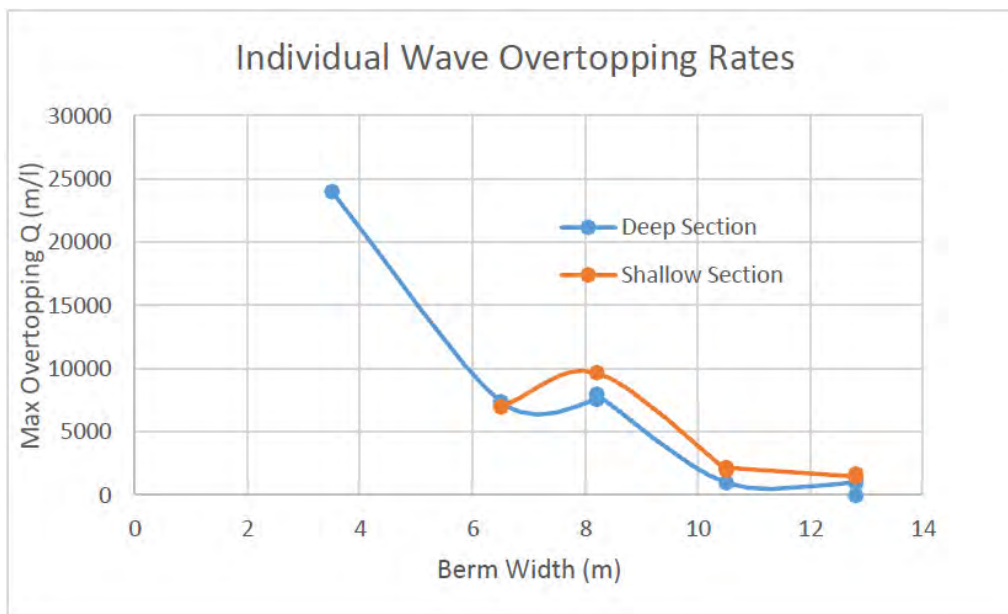


Figure 11. Individual overtopping volume for various berm widths

4 CONSTRUCTION

The final construction drawings with all the design changes, after the physical models carried out the NRC, was completed at the end of December 2016, before the contractor finished the approach to the breakwater. Previous to the placements of the Tetrapods on the breakwater, a test cross section was done in land to review the tolerances and packing density as required in the specified special placement pattern. Tetrapod placement in the water initiated in early March 2016. The redesigned wide berm breakwater reduced the overall cost by more than 3 million euros, further the increase in available area eased the construction since additional turning bays for the trucks transporting the stone materials are not needed and a “bottle neck” effect is not created for the 1 km long breakwater, the total width considering the road way and parking of the crest allows for different equipment and parallel construction.



Figure 12. Test Cross Section in Land and Tetrapod Placement in the water.

4.1 Toe Trench Construction

The results from the second physical model at the NRC proved that the breakwater's toe trench is very important for the stability of the breakwater and could not be avoided. The toe trench construction at the beginning of the project was done with a 5-ton heavy chisel that was dropped from a height of 10m into the water to loosen the hard calcarenite and then a clam shell bucket with teeth was used to scrape the calcarenite. This initial method proved to be difficult to attain the trench precision and tolerances as required by the design, less than 100m were excavated with this method. The construction methodology of the trench was changed to attain a better precision; a large backhoe dredger was mobilized to complete the toe trench excavation with better results. Nevertheless, a small gap between the leeward row Tetrapods and the trench's vertical wall was inevitable, as shown in figure 13. During construction, large 5m waves impacted the breakwater and the Tetrapods in the trench. The shallow water section had a minor slide towards the front wall of trench, validating the conclusion found in the physical model, which is that a Toe Trench is of utmost importance for the stability of the shallow water section of the breakwater.



Figure 13. Prototype excavated trench and confinement of Tetrapods by the trench at the shallow section.

4.2 Tetrapod Placement Pattern

The performance of the Tetrapod stability with the specified special placement pattern has proven to be stable. During construction the placement pattern was easily achieved by the contractor (figure 14) and no movement or rocking of the Tetrapods has been recorded.



Figure 14. Prototype Tetrapod placement pattern

The construction of the breakwater has progressed based on the redesigned cross section after the physical model carried out at the NRC. Approximately 500 meters of the 1-kilometer long breakwater has been constructed thus far. A wave gauge was installed at a depth of 17.5 m to monitor the performance of the breakwater. The 17.5 m depth matches the approximate depth of where the waves were generated in the physical model. Several large storms have impacted the breakwater during the construction comparable to the 50-year return period event. Since the berm and the crown wall have not yet been built the performance of overtopping is still indicative, nevertheless the design has proven satisfactory under these conditions.

5 CONCLUSION

The crest-height reduction of the breakwater of the Ayia Napa Marina was achieved through creating a wide-berm breakwater section. The combination of an outer Tetrapod section with an inner rock berm to reduce the overtopping rates, proved to be the key to lowering the crest height of the breakwater creating an innovative solution to the obstruction of views by a common breakwater section. The additional length of the required top berm was determined through physical model tests at the NRC, carrying out 14 variations of the berm width and water depth. The additional width of 10.5 meters allowed for a reduction of 2.5m of the crown height, allowing for unobstructed views for the resort-style development on the lee side of the breakwater.

The two-dimensional physical model studies carried out to support the design changes of the breakwater were crucial to obtain a safe reliable solution. The low crested wide berm breakwater will protect the new mega-yacht marina for 100-year return period storms. An expedited physical model was used to investigate key issues that were raised during early stages of construction, including potential elimination of the toe trench and lowering of the breakwater crest. The model was used to assess these changes to the initial breakwater design, and the knowledge and results gained from the physical model study have been used to support and optimize the final design of the new breakwater.

The lowering of the breakwater's crest height provided more harmonic integration with the development's landscape and users, and allowed for substantial cost savings for the owner. Design performance and development economic performance were both enhanced as a result. The design changes have also eased the construction impacts, providing better access and additional valuable, developable areas for the Ayia Napa Marina.

6 REFERENCES

Cox, J and H Clifford 2014, "Inferring Breakwater Overtopping and Wave Transmission Performance Based on Armor Type", Coastal and Marine Research, 2(2):23-36

EurOtop, 2016. Manual on wave overtopping of sea defences and related structures. Van der Meer, J.W., Allsop, N.W.H., Bruce, Kortenhaus, A., Pullen, T., Schüttrumpf.

Boshek, M. R. and Cox, J. C (2016). Design and Engineering of a Breakwater in Cyprus. Ports 2016, 14th Triennial International Conference, New Orleans

Hirayama, K. (2002). Utilization of Numerical Simulation on Nonlinear Irregular Wave for Port and Harbor Design, Port and Airport Research Institute of Japan Technical Note 1036.

Provan, M., and Knox, P., 2017. 2D Hydraulic Model Study of the Cyprus Makronisos Breakwater, National Research Council of Canada Controlled Technical Report OCRE-TR-2017-002

Van Gent, M. R. (2013). Rock stability of rubble mound breakwaters with a berm. Coastal Engineering, 78, 35-45,

SITE CONDITIONS FOR PORT DEVELOPMENT IN CENTRAL PANAMA'S ATLANTIC COAST

by

Luis D. Alfaro¹

ABSTRACT

The purpose of this paper is to present a general description of the geological and seismic conditions in the Atlantic coast in the vicinity of the Panama Canal. Geologic conditions involve very soft marine sediments, as well as a predominant rock formation that presents distinctive characteristics. Seismic conditions were revised in 2016, based on studies made in support of the Panama Canal Expansion Program. This paper describes proven best practices and analyzes the potential impact of the stronger ground motions on such practices.

1. INTRODUCTION

The construction of the Panama Canal has motivated the development of multiple ports at both ends of the 80-km long Canal. With the expansion of the Canal, and its new NeoPanamax-size locks, it is likely that additional port facilities will be built in the near future. Container Traffic in 2016 on the Atlantic coast of central Panama reached 3.2 MTEU (million twenty-foot equivalent units) (2). CAF Banco de Desarrollo de America Latina estimates that this traffic will grow to 13.5 MTEU by 2040 (2). Such forecasts imply the need for a significant increase in port facilities in the area. Figure 1 presents a map of the Atlantic Coast of central Panama (Canal area), with existing ports and other facilities.

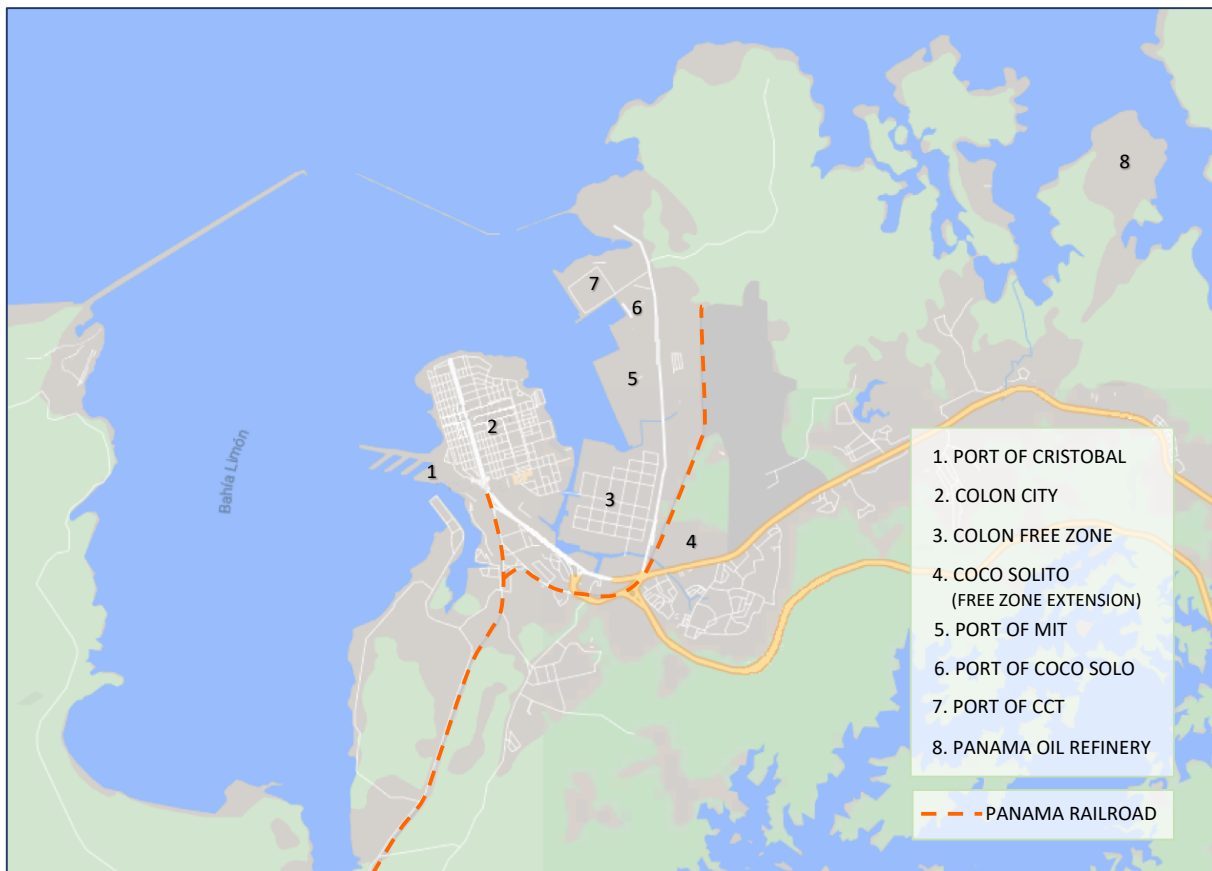


Figure 1: Area of interest with main facilities

¹ Ingenieros Geotécnicos, S.A., Consulting Engineer, Panamá

2. GEOLOGIC CONDITIONS

Figure 2 presents an extract of the Geologic Map of the Panama Canal and Surrounding Areas prepared by Stewart et al (15) for the Atlantic region. Three dominant geologic formations are of interest: The Gatun Formation (Tg), The Undivided Holocene sediments (Qa), and the Holocene fringing coral reefs (Qr). Appendix A presents a legend and a correlation diagram that indicates the placement of these formations in the geologic history of the area. Following is a brief characterization of the three formations identified.

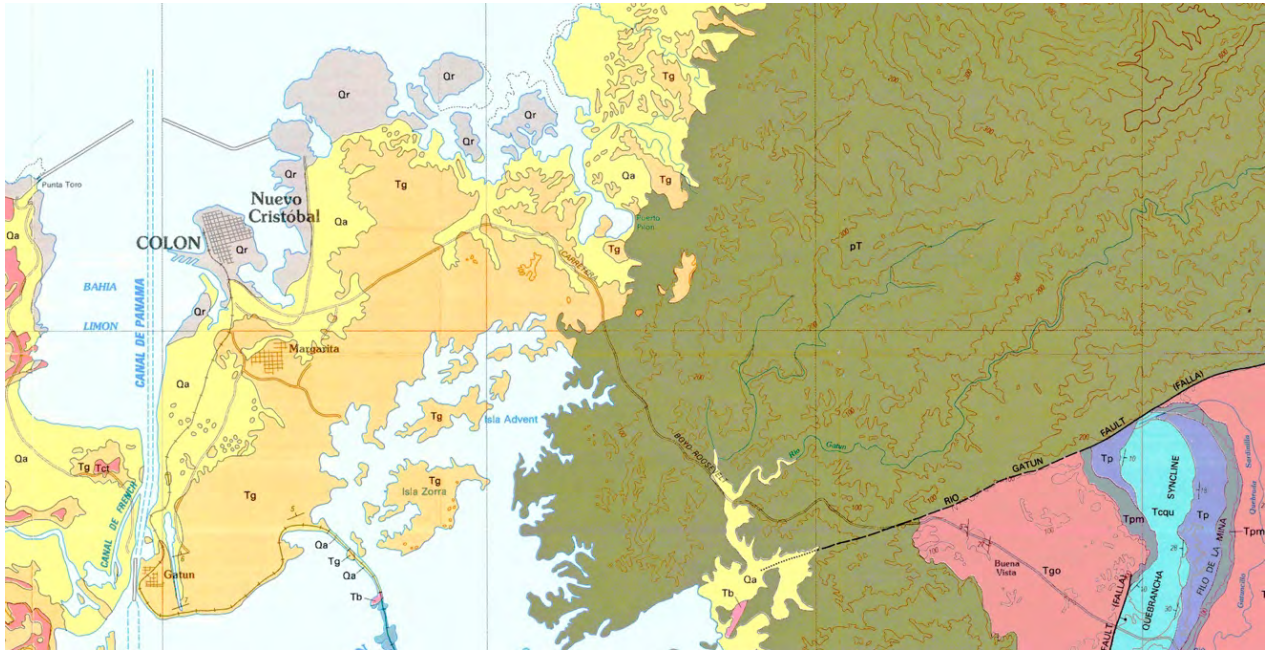


Figure 2: Geologic map – Atlantic Region

2.1 Gatun Formation (Tg).

This is a middle Miocene sedimentary formation composed of sandstones, siltstones, tuffs and conglomerates.

Jones (8) describes the Gatun as “mudstones, siltstones, conglomerates and tuffs, all thickly and massively bedded. The siltstones, sandstones, and conglomerates are variably marly and tuffaceous, highly fossiliferous and massively jointed... The tuffs are uniformly grained siltstones and claystones except for local streaks, sparsely scattered with pumice pebbles and cobbles. The formation has a thickness known to exceed 1,400 feet and probably much more. The beds dip north-westerly to northerly at angles ranging uniformly from 2° near the shore of Limon Bay to as much as 20° in a few places near their south-eastern border. The depth of overburden and weathered rock averages about 30 feet on this formation. The weathered rock is soft and grades imperceptibly into red clay soil.” Appendix 1 in this reference, provides a detailed description of the sequence of the lithologic units contained in this formation.

De Puy (7) presents a summary of material parameters for the Gatun Formation, based on extensive testing performed by the Autoridad del Canal de Panama in their geotechnical laboratory. Table 1 presents various statistics that provide a sense of the range of values for these material’s parameters. These statistics incorporate the various lithological groups contained in the formation, without any segregation. These groups include the following rock types: sandstone, sandstone fossiliferous, sandstone conglomeratic, sandstone pumiceous, siltstone, tuff, and conglomerate.

De Puy (7) also reports geophysical tests which reveal that the shear wave velocity ranged between 400m/s to 900m/s for sound rock, and between 300m/s and 600m/s for weathered rock. Triaxial testing of intact samples revealed an average internal angle of friction of 56°, and an average cohesion of 3.3 MPa.

Table 1: Parameters for materials of the Gatunn Formation

| Parameter | Number of tests | Mean | Mode | Standard deviation | Coefficient of Variation | Minimum value | Maximum value |
|---------------------------------------|-----------------|-------|-------|--------------------|--------------------------|---------------|---------------|
| Unit weight (kg/m ³) | 466 | 1,859 | 1,900 | 179 | 9.6% | 1,313 | 2,435 |
| Unconfined compressive strength (MPa) | 532 | 5.5 | 4.0 | 3.7 | 67.3% | 0.6 | 42.4 |
| Elastic Modulus (MPa) | 466 | 1,228 | 800 | 786 | 64.0% | 149 | 6,462 |

2.2 Undivided Holocene Sediments (Qa).

This is a Quaternary formation composed of marine and fluvial sediments. Stewart et al. (15) included man-made fills in this formation. This formation is commonly referred to as Atlantic Muck in technical documents and in general practice.

A general characteristic of this formation is that it is very heterogeneous. Mesa (12), through a systematic program of laboratory tests, provides ranges of material parameters measured for marine sediments in central Panama. Table 2 summarizes these parameters for the Atlantic Muck.

Table 2: Parameters of the Atlantic Muck

| Parameter | Low value | High value |
|---|-----------------------|-----------------------|
| Natural water content – w(%) | 43 | 138 |
| Liquid Limit - LL | 45 | 83 |
| Plasticity Index (PI) | 17 | 35 |
| Specific gravity of solids (Gs) | 2.46 | 2.79 |
| Moist unit weight – γ_m (T/m ³) | 1.44 | 1.84 |
| Dry unit weight – γ_d (T/m ³) | 0.73 | 1.28 |
| Preconsolidation pressure – p'_c (kg/cm ²) | 0.22 | 0.80 |
| Coefficient of consolidation – c_v (cm ² /s) | 0.11×10^{-4} | 20.9×10^{-4} |
| Oedometric modulus – m_v (cm ² /kg) | 0.001 | 0.202 |
| Compression index – Cc | 0.20 | 1.71 |
| Vertical Coefficient of Permeability – k_v (cm/s) | 0.1×10^{-9} | 1.97×10^{-7} |
| Horizontal Coefficient of Permeability – k_h (cm/s) | 9.9×10^{-8} | 1.25×10^{-7} |
| Cohesion – c (T/m ²) | 0.2 | 1.95 |
| Angle of internal friction – ϕ (degrees) | 2 | 13 |
| pH | 6.8 | 7.0 |

2.3 Holocene fringing coral reefs (Qr).

Kennedy et al. (10) state in their abstract: “Fringing reefs are generally not simple veneers of coral growth along tropical shorelines. Extensive research over the past few decades, based on radiocarbon dating of Holocene reef deposits, has indicated that they can develop in a complex variety of ways even though the surface morphology may appear relatively simple. The principal factor that appears to determine the growth and morphology of fringing reefs is the available accommodation space. Sea-

level fluctuations are important, primarily because the sea surface determines the absolute accommodation space for a given reef. This means that a reef established during a period of sea-level rise will be able to accrete vertically as space is created above it. If, however, the reef establishes at, or grows to, the sea surface, thereby occupying all the available accommodation space, it can no longer accrete vertically and begins to build laterally.”

This formation has not figured prominently in projects developed in the area, except in two instances: (a) dredged coral reefs are stored by Canal authorities and used as competent fill material when required; and (b) driving concrete piles through these materials may require pre-drilling. Apart from these comments, this formation will not be addressed further in this paper.

3. SEISMIC CONDITIONS

Central Panama has been subjected to two important earthquakes. Figure 3 shows a map (6) indicating the estimated location of the earthquake of 7 September 1882. Intensities are in the Modified Mercalli scale.

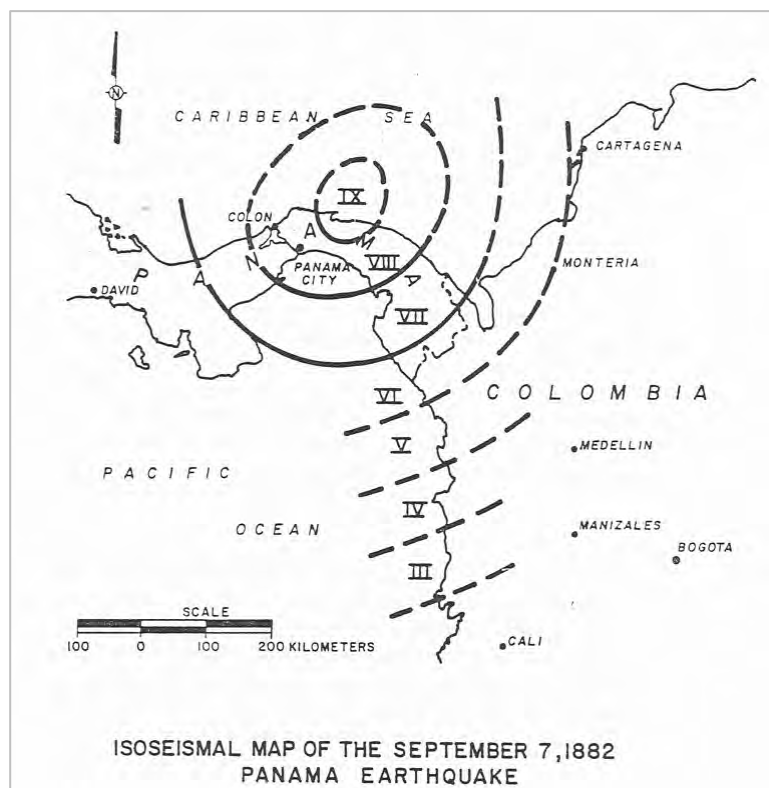


Figure 3: Estimated location of Epicenter – 1882 Earthquake

It originated on a subduction zone called the North Panama Deformed Belt, which is shown in Figure 4 (19).

Figure 5 shows an extract of the Geologic Map of the Panama Canal and Surrounding Areas prepared by Stewart et al (15) for the Pacific region. Crustal Fault Pedro Miguel, shown on this map, is believed to be source of the 2 May 1621 earthquake.

Historical accounts of these earthquakes (4, 5, 6, 11, 13, 20) led the *Autoridad de Canal de Panamá* to perform a detailed characterization of the seismicity of the region. This information was used for the design of the new Pospanamax locks and the new earth dams required for the Canal Expansion Program. Association of the Pedro Miguel Fault and the 2 May 1621 earthquake is presented in (14).

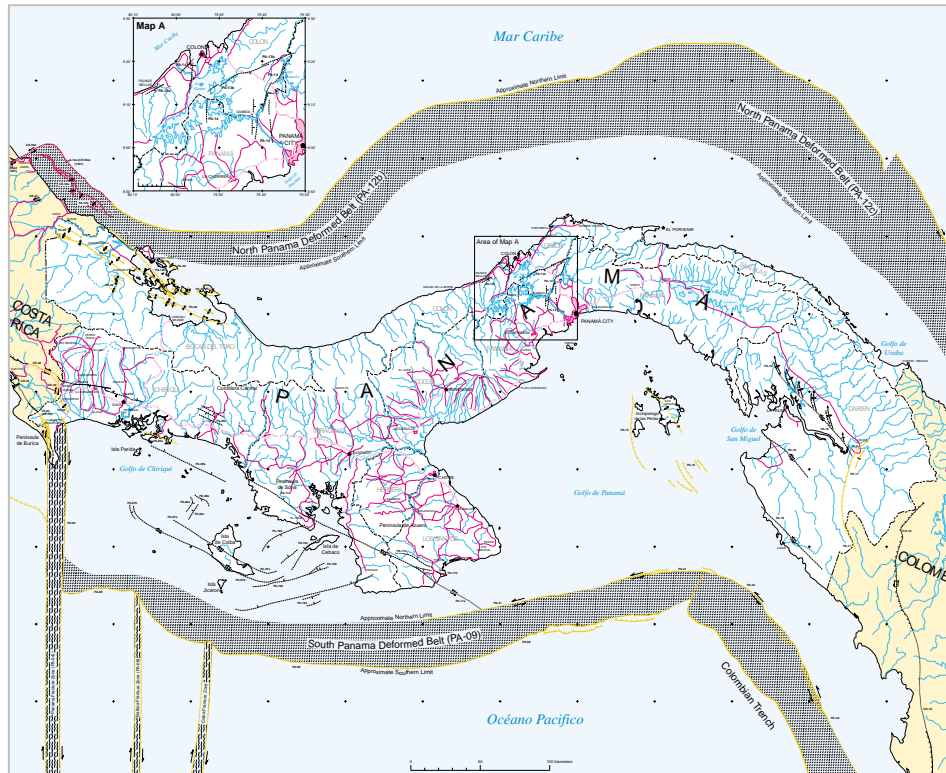


Figure 4: USGS map of faults and folds - Panama

Later, the information was transmitted to the *Junta Técnica de Ingeniería y Arquitectura*, institution that regulates the practice of engineering and architecture in the country, and created and maintains the Panamanian Structural Design Code, or REP which is its acronym in Spanish (9). The new ground motion assessments were incorporated in the 2014 version of the REP, which was published in 2015 and enforced in 2016.

Figures 6 present s a map with peak ground accelerations, from a Probabilistic Seismic Hazard Analysis, for a recurrence period of 2,500 years (16, 17). We note that in addition to the higher ground motions, the code also incorporates the use of a recurrence interval of 2,500 years, instead of the 475-year recurrence interval used by previous versions of the codes. The new ground motions also increase the seismic design category for structures in many areas.

The increase in ground motions identified by the new code, has a direct impact on ground response, structural response, and associated phenomena such as liquefaction. These issues must now be given greater attention.

This map reflects the influence of the North Panama Deformed Belt, and of the crustal faults, believed to be active in the area (14). These are the Pedro Miguel Fault (shown in Figure 5), the Gatun Fault (shown in Figure 2) and the Limón Fault (not shown but believed to be a possible extension of the Pedro Miguel Fault to the North).

This map provides an integral conception of the seismicity of the area. It was later complemented by a Deterministic Seismic Hazard Analysis, which was used to “cap” the probabilistic analysis near the three crustal faults mentioned. The resulting maps for peak ground accelerations, spectral accelerations for 0.2 s, and spectral accelerations for 1.0 s are included in (9). These are the maps that should be used for design.

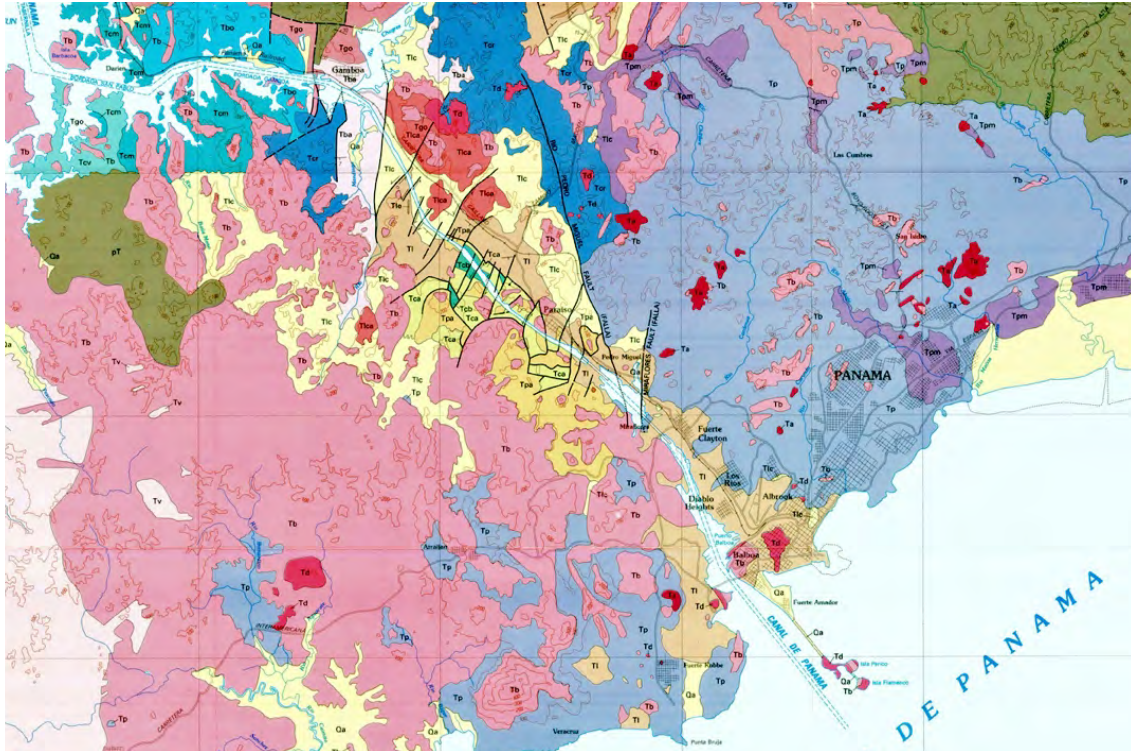


Figure 5: Geologic map – Pacific Region

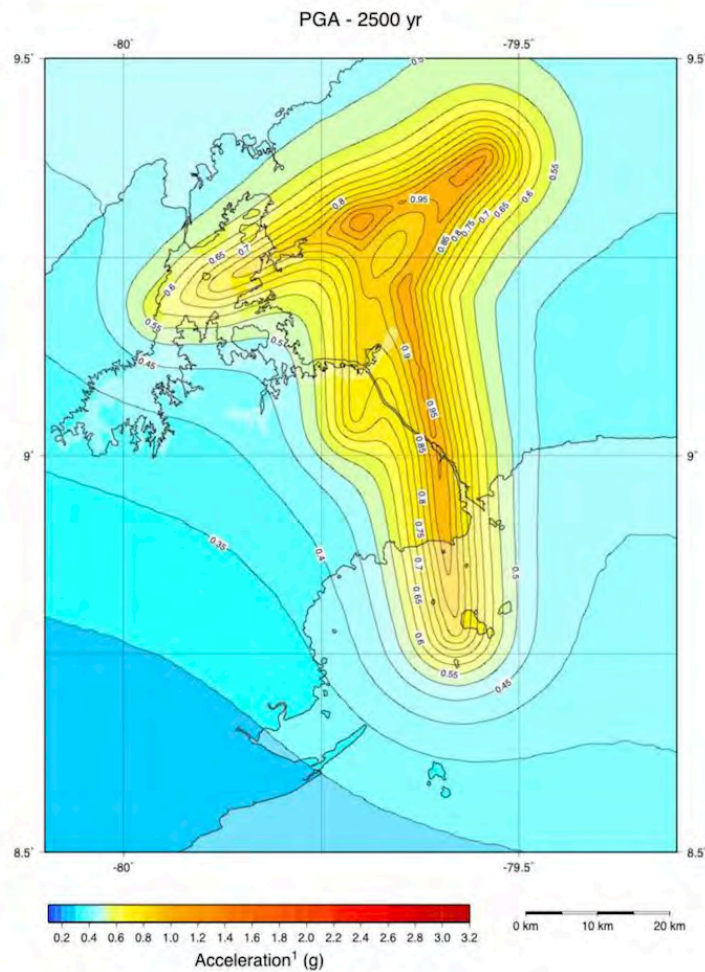


Figure 6: Peak ground accelerations 2,500 return period – Canal area

4. EXPERIENCE WITH THE GATUN FORMATION (Tg)

For over a century, large civil works have been developed on the Atlantic area, as shown in Figure 1. This has required an understanding of the characteristics of the Gatun Formation (Tg) and the Undivided Holocene Sediments (Qa). Engineering practices for dealing with these materials have progressively evolved with each major project. This experience provides a wealth of information that is beneficial to the development of future projects. Following are the principal learnings with various types of situations and problems.

4.1 Excavation process in the Gatun Formation

The Gatun formation does not present a significant amount of weakness planes that control its behavior, as is common in many other geologic formations in the region, which are of volcanic origin. Therefore, relatively steep slopes can be excavated without much risk of instabilities. The first excavations performed for the Third Set of Locks in the Panama Canal, began in 1940, but were stopped in 1942 due to World War II. The excavations were left in place since then. Of the almost 5 km of slopes left in place (including both banks of the 2,400m channel), only a minor wedge-type slide took place in the stated period. When the Third set of Locks project was restarted on the Atlantic side in 2009, excavations continued, as the new locks are much larger than those envisioned in the 1940s) from where they were left in 1942. Again, no significant instabilities took place.

With modern excavation equipment, excavating sound Gatun Formation usually does not require the use of explosives. The latest deepening of the Atlantic Entrance of the Panama Canal was performed with a large cutter-suction dredge, without prior blasting.

The same has been observed with dry excavation on land. Explosives are not necessary and are only used when a higher productivity is warranted. It becomes a matter of economics: time and cost of excavation with explosives versus time and cost of excavation without explosives.

In general, excavation in the Gatun Formation is a relatively simple process, with none of the ubiquitous landslide problems present in the Canal's Gaillard Cut, where the Canal crosses the continental divide in the isthmus.

4.2 Foundations on the Gatun Formation

The material parameters presented in Table 1 indicate that this material can be considered a soft rock. Shallow foundations on rock outcrops can usually be designed for an allowable bearing capacity of 2,000 kPa.

Drilled pile foundations can be designed for a similar tip resistance if the pile has little penetration into sound rock. A pile socket into bedrock would require a more detailed analysis to establish consistent tip resistance and shaft friction resistance in the socket. Drilling into the Gatun formation poses no difficulties for pile drilling equipment.

Driving piles into the Gatun formation is another matter. Even with hardened steel tips, it is difficult to drive concrete piles or steel piles (pipes or HP sections) into the Gatun Formation. Concrete piles do not penetrate into the Gatun formation. Excessive driving will damage them. Similarly, steel piles will suffer buckling and rupture before penetrating into sound Gatun. If driving piles into sound Gatun is required to achieve a condition of fixity, pre-drilling is necessary. The use of test piles is very convenient for a large project, to determine realistic construction needs before beginning production pile driving.

The higher ground motions in REP-2014 favor the use of more flexible structures, so the use of batter piles is, in general terms, undesirable.

4.3 Using Gatun Formation materials as fill

Materials of the Gatun formation have been used extensively for constructing fills in many of the projects shown in Figure 1. This includes the city of Colon, the Colon Free Zone, the Oil Refinery, all of the ports, the railroad and various highways.

Fills constructed with materials from the Gatun Formation are excellent, if proven practices for construction, as outlined below, are followed.

- The material should be used as soon as it is extracted from the borrow area. This limits exposure time that promotes weathering. The clay content of these materials deteriorates when in contact with air and water. The excavated materials from the Gatun Formation should not be stored temporarily in stockpiles. Cutting from the source and filling at the project site should be a continuous operation.

- The equipment used to excavate the material should be such that, the largest block size is 40 cm.
- The fill must be placed in layers that are 30 cm thick. It has been observed that material with a largest block size of 40 cm will result in a layer of 30 cm when compacted.
- The fills must be compacted using optimal water content, achieving a dry density of 98% of the maximum given by Standard Proctor test. The degree of compaction must be verified in the field based on requirements defined by the Ministry of Public Works (MOP).
- At all times during fill placements, the top surface of the fill must have a slope greater or equal to 2% to avoid the infiltration of runoff during and after periods of precipitation.
- If the surface on which the fill is to be placed is soft, a woven geotextile, performing a separation function, must be placed at the site before filling commences. Afterwards, the fill can progress as indicated above. In no case can a layer of boulders be placed over the soft soil, with the supposed intent of “stabilizing the area” before fill construction.

Large shear box testing of crushed Gatun formation samples (7) revealed an average internal angle of friction of 33° and an average cohesion of 0.025 MPa. De Puy.

Berman et al. (3) present a project in which materials from the Gatun formation were used to construct a fill, utilizing the procedure outlined above. The resulting compacted fill exhibited Standard Penetration Test results with an average of $N = 33$ blows/foot. A mat foundation 8.0 meters wide was selected by the client to support a series of low-rise buildings, and a Plaxis 2D model was used to estimate potential settlement under a uniform load of 50 kPa. The prediction was that settlements would be limited to 10.0 mm. Actual performance of the structures has been excellent. Measured settlements have not exceeded 7.0 mm.

5. EXPERIENCE WITH THE UNDIVIDED HOLOCENE SEDIMENTS (Qa)

5.1 Consolidation of the Sediments

The material parameters shown in Table 2 evidence the high compressibility of these sediments. Compression indexes as high as $C_c = 1.71$ are indicative of very large void ratios and very significant potential settlements under load.

Light structures built on these materials, or on several meters of fill placed over these materials, have exhibited significant damage, and in some cases collapse, when a site is not prepared (stabilized) properly.

5.2 Liquefaction potential in the Sediments

The 1882 earthquake caused extensive liquefaction in zones of predominantly sandy materials. Figure 7 presented in (4) shows the general area (hatched) where liquefaction was reported. The figure also shows the areas affected by Tsunami, which was the main cause of death during the earthquake.

It is interesting that the term liquefaction was not yet in use at that time. Camacho and Viquez (4) quote The Star and Herald, the local newspaper of the day, stating (translated to English): “In Donoso (a town) on the coast of Colon...craters were observed from which gushes of water were ejected, reaching almost the height of a house. In (another location) close to this town, a 10-meter wide crack opened in the ground.”

In 1991, the Limon M7.6 earthquake in Costa Rica (also generated on the North Panama Deformed Belt) caused extensive liquefaction in similar coastal sediments along the Atlantic coast of the province of Bocas del Toro, the westernmost part of the Panamanian Atlantic coast.

The higher ground motions in REP-2014 increase the importance of performing appropriate liquefaction triggering evaluations for sites in which the materials may be susceptible to this phenomenon.

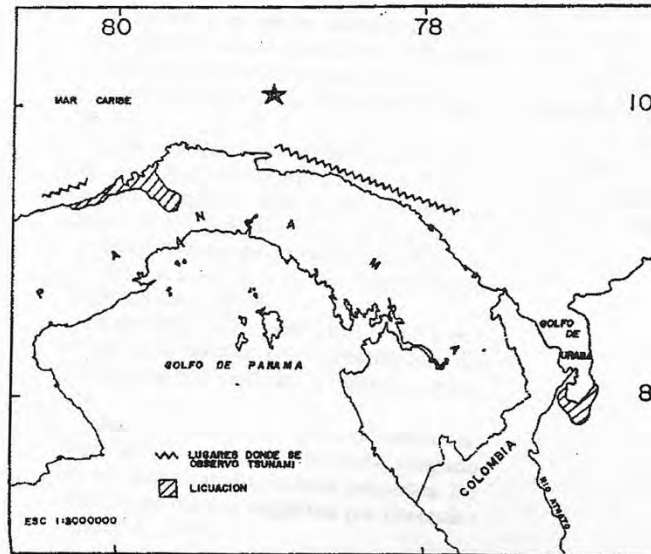


Figure 7: Areas of Liquefaction and Tsunami – 1882 Earthquake

5.3 Construction on Sites with Soft Sediments

Container yards, roads, dredge disposal sites and light structures have been built in areas that present soft sediments in their geologic profile. All can be safely built with the proper site preparation. The opposite is also true. In some cases, structures are supported on piles, but the ground slab is supported on grade. The differential settlements generally cause damages to the affected structures.

Preloading has worked well in the past to increase the strength and reduce the compressibility of these materials. The use of vertical wick drains, piezometers and settlement plates make it very straightforward to prepare a site for its reliable use.

Furthermore, experience has shown that consolidation under preloading is relatively quick. Often 6 to 12 months will suffice to make a site adequate if vertical drains are not used. If they are used, it would take significantly less time. Plotting the performance of settlement plates, and the reduction of excess pore pressures in piezometers, make the process very reliable. The end of consolidation is readily detected, and the site can perform well under loads that are lower or equal to the preloading applied.

Alfaro et. al (1) describe the difficulties that these sediments posed for the construction of the Gatun Dam in the early XX Century. This is a key structure of the Panama Canal, as it impounds the Gatun lake to enable the use of the Canal's locks. A model dam was constructed to validate solutions to these very adverse conditions. The success of the dam is indicative that construction on these soft materials is feasible if proper methods are used. The fact that this complex structure was built in this era, is a testament to the genius of Canal designer and builders.

5.4 Navigation channels in the Sediments

Very soft sediments usually require very flat slopes to maintain their stability. Experience shows that commonly slopes (vertical: horizontal) of 1:3 or 1:4 are required. On occasions, flatter slopes may be required. However, since these slides are usually not critical, it becomes an issue of economy between initial costs and maintenance costs.

6. CONCLUSIONS AND RECOMMENDATIONS

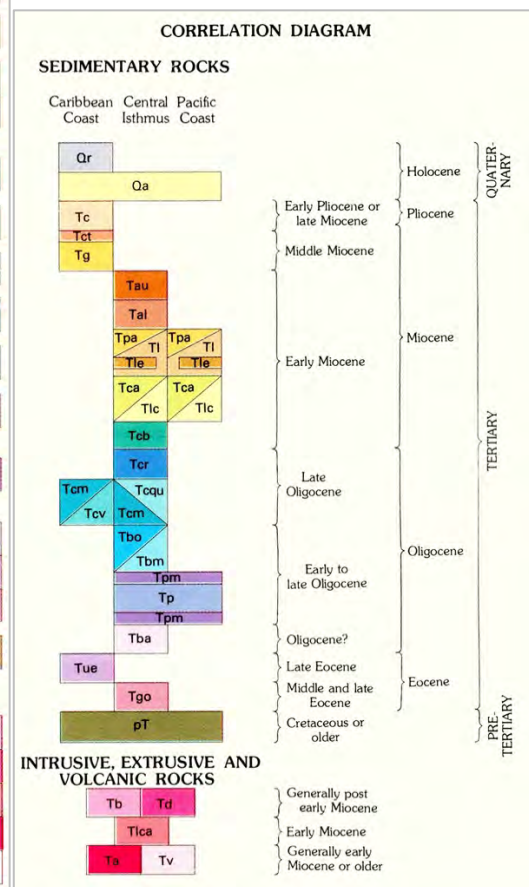
- Gatun formation materials have been used successfully in many large projects; as in-situ competent rock, and as compacted fills.
- Gatun formation materials constitute a promising resource for developing future engineering projects in the area. This paper describes its peculiarities, and recommendations for its effective use.
- The problems associated with the presence of soft sediments along the coast, can be mitigated if proper and proven procedures are used in design and construction.

Appendix A: Geologic legend and correlation diagram (15)

The geologic formations discussed in the paper are included in the following legend and correlation diagram for all the formations present in the Canal area.

LEGEND

| | |
|--|------|
| Undivided Holocene sediments, principally alluvium or fill | Qa |
| Holocene fringing coral reefs | Qr |
| Chagres Sandstone, late Miocene or early Pliocene. Massive, generally fine-grained sandstone | Tc |
| Toro Limestone, basal member of Chagres Sandstone. Coquina | Tct |
| Gatun Formation, middle Miocene. Sandstone, siltstone, tuff and conglomerate | Tg |
| Alhajuela Formation, upper member, late early Miocene. Tuffaceous sandstone, calcareous sandstone and limestone | Tau |
| Alhajuela Formation, lower member, late early Miocene. Calcareous sandstone | Tal |
| La Boca Formation, early Miocene. Mudstone, siltstone, sandstone, tuff and limestone | Tl |
| Emperador Limestone, member in lower La Boca. Coraliferous limestone | Tle |
| Pedro Miguel Formation, early Miocene. Fine-to coarse-grained agglomerate | Tpa |
| Cucaracha Formation, early Miocene. Bentonitic clay shale, carbonaceous clay shale and in lower part, a thin ash flow tuff | Tca |
| Las Cascadas Formation, early Miocene. Agglomerate and soft, fine-grained tuff | Tlc |
| Culebra Formation, early Miocene. Calcareous sandstone and siltstone | Tcb |
| Caraba Formation, late Oligocene. Principally a dacite porphyry agglomerate. In type area, conglomerate, fossiliferous calcareous sandstone and limestone | Tcr |
| Caimito Formation, late Oligocene, marine. Tuffaceous sandstone, tuffaceous siltstone, tuff and foraminiferal limestone | Tcm |
| Caimito Formation, volcanic facies, late Oligocene. Agglomerate and tuffaceous graywacke | Tcv |
| Quebrancha Limestone, member of Caimito Formation, late Oligocene. Foraminiferal limestone and calcareous siltstone | Tcqu |
| Bohio Formation, early to late Oligocene. Conglomerate, principally basaltic and graywacke sandstone | Tbo |
| Bohio Formation, marine facies, early to late Oligocene. Calcareous sandstone and small-pebble conglomerate | Tbm |
| Panama Formation, early to late Oligocene. Principally agglomerate, generally andesitic in fine-grained tuff. Includes stream-deposited conglomerate | Tp |
| Panama Formation, marine facies, early to late Oligocene. Tuffaceous sandstone, tuffaceous siltstone, algal and foraminiferal limestone. Sandy siltstone in basal part of formation in Quebrancha syncline | Tpm |
| Bas Obispo Formation, Oligocene(?). Agglomerate and hard tuff | Tba |
| Marine rocks, late Eocene. Sandstone and siltstone | Tue |
| Gatuncillo Formation, middle and late Eocene. Mudstone, siltstone, quartz sandstone, algal and foraminiferal limestone | Tgo |
| Pre-Tertiary. Altered basaltic and andesitic lavas and tuff. Includes dioritic and dacitic intrusive rocks | pT |
| INTRUSIVE, EXTRUSIVE AND VOLCANIC ROCKS | |
| Intrusive and extrusive basalt, middle and late Miocene | Tb |
| Intrusive dacite and dacite porphyry, Miocene | Td |
| Andesite, equal in age to Las Cascadas Formation, early Miocene | Tlca |
| Intrusive and extrusive andesite, Oligocene and early Miocene | Ta |
| Volcanic rocks, undifferentiated, generally early Miocene or older | Tv |



REFERENCES

1. Alfaro, L.D., Barrelier, M.H. and De Puy, M. Gatun Dam History and Developments. Engineering the Panama Canal. A Centennial Retrospective, Edited by Bernard G. Dennis, Jr. p.367-383 ASCE (2014)
2. Arroyo Crejo, F. Desarrollo Portuario en América Latina y Caribe, Horizonte 2040. Presentacion hecha en AAPA XXV Congreso Latinoamericano de Puertos en Mérida México (2016).
3. Berman, G. and Rangel, T. Ingenieros Geotécnicos, S.A. report on foundation design for Building in Renovación Urbana de Colón (2016).
4. Camacho E. and Víquez, V. El Terremoto de San Blas del 7 de septiembre de 1882. Fecha
5. Camacho, E. y Víquez, V. Historical Seismicity of the North Panama Deformed Belt, Rev. Geol. America Central No. 15 fecha
6. D'Appolonia Project No. 81-563. Report on the Seismicity Evaluation of the Tabasará Hydroelectric Project in Western Panama for Acres International Ltd. Niagara Falls, Ontario Canada December (1981).
7. De Puy, M. Gatun Formation Engineering Properties. Internal presentation given in *Autoridad del Canal de Panamá* (2011)
8. Jones, S.M. Geology of Gatun Lake and Vicinity, Panama. Bulletin of the Geologic Society of America, Vol. 61, pp.893-922, September (1950).
9. Junta Técnica de Ingeniería y Arquitectura. Reglamento Estructural de Panamá – REP-2014. Resolución No-JTIA-187-2015 (2015).
10. Kennedy D.M. and Woodroffe C.D. Fringing reef growth and morphology: a review. School of Geosciences, University of Wollongong, Wollongong, NSW 2522, Australia Earth-Science Reviews 57 p. 255–277 (2002).
11. Mendoza, C. and Nishenko, S. The North Panama Earthquake of 7 September 1882: Evidence for Active Underthrusting. Bulletin of the Seismological Society of America, Vol. 79, No. 4, pp1264-1269, August (1989).
12. Mesa, C. Características del Suelo Marino (Lama) en Panamá. Reporte Técnico No. CEI-01-002, Universidad Tecnológica de Panamá, Vicerrectoría de Investigación, Postgrado y Extensión, Centro Experimental de Ingeniería. Noviembre (2001).
13. Requejo Salcedo, J. Historical and Geographical Report about Panama from 1640. Original manuscript from the Museum-Library, Seville, Spain. Translation into English by Alice E. Westman in 1947, available at http://bruceruiz.net/PanamaHistory/panama_report_1640.htm.
14. Rockwell, T., Gath, E., González, T., Madden, C., Verdugo, D., Lippincott, Dawson, T., Owen, L.A., Fuchs, M., Cadena, A., Williams, P., Weldon, E., Franceschi, P. Neotectonics and Paleoseismology of the Limón and Pedro Miguel faults in Panamá: Earthquake hazard to the Panamá Canal Article in Bulletin of the Seismological Society of America 100(6):3097-3129 · December 2010
15. Stewart, R.H., Stewart, J.L. and Woodring, W.P. (1980). Geologic Map of the Panama Canal and Vicinity, Republic of Panama. Department of the Interior, United States Geological Survey, Miscellaneous Investigation Series, MAP I-1232.
16. URS Corporation, Development of Design Earthquake Ground Motions, Final Report Prepared for the Panama Canal Authority (2008).
17. URS Corporation, Explanatory Notes for the Probabilistic Seismic Hazard Maps of Panama, Final Report Prepared for the Panama Canal Authority (2009).
18. URS Corporation. Report on “Geotechnical Evaluation of Gatun Dam” ACP Contract No. CMC-172538, Task Order No. 8. (2012)
19. U.S. Geological Survey. Map of Quaternary Faults and Folds of Panama and its Offshore Regions. Open File Report OFR-98-779 (1998).
20. Víquez, V. and Camacho, E. El Terremoto de Panamá la Vieja del 2 de mayo de 1621: Un Sismo Intraplaca. Boletín de Vulcanología No. 13 (1994).

CONTAINER PORT DEEPENING IN CARTAGENA

Brian E. Shaw, PE ¹

ABSTRACT

Manga Terminal, operated by SPRC in the heart of Cartagena, Colombia, expanded at a moderate pace through the late 20th century to incorporate products ranging from cruise to Ro/Ro, and the first container handling berths were retrofit in 1985. Growth surged in recent years, precipitated by the expansion of the Panama Canal and consequent demand for nearby, deep water berths and container transshipment terminals. The two terminals operated by SPRC in Cartagena, Manga and Contecar, are now one of the top five container handling entities in Latin America.

After Berth 9 was constructed in 2011, the terminal could not expand significantly due to land constraints, so operators turned to modernization projects to increase throughput capacity. This paper discusses port improvements which will allow docking of New Panamax vessels alongside four berth segments, totaling 700m in length, originally designed and equipped for Panamax class ships. The increase in mooring and berthing load required upgrades to fenders and localized strengthening of the mooring hardware and berth structures. Dredging at the berth face was enabled through installation of toe walls to retain the existing under-wharf slope – a particularly challenging design for one segment with an existing toe wall. Ship to shore operations will be improved through procurement of larger gantry cranes in the future.

Innovative engineering allowed cost-effective upgrades which maximized reuse of existing infrastructure, with the constraint of maintaining container throughput during the construction period.

This discussion will be of interest and benefit to port planners and design engineers, specifically those adapting existing infrastructure to the ever-larger needs of the shipping industry.

¹ Moffatt & Nichol, USA, bshaw@moffattnichol.com

INTRODUCTION

The Manga Marine Terminal is located within Cartagena on the northern coast of Colombia, approximately 650 miles north of the Capital at Bogota and 330 sea miles east of the Atlantic mouth of the Panama Canal. Sociedad Portuaria de Cartagena (SPRC) owns, operates, and maintains this terminal in conjunction with nearby Contecar to the southeast. Together, they are one of the top five container handling entities in Latin America.

The Manga Marine Terminal was originally constructed in 1934 and expanded at a moderate pace through the late 20th century to incorporate products ranging from cruise to Ro/Ro, with the first container berth retrofits in 1985. Port operations are now focused around container transshipment along the marginal wharf and cruise ship services at two piers.

Growth in container handling has surged in recent years, precipitated primarily by the expansion of the Panama Canal and consequent demand for nearby, deep water berths and transshipment terminals. As the Manga Marine Terminal has reached its expansion capacity, SPRC is turning to modernization projects in response to increase throughput capacity. This paper discusses structural improvements which will allow docking of New Panamax vessels alongside four marginal wharf segments, totaling 700 meters in length, originally designed and equipped for Panamax class ships.

EXISTING CONDITIONS

The container wharf at the Manga Marine Terminal is 700 meters long and is comprised of three berths, designated as Berths 7, 8, and 9. Berth 8 is further subdivided into two sections, Berth 8 East (8E) and Berth 8 West (8W) which were constructed in different time periods using substantially different structural sections. The locations of these berths are shown in Figure 1. Each is a marginal, pile-supported wharf.

Berths 7 and 8, together totaling 538 meters in length, were designed and equipped for Panamax ships with a dredged depth of 13.2 meters, overall vessel length (LOA) of 295 meters, and vessel displacement of approximately 75,000 metric tons (MT). Mooring bollards at each berth were rated to 100 metric tons. Berth 7, part of the original terminal expansion, was converted to a container wharf in 1985; this retrofit included an outboard sheet pile toe wall and crane beams supported by concrete piles for the transition to container use. Both segments of Berth 8 were constructed for container vessel use.

Berth 9, completed in 2011 and 162 meters in length, was designed to accommodate Super Post-Panamax ships with a dredged depth of 16.5 meters, LOA of 366 meters, and vessel displacement of approximately 200,000 MT, on the assumption that Berths 7 & 8 would be upgraded in the future to allow full utilization of this capacity. Berth 9 was equipped with the same fender system as the adjacent Berths 7 and 8 to maintain a straight berthing alignment, but was designed to accommodate higher reactions and larger mounting surface required for a future upgrade to all fenders. Similar to the other berths, 100-MT bollards were provided along its length, with the exception of three (3) 225-MT bollards located at the west end. Again, these high strength bollards anticipated future upgrade to Berth 7 & 8.

DESIGN CRITERIA

The primary design criteria for the deepening project was the safe mooring and berthing of New Panamax container vessels at either end of the wharf. These two positions were selected in order to maximize operational flexibility, without the need to upgrade every bollard or the accompanying disruption to terminal throughput. The increased ship size, approximately 250% increase by displacement over the Panamax class, necessitates the following works:

- Dredging of the berth pocket and toe walls to support existing slopes and structures in place
- Fender upgrades for added berthing energy
- Mooring bollard upgrades to maintain operational wind criteria with larger vessels at berth
- Future upgrades to ship-to-shore (STS) cranes for additional outreach

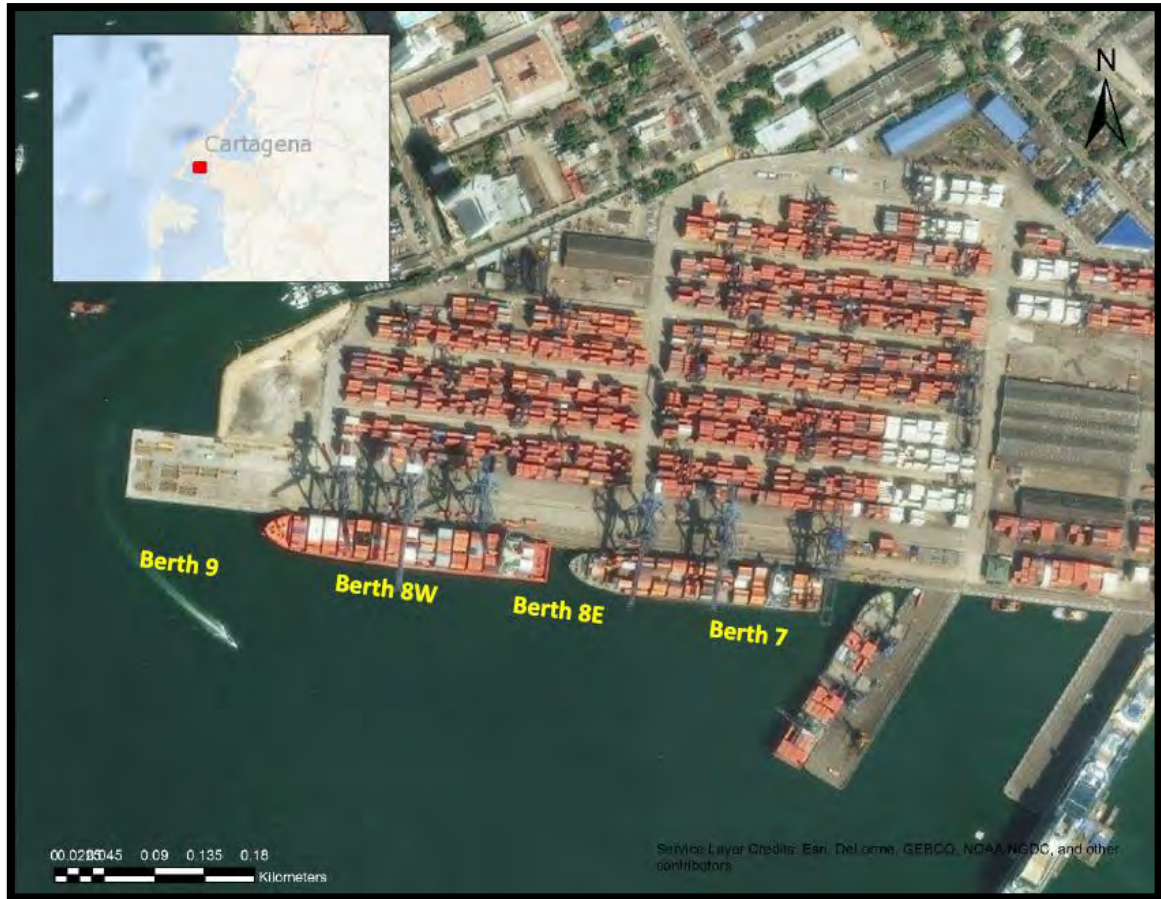


Figure 1: Manga Marine Terminal & Berth Locations

Design Vessels & Dredge Depth

The MSC Beryl was identified as a suitable design vessel in the New Panamax class, as described in Table 1. Design dredge depth was set to 16.5 meters for the required underkeel clearance (UKC) for both New Panamax and Super Post-Panamax classes. Based on berth geometry and vessel proximity limitations, the largest ship which can be berthed concurrently is a 200-meter LOA feeder vessel.

| Vessel Parameter | Units | MSC Beryl |
|-------------------------------------|----------------|--------------|
| Length Overall (LOA) | m | 366 |
| Length Between Perpendiculars (LBP) | m | 350 |
| Width/Beam (B) | m | 48.4 |
| Moulded Depth (D) | m | 23 |
| Design Draft (T) | m | 13.5 |
| Displacement at Design Draft | MT | 182,665 |
| Loaded Lateral Wind Area | m ² | 11,500 |
| Loaded Frontal Wind Area | m ² | 1,550 |
| Number of Mooring Lines | - | 16 |
| Mooring Line Type | - | Double Braid |
| Mooring Line Material | - | Nylon |
| Mooring Line MBL | MT | 135 |

Table 1: Design Vessel Parameters

Environmental Limits for Operations

The design wind speed of 90 kilometers per hour (30-second average) was considered, in accordance with United Facilities Criteria (UFC) 4-159-03 *Type IIA, Standard Moorings* and the existing operational criteria. Hurricanes do not occur in Cartagena, and this design wind occurs with a return period greater than 1 year. Winds from the northeast to northwest quadrants cause the largest mooring loads and vessel motions, as the wind acts to push the vessel away from the berth. Due to the sheltered location, analysis demonstrated that the wave and current loads were not controlling criteria.

Fender Design Criteria

Berthing energy requirements were calculated in accordance with the recommendations of PIANC Maritime Commission Working Group Report No. 33, *Guidelines for the Design of Fenders Systems*. Maximum allowable hull pressure was limited to 200 kilopascal (kPa) for design of the steel fender panel. Results are shown in Table 2.

| Design Parameter | Value |
|--|---------------------------------------|
| Abnormal Berthing Energy of New Panamax (kN.m) | 1430 |
| Recommended Fender | Trelleborg SCN1600 E1.2 or Equivalent |
| Rated Energy Absorption (kN.m) | 1618 |
| Rated Reaction Force (kN) | 1955 |
| Maximum Allowable Hull Pressure (kPa) | 200 |
| Minimum Required Fender Panel Area (m ²) | 10.8 |

Table 2: Recommended Fender Parameters

Mooring Point Design Loads

A dynamic mooring analysis was conducted for the design vessel using aNyMoor software. 225-MT single bitt mooring bollards were selected for New Panamax bow and stern line locations, matching the type and capacity of the larger bollards installed at Berth 9.

For structural analysis of a mooring system, designers typically consider an allowable pull on each bollard equal to the safe working load (SWL). This ensures that the weakest link in the load path is the mooring line, followed by the bollard, then the structure. For the existing berths at Manga, the mooring points were envisioned as a closely spaced cluster of three bollards to reduce construction footprint, with approximately 6m between bollards in lieu of more conventional 18 to 24 meter spacing. Simple addition of the SWL for each bollard proved unrealistic and unmanageable for the existing structure with such close proximity between bits.

In general accordance with PIANC Maritime Commission Working Group Report No. 153, *Recommendations for the Design and Assessment of Marine Oil and Petrochemical Terminals*, the total allowable bollard pull on each mooring point was ultimately determined by the following equation:

$$\text{Mooring Load, } M = SWL [1 + 0.6 (n-1)]$$

$$M = 495 \text{ MT}$$

Where:

$$SWL = \text{Safe Working Load of individual bollard, 225 MT}$$

$$n = \text{number of bollards in cluster, 3}$$

While this method was conceived for quick release hooks, it has similar application to the Manga upgrades as it presumes that all three bollards in a mooring point will not experience maximal loads concurrently. The individual anchorage for each bollard was designed for the full SWL, maintaining the standard design practice of the mooring line being the weak link in the system.

GEOTECHNICAL ANALYSES & STRUCTURAL UPGRADES

Toe Walls

It was critical to preserve the existing slope under each wharf after dredging to maintain bearing pile support conditions and preclude lateral forces from downslope soil displacement. A toe wall was therefore required, both to accomplish the change in grade between existing and proposed mudline and for global stability of the existing wharf structure.

Slope Stability

Each section of wharf was evaluated for the existing and future dredge depth, including analysis of the existing cutoff wall, where applicable, and proposed toe wall. The effects of surcharge loads on the wharf structure and in the container yard behind the wharf were also investigated. Results show that the proposed deepening to 16.5 meters could be safely accomplished through installation of a toe wall at each berth with suitable embedment into the Cartagena Formation, the bearing stratum in this locality which is comprised primarily of hard clays.

Existing Foundation Capacity

Analysis showed that the existing pile foundations, especially the critical waterside crane beam (WSCB) piles, were embedded almost entirely in the active wedge of the retained soil mass and provide negligible restraint to the soil mass for small deflections. As such, the new toe wall would be the stiffest element in the global system and dictate the slope stability under the structure. To determine required toe wall moment of inertia, which in turn determines slope displacements, idealized deflections from bulkhead models were entered in the finite difference model of the WSCB piles as soil displacements. The resulting design moment and concurrent axial demand on the bearing piles were compared to the interaction diagram of the existing concrete piles to determine the maximum allowable toe wall deflection equal to 6 centimeters.

Retaining Wall Design

Improvements to the Berth 7 berth to accommodate the New Panamax vessel loads included addition of a new toe wall, landward of the existing toe wall, and a supplementary deadman system. The new toe wall at Berth 7 replaced an older generation of sheet piling (which was demolished and removed) and retains substantially more soil than Berth 8 toe walls. To maintain stability, it was determined the limits of the toe wall should extend from the active mudline to EL -29.0 meters at the tip, which is approximately equal to the tip elevation of the existing piles. A king pile wall system was selected to obtain appropriate stiffness; however, even the largest commercially available sections exceeded the soil deflection criteria of the existing bearing piles (6 centimeters) when used as a cantilever retaining wall. Consequentially, alternatives were investigated to anchor the bulkhead.

Ultimately, the king piles were extended to the deck elevation and incorporated into the fascia beam to provide lateral restraint to the bulkhead. Intermediate sheet piling was cut off at the active mudline to save material costs. This design allows for king pile installation fully above water. Intermediate sheet piling is also threaded into the interlock above water, then driven to grade using a follower. Subsea soil anchors were considered as an alternate anchorage method but were ultimately discarded due to capital cost and equipment availability. Overall lateral capacity of the wharf was augmented with new tie rods and landside deadman pile pairs. See Figure 2 for a typical Berth 7 section view.

Further complicating the toe wall installation, the Berth 7 structure included existing batter piles, with the pile inclining toward the waterside and penetrating the toe wall alignment at approximately the design dredge depth. Soil exfiltration at the penetration was minimized by arranging bulkhead elements to frame each batter pile with minimal tolerance. This was accomplished using AU 20 intermediate sheet piles, which are nearly equal in width to the existing batter pile, and alternating single/paired HZM king piles. This unique arrangement, as shown in Figure 3, also fits the existing structure bent-to-bent spacing of 6.0m exactly, allowing uniform detailing down the length of the wharf.

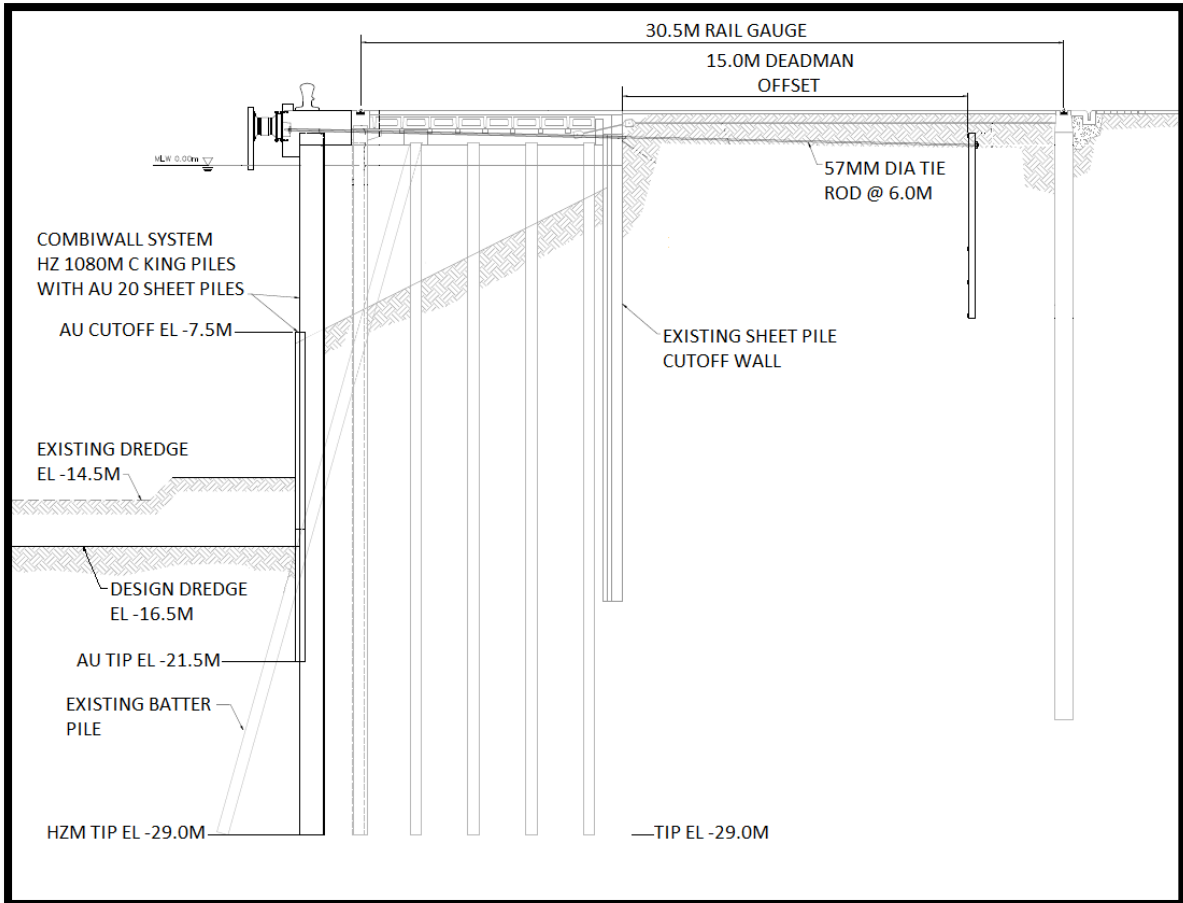


Figure 2: Berth 7 Section

Installing the toe wall landward of the existing berth face provided ancillary benefits in the form of additional vertical support to the WSCB, which may be required for future STS crane upgrades, and zero extension into the berth pocket – maintaining the same berth face as the current berth configuration. For a king pile toe wall in particular, the depth of the section is significant. Installation waterside of the fascia would have relocated the berthing line substantially, reducing the STS crane efficiency and relative reach.

Conversely, toe walls for Berths 8E and 8W were designed as conventional, cantilever steel sheet pile bulkheads, installed immediately outboard of the fascia beam. The difference in design section compared to Berth 7 was primarily due to the existing slope under these wharf segments, which was both steeper and dredged deeper, minimizing load imparted on the toe wall. The pre-existing toe wall at Berth 7 had a cutoff elevation of -8.0 meters, whereas the Berth 8 slope toe elevation was -13.5 meters.

Installation of the Berth 8 toe wall outboard of the fascia beam reduced disruption to wharf operations, requiring temporary removal of fenders but no additional work on the concrete wharf elements. See Figure 4 for a representative typical section view of Berth 8.

A toe wall was not required for Berth 9 by original design.

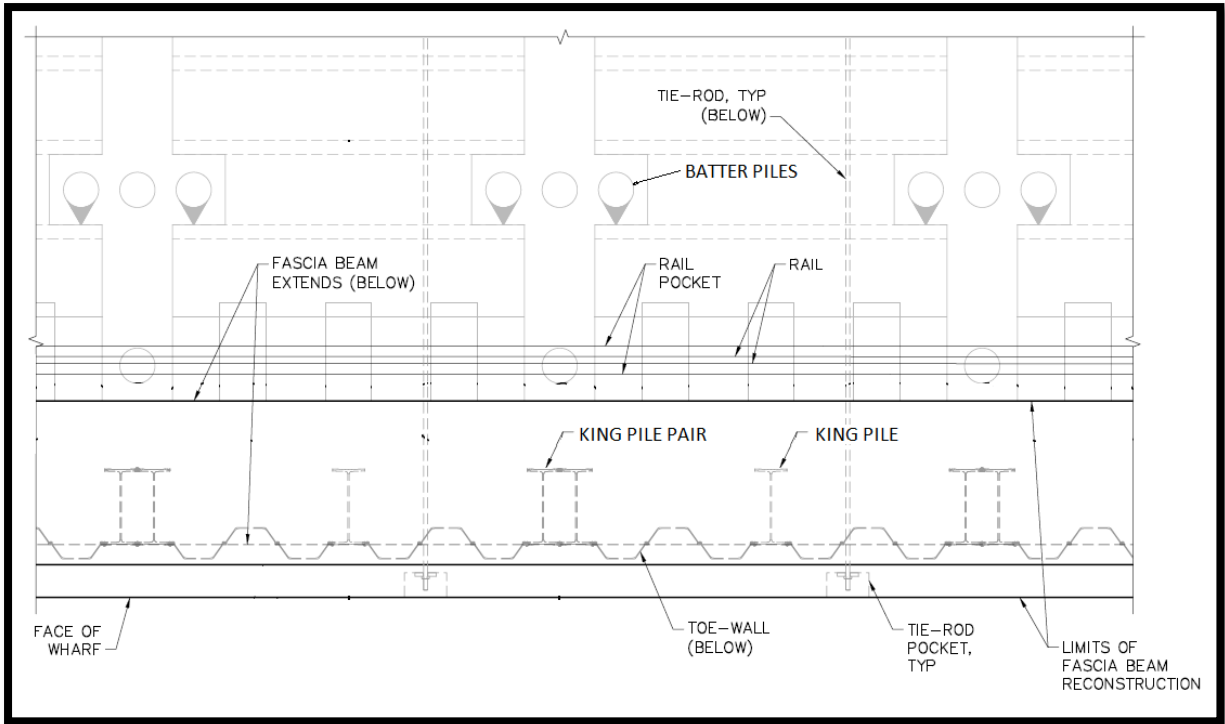


Figure 3: Berth 7 Toe Wall Arrangement

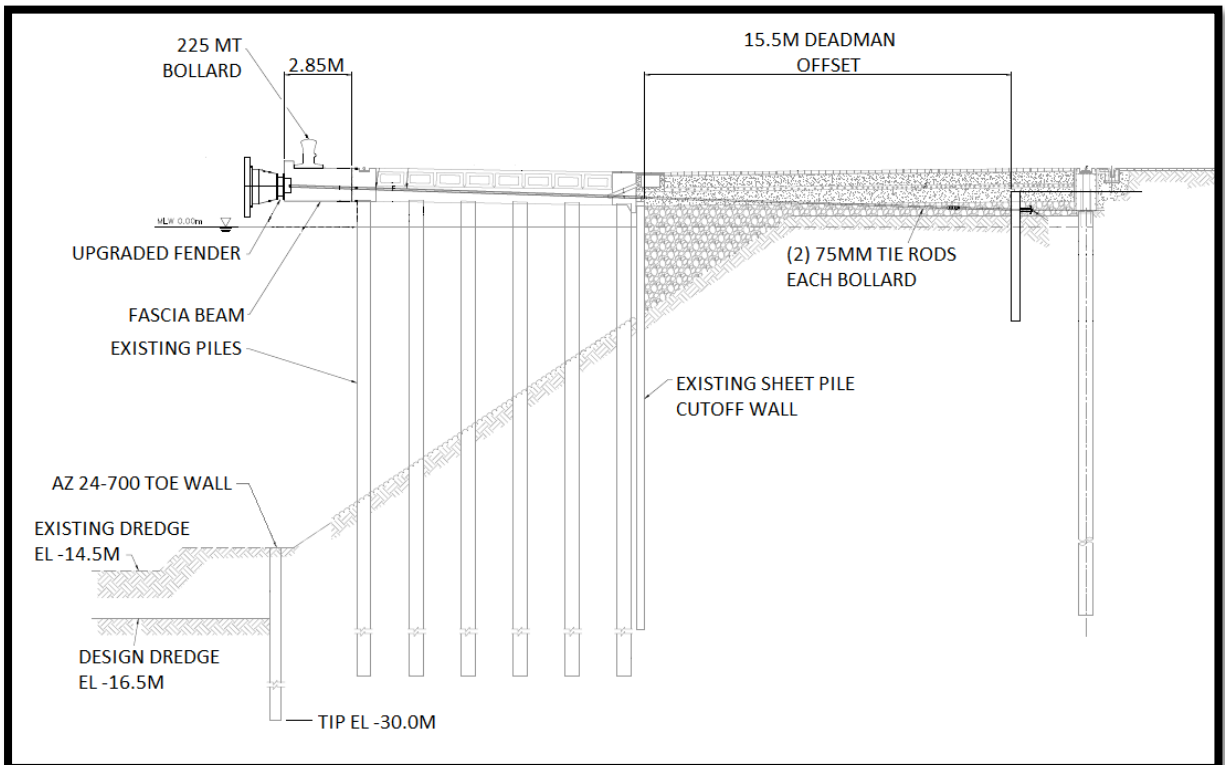


Figure 4: Berth 8 Typical Section after Upgrades

Fenders

Existing fenders were a combination of Bridgestone SUC 1000H and Marine International MCS 1000 cell fenders, spaced 6 to 18 meters on center typically. Based on the berthing energy calculation, the existing fenders do not have sufficient capacity to accommodate the New Panamax; therefore, a new fender program was selected for the berths.

To limit the required crane outreach, reduce fender submersion, and fit elements to the small existing fascia, a dual system was selected with two SCN 1100 fenders sharing a single panel, depicted on Figure 5. The existing cell fenders were removed and replaced with these cone fenders. The new fender systems were located approximately 18 meters on center. This was determined to agree with bent-to-bent spacing of approximately 6 meters.

The change in fender system type increased the load imparted on the structure from vessel berthing impact. Additionally, the dual system required individual elements to be located on either side of the existing bent caps, whereas existing fenders were located directly at transverse beams. Therefore, localized reinforcement of the fascia beam was also required.

Fender element design also included a small spool piece, which increases standoff and maintains safe ship clearance to the fascia and toe wall. This is especially important at Berth 8E and 8W, where the toe wall was driven immediately outboard of the fascia beam. The spool piece also permits slightly larger spacing between fender elements, thus reducing the total number required.

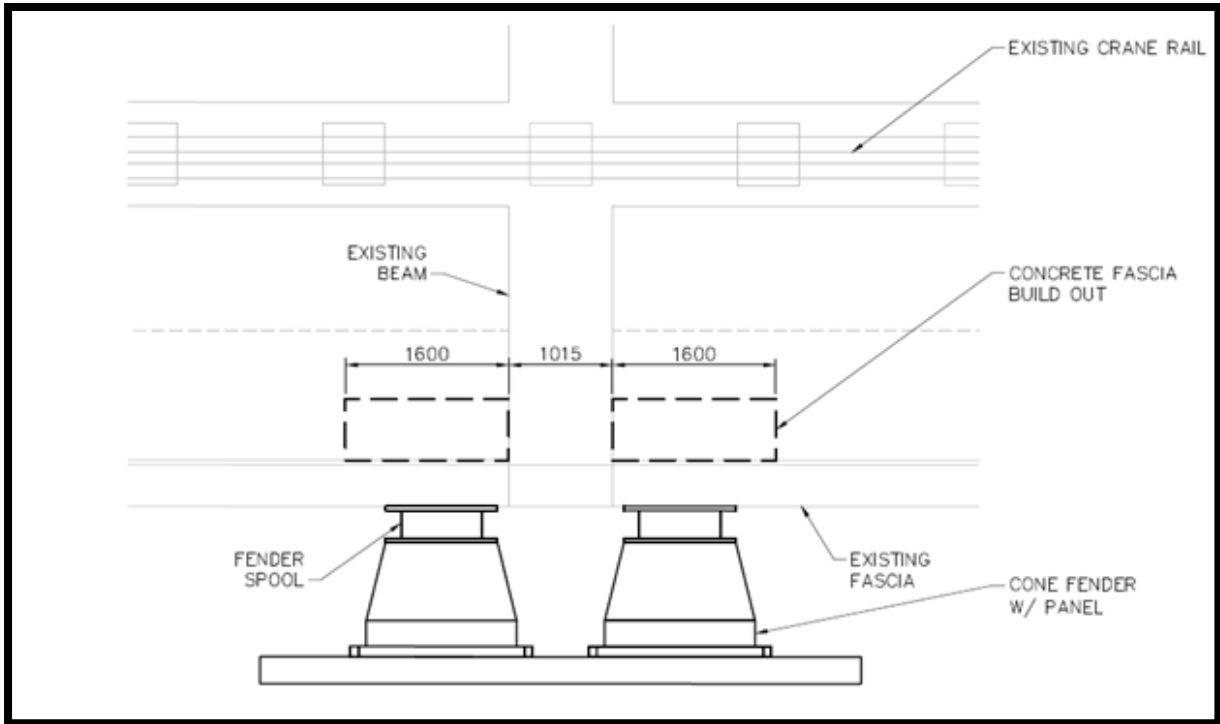


Figure 5: Fender System Layout

Mooring Points

To facilitate the plan for berthing of the New Panamax ships at either end of the terminal, additional 225-MT three-bollard groups were added at 3 locations (9 total new bollards). These larger capacity mooring points resulted in higher loads imparted on the wharf structures. To resist the lateral load, reconstruction of approximately 18 meters of the fascia beam and installation of additional anchors – tie rods and sheet pile deadman – was required at each cluster location. The existing plumb piles were determined sufficient to absorb the increased longitudinal loads at each cluster in Berth 8E and 8W.

Variations on the theme were required for each mooring point. At Berth 7, given the age of the structure and uncertainty in the as-built details and condition, cased drilled shafts were added to support the

additional longitudinal loads. At Berth 8W, the existing pile caps run parallel to the wharf face, and short transverse beams were added to balance vertical loads and moments at the fascia beam.

The existing 100-MT bollards were left in place along the remainder of the structure as they were determined to be suitable for spring lines for the New Panamax vessels and as mooring points for smaller vessels utilizing the berths.

Future Gantry Crane Upgrades

Evaluation of the existing gantry crane rail foundation system was completed. Currently, each berth is outfit with crane rails at 30.5-meter gauge, suitable for the current generation of Post-Panamax STS cranes. Vertical capacity of the berths was originally designed considering 46 ton per meter crane wheel loads and 50 kilopascal (kPa) uniform live load. The larger container cranes required to serve the newest container ships have wheel loads ranging from 74 ton per meter to 97 ton per meter, depending on the manufacturer and specific operational requirements. As these higher wheel loads exceed the allowable capacity of the existing pile foundations, before larger cranes are employed at Manga, localized strengthening of pile foundations at each crane beam will be required.

Alternatives investigated for future crane rail improvements included additional piles and crutch bents or installing new steel pipe pile sleeves over the existing concrete piles. A determination of the optimal course will be made during final design.

CONCLUSION

The deepening project will greatly expand the operational capabilities of the Manga Marine Terminal and enhance Cartagena's reputation as one of the top transshipment locations in Latin America. Through targeted structural modifications, the existing wharves will meet new demands economically and with minimal disruptions.

At the time of this writing, the upgrade projects are partially complete. Toe walls have been installed and the fascia of Berth 7 has been reconstructed and anchored. Since initial analysis and design, a mooring buoy has been installed approximately 40 meters west of Berth 9. Mooring point construction is pending, with potential layout modifications accounting for the additional buoy. Fender design will also consider reuse of fenders recently removed from the Contecar facility.

REFERENCES

- PIANC (2002) Maritime Commission Working Group Report No. 33, *Guidelines for the Design of Fenders Systems*, PIANC, Brussels.
- PIANC (2016) Maritime Commission Working Group Report No. 153, *Recommendations for the Design and Assessment of Marine Oil and Petrochemical Terminals*, PIANC, Brussels.
- United Facilities Criteria (2012) UFC 4-159-03, Design: Moorings, U.S. Army Corps of Engineers.

Keywords:

Port Engineering

Container Terminal

Dredging and Port Deepening

Fender

Mooring Bollard

BAHIA BLANCA 2040 MASTER PLAN, FLEXIBLE PLANNING FOR WATERWAYS

by

Eng. Gerardo Bessone¹, Lic. Juan Linares²

ABSTRACT

Up-to-date development of the Bahia Blanca Estuary and region was tied to the improvement of the access channel to the main Ports located in the innermost section. Since the late 19th century the Ports constituted one of the main gates to distribute the agricultural produce of a vast region to the world markets. As the traffic and size of bulk carriers grew, it became apparent that the waterway needed to be adapted. In the early 90's, because of a change in policy, Bahia Blanca became the first Self-administered Port in Argentina. This provided the possibility to plan and invest directly on the port system the revenues generated by the Port itself. This circumstance leads to a considerable improvement of the facilities and services, which in time promoted the arrival of new terminals and industries to the region.

A great portion of the revenues have been applied to the maintenance of its waterways. Today dredging represents roughly some 60% of the total budget. It becomes paramount to make a comprehensive planning of the waterways to promote adequate depth and sizes for the current fleet, thus lowering dredging volumes.

Since 2017 the CGPBB has taken a big step in Port Planning. For the first time in its history it has undergone, with the help and supervision of Port Consultants of Rotterdam, a thorough process of devising a Plan looking at 2040. This means a change of paradigm, were the actual waterways will be defined by the needs of its users.

This change will lead to a more flexible channel design, where the actual size of the waterways will be that that is required at the time by its users. As a result, the dredging volumes will be limited to maintain the necessary depth, thus proving more sustainable both economically and environmentally.

1. LOCATION AND MAIN CHARACTERISTICS OF THE WATERWAYS OF BAHIA BLANCA

The Port of Bahía Blanca and its waterways are located in the estuary of the same name some 500 km south west of the city of Buenos Aires. The estuary has over 2400 square kilometres of wetlands and shallow waters and its coastline totals some 400 km on both margins. On the northern shore there are three main ports (Puerto Rosales, Belgrano Naval Base and the Port of Bahía Blanca) all located along a strip of some 25 km.

¹ In Charge of Dredging and Aids to Navigation Department, CGPBB
gbessone@puertobahiablanca.com

² Manager of Land and Maritime Logistics, CGPBB jlinares@puertobahiablanca.com

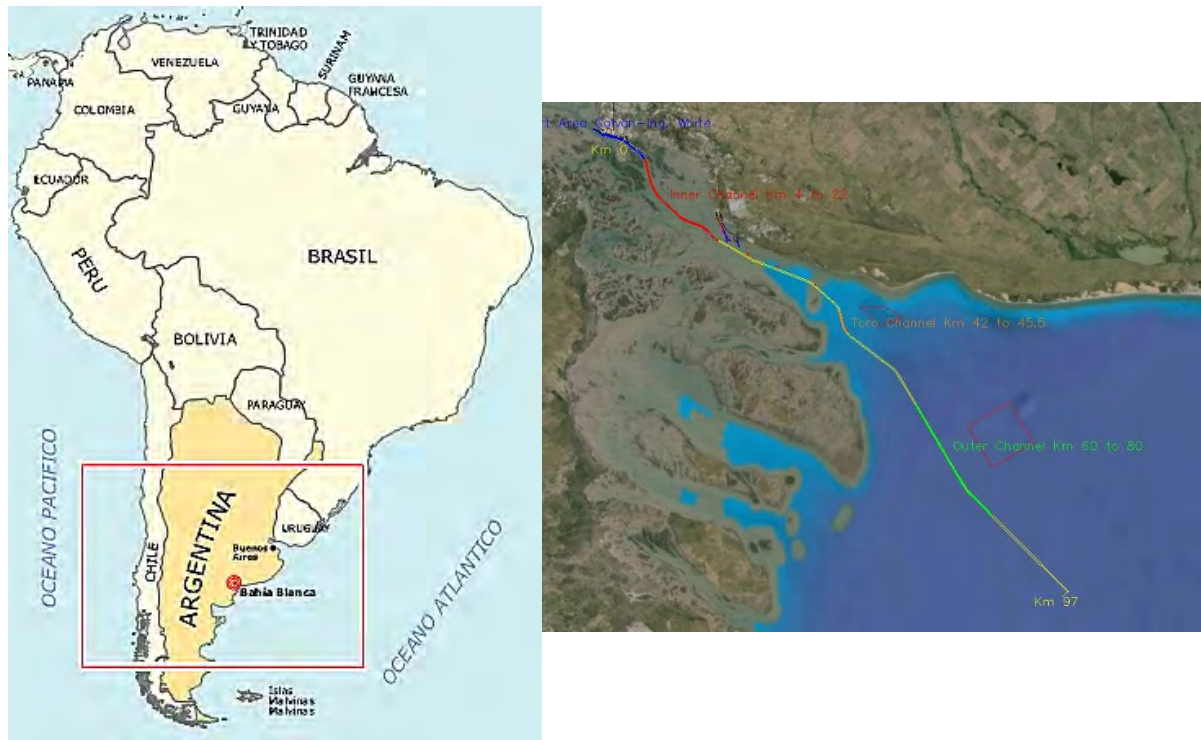


Figure 1: Location of Bahía Blanca Estuary

The extensive wetlands and tidal plains are connected by a series of side channels which flow to the Main Channel that runs on a NW-SE direction. The shape of the Estuary is roughly a triangle, with its base oriented to the SE.

One of the main characteristics is the tidal amplitude, which varies throughout the estuary, ranging from 2.5 m in the outer portion to up to 4.5 m in the inner port area. This great amplitude renders Bahía Blanca as one of the major deep-water ports of the region, since it allows with the use of high tide window the navigation of vessels with a draught of up to 45 feet.

Wave climate is dependent of wind conditions, especially in the outer estuary, where the open waters provide enough fetch, which added to the relatively shallow depth result in waves of up to 3 m when persistent high intensity winds from the southern quadrant blow. The wave heights drop dramatically further into the estuary, providing a sheltered natural port that was the main reason for the settlement of what today is Bahía Blanca Port.

The distribution of sediments along the estuary is a direct consequence of the surrounding availability of the sea bottom materials and of the hydrodynamics present locally.

When the sediments are mobilized, because of lateral erosion, the finer proportion (clay and silt) is kept in suspension in the entire water column causing high turbidity, a characteristic of the inner portion of the estuary. Coarser materials (sands) are mobilized by the currents near to the sea bottom and deposited in the channel area.

The dominant hydrodynamics results in the formation of sand bars on the outer portion of the estuary, and of highly movable bottom sand dunes, which sometimes cross the navigation channel, generally without affecting navigation.

The morphology of the estuary and its waterways has been modified throughout the decades, due to the shifting of the sand bars and bottom dunes, which alters the layout of the channel as they protrude into them. This calls for constant monitoring and survey of the area, besides maintenance dredging of some portions of the channels.

2. EVOLUTION OF BAHIA BLANCA AND ITS WATERWAYS

What today is known as Bahía Blanca Port can be traced back to the 1820's, when colonization of aboriginal land and the threat of war with the Brazilian Empire motivated expeditions to the Bahia Blanca Estuary, with the intention of establishing a small port and a fort to proclaim sovereignty. Favourable conditions for settlement (nearby fresh water) and a sheltered natural port resulted in the establishment of a minor outpost which served as the sole connection to the rest of the country for the incipient town of Bahia Blanca.

Along its history the port and its channel received sprouts of quick development followed by decades of apparent stagnation. It was not until the 1880's when the port and its channel as we know it today began to take shape.



Figure 2: Ing. White Port ca. 1930s

The expansion of the railroads was the kick off to a spectacular development from mid-1880 till the 1920's. Alongside the development of the port infrastructure, the waterways of the time were the natural channels available within the estuary. Primitive and partial surveys, conducted by the hydrographic department of the Argentina navy, allowed the navigation with relative safety of ships of drafts of up to 25 feet. Later around the 1920's improved survey and primitive aids to navigation allowed the drafts to be augmented to 33 feet.

Political and economic swings and lack of well-defined policies and legislation prevented the Port to achieve a sustained development. It was not until the 1960's and 70's that new berths were constructed, but no intervention was carried out in the waterways which maintained its natural depth allowing the sailing of vessel with a draft of up to 33 feet.

By the late 60's ships growth called for deeper ports and waterways. Consequently, the National Government started to analyse possible alternatives. These included the building of a totally new port on the Atlantic shore of the Province of Buenos Aires, the deepening of existing waterways and ports up the Parana River (Argentina's main waterway and where 80% of the agricultural produce is concentrated) among others. Finally, the decision was adopted by the Government at the time (beginning 1970's) to turn Bahía Blanca as the main deep-water port in Argentina. First step in this direction was the capital dredge conducted that gave the port facilities and the main Channel an operational depth of 40 feet.

Such policy has been maintained since, not only under national administration, but also when it became self-administered in 1993. Another major landmark was the deepening of the port and Main Channel to 45 feet (using the appropriate tide window), giving Bahia Blanca yet another competitive boost. This called for the dredging of fifty million cubic meters, with an investment of over two hundred million US Dollars (at the time). This capital dredge was carried out from 1989 to 1992.

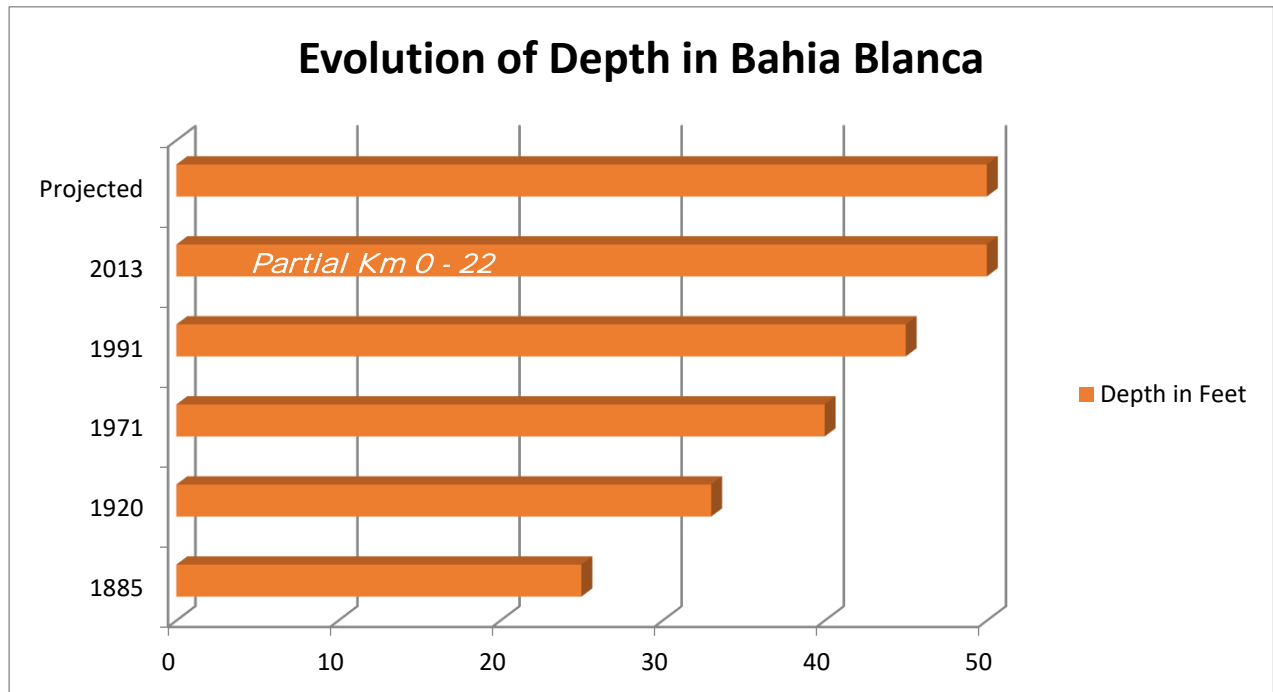


Figure 3: Depth evolution in Bahia Blanca

The current layout of the Channel is a consequence of the studies carried out in the 80's by NEDECO Consulting of the Netherlands which concluded that such was the best option, considering all the relevant factors (sedimentation, currents, navigation time, etc.).

Thanks to all the data gathered several layouts were considered and sediment models were proposed. After careful consideration, a layout was chosen evaluating different channel depths being the chosen design vessel a Panamax Bulk carrier, thought at the time to be the biggest ship to call upon the port at time.

Thus, we arrive at today's Main Access Channel to Bahía Blanca, which is located close to the northern shore of the estuary; its total length is 97 Km beginning in the Bahia Blanca Port Area.

Connected to Main Channel are two other side channels: the 4 kilometres long Access Channel to de Belgrano Naval Base located at Chainage Km 22 and Puerto Rosales Access Channel, 1.7 kilometres long, at Chainage Km 23.5.

Consequently, the actual design of the channel is the result of the above-mentioned study. The Main Channel has a width of 190 m throughout the whole extension, except between kilometres 14 to 22 where it has 205 m due to the presence of consecutive curves. The side slopes vary according to the stability of the banks ranging from 1 to 5 to as much as 1 to 15.

| BAHIA BLANCA MAIN ACCESS CHANNEL DESIGN | | | | |
|---|------------------------------------|----------------------|--------|-------|
| Chainage (Km. a Km.) | Nautical Depth (m.) | Bottom Width (m.) | Slopes | |
| | | | RED | GREEN |
| 0,0 a 4,0 | 13,50 m. Width and slopes variable | | | |
| 4,0 a 8,9 | 13,50 m. | 190 m. | 1:5 | 1:5 |
| 8,9 a 14,2 | 13,50 m. | 190 m. | 1:10 | 1:10 |
| 14,3 a 21,0 | 13,50 m. | 205 m. | 1:10 | 1:10 |
| 21,0 a 40,3 | Natural Width and Depth | | | |
| 40,3 a 45,3 | 12,80/13,20 m. | 190 m. | 1:10 | 1:10 |
| 45,3 a 52,0 | Natural Width and Depth | | | |
| 52,0 a 63,2 | 12,80 m. | 190 m. | 1:10 | 1:10 |
| 63,2 a 72,0 | 12,80 m. | 190 m. | 1:10 | 1:10 |
| 72,0 a 75,0 | 12,80 m. | 190 m. | 1:15 | 1:10 |
| 75,0 a 85,0 | 12,80/13,10 m. | 190 m. | 1:15 | 1:10 |
| 85,0 a 97,0 | 13,10 m. | 190 m. | 1:15 | 1:10 |

Figure 4: Bahia Blanca Channel Design (as of 2013)

The Main Channel is divided into three sections:

- Inner Channel (Km 4 to Km 22) One way, no crossing permitted except for vessels with a Beam under 25m.
- Toro Channel (Km 42 to Km 46) One-way same restrictions apply.
- Outer Channel (Km 60 onwards) One-way until Km 80, from there onwards no restrictions applied.

Between these sections the channel has naturally a great depth, not requiring any maintenance work and posing no restriction to navigation.

The *Inner Channel* runs along banks of great stability, presenting little to no sedimentation at all. The predominant material is coarse sand with migrating bottom sand dunes. These occasionally interfere with the channel requiring small dredging campaigns to restore design depth.

This portion of the Main Channel received capital dredge in 2013 (known as stage 1 of the deepening project), going from an initial depth of 12.20 m to 13.50 m (referred to local Datum) thus improving port operation and allowing navigation at maximum depth (45+ feet) regardless tide condition.

Between this section and the Toro Channel natural depth is over 15 m, reaching a maximum of up to 25 m. The channel widens to as much as 1000 m. This provides a safe zone for overtaking and crossing manoeuvres.

The *Toro Channel* runs along the Toro Bank, South and West Banks. These are advancing towards the channel. Consequently, the area presents high volumes of sedimentation. The sediments are medium sand with silt in different proportions. Along the years this section of the channel has suffered several changes (minor) to its layout, adapting to the dynamics of the mentioned banks.

Design depths in this section vary from 12.8 meters at Chainage Km 42 to 13.1 meters at progressive Km 45.5. From there until Km 60 natural depth is above 15 meters requiring no maintenance dredging at all.

The *Outer Channel* runs on a NW to SE orientation and generally is aligned with the current, thus sedimentation is moderate. Between Km 67 to 73 the presence of a curve and a slight change in current alignment causes sedimentation to rise. The bottom material in this area is fine sand, with different grades of silt.

The Outer Channel has a depth of 12.8 m from Chainage Km 60 to Km 75. From there onwards it varies reaching 13.1 m on Chainage Km 85, maintaining that value till the end. All the depths mentioned are referred to local chart Datum.

3 FACTORS INVOLVED IN WATERWAYS EVOLUTION

Change in legislation and port related policies permitted Bahia Blanca to become in 1993 the country's first self-administered Port with the creation of the **Consortio de Gestión del Puerto de Bahía Blanca (CGPBB)**. With it came also the responsibility to maintain the waterways financed through the fares and tariffs for the usage of the waterway and other services provided by the Port. Today maintenance dredging constitutes the main expense to be afforded by the CGPBB drawing roughly up to 60% of its annual budget with ever rising costs.

3.1 Evolution of Maintenance Dredging

Since 1999 all dredging conducted in the waterways was contracted and paid for by the CGPBB, with no further financing from the Government.

Since maintenance of navigation draft is paramount to keeping its comparative advantage against other ports in the region, from the beginning it was devised that the best bet was to pursue a Performance Based Contract (PBC), ensuring at all-times (and regardless the volume to be dredged) the design depths in the Main Channel.

Because the layout of the channel has been almost the same since it was originally plotted in the 80's, considerable data is available regarding the sedimentation along the channel and the hot spots where it peaks. Moreover 25 years of continual surveys allows to form a good picture in terms of the evolution of the waterways morphologically. This can be translated to a fairly good understanding of the sedimentation process and the expected volumes.

Statistics show that the annual sedimentation is close to three million cubic meters, of which some two million are contributed by the Outer Channel (Chainage Km 60 to 80), another 700.000 cubic meters to the Toro Channel (Chainage Km 42 to 45.5) and the rest correspond to the Inner Channel (Chainage Km 4 to 20) and the access channels to the Belgrano Naval Base and to Puerto Rosales. The rest of the waterways, as mentioned before, because of their natural depth or due to the local hydrodynamics and morphology, do not require any maintenance work.

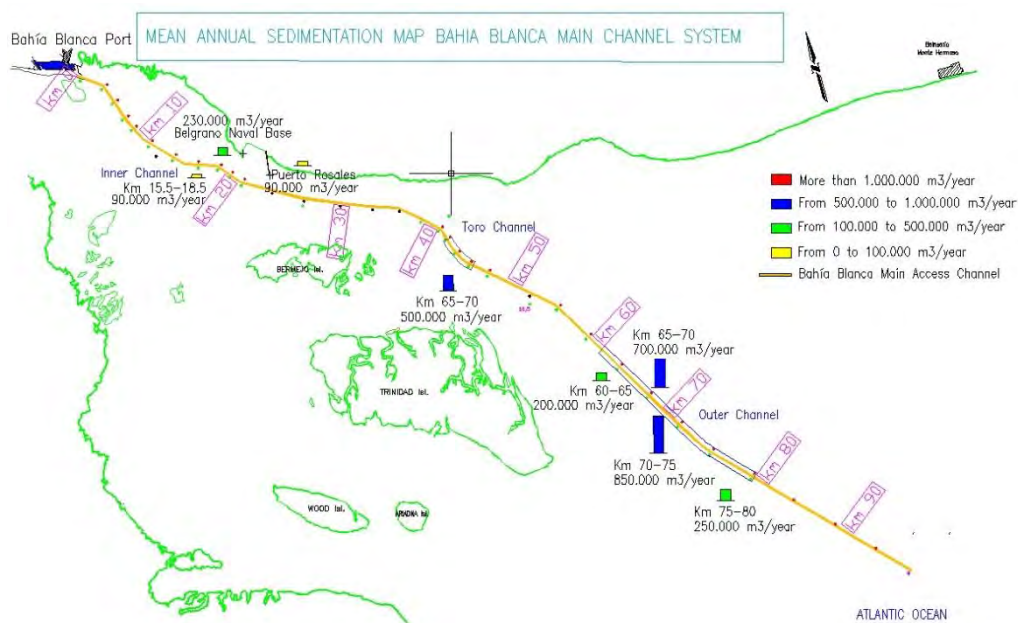


Figure 5: Mean Annual Sedimentation along the Main Channel

Due to the characteristic of the material deposited (sand and silt in various proportions), the work is carried out using Trailing Suction Hopper Dredges (THSD). Depth limitations outside the channel area and the volumes removed determine the size and capacity of the equipment used. In general, the dredgers employed are of medium to small dimensions, with a hopper capacity of around 3 to 4 thousand cubic meters.

3.2 The cost of Dredging

As mentioned above, volumes dredged annually have been constant throughout the last 20 odd years, with some variation related to climatological harsher years. Nevertheless, these differences have been within an interval of some 30%. But when we look at the evolution of the cost of dredging its obvious that the price per cubic meter has risen dramatically in subsequent contracts.

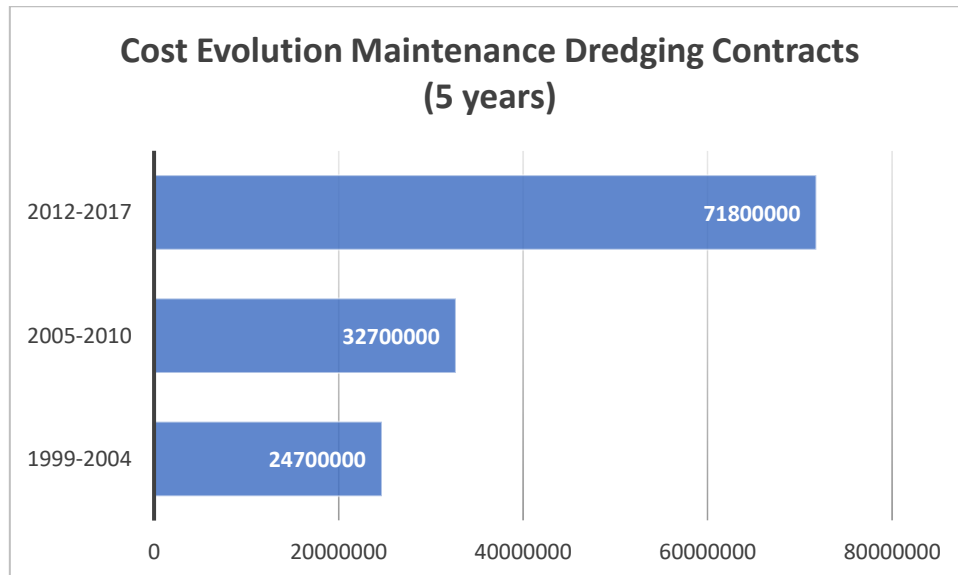


Figure 6: Maintenance Cost evolution in Bahia Blanca

Reasons for this steep rise are several, amongst others a big component is the uncertainty posed by the country's economy (with recurrent crisis and changes in policy), the price of oil, availability of equipment in the area etc.

What is clear enough is that the tendency that costs will most likely keep growing, and with it the resources that the CGPBB will have to allocate to maintenance. This could in the long run affect competitiveness, since fares for usage of waterway might be affected to provide for the necessary funding to pay for the higher cost.

3.3 Traffic analysis

Looking at the evolution of traffic since the CGPBB was created, it becomes apparent that the total numbers haven't varied much (some 30%) compared to the volume handled which has more than doubled in the same period.

Reasons for this disparity can be found in the size of the ships calling on the port, also on the amount of cargo carried in each vessel (due to the increase in draft).

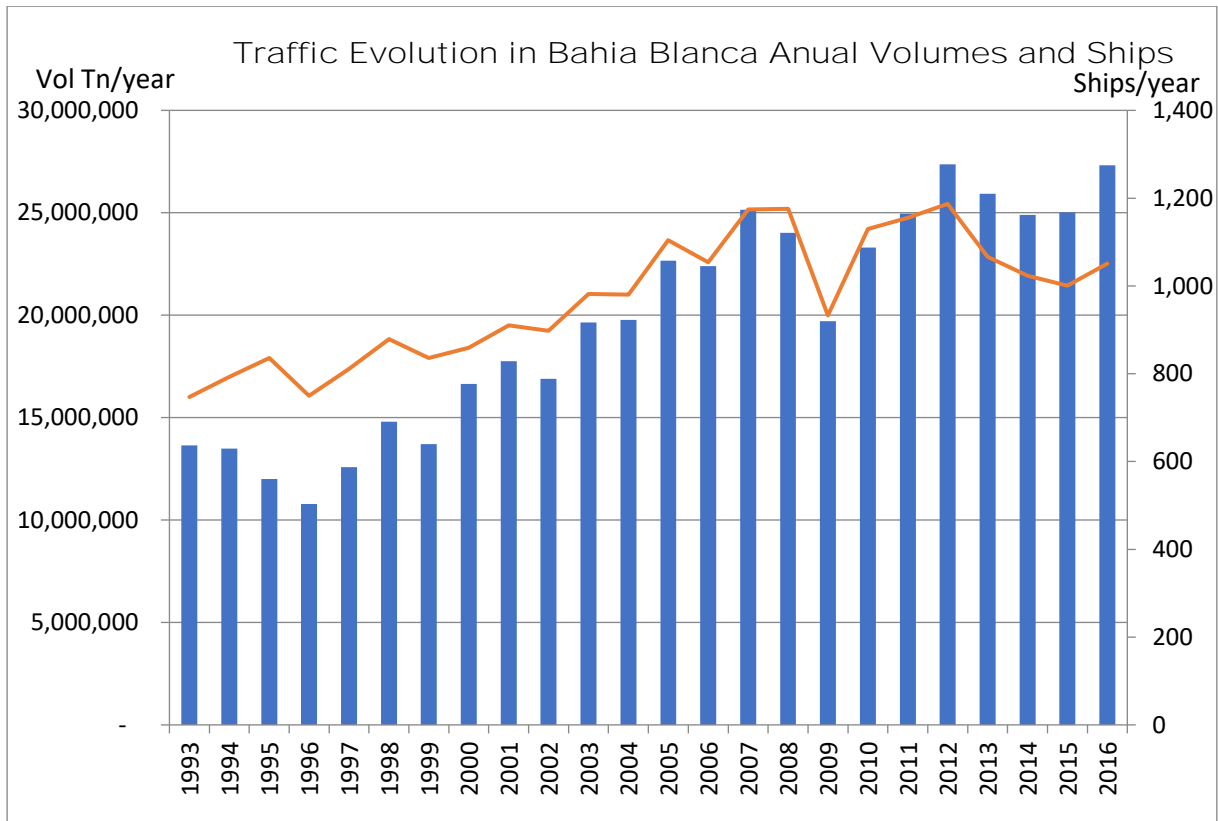


Figure 7: Traffic evolution in Tons and number of ships

One key factor to consider is that Bahía Blanca has positioned itself as one of the country’s leading top off ports for solid bulk (mainly grains). Today the bulk of the more than 100 Mill tons of the grains produced in Argentina (close to 80%) is exported through the ports located up the Parana River in various terminals along several hundred kilometers. The main reason for this volume is the closeness of the main production zones, which in turn means less land transportation cost compared to the ports located in the Atlantic coast.

But drafts in up river ports is today limited to 34 feet and subject to the variations (which can be sudden) in the Parana river level. Hence the necessity to top off the Panamax and Post Panamax bulk carriers which constitute the gross of the fleet currently used.

Bahía Blanca results (along with Quequen some 250 km NE in the Atlantic coast) the main Argentinian top off port. Together they round off the 20 odd % of the exports, being today roughly Bahia Blanca volume 60% more than Quequen’s (considering only grain exports).

When analyzed, in 2016 and 2015 all the Panamax Dry Bulk carriers that called upon Bahía Blanca came to top off, averaging some 20.000 tons per ship.

Another interesting fact is the number of ships with drafts above 44-45 feet that call on Bahía Blanca (Dry Bulk carriers leave port fully loaded), including incoming Panamax tankers that operate unloading crude oil to booth CALM buoys near Puerto Rosales which usually sail with draft of 45 feet (13.70m). They represent roughly 35% of the total traffic. The maximum draft ever operated was 47 feet using a particular tide window and favourable weather conditions.

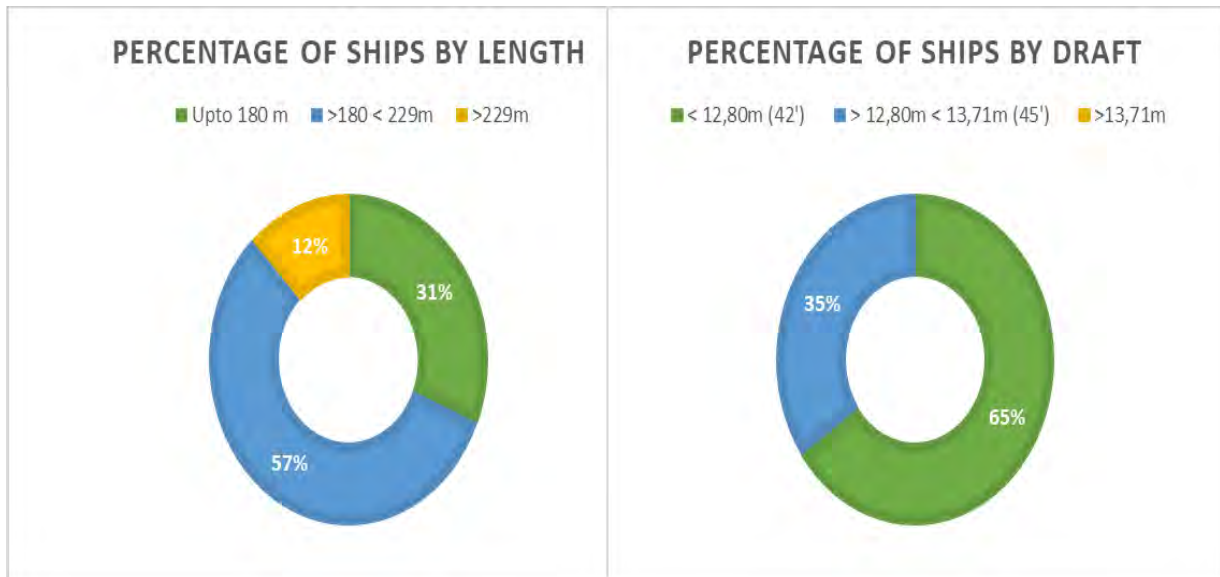


Figure 8: Traffic share by Dimensions in 2017

When considering extreme dimensions beside draft, since 2008 Bahia Blanca receives LNG ships with some 277 m in length, 43,5 m breath and a maximum draft of 12.1m. Although the channel was originally designed for a Panamax, simulations carried out and almost 10 years of continual operations have shown that with minimal restriction to the rest of the traffic these vessels can operate without inconvenience. Further simulation even allowed safely sailing of ships up to Q Flex size, though up to now no such vessel has called on the port.

When looking at the traffic it is also necessary to consider not only the port itself, but also the destination port and its facilities. The fully loaded dry bulk carriers have as destination ports in the east (mainly China) and Middle East. Those ports nowadays have capacity to operate with ships with drafts of up to 45 to 48 feet, thus the size of ships that call upon Bahia Blanca has maintained for the past 15 years.

4 WATERWAYS PLANNING

Since CGPBB came to be, all the responsibility for the operation and maintenance has befallen solely upon itself, including the planning of possible enhancement or modification to its layout.

4.1 Reasons for a deeper system

In 2007 owing to the increasing traffic in the port area and with the perspective of the establishment of future terminals, the Board of Directors required the Technical Areas within the CGPBB to begin feasibility studies to improve operations and availability of berths.

Early on it was decided to tackle the system in two stages, since the cost involved in doing the whole capital dredge was rendered too high considering that the entire works were going to be afforded by the CGPBB, with no financial help from the government.

At the time the priority was set on avoiding congestion in port operation caused by the cramming of all the operations (dockings and un-dockings) in just a few hours a day (using high water in case of the completed ships). This fact stressed to the limit the capacity of the services in the port (tugs and pilots) and led to increasing downtimes, a matter that would worsen quickly if the projected arrival of new terminals were to have happen.



Figure 9: Port Congestion

At the time it was deemed that continuous increase in grain production (specially soy bean) destined to the ever-demanding Chinese market could drive to the arrival of greater ships, requiring thus deeper drafts, enhancing the possibility of Bahia Blanca to attract not only top off operations but also complete loads of post Panamax or even cape size bulk carriers. All of this would benefit if the system was prepared to handle drafts of up to 50 feet (using the tide window). Already back in the 80's NEDECO had determined that 50 was the ultimate scenario to be analysed.

4.2 First Stage Port Area and Inner Channel, avoiding Congestion

The result of the work carried out by the specialists at the CGPBB was a project to carry out capital dredge in the port area from the former 12.20 to 13.50 meters; this would allow vessels to operate at 45 feet regardless of the tide condition.

Furthermore, it was also determined to dredge the Access Channel from Km 4 to 20 to a depth of 13.50 meters maintaining the overall width of 190 meters. This would allow the operation of vessels of up to 50 feet draught with the use of the appropriate tide condition or 45 feet at any time within the mentioned sector. This meant that ships could cast off at any time, sail the one-way channel up to one of the three available anchorage areas near the Toro Channel and await there the tide window to continue sailing outwards. Doing so would increase the number of operations per day, employing the services available in an orderly manner thus reducing downtimes significantly.

The project called for a total volume of 5.700.000 cubic metres to be dredged. Due to the characteristics of the material, (determined by seismic profiling and obtaining soil samples using coring), large trailing suction hopper dredgers (THSD) and cutter suction dredgers (CSD) were needed.

Financing was secured through a loan of the CAF (Corporación Andina de Fomento), for an amount of over sixty million dollars, to be repaid by the Consorcio during the following ten years.

An international tender was called in 2011, by which the joint venture between Boskalis International and Jan de Null was awarded the contract that amounted to a total of over 120 Million U\$S Dollars, this included the capital dredge and the maintenance of the waterways for a period of five years (2012-2017). Deepening works were carried out throughout nine months in 2013, within the planned schedule.

As it was shown on the preceding section, traffic didn't experience the forecasted increase, mainly due to internal and external factors (2008 world economic crisis and, in 2009, a bitter taxing dispute between agricultural producers and the government). Nevertheless, the deepening of this portion of the main channel and the ports basin proved a success lowering downtimes to almost 0.

5 2040 MASTERPLAN AND FLEXIBLE WATERWAYS

5.1 Lessons learnt, needs to change

The biggest lesson learnt after the 2013 deepening was that forecasts are dependant on factors that are out of reach of local port authorities. In an ever-increasing globalized world, one must expect the unexpected. This turns even more critical when decisions taken could severely affect the financial health of the port considering it does not have the backing of the State.

To date (in Bahia Blanca), waterways were built (dredged) in answer to what the government thought (or planned) without knowing first-hand the actual needs or perspectives of the prospective users, only acknowledging what central planners thought would be best for the country. Once it was operational then the port and its stakeholders made the best of what was available, with little or no possibility to have a saying at what are the needs in terms of channel design.

Changes began once self-administration was obtained. The CGPBB started to analyse the operations, traffic and tendencies in shipping to evaluate possible needs to be filled, and whether the waterway's design fulfilled the current necessities.

A major step forward was the realization of a Vision for the long term (2040). This Vision was not only from the perspective of the Port, but what was innovative compared to prior works, is that all the stakeholders were considered. With the supervision and help of Port Consultants Rotterdam (PCR), a thorough and comprehensive work was carried out during 2017. As a result of more than 500 interviews, workshops and data gathering and processing the Goals for 2040 were set. As part of these goals the definition of what waterways would be needed and when was obviously resolved.

5.2 Reasons to be flexible

As mentioned forecasts seldom become true, specially when we consider politics in a country prone to sudden shifts in economic horizons and ideologies and with no long-term planning. This makes planning ahead and investing a hard job. On the other hand, waterways need careful planning and study to design the best scenario, and this obviously takes time to carry out. So, the balance between thinking too far away (with high probabilities of not being feasible) and not having time to gather the required information and planning to take good decisions is being halfway. In other words, be flexible in the planning, have several scenarios and what is required to trigger the actions needed with enough time for carrying out all the necessary works will result in the best possible option at the desired time.

Other very important reason to be flexible is cost. Dredging is not cheap, and the prices have consistently gone up, with no sign of subduing. So, only dredging when is strictly necessary will save money, not only in the capital dredge, but specially afterwards in maintenance.

In waterways like Bahía Blanca every centimetre constitutes tens of thousands of cubic metres, thus just half a foot turns into millions of dollars. With this predicament, it is easy to see why one must consider all the alternatives possible before getting involved in deepening the existing waterways.

Another no less important factor to consider is the environment. Dredging has become an activity (even in developing countries) subject to ever increasing controls and regulations. This calls for careful planning of works to be carried out minimizing the impact (all anthropic activities have to a certain extent) on the Environment.

For instance, deepening the channel will not only result in higher volumes to extract and later to maintain, but also it will affect larger portions of the Channel. Every foot deepened turns into in several kilometres added to maintenance works and may lead to requiring new dump areas to cope with the extra volume extracted. This constitutes additional strain on the estuaries ecosystem and execution of a greater monitoring program.

Bottomline being flexible is not only cost-friendly but also environmentally reasonable.

5.3 Flexible contracts

Up to date (during the last 20 years), dredging contracts have been Performance Based owing to the need of securing the depth at all times. This was important due to past struggles and difficulties when the state was in charge.

Experience has shown that volumes tend to be circumscribed to a certain amount, with a variation of around some 30 %. Also, since the late 90's the equipment used in the maintenance has been a THSD (trailing suction hopper dredge) for the waterways, and a WID (Water Injection Dredge) for the berths and port basins.

This means that one could consider two contracts instead of just one for all the dredging works, drafting them according the type of equipment used. The advantage is that by doing so more offers could be received (specially from smaller or local companies), since there are few dredging companies with the capacity to carry out all the works that requires specific equipment. Also, time span for the contract can vary since maintenance of berths calls for frequent interventions as opposed to outer channel where one could even plan just a single campaign per year, provided sufficient over dredging allow to cope with the expected annual sedimentation.

Another way of making contracts smaller and thus open to more participants is to minimize the additional task to be performed by the contractor, for instance maintenance of tide gauge system, and all which is not directly concerned with dredging.

Being flexible also means that the CGPBB has begun to listen what the companies have to say regarding the tendering process. Among others, a revision of requested paperwork to minimize bureaucracy, providing constant feedback and consulting all the parties throughout the entire process. All this with the goal of obtaining the best contract that will satisfy all parties involved in terms of time span, reach and (of course) costs.

As a first approach to attain this goal and the change in the dredging contract paradigm, in 2018 the partial tender was placed reducing paperwork and performing a partition in the works carried out (considering the equipment used THSD or WID). Allowing an offer to be made for one or the other or both if possible. Direct contact and briefing was maintained all through the process, and special meetings were maintained with all the companies at the same time, giving all the contenders the required information that would lower the uncertainties, thus providing the grounds for an adjusted offer.

5.4 Being ready to be flexible

The Bahia Blanca 2040 Port Vision has provided the basis for the ongoing Master Plan, and amongst the various tasks to be performed, one of the highest priorities is the gathering and improving of all the basic data available, to be able to conduct the studies that will provide grounds for the development of future projects.

When it comes to waterways and its design, in the 80's a thorough study was carried out by a group of Dutch consulting companies, applying what was at the time state-of-the-art tools (including computational sedimentation models). Also, it included hundreds of field measurements of current, suspended sediments, bottom sediment, wave climate and tide at several sample points. Besides this, a comprehensive bathymetric survey was carried out along several potential layout areas.

But although the data is still used today, a lot has changed since. Not only in the equipment and methods used in the data collection and processing, but moreover in the estuary itself. More than 30 years have seen big morphological changes in the estuary. So, there is dire need to update and improve data to be able to have a better understanding of the estuary today, and the future development of its waterways.

Back in 2012, and because of the ever-increasing sedimentation in the Toro channel, a minor correction was carried out in the layout that meant shifting some 80 meters further south the curve near an advancing sand bank and adjusting the layout to maintain the curve radius and navigation conditions. This sole action meant cutting by half maintenance dredging at the zone. This proves the necessity of knowing what is happening not only in the waterways but also in its surroundings.

To improve such knowledge, and to have further control on the dredging works, the CGPBB has developed in 2018 its own Survey Department with state of the art Multi Beam and Inertial GNSS equipment. This will ensure a better understanding through periodical soundings of the changes in morphology, also providing data to conduct accurate volume calculations.

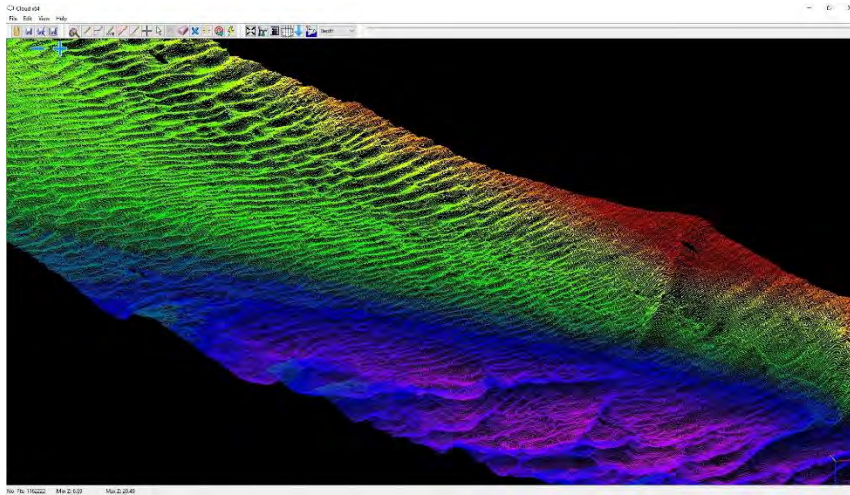


Figure 10: Multibeam Survey

Another action derived from the 2040 Vision is to initiate studies and data collection that will enable to set up, calibrate, validate and eventually run a Hydrodynamic mathematic model of the Estuary, including its waterways. It will provide enough detail to evaluate currents and water heights at every place and at all times. Having such a tool will generate useful information for setting up a Sedimentation model and Environmental one. All these tools will serve as the basis for layout and geometrical design of future waterway or the modification or deepening of the current ones. Enabling the analysis of multiple scenarios and, by comparison, the arrival of the best solution. Adding to these, a cooped manoeuvre simulator could provide information that could provide how vessels would react to modifications, or even be used to train pilots to sail new vessels that have not yet visited the system.

Being able to own and operate such a tool will give the CGPBB an unparalleled flexibility to analyse all possible requirements in a fast and trustworthy manner, provided the needed information to carry out the works (dredging, modifications in AtoN etc.) or eventually provide the basis to prepare tenders to achieve the desired goals.

Not only can mathematical modelling help with the analysis of future designs. Increasingly in other channels throughout the world the concept of Dynamic Under Keel Clearance (DUKC) is being used as a way of allowing safe sailing without over dredging. The waterways in the Bahia Blanca Estuary could profit immensely from its adoption.

Today every foot turns into almost a million cubic metres of annual sedimentation, which constitutes several million USD. So, having a reliable tool to forecast high waters and wave climate and being able to have an improved management of the tide window and drafts could provide a deeper waterway without dredging, meeting the requirements of the users with a fraction of the cost as compared to deepening.

As a summary one could say that being ready is having the information and the possibility of developing the tools in a short amount of time. Also, not less important, is to have the staff prepared to handle and to analyse these data. Training the personal at the CGPBB to cope with the required new skills, then becomes a task to tackle immediately.

5.5 When to change

As with dredging contracts, the time has come to exercise a change in paradigm when it comes to waterway planning. And as mentioned before, hearing what others have to say is perhaps the most important factor. In line with what was promoted in the Port's 2040 Vision and Master Plan all the stakeholders have something to say and must be heard. Of course, some of them will request deeper or wider channels, or better signalling, or lower fares, it is then up to the CGPBB to correctly analyse all these requests and promote those actions that sees fit to improve the waterway accordingly. There won't be complete satisfaction, but from interaction there will surely be a better understanding between the parties.

But change won't come only from local or regional request, worldwide shipping must be considered. In the past changes in the world fleet were slow to be acknowledged, leading to loss of cargo, greater downtimes or hasty works to adequate to newcomers with greater dimensions. Today the access to information allows to keep track of tendencies regarding the types of ships likely to call upon port, considering new orders placed on the main shipyards, or the constitution of the actual fleet. This is done regularly to ensure that the system will be able to cope in the foreseeable future with the traffic expected.

Nevertheless, a Port must also be prepared, should the case arouse of a different type or cargo, which in term will require a different kind of ship. For this reason, definition in waterways is a subject to which all areas within the CGPBB should relate. It takes a couple of years to build (depending its size), approximately the same time required to make changes to the waterways.

So, the time to change will be promoted by the need to change, but to be able to do so one has to be willing and prepared.

6 CONCLUSIONS

Up to recently, planning of waterways was mainly done considering what others (the government) stablished as the goals to achieve. This partially was modified once the CGPBB began to operate (and maintain) the waterways. The requirements of potential operators were seldom considered or evaluated.

A first attempt came when in 2013, when partial capital dredge was carried out to improve congestion in the port area and the associated increasing downtimes. Assumptions and forecast made at the time concerning rise in traffic turned out to be too optimistic. Conditions in and out of the country prevented the envisioned development to happen.

A great landmark came in 2017 with the realization of the 2040 Port Vision as the stepping stone to making a Master Plan. This innovative tool provided much needed feedback of all the port's activities, in particular, what the stakeholders needs are and the requirements for the future in all aspects.

Another important issue is the ever-increasing maintenance dredging cost and how it affects the port competitiveness, consuming an increasing share of the budget. This calls to address a change in paradigm when it comes to Dredging Contracts, modifying the way tenders are conducted and the interaction with offering companies, partitioning tasks, time span, avoiding unnecessary bureaucracy etc.

Providing due time for studying all the information and analyses of potential scenarios, to be ready to react to new needs is of the utmost importance. Also, having a constant oversight of the world's trend in fleets likely to call port and interacting fluidly with all the stakeholders on a regular basis.

Being flexible when it comes to waterways is to be prepared to adapt to the immediate needs, to be cost effective and, not less important, environmentally aware. Not performing unnecessary capital dredging that will entail greater maintenance afterwards. In all, dredging should be the last resort, after improving aids to navigation and operational management tools.

The Port of Bahia Blanca began to implement measures that hopefully will set the bases for achieving flexible planning when it comes to its waterways, in a cost effective and greener way.

7 REFERENCES

ABITANTE O., LINARES J. and SCHNEGELBERGER M. (2007): Anteproyecto Conectividad Marítima del Sistema Interior

NEDECO Netherland Engineering Consultants and ARCONSULT Consultores Argentinos (1983): Estudio de Dragado del Canal de Acceso al Puerto de Bahía Blanca

OPERATIONS DEPARTMENT CGPBB (1993-2015): Anuario Portuario years 1993-2017
Traffic statistics

PHYSICAL AND NUMERICAL MODELLING OF SHIPS MOORED IN PORTS

by

Pierre-François Demenet¹, Lionel Guisier² and Cyrill Marcol³

ABSTRACT

The study of a moored LNG carrier vessel in presence of waves by numerical and physical modelling is presented in this paper. The objective is to compare the numerical modelling of this vessel in presence of an harbour structure (as a vertical quay or rubble-mound breakwater) with the results obtained with a physical model in order to improve our confidence and our practice when using the numerical model for engineering applications. The paper describes in details the model set-up, the instrumentation, the ship model characteristics to comply with Froude scaling and the results obtained.

Among the different harbour structures tested by physical model, the vertical quay quite far from the vessel is the structure which has a clear impact on vessel behaviour by increasing significantly the mooring lines tensions and the vessel motions comparing to a configuration without any structures. In addition, mooring lines tensions are in good agreement between the two models as well as motions, except for roll, which is twice larger in the numerical modelling and which requires to be further analysed in a next phase of the project.

1. INTRODUCTION

Study of moored vessel motions in presence of waves is a very important issue for all harbour design project as vessel dynamic behavior has a direct impact on safety of (un)loading operation as well as on berth equipment (mooring lines & fenders) integrity. In addition, wave conditions are one of the main factors which could affect the berth operational downtime. As this downtime shall be very low to ensure cost-effectiveness of the berth, it shall be demonstrated that wave-induced motions are acceptable to enable (un)loading operations in presence of the most frequent wave conditions.

Several numerical tools are available to perform dynamic mooring analysis of ships exposed to waves. However, despite the fact that these tools are very efficient to simulate rapidly a large amount of different environmental and mooring conditions, some parameters used in these numerical models need to be calibrated from physical model tests measurements. Physical model tests are hence required to calibrate numerical simulations but are also necessary to model some specific and complex hydrodynamic configurations for which a numerical approach is not sufficient such as moored vessel close to rubble-mound breakwater, with complex bathymetry for instance. In a general way, a vessel moored at berth inside a port can be exposed to a very complex wave disturbance pattern which could include several wave trains issued from reflective structures as quays or rubble mound breakwater or issued from diffraction of waves at the main breakwater roundhead.

In order to improve the reliability and relevancy of numerical mooring analysis as well as to improve our understanding of some specific hydrodynamic complex configurations, a research project has been launched in ARTELIA hydraulic laboratory which consists in carrying out series of physical modelling tests (a) to provide relevant experience feedbacks for numerical modelling and (b) to improve the methodology deployed in our laboratory for floating bodies physical modelling.

¹ ARTELIA Eau & Environnement, France, pierre.francois.demenet@arteliagroup.com

² ARTELIA Eau & Environnement, France, lionel.guisier@arteliagroup.com

³ ARTELIA Eau & Environnement, France, cyrill.marcol@arteliagroup.com

2. DESCRIPTION OF THE PHYSICAL MODEL TESTS

2.1 Methodology

Using physical modelling for study of dynamic behavior of vessels moored at berth is a classical approach which is well described in several standards, guidance and literature (e.g. Sutherland, 2013; British Standards, 2013)

Froude's law is the similarity law applied, due to the fact that gravity forces predominate over the other forces (e.g; viscosity). However, it is necessary to verify that the Reynolds number is greater than 104 in accordance with Hydralab guidance (Sutherland 2013), to ensure that the forces of viscosity are sufficiently representative. The above criteria have been verified for the different waves and depth conditions which have been tested.

The modelled vessel is a LNG carrier which represents a type of vessels which is frequently studied by ARTELIA for mooring analyses we have to carry out as part of marine terminal design projects.

As one of the main objectives of this physical model tests campaign is to enable a direct comparison with numerical model results, some simplifications have been decided at the beginning of project:

- The bathymetry is represented in the wave basin as a flat bed at 0.225m depth (18m nature), in order to perfectly correspond to the numerical model.
- A linear behavior is modelled for stiffness of mooring lines as well as for fenders. This is to avoid a too complex model (as regard to construction aspects) and hence to facilitate understanding of dynamic behavior of physical model in comparison to numerical model.

2.2 Model set-up

The model tests were performed in one of the wave basin of the Hydraulic Laboratory of ARTELIA, in Pont-de-Claix, near Grenoble (France). The basin is 16m wide, 30m long, 0.8m high and is equipped with a piston-type wave paddle driven by a hydraulic jack, which generates long-crested waves. The model was built at 1/80 scale, based on Froude scaling.

A simplified flat bathymetric profile was built in hard cement in the basin slab. The seabed is reproduced as a non-erodible surface. Wave-absorbing beaches have been placed at the boundaries of the basin, to prevent as much as possible unwanted reflections (boundary effects).



Figure 1. Overview of model implemented in the wave basin

The following components, representative of a typical LNG terminal berth have been implemented as follows:

The vessel, modelled with representative geometry, displacement, draught, COG, metacentric height & inertia

- The berth, modelled by 8 mooring dolphins and 2 breasting dolphins
- 8 mooring lines (representing actually 16 mooring lines, as two real mooring lines are represented in the model by a unique bundle).
- 2 fenders (representing actually 4 fenders)

The following figure details the studied berth and provides an overview of the deployed instrumentation:

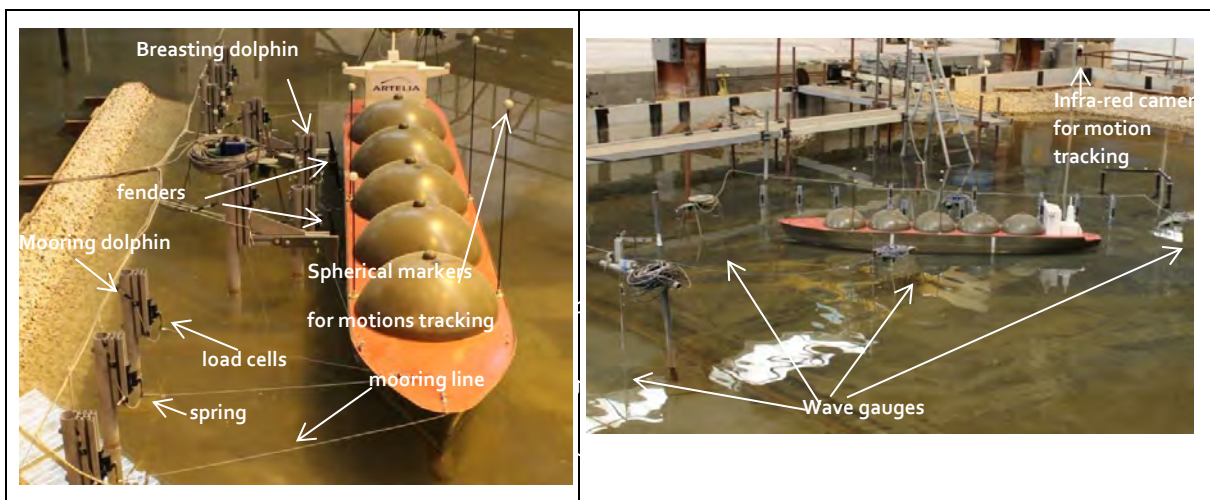


Figure 2. detailed view of berth & overview of deployed instrumentation

The modelled vessel is a 130 000m³ capacity LNG carrier, in loaded configuration, with the following characteristics:

| Vessel characteristics | At prototype scale | At model scale |
|-------------------------------|--------------------|----------------|
| Length overall (m) | 287.5 | 3.6 |
| Lpp (m) | 274 | 3.425 |
| Breadth (m) | 43.4 | 0.542 |
| Depth (m) | 25 | 0.312 |
| Displacement (t) | 92 365 | 0.176 |
| Mean Draft (m) | 10.8 | 0.135 |
| Natural roll period (s) | 16.40 | 1.83 |
| Metacentric height GMt (m) | 5.02 | 0.063 |

Table 1. Vessel model characteristics

2.3 Instrumentation

For each test, the following parameters have been monitored and recorded:

- Tensions in each of the 8 mooring lines
- Forces in the 2 fenders
- Motions of the ship in the six degrees of freedom
- Water surface elevation at five locations in the vicinity of the ship

Tensions in mooring lines and forces in fenders have been measured by strain gauge technology sensors (bending beam load cells utilized in compression) and motions of ship in the six degrees of freedom have been measured by the combination of 4 infrared cameras for motion tracking (Qualisys system).

Waves conditions have been assessed from omnidirectional and directional gauges. Omnidirectional wave gauges measure the water surface elevation. These capacitive gauges are made of two thin vertical wires, and relate voltage to water level. The directional wave gauges measure the wave orbital velocities, based on the principle of electromagnetic field distortion in the presence of currents. Coupled with omnidirectional wave gauges at given locations, they are used for separating incident and reflected wave energies (and then to determine reflection coefficients of the structures). The different types of gauges are used: for directional wave gauges to check the target input conditions at specific reference/control points and for omnidirectional gauges to measure local wave disturbance at specific areas.

The wave generator is controlled by the GEDAP comprehensive software system for the analysis and management of laboratory data. This state-of-art software, developed by the Canadian Hydraulics Centre of the National Research Council (NRC-CHC), enables wave generation, real-time data acquisition and post processing wave analysis.

All measurements have been synchronised and performed at a sampling frequency of 60Hz.

2.4 Tests procedure and program

Different water depths (18m and 14m at prototype scale) and wave conditions (H_m0 in the range [0.5m – 1.5m] and T_p in the range [8s – 18s]) have been tested together with two wave incidences: (a) Waves coming abeam and (b) Quartering seas: waves coming from 45° with reference to the bow. Modelled wave spectrum is Jonswap type with a gamma factor of 3.3.

In addition, two harbour structures (vertical quay and a rubble mound breakwater) have been implemented for some tests into the model to analyse the impact of different kinds of structures (fully or partially reflecting the waves) on moored vessel behaviour. This mooring configuration in shallow water and in presence of harbour structures represents the context of typical harbour design project performed in ARTELIA.

For this purpose, four configurations have been tested as follows:

- Configuration A: a berth without any structure
- Configuration B: a berth with a vertical quay very close to the ship (distance of 4m between ship hull and quay at prototype scale)
- Configuration C: a berth with a vertical quay quite far from the ship (distance of 110m between ship hull and quay at prototype scale)

- Configuration D: a berth with a rubble-mound structure (typically half of a breakwater) far from the ship (at prototype scale distance of 100m between ship hull and intersection of rubble-mound structure with still water level)

It shall be noted that configuration B does not represent a realistic situation for LNG carrier, as this kind of vessel is generally not moored directly alongside and close a vertical quay. LNG carrier ships are rather moored at a dedicated berth where main mooring dolphins are at a distance of typically 50m from berthing line (as modelled in the present project and as presented in above Figure 2). However this configuration “B” is studied in order to provide a relevant feedback for numerical model representing a vessel moored alongside and close to a vertical quay as it is a common practice for general cargo, ferries or container vessel.

These four configurations are presented in the following figure:

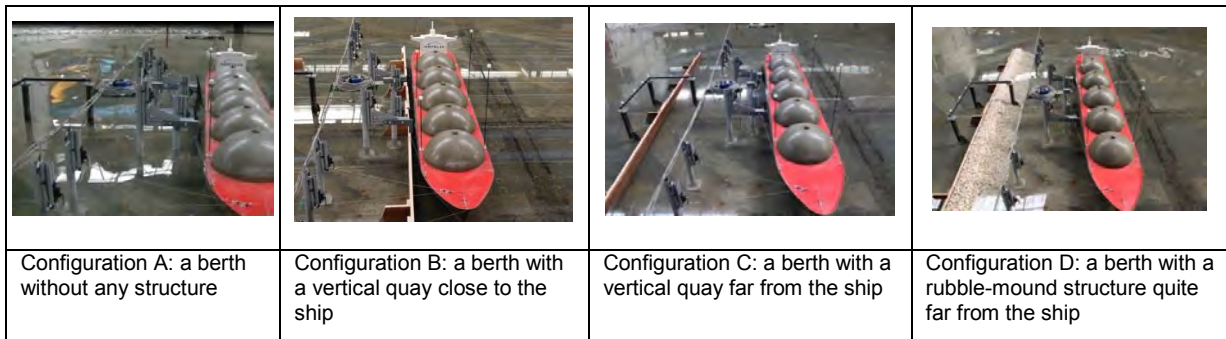


Figure 3. Views of the different studied configurations

Tests have been performed in regular waves conditions as well as in random waves conditions. For random waves, tests are performed considering a 3 hours duration (prototype scale). At model scale, this represents a test duration of about 20 minutes. After completion of each test, a time-domain analysis of the measured data is carried out. For tensions in mooring lines, forces in fenders and motions for each of the 6 degrees of freedom, the following statistical results are output:

- F+1/10: Average value of the highest 1/10th of the peaks;
- F+max: Maximum value of the peaks;

The same statistical study is performed for the troughs (F-). Statistical analysis for post-processing of data is performed using WaveLab software, developed by the Hydraulics and Coastal Engineering Laboratory of Aalborg University (Denmark).

3. NUMERICAL MODEL AND SOFTWARE DESCRIPTION

Several configurations tested in wave basin were modelled in DIODORE™ software which is a general purpose hydrodynamics software package designed to solve a large number of problems in offshore and marine applications, such as stability, sea keeping and mooring analyses. DIODORE™ includes several modules:

- A Pre-processor, that defines the physical and geometrical characteristics of the floating body and its hydrostatic characteristics.
- An Hydrodynamic processor, which computes, from a mesh-model of the vessel hull shape, the hydrodynamics of the floating body and the corresponding wave diffraction/radiation loads. This software is based on the potential theory. Such

approach allows to compute, from a mesh-model of the immersed volume of the hull, the hydrodynamic characteristics of the floating structures in terms of diffraction (disturbance of the wave field incident to the fixed structure) and radiation (as generated by the wave field induced by the movement of the structure). Radiation is measured in the form of added masses and radiation damping. Diffraction is evaluated in the form of transfer functions of wave loads. The main assumption of the Potential theory is to neglect viscous effects. It is therefore necessary to use additional models to reproduce the effects due to the viscosity, especially for those degrees of freedom where radiation provides very little damping, as in roll. Viscous damping in roll is therefore added, based on coefficients found in the literature (or from basin model tests, when available). In the present case, the linear and quadratic damping coefficients which have been input in the numerical model have been evaluated by the physical modelling and dedicated decay test (see section 4).

- A Mechanical processor, which computes the linear and non-linear motions of the floating body, induced by waves (wave frequency and low frequency 2nd order drift), wind and current. It includes a time domain solver to analyse, over typically a 3 hours simulation, the dynamic motions of the floating structure, taking into account the (non-linear) stiffness of the mooring lines and the fenders.
- Post-processor, which is used to visualize the results and which provides statistical analysis of key parameters, such as tensions in the mooring lines, motions of particular point along the hull ...etc.

In the present case, for assessment of slowly-varying drift forces, the Newman's approximation is used (Newman, 1974).

The Diodore™ solver enables to model multi-body systems. Hence it is possible to model another (fixed) structure (e.g; a vertical quay) in presence of the vessel to take into account a coupling between hydrodynamics of the structure and of the vessel. This modelling enables to take into account of the reflective wave trains generated by the quay (fully reflective) on the vessel dynamic behavior in addition to the incident wave trains.

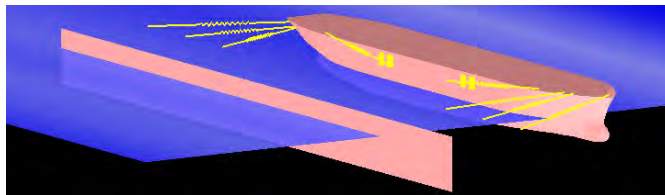


Figure 4.: Numerical model (including a vertical quay)

When the vertical quay is very close to the vessel, the close proximity of the ships creates a narrow volume of water in the gap between the ship and the quay. As it is a confined volume of water, hydrodynamic resonances in this area could occur. The method to handle correctly these phenomena numerically is presented in the article of Lecuyer et al (2012). The aim of this method (which has been originally developed to represent ship-to-ship configuration) is to model a free-surface with some additional damping representing the viscous effects due to the vortex shedding along the bilge of the ship. This is made in DIODORE™ by a specific lid method, consisting in setting rigid dummy plates at the free surface in the narrow part of the gap. However, lid method, results obtained with numerical model and comparison with corresponding model tests cannot be further exhaustively presented in the frame of this article.

4. MODEL CHARACTERISTICS VERIFICATION

In order to ensure a correct representation of the vessel at laboratory scale, it has been verified that the target characteristics of the ship model have been checked.

Displacement, draft, as well as trim and heel angles have been verified using the measurements taken on 4 draft scale implemented on the hull of the ship at aft, bow, portside and starboard side.

In addition metacentric height (GM) was determined and verified by inclining test (method consisting in the displacement of a known weight from a side to the other side by a known distance and by measuring the induced modification in heeling angle)

Then, free decay tests in roll have been performed in order to check (a) the roll eigen period of ship and (b) to assess the roll damping coefficients. Each test (defined by an heel departure angle for starboard side and for portside) have been repeated twice. From free decay tests results, the roll damping coefficients have been assessed with reference to methodology exposed in ITTC standards procedures (ITTC 2011).

Once the damping coefficient have been evaluated from specific decay tests, these coefficients have been input in the numerical model and then a numerical decay test has been performed in the same conditions than physical model. The calculated roll motions have been observed to be in very good agreement as shown in the following figure:

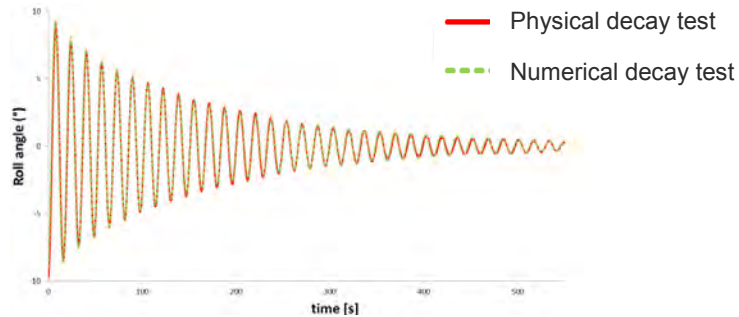


Figure 5.: Comparison of numerical model with physical model – decay test

5. REPEATABILITY OF PHYSICAL MODEL TESTS

In order to assess the variability of the results (in terms of motions as well as in terms of tensions in the mooring lines), some repeatability tests have been performed:

- For the same defined (H_{m0} , T_p) conditions, repetition of the same time series of wave trains
- For the same defined (H_{m0} , T_p) conditions, performance of a test with another time series of wave trains (randomly generated).

The following figure presents the results of two tests (with different time series of wave trains), performed in beam seas configuration, for a water depth of 18m, and considering that each mooring line is actually a bundle of two mooring lines. The results presented are $F+1/10$ values.

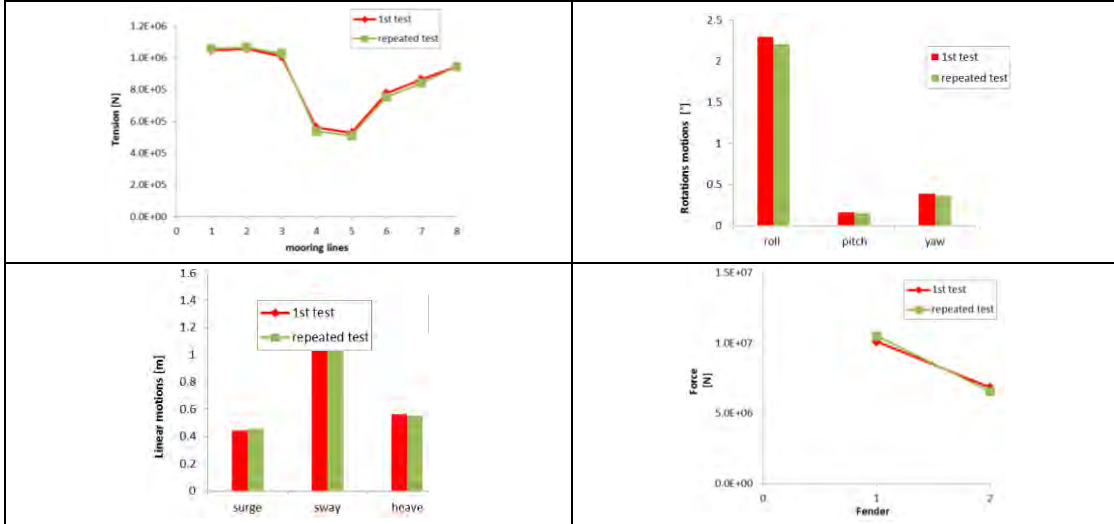
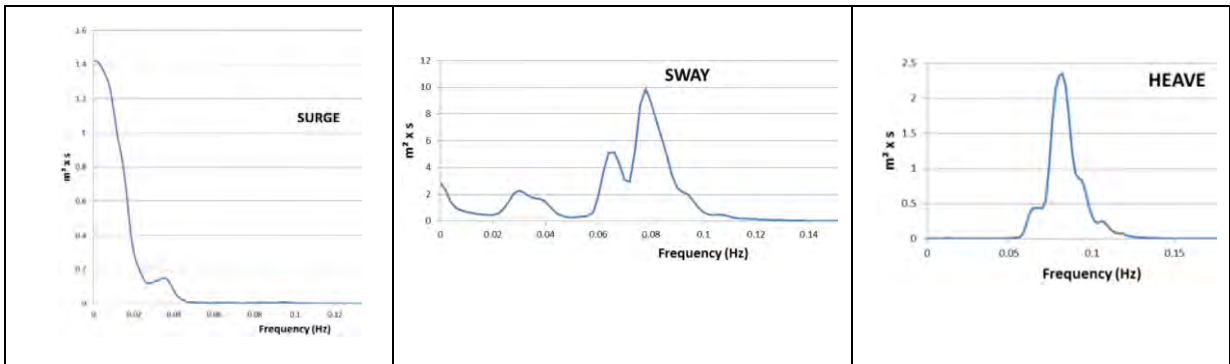


Figure 6. Repeatability tests (for Hm0= 1m /Tp=12s)

In above figure (as well as in this paper), the lines (bundle) n°1,2 & 3 refer to head lines, n°4 & 5 to spring lines and n°6, 7, 8 to stern lines. Regarding fenders, fender n°1 refers to fore fender and n°2 refers to stern fender. Variability from a test to another is low (about 4% for forces and 5% for motions). From the same performed tests, it has been observed that, for maximum values (F+max), the variability is increased (about 15% for forces and 7% for motions).

In addition, for variability tests based on similar wave trains the observed variability is about 3% for forces and 2% for motions for F+1/10 values and is about 9% for forces and 4% for motions for F+max values. F+1/10 values are less sensitive to random aspects of tests (comparing to F+max), hence, unless otherwise specified, results presented in this paper will be related to the F+1/10 values.

In addition, for these test conditions, a spectral analysis has been performed on the time series of motions, in order to evaluate the energy distribution for the six degrees of freedom. Results are presented in the following figure:



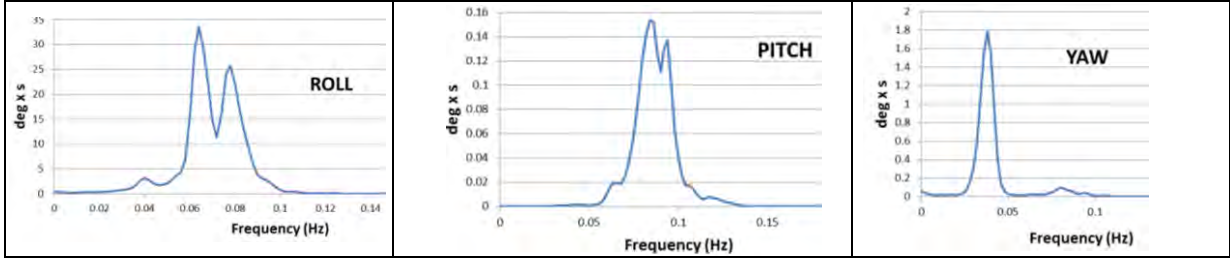


Figure 7. motions spectra for repeatability test ($H_m0= 1m /T_p=12s$ – beam seas) at prototype scale

For these test conditions, the wave spectrum (issued from wave gauge located at wave control point) is presented in the following figure as well as the distribution of wave height (with comparison to a Rayleigh distribution).

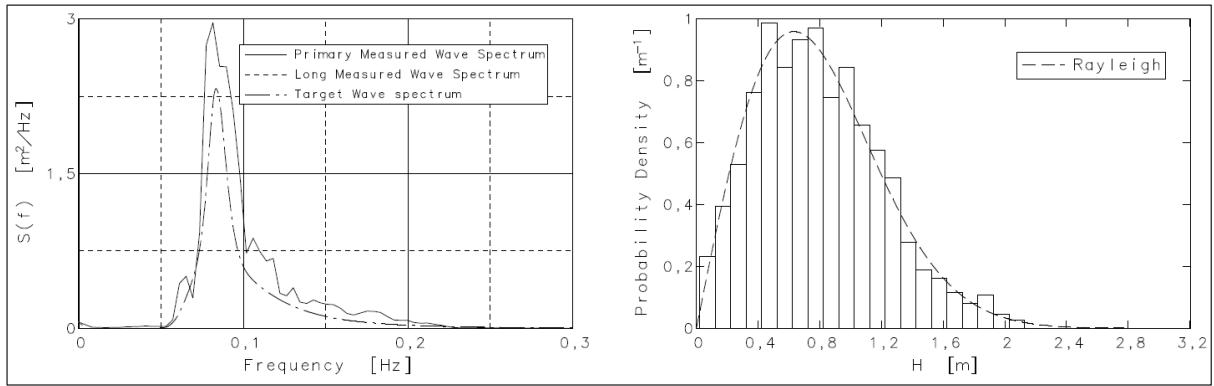


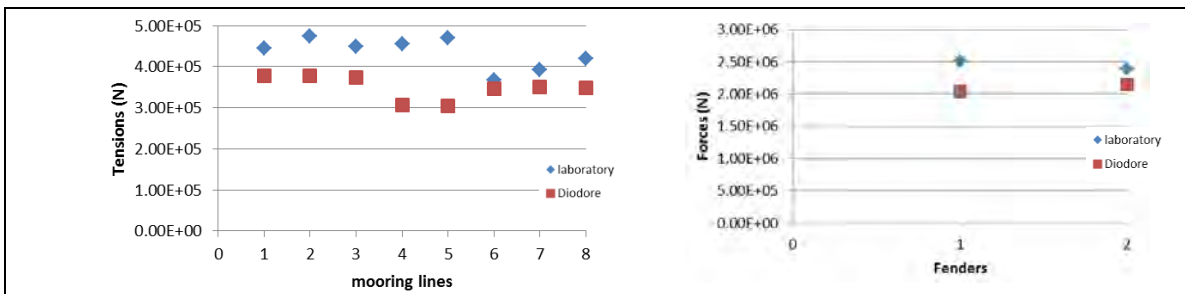
Figure 8. wave spectrum for repeatability test ($H_m0= 1m /T_p=12s$ – beam seas) at prototype scale and distribution of wave height

6. SIMULATIONS WITH NUMERICAL MODEL AND COMPARISON WITH PHYSICAL MODEL TESTS

At this stage, the physical modelling tests campaign is just finished. All the performed tests have not been exhaustively post-processed and analyzed. Thus, the results presented in the following sections correspond to the first tests which have been analyzed.

6.1 Without structure

The following figure presents some of the results of the numerical modelling in comparison to the physical modelling for quartering seas conditions.



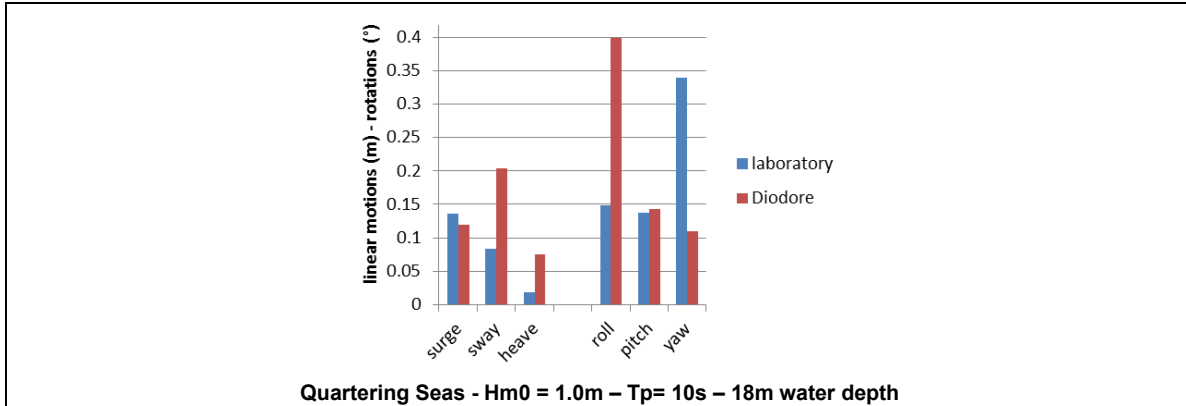


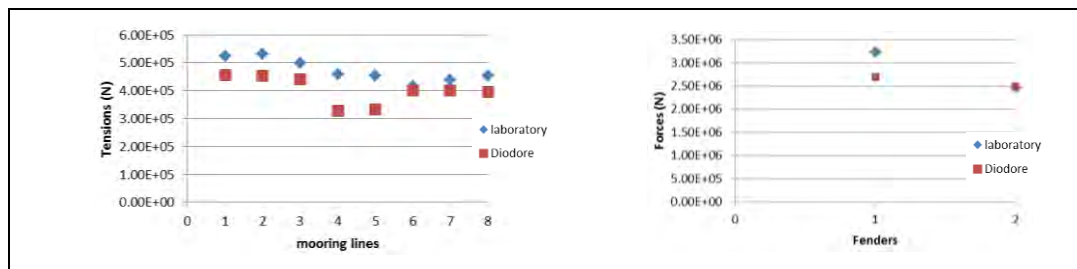
Figure 9.: Comparison of numerical model with physical model – without structure

The above results show that

- Tensions are in fairly good agreement in the two models (physical and numerical). This is particularly true for head and stern lines for which the difference between the models is about 20% to 25%.
- Forces in fenders are quite in good agreement too. Maximal difference between the models is 20%.
- The motions are quite in good agreement for surge and pitch, but for the other degrees of freedom, some discrepancies are observed.
- For roll motion, the values are more than twice larger in the numerical model than the values assessed with physical model. This is quite surprising as the numerical model uses the quadratic and linear damping coefficients specifically evaluated from decay test (following roll axis) performed with the physical model (as explained in above section 4)

6.2 In presence of vertical quay far from vessel

The following figure presents some of the results of the numerical modelling in comparison to the physical modelling



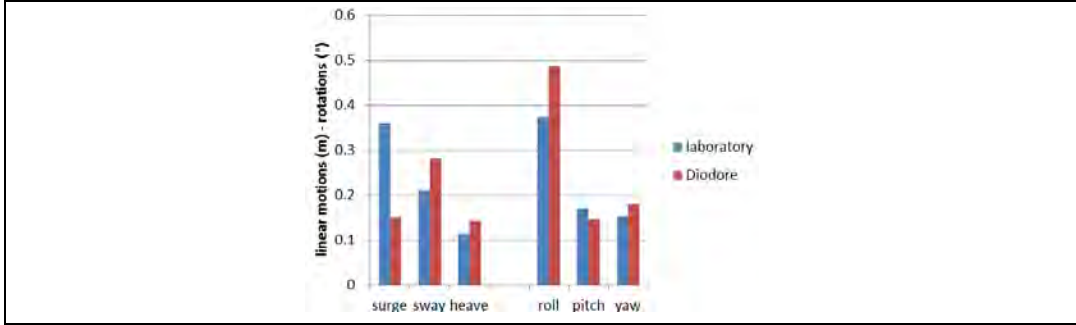


Figure 10.: Comparison of numerical model with physical model – with a vertical quay far from vessel

These results show that:

- The mooring line tensions are in good agreement for head lines and stern lines (maximum discrepancies of 15%). For spring lines, tensions assessed from physical model are up to 35% larger than tensions from numerical model
- Forces in fenders are in very good agreement as well.
- Regarding motions, except for surge and for roll, the results obtained for the two models are quite in good agreement

7. PHYSICAL MODELLING AND INFLUENCE OF HARBOUR STRUCTURES

For the four configurations studied (one configuration without structure and three different structures, as shown in above Figure 3), the tension in mooring lines as well as motions are plotted in the following figures for the quartering seas direction and for a water depth of 18m.

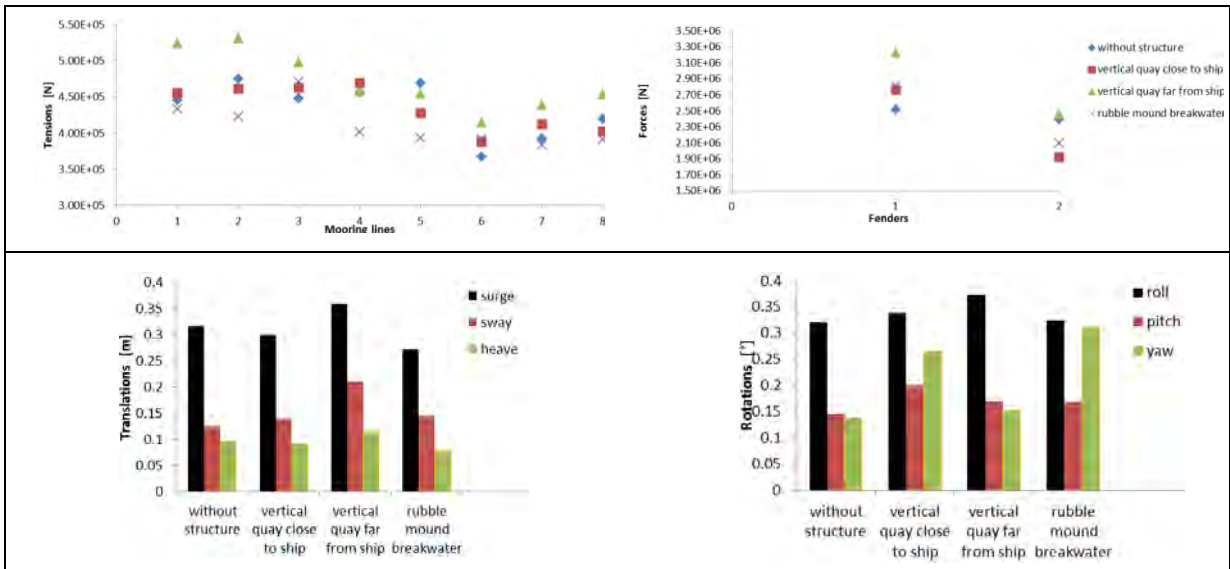


Figure 11.: Influence of harbour structures - quartering seas - $H_m0 = 1m$ – $T_p = 10s$ - 18m water depth

From these tests, the following findings can be drawn:

- For the four studied configurations, the structure consisting in a vertical quay far from the ship is the harbor structure which leads to the largest tensions in mooring lines and to the largest forces in fenders and as well as the largest motions of vessels. Depending on the mooring line location, the tension is up to 20% larger in presence of a vertical quay far from the vessel comparing to a configuration without structure.
- The three other studied configurations induce mooring lines tensions rather in the same range of values, even if the configuration consisting of a vertical quay close to the ship seems to induce slightly larger values.
- The structure which leads to the lowest tensions in mooring lines is the rubble mound breakwater. This result is quite surprising as this (partially) reflective structure leads to tensions slightly lower than tensions observed for a configuration without any structure. At first glance, it could have been expected, that this (partially) reflective structure increases wave disturbance in the area between vessel and rubble-mound and thus increases wave energy reaching the vessel and as a consequence increases motions of vessels as well as tensions in mooring lines.

Regarding the wave pattern in front of a reflective structure, in case of normal (i.e. frontal) attack, the significant wave height oscillates, featuring nodes and antinodes which reduce when moving away from the structure to reach an asymptotic value (typically 1.4 time the incident significant wave height for a vertical structure) for a distance from structure equal to about 1.5 time the wave length (Goda, 2010 and Klopman et al, 1999). Spacing between nodes and antinodes is $0.25 \times L_p$ (with L_p : the wave length).

With oblique waves, there is again a system of nodes and antinodes with a spacing of $0.25 \times L_p \times \sin$ (angle of attack).

In the present case:

- The angle of attack is 45° .
- The wave length (for a water depth of 18m and a period of peak of 10s) is 117m.

Hence, in the present case, the distance from which the significant wave height oscillations are damped is 124m. This distance corresponds roughly to the distance between structure and vessel Center of gravity (131m for the vertical structure and 121m for the rubble mound breakwater). Therefore, it can be considered that the vessel is out of the area where large oscillations of significant wave height can be observed.

8. ACCURACY, SCALE EFFECTS AND MODELS LIMITATIONS

In addition to the usual scale, laboratory effects and limitations inherent to physical modelling of floating structures (Hydralab, 2013; Goda, 2010; Hughes, 1993), this physical model tests campaign has highlighted some limitations and some constraints:

- Generation of small waves conditions: the waves conditions which have been tested are typical waves values which could be observed inside harbour in presence of moored vessel (i.e. in waterways protected by breakwaters). Hence the tested wave heights are quite small (H_{m0} up to 1.5m). At the scale model (1/80), the corresponding wave height is small (19mm). In this context, the verification of the waves generated and reaching the vessel model is less accurate for these small waves than it would be for higher waves. This is induced by the deployed instrumentation (directional wave gauge) with which the assessment of coefficient of reflection is less accurate for small waves conditions. This is due to the accuracy of current measurement in presence of very low values of velocities, for these gauges

which in most cases measure larger wave height. In addition, the maximal significant wave height modelled in our campaign (2cm) represents the limit commonly used (Wolters 2007) for the lowest waves modelling to avoid significant model effects.

- Influence of temperature: the tests campaign has been carried out during a period of several months, with different temperature conditions for the water used for the tests. Particularly, the decay tests have been performed in winter with a water temperature of 8 to 10°C, and some of the tests with the moored model have been performed during a hot summer period with sea water larger than 20°C. It is possible that this situation could have induced some distortions on results obtained in summer comparing to results obtained in winter as regard to the difference in viscosity (reduction of about 25%) which is observed when the temperature is increased from 10°C to 20°C. However, this phenomenon should need to be further studied to assess the real impact of water temperature on model behavior.

9. CONCLUSIONS, EXPERIENCE FEED-BACK AND FUTURE WORKS

At completion of this first stage of in-house research project, the following findings have been provided:

For the case where a vessel is moored at berth without any port structure at proximity, above results have shown that a good agreement between numerical and physical models can be obtained. This configuration (typically a terminal in open sea, with a very simple bathymetry) can be modelled and studied by dedicated numerical tool for instance to determine operational thresholds induced by waves with relevant criteria regarding mooring line tensions.

In addition, for berth and port designers, another usual situation consists in a vessel moored at vicinity of an harbour structure which could modify the wave pattern reaching the vessel. In this configuration, impact of these reflective structures (e.g. a vertical quay) is not marginal as for instance for the mooring lines tensions which could be significantly increased. In this context, comparison between numerical and physical modelling shows that we could be quite confident in the numerical model to analyze the behavior of a vessel moored in presence of a vertical structure (typically a quay) far from the vessel.

However, results show that roll motions seem to be over-estimated in numerical modelling (compared to motions measured on physical model). The impact is marginal for mooring lines tensions and also for forces in fenders, but this could induce potentially conservative results in numerical analysis for which a strict criteria is to be fulfilled as regard to roll motion (e.g. when (un)loading operations could be governed by roll motions).

Analysis of a moored vessel in presence of other port structure as quay close to the vessel and rubble-mound breakwater by numerical modelling is quite more complex and requires an additional work we intend to perform in a next stage of our project.

In addition, comparisons by physical modelling of the different configurations of a moored vessel (without structure, with rubble mound breakwater and with vertical quay close to the vessel or far from vessel) have shown that the vertical quay is the structure which leads to the largest tensions in mooring lines as well as the largest motions.

However, the post-processing and the analysis of all performed tests need to be completed to potentially draw additional findings.

This campaign is a first step and some further developments could be envisaged. For numerical approach: to go on the modelling of vessel behavior in presence of partially reflective structure (as rubble-mound breakwater), on the basis of the performed physical model tests or additional tests to be performed. Regarding physical modelling, the following future actions are envisaged:

- To model non-linear stiffness for mooring lines and fenders, as it is recommended for an accurate modelling of hydrodynamic behavior (Sutherland et Al, 2013)

- To extend analysis to other harbor structures or others ports configuration (e.g. complex bathymetry with steep slope).
- To go on the identification and mitigation (when possible) of laboratory effects we experienced in our facility.

10. ACKNOWLEDGEMENTS

The authors would like to thank Dr J.M. Rousset (Centrale Nantes Engineering School) for his constructive assistance for motions capture system set-up as well as Dr L. Hamm (ARTELIA) for his fruitful comments.

11. REFERENCES

British Standards, 2013. BS 6349-1-1, maritime works Part 1-1: General – code of practice for planning and design for operations.

Goda Y, 2010. Random Seas and design of maritime structures 3rd edition, Singapore, ISBN-13 978-981-4282-39-0

Hughes S.A., 1993. Physical models and laboratory techniques in coastal engineering, Singapore, ISBN 981-02-1540-1

ITTC, 2011. Numerical estimation of roll damping, recommended procedures and guidelines

Klopman G., Van Der Meer J.W., 1999. Random wave measurements in front of reflective structures, Journal of waterway, coastal, and ocean engineering, 125, 1, 39 – 45.

Lecuyer B., Ledoux A., Molin B., Le Boulluec M, Heguiaphal B., 2012. Hydro-mechanical issues of offloading operations between a floating LNG terminal and a LNG carrier in side-by-side configuration - International Conference on Ocean, Offshore and Arctic Engineering (OMAE)

Newman, J.N. (1974) "Second Order, Slowly Varying Forces in Irregular Waves". Proc. Int. Symp. Dynamics of Marine vehicles and Structures in Waves, London

Sutherland J. Evers K-U (lead authors), 2013. Foresight study on laboratory modelling of waves and ice loads on coastal and marine structures, deliverable D2.3 – EC contract n°261520, HYDRALAB-IV,

Wolters G. (Lead Author), 2007. Guidelines for physical model testing of breakwaters – deliverable NA3.1-2 -2007 - HYDRALAB III

AN INTEGRATED APPROACH TO PORT PLANNING, OPERATIONS & RISK MANAGEMENT THROUGH TECHNOLOGY

by

*Brendan Curtis*¹

ABSTRACT

Ports and shipping channels are critical components of many nations' transport infrastructure, and make a significant contribution to the economy. With increasing global trade comes further pressures on ports through greater volumes, larger vessels, and more demanding shipping schedules. This is occurring against a backdrop of increasing regulatory, environmental, and social requirements for port authorities and operators that makes development more challenging. Furthermore, port authorities often hold the dual responsibility of facilitating trade and ensuring port safety.

Advancements in technology from a range of fields in the maritime sector are enabling new solutions to these challenges. Developments include improvements in hydrodynamic modelling capabilities, high density bathymetric surveys, improvements in weather forecasting, cost effective access to real time met-ocean data, advancements in environmental data assimilation techniques, broad adoption of AIS and Electronic Navigational Charts (ENCs), and high precision measurement of vessel motions in full scale and real time using DGPS and IMU technologies. Each of these developments individually has provided benefits to the industry. However, the greatest benefits, from the dual perspectives of risk management and efficiency, are realised when they are integrated and implemented across both the planning and operations of a port.

Changes across the industry, and within specific port environments, such as vessel sizes, transit speeds, channel depth profiles, transit times, and changes to port layouts resulting from new berths or dredging can influence the applicability of long standing port procedures and risk management functions, particularly static UKC regimes.

To highlight the changing nature of the port operating environment, this paper presents three separate examples where assumptions about port operations have been incorrect, and consequently, the design or operating procedures have required amendment.

The paper culminates with case studies for the Ports of Port Hedland, Whyalla and Geelong, to examine how a suite of integrated software solutions deliver increased safety and improved operational performance. This is achieved through a consistent approach to port planning, capital and maintenance dredging, vessel fleet planning and chartering, vessel transit planning, and real time in-transit monitoring.

¹ GM Business Development, OMC International, b.curtis@omcinternational.com

1. INTRODUCTION

Ports and shipping channels are critical components of many nations' transport infrastructure, and make a significant contribution to the economy. In Australia, the daily trade flows through ports is estimated at \$1.2 billion (Ports Australia, 2017). With increasing global trade comes further pressures on ports through greater volumes, larger vessels, and more demanding shipping schedules. This is occurring against a backdrop of increasing regulatory, environmental, and social requirements for port authorities and operators that makes development more challenging. Furthermore, port authorities often hold the dual responsibility of facilitating trade and ensuring port safety.

Advancements in technology from a range of fields in the maritime sector are enabling new solutions to these challenges. Developments include improvements in hydrodynamic modelling capabilities, high density bathymetric surveys, improvements in weather forecasting, cost effective access to real time met-ocean data, advancements in environmental data assimilation techniques, broad adoption of AIS and Electronic Navigational Charts (ENCs), and high precision measurement of vessel motions in full scale and real time using DGPS and IMU technologies. Each of these developments individually has provided benefits to the industry. However, the greatest benefits, from the dual perspectives of risk management and efficiency, are realised when they are integrated and implemented across both the planning and operations of a port.

2. THE UKC CHALLENGE

The problem of underkeel clearance is not new; since time immemorial navigators have been concerned to know the minimum depth of water in which they can sail with a ship of given draft. Until quite recently, underkeel clearance requirements were determined almost entirely empirically, and in many cases the rule of thumb values used can be shown to be greater than the requirement of navigational safety would dictate.

In the years since the war the pattern of the oil industry has changed and very large ships are now commonly used to carry crude oil cargoes to a large number of ports around the world. It is obvious that use of these ships, with their deep drafts, has meant that a number of expensive dredging projects have been put in hand to provide adequate access to the ports served. Continuing escalation in size means this will probably continue. (Dickson, 1967)

The above quote was published in 1967, and remains equally true today. Static rules are the mechanism by which most shippers and regulatory authorities manage the under keel clearance (UKC) of a vessel. Static rules typically comprise a fixed UKC requirement to determine times of sailings and/or maximum sailing drafts. This fixed UKC requirement must account for a range of conditions, and does not consider individually the factors that influence UKC.

In reality, these factors change dynamically depending on vessel, channel and environmental conditions (PIANC, 2014). The implication is that the static UKC rules typically must account for some level of uncertainty to accommodate the expected range of scenarios and conditions. Adopting a one size fits all approach generally results in an inefficient operation. Furthermore, the assumptions on which the static UKC rules were originally based also change over time. Often, the static UKC rules themselves are not reviewed in line with the changes to the underlying assumptions. Examples of changes to port operations that may influence the applicability of a static UKC regime include vessel size, transit speed, channel depth profile, transit time, and changes to port layout resulting from new berths or dredging.

A general summary of the factors that influence UKC is presented in Figure 1. For a non swell exposed environment, squat is the generally dominant UKC component. While many various squat formulas exist, actual squat depends on characteristics of the vessel, the channel being traversed, speed through water as well as water depth.

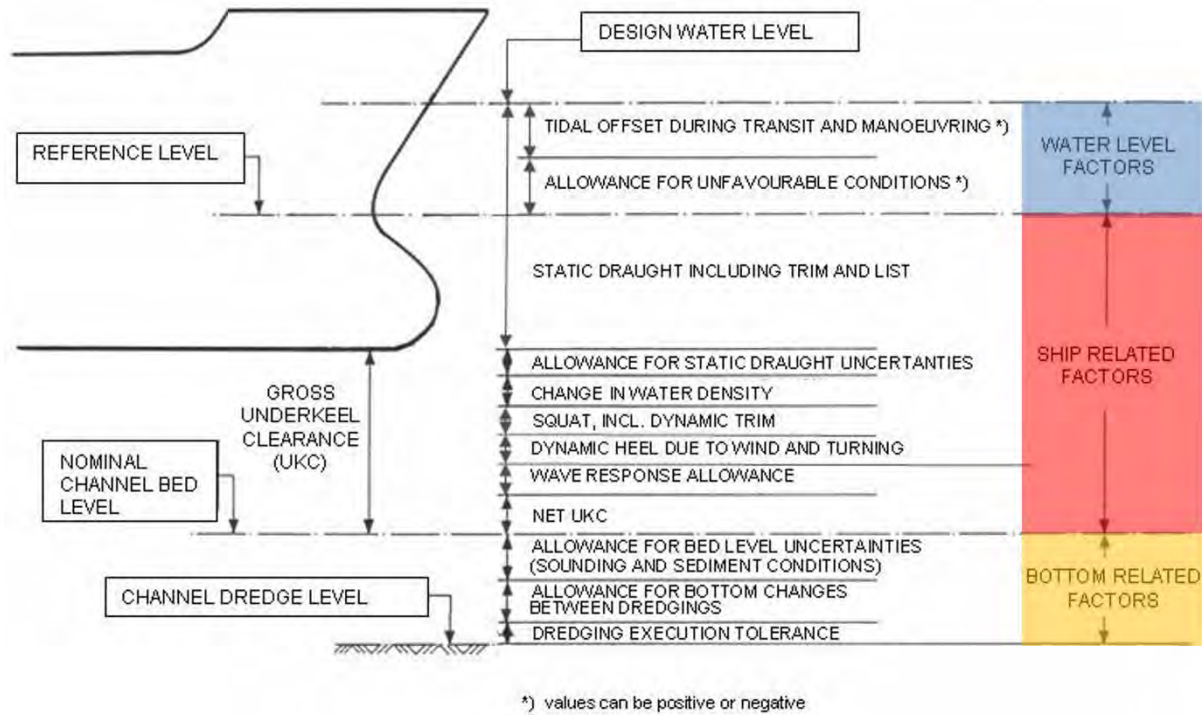


Figure 1 Channel Depth Factors (PIANC, 2014)

Applying static rules is effectively a variable risk approach to UKC management, as the gross allowance is allowed for and assumed to be sufficient to cover all cases but at any particular time the nett UKC is effectively unknown. This yields two implications.

Firstly, as the static UKC margin is assumed to cover all situations, the actual nett UKC varies and thus the risk of grounding for any given sailing is unknown. Furthermore, situations may exist where the gross allowance is actually inadequate to ensure the risk of grounding remains acceptably low.

Secondly, the static allowance is determined with some level of conservatism to account for the individual, but otherwise unknown, UKC factors. This results in inefficiencies when conditions are favourable, as the sailing draft or departure time is restricted by the conservative static rule, with obvious economic implications.

3. INCORRECT ASSUMPTIONS

The application of a static UKC rule to the safe operations of a port has inherent assumptions regarding each of the UKC factors and contributing variables. As those variables change over time, the UKC rules should also be reviewed. To illustrate the changing nature of the port operating environment three examples are provided from projects in which the author has been involved where assumptions about the operations have been incorrect, and consequently, the design or procedures have required amendment. Given their nature, these examples are presented anonymously.

Example 1: Vessel Speed

The author was involved in a UKC assessment for a port. The study involved assessing the risk of grounding. The client provided the vessel speeds for which the analysis should be completed as 10 knots, but allowing for a +/- 1 knot variation. However, when these speeds were later validated against AIS, it showed that the vessels actually often transited at 3 to 4 knots faster than the client had assumed. This variation resulted in 0.60m to 0.90m extra squat than initially calculated, thereby changing the risk profile of the transit considerably. **Error! Reference source not found.** shows the nominated speed profiles plotted against the AIS derived speeds. The Eryuzlu squat curve (PIANC 2014) for the design vessel and channel profile is shown in **Error! Reference source not found.**. The impact on the calculated squat of increasing speed from 10 knots to 12 or 13 knots is clearly evident.

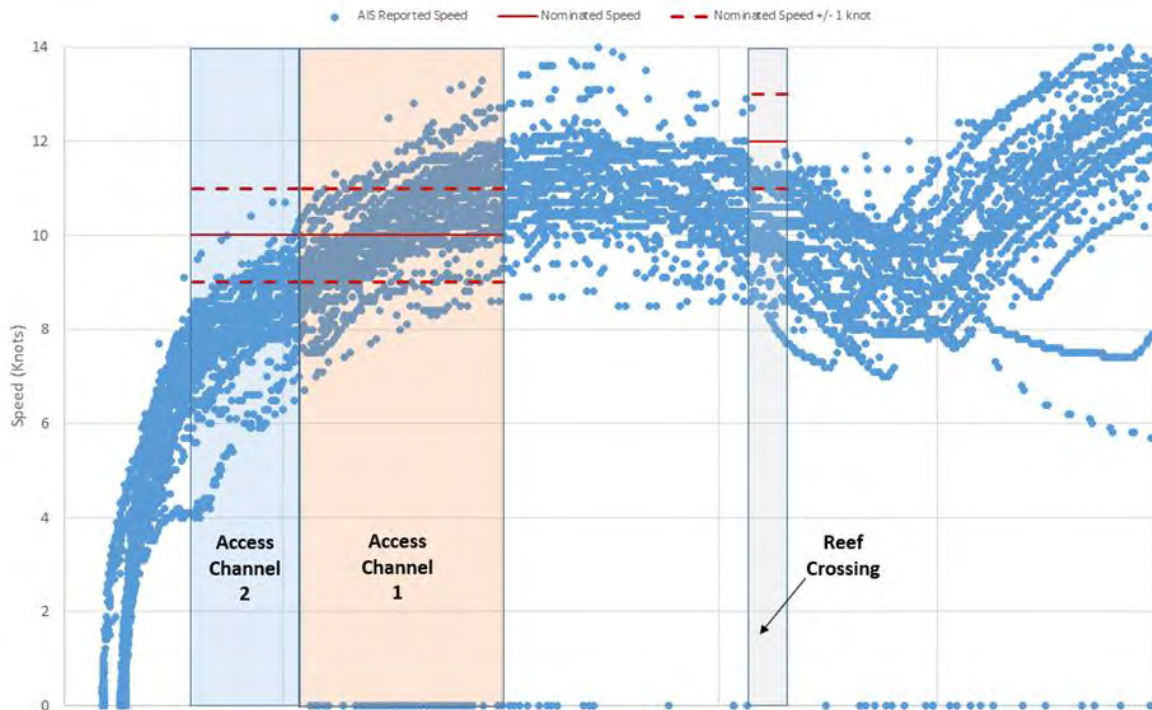


Figure 2 Vessel Speed Analysis. AIS analysis indicates that vessels transit considerably faster than assumed

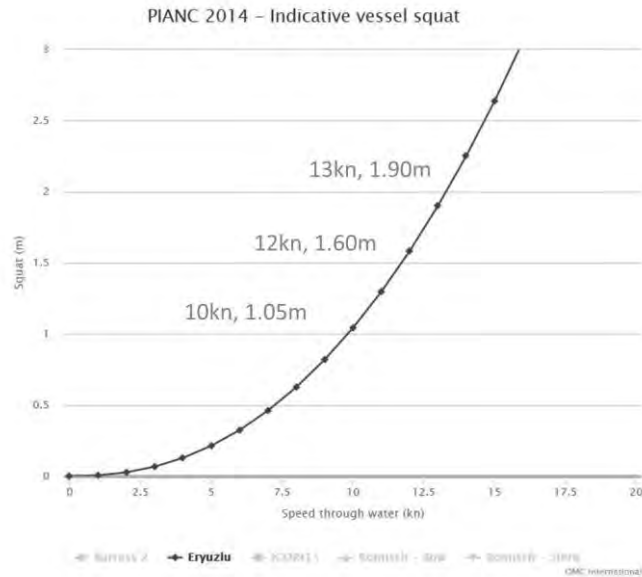


Figure 3 Eryuzlu Squat Curve. Increasing speed from 10 knots to 12 or 13 knots significantly increases the calculated squat.

Example 2: Tidal Assistance

The second example relates to a port which typically operated with a fixed departure time relative to high water. Their static UKC calculation was based on the high water tide. Operations evolved over time such that the transits commenced up to one hour earlier. Given the large tidal range experienced at the port, the actual tide at departure time could be 0.90m to 1.0m less than the high water tide. Instead of the assumed static UKC of 10% of draft, the actual static UKC was 4% of draft. This had resulted in manoeuvrability issues for some vessels.

Example 3: Wave Response

The third example is for a port which experiences beam on swells for Capesize bulk carriers. Following concerns over the wave response, an analysis of the vessel fleet profile highlighted that the typical beam had increased from 45m to 54m. For the same angle of roll, the measure by which the pilots indicatively monitor the wave response, the reduction in UKC for these larger vessels was 20% more than for the vessels for which the static UKC rule was intended.

4. INNOVATIONS

DUKC®

An alternative approach to UKC management is a dynamic UKC regime, which can be described as a fixed risk approach. This approach defines a minimum nett UKC allowance that must be maintained throughout the transit. Allowances for each of the relevant UKC components are then computed individually, considering the unique specifics of the transit. The transit specifics include depths, speeds, vessel type and characteristics, and environmental conditions. The final UKC requirement is a summation of the individual component allowances and the nett UKC allowance. By varying the UKC allowance to accommodate the prevailing conditions, the dynamic approach can ensure that the safety margin is not breached. Through a more comprehensive understanding of the risk profile, the risk can be maintained at the required level, whilst maximising operational efficiencies with respect to vessels' drafts and sailing windows.

The concept of a dynamic approach to UKC management is not new, with the first Dynamic Under Keel Clearance System (DUKC®) being operational at the coal export terminal in Hay Point (Queensland, Australia) since 1993. The DUKC® has evolved considerably since then as the supporting technologies have advanced, and has safely facilitated over 159,000 deep draft transits throughout more than 120 port facilities, terminals, and waterways.

The core functionality of the DUKC® is to provide ports, regulators and shippers with dynamic passage planning advice regarding:

- Maximum sailing drafts for known or fixed sailing times;
- Sailing window times for known or fixed sailing drafts;
- UKC and vessel motion information for a specific transit with a known departure time and draft.

This planning functionality is complemented by critical risk management functions such as vessel speed control, and real time UKC monitoring capabilities through AIS, including dynamically updated chart overlays which display high risk areas within the channel on the portable pilot units (PPUs) as shown in Figure 4, or via the DUKC® website. This functionality provides critical real time data to pilots and harbour masters during emergency scenarios (such as engine slowdowns or steering failures) to enable the optimal response to the situation.

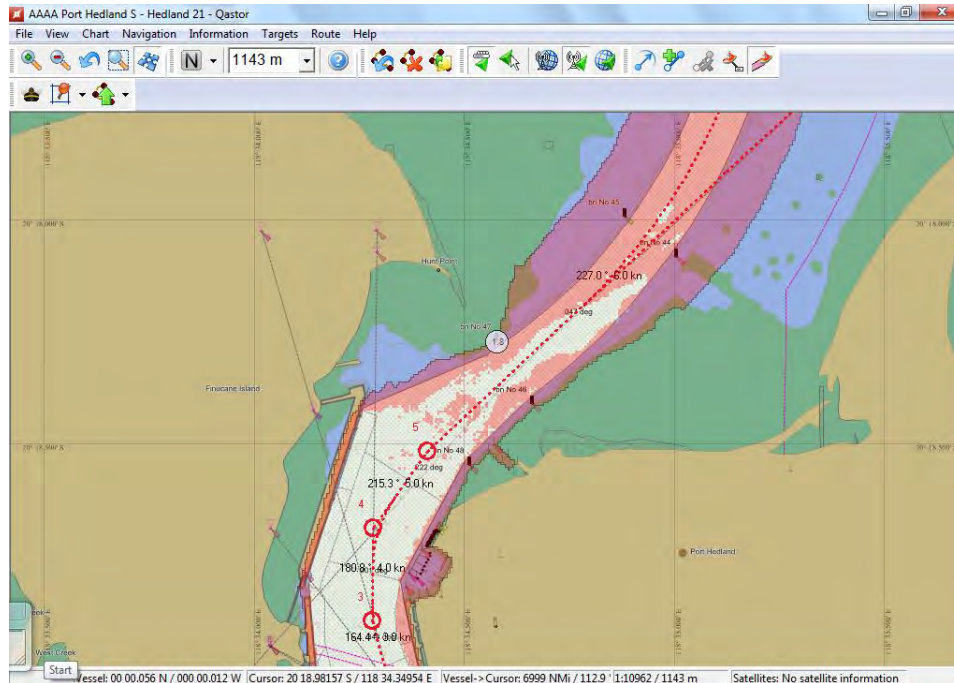


Figure 4 Chart Overlay (Source: Internal). Pilots have direct access to real time UKC information via the PPU.

DPCM®

An advancement of the DUKC® has been into the area of Port Capacity Modelling. The Dynamic Port Capacity Model (DPCM®) is the world's first discrete event simulation model that incorporates the dynamic under-keel clearance calculations. The purpose of the DPCM® is to provide a tool to assess the impact on port capacity of changes to variables such as ship loader rates, vessel fleet profiles, cyclones, asset availability (tugs, pilots, etc.) as well as capital projects including dredging, and new berths.

Dredge Optimisation

The DUKC® is also utilised in channel design and dredge optimisation. This involves individually calculating each of the factors (wave response, squat, heel, etc...) that contribute to reducing UKC at all points of a transit through a restricted waterway. Consideration is given to the actual environmental conditions (waves, tides), vessel dimensions, stability characteristics and speeds, and actual channel configuration. The result of this analysis is a nett UKC profile for each vessel transit.

To capture a true representation of the concurrence of environmental events and vessel sailings, thousands of vessel movements are simulated using DUKC® under a time series of environmental conditions to determine UKC requirements along all points of the channel. From this analysis, the optimal channel depths required to achieve the desired channel accessibility can be determined.

5. CASE STUDIES

Case Study 1: Port Hedland

The Port of Port Hedland is the world's largest bulk export port by volume, and has seen considerable growth over the past decade. Figure 5 shows the annual export tonnages, and total vessel movements.

Facilitated by innovative port optimisation and risk management technologies implemented by PPA, the port set a number of trade records in 2017 (Pilbara Ports Authority, 2017):

- Annual throughput of 500.9 million tonnes (an increase of ~40m tonnes or 9%);
- A monthly throughput of 47.25 million tonnes;
- A total of 272 vessel visits in a month;
- Exports of 2,183,611 tonnes in 24 hours;
- A total of 1,589,061 tonnes across 8 vessels on a single tide, an increase on the previous record of 77,084 tonnes.
- Sailed more than one million tonnes on a single tide over 60 times, having only achieved one million tonnes on a tide for the first time ever in 2012.

Additionally, the deepest draft to sail is 19.95m for a total of 270,006 tonnes.

Iron ore dominates the port's trade, representing 98% by volume. This is significant not only in the context of the port, but also nationally. The Port of Port Hedland accounts for just under 60% of Australia's iron ore exports, equating to more than a quarter of the global seaborne iron ore exports (Government of Western Australia Department of State Development 2016).

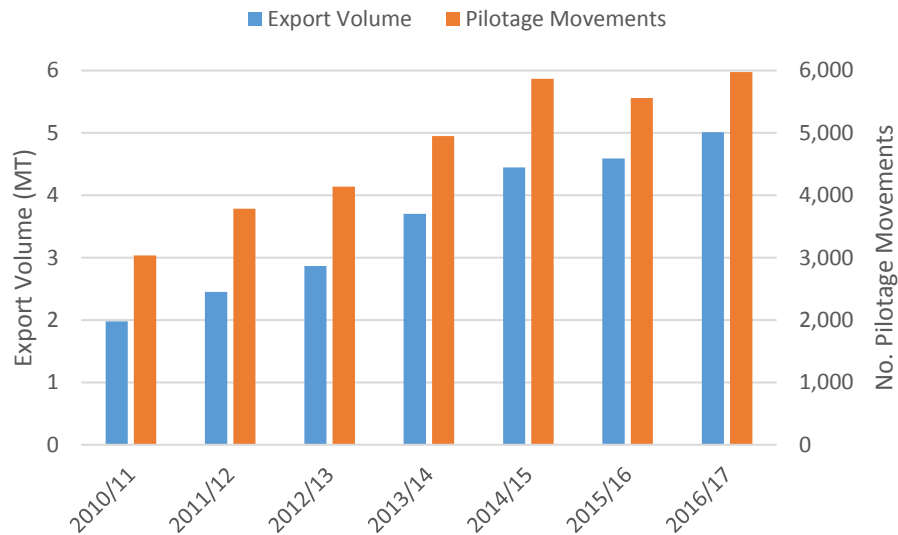


Figure 5 Port Throughput (Pilbara Ports Authority, 2016, 2017). The volume of trade through the port has grown significantly since 2010/2011.

Whilst the sheer volume makes the shipping challenging, the operations are further complicated by the geographic layout, and environmental conditions of the port.

Figure 6 shows the layout of the channel, which is approximately 42km long and uni-directional.

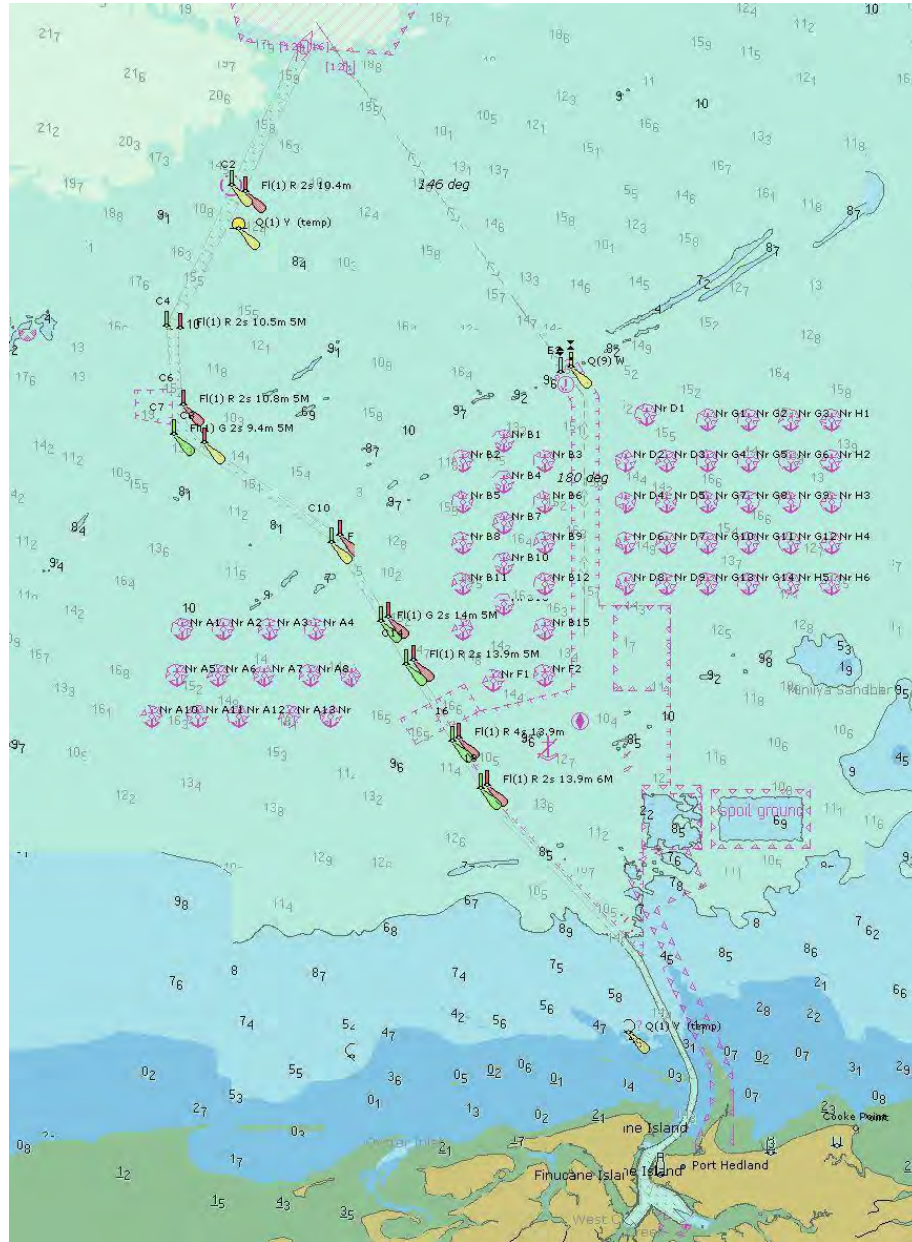


Figure 6 Channel Layout. The 42km, uni-directional, tidally restricted channel creates a challenging operating environment.

Access to the harbour is constrained through a single entrance with a minimum channel width of 162m. Furthermore, with a minimum channel depth of 14.6m, the departures are tidally restricted. The tidal range is up to 7.4m and tidal currents up to 3.5 knots (Ayre 2016).

In addition, the profile of vessels calling the port have also changed dramatically in the past 30 years. Specifically, they have become, wider, longer and deeper as shown in **Error! Reference source not found.**

| Year of Build | DWT (kt) | Beam (m) | LOA (m) | Draft (m) |
|---------------------|----------|----------|---------|-----------|
| 1981 | 138 | 43 | 270 | 16.8 |
| 1990 | 149 | 43 | 270 | 17.3 |
| 2000 | 171 | 45 | 288 | 17.7 |
| 2010 | 180 | 45 | 292 | 18.2 |
| 2011 Wozmax | 250 | 57 | 330 | 18.2 |
| 2011 'N' Class VLOC | 297 | 55 | 327 | 21.4 |
| 2017 | 260 | 57 | 327 | 19 |

Table 1: Evolution of Capesize Vessels. The trend is vessel sizes has been towards longer, wider, and deeper. (Ayre 20016)

As vessel sizes have increased, the port has seen an corresponding increase in the proportion of large vessels calling, as shown in Table 2.

| Vessel Size | 2009/10 | 2015/16 | 2016/17 |
|-------------|---------|---------|---------|
| >200k DWT | 10% | 31% | 33% |
| >250k DWT | nil | 7% | 9% |

Table 2: Port Hedland Vessel Fleet. Vessels greater than 200k DWT account for one third of total vessels. (Fernandes 2018)

To achieve the current port volumes, laden capesize bulk carriers transit in convoy, with up to eight vessels on a tide. The vessels typically transit with 30 minutes separation between them. If a vessel towards the front on the convoy breaks down, there is a risk of the following ships grounding or colliding with the lead vessel (Finch 2016). There are currently two shallow escape areas where a vessel can anchor outside of the channel. However the ability of a ship to safely reach an anchorage is dependent on numerous factors including the time available to react, the availability of tugs, the sailing window, and the prevailing environmental conditions.

The practical implication is that any incident within the channel has the potential to block access to the port. Given the value of trade through the port, approximately \$100 million per day, this would have far reaching consequences to not only the operation of the port and its customers, but also the economies of the State, and Australia (Pilbara Ports Authority 2017). Therefore, the risks must be carefully managed having consideration for all the operational factors, including the channel profile, environmental conditions, geographic constraints, and vessel characteristics.

For the Port of Port Hedland, the dominant UKC components are typically tide, squat and, with prevailing swells, wave response. The speed of a vessel can have a significant effect on the UKC as it directly influences squat. While many various squat formulas exist, actual squat depends on characteristics of the vessel, the channel being traversed, speed through water as well as water depth (PIANC 2014). Furthermore, given the length of the channel and tidal range, the speed is critical in determining the position of vessel along the channel at any time, and therefore the available water.

As an example, consider a vessel departing at five hours before high water, with a high water tide of 6.35m. The tide level at the start of the transit is 1.83m. By the time the vessel reaches the end of the transit, the tide is 4.93m. A vessel departing at high water on the same tide has 6.35m at the start of the transit, but only 3.20m tide at the end of the channel. Each of these vessels will have extremely different UKC profiles, and therefore, different risk profiles. Furthermore, assume circumstances are such that the vessel sailing at high water arrives at the final waypoint 20 minutes later than expected. In this case, the available tide will be 2.84m, resulting in 0.36m less UKC than originally planned. If not managed effectively, this could pose a significant risk to the safety of the vessel.

PPA uses DUKC® to mitigate the risks of the port, including the Transit Monitoring and Chart Overlay functionality (Finch 2016). DUKC® assists in managing vessel drafts and sailing windows delivering on average 0.60m to 0.80m additional draft, equating to up to 12,000 tonnes per vessel. Furthermore, as every transit is monitored in real time via AIS, subtle differences or changes in the operating parameters, such as the speed profiles associated with particular vessel classes, can be tracked over time.

An additional key strategy in managing the channel risk currently under development by PPA is the \$120m Channel Risk and Optimisation Project (CROP), the budget for which received approval in May 2016. CROP involves the delivery of an emergency passing lane alongside the shipping channel to mitigate the risk of disruption to the port's operations in the event of an adverse incident by allowing vessels in the convoy to continue safe navigation. Furthermore, an existing refuge zone will be enhanced to allow anchorage over low water. Targeted dredging will also enable existing channel depths to be fully utilised, increasing the available draft and tonnage to laden outbound vessels, and extending sailing window (Government of Western Australia Minister for Agriculture & Food; Transport 2015). The wider sailing window creates opportunity for increase separation times between vessels, thereby providing optionality in an emergency scenario.

PPA used DUKC® technology in evaluating the proposed CROP channel design depth profiles, and to ultimately quantify the benefits of the project.

For the CROP analysis, a baseline scenario was first established by using the existing Port of Port Hedland DUKC® configuration and bathymetry. Vessel transits were simulated over the analysis period for each tide cycle. From each simulation, the available departure drafts were calculated over a tide cycle.

PPA initially presented four draft channel design profile options based on their initial assessment of what would likely be achievable from a capital dredging perspective based on existing depths and geography of the channel, their historic knowledge of the geotechnical properties of the seabed, the overall dredge volumes, and their budget targets. OMC performed a preliminary study yielding a preferred profile. From this preferred channel profile, further refinement by the PPA produced an additional four channel profiles for analysis by OMC. Comparing the simulation results with the baseline scenario yielded the expected benefits of each proposed channel profile.

The value of the DUKC® approach to the channel design process was that the PPA's Operations Team was able to identify a channel depth profile that significantly reduced dredging of geotechnically challenging, and therefore costly, areas by over 90,000m² without any reduction in benefits.

In assessing the value of applying DUKC® methodology to the channel design in conjunction with using DUKC® operationally, an analysis against the static UKC was performed. This analysis highlighted that utilising DUKC® for dredging optimisation resulted in a considerable benefit over a traditional static UKC approach. To achieve the same level of accessibility would have required a channel profile on average 0.63m deeper, and up to 1.4m deeper.

From a port planning perspective, PPA also utilise the DPCM® innovation. The performance of the DPCM has been validated each year since its development against the actual port throughput. Analysis undertaken utilising the DPCM® was the basis by which the declared port capacity of Port Hedland was increased by 16 per cent from 495 mtpa to 577mtpa in 2015 (Government of Western Australia Minister for Agriculture & Food; Transport 2015). This increase is one third of the additional capacity proposed by the now shelved Outer Harbour project, which had an estimated cost of \$20b (Environmental Protection Agency 2012).

Case Study 2: Whyalla / Spencer Gulf

In contrast to Port Hedland, Whyalla is a regional port operated by Liberty OneSteel, a steel manufacturer and iron ore exporter. The port handles on average 10 ships per month through two channels and 3 berths, and a transshipment operation. With a tidal range of 2.7m, complex tidal phasing, and residuals that can reach in excess of ±1m, the challenges facing the operations at Whyalla are significantly different from those at Port Hedland.

The iron ore is exported through two operations: direct loading from the Outer Harbour in Handymax vessel, and transshipment to Capesize vessels which then transit the Spencer Gulf.

The Spencer Gulf is located in the state of South Australia and faces the Great Australian Bight. It is 322 km long and 129km wide. The piloted capesize shipping route from north to south is approximately 85km in length with a transit duration of about 4.5 hours.

The tidal regime in the Spencer Gulf is critical from a shipping perspective for a number of reasons. The tidal ranges reach 2.7m, but given the narrowing of the Gulf towards the north, the tidal ranges are greater at the start of the transit near Whyalla than at the end of the transits at Middlebank. Furthermore, the phasing of the tides is inconsistent such that the time between high waters varies. This complicates transit planning as any variations in the planned vessel speed or transit duration will result in less available water at the end of the transit. An example is shown in Figure 7.

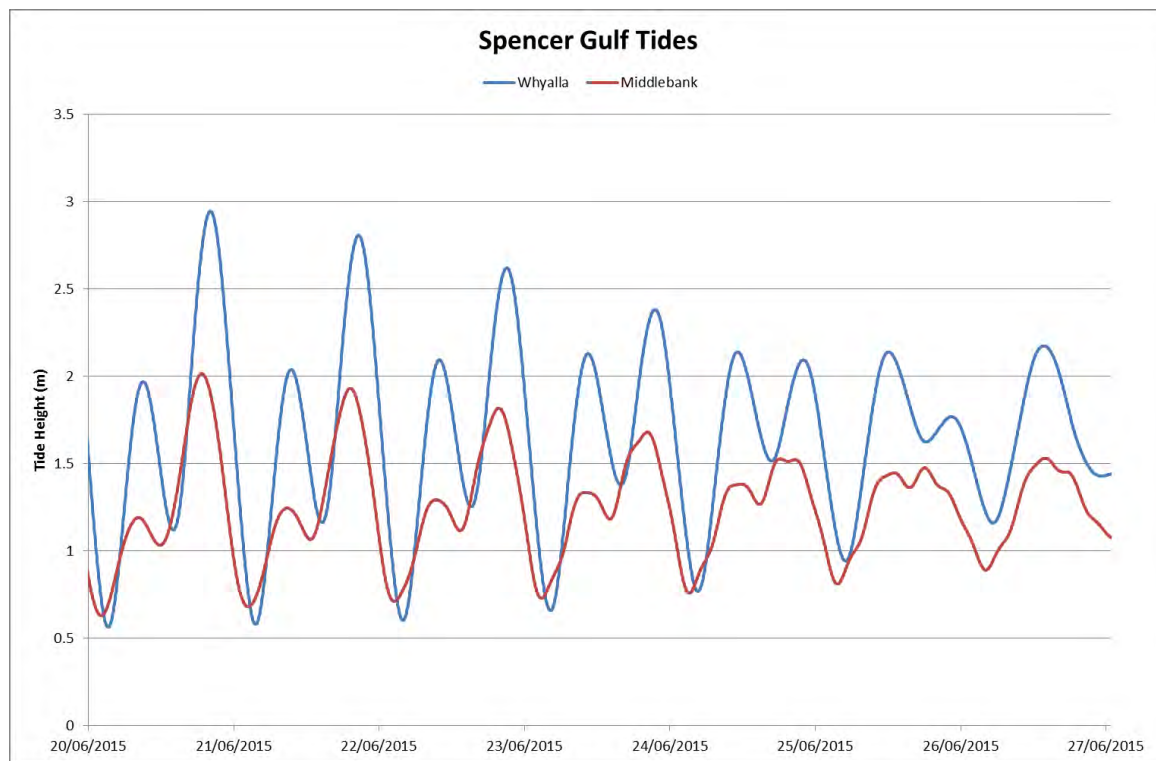


Figure 7 Spencer Gulf Tides: Complex tidal phasing impacts transit planning (OMC 2014).

The second key issue with tides is that local weather systems can result in significantly depressed tides (negative residuals). It is not uncommon for these residuals to be in excess of 30cm, which can equate to between 15% and 30% of the total tide, and as much as 1.0m. Failing to account for this loss of water when planning sailing drafts can have potentially serious consequences for safety.

The third key issue for tides is what is locally coined *dodge* tides. A dodge tide is an event where a neap tide has minimal variation of the course of the tidal cycle. This results in a very flat tidal plane. From a shipping perspective this can result in a vessel being unable to sail whilst waiting for a sufficient high water.

The Recommended Track, shown in Figure 8, is mostly deep water. However, there are two locations where underkeel clearance is critical. The first is Yarraville Shoal, which is approximately 9 nautical miles from the transshipment point and has a declared depth of 19.4m. The second shoal is at Middlebank, which is approximately 40 nautical miles from the transshipment point and has a declared depth of 20.1m.

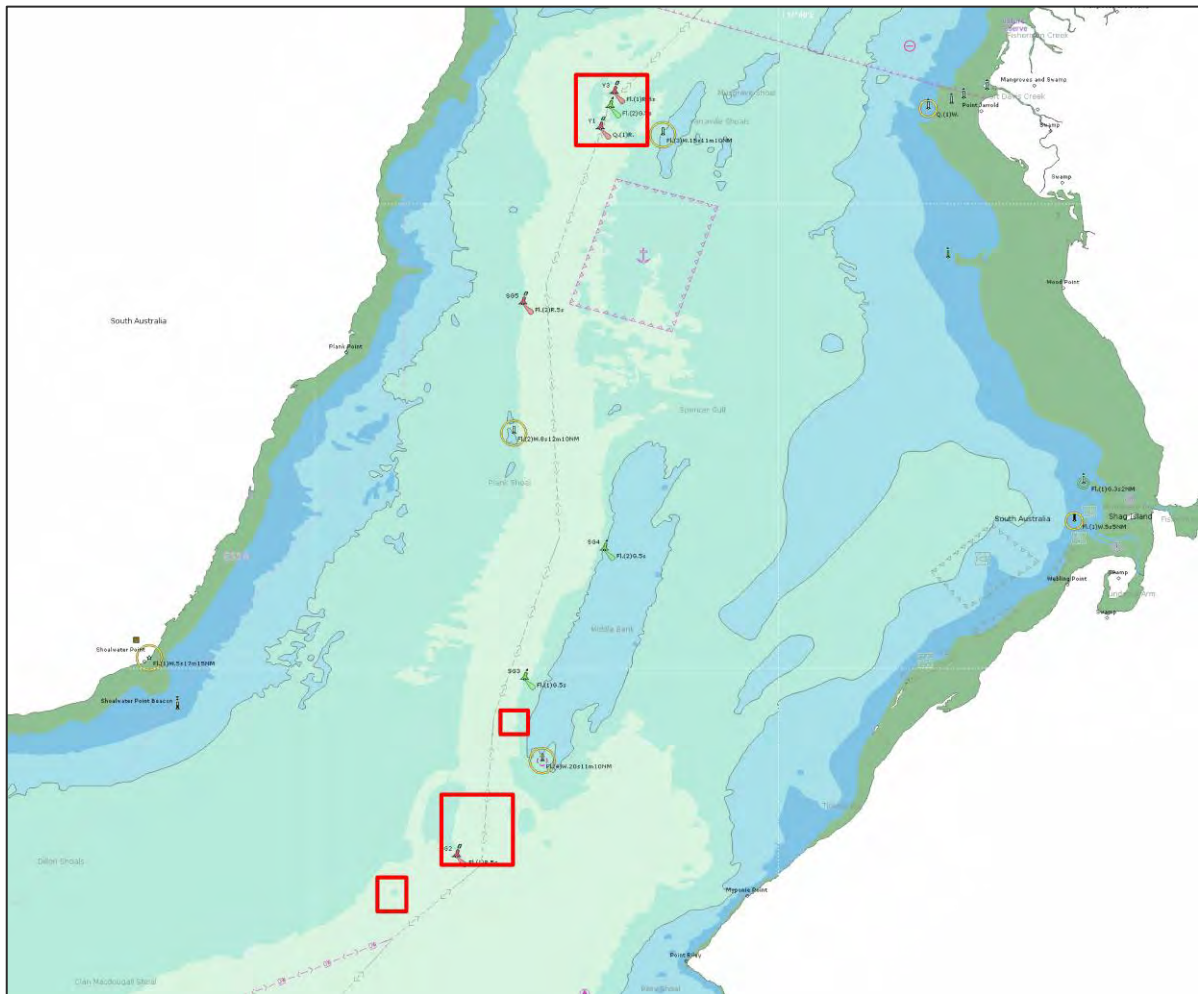


Figure 8 Spencer Gulf Route: UKC critical locations are several hours apart.

These known shoals are surveyed to a tolerance of 0.25m and 0.40m respectively. Outside of the areas, the depths are applied as per the hydrographic charts. However, these surveys are known as Class A2, which implies a Zone of Confidence (ZOC) margin of 1m plus 2% of depth. Therefore, a depth reading of 21m could in fact be as shallow as 19.58m.

To account for these uncertainties, the Capesize vessels required a static UKC rule of 15% of draft, with a maximum draft of 18.2m imposed. With the improved risk management functionality achieved with the implementation of DUKC®, the efficiency of the port operations improved significantly.

The Spencer Gulf DUKC® was the first ever application of Dynamic UKC technology to a transshipment operation (Saltbush to Steel, 2015). The technology has improved efficiencies allowing increased drafts and tonnages, leading to new records being set for both. In the first year of operations, a total of 34 vessels were able to load beyond the previous maximum draft of 18.2m. The average increase in draft was 0.11 metres, with the greatest increase being 0.27m. Note that this result was limited by the size of the vessel. The DUKC® could deliver even deeper drafts should larger vessels frequent the port.

In total, the freight savings amounted to US\$738,000, far exceeding the base case estimates. Furthermore, an additional tonnage in excess of 50,000t was shipped, providing an increase in revenue of US\$2.5m (Curtis 2016).

On October 24th 2015, the MV FPMC B Nature was loaded to 205,700 wet metric tonnes, setting both new record for tonnage and draft at 18.43m (Whyalla News 2015). The draft record was broken twice in December 2015, and again in February and March 2016, with the Lavinia Oldendorff, Lydia Oldendorff, and Leopold Oldendorff all sailing at 18.47m.

This case study highlights the economic benefits available when an investment is made in identifying operational inefficiencies, and understanding the accretive value of improving these inefficiencies. It demonstrates that improved technology can yield significant value even for relatively low volume ports that are naturally deep and not swell exposed.

Case Study 3: Geelong Port

The third case study to be reviewed is the Port of Geelong. Major port customers include Viva Energy, GrainCorp, and Midway Limited, a publicly listed woodchip exporter. Geelong Port handles over 600 vessel visits every year. The majority of the shipping activity is linked to the bulk liquid berth at Refinery Pier, which serves as an import destination for the Viva Energy refinery. The refinery supplies about 55% of the fuels needs for the state of Victoria, and accounts for 20% of ship visits and 50% of the port's trade. Recognising a need to attract larger vessels, improve operational efficiency, and increase their competitiveness, the port implemented DUKC®.

In its endeavour to accept larger and deeper vessels, the port faced several challenges including depth and width restricted channels, and a complex tidal regime with a seiching effect and the potential for rapid changes in water levels influenced by local weather systems.

A key innovation for the Geelong Port DUKC® was the implementation of TideCaster. TideCaster is a new approach to water level forecasts that incorporates numerical forecasts with in-situ environmental observations on an operational basis. TideCaster provides the ability to tailor a forecast to achieve a desired level of conservatism across a planning horizon, and can improve the accuracy when compared with astronomical tides, numerical forecasts, and persistence based forecasts (Uslu et al. 2017).

The core DUKC® functionality of the determination of tidal windows and maximum sailing drafts at Geelong Port is complemented by advanced in-transit risk management including Chart Overlays and Transit Monitoring. This enables pilots or VTS operators to adjust the planned vessel speeds in order to achieve a safe UKC profile, monitor the actual transit speeds, and identify the exact location within the channel of low UKC areas (Abraham, 2018). An example of the Chart Overlay function is provided in Figure 9.

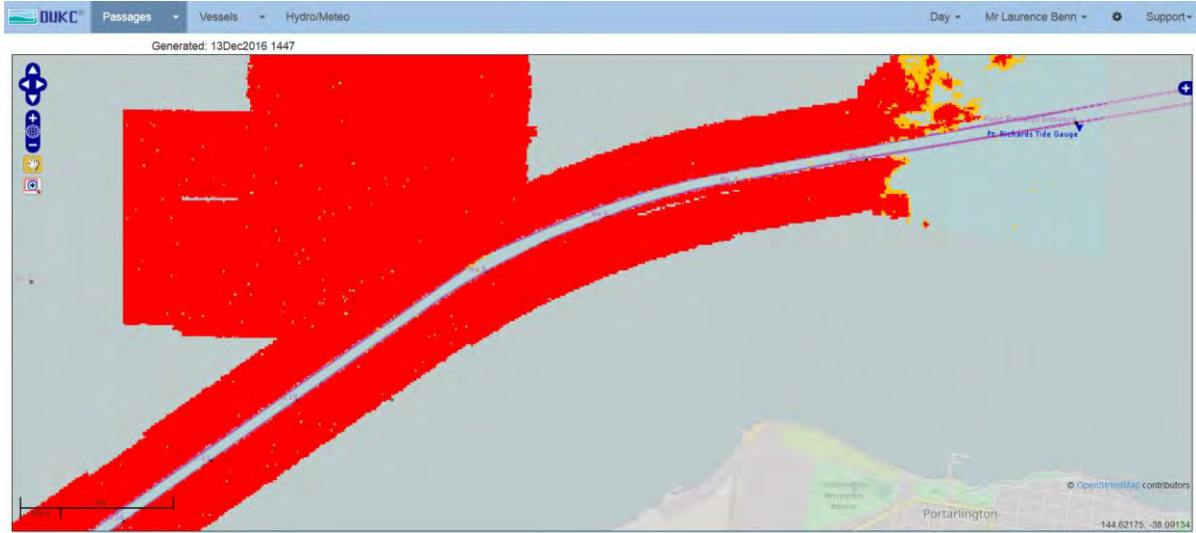


Figure 9 Geelong Chart Overlays: UKC critical locations are highlighted.

The port adopted a phased approach to the implementation of DUKC®, whereby drafts were incrementally increased by 0.10m on subsequent vessels. The first six vessels that sailed at a draft beyond the static UKC rule underwent a full scale validation using high precision differential GPS units on board. This enabled the port to compare the DUKC® computed vessel motions and UKC with the actual vessel motions. In addition to providing evidence as to the accuracy and safety of the DUKC®, the full scale validation gave confidence to the various stakeholders within the port. Some examples of the validation results are provided in Figure 10

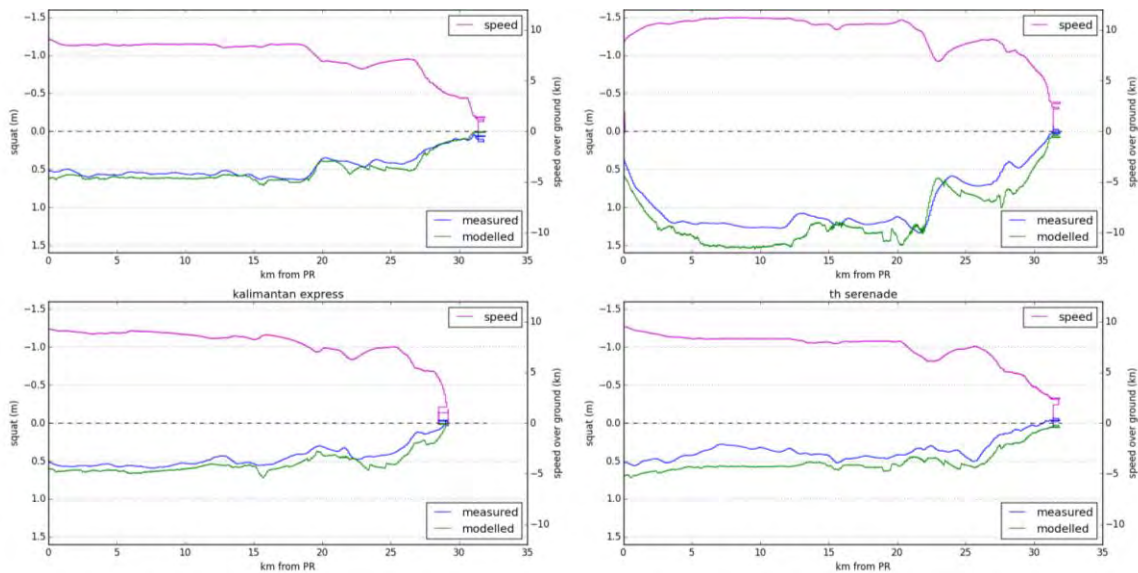


Figure 10 Geelong Full Scale Validation Results (Abraham, 2018).

Since the implementation of DUKC®, the port has set several records. The technology has allowed inbound tankers to safely increase their drafts beyond what was previously achieved. With annual cost reductions in the order of \$1m for every additional 10cm in draft (Lannen 2016), the DUKC® has delivered multi-million dollar benefits for the port and its customers.

Additionally, the export customers have been able to ship an additional 7,000 to 9,000 tonnes of cargo per ship, thereby increasing revenues and reducing the per tonne freight costs (Lannen 2016). The practical benefits of DUKC® to the shippers are evident in the record tonnages that have resulted since its implementation, including:

- Largest ever draft with the oil tanker *Phoenix Advance* in August 2016 (Lannen 2016);
- Record cargo of woodchips on the *Fujian Express* in January 2016 (Shand 2016);
- GrainCorp's biggest single shipment of canola from Geelong, with the Nord Pollux sailing with more than 61,900 tonnes;
- Its biggest single shipment of wheat fully loaded in Geelong, with the Tomahawk departing carrying almost 61,800 tonnes;
- Its largest shipment of barley fully loaded in Geelong, with the Twinkle Island sailing with about 62,500 tonnes;
- Exporting the most grain ever in a month, more than 393,560 tonnes;
- The Port recording the largest month of exports – grain and woodchips – with total shipments topping 412,750 tonnes. (Victorian Regional Channel Authority 2017)

6. CONCLUSION

The ports of Geelong, Whyalla, and Port Hedland differ significantly in terms of operations, volumes, trade, environmental conditions, channel profiles, and port layouts. Despite these differences, and the unique challenges they present, the same risk management technology has been tailored for use at each to improve the shipping efficiencies, thereby achieving significant increases in throughput, reduced dredging requirements, and reductions in freight costs.

With ever increasing scrutiny on the financial and environmental credentials of ports, and higher expectations from ports' customers, stakeholders and local community, particularly with respect to dredging, it is imperative that ports continue to apply best practice with respect to risk management, and be in a position to demonstrate the value delivered from capital investments and operational decisions. The suite of tools presented herein provides port authorities, terminal operators, and shippers with a comprehensive solution to manage risk, and analyse and evaluate decisions, both planning and operational. This helps ports meet their commercial demands whilst always ensuring vessel safety and channel integrity.

7. REFERENCES

- Abraham, D. (2018). *Victoria Regional Channel Authority - Geelong DUKC*.
- Ayre, M. (2016). Best Practises Pilotage Standards in Port Hedland, Proceedings of the Safe Ships, Safe Port Forum (8 September, Perth).
- Curtis, B. (2016). The Value of a Centimetre: Improving Shipping Efficiencies Through Underkeel Clearance Management Technology. In: *The Maritime Transport of the Future: The Role of Innovation*. Hamburg: International Association of Maritime Economists.
- Dickson, A. (1967). Underkeel Clearance. *Journal of Navigation*, 20(04), pp.363-387.
- Environmental Protection Authority, WA (2012). *Statement No. 890 Outer Harbour Development - Port Hedland BHP Billiton Iron Ore*. Perth.
- Fernandes, M. (2018). *DUKC at Port Hedland: Improving safety and efficiency outcomes*.
- Finch, J. (2016). Managing Growth and Channel Risk, Proceedings of the Safe Ships, Safe Port Forum (8 September, Perth).
- Government of Western Australia Minister for Agriculture & Food; Transport (2015). Extra capacity for Port Hedland channel, media statement (13 November).
- Lannen, D. (2016). Record tanker depth points to new Geelong shipping heights. *Geelong Advertiser*. [online] Available at: <http://www.regionalchannels.vic.gov.au/index.php/8-news/108-record-tanker-depth-points-to-new-geelong-shipping-heights> [Accessed 29 Mar. 2018].
- OMC International (2014). *Arrium DUKC Scoping Study*. R5600.
- PIANC (2014). *Harbour Approach Channel Design Guidelines*. Working Group 49 Report No. 121.
- Pilbara Ports Authority (2016). *Pilbara Ports Authority Annual Report 2015/16*.
- Pilbara Ports Authority (2017). *Pilbara Ports Authority Annual Report 2016/17*.
- Ports Australia (2017). *Strengthening the National Security of Australia's Critical Infrastructure*.
- Saltbush to Steel (2015). Technology Brings Range of Improvements. p.4.
- Shand, J. (2016). Geelong welcomes one of the biggest chip ships as new era for port opens. *Lloyd's List*.
- Uslu, B., Taylor, A., Hibbert, G. and Soutelino, R. (2017). Connecting Sea Level Forecasts with the Bulk Export Industry. In: *Australasian Coasts & Ports 2017: Working With Nature*. [online] Barton, ACT: Engineers Australia, PIANC Australia and Institute of Professional Engineers New Zealand.
- Victorian Regional Channel Authority (2017). *VRCA welcomes GrainCorp's fleet of new records at Geelong's port*. [online] Available at: <http://www.regionalchannels.vic.gov.au/index.php/news-publications/media-releases> [Accessed 29 Mar. 2018].
- Whyalla News (2015). Arrium set marine record. [online] Available at: <https://www.whyllanewsonline.com.au/story/3553212/arrium-sets-marine-record/> [Accessed 28 Mar. 2018].

STAD SHIP TUNNEL – THE WORLD’S FIRST FULL SCALED SHIP TUNNEL

by

Terje Andreassen^{1,2}

Background for the Stad Ship Tunnel

Historic

Even the Vikings feared the fairway outside Stad peninsula. There is a pass at Stad peninsula called “Dragseidet”, which in English means: “A pass where you pull boats over land”. In the Viking age “Dragseidet” was used as an alternative route to avoid the infamous Stad Sea.

In the year of 1874, there was an article in a Norwegian newspaper about the need and possibility of caving a tunnel through the Stad peninsula. The estimated cost at that time was 1.6 million NOK (\$200.000)

Johannes Balderhaug, often referred to as the “father” of the Stad Ship Tunnel, was very keen to realize many years of ideas about building Stad Ship Tunnel. In 1984 his efforts resulted in serious conversations with the Mayor of Selje Municipality and, consequently, the concretization of a feasibility study of the project

Since then, there have been several studies. The first feasibility study by the NCA (Norwegian Coastal Administration) took place in 2000. This was based on a tunnel with a smaller cross section than the present one.

The 14th of December 2003 there were a serious incident outside Stad peninsula. In stormy weather and with 8 meter waves, the coastal ferry MS Midnatsol got machinery problems which caused a total blackout. The ship was drifting towards land and all passengers were evacuated to the rescue area on deck, waiting for orders to enter the lifeboats. However, only 150 meters from the shore, the captain were able to drop both anchors which enabled the ship to stop drifting.

Because of this incident, suggestions arose about increasing the size of the Stad Ship tunnel to enable coastal ferries to avoid the Stad Sea and sail safe through the tunnel as well. Studies in 2000-2001 and 2007-2008 have analyzed a number of alternative cross sections and routes for the tunnel. The final route has been selected because the Stad Peninsula is at its narrowest point here, and the waters are sufficiently shielded to allow shipping to use the tunnel in most weather conditions.

Picture 1: Trace for Stad Ship Tunnel Studies – as a foundation for the selection of the route and cross section – took place in connection with the concept selection report (KVU) and the subsequent external quality assurance process KS1.

In connection with White Paper 26 (National Transport Plan 2014-2023), the Storting (the Norwegian parliament) opted to proceed with the large tunnel alternative.



Picture 1: Trace for Stad Ship Tunnel

¹ Norwegian Coastal Administration, terje.andreassen@kystverket.no

² Project Manager Stad Ship Tunnel

Navigational conditions

The Stadhavet Sea is the most exposed and dangerous area along the coast of Norway. The Kråkenes lighthouse, just south of Stad, is the meteorological weather station with the most stormy days, which can be anything from 45 to 106 days per year. The combination of wind, currents and waves around this part of the coastline make this section a particularly demanding part of the Norwegian coast.

The combination of sea currents and subsea topography creates particularly complex and unpredictable navigational conditions. Very high waves come from different directions at the same time and can create critical situations. **Picture 2: Challenging navigation outside Stad peninsula**

The conditions also cause heavy waves to continue for a number of days once the wind has died down. This causes difficult sailing conditions even on less windy days.



Picture 2: Challenging navigation outside Stad peninsula

Safety

The aim of the project is to improve accessibility and safety for shipping past Stad. Luckily, there have not been any accidents with loss of life since 1984, but there have been a lot of serious incidents. The last incident was in March last year. The cargo vessel Nyksund was hit by a huge wave, which led to displacement of cargo and that the vessel became listed at around 20 degrees.

Predictable voyage

The Stad Sea is very unpredictable due to weather conditions and is in a way a barricade for transport of cargo and passengers. Speed ferries do not have permission to sail with passengers past Stad Peninsula. Today many vessels that sail in this area have to wait, several times a year, for weather conditions to improve. When the tunnel is operative, the journey becomes much more predictable so cargo can arrive on time. This is especially important for transport of living fish and transport of caught fish.

To eliminate waiting time for sailing past Stad peninsula will have a huge economic impact. This will also gain the process of transferring more cargo from vehicles to vessels. The Stad Ship Tunnel will also have a social impact as it will make it possible to establish a speed ferry route between two main cities in Norway, Bergen and Ålesund. Also for leisure crafts the tunnel will open for new possibilities. Finally, by establishing a new fairway in a protected area it will become much more comfortable for passengers and crew.

Environmental effects

Sailing distance is 3 nm longer through the tunnel than sailing outside Stad peninsula. Therefore, you gain nothing in good weather conditions. In bad weather conditions vessels often use three times longer time to sail past Stad than in good weather (if they manage to sail at all). That means significant more consumption of fuel and much more exhaust emissions. If vessels wait for weather to improve, their engines are still running and polluting the air.

If an accident should happen, the environmental impact caused by an oil spillage would be tremendous and impossible to handle in such weather conditions. Close by we have the southernmost seabird island in Norway called Runde, also known for having most species of seabirds in all of Scandinavia.

Feasibility study

Traffic situation

Stad Ship Tunnel will be a part of a new main fairway from Ulvesundet to Vanylvsfjorden. **Figure 1: Overview fairway past Stad**

Most of the navigation aids will be concentrated close to and inside the tunnel. There will be one-way traffic through the tunnel, which alternate every hour. All motor-driven vessels may use the tunnel. The maximum speed is 5 knots for all vessels, except speed ferries that are allowed a maximum speed of 8 knots. In the fairway close to the entries of the tunnel, a maximum speed of 8 knots will be allowed. All vessels which intend to sail through the tunnel must apply for a slot-time two hours ahead of ETA. Vessel Traffic Services (CTS) will manage slot-time allotments and vessel monitoring. The capacity will be five large vessels per hour.

West of the tunnel there is a narrow strait called Saltasundet. This strait will be made deeper and wider by underwater dredging.



Figure 1: Overview fairway past Stad

Computer simulated voyages

In order for the pre-project to Stad Ship Tunnel to have the best possible basis for describing a project that is "Good", it was decided to carry out a computer simulation in a ship simulator. The ship simulator focused on sailing in areas that would be affected, while testing the effect of necessary safety and navigational measures when approaching and entering the tunnel.

The simulations took place in Copenhagen at Force Technology in 2016 May 30th to June 2th.

In order to make the simulations as realistic as possible, we used navigators who are familiar with the relevant vessel types that would be dimensioning for the tunnel.

Two marine pilots with certificates for the area, a captain at MS Midnatsol, and a navigator from North Sea Container Line navigated vessels in the computer simulation. In addition two nautical experts from the NCA participated. **Picture 3: View inside tunnel from the bridge onboard MS Midnatsol**

We did several simulated voyages with vessels that are most relevant to potential and expected challenges in relation to dimensioning vessels, weather and timing.

The voyage of the largest vessels were carried out by a team of two people from the group of selected pilots, captains and navigators who participated in the simulations. Simulations with smaller vessels were carried out by one navigator only.



Picture 3: View inside tunnel from the bridge onboard MS Midnatsol

The simulator was well equipped, both in relation to optical sailing and instrumental navigation. All exercises were relevant to test challenges in relation to ship dimensions/design, and weather conditions one can expect in this area.

During some voyages, issues and events, such as fire onboard and machine problems, were added to test their effect on other ships in the convoy. Those simulations provided useful information on potential challenges, especially in relation to convoys.

Entering from Vanylvsfjord with large vessels and simple equipment with regard to maneuverability, can be challenging with heavy wind from NNE.

The simulator voyages showed that dimensioned vessels could safely use the tunnel during all relevant weather conditions without excessive risk of accidents. One exception is the maximum size vessel (Container vessel) that has huge drift and limited maneuvering capability. In this case, it will be challenging to enter from Kjøddepollen in heavy wind from NNE.

Further studies must be conducted to evaluate fendering; the distance from fender to tunnel wall at the junction where entering construction turns into leading construction.

By convoy, the largest vessels should have priority when entering, either by leading or having more space to the next vessel in the convoy. Otherwise, large vessels should be the last incoming vessel, as it would require more length to stop, hold position and get in position for entry, and thereby more space to do so.

Model test

In the model test, we used the same vessels as in the computer-simulated voyages. However, this time we wanted to study the hydrodynamics inside the tunnel, which, from a maritime point of view, in reality is a channel. **Picture 4: Model test of MS Midnatsol in the tunnel/channel**

In Marintek's harbor basin, we rigged part of the channel to a length corresponding to 1250 meter. The scale of both channel and vessels was 1:27,5.

The tests were done in three different depths of water similar to the tide. There were also arranged currents of one and two knots and we sailed both directions.

The study gave the following observations and conclusions:

- The vessels had a speed equivalent of 5 knots of speed outside the channel, but due to channel effects, the speed was reduced by 20-25% for MS Midnatsol, and 35-45% for the container ship.
- The speed reduction decreases slightly when the water level drops, especially for the container vessel where the channel effects are greatest.
- The efficiency requirement increases by about 10% for MS Midnatsol, while the increase is in the order of 50% for the container vessel, compared to voyages at 5 knots in open water outside the channel.
- None of the regular test conditions gave significant maneuvering problems to any of the vessels.



Picture 4: Model test of MS Midnatsol in the tunnel/channel

CFD study of bank and squat effects

The company Force Technology ran the CFD-study based on the same vessels and scale as the model tests. The study was done with and without currents in two different depths.

The plots clearly show that the speeds around the vessel are significantly reduced when sailing in a current-free environment, compared with voyages with currents in place. The speed range also changes around the ship. In addition, it is clearly seen that the waves generated by the vessel are slightly higher when the vessel is situated close to the fender compared to when the vessel is located in the middle of the channel.

There seems to be a slight increased tendency for the squat as a function of velocity. There is not a big difference between the squat in front and in rear of the vessel, i.e. the vessel gains only a rather weak trim. The deviations in current situations are assumed to be due to the increased cross flow due to the current. However, the real variation is quite small and the vessel does not exhibit the risk of ground impact.

Construction

The construction of the tunnel will be done by traditional drill and blast methods. In the roof of the tunnel, there will be horizontal drilling and blasting. The roof will be secured with bolts, anchors and shotcrete before blasting the next levels downwards. Those levels will be done by vertical drilling and blasting as in open mining. We will leave a part of the rock in both ends of the tunnel to enable dry conditions down to level -12. **Figure 2: Principle sketch of the construction of the tunnel**

After establishing pillars for the guiding construction, the remaining rock will be blasted so that seawater can flow in.

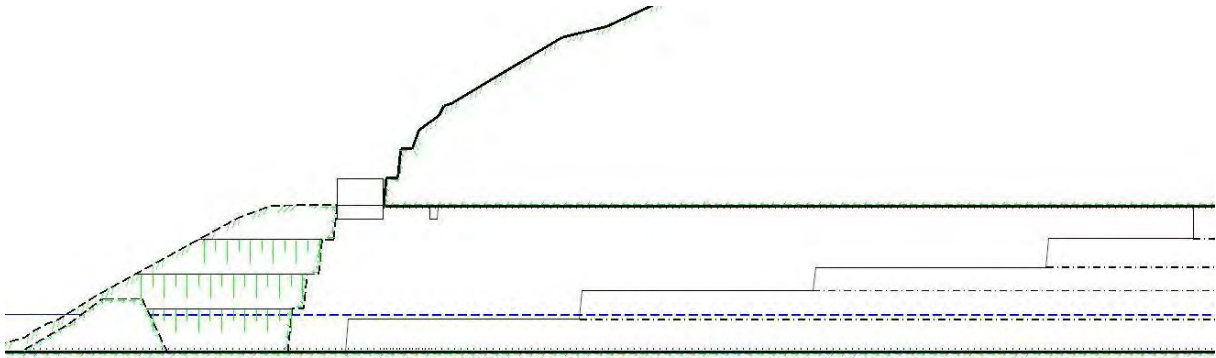


Figure 2: Principle sketch of the construction of the tunnel

On both sides of tunnel, 3 meters above the sea level, there will be a guiding construction applied with fenders. **Figure 3: Principle sketch of guiding construction and roof catwalk**
 The main purpose for this guiding construction is to prevent the bridge wing from smashing into the rock. Secondly, this guiding construction can be used as a evacuating path in case of emergencies inside the tunnel. **Figure 4: Principle cross section of quay and friction** There will be established a catwalk up beneath the roof along the whole length of the tunnel in order to do inspections of the tunnel roof.

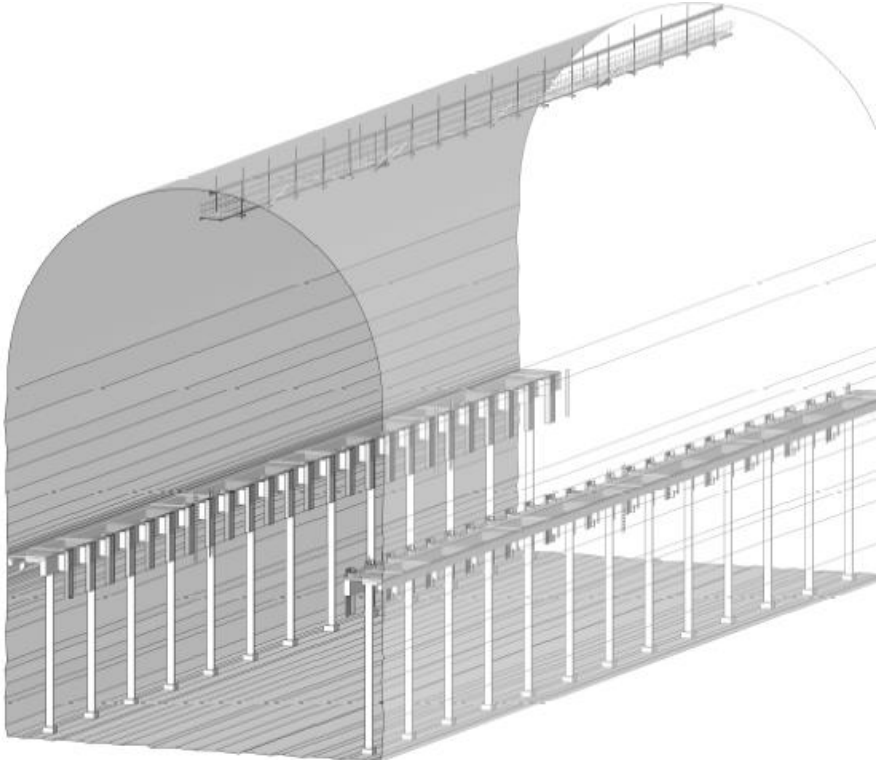


Figure 3: Principle sketch of guiding construction and roof catwalk



Figure 4: Inside tunnel

In both ends of the tunnel, there will be established entrance constructions with an angle of 9 degrees to the centerline. Where the entrance construction meets the guiding construction there will be established three rolling fenders. **Figure 4: Principle sketch of entering construction and rolling fenders**

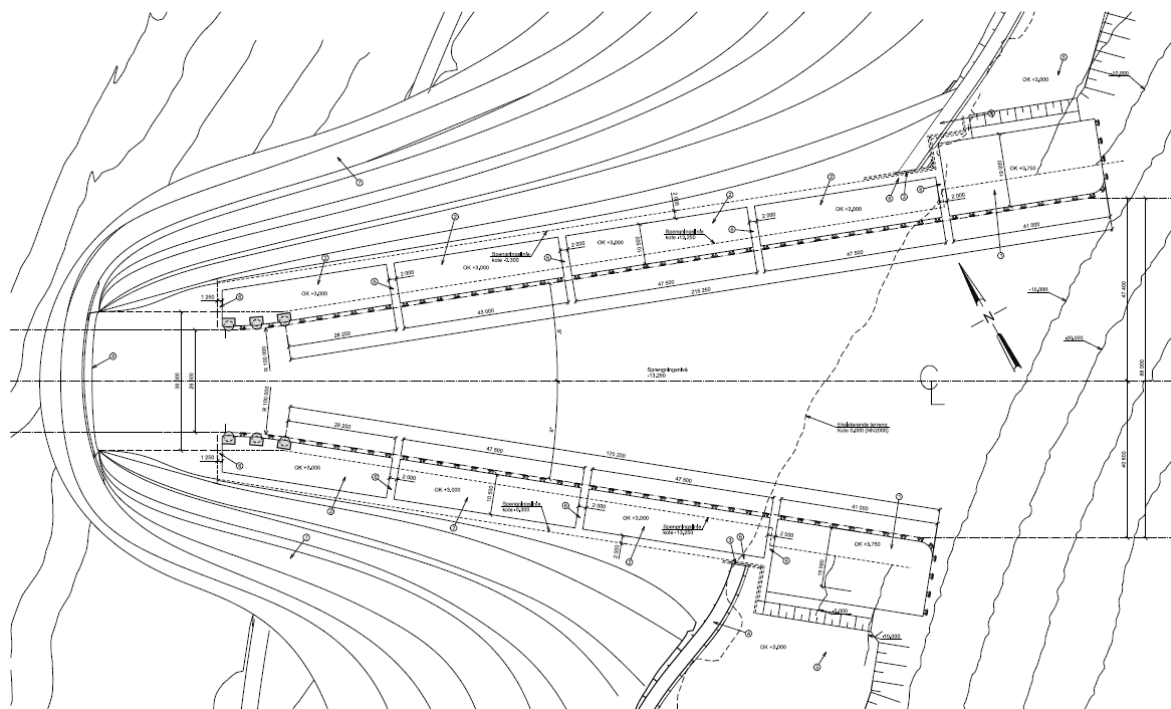


Figure 4: Principle sketch of entering construction and rolling fenders

The idea of the entrance construction is to shield the construction, i.e. in case a vessel unfortunately should crash into the construction. To achieve this, the upper part of the entrance construction is made by frictions boxes with fenders. **Figure 5: Principle cross section of quay and friction** The friction boxes is made of concrete and filled up with ballast of stones. The friction boxes are supported by wire sawed rock in the inner part of the entering construction and by a quay of concrete in the outer part.

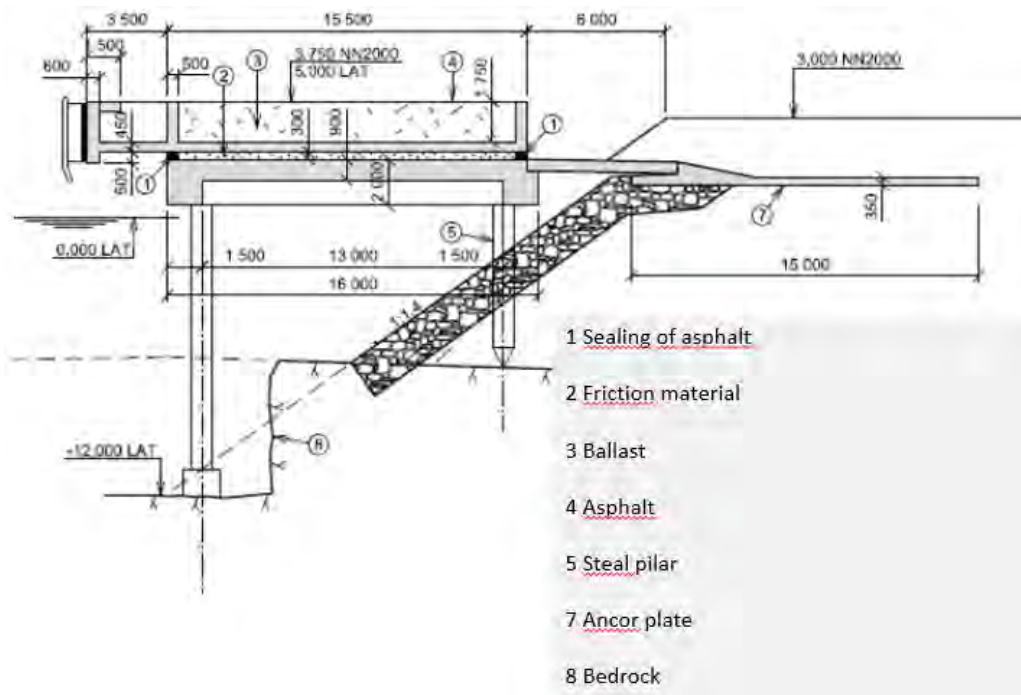


Figure 5: Principle cross section of quay and friction boxes

One of the biggest challenges is to establish a significant infrastructure during the construction time. The landscape is very steep, which forces us to establish an area for rigging in both ends of the tunnel entrances. After the tunnel is caved out, this area must be grabbed and dredged before the construction of entry points can take place. All blasted rock must be transported from the site at huge barges. In addition, there are public roads on both sides that have to be relocated. At the entry in Moldefjorden, a bridge will be made above the tunnel entry. This bridge must have a roof and the area above have to be secured with fences to protect it from landslides and avalanches.

Navigation aids

To help navigation inside the tunnel there will be center marker lights each 50 meters in the roof. In addition, there will be indirect lights at the edge of the guiding construction. **Figure 6: Navigation aids** At the entrances, there will be lateral lights and center lights. Along the fairway to and from the tunnel, there will be some new navigational aids as well.

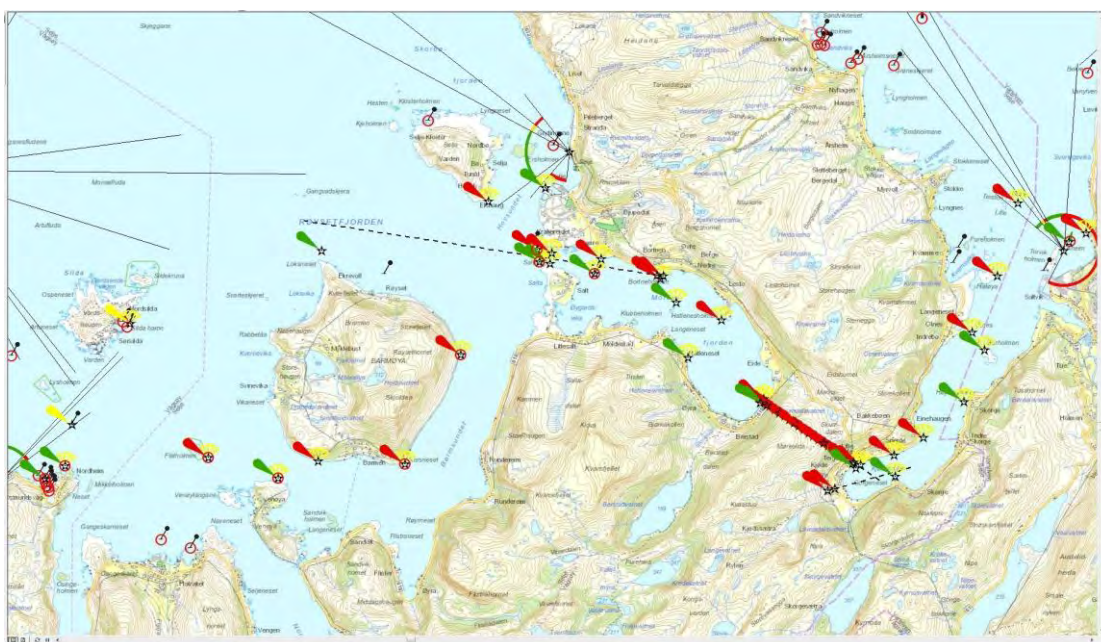


Figure 6: Navigation aids

Landscape and terrain design

Kjødepollen is a small place with characteristic fjord landscape, scattered settlements and smaller farms. The landscape slopes evenly from the wooded mountainside through the open farmland that meets the fjord.

In the transition between the entrance structures and the shoreline, there will be an extensive area affected by fillings during the construction phase. We have looked at the relationship between the construction phase and the finished situation to find a solution that will both work temporarily, and also become part of the new situation for the site. **Picture 4: Entrance Kjødepollen**

At Moldefjorden, the landscape is steeper and therefore also has less agricultural area and fewer dwellings. The landscape is facing west with a great view of the Stad peninsula. No buildings are directly affected by the operation, but in the upper part of the recess, the existing road must be moved and established in an overlying new bridge. The solution has many common features with Kjødepollen, but visually they will appear quite different. The steep terrain in the face of the terraces gives a more close and dramatic impression.



Picture 4: Entrance Kjødepollen

Risk analyses

The risk analysis looks at the effect of Stad Ship Tunnel on collision and ground impact risk in the area from Ålesund to Måløy. The risk analysis consists of a frequency analysis and impact assessment.

The frequency analysis uses the IWRAP navigation risk program to calculate the grounding and collision frequency before and after the action. The measure in this analysis is Stad Ship Tunnel. The frequency analysis has been based on AIS data from 2015, and there are no prognoses for changes in shipping traffic, so the total traffic volume is equal before and after construction. The frequency analysis has included a traffic transfer from the outer fairway to the inner fairway after construction, as it is assumed that the vessels that want to use the tunnel will choose to sail the inner fairway, especially in bad weather.

The frequency analysis shows that there will be a slight decrease in the collision frequency in the area after construction. This is because traffic will be allocated different sailing routes for use of the tunnel.

Figure 7: Different sailing routes

The grounding frequency will increase after construction, as more vessels will use the internal sailing routes than before construction. As there is risk of more groundings than collisions, the total accident rate will increase. An increase in total accident rate is estimated as 0.23 accidents per year.

The impact analysis has evaluated how the traffic-specific conditions around Stad peninsula will affect the outcome of a grounding or collision. The risk analysis has calculated the potential serious consequences, such as loss of life, personal injuries, serious property damage and emissions based on the frequency analysis and impact assessment. The risk analysis shows that, with the fairway

specific assessments, a reduction in the number of deaths, personal injuries and emissions is expected, as well as a marginal increase in serious material damage for utility vessels during ground impact or collision.

For capsizing and stability failure without capsizing, a simplified analysis has been conducted, based on the fact that smaller vessels – that are particularly vulnerable to these types of accidents – are largely transferred to the Stad Ship Tunnel. This will result in a significant risk reduction for the fairway past Stad.

Risk change for the leisure fleet has been considered qualitatively. The main differences between utility vessels and recreational crafts are that sailing distances are not expected to be equally important, and it is assumed that a large proportion will choose to use the Stad Ship Tunnel. The conditions at Stad are considered to increase both the frequency and consequence of a leisure boat accident, and it is therefore considered that the Stad Ship Tunnel will have a major maritime safety effect for the leisure fleet.

The analysis has assessed traffic transfer and fairway-specific conditions on both frequency and impact side. Overall, it is considered that the Stad Ship Tunnel will have a positive marine safety effect for utility vessels for ground impact, collision, capsizing and stability failure without capsizing. In addition, a qualitative assessment of the marine safety effect for recreational crafts has been made, which shows that a major positive impact on the marine environment is assumed.



Figure 7: Different sailing routes

Fire protection

The primary contingency concept for the tunnel is that, if possible, the vessel shall attempt to sail out of the tunnel in the event of fire. Evacuation inside the tunnel itself will therefore only happen if the vessel fails to sail out of the tunnel. In the event of an event within the tunnel, the concept is that evacuation should not depend on external resources (self-sufficiency).

Evacuation takes place via gangway / ladder to the lanes that are located on both sides of the tunnel. It should be possible to evacuate in both directions along the lane to the portals. **Figure 8: Illustrating evacuation situation from a coastal ferry to emergency path (Pathfinder)**

The areas outside the portals could be arranged as emergency shelters and are available for emergency services via access routes.



Figure 8: Illustrating evacuation situation from a coastal ferry to emergency path (Pathfinder)

A walkway is facilitated for evacuation by establishing railings, handrails and emergency lights. The tunnel will not have mechanical ventilation. Mooring possibilities are established for larger vessels in connection with entry construction at each portal to facilitate evacuation of ships at the portals. There is no need for mooring of larger vessels inside the tunnel.

CORROSION EVALUATION WITH MEASUREMENTS OF MARITIME STEEL STRUCTURES IN COSTA RICA

by

Millan Solorzano, L.O.¹ Costa Rica

1. INTRODUCTION

Due to the easiness of construction, many maritime structures, principally, foundation piles and earth retaining walls are made of steel. Consequently, these structures are subject to corrosion that could be severe because of the direct contact with seawater and/or spray.

For such structures, some inspection and measurements, are accomplished as quality control during construction. However, in most cases, corrosion assessment, during service life, is negligible. Afterwards remediation countermeasures, are often costly and done with poor knowledge of which areas are critical.

Nevertheless, there are some advantages in doing measurements for maintenance evaluations. Maybe the most important is to detect differences in the behavior of similar-type elements, and establish the priorities for maintenance.

This paper considers three study cases, located in the Pacific of Costa Rica, with after construction evaluation or follow up of maritime structures, including thicknesses of steel elements and electrical potential measures of cathodic protection systems. These cases are a) A Cellular Cofferdam Breakwater at Quepos, b) A Sheet-pile wall at Caldera Port and c) A Trestle at Punta Morales Pier.

Key words: Monitoring of structures, steel maritime structures, corrosion, ultrasonic thickness measurements, cathodic protection.

2. CELLULAR COFFERDAM BREAKWATER AT QUEPOS

2.1 Descriptions



Fig. 1 (Left) Aerial view of the Marina from 2010 (Right) Arrangement and numbering of cells

¹ Millan Ingenieria, MSc/MPE Cand., luis@millaning.com

The first phase of a marina in Quepos, Costa Rica, finished construction in 2010. This phase included two mix breakwaters, both with rubblemound and circular cells of sheet piles, on marine steel and filled with sand and gravel. These breakwaters are 956 meters long and have 25 circular cells from 12 to 18 meters in diameter, with interconnection arches, in water depths from 1-6 m below low water level or LWL (*Fig. 1*).

The sheet piles were not protected by a barrier, i.e. do not have paint or coatings prior to their installation, nor concrete or other material once constructed. Also, no anodes were placed for cathodic protection of submerged parts. As result, of these design decisions, corrosion is expected to occur without restrictions.

Therefore, the designer considered for the tidal and splash zone, as well for the submerged part, an over-thickness that could corrode during the lifespan of the structure, keeping the real capacity of the cells unaffected. The maintenance plan for the marina, considers tracking the corrosion experienced by the steel sheet-piles, and comparing 'actual' against expected corrosion rates. An analysis is then required to check that the structural limits for the corrosion additional thickness are not exceeded.

2.2. Method Statement

Specific control sections, distributed along the breakwater, were considered both inside and outside the marina basin, being one section per cell or arch inside, and two sections per cell or arch outside. In this way, a general distribution of the corrosion condition around the breakwaters, with different exposition for the cells, could be surveyed. The sections are to be controlled annually, although not all the sections were taken in each campaign.

Also, other few measurements were done behind rock revetments, provisionally withdrawing rubble mound, and in diaphragm sheet piles, which are the cell elements within the fill, in this case by previously excavating the gravel and sand fill of the cell. This was made to understand the behavior of these sections compared to exposed cells.

In each section, thicknesses were measured, using ultrasonic equipment and a special underwater transducer, every meter from the top of the cell, about +4 m LWL to the seabed. When the measurements were above the water, access to the points was done with stairs and platforms. On the other hand, measurements below the water required divers.

A nomenclature was adopted to define every measurement location, including the cell number, the specific sheet-pile (starting from the joint), and measuring the height from top of the cell down. At each elevation, 4 points were measured as shown in *Fig. 2*, so that minimum and average values could be considered for statistical purposes. Relating the measurements to a specific location, allows re-staking each section and points in a simple way, so that they could be repeated during annual measurements.

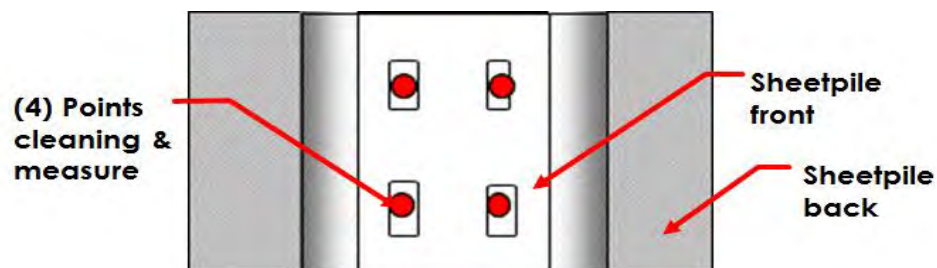


Fig. 2 Scheme of points measurements at each elevation.

Update annual campaigns measurements, are from 2011 to 2013, and 2015 to 2017. The campaign, included in this paper, was the one from April 2016, when the sheet piles had from 7-8 years of being installed. This year was chosen over 2017, since in 2016 all the sections were measured, which did not happen in 2017, when the measures were partial.

An air needle powered by a compressor was used at each measurement point to clean the sheet-pile surface from marine life and corrosion. The cleaning was done in a circle with no more than 10 cm in diameter. This cleaning was executed also above water, likewise with the same equipment.

The thickness measurements were made with a UT (ultrasonic equipment), having a nominal frequency of 5 MHz, and a straight ½ in. diameter underwater transducer, with a 15 m in cable, so that the measuring device was at the upper part of the cell all time. *Fig. 3* shows the cleaning and the installation of the underwater transducer at the surface during the measurement of one of the points.



Fig. 3 Underwater Procedures at the Marina in Quepos (Above) Cleaning of measurement points (Below) Thicknesses measurement with ultrasonic sensor.

2.3 Minimum Structural Thicknesses

To calculate the minimum admissible thicknesses, design loads are used to estimate the sheet pile hoop tensions, using the procedure from the Corp of Engineers and Pile Buck Manuals [2, 3]:

$$F_{t,Rd} = \min\left(\frac{0.8 \cdot R_{k,s}}{S.F.}, \frac{t_w \cdot f_y}{S.F.}\right) \quad F_{t,Ed} = p_{m,Ed} \cdot r_M \quad F_{t,Ed} \leq F_{t,Rd} \quad (1) (2) (3)$$

Where,

- $P_{t,Rd}$ is the admissible tension;
- r_m is the cell radius;
- t_w is the sheet-pile thickness;
- f_y is the sheet-pile material yield stress;
- $p_{m,Ed}$ is the maximum tension, which can be calculated with several formulas;
- $P_{t,Ed}$ the maximum cell tension force/length;
- $R_{k,s}$ interlock tension force;
- $S.F.$ is a safety factor.

For simplicity, the pressure in the splash zone was considered half of the pressure in the immersed zone, the last calculated as per the analytical formulation. About this must be considered that critical elevations vary from cell to cell and could be either above or underwater. To explain, corrosion levels are higher at tidal zone, but tension forces diminish. Opposed to this, below water, the highest tension of the sheet-pile occurs around or just above the seabed level, but corrosion rates are smaller.

It must be recognized that, joint interlock tension loss due to corrosion is difficult to measure, so an alternative approach was considered. It was assumed a linear relationship between the measured thickness and the maximum tension that theoretically can support the connection. This is based on ARCELOR design manual [4]. Then, the thickness of the sheet pile corresponding to the tension calculated for the joint is extrapolated. The safety factor used in the formulas was 1.5.

In *Table 1*, summarizes the minimum calculated thicknesses for the combination of inner and outer exposed cells, main and connecting arches, as well for the connecting yees (or joints). In this calculus, besides cell filling, other interactions, such as the presence of concrete parapets, or the effect of external waves, may be neglected, since they do not affect the internal pressure toward the outside of the cell which drives the hoop tension of the sheet-piles.

Table 1 Minimum thickness (mm) to comply with cell hoop tension and a 1.5 safety factor [5].

| Location | | 12.2 m cells | 18.6 m cells | |
|-------------------|-----------|--------------|--------------|-----|
| Outside the basin | Above LWL | Sheetpile | 1.8 | 1.4 |
| | | Joint | 2.5 | 1.9 |
| | Below LWL | Sheetpile | 1.4 | 2.4 |
| | | Joint | 2.2 | 3.4 |
| Inside the basin | Above LWL | Sheetpile | 1.3 | 1.6 |
| | | Joint | 2.0 | 1.9 |
| | Below LWL | Sheetpile | 1.2 | 2.5 |
| | | Joint | 1.9 | 3.5 |

It could be concluded from the previous table that the thicknesses for having failure, compared with the theoretical thicknesses of the piles, are in fact low, about 25%-30% of theoretical thickness. Thicknesses are greater for the joints compared to other sheet-piles. For the 18.6 m cells, sheet-piles above water require higher thicknesses compared to those below water, and the opposite is true for the 12.2 m cells.

2.4 Thicknesses measurements

The measurements from 2016, for the inside of the north breakwater, could be seen graphically in Fig. 4. In this graph, one section is considered per cell, so in cases with two sections measured per cell, conservatively the one with lower thicknesses was included in the figure. Levels are in meters from the LLWL (lowest water level) so that effects of tides are recognized. Similar graphs were considered for the other exposition conditions i.e. south breakwater, and outside the basin.

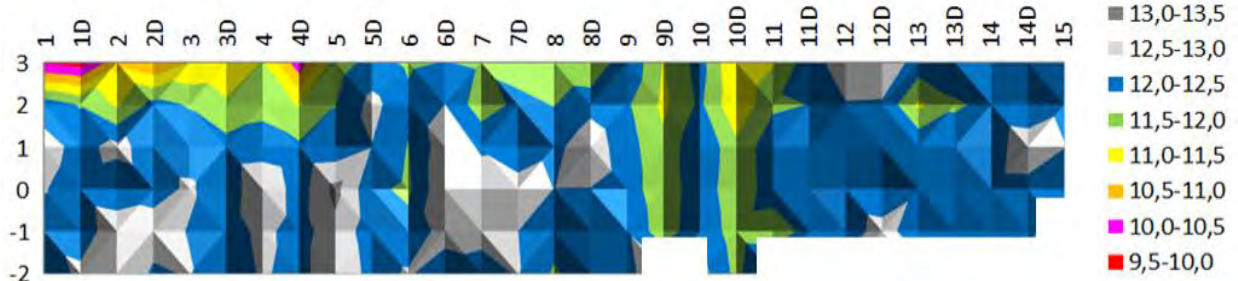


Fig. 4 Thicknesses (mm) at different elevations (from LLWL) and sections (one per cell) for the north breakwater inside the basin, 2016.

From these graphs, specific cells with lower thicknesses, i.e., higher corrosion could be identified, for example, above +1 m LWL inside cells 1-5 and above +1 LWL for outside cells 1-8. Also, statistically, the distribution of quantity of measurements for given ranges is also considered, as shown in Fig. 5. This graph shows the thickness measurements distribution for the north breakwater outside the basin, but similar graphs were calculated for other exposition conditions.

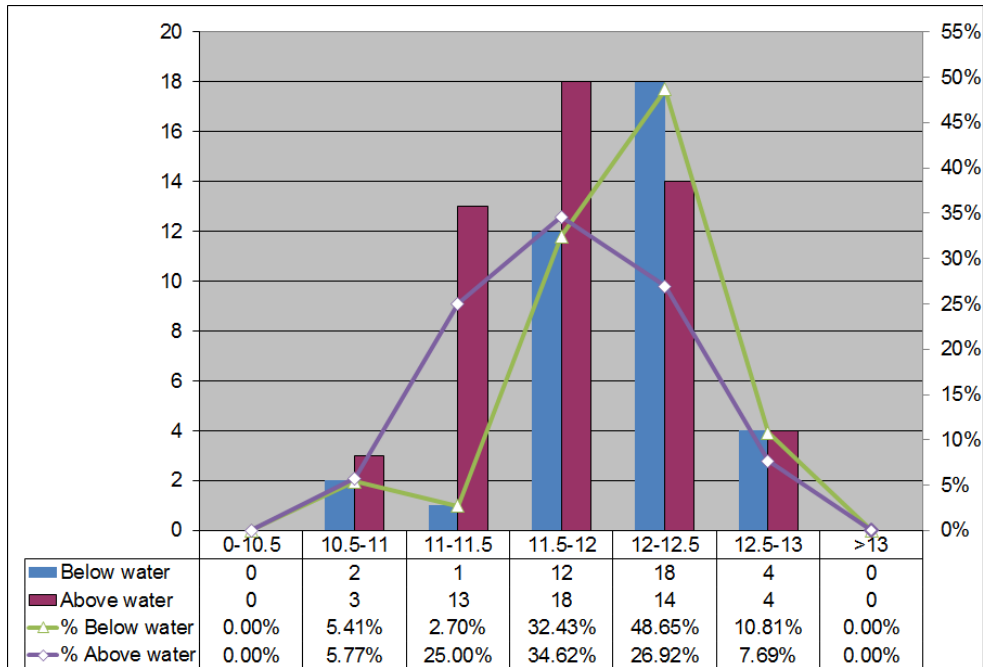


Fig. 5 Thicknesses measurements distribution for north breakwater outside the basin, 2016.

Inside the north breakwater, 49% of measurements above LWL and 60% below LWL are between 12.0-12.5 mm, with a minimum measured thickness of 9.8 mm. Meanwhile, outside the north breakwater, 35% of measurements above LWL are from 11.5-12 mm, and 49% below LWL, are from 12-12.5 mm, with a minimum measured thickness of 10.6 mm. From the previous, and as expected, corrosion attack is higher above LWL, and lower below LWL.

2.5 Thicknesses versus time

The measurements of the all the campaigns carried out, were plotted against the years between measurement and sheetpiles construction. This comparison considers the generalized behavior of sheet piles over time. *Fig. 6* shows the case corresponding to the inside part of the north breakwater. Similar cases were addressed for the other conditions i.e. north and south breakwater, and inside or outside the basin.

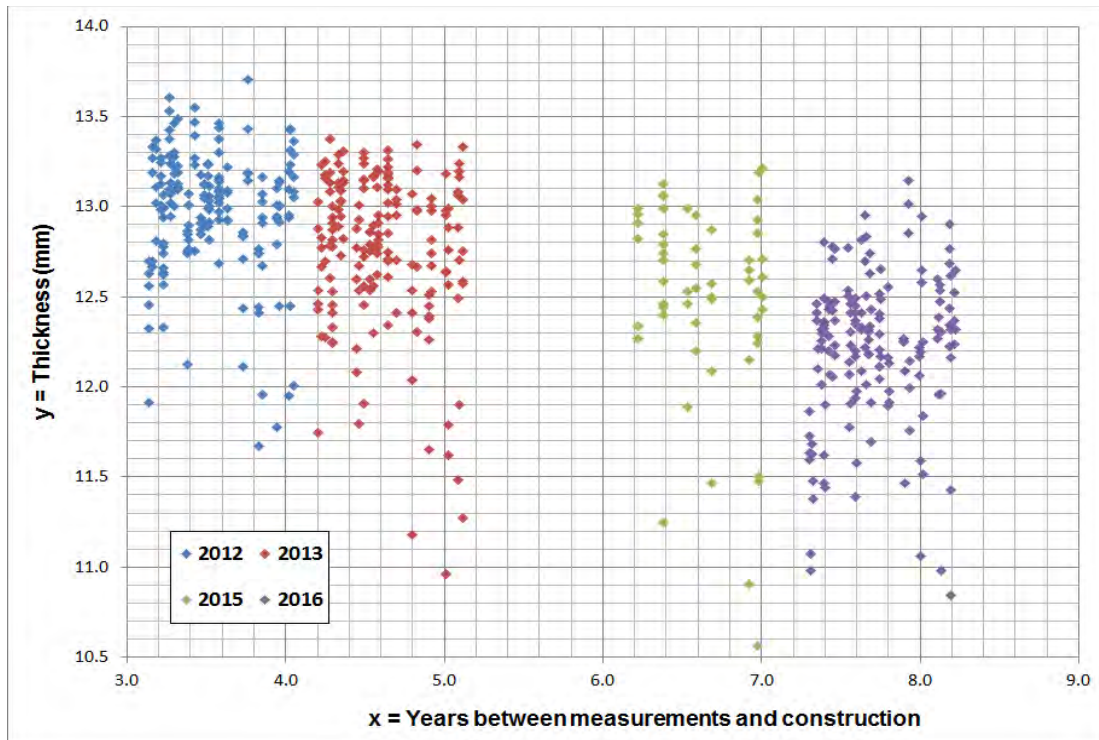


Fig. 6 Set of all thicknesses inside north breakwater vs. construction time, 2012 to 2016.

Because the construction of the breakwater cells was executed over a period of several months, the graph ends up having a distribution of points that allows to validate the observations and the calculations made in this way.

As expected, it is concluded that the general behavior of the sheet-piles after the construction of the breakwaters is loss of thickness (or corrosion), this no matter the exposition condition, North or South breakwater, inside or outside the basin. In general, in the north and south breakwaters, the lower thicknesses are in the sheet piles above +0 m LWL. The trend seems to be that higher up on the sheet-pile corrosion is greater.

In the north breakwater, the losses outside and inside the basin are in the same magnitude order. But on the south breakwater, this cannot be concluded because there is only one section in the inner part because rubble mound is laying in almost all the internal cells. Inside the basin, there is more corrosion in the curved part of the north breakwater, compared to the rest of the sheet piling. Outside this same breakwater, the corrosion is greater on the most exposed cells to waves.

Besides the general comparison, differences between data of the same measurement points from 2012 and 2016, were calculated. For the same point, the average differences are from 0.46 to 1.10 mm and maximum from 1.22 to 2.61 mm. Those differences are summarized on *Fig. 7*.

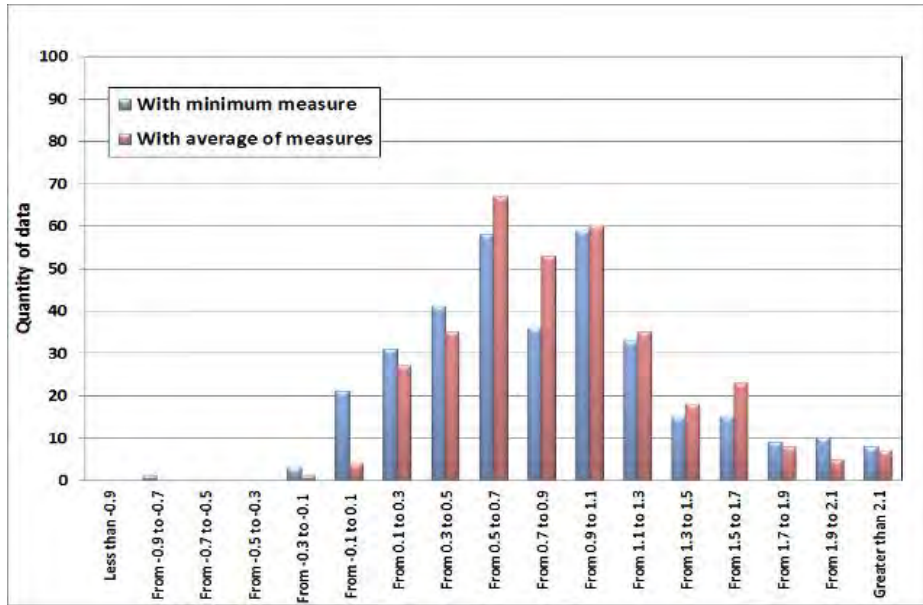


Fig. 7 Thicknesses differences of measurements, 2016-2012.

As shown, few measurements were higher in 2016 compared with the ones from 2012. That may be due to differences in equipment or cleaning, but also because, by procedure, measurements are directly on site, which never happens in the same exact spot. This is, for each measurement, an area of the sheet pile surface about 10 cm diameter, is cleaned, and the transducer is placed within this area. As the surface is irregular, some differences between measurements from different years are expected central cells.

2.6 Corrosion Rates

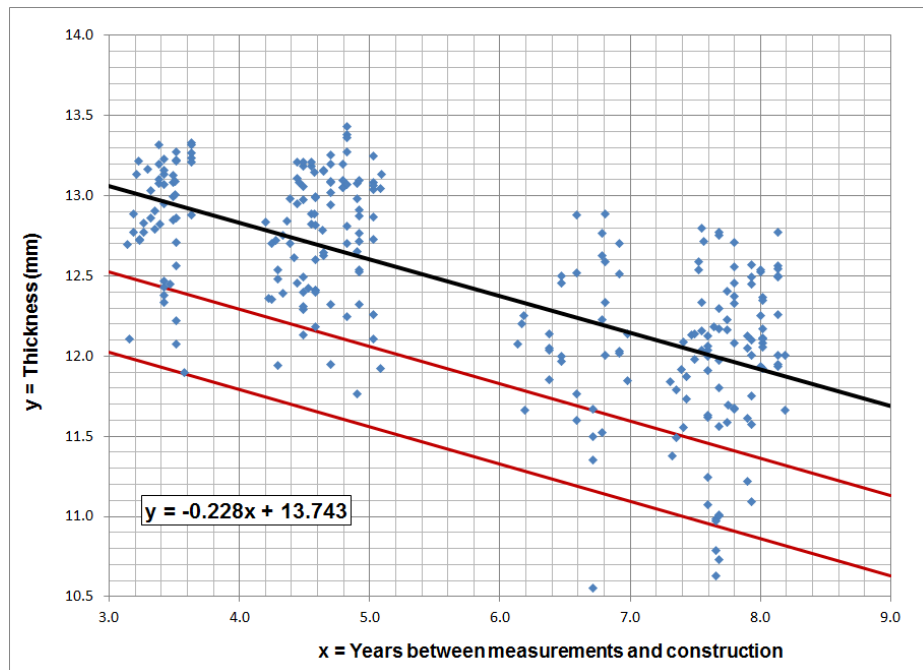


Fig. 8 Adjustment lines for the north breakwater outside and above waterline, 2012 to 2016.

With measurements from different years, corrosion rates could be calculated, as an average for some structure sectors, or for each measured point. Differences on thicknesses loses and corrosion rates were identified for conditions of exposition, i.e. outside and inside basin, above and below LWL, and due to the location along the breakwaters.

Linear best fit lines were determined, with the measurements from 2012 to 2016 as part of the same set of data. For considering lower limits for the best fits, two other parallel lines to the fit line were included with a separation between them of 0.5 mm. *Fig. 8* shows the data and adjustment lines for the inside section of the north breakwater. The same was done for other combinations north-south breakwater, inside-outside sections and over-under water.

These comparisons are intended to consider the general behavior of the breakwater. Low correlations are expected, as they include different levels and locations along breakwaters, where individual corrosion rates are not the same. The slope of the adjustment lines can be considered as an average corrosion rate of the structure section. In the case, for the external north breakwater above the water, it is 0.23 mm/year, which is high, but expected for tropics with no barrier or cathodic protection.

On the other hand, the estimates of the corrosion rates for each of the measured points, are based whether on the average of the measurements in each of the elevations or the minimum in the same section and elevation. For all the cases, the corrosion rates averaged from 0.11 to 0.26 mm/year, which are also high. It should be clarified that these rates have been calculated with a four-year term (2012-2016), and it is expected that the estimates will improve over the years, and more data.

2.8 Estimated Lifespan

Considering that the best fit lines, their parallel lines, and intersection with the minimum thicknesses, is possible to establish general lifespans (or useful lives) for the steel breakwaters, considering each of the analyzed exposition conditions (combinations of north-south breakwaters, inside-outside the marina, or above-below sea level). The calculation shows estimated lifespans greater than 30 years in all cases, which is the about the time for ending the marina concession.

Also, from the safe structural thickness for each sector, lifespans could be calculated, based with the differences between the average measurements of 2012 and 2016 for each point. In general, these complies with the designed lifespan for the whole structure, however there are specific sectors with lifespans that are lower than required.

For each cell, the difference between the current measurement of the point, and the minimum safe thickness according the structural calculation, is a remnant of corrosion (available thickness that could corrode without failure of the structure). The time in years required for the estimated measurement thickness to corrode the remaining material up to the minimum thickness, in the calculated corrosion rate, is related to the lifespan for the sheet pile at that specific point.

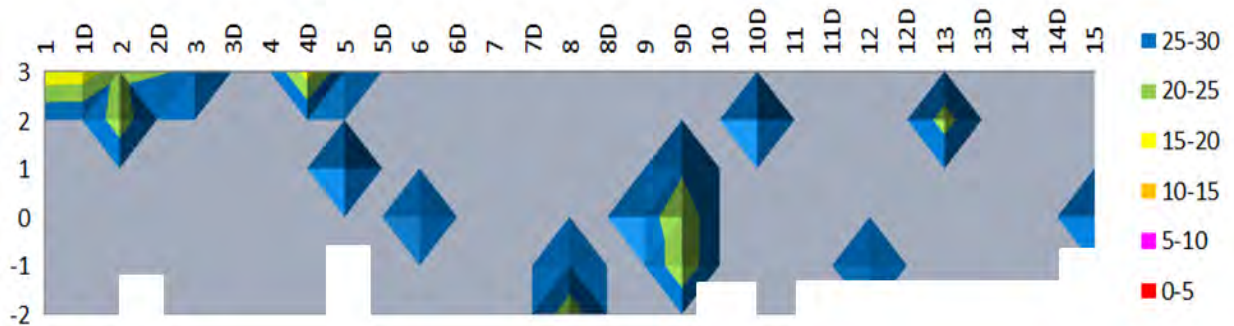


Fig. 9 Lifespans (years) for different elevations (from LWL) and sections (one per cell) for the north breakwater inside the basin, 2016.

The previous is summarized in Figs. 9 and 10, respectively for the north breakwater inside and the same breakwater outside. From these graphs it could be inferred that most of the points would have lifespans over 30 years. Similar graphs were obtained for all the combinations of expositions analyzed i.e. north-south breakwater, inside-outside of basin, and above-below LWL.

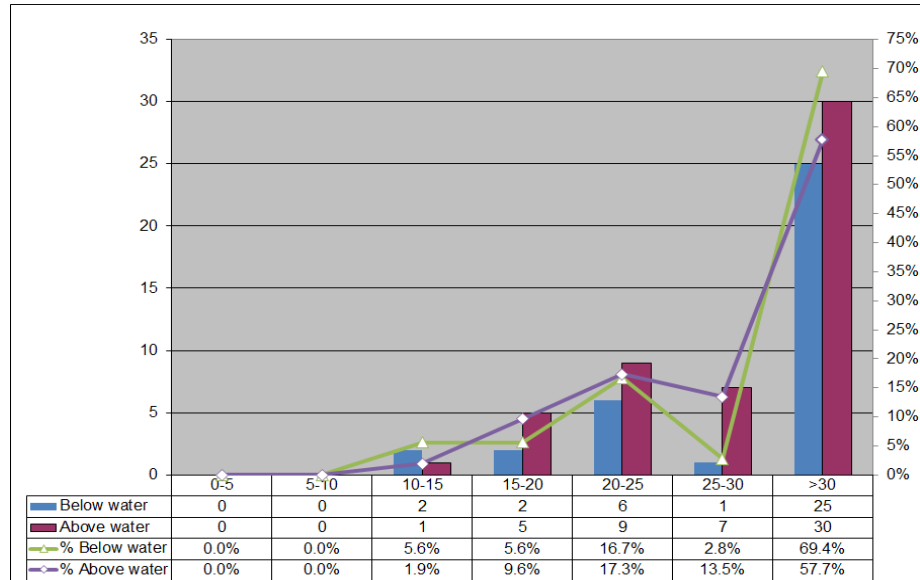


Fig. 10 Lifespans for individual measurements at north breakwater outside the basin, 2016.

The analysis shows that there are critical cases with lifespans between 10-20 years. Among the conditions under-over water and inside-outside the marina, the conditions over water and outside the marina have lower lifespans. For example, in the north breakwater, 86-89% of inside cells have lifespans of more than 30 years, with minimum individual lifespans form 15-20 years. Meanwhile, outside 58-69% of cells have more than 30 years with minimum individual lifespans 10-15 years.

3. SHEET-PILE WALL AT CALDERA PORT

3.1 Descriptions

The principal bulkhead of Port of Caldera, includes three berthing positions Berth N.1-N.3 depths from -7.5 to -11 m LWL with a total length of 500 m, and was constructed in 1980 i.e. have 38 years of service (Fig. 11). An additional Berth N.4, which starts operation in 2014, corresponds to a pile supported pier, and is not included in this analysis.

The bulk-head is a steel sheet-pile retaining wall, with back filling composed of stone, and granular materials in the upper part. The sheet pile is anchored at +2.0 LWL level. An end cap of 2.6 m width was constructed between the levels +0.50 to +5.0 LWL, with the sheet pile embedded up to the level +3.0 LWL. These caps provide a barrier protection for the steel sheet-piles on the splash zone. Below water, sheet-piles are protected by sacrificial aluminum alloy anodes providing passive cathodic protection. In the attached Fig. 12 there is a cross section through the Berth N.1.

According to construction plans sheet piles used were Z-25 type with 305 mm depth for berth N.3, and Z-45 with a depth of 360 mm for berths N.1 and N.2, both types of sheet-piles 400 mm wide. Regarding the galvanic anodes for the submerged part there are two rows of anodes for berth N.3 and 3 rows for berths N.1 and N.2. Each of the anodes weighs 137 kg, with external dimensions of 730 x 300 x 260 mm, and are placed on a steel plate welded to the sheet pile.



Fig. 11 Quay wall at Puerto Caldera, taken from the end of Berth N.3.

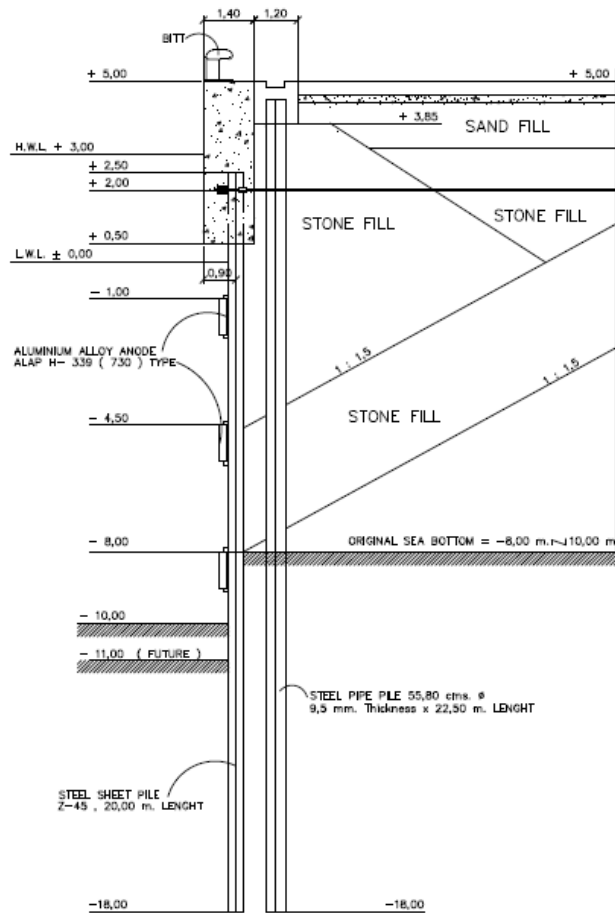


Fig. 12 Cross section trough sheet pile wall at Berth N.1.

3.2. Method Statement

Evaluations of sheet-pile thicknesses and electrical potential generated by the cathodic system were performed by others in 2003. Additional measurement campaigns, were executed from 2011 to 2015, and the last one in 2017. For horizontal location there were defined on 2011, reference points denominated W, P, E and located respectively in the west closure wall (E), main wall (P) and east closure wall (E), of the quay, located about 5 meters apart one from another.

Steel thicknesses measures, follows an analogous methodology as in the previous case study, with the difference that only measurements below water were executed, where there is no concrete cap. (Fig. 13) Since the measurements from 2011, were taken as a base, longitudinal measurements were performed that year on sections every 10 meters. Based on the information from the campaigns of 2003 and 2011, follow up thicknesses measurements for following campaigns were executed at 8 control chosen sections.



Fig. 13 Example of thickness measurement at Caldera sheet-pile wall, 2017.

Electrical voltage assessment of the potential generated by the anodes of the quay wall, is used as maintenance evaluation to detect areas not complying with what is required for corrosion inhibition. Measurements are done in sections every 5 meters alongside the main and closure walls, and vertically every 50 cm from top to sea-bed. Also, on the campaign of 2011, a survey of the location of existing anodes on the wall was done.

Electrical potentials are measured with a voltmeter, in which the negative phase is connected to a special Ag/AgCl reference electrode and placed in the water, and the positive part to a plate that is connected inside the cap to the sheet-pile, as was originally planned by the Japanese to make these measurements. And scheme of the measurements and the equipment used is shown in Fig. 14.

In the procedure, first, the sea bottom is obtained measuring using a 30 m tape with a ballast weight. For the voltages measurements, with all connected, the reference electrode is located at the elevation +0.0 m LWL and lowered every 50 cm until the sea bottom previously measured is reached. With each increase in depth, the voltage value in the voltmeter is recorded. It was noted that the values were stable so it was not required to make several measurements at the same elevation.

The potential is adequate if it is more negative than -850 mV compared to a CSE reference electrode, which is equivalent to -800 mV to a Ag / AgCl electrode, or at least there is a negative change of 100 mV from the potential without anodes (in this case this information is not available). This is per the specifications established by the National Association of Corrosion Engineers (NACE) of USA [6], [7].

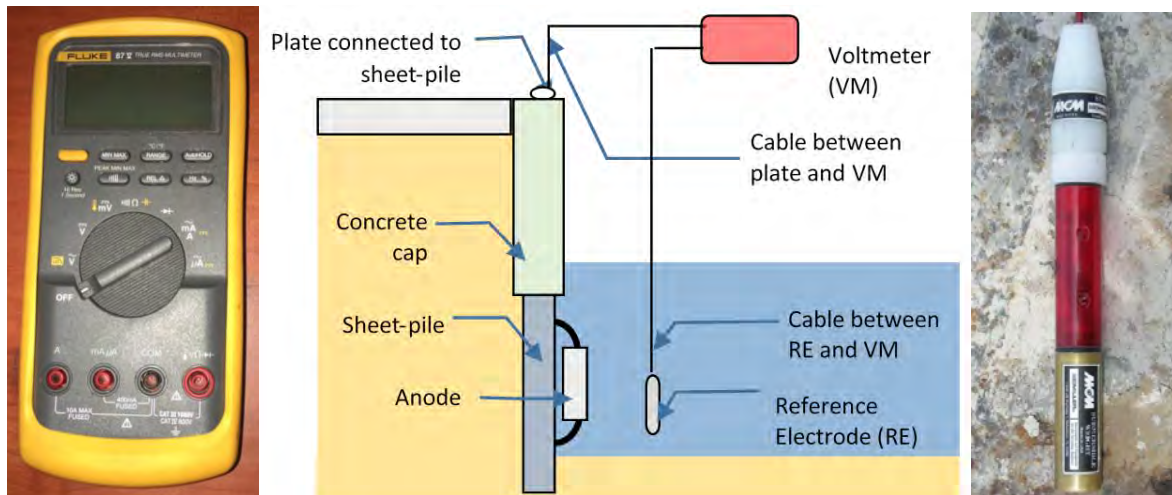


Fig. 14 Measurement of Anodes Potential (Left) High Impedance Voltmeter (Center) Equipment connection and Measurement Scheme (Right) Ag/AgCl Reference Electrode

This same procedure is repeated for the other sections beyond half the distance to the next plate. The previous so that the measurements could be verified, by overlapping measurements between plates, which did give similar results.

3.3 Thicknesses measurements

The averages of the four points measurements at each considered elevation, were calculated. The lowest average thickness in the sheet piles of Berths N.1 and N.2 is 20.01 mm, which is 1.79 mm less than the theoretical thickness. On the other hand, the smaller thickness in the sheet piles of Berth N.3 is 12.26 mm, 0.74 mm less than the theoretical. Thicknesses greater than the theoretical were also measured, which is possible considering the manufacturing tolerances of steel sheet piles.

Despite this is a structure with 38 years of construction, steel thicknesses compared to sheet-pile original specifications remain similar. It is then noted that in general, there has not been a significant loss of sheet pile thickness which is probably due to an effective cathodic protection.

3.4 Corrosion rates

For the corrosion calculations, the theoretical thickness of the sheet pile were taken as a basis, namely 21.9 mm for the sheet piles of the West closure wall and for Berths N.1 and N.2 walls, and 13 mm for Berth N.3 wall. To be consistent with the information presented, the corrosion rates have been calculated with the averages at each elevation. The corrosion rates calculated with the average are 97% less than or equal to 0.03 mm / year.

In addition to the rates calculated with averages, corrosion rates from the minimums measurements at each elevation were also carried out. These calculations are more conservative, considering not only that it is done with the minimum, but because between two measurements at a given elevation, the minimum does not necessarily occur at the same point between annual or a previous measure.

Due to the time that has elapsed from the construction of the quay (38 years), it is considered that the rates considering the theoretical thicknesses of steel sheet piles as calculated are reliable. The premise is that, if up-date there have been no significant losses in the sheet piles, there is no reason for them to occur, as long as the required potential is maintained throughout the sheet-pile.

3.5 Potential measurements and countermeasures

As indicated before, the measurements of the voltages generated by the cathodic system, could be used to evaluate the provided protection to the sheet-pile. The campaign from 2011, is interesting since, the locations of the existing anodes were surveyed. When these locations are compared with the interpolation of the potential through the wall, it could be seen that the variations of the voltages ranges are related to the anodes location (*Fig. 15*). For example, an area outside specification was detected at middle of Berth 1, which is due to the lack of sacrificial anodes in the area.

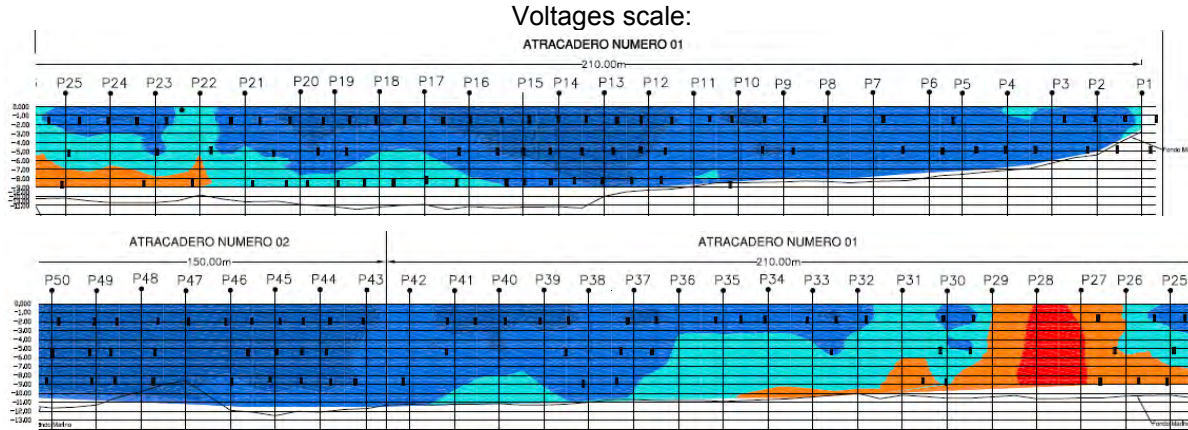


Fig. 15 Potential distribution and location of anodes in the sheet-pile wall on berth N.1, 2011.

If the potential is not what is required, additional anodes are welded to regain it. Also, after the new anodes were installed, electrical measurements are performed to confirm the protection. This approach minimizes maintenance costs since only the sections that need anodes would be re-protected with them, compared to replace anodes after certain mass loss despite the generated potential.

There had been other cases in which this happened. One was after the construction in 2012 of the underwater rock revetment at the Berth 3 corner, which was required for the slope protection between this corner and the dredging Berth 4. Because of the construction method for rock layers conformation, most of the anodes from the wall were ripped and potential measurements became inadequate.

After la installation of only 21 anodes in the bottom of the wall, the potential was regained. These could be seen in on *Fig. 16* for a portion of Berth N.3, with the location of the new anodes for more clarity. Above and below graphs are the conditions before and after the installation of the new anodes.

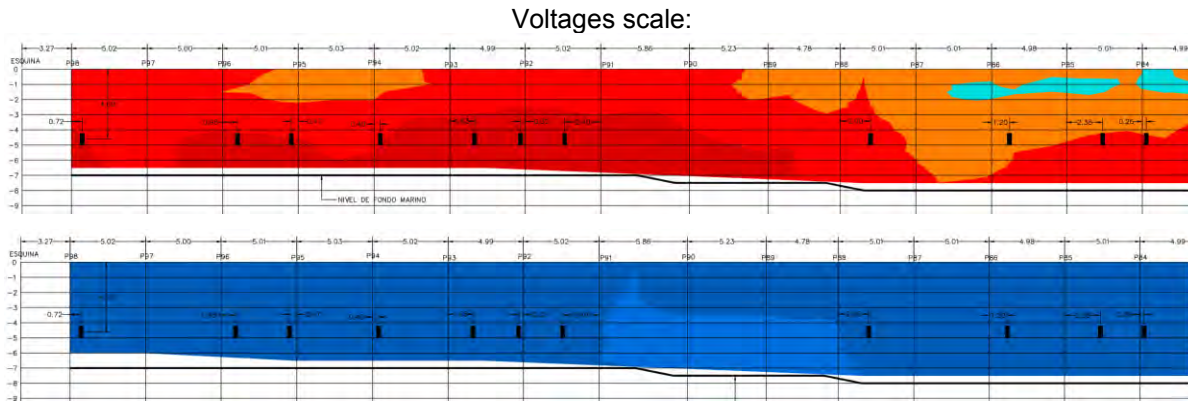


Fig. 16 Potential voltage measurements at a portion of Berth N.3 (Above) Before installation of anodes. (Below) After installation.

4. TRESTLE AT PUNTA MORALES PIER

4.1 Descriptions

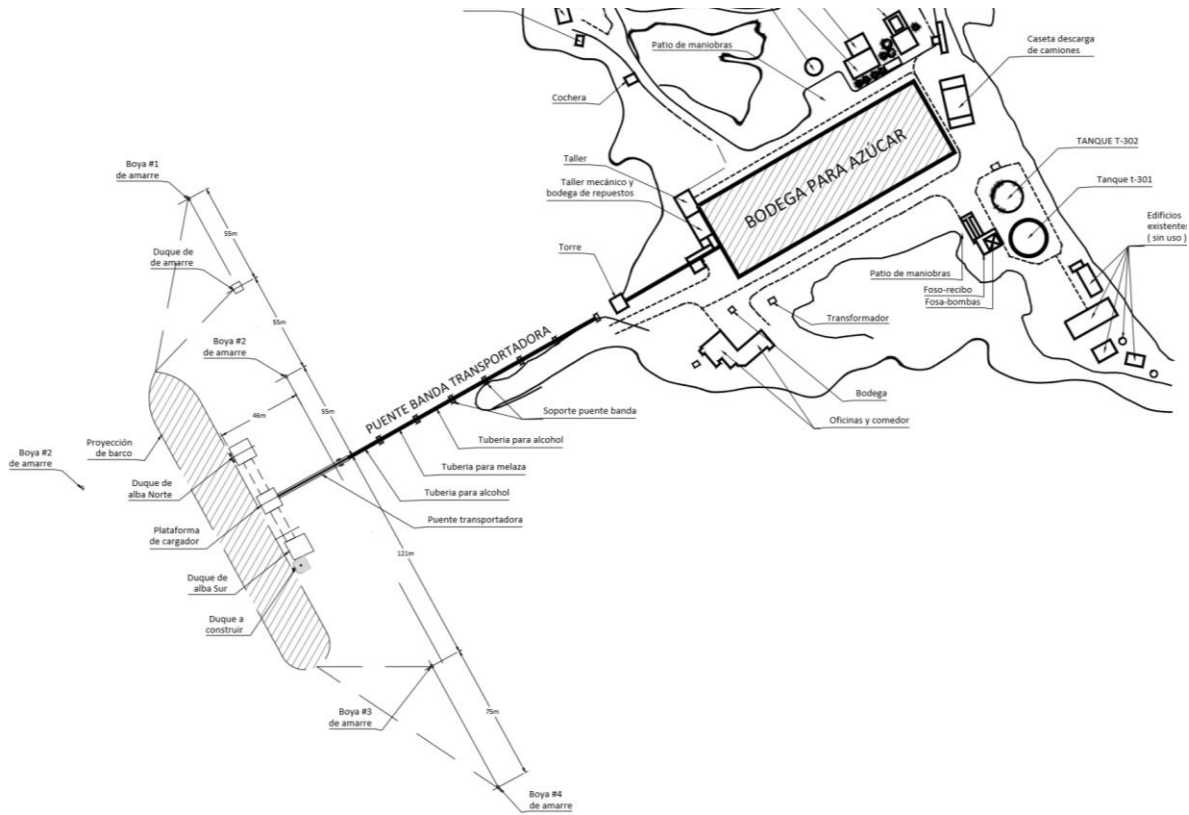


Fig. 17 Punta Morales Pier (Above) Layout of the pier including Charging Platform, Berthing Dolphins and Conveyor supports (Below) General View of Trestle Supports from land.

The Punta Morales pier, principally for sugar export, was constructed in 1980, and is a dolphin-type pier with a loading platform, all steel pipe piles. The sugar is transported from a warehouse on land to the loading platform by means of a conveyor belt. This belt is supported on (9) concrete caps, each one with (4) H-beam steel piles. In general, the piles were located with a certain horizontal inclination with respect to the axis of the conveyor belt, although the majority are with the flanges oriented in the direction of the belt axis. The layout of the pier including the conveyor support is shown on Fig. 17.

The first support of the conveyor belt from the pier, is different from the others, in cross section of the piles, and because there are some reinforce diagonals between piles. This support is in the deepest part, in addition to the band and catwalk are raised about 15 meters above the upper level of the upper part of the slab of the support, which probably explains the more braced structure.

The piles of the supports are protected with an active cathodic protection system of impressed current, wired at the top interconnected with the trestle superstructure. Cathodic protection condition would not be addressed in this paper.

In addition, piles are painted with epoxy products, with thicknesses from 0.2-0.4 mm as measured with the ultrasonic equipment. This represents an additional protection, whose effectiveness depends on how impermeable and continuous the layer is, so that it being effective as a barrier protection for piles.

During routinely inspections, sections losses were viewed on the belt support piles, mostly near LWL, and possible due to abrasion. However, extend of the damages were unknown, especially below water. So, the recommendation was to measure steel thicknesses at each pile, every meter from top to sea-bottom, in the five outermost supports, which pile does not discover on low tide. According to measurements made on site, in these first (5) supports, the depths of the seabed from LWL are 9.0 m, 4.5 m, 3.0 m, 1.5 m and 1.0 m.

It should also be noted that this seems not to be a recent problem, since some piles have steel plates reinforcements welded principally in the flanges and the upper part of the piles. Its known that the site have important tide currents that carries nearby rivers sediments provoking abrasion and poor visibility.

4.2. Method Statement

Pile thickness measurements were made, vertically, at five points per elevation, each meter starting from the top of the pile below the support head (approximately at +3.0 m NMBS level) until it was closest to the bottom marine, or as far as visibility would allow.

In the scheme points 1,2, 4 and 5 are points taken on the pile's wings, while point 3 is taken at the beam's web, to differentiate conditions around the pile. By easiness to measure outside of the beam, was preferred, although in some cases, especially when there were existing reinforcement plates the measurements were done from the internal side (Fig. 18).

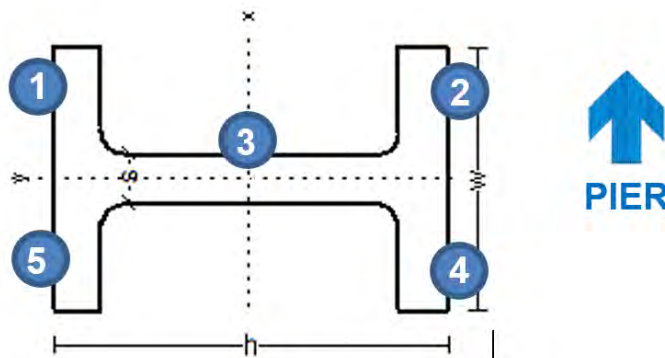


Fig. 18 Location of measurement points on H-pile flanges and web at each elevation

Due to visibility issues, it was not possible to reach the first of the supports from the ground to the seabed, but up to the level -7 m NMBS, which is about 2 meters above sea-bottom. In all other supports, measurements were made to the seabed. *Fig. 19* shows a thickness measurement in one of the piles on the first support from the pier.



Fig. 19 Thickness measurement in one pile of the first support from the pier

4.3. Thicknesses measurements

The thickness of the wings of the H-beams, are on average 20-21 mm, and 13-14 mm in webs. In general, from the analysis of the information there are piles that had lost 2 mm in thickness, compared with other measured elevations in which no corrosion is detectable. A single point on one of piles, gave a thickness of 17 mm, that is 3 mm less than the average.

The main losses are located coinciding with the low tide level (0 m of the NMBS), and about 3-4 meters below the level of the low tide. As demonstrated, thicknesses measures helped to detect areas with severe losses, and showed some losses below water, not necessarily detectable by divers.

As clarified, in some cases, there were some previous repairs with steel plates, for which there would be no problem, even if the thickness of the pile is much lower if some conditions are complied. These are that the plates are fairly welded, and that the plate reinforcement overlap to lower and upper sections of a pile in good condition.

4.2. Piles repair

Instead of prescribing substitution of the piles, which would probably be the recommendation without data, reinforcement of the piles with steel plates was proposed. Location of these reinforcements were accordingly, with the distribution of lower measurements from the study and in places without previous welded plates. These plates reinforcements were calculated following the shear flow concept [8], [9].

All this was implemented some months after the evaluation, and included underwater welding in difficult current and visibility conditions, but at low cost compared to a full substitution of piles. The piles were reinforced locally with 150 mm long 13 mm thick steel plates and with a width that allowed fillet welding between the plates and the top of the flanges or on the sides of the web. 21 plates were welded in the first 4 support H-piles in flanges, webs and in some cases in both. No intervention was considered for the fifth bent. *Fig. 20* shows the proposed reinforcement on Bent N.3 taken from the pier.

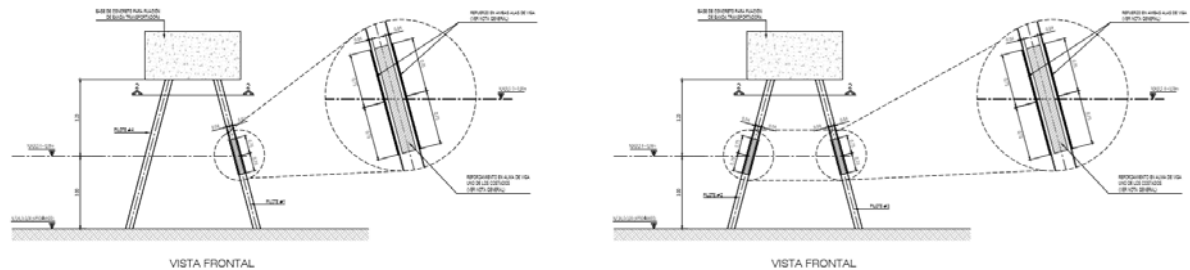


Fig. 20 Example of the proposed pile reinforcement at Bent N.3.

For additional protection, plates were painted with marine coating before installation, and the pile surface, where a plate goes, was cleaned from maritime life and corrosion, manually and using pneumatic tools.

Plates were placed in the intended position, secured and welded. Once the reinforcement plates were welded, the welds were toughly cleaned from slag, and from incipient marine life and corrosion. The borders of the plates were protected by a coat that could be placed and cured below underwater. This operation was performed once the welding was finished, which justifies the additional cleaning before coating. *Fig. 21* shows the general procedure of installation of reinforcement plates underwater.

5. CONCLUSIONS

In all these three study cases, thicknesses and electrical potential determination with maintenance measurements, helps to differentiate sectors of steel structures, where the phenomenon of corrosion and/or abrasion occurs with varied attack levels. With several campaigns of thicknesses measurements, along the years, it is possible to estimate corrosion rates and useful lives or lifespans, both general for structures, and specific for each level and section.

In turn, this allowed to identify maintenance priorities, defining possible sites where measures of corrosion protection should initiate, with barrier protection, or active or passive, cathodic protection systems, the need to apply other countermeasures as reinforcement or substitution of elements, as well in general, to have confidence in the structural capacity and safety of structures. Moreover, evaluation with discrete measurements along the structures had shown to be cost-effective reducing the costs for repairs and maintenance of the steel elements and cathodic protection systems.

6. REFERENCES

- [1] Coburn, S. K. (2003). Corrosion Factors to be Considered in the Use of Steel Piling in Marine Structures. Pittsburgh: Pile Buck, Inc.
- [2] U.S. Army Corps of Engineers (1989). EM 1110-2-2503 Design of Sheet Pile Cellular Structures Cofferdams and Retaining Structures. Washington, DC.
- [3] Pile Buck, Inc. (1990). Cellular Cofferdams. Jupiter, Florida: Pile Buck, Inc.
- [4] Arcelor RPS (Rails, Piles & Special Sections). Arcelor Group (2005). Piling Handbook. 8th ed.
- [5] Bardi, J. (2012). Marina Pez Vela Cellular Cofferdam Evaluation. Washington: Berger Abam.
- [6] National Association of Corrosion Engineers-NACE (2013) SP0169 Control of External Corrosion on Underground or Submerged Metallic Piping Systems.
- [7] National Association of Corrosion Engineers-NACE (2012) STD TM0497 Measurement techniques related to criteria for cathodic protection on underground or submerged metallic piping.
- [8] Creviston, Jonathon C. (2012) PDHonline Course S245 Steel Beam Reinforcement. PDHonline, PDHCenter, Virginia.
- [9] Dowswell Bo (2014). Reinforcing the point in Steelwise, January 2014.

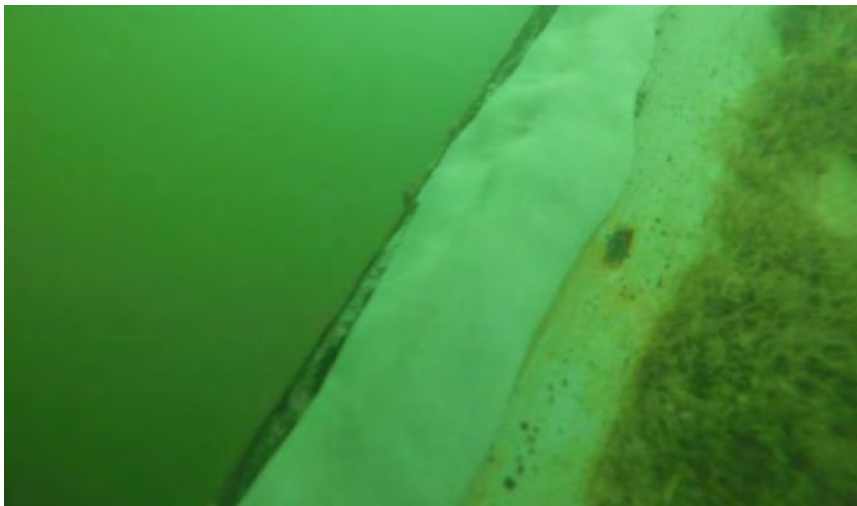


Fig. 21 Procedure for reinforcement of H-piles (Above) Installation of plates (Center) Underwater welding of plates (Below) Underwater coating of welds and plates borders.

SOHAR BREAKWATERS – COST BASED RISK ASSESSMENT

J.C. van der Lem¹, R.J.H. Stive², P.J.J. Groenewegen³

ABSTRACT

The Port of Sohar (Oman) is protected by two breakwaters which were damaged during the 2007 tropical cyclone Gonu. Extensive surveys were carried out in the past to determine the extent of the damage and studies were made for repair and upgrade designs. However, the costs for the proposed repairs showed so large that in 2016 repairs still had not been carried out.

When asked for its opinion, Royal HaskoningDHV advised the port that in the decision making process to repair the breakwaters an important item was overlooked, i.e. that also the repaired breakwaters would have a certain risk to be damaged. Consequently, the repair should only be made in case the benefits from the repair (reduction of risk) would outweigh the costs for such repair.

Following these observations, Royal HaskoningDHV was requested to quantify this in a cost based risk assessment. An important element in this quantification was finding a relationship between the damage to the concrete armour units (predominantly showing settlement) and the occurring wave conditions. Such relationship was established based on the model tests carried out in the past and relates the number of settling armour units (N_{od}) to the incident wave conditions (H_{m0} , T_p), the packing density of the armour units (ϕ) and the number of waves in a storm (N_w). Using this established relationship the present and future risk of the breakwaters could be quantified, taking into account the probability of the occurring wave conditions. The approach to the cost based risk assessment, the damage function and the results of the analysis are presented below.

1 SOHAR BREAKWATERS – HISTORY

1.1 The Port of Sohar

The Port of Sohar is located in the North of Oman, some 250 km south of the Strait of Hormuz (Figure 1).



Figure 1 The Port of Sohar, Oman (situation in 2007)

Construction of the port commenced in 2000 and the breakwaters were completed in 2002. The breakwaters are built as rubble mound breakwaters provided with CORE-LOCTM armour units. Typical cross sections of the north and south breakwater are presented in Figure 2 and Figure 3. The north breakwater is provided with 1.6 m³ CORE-LOCTM and the south breakwater with 3 m³ CORE-LOCTM.

¹ Royal HaskoningDHV - Senior Port Consultant, PO Box 8520, 3009 AM Rotterdam. Cock.van.der.Lem@rhdhv.com

² Royal HaskoningDHV - Senior Port Consultant, PO Box 8520, 3009 AM Rotterdam. Ronald.Stive@rhdhv.com

³ Royal HaskoningDHV – Coastal / Port Engineer, PO Box 8520, 3009 AM Rotterdam. Perry.Groenewegen@rhdhv.com

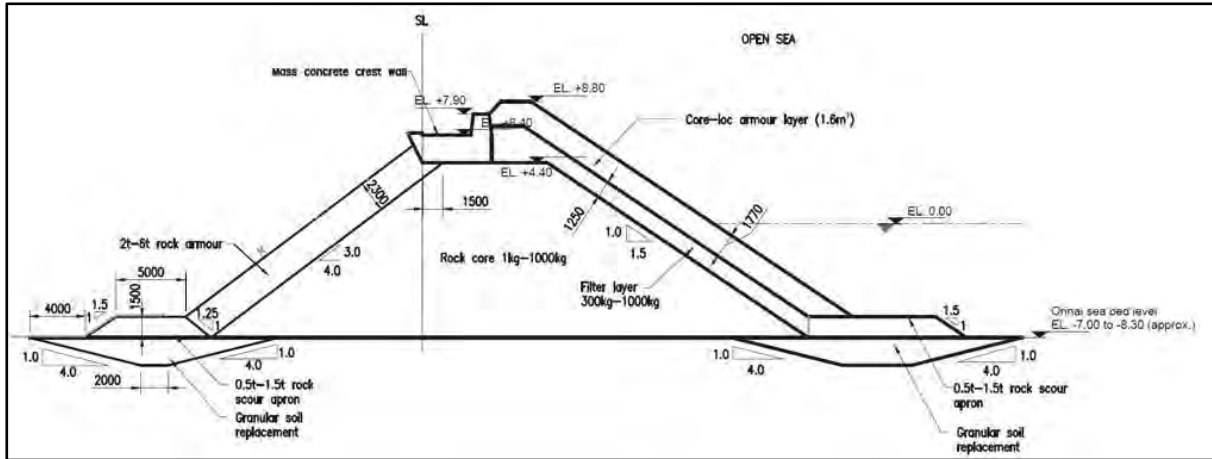


Figure 2 Sohar north breakwater (2007)

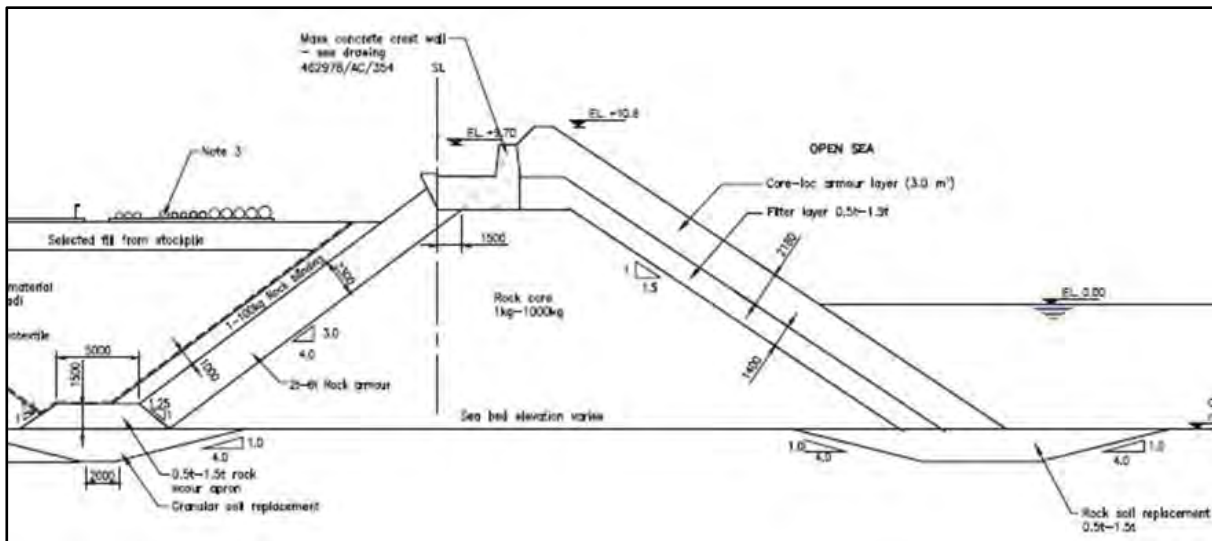


Figure 3 Sohar south breakwater (2007)

1.2 Tropical cyclone Gonu

In May 2007 tropical cyclone (TC) Gonu occurred on the Arabian Sea and was ultimately classified as a super cyclonic storm. Due to interaction with the dry Arabian Peninsula, TC Gonu decreased in intensity by the time it emerged in the Gulf of Oman and was degraded to a severe cyclonic storm and subsequently to a cyclonic storm on 7th of June just before it made landfall in Iran (Figure 4).



Figure 4 TC Gonu track, passing Sohar at 166 km distance (Source: Joint Typhoon Warning Centre)

1.3 Damage to the breakwaters

When TC Gonu passed the Port of Sohar, large waves hit the breakwaters resulting in large wave overtopping (Figure 5). Although no measured wave data are available during the passage of tropical cyclone Gonu, anecdotal evidence suggests that waves were up to 3-3.5 m in height lasting over a 48-hour period, with a wave period of about 7s (Ibn Khaldun-Halcrow, 2007).



Figure 5 Heavy wave attack and overtopping on the south breakwater during TC Gonu

A visual inspection of the breakwaters undertaken immediately after the passage of TC Gonu revealed the following damage to both the north and south breakwaters (Ibn Khaldun-Halcrow, 2007), (Baird, 2010):

- The inside roadway on the south breakwater (approximately between Ch. 1400-1900) was impacted by wave overtopping, with the platform corridor material, rock fill, and geotextile interlayer being displaced.
- Some of the pipelines on the inside of the south breakwater were displaced by rock fill moved during the storm. The inside face of the south breakwaters did not sustain any damage between Ch. 1900 and the roundhead.
- Several CORE-LOC™ units were displaced on the south breakwater, mainly between Ch. 1800 and 2900.
- The filter/under layer became significantly exposed in certain areas, specifically between Ch. 2060 and 2130 on the south breakwater. In other areas, the damage was not quite as significant; however, there are “fault lines” or seams between sets of units where the filter layer is exposed.
- It appeared that there was some settling of CORE-LOC™ units down the slope of the seaward side for both breakwaters.
- A few CORE-LOC™ units were broken on both breakwaters.
- The dive inspection did not show any real displacement of units underwater, nor did it show any broken units, nor did it show any units being deposited at the toe of the structure.

1.4 Investigations 2007 - 2014

The damage inflicted on the breakwaters was such that extensive surveys, studies and investigations were performed in the years 2007 – 2014 to record the damage to the breakwaters in detail, explain why tropical cyclone Gonu had such large effect on the breakwaters and provide recommendations for repair.

It goes beyond the scope of this paper to reflect on all these studies, but to repair the breakwaters it was basically recommended to remove all CORE-LOC™ armour units from the slopes of the north and south breakwater and replace them at a higher packing density (Halcrow Middle East LLC, 2014).

The cost implication of this recommendation was large. Cost estimates for repositioning of all CORE-LOC™ units ran into millions of Omani Rial (OMR) and consequently these repairs were not immediately carried out.

1.5 New tender

As the costs for the recommended full repair are so large, Sohar Industrial Port Company in 2016 launched a new tender for consultancy services to upgrade the breakwaters, with the clear objective to optimize the costs for repair. The services were awarded to Royal HaskoningDHV, primarily as the

proposed “cost based risk assessment” for the breakwaters aimed to identify whether the repairs recommended in the past could be justified from an economical point of view. The approach thereto and the outcome thereof are further discussed below.

2 METHODOLOGY TO THE COST BASED RISK ASSESSMENT

2.1 Repairs decision process

With the breakwaters clearly being damaged by TC Gonu it makes common sense to expect that there is a risk of further damages. The more important question is though whether this risk is small or large. In case of a small risk, one may decide to accept the risk. But in case the risk is (very) large, one would likely decide to repair the breakwater. Hence it is required to quantify the risk.

In order to quantify a risk there are two components to be addressed: the probability that an event happens and the consequences of that event. If an event is to happen frequently, one would like to see that (negative) consequences such as casualties, damages and economic loss due to such event are low or non-existent. High (negative) consequences are essentially never acceptable which in practical terms implies that the probability of occurrence of such event should be (very) small. So, assuming that the future damage risk of the current breakwaters can be quantified (being either high or low), the question remains: “when to decide to invest in a repair of the breakwaters?”

A repair of the breakwaters at this moment will require a substantial amount of money. But once the breakwaters have been repaired there will still be a risk that the repaired breakwaters could be damaged, even when there is a clear objective of the repair to reduce the remaining risk. Adopting that the investment in a repair should result in at least a reasonable reduction of the risk, it makes sense to do this repair only in case the present day repair costs are reasonably lower than the reduction in risk due to that repair. Assuming that the risk can be expressed in money (in this case OMR), the repairs would only be justified if:

$$\text{Repair costs} < \text{Present risk} - \text{Future risk}$$

2.2 Risk

2.2.1 Cost based risk

As discussed above a risk consists of two components: the probability of an event and the consequence of that event. Consequences of an event could be casualties, direct damages and indirect damages.

When looking at the TC Gonu type of environmental conditions (Figure 5) it is assessed that under extreme conditions no staff will be on or near the breakwaters and for the risk assessment of the breakwaters it will be assumed that the risk of casualties on the breakwaters will be extremely low. Hence loss of life or other casualties has NOT been taken into account in the risk assessment and breakwater repair decision process.

The risk assessment therewith becomes a cost based risk assessment in which the consequence of an event (like TC Gonu) is expressed in OMR. Based on this approach the risk is calculated as:

$$\text{Risk}_{\text{OMR}} = P_r(\text{event}) \times C_{\text{OMR}}(\text{event}) \quad (1)$$

Where the risk is expressed in OMR, P_r is the probability of occurrence of an event and C is the cost consequence of the event expressed in OMR.

The cost consequence of an event not only addresses the costs of damage to the breakwater itself (direct damage to the civil structure), but may also include the consequential damages. For instance in case the port or a terminal cannot be used for a certain period of time until repair has been carried out. It is assumed that these consequential damages can also be expressed in costs.

2.2.2 Proposed repairs and future risk

The studies that have been carried out in the past included different methods of repair. (Halcrow Middle East LLC, 2014) in particular mentions 3 methods:

- Base repair, i.e. rebuild the breakwater to the original design with a packing density of the armour units of $\phi = 0.57$.

- Repack all armour units above LAT to the latest recommended packing density of about $\phi = 0.63$ (CLI, 2012).
- Repack the full existing slope to latest CLI packing density about $\phi = 0.63$.

When such repairs are considered, the effect of such repairs on the future risk needs to be taken into account. Hence, also for these repairs a (future) risk assessment will be required.

2.2.3 Direct damage

To assess the risk, both the occurrence of an event and the consequence of an event need to be addressed. With respect to the latter, the consequences of TC Gonu in terms of direct damages to the breakwater can be summarized as follows (Baird, 2010):

- Displacement of CORE-LOC™ units along the slope of the breakwaters, resulting in “a higher than expected packing density in most areas on the underwater slope of the breakwaters” and “a general reduction in the packing density of CORE-LOC™ units on the above water breakwater slope” (Figure 6). Hence, the change in packing density is a consequence of the displacement of the armour units down the slope under the influence of incident wave conditions. This applies to both breakwaters (north and south).
- Another type of damage identified during the assessment relates to areas where the toe of the breakwater armour layer has been compromised. This deficiency exists at several locations on both the north and south breakwaters. This type of damage was observed in areas where it was apparent that there was a mass accumulation of units at the bottom of the slope.
- Approximately 35 broken CORE-LOC™ units were observed within the study area. Most of these remain within the interlocking grid and would only need to be replaced in areas where the repacking is required.
- The final type of damage or as-built non-conformance relates to armour units that were observed sitting on top of and outside of the interlocking grid.

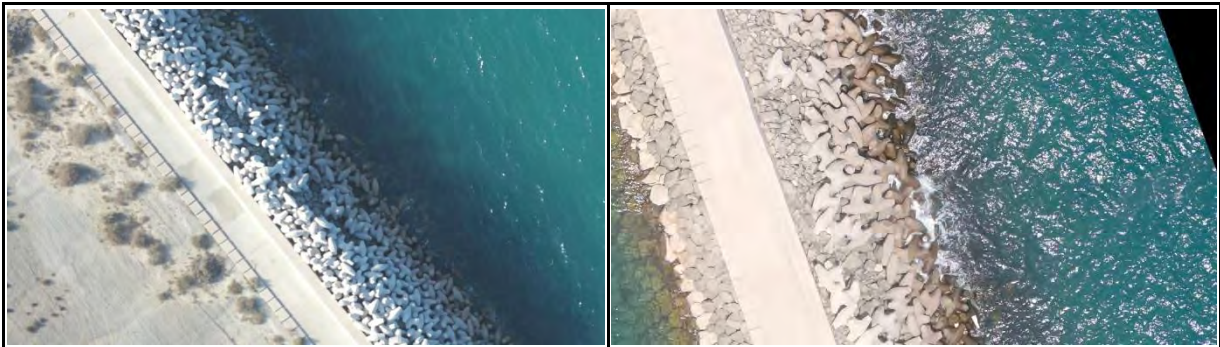


Figure 6 Impression of (local) damages after TC Gonu
Left: north breakwater. Right: south breakwater

Further, (Baird, 2010) observes that the main cause of damage is formed by the wave and water level conditions that occurred during TC Gonu.

Based on the above it is concluded that the risk of damage to the breakwaters is dominated by the probability of wave and water level conditions to occur. The consequences of these events are predominantly driven by the displacement of armour units. The latter in turn are affected by the (as constructed) packing density of CORE-LOCTM units. Displacements of the armour units in turn result in higher packing density and accumulation of armour units under water, a reduction in packing density above water, as well as a higher probability that armour units hit each other and break.

For a proper risk assessment in relation to this type of damage it will be required that:

- A clear relationship is established between the wave and water level conditions and the displacements of armour units or changes in packing density.
- The damage level is defined e.g. in terms of number of displaced armour units, for both the present and the repaired breakwater condition.
- A proper joint probability assessment of wave and water level conditions has been carried out and is available.

2.2.4 Indirect damage

No indirect damages are reported by (Baird, 2010) nor by (Halcrow Middle East LLC, 2014). But most likely indirect damages are to be expected in case overtopping of the breakwater becomes too high. In such event the operations behind the breakwaters will be affected (e.g. shut-down). For the north breakwater the (future) container terminal operations might be under threat in such an event and for the south breakwater the pipelines and/or the inside revetment rock layers might be under threat in such a case. Overtopping and how it relates to the indirect damage has been addressed in the studies by Royal HaskoningDHV, but does not form part of the present paper.

3 THE DAMAGE MODEL

3.1 Damage development

As discussed above, for the risk assessment of the breakwaters a relationship between wave and water level conditions and displacement of armour units and/or packing density will be required. But such damage function is not a priori defined. This is illustrated by the (2012) design guideline for CORE-LOC™ (CLI, 2012), which applies the Hudson formula to determine the size of the armour unit:

$$\frac{H_s}{\Delta \cdot D_n} := (K_D \cdot \cot \alpha)^{\frac{1}{3}} \tag{2}$$

The ratio between design wave height H_s (m) and unit size D_n (m) and relative density Δ (-) is a fixed value based on slope gradient and stability coefficient K_d .

Hence, in case the incident waves increase beyond the design wave and the size of the CORE-LOC™ is fixed, there is no indication what is to be expected for the damage to the breakwaters.

But it is obvious that damage has been inflicted by TC Gonu and one may question whether damage will not develop further. As literature does not provide information on the damage development to be expected, results of the available 2-D model tests for the 2013 base and upgrade repair method of the Sohar breakwaters have been used to develop such damage function.

When looking at concrete armour units, the Rock Manual (CIRIA; CUR; CETMET, 2007) provides the following relationships between damage and incident wave conditions for cubes and Tetrapods in a double layer:

| Type of armour | Design formula / relationship |
|---|--|
| Double layer of randomly placed cubes | $\frac{H_s}{\Delta D_n} = \left(6.7 \frac{N_{od}^{0.4}}{N^{0.3}} + 1.0 \right) s_{om}^{-0.1}$ |
| Double layer of randomly placed Tetrapods (surging waves) | $\frac{H_s}{\Delta D_n} = \left(3.75 \left(\frac{N_{od}}{\sqrt{N}} \right)^{0.5} + 0.85 \right) s_{om}^{-0.2}$ |
| Double layer of randomly placed Tetrapods (plunging waves) | $\frac{H_s}{\Delta D_n} = \left(8.6 \left(\frac{N_{od}}{\sqrt{N}} \right)^{0.5} + 3.94 \right) s_{om}^{0.2}$ |

Table 1: Relationships between damage and wave conditions for cubes & Tetrapods (CIRIA; CUR; CETMET, 2007)

From these formulae it follows that:

- The damage (N_{od} = number of displaced⁴ armour units in a D_n wide strip of the breakwater) is non-linearly dependent on $H_s/\Delta D_n$.
- The damage is non-linearly dependent on the number of waves N .
- The damage is non-linearly affected by the steepness (s_{om}) of the incident waves and thus dependent on the wave period (T_m).

⁴ Displaced here actually should be read as “extracted” instead of “settled”.

As these formulae do not only include the wave height, but also the wave period and the duration of the storm (i.e. number of waves), this type of formula has been taken as a starting point to develop a relationship between wave parameters and damage to the Sohar breakwaters, i.e.:

$$N_{od} := \left(\frac{H_s}{\Delta \cdot D_n} \right)^{\alpha_2} \cdot s_{0p}^{\alpha_3} \cdot N_w^{\alpha_4} \quad (3)$$

where the coefficients α_1 to α_4 are to be determined. To do this, a decision must be made which damage parameter to select, where particularly the available 2-D model test reports (HR Wallingford, 2013) on the base repair and upgrade repair provide data on:

- Displaced armour units, within different categories of displacement⁵:
 - Category 1: $0.1 \cdot D_n < \text{displacement} < 0.5 \cdot D_n$
 - Category 2: $0.5 \cdot D_n < \text{displacement} < 1.0 \cdot D_n$
 - Category 3: $\text{displacement} > 1.0 \cdot D_n$
- Rocking armour units.
- Extracted armour units.

Looking at the available model tests results, the amount of extracted units and rocking units showed to be so small that this data provide insufficient information to develop a clear dedicated damage function. Hence the number of displaced armour units has been taken as damage parameter.

To demonstrate the viability to select the number of displaced (settled) armour units as “damage parameter” in relation to the observed damages at the Port of Sohar, the following model of thought discusses the relations between packing density and armour unit displacements.

3.2 Relation between upslope and downslope packing densities

Assuming that no armour units are being extracted and that the units mostly displace downslope, the average packing density upslope (ϕ_1) is affected by the change in packing density downslope (ϕ_2) relative to an initial packing density (ϕ_0) and to the length of the (compacted) downslope L_2 relative to the total slope length L_0 (all based on continuity). Based on this approach the mean upslope packing density can be computed by the following relationship:

$$\phi_1(L_2, \phi_2) := \phi_2 + \frac{L_0}{L_0 - L_2} \cdot (\phi_0 - \phi_2) \quad (4)$$

Starting with $L_0 = 100$, L_2 can be interpreted as the percentage of the total slope (as $L_0 = 100$) having an increased packing density ϕ_2 . Starting with $\phi_0 = 0.58$ the effect of an increasing downslope packing density ϕ_2 on the upslope packing density ϕ_1 is shown in Figure 7:

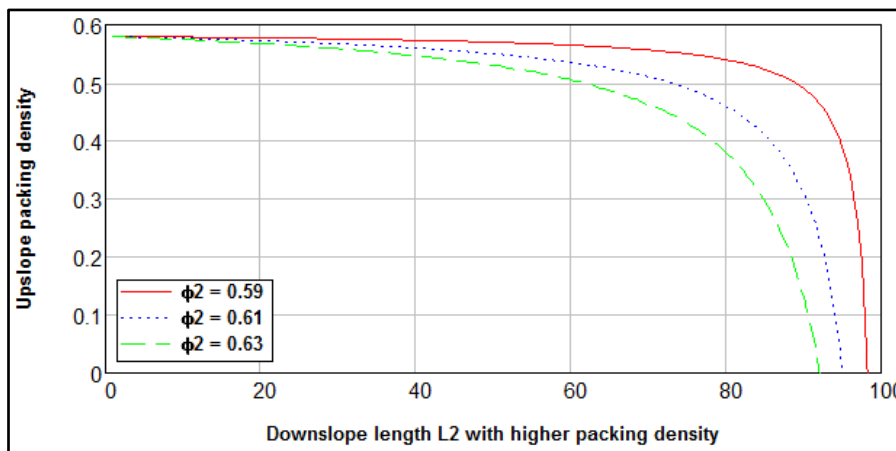


Figure 7: Theoretical effect of downslope packing density (ϕ_2) on upslope packing density (ϕ_1). Initial packing density is $\phi_0 = 0.58$.

⁵ Here displacement should be read as “settlement” instead of “extraction”.

Figure 7 indicates that very low packing densities in the upslope region should result in case the packing density in the lower slope region increases AND in case the length of this part of the slope increases (meaning that more and more units have moved down the slope).

3.3 Packing density and armour unit displacements

By definition, the packing density can be calculated as:

$$\phi := \frac{D_n^2}{D_h \cdot D_v} \tag{5}$$

Where D_h and D_v represent the horizontal and vertical placing distances of the armour units and $D_n = V^{1/3}$ where V represents the volume of an armour unit. Further using $D_v = D_h / 2$, this gives:

$$\phi := \frac{2 \cdot D_n^2}{D_h^2} \tag{6}$$

Given an aimed value for the packing density, the placing pattern D_v and D_h can be expressed in terms of D_n . This is shown below in Figure 8.

A packing density of $\phi = 0.57$ would result in $D_h = 1.873 \cdot D_n$ and $D_v = 0.936 \cdot D_n$. It is to be observed though that in the observations on the displacement of CORE-LOC™ units in the 2-D model tests, the minimum displacement considered is $0.1 \cdot D_n$ (lower limit Category 1 displacement). However, a change of $\pm 0.1 \cdot D_n$ in above figure (around $\phi = 0.57$) results in a variation in packing density of 0.52 to 0.63 (for D_h) and between 0.47 and 0.71 for D_v .

Hence, in case vertical displacements of $0.1 \cdot D_n$ result in compaction of the armour layer (typically under water) the packing density would increase theoretically to nearly 0.71. However, in case vertical displacements result in loosening of the armour layer (typically above water), the packing density may reduce to 0.47. Larger displacements obviously have an even larger impact on the packing density.

Albeit that this is a theoretical result and assumes that all (or many) armour units displace, the results are in fair agreement with the model tests and prototype observations. The warning is that the displacement of the armour units appears to have a large effect on the packing density. Many armour units showing even a small displacement may have a positive impact on the stability of the armour units when the armour layer compacts (lower part of the slope), but a negative impact when the armour layer loosens up (upper part of the slope). For larger displacement this effect becomes larger.

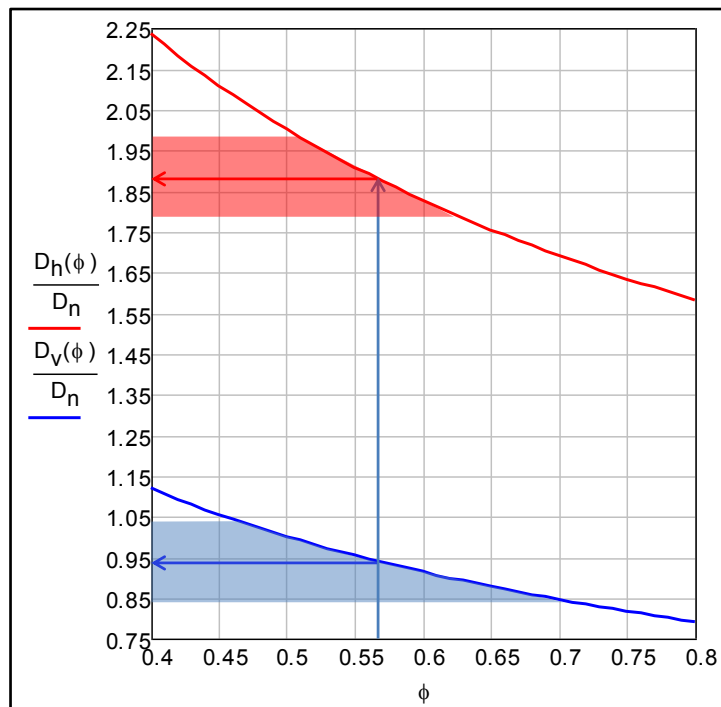


Figure 8: Effect of packing density on placing distances and vice versa

Using the above two theoretical models on the packing density, it is possible to couple downslope displacement of armour units (resulting in a compaction of the armour layer) with an upslope reduction in packing density, as shown in Figure 9.

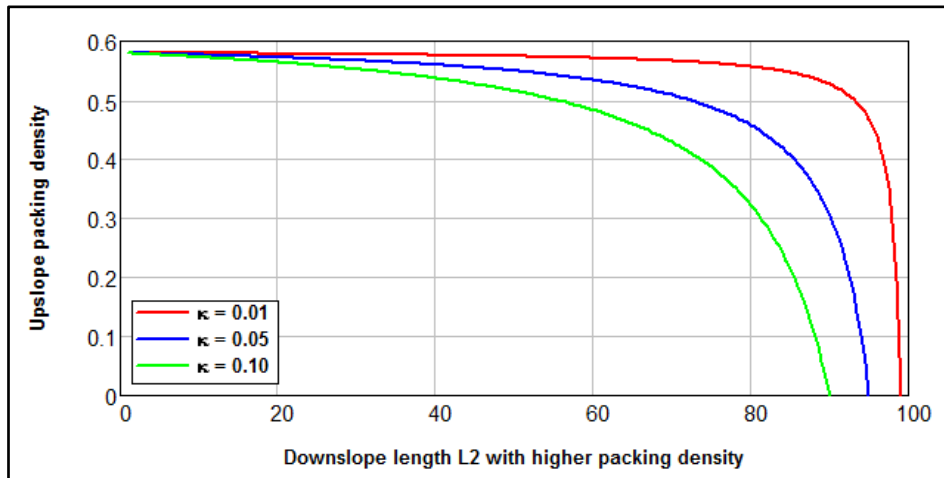


Figure 9: Effect of downslope displacements ($\Delta D_v = \kappa \cdot D_n$) on upslope reduction in packing density. Initial packing density is $\phi_0 = 0.58$.

Figure 9 demonstrates that, assuming a change in downslope packing density due to displacements of say $\kappa = 0.05 \cdot D_n$, the average upslope packing density reduces to about $\phi = 0.45$ in case 80% of the downslope armour is being compacted. When κ increases to $0.10 \cdot D_n$ such low upslope packing density is already reached when 2/3 of the total slope is compacted due to such displacements. Theoretically the upslope packing density only remains unaltered when there is no compaction (settlement) in the downslope area at all.

The conclusion to be drawn from this “model” is that even small displacements of many armour units (often interpreted as “initial settlement”) may have a large effect on the packing density of the armour units in the upper regions of the slope. Hence, selecting displacements larger than $0.1 \cdot D_n$ (rather than $0.5 \cdot D_n$ or $1.0 \cdot D_n$) as damage parameter in the envisaged damage model makes sense.

Apart from this it may be questioned whether the classification of the displacements in the model tests (not addressing displacements less than $0.1 D_n$) has been chosen wisely as smaller displacements may also result in reduced packing densities on the upper slope. Finally it may be questioned whether the common practise to neglect “initial settlement” as damage is justified. The above model suggests that any displacement after construction of the armour unit layer should be interpreted as damage.

3.4 Modified damage function

From the investigations into the damage of the Sohar breakwaters and above considerations it has become clear that the initial packing density of the CORE-LOC™ units affects the stability of the armour units. Therefore the initial (as-built) packing density (ϕ) preferably should be included in the damage function as well. This can be done in different ways, but as a lower packing density is assessed to affect the stability of the armour units in a negative way, the following basic relationship has been applied:

$$N_{od} := \left(\frac{H_s}{\alpha_1 \cdot \phi} \right)^{\alpha_2} \cdot s_{op}^{\alpha_3} \cdot N_w^{\alpha_4} \quad (7)$$

- where: N_{od} = Number of displaced (settled) CORE-LOC™ armour units in a strip D_n wide, accumulated during the test
 H_s = H_{m0} = significant wave height
 s_{op} = Wave steepness = $H_{m0} / (g T_p^2 / (2\pi))$
 N_w = Number of waves
 ϕ = Packing density at the start of the test
 α_i = Coefficient (to be determined)

It is emphasized that the packing density is the initial packing density of the armour layer. The effect of reduced packing densities in the armour layer due to settlement in the layers is implicitly included in the results of the model tests themselves.

3.5 Final damage model

Taking equation (7) as a starting point, coefficients α_i were established by finding the fit resulting in the least squared error between calculated and observed N_{od} numbers. The best fitted results and coefficients are presented in Table 2:

| | α_1 | α_2 | α_3 |
|--|------------|------------|------------|
| ■ North breakwater (repair full slope) | 5.0491 | 2.1309 | -0.3671 |
| ■ South breakwater (repair full slope) | 5.4503 | 1.829 | -0.2736 |
| ■ South breakwater (repair above LAT) | 7.7803 | 4.452 | -0.8383 |

Table 2: Best fit α coefficients for damage function

The result of the fitting analysis reveals that:

- There is a strong non-linear relation between N_{od} and H_{m0} ($\alpha_2 > 1$) which is in line with stability relationships for other armour units and rock.
- There is an inverse proportionality with s_{op} ($\alpha_3 < 0$) indicating that lower steepness results in more damage. In turn this implies that longer waves (higher wave periods) result in more damage, which also is to be expected (based on experience).

The fitting procedure revealed that there was no clear relationship with the number of waves ($\alpha_4 = 0$), most likely since the number of waves in the model tests is more or less the same for all tests. Hence the number of waves is not included in the present damage function. From the figure included in Table 2 it can finally be observed that the resulting functions give a very reasonable prediction of the damage to be expected, but that there is still some scatter around the calculated values.

It is to be noted that, theoretically, this damage (or better: settlement) function could be applied to design CORE-LOC™ armour layers, however this is not advised and supported by the authors of this paper for the following arguments:

- Results and coefficients are based only on series of tests for this dedicated, single project.
- Results and coefficients are site dependent (e.g. affected by the specific particulars of the site like wave conditions and/or bathymetry and water level).
- It is unclear what damage number to use for “acceptable damage” or “failure”.

Still, given the relationship found between damage and incident wave conditions, it seems worthwhile (in general) to carry out additional investigations into this “damage” function. Not only for the CORE-LOC™ armour unit, but also for other single layer armour units as it is expected that the found trend may apply to other armour units as well.

4 QUANTIFICATION OF THE COST BASED RISK ASSESSMENT

The cost based risk assessment for the CORE-LOC™ armour layer requires the probability of an event and the consequences of the event (damage) expressed in OMR. The probability of an event is dominated by the probability of occurrence of the wave conditions. The consequences are dominated by the expected damage to the CORE-LOC™ armour layer.

4.1 Wave conditions and probability

4.1.1 Nearshore wave statistics

The nearshore wave conditions at the locations of the north breakwater trunk and the south breakwater are presented in Figure 10 and Figure 11.

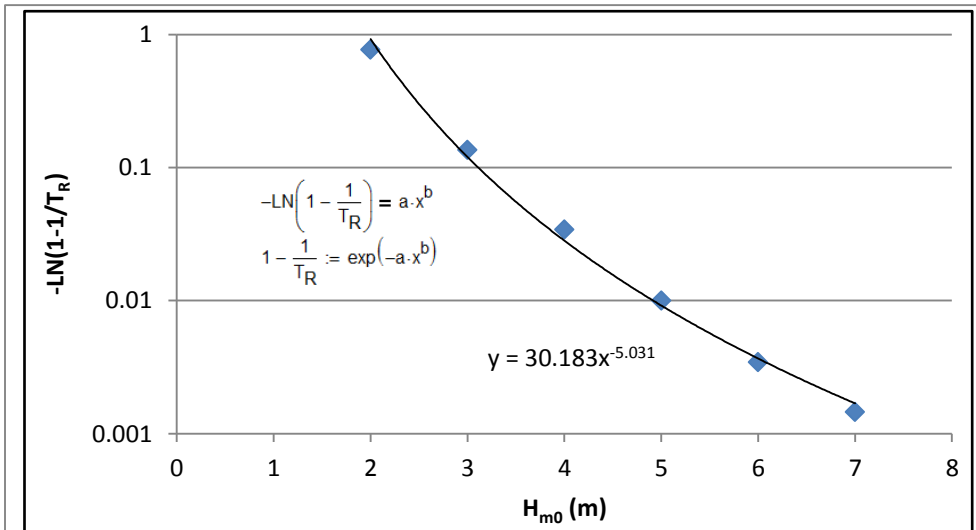


Figure 10 Non-exceedance probability function for the north breakwater.
 T_R = return period, H_{m0} = spectral significant wave height

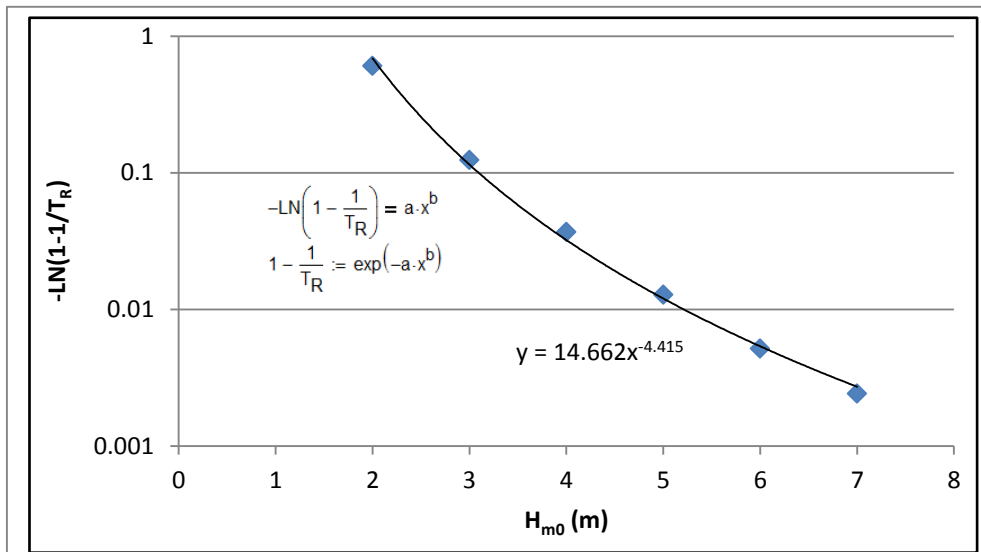


Figure 11 Non-exceedance probability function for the south breakwater.
 T_R = return period, H_{m0} = spectral significant wave height

The above probability functions represent the long term average probability on an annual basis. When the lifetime of the structure is to be included, the probability that a wave condition is NOT being exceeded in this lifetime $K(H_{m0})$ can be calculated by:

$$K(H_{m0}) = (F(H_{m0}))^{N_{yrs}} \tag{8}$$

where N_{yrs} is the lifetime of the breakwaters in years. The probability density function $k(H_{m0})$ is by definition the derivate of $K(H_{m0})$. An example of these functions is presented below for the south breakwater:

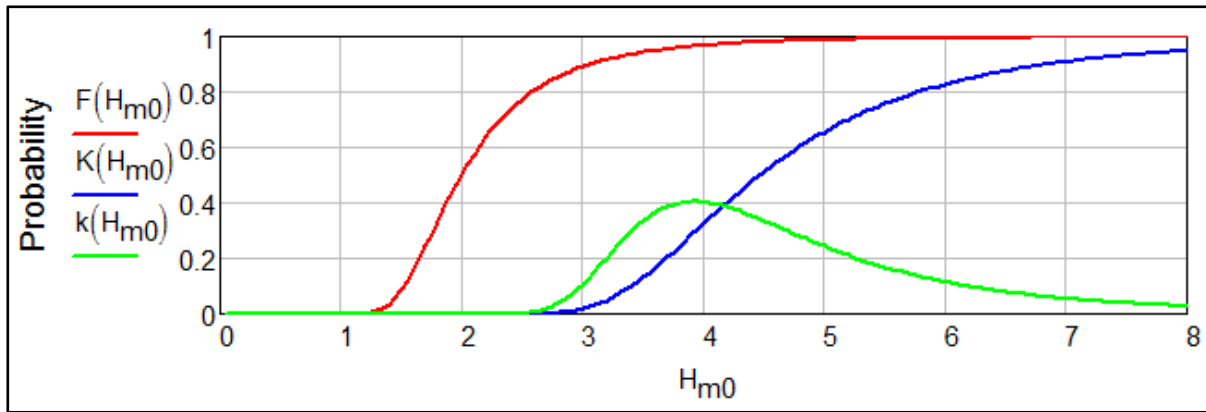


Figure 12 Probability functions for the south breakwater (similar for the north breakwater)

From Figure 12 it can be interpreted that the probability per year (■) that a wave height H_{m0} is smaller than 4m is 97% (hence a very small chance that it will be larger than 4m). But the probability that it will (always) be smaller than 4m during the (remaining) lifetime of the breakwater of 35 years (■) is 32% (hence a fairly large chance it will happen at least once in the lifetime that a wave height H_{m0} will be larger than 4m).

The probability density function (■) indicates that of the higher waves ($H_{m0} > 2.5m$) to occur during the remaining lifetime of the structure, most of these wave will be in the order of 4 m. The probability that these waves will reach wave heights in the order of 7 to 8 m is small.

4.1.2 Wave height – wave period relationships

The nearshore $T_p \sim H_{m0}$ relationships as given in Table 3.

| Location | $T_p \sim H_{m0}$ relationship |
|------------------|---|
| North breakwater | $T_p(H_{m0}) := 5.9847 \cdot H_{m0}^{0.467}$ |
| South breakwater | $T_p(H_{m0}) := 5.4788 \cdot H_{m0}^{0.4561}$ |

Table 3: Relationships between peak wave period T_p and near shore significant wave height H_{m0}

As the differences in coefficients at the two locations are small, also the differences in wave periods and wave steepness's between the two breakwaters are small.

4.2 Damage as function of wave height

Filling in the $T_p \sim H_{m0}$ relationship in the damage function (7), the damage function becomes a function of H_{m0} only (for a fixed value of N), as shown in Figure 13. From this figure it can be observed that for a given wave height H_{m0} and more or less the same T_p (see Table 3) the north breakwater shows much more damage than the south breakwater. This is obvious since the CORE-LOC™ armour units on the north breakwater are smaller than those on the south breakwater. Apart from this, changing the packing density from $\phi = 0.57$ (Base Repair) to $\phi = 0.63$ (Upgrade Repair UR3) indeed reduces the damage to be expected, but not that much.

Also the south breakwater shows that a lower packing density ($\phi = 0.57$, Base Repair) results in more damage than in case of a higher packing density ($\phi = 0.63$ Upgrade Repair UR2). But more interesting to see is that the Upgrade Repair 1 (UR1, repacking above LAT with $\phi = 0.63$) results in less damage compared to the Base Repair and UR2 in case the wave heights remain below about 6.5m. For wave heights larger than 6.5m the damage for UR1 will be larger than for Base Repair and UR2.

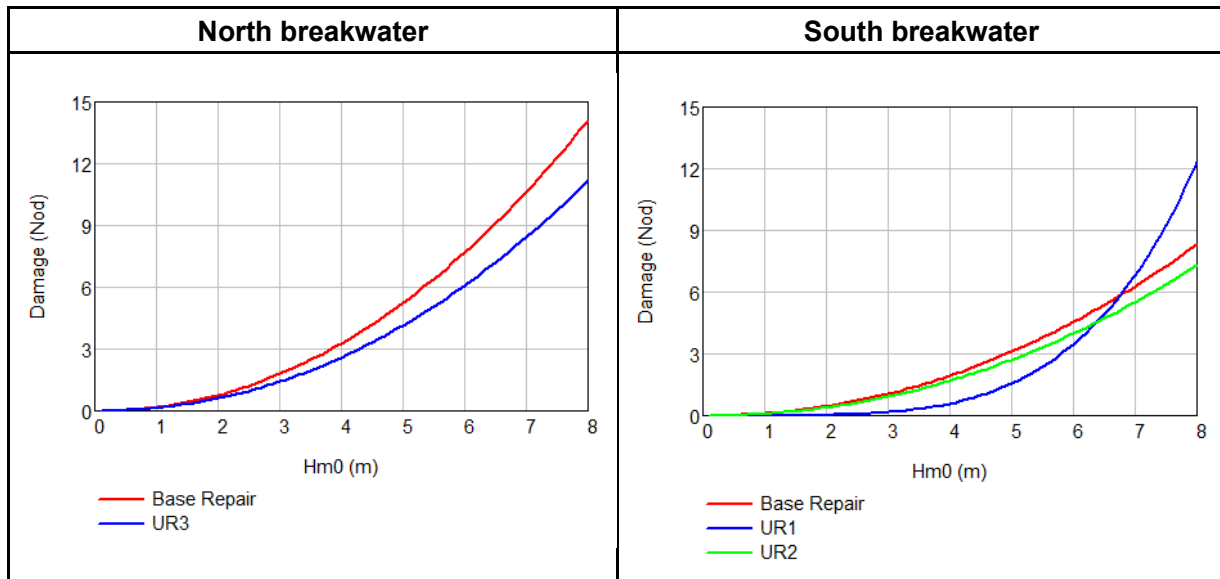


Figure 13 Damage as function of H_{m0} (Base repair: $\Phi=0.57$ full slope, UR1: $\Phi=0.63$ above LAT, UR2: $\Phi=0.63$ full slope, UR3: $\Phi=0.63$ full slope)

4.3 Development of damage cost functions

From the above it is clear that the physical damage, i.e. settlements expressed as N_{od} value, to be expected as function of the wave conditions can be calculated (Figure 13). However, for the cost based risk assessment this physical damage needs to be converted to damage costs.

The best guidance for the assessment of the damage costs being equivalent to the repair costs is provided by studies carried out between 2008 and 2014 (Halcrow Middle East LLC, 2014). These costs have been increased to a 2016 price level taking into account a 3% indexation (Table 4). It is noted that in the year 2016 one OMR equalled about 2.6 USD.

| Repair method | North breakwater | | South breakwater | |
|----------------------------------|------------------|-----------------------------------|------------------|-----------------------------------|
| | Full slope | Partial slope = 60% of full slope | Full slope | Partial slope = 60% of full slope |
| Repack CORE-LOC™ armour units | | | | |
| Base repair ($\phi = 0.57$) | 2480 | - | 3010 | - |
| Upgrade repair ($\phi = 0.63$) | 2590 | 1760 | 3120 | 2045 |

Table 4: Costs for repair (OMR per running meter breakwater, 2016 price level) as input to cost based risk assessment

These repair costs typically apply for the condition of the breakwater as presently observed. However, it is to be expected that the repair costs will increase in case the damage to the breakwater CORE-LOCS™ would increase in case of future higher waves (H_{m0}), inflicting additional damage. As this damage is mostly correlated to the further displacement of armour units, for the cost based risk assessment it has been adopted that the direct damage costs increase proportionally with the damage assessment (N_{od}) relative to the present damage. The present damage is formed by the damage due to TC Gonu corresponding to an incident wave height of about $H_{m0} = 3.8m$. Combining the damage costs with the damage functions shown in Figure 13, the found damage cost functions are shown in Figure 14.

The damage cost functions demonstrate that, assuming the same wave height, the economic damage to the north breakwater will be larger than to the south breakwater. This is primarily driven by the higher physical damage (N_{od}) due to the smaller CORE-LOC™ armour unit. The damage costs will be higher for UR3 as the higher packing density requires more armour units to be placed.

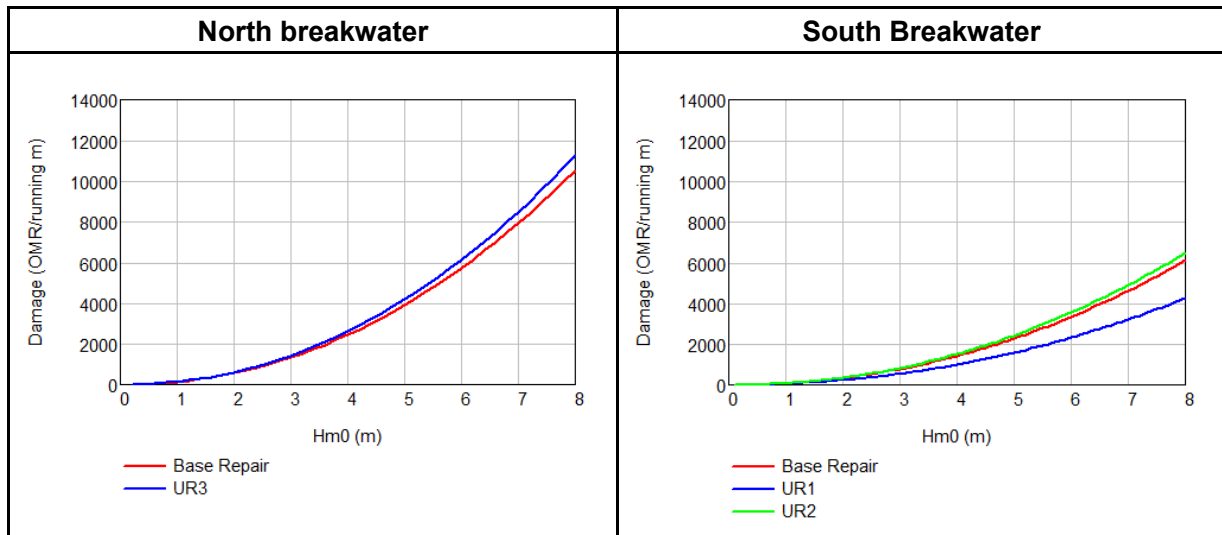


Figure 14 Damage costs as function of H_{m0} , 2016 price level. (Base repair: $\Phi=0.57$ full slope, UR1: $\Phi=0.63$ above LAT, UR2: $\Phi=0.63$ full slope, UR3: $\Phi=0.63$ full slope)

The same observation can be made for the south breakwater. The damage costs overall are smaller compared to the north breakwater due to the larger armour unit and next to that the variation in packing density affects the costs as well. As the UR1 repair only includes a repair above LAT, the damage costs are lower than for Base Repair and UR2.

When including the above indicated costs in the cost based risk assessment, these costs shall be interpreted as “loss of value” due to (future) damage to the repair alternative addressed, irrespective of the actual repair action. For example, in case a future damage would result in an assessed cost of 3000 OMR/running meter and this damage would not be repaired (for whatever reason), then still the damage = “loss of value” = 3000 OMR/running meter even though no money is spent on such repair.

The above costs reflect direct cost linked to the repair of the breakwater armour layers. As mentioned earlier, no indirect damages resulted from TC Gonu, hence it is assessed that the amount of indirect costs related to an armour repair of the settled armour units will be limited.

4.4 Cost based risk assessment

The final step in the cost based risk assessment is combining the occurrence of an event with the damage costs of such event. The procedure is demonstrated in Figure 15 below. The damage costs due to a wave of e.g. $H_{m0} = 4.5\text{m}$ to the Base Repair of the south breakwater is multiplied with the probability (density) that this wave height will occur⁶ once in the 35 year lifetime of the structure. This is repeated for all possible wave heights to occur. Adding all contributions results in a **cumulative risk**, expressed in money (OMR).

⁶ As damage increases for increasing wave height, the probability of occurrence in 35 years is to be used, not the probability of exceedance. Hence the probability density function $k(H_{m0})$ needs to be used.

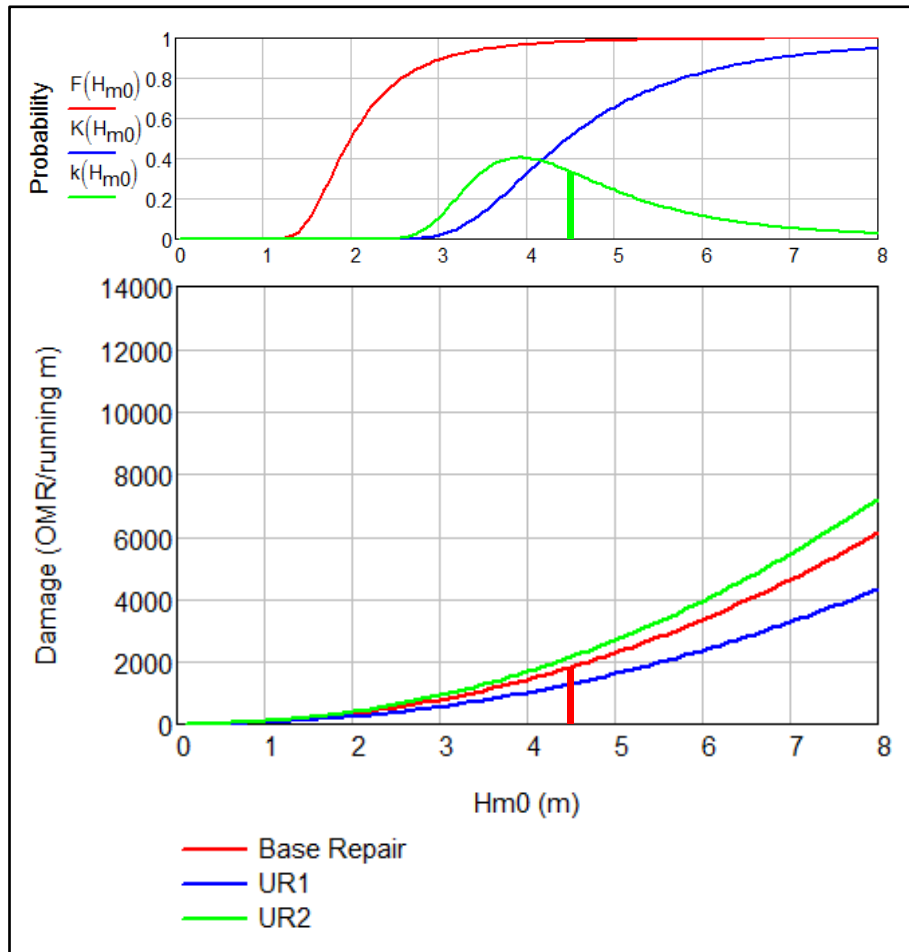


Figure 15 Procedure cost based risk assessment (2016 price level)

As the damage functions have been determined on the basis of the 2-D model tests, the risks typically apply to the repair solutions as included in the available Base Repair and Upgrade Repair model test reports. In short these can be summarized as:

- **No Repair**

In case the present (damaged) breakwaters are not being repaired, the risk over the remaining lifetime of the breakwater needs to be added to the damage that has already been inflicted on the breakwater. The present damage cost results from the damage cost functions (for the Base Repair) using a wave as occurred during TC Gonu, which is in the order of $H_{m0} = 3.7$ to 3.8m . For the risk assessment in case of No Repair then only larger wave heights need to be taken into account based on the damage cost function for the Base Repair (original packing density).

- **Base Repair - repack full slope, $\phi = 0.57$**

This breakwater repair alternative particularly represents the original design (and original packing density) of the breakwaters. For the cost based risk assessment it is adopted that the damage development of this alternative is representative for the current breakwaters.

- **No Repair**

In case the present (damaged) breakwaters are not being repaired, the risk over the remaining lifetime of the breakwater needs to be added to the damage that has already been inflicted on the breakwater. The present damage cost results from the damage cost functions (for the Base Repair) using a wave as occurred during TC Gonu, which is in the order of $H_{m0} = 3.7$ to 3.8m . For the risk assessment in case of No Repair then only larger wave heights need to be taken into account based on the damage cost function for the Base Repair (original packing density).

- **Repack full slope, $\phi \approx 0.63$**

In this repair approach all armour units have to be removed and placed back with a higher packing density.

- **Repack above LAT, $\phi \approx 0.63$**

In this repair all armour units have to be removed and placed back with a higher packing density, but “only” above LAT level.

The results of aforementioned costs based risk assessment are presented in Table 5.

Table 5: Accumulated economic risk for armour displacement (OMR per running metre breakwater) over 35 years lifetime of the breakwater. 2016 price level.

Note: Differences in risk (Δ risk) taken relative to the No Repair alternative

| Option | North breakwater | | South breakwater | |
|--|------------------|---------------|------------------|---------------|
| | Risk | Δ Risk | Risk | Δ Risk |
| No Repair | 5,487 | - | 5,227 | - |
| Repack full slope, $\phi = 0.57$ | 3,776 | -1,711 | 3,564 | -1,663 |
| Repack full slope, $\phi \approx 0.63$ | 3,122 | -2,365 | 3,085 | -2,142 |
| Repack above LAT, $\phi \approx 0.63$ | 3,492 | -1,995 | 4,059 | -1,168 |

From Table 5 it can be observed that, as the breakwaters are already damaged, the economic risk itself is the highest for the damaged breakwater and all repair options result in a reduction of that risk. This is in line with the expectations. The biggest risk reductions are achieved when the armour units would be repacked with a density of 0.63 over the full length of the slopes of the north and south breakwater. In such event the risk reduction on the north breakwater is slightly higher (per running meter) than on the south breakwater. Whether the assessed reduction in risk justifies the investment in repair is discussed below.

4.5 Economic benefit of potential breakwater repair or upgrade

Using the cumulative economic risk values of Table 5 it is possible to quantitatively indicate whether a potential repair or upgrade of the damaged primary armour slopes of the north and south breakwater is beneficial from an economical point of view.

There to it is additionally required to incorporate the anticipated inflation over a period of 35 years (i.e. the remaining design life) and thereupon discount the inflated economic risk to a 2016 price level (i.e. incorporate an average interest rate over 35 years). When a long term inflation rate of 3% is chosen and an interest rate of 4%, the quantitative results presented in Table 6 show that:

- It is not beneficial to fully re-pack any of the two breakwaters with the originally applied packing density of 0.57 (i.e. Base Repair full slope): it would lead to a negative investment of about 3 million OMR for the south breakwater and of about 2.5 million OMR for the north breakwater, given the length of both breakwaters.
- Also upgrading the complete armour slope to a packing density of 0.63 (i.e. Upgrade Repair full slope) is economically not attractive: it would lead to a negative investment of about 2.7 million OMR for the south breakwater and of about 1.8 million OMR for the north breakwater.
- Upgrading the damaged breakwaters with a packing density of 0.63 at only that part of the primary armour slope which is located above LAT, gives in total the lowest negative investment: at the south breakwater a negative investment of about 2 million OMR is found, whereas upgrading the north breakwater leads to a negative investment of about 660,000 OMR; thus in total a negative result of 2.66 million OMR.

| Design life = 35 years | Cumulated risk in design life [2016] | Cumulated risk discounted | Reduction in cumulated risk relative to 'No Repair' | Present day repair investment | Repair benefit in design life |
|---|--------------------------------------|---------------------------|---|-------------------------------|-------------------------------|
| South breakwater (OMR/m') | | | | | |
| Option: | | | | | |
| No repair | 5227 | 3727 | 0 | 0 | 0 |
| Base repair full slope ($\phi = 0.57$) | 3564 | 2541 | 1186 | 3010 | -1824 |
| Upgrade repair above LAT ($\phi = 0.63$) | 4059 | 2894 | 833 | 2045 | -1212 |
| Upgrade repair full slope ($\phi = 0.63$) | 3085 | 2200 | 1527 | 3120 | -1593 |
| North breakwater (OMR/m') | | | | | |
| Option: | | | | | |
| No repair | 5487 | 3913 | 0 | 0 | 0 |
| Base repair full slope ($\phi = 0.57$) | 3776 | 2693 | 1220 | 2480 | -1260 |
| Upgrade repair above LAT ($\phi = 0.63$) | 3492 | 2490 | 1423 | 1760 | -337 |
| Upgrade repair full slope ($\phi = 0.63$) | 3122 | 2226 | 1686 | 2590 | -904 |

Table 6: Economic “benefit” (in OMR per running metre breakwater) of repairing or upgrading the ‘damaged’ breakwaters

4.6 Actual breakwater repair

Based on the above cost based risk assessment it has been concluded that the considered repair methods are not justified. The economic benefit of any of these considered options is less than the investment cost for present day repair. However, this does not imply that the breakwaters are not being repaired at all. As discussed and agreed with the owners of the port, it was decided to do so-called “no-regret” spot repairs at several isolated locations. These small scale repair actions do focus on areas along the slope above LAT level where the interlocking between adjacent armour units has disappeared completely and moreover the secondary armour stone at these spots is fully exposed beyond an agreed area (leading to a far too low local packing density).

5 CONCLUSIONS

From the early ages of the introduction of single layer armour units, breakwaters with these units, like the breakwaters for the Port of Sohar, are typically designed on the basis of the Hudson formula (2). Drawback of this formula is that it does not provide a relation between incident wave conditions and damage to the armour layer. Model tests performed to confirm such breakwater designs apply criteria like “no extractions” and “minimum rocking”. Model tests for the Port of Sohar confirmed that these criteria were being met.

Still, after the passage of TC Gonu, clear damages were inflicted on the breakwaters of the Port of Sohar, mostly in the form of displacement (settlement along the slope) of the concrete armour units. This shows that, apart from “extractions” and “rocking”, displacement of armour units is to be interpreted as damage. The displacement of the armour units on the breakwater of the Port of Sohar resulted in reduced packing densities above water and increased packing densities under water. Expectedly, the reduced packing densities above water may even form the onset to (higher risk of) extractions and rocking (Lem, Stive, & Gent, 2016).

The cost based risk assessment for the breakwater repair for the Port of Sohar confirms that the displacement of the armour units appears to have a large effect on the packing density of the armour layer. Many armour units showing even a small displacement may have a positive impact on the stability of the armour units when the armour layer compacts (lower part of the slope), but a negative impact when the armour layer loosens up (upper part of the slope). For larger displacement this effect becomes larger. The conclusion to be drawn from this is that even small displacements of many armour units (often interpreted as “initial settlement”) may have a large effect on the packing density of the armour units in the upper regions of the slope. Hence, it may be questioned whether the common

practise to neglect “initial settlement” of armour units in terms of damage is justified. The present analysis suggests that any clear displacement i.e. settlement after construction of the armour unit layer should be interpreted as damage.

Taking this as a starting point and using available model test results, a relation was sought and found between the displacement of the armour units applied for the Sohar breakwaters (CORE-LOC™), the incident wave conditions, the size of the armour units and the packing density of the armour units. Theoretically, the resulting damage function (7) and coefficients (Table 2) can be applied to design CORE-LOC™ armour layers, however this is not advised and supported by the authors of this paper (and likely not permitted by the licensee as well) for the following arguments:

- Results and coefficients are based only on series of tests for this dedicated, single project.
- Results and coefficients are site dependent (e.g. affected by the specific particulars of the site like wave conditions and/or bathymetry and water level).
- It is unclear what damage number to use for “acceptable damage” or “failure”.

Still, given the damage function found it seems worthwhile (in general) to carry out additional investigations. Not only for the CORE-LOC™ armour unit, but also for other single layer armour units as it is expected that the found trend applies to other single layer armour units as well. Once the damage function has been confirmed, it is anticipated that it can be applied to design single layer armour units, by taking appropriate damage i.e. settlement criteria, as a function of the incident wave conditions. By limiting the number of displacements (settlement) it is anticipated that implicitly other criteria like “extractions” and “rocking” will be met.

In the present analysis, dedicated to the Port of Sohar, the damage function has been used to assess the damage development for the (already) damaged breakwaters of the Port of Sohar and for a number of repair strategies. As the found damage function also predicts the damage development of the repaired breakwaters, the effectiveness of these repair options could be assessed in terms of (repair) cost versus benefit (reduction in economic risk). The outcome of the cost based risk assessment shows that the proposed (large scale) repairs are not economically justified. Instead the repairs presently in progress only address local spots on the breakwater slope above water where repairs are deemed necessary anyhow.

CORE-LOC™

In this document the name CORE-LOC™ is used frequently. The concrete unit has been developed and patented by the US Army Corps of Engineers (USACE) in the mid 1990's, and is nowadays also licensed by Concrete Layer Innovations (CLI). Wherever “CORE-LOC” is written this should be read as “CORE-LOC™”.

References

- Baird. (2010). *Post-Gonu Damage Assessment and Remedial Action*.
- CIRIA; CUR; CETMET. (2007). *The Rock Manual. The use of rock in hydraulic engineering (2nd edition)*. London: C683, CIRIA.
- CLI. (2012). *Guidelines for design - CORE-LOC™*. Concrete Layer Innovations.
- Halcrow Middle East LLC. (2014). *Consultancy services for the base repair and upgrade repair of the Sohar industrial port breakwaters - Upgrade design final report*. Muscat, Oman.
- HR Wallingford. (2013). *Sohar industrial port breakwaters - repair and upgrade. 2D physical model base repair testing report*. CAR5064.
- Ibn Khaldun-Halcrow. (2007). *Sohar Industrial Port: Cyclone Gonu*. Sultanate of Oman.
- Lem, J.C. van der; Stive, R.J.H.; Gent, M.R.A. van. (2016). *Sal Rei breakwater with single layer cubes. PIANC-COPEDEC IX*. Rio de Janeiro, Brazil: PIANC.

INTEGRATED ASSET MANAGEMENT: PREDICTIVE & FUTURE RESPONSIVE

by

Henk Voogt¹

1. INTRODUCTION

In the recent years Port of Rotterdam worked on a higher level in Asset Management of its maritime infrastructure, which is confirmed by achieving the ISO 55000 certification. The currently running program Integrated Asset Management adds to this basis to look at the assets as part of the logistics chain and/or nautical process and ensure the availability of (asset related) information for all in the chain involved parties, not only within the Port of Rotterdam organization but beyond, such as customers and other stakeholders.

The customers and stakeholders want to know more about the assets, but we want to know more about how customers use and need the assets with the aim of increasing efficiency in all parties. In society and the world around us we see increasingly challenges that result in threats and opportunities, not just for individuals and the environment, but also for organizations such as the Port of Rotterdam. This includes issues such as climate change, world population growth and more specific issues for the port authority like energy transition, autonomous sailing, alliances in the container transport and the demand for mobility.

At the same time, there is exponentially increase in digitization. Everything is measured or can be measured and is available digitally. Port of Rotterdam will have to prepare for major changes in the field of digitization and robotization in the port, which is already recognized in the ports digitization strategy: Port of Rotterdam's aim is not only to have the best port infrastructure, but also the smartest. Same goes for the assets of Port of Rotterdam in the future. Where the assets are "dumb" now, they will be in the future equipped with smart sensors. These sensors monitor continuously the assets of Port of Rotterdam Integrated, anywhere in the Port, all at the same time, all together and on every second of the day, assets will cooperate with each other. Hence: "the inspector of the future is a sensor."

No longer doing things right, but doing the right things in asset management. Using smart and integrated analyses (Analytics) that make it possible to understand and anticipate better and that now are still unknown and unforeseen. Analytics within Asset Management is seen as one of the critical success factors to assets and modalities to make timely measures and developments in the port. Analytics allow us to make future-oriented decisions based on facts, so called ' what-if ' scenarios and to develop aging models based on actual use. This allows us to optimize the performance of assets and modalities based on real time and future use (like predictive maintenance and future-responsive). Analytics will also tell us on which areas still insufficient information is available to support adequate decision-making. Also analytics will trigger for the tuning of appropriate information based on, among other things, sensors, external data sets, and big data.

The availability of (real time) data will also provide benefits in the design of new assets. Integrated asset management does not start when a new asset is built and delivered, but gives added value in the design process, by making clear what the longer term effects are of choices in the design, based on data from actual use. In the end it delivers a saving of deployment of hours and money.

On several areas there is now talk about scaling up, so also in asset management. Eventually, the shared information, lead to systems that are associated with each other and communicate with each other independently, a complex of systems, where plans, information and so on is shared between organizations and leads to more cooperation and decision making based on the interests of the entire

¹ Port of Rotterdam, Asset Management Constructions, h.voogt@portofrotterdam.com

chain of systems. What eventually leads to an even more efficient port management. The benefits are evident.

2. AT THIS POINT: DOING THE THINGS RIGHT

Since the early days The Port of Rotterdam is building waterfront assets to facilitate the processes of her clients and to guarantee a safe and smooth mooring process of the ships that call Rotterdam. Maintaining the assets is bound to building the assets.

The traditional asset management will change on important points in the coming years drastically due to digitalization and robotizing In the past ten years ever growing effort was put in implementing asset management processes and tools to deal with ever deteriorating assets, risks, investments and service levels.

Based on this effort the Port of Rotterdam was rewarded as the world's best waterfront infrastructure by the World Economic Forum (see: 2015/2016 Global Competiveness Report). Besides that the Port of Rotterdam was the first port authority ever to achieve the PAS55 / ISO55001 certificate for the quality of its asset management process.

3. BUT: TIMES ARE CHANGING:

In the world around us and we experience ever increasing challenges that result in threats and opportunities, not exclusively for individuals and the environment but also for organizations like the Port of Rotterdam. Think about the climate change and the growth of the global population and more specific for the Port of Rotterdam: the energy transition, autonomous sailing ships, alliances in the container transport and the demand for mobility. Asset Management has a challenge.

Performance, risks and costs of assets and modalities need to be optimized. Changes in asset management will effect assets, logistic chains and modalities. New technologies will be developed and will lead to changes in data needs, intelligence and knowledge of the employees. Asset management will use new technology and possibilities in data to extend her service level towards the tenants.

The impact and the pace of these changes demands the asset management department and the asset management process to anticipate on the consequences that the changes have on the asset portfolio. And knowing that the changes will reveal itself increasingly faster and with growing impact on the processes of asset management.

4. AT THE SAME TIME: EXPONENTIAL GROWING DIGITALIZATION

We are living in a world that is rapidly being digitalized and robotized. In the two years more changes were made than in the ten years before that. Everything can be recorded or is digital available. Not only the Port of Rotterdam needs to be ready for the big changes that digitalizing and robotizing will bring. Which is already recognized in the ports digitization strategy: Port of Rotterdam's aim is not only to have the best port infrastructure, but also the smartest. "Dumb" asset therefore will be equipped with smart sensors.

Sensors but also satellite's, drones and the internet of things (IoT) will deliver data that will give us a deep insight in the way we are working in asset management. Different types of data can and will be brought together and the data (like is being done with the current inspections) will be no longer recorded once or twice a year but will be real time available, 24/7.

That opens the possibility for the assets of the Port of Rotterdam to work together. Where the assets are dumb at this moment, they will be made smart by adding smart sensors to the assets. These sensors will continuously monitor the status and condition of the assets of the Port of Rotterdam. Integrated, which means on all spots in the port, all together and every second of the day. The assets of the Port of Rotterdam will work together integrated, that is way the slogan is: “the inspector of the future is a sensor”

5. ANALYTICS ARE THE KEY TO SUCCESS: FOR EVERYONE, BY EVERYONE

The power of integrated asset management will be visible in the availability of information for everyone and to use the information made available by others. Not only within our own organizations. On the contrary: tenants, stakeholders and big data will provide information . Information needs to be in a way that everyone speaks the same language. No longer, we are evaluating whether we do the things right, but we evaluate whether we do the right things. With the help of smart and integrated analytics it will be made possible to understand things and to anticipate on changes that now are unknown or unrevealed.

Analytics is within the asset management considered to be one of the key success factors to connect assets and modalities in time on the demands and developments (like the earlier mentioned energy transition) in the Port of Rotterdam. Analytics will facilitate us to make future responsive decisions based on facts, to calculate so called “what-if” scenarios and to develop models. By doing so we are able to optimize the performance of assets and modalities, based on current use and predicted future use of the assets (predictive maintenance). Analytics will show us the areas in which insufficient information is available to make adequate decisions. In that way analytics will be the trigger to implement needed information bases on sensors, external data sets and big data.

Increasing availability of data and possibilities to record real time continuously, example given the loads on assets, will make it possible to predict the remaining lifetime of a structure more accurately than the current methods that are based on physical research and vendors information. Predictive models are of extreme value to plan the maintenance activities “just in time”, so no expenses or work will done to early or to late.

6. FRAMEWORK: FROM DATA TO THE RIGHT DECISION

Integrated asset management will not only give the asset manager insight on the performance , risks and costs of the individual assets, it will also show the connection of all the assets in a logistic chain or the nautical process. Data on these assets must deliver useable information that can be shared among other asset managers and departments within the Port of Rotterdam, but also among stakeholders like terminals, transport firms and nautical service providers.

Integrated asset management will also provide a framework in which data management is integrated in the processes and information is made visible in an understandable way, so it can be used for modeling and analyses. These so called analytics are giving the opportunity to predict, to plan predictive maintenance and to warn for trouble in an early stage inside and outside the organization of the Port of Rotterdam. In cooperation the most favorable scenario can be chosen to act on. Integrated asset management will bring change in how we think and in which way that thinking will be translated into actions and cooperation.

7. PLATFORM: INTEGRATION OF PEOPLE, PROCESSES, ASSETS AND DATA

Besides a framework integrated asset management will also provide a platform on which people, processes and assets are connected to data and information as a result from analytics and modelling

and also connected to data and information coming from other stakeholders, like tenants, nautical service providers, harbor master etcetera. Not look at the assets as assets but as part of bigger picture, the logistic chain or the nautical process, a holistic approach.

Integrated asset management is in the momentum of changes, not only in the availability of huge amount of data and the possibilities that digitalization and IT infrastructure offers, but also innovations in asset management in the field of among others deterioration models and risk management are developing. This offers opportunities to people, as well as individual as team, department or organizations to work together more intensively and finally be more efficient and effective and achieve better results in service level, risk profile and costs.

8. ALSO FOR THE DESIGN OF NEW ASSETS

The availability of (real time) data will also benefit the design and building of new assets. Integrated asset management doesn't start when an asset has been build, but gives added value in the design process, by making clear what the long term effects are of choices made in the design. The optimal use of data at the begin of the design process will eventually lead to a save of money and hours. The same goes for so called indirect assets of the Port of Rotterdam, for instance participations in pipeline areas and glass fiber networks.

9. MORE EFFICIENT PORT MANAGEMENT

Integrated asset management and the way of working and communicating that goes with it, makes it possible to incorporate the tenants and terminals in the asset management that still has an internal and technical focus. The tenants and terminals want to have more data on the assets, the asset manager wants to have more data on the activities on the terminals. In the end all the parties involved will benefit. Optimal data management results in more efficient use of the port infrastructure. Making the port more efficient, reduction of down time, reduction of turnaround time is necessary to maintain the competitive position of the port now and in the future

10. TOWARDS A LARGER SCALE: A SYSTEM OF SYSTEMS

In different areas there is an upward movement in scale, also in asset management. Eventually the shared information, will lead to systems that are connected and independent communicate with each other, call it a system of system, where plans, information etcetera is being shared between organizations and will lead to more cooperation and decision making based on the interest of the complete logistic chain.

APPLICATION OF A MANEUVERING SIMULATION CENTER AND PILOTS EXPERTISE TO THE DESIGN OF NEW PORTS AND TERMINALS AND INFRASTRUCTURE OPTIMIZATION IN BRAZIL

by

E. A. Tannuri¹, G. H. A. Martins²

ABSTRACT

In a recent initiative, the Numerical Offshore Tank Laboratory of the University of São Paulo (TPN-USP) established a research partnership with the Brazilian Maritime Pilots Association (CONAPRA) for the development and enhancement of a Maneuvering Simulation Center for port, rivers and offshore operations. The name of the core simulator code is SMH (Portuguese acronym for Maritime and Waterways Simulator) and it is an engineering tool used for the analysis of new operations in the Brazilian ports, to improve their efficiency in the context of the increasing oil and gas production and commercialization as well as the enhancement of international commercial trades. The accuracy of the mathematical model is an important requirement for a maneuvering simulator dedicated to engineering projects. The engineers, pilots and captains must rely on the dynamics of the simulator since it will be used to give answers to questions related to maneuvering analysis. The simulator is a tool to evaluate new channels design, tugboats requirements, environmental window, DP system analyses, or even to define the maximum dimensions of vessels in an approach channel or basin, among others questions. Therefore, the joint work of the simulator development team and the pilots is crucial to obtain such a calibrated and reliable simulator, combining the local expertise of the pilots and their knowledge about ship handling and behavior in confined waters to the technical skills of the researchers. This paper will present the mathematical model adopted in the simulator and the calibration procedure based on results from sea-trials and pilots' feedback. The tugboat operation both in vectorial and manned simulation models will also be detailed. Several applications in Brazilian coast will be described, including ship-to-ship operations, maneuvering analysis of larger containerships in the existing infrastructure, evaluation of new terminals in design stage with unsheltered turning basin among others.

1 INTRODUCTION

Ship maneuvering simulators are used for predicting the navigation safety in restricted areas (ports and channels) and training. The following paragraph, taken from Webster (1992), summarizes the concepts to be studied. "A limited number of simulations using a less-than-perfect simulator, a few select (design) ship types, a few select environmental conditions over extreme ranges characteristic of the local area, and a few pilots with representative local expertise and ship handling proficiency are sufficient to obtain a useful appraisal of waterway design..."

Some points should be stressed in this statement, which illustrate the benefits and proper way of using simulators. The simulators are never perfect, since mathematical models are simplifications of reality. Therefore, they must always be used in conjunction with the knowledge and experience of local conditions. The use of standards and recommendations (such as PIANC, USACE, ROM, etc.) must also accompany the port studies, corroborating and/or discussing the results of the simulations.

In a recent initiative, Transpetro and Petrobras established a research partnership with the Numerical Offshore Tank Laboratory of the University of São Paulo (TPN-USP) for developing a maneuvering simulator for port, rivers and offshore operations, with the technical collaboration of Brazilian Maritime Pilots Association (CONAPRA). The simulator name is SMH (Portuguese acronym for Maritime and Waterways

¹ Numerical Offshore Tank, University of São Paulo, Brazil, eduat@usp.br

² Brazilian Maritime Pilots Association, CONAPRA, Brazil

Simulator) is an engineering tool used for the analysis of several new operations in the Brazilian ports to improve their efficiency, due to the increasing oil and gas production and commercialization.

The accuracy of the mathematical model is an important requirement for a training simulator, but even more important for an engineering tool. The engineers, pilots and captains must rely on the ship dynamics represented by the simulator, since it will be used to give answers to questions related to maneuvering analysis. The simulator can be used to evaluate new channels design, tugboats requirements, environmental window, DP system analyses, or even to define the maximum dimensions of vessels in an approach channel or basin, among others questions.

This paper presents the mathematical model of SMH, adequate for low-speed maneuvering. The software is based on the TPN (Numerical Offshore Tank) numerical code (Nishimoto et al., 2002) which had several modifications to perform real-time simulations. The present simulator applies a Modular Mathematical Model, gathering a large number of models to represent the complete behavior of a ship during the navigation in restricted waters. Other time-domain maneuvering simulators are presented by Ankudinov et al. (1993), Koh et al. (2008), Fossen and Smodeli (2004), among others.

The simulator was developed using modern software engineering concepts, guaranteeing a flexible architecture, easy communication between different stations and external equipment and modularity, that enables new developments and improvements. The simulator supports different versions of hardware, such as part-task simulators with 3 or 6 visualization, tugboat stations of full-mission simulators using screen or projection technology.

Several Brazilian ports and rivers have already been studied and, in cooperation with pilots and captains, the simulator has been constantly improved. The feedback from the pilots and captains are used to perform a "fine-tuning" of the maneuvering models and environmental conditions in each port. This synergy between the theoretical background and field expertise has proven to be very effective. Some illustrative results of simulations and important results are exposed.

2 SMH MATHEMATICAL MODEL

2.1 General

This section summarizes the mathematical model implemented in the SMH simulator. The description is based on the paper by Hwang, (2004), that tried to define a standard documentation for maneuvering simulator models. Tannuri et al. (2014) and Queiroz Filho et al. (2014) present a more detailed description of the mathematical formulation and physical fundamentals of the SMH models. This section also presents the model calibration and validation procedure.

2.2 Outline of the Mathematical Model

The mathematical models represent the motion of a floating vessel at low speed in 6 DOF (degrees of freedom), subjected to the external forces due to the environmental and tugboats and to the control forces provided by the thrusters, propeller and rudder. The 6DOF floating vessel dynamics differential equations (already considering the interaction with the fluid and the external forces acting on the hull) are solved using 4rd order explicit Runge-Kutta integration method. However, as a matter of simplicity, this section will only present the equations of motion for the horizontal plane.

We adopt two different coordinate systems to derive the ship equations of motions, as shown in Figure 1. The system $OXYZ$ is earth-fixed (inertial system) and the system $oxyz$ ship-fixed, with the origin on central point of the keel midship section. The center of gravity G is at the distance x_G ahead from the point o , ox is the longitudinal axis of the vessel directed to the bow, and oy is the transversal axis, pointing to port. The heading of the vessel ψ defines the angle between the ox and OX axes.

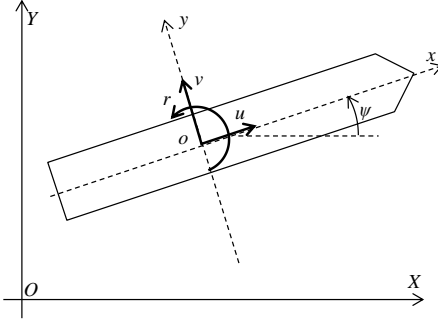


Figure 1 Coordinate system and basic definitions (for the 3 horizontal DOF)

The potential forces due to water-hull interaction are evaluated by means of added-mass and potential damping matrixes. The potential damping for horizontal motions is negligible, and can be simplified if the vessel is symmetrical along ox . Applying Newton's law of the motion, one can obtain the differential equations describing the relationships between the motion equation, given by:

$$\begin{aligned} (M + M_{11})\dot{u} - (M + M_{22})vr - (Mx_G + M_{26})r^2 &= X_{ext} \\ (M + M_{22})\dot{v} + (Mx_G + M_{26})\dot{r} + (M + M_{11})ur &= Y_{ext} \\ (I_z + M_{66})\dot{r} + (Mx_G + M_{26})(\dot{v} + ur) + (M_{22} - M_{11})uv &= N_{ext} \end{aligned} \quad (1)$$

where M is the vessel displacement (mass), I_z is the yaw moment of inertia of the ship, u and v are the surge and sway velocities respectively and r is the yaw angular velocity. The term M_{11} and M_{22} are the ship added masses in the surge and sway directions, M_{66} is the ship added moment of inertia and M_{26} is coupled sway-yaw added inertia. The last term on the right side of the yaw equation is the Munk's moment.

The subscript ext represents the external loads, that may be expressed in terms of different factors:

$$X_{ext} = X_h + X_w + X_{wv} + X_p + X_{tug} + X_M \quad (2)$$

where X_h represents the hydrodynamic non-potential forces, including the current and maneuvering forces, X_w , X_{wv} represent the wind and wave forces, respectively X_p represents the thrusters, propeller and rudder forces, X_{tug} represents the external action of the tug boats, either in contact with the hull or connected by a cable and X_M represents the forces due to mooring lines, fenders or anchor lines.

2.3 Modeling Phenomena and Valid Application Range

This section provides information about the physical effects modelled in the simulator, as well as the application and validity range, in a tabular and simplified format.

| Modeling Phenomena | Description / Application Range |
|--------------------------|--|
| Steering Gear | <ul style="list-style-type: none"> Rudder Angle Velocity is configurable (default value 2.3 deg/s) Constant rudder angle velocity Maximum rudder angle is configurable (default value 35 deg) |
| Main Engine | <ul style="list-style-type: none"> Model 1: The balance between hydrodynamic propeller torque and motor torque is calculated at each time step and is applied to the shaft equation (second order system). User must provide the shaft moment of inertia. The motor torque is assumed to be proportional to the telegraph command. This model better represents the behavior of the engine. Model 2: The machinery model (relation between commanded and effective RPM) is represented by a second order linear dynamics with no speed overshoot. User must provide the time to accelerate the axis from zero to full rpm. |
| Hull Hydrodynamic Forces | <ul style="list-style-type: none"> 6-DOF model with wave motion Hydrodynamic forces action on the hull are based on the current coefficients obtained by towing tank tests or CFD. Those coefficients must be provided for the complete range of angles (from 0° - stern incidence; to 180° - bow incidence). |

| Modeling Phenomena | Description / Application Range |
|-------------------------------|--|
| | <ul style="list-style-type: none"> Sectional integration of the hydrodynamic along the hull (Obokata, 1987). The model can take into account the influence of the yaw rotation and non-uniform current field near a port area. |
| Propeller Hydrodynamic Forces | <ul style="list-style-type: none"> Fixed Pitch Propeller (FPP) or Controllable Pitch Propeller (CPP) A four quadrant model for the propellers is adopted, including an extra ad-hoc correction for the yaw motion induced by the reverse action of the main propeller (paddle effect). User must provide the Thrust (KT) and Torque (KQ) coefficients as a function of the advance ratio (J) and Pitch (P/D). Those coefficients must be in tabular or polynomial format. For CPP propellers, a constant (configurable) pitch variation velocity is assumed. Wake and thrust deduction factors are input data. |
| Rudder Hydrodynamic Forces | <ul style="list-style-type: none"> - A four quadrant model for the rudder action is adopted, including the interaction between the propeller and the rudder. - The rudder Lift and Drag curves must be provided. The simulator database includes standard coefficients for all-movable, flapped and Schilling rudders. |
| Shallow-Water Effects | <ul style="list-style-type: none"> The shallow water corrections are applied to the hydrodynamic potential and non-potential forces following two options: Option 1 (Pre-Calculated): The potential hydrodynamic properties (added masses and potential damping) and forces (first order and drift coefficients) are obtained by potential codes already considering the bottom in the mesh grid, and are provided as input to the simulator. The non-potential forces (represented by the current coefficients) are obtained by towing tank or CFD tests with the bottom already included. The validity of this approach is dependent on the quality of the pre-calculation procedure, and may reach up to $h/T=1.05$ (h is the water depth; T is the ship draft). Option 2 (Real-Time Corrections): Ad-hoc corrections to the potential and non-potential forces are performed in order to account for the shallow water effects. Those corrections are valid up to $h/T=1.2$. |
| Bank and Passing Ship Effects | <ul style="list-style-type: none"> The effects of obstacles, such as banks or passing ships, are evaluated by the real-time calculation of the distance between the vessel hull and the external obstacles. Tabulated suction forces and yaw moments are used in order to provide the adequate physical effect expected by the pilots. |
| Wind Effects | <ul style="list-style-type: none"> The wind effect is simulated by using the aerodynamic force and moment equations which are expressed as functions of aerodynamic force coefficients, above-water projected areas of the ship, the effective wind force and the effective wind direction. Those coefficients are obtained by wind tunnel tests of CFD calculation. The simulator allows constant or gusty wind. The wind spectra implemented in the code are Harris, Wills, API and NPD, among others. |
| Wave Forces / Motions | <p>The following wave effects are implemented:</p> <ul style="list-style-type: none"> Second order drift forces (Slow and mean drift forces - that induces low frequency wave oscillations and drift) 6DOF First order forces (that induces the oscillatory vertical motions) Wave-current (or vessel speed) interaction, that modifies the wave drift forces and the frequency of incidence. Irregular wave spectrum models (JONSWAP or Pierson-Moskowitz) with directional spreading and bimodality. The effect of the breakwaters that changes the wave pattern into the sheltered area is considered. A spatial map of wave height and direction may be defined as an input to the simulator. The simulator then calculates an average wave height and direction for the vessel instantaneous midship position, and these wave properties are used for obtaining the forces at that time. Wave potential coefficients can be imported from different commercial softwares (Wamit, Acqua, Hydrostar). |
| Bow and Stern Thrusters | <ul style="list-style-type: none"> The net thruster forces are dependent on the RPM and is reduced due to the ship longitudinal and lateral speed at the bow or the stern. The influence of the longitudinal speed is configurable, and the default reduction is zero net-thrust for 6knots. The influence of the lateral speed at the bow or stern (inlet speed) depends on the thrust coefficient (Kt) as a function of advance ratio (J) |
| Tugs | <p>Option 1: Simplified Vector Model</p> <ul style="list-style-type: none"> No limitation in the number of tugs Push-pull and Online assisting methods Correction due to current, wave and vessel speed on the net thrust Reduction of the efficiency when force astern (configurable) |

| Modeling Phenomena | Description / Application Range |
|---------------------------|--|
| | <ul style="list-style-type: none"> • Time to connect the line, to change force and to change direction are configurable. Option 2: Multiplayer simulation • Tugboat is modeled as vessel and is controlled by the part-task simulators. (up to 4 tug boats allowed) • Conventional of Azimuth tugboats • Push-pull, Online and indirect assisting methods |
| Mooring Lines and Fenders | <ul style="list-style-type: none"> • No limitation in the mooring line numbers, that are modeled as catenary equation, with linear restoration. • Winches are commanded by the operator interface, with constant (and adjustable) speed. • Fenders are modeled as non-linear restoration elements with contact friction. |

2.4 Outline of the Mathematical Model

For each vessel modeled in the simulator, several standard maneuvers are executed and documented in order to check the model. These tests are done in the simulator running in fast time mode, with an automatic procedure for actuating on the rudder and propeller. Those maneuvers include at least:

- Turning Circle
- Stopping Ability (Crash Stop)
- Inertia Test
- Yaw-Checking and Course-Keeping Ability (10/10 And 20/20 Zig/Zag)
- Turning Circles in Shallow Water
- Turning Circles in Wind
- Deceleration Performance
- Pull-In and Spiral Tests
- Accelerating and Coasting Turns
- Low Speed Maneuver - Lateral Thruster Capabilities

The maneuvers must be executed preferable at half-speed, since it is closer to the actual speeds used close to a port area. However, the velocity will depend on the available results from the Sea-Trial report of the actual vessel. The main parameters of each maneuver are calculated and are compared to the results of the real vessel sea-trial. The most important parameters compared are:

- 10/10 And 20/20 Zig/Zag
 - 1st and 2nd overshoot - angle and time
- Turning Circle
 - Tactical Diameter, Advance, Transfer, Speed at heading 90°, 180°, 270°, 360°
- Stopping Ability (Crash Stop)
 - Head / Side Reach and Travel Distance until stop, Time to stop
- Lateral Thruster Capabilities
 - Time to turn the vessel with bow/stern action with / without speed

If the comparison results a difference larger than 20% in any of those parameters, we do the calibration procedure. Specific vessel parameters are multiplied by a factor from 0.8 - 1.2 to match the model to the actual vessel. The parameters we mostly tune are the sway added mass, rudder lift, current/hydrodynamic forces for bow incidence (that are equivalent to the linear Y_v or N_v hydrodynamic derivatives) and propeller efficiency for astern action. When we change any parameter, all tests must be repeated. An automatic software executes such a process. The vessel parameters allowed to be changed are those estimated/calculated by the laboratory. We do not change the actual vessel parameters (for example, rudder area).




Of course, a comprehensive knowledge of the mathematical maneuvering model is required in this calibration procedure, since the researcher must know, a priori, the effect of any change that is being done. The calibration procedure requires the supervision of the coordinator or the main simulator operator.





In most cases, the vessel documentation provides no sea-trial results for shallow water, and the calibration procedure is only executed for deep-water maneuvers. The hydrodynamic coefficients for shallow water are the applied to the "deep-water calibrated" model, and the results of the vessel in shallow water are compared to those in deep-water. The relation between the deep water and shallow water parameters are compared to results of similar vessel or from literature, in order to verify the model in shallow water. If there are sea-trial results for shallow water maneuver, the calibration procedure is expected to be better since the shallow water maneuvers from the simulator are directly compared to the actual results of the vessel.

After this process, experienced pilots maneuver the vessel in the simulator, performing some typical harbor-like maneuver, such as navigate along a channel, to execute a bend and to stop the vessel. The pilot's expected rudder efficiency, rate of turn, and stopping ability are compared to the simulator and we do some extra adjustments.

3 TPN-USP MANEUVERING SIMULATION CENTER INFRASTRUCTURE

The TPN-USP Maneuvering Simulation Center has 6 simulators, being 3 classified as full-mission (immersive system with more than 270° angle of projection). All simulators can run together in the same run (multiplayer simulation). The following chart presents the main characteristics of each simulator:

| | |
|---|---|
| <p>General features</p> | <ul style="list-style-type: none"> • Commands for rudder, fixed or controllable pitch propellers, tunnel and azimuth thrusters • DP System and AutoPilot • GPS, Anemometer, rate of turn, compass, Doppler log, Echo-sounder, Radar, ECDIS, Echo Souder, Speed Log (bottom and water related) • Portable Pilot Unit (PPU) • Rudder Repeater, Girocompass repeater, Binoculars • RIPEAM interface • Radio communication • Alarms and Anchor, Mooring lines |
| <p>Full-Mission 1</p>  | <ul style="list-style-type: none"> • 12m diameter screen, 30 projectors, 270° field of view, Floor Projection • 10 panels for commands and instruments, 4 overhead screens • 2 wings and automatic change of point of view when the pilot is in the wing |
| <p>Full Mission 2</p>  | <ul style="list-style-type: none"> • 25 visualization screens, 360° field of view • 7 panels for commands and instruments, 3 overhead screens • Stern bridge for PSV operation  |

| | |
|---|--|
| <p>Full Mission 3</p>  | <ul style="list-style-type: none"> • 21 4K visualization screens, 360° field of view • 2 panels for commands and instruments • Customizable simulator, can be used in either mode <ul style="list-style-type: none"> ○ Tugboat ○ Offshore Crane  |
| <p>Simulator 4D</p>  | <ul style="list-style-type: none"> • 1 large stereo visualization screen • Moving 6DOF platform for complete immersion • 2 panels for commands and instruments • Used for tugboat simulation |
| <p>Part-Taks Simulators (2 units)</p>  | <ul style="list-style-type: none"> • 6 visualization screens • 5 panels for commands and instruments |

4 APPLICATIONS

The simulator helps in performing various maneuverings in extreme conditions, with different ships and in damaged conditions and/or command failures. The envelope of the ship's course is obtained in extreme and operating conditions that, in reality, occur seldom during the year. In this way, it is possible to dimension the channels, maneuvering basins and escape routes.

The simulator can also be used to verify the impact of civil works, such as new berths and breakwaters construction. Often, the maneuvering simulation should be associated with a hydraulic and wave diffraction study to predict the alteration of the field of waves and current because of such works.

Dredging studies relate to the same context. Deepening a channel does not directly reflect on increasing the draft permitted for navigation. A study should be undertaken with the help of simulators, inasmuch as the maneuverability of the ship with this new draft is altered, as well as other physical phenomena that define the maximum draft, such as squatting, wave motion and current in the channel.

Non-conventional operations, such as ship-to-ship berthing and maneuvering of hulls of future FPSO platforms (without propulsion), can also be examined beforehand using simulation. Moreover, when the dimensions of channels and access bends are very close to or less than obtained by standards or recommendations, it is essential to perform simulations to check the risks associated with extreme operating conditions, and to define environmental windows for operation.

The analysis of the results of simulation can also be used to define the navigation signals and lights design (location and type of buoys) and contingency plans. The number, layout and bollard-pull of tugboats to guarantee the safe positioning of ships can also be appraised using simulators.

4.1 Quantitative evaluation of the simulations executed from 2012-2017

During the period from 2012-2017, TPN-USP executed 94 maneuvering simulation studies, with the participation of over 140 pilots from Different Zones. The Figure 2 shows the number of simulations executed per year and per Brazilian states.

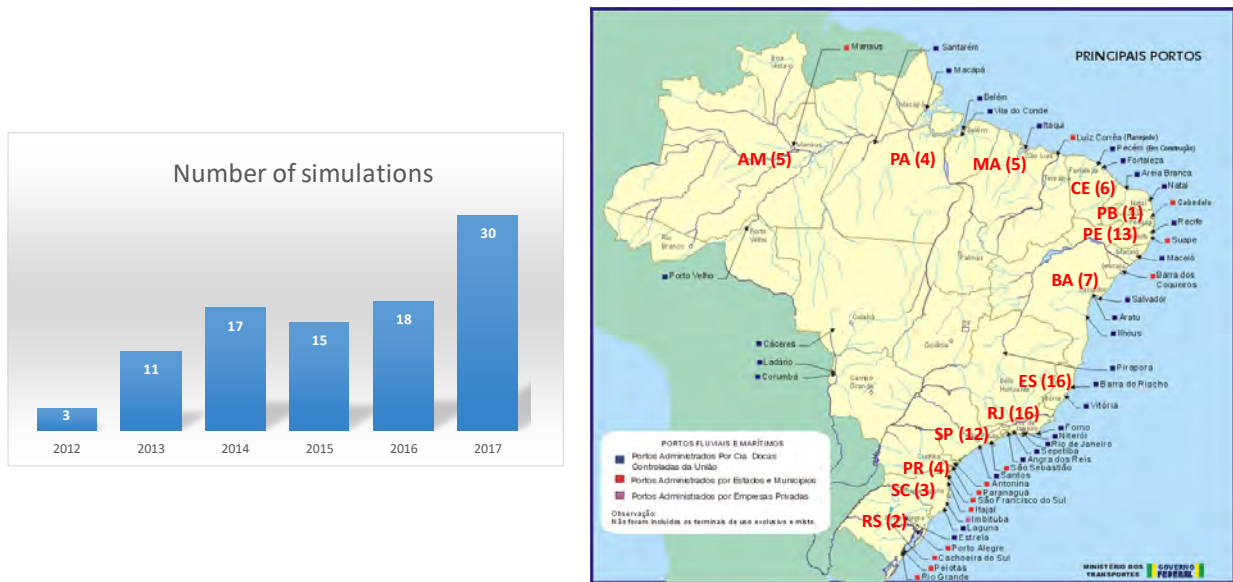


Figure 2 Maneuvering simulations performed at the TPN-USP during 2012-2017: (left) number per year; (left) Distribution by type; (right) Distribution per Brazilian states

The simulations have different levels of complexity and realism and different purposes. The Figure 3 shows the distribution of the simulations among different types and purposes. The classification of the simulation level is:

- **Fast-Time Simulation (17% of the total):** the simulator operates with algorithms that represent the behavior of the pilot, controlling the ship and tugs. One or more local pilot take part in the initial meeting, defining the maneuvering procedure that the control algorithm must mimic. The maneuvers run in accelerated mode and the execution of a large number of runs is possible. The statistical analysis of the ship tracks can define the optimal layout of the maneuvering area or the limiting conditions.
- **Real-Time Single Player (67% of the total):** real-time simulation controlled by the local pilot, using a full-mission simulator. The simulator operator uses the so-called vector tug models to control the tugs. Simplified model based on efficiency curves calculates the effective force applied by the tugboat, for different conditions (speed, current, wave and towing angle). To compensate the short comings of using simplified models, sometimes one tug captain attends the simulation campaign

and advise the simulator operator on which tug forces or position could be applied realistically, on the limitations of the tug, the tow line length, requirement for space, reaction time, etc..

- Real-Time Multi Player (*Interactive tugs* – 16% of the total): the main simulator is the assisted ship, controlled by the pilot, and one or more simulators are the tugs, controlled by tug captains. A 6DOF maneuvering model calculates the tug motion and behavior; in such a way the simulator considers almost all aspects: tug type and characteristics, influence of speed and towing direction, required space, reaction time and pilot-tug captain communication. Since the ship is often assisted by 3 or 4 tugs, it is not practical and very expensive to have such number of interactive tugs during the simulation. Therefore, we use vector tugs combined to interactive tugs. Normally, 1 or 2 most critical tugs are operated in the interactive mode.

The different purposes of the simulations are:

- New Operations (incl. STS): feasibility assessment and definition of environmental window for new operations in an existing port, such as a different type of vessel or ship-to-ship operation alongside the berth.
- New Port and Terminals (Design): evaluation and optimization of the horizontal design of a navigation channel or harbour basin, as suggested by PIANC (2014) in the Detailed Design stage.
- New Port and Terminals (Verification): evaluation of environmental window, operational procedure and pilots' familiarization for a newly built port or terminal or for an existing port that was subjected to dredging or expansion.
- Increase Ship Size: verification if the horizontal dimensions of existing channel and basin are compatible to ships with larger dimensions.
- Increase Draft: the increase in draft is associated with reduction in the maneuvering margin (MM) and increase in the vessel inertia. The maneuvering simulator can be used to verify the impact of those changes in the safety of the maneuver.
- Dredging design: verification of the horizontal dimensions of the area to be dredged, including channels, basins and stopping areas.
- Tugboat specification: verification of the tugboats number, layout, bollard pull and type.

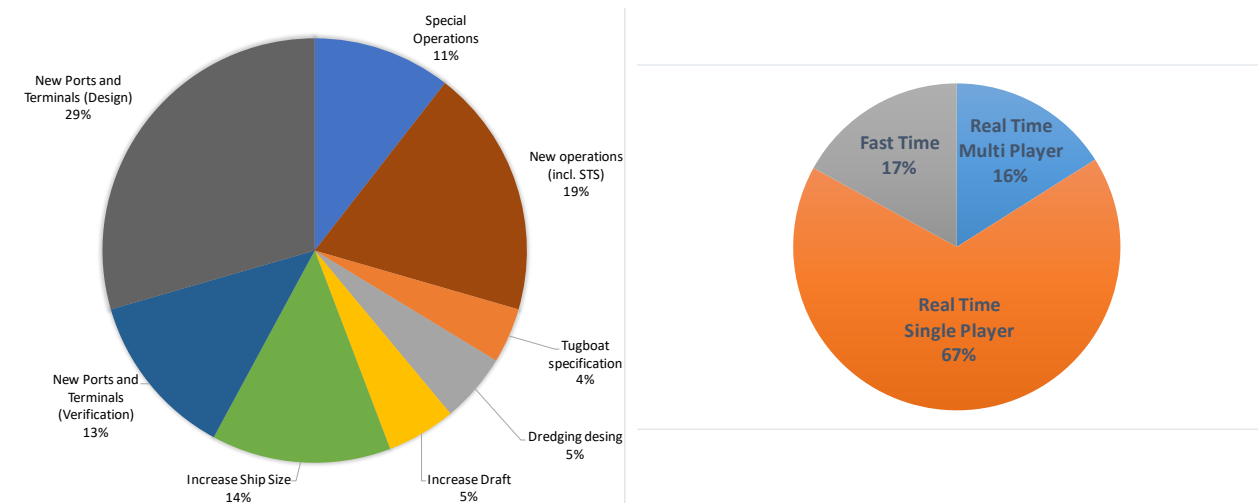


Figure 3 Maneuvering simulations performed at the TPN-USP during 2012-2017: (left) Distribution by type; (right) Distribution by each category

4.2 Case Study 1: Feasibility analysis for larger containerships

The Port of Santos, located in the State of São Paulo - Brazil, is the most important Brazilian port, representing an economic influence greater than 50% of the national gross domestic product. In total, the port counts on 65 berth quays, spread on its both margins, and receives multiple types of ships, including containers, solid and cargo bulk carriers, cruises and Ro-Ro. The nominal access channel water depth is 15 m and the current draft rule in place limits ships with drafts larger than 14.2m, considering 1m of tide.

Despite its local importance, the Port of Santos infrastructure does not enable the traffic of the most recent container vessels in operation by limiting the port access to vessels with maximum lengths of 336m, able to carry around 10.000 TEUS. Notwithstanding, the search of the shipping line companies to achieve economies of scale has given rise to sharply growths of container ship sizes in the last years, increasing the port challenges to improve its capabilities. For comparison, the highest-capacity ship current in operation is able to carry around 19.000 TEUS and is 395m long, 59m wide with a design draft of 14:5m

Based on this scenario, the Port of Santos has been planning to reduce the port restriction and start attending a new class of container ships with maximum length of 366m (13,800 TEU). With this purpose, a series of studies covering different aspects are required to evaluate the manoeuvring feasibility of this novel ship size in the port, such as: suitability of the present horizontal and vertical dimensions of the navigation channel, impacts on the maintenance dredging necessity, dimensioning of new turning basins, ship manoeuvring challenges, new tug bollard pull requirements and impacts induced by its passing speed and distance to moored ships, these last ones being the focus of the present analysis.

Motivated by the studies performed by the Port of Santos, several Brazilian ports executed studies with TPN-USP to evaluate the manoeuvring feasibility of the 366m long containership (Figure 4). They know that if this new class of containerships is allowed to operate in the Port of Santos, they will need to receive those vessels to guarantee their market share. The Figure 4 also shows the number of simulations of containerships carried out by TPN-USP, with a clear tendency of increasing number of vessels with LOA larger than 349m.

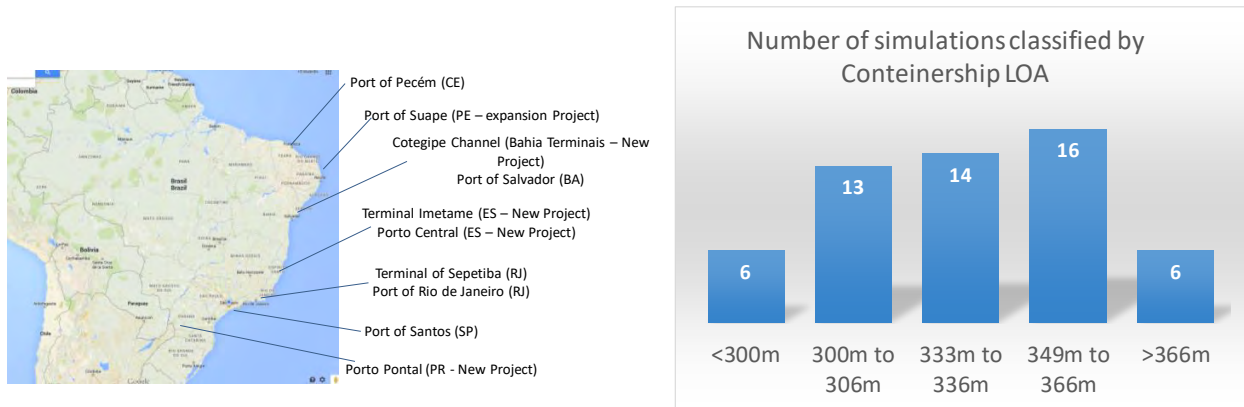
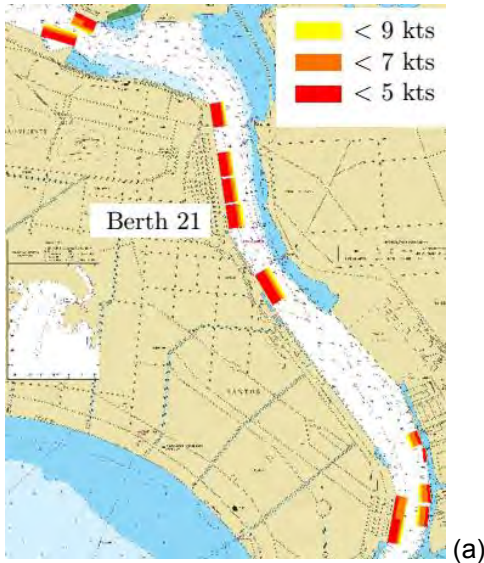


Figure 4 (left) Ports that executed studies with TPN-USP to test the manoeuvring feasibility of the containership with LOA larger than 336m; (right) number of simulations classified by containership LOA

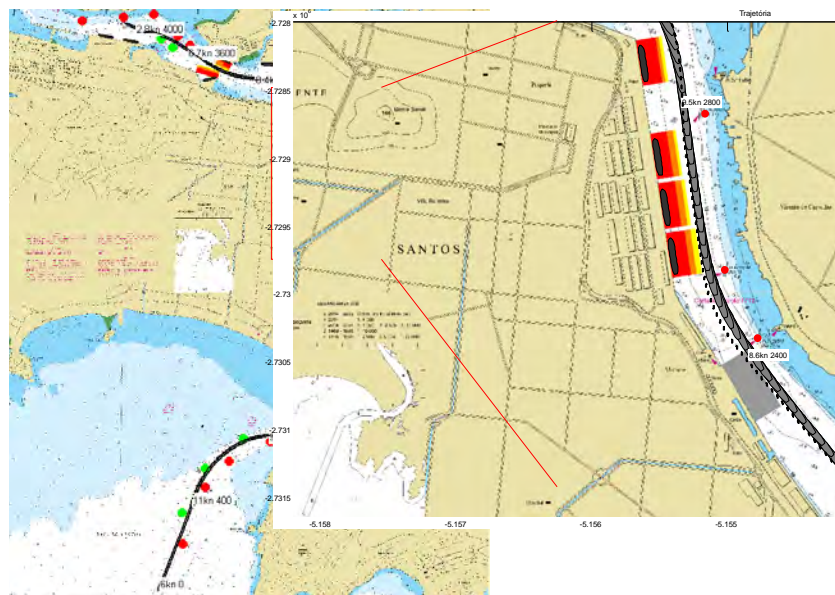
Assessing whether an existing infrastructure can accommodate a larger vessel involves maneuvering simulation. The study should define contingency measures in case of failures, number and types of tugs, environmental limits and operational restrictions.

The Port of Santos is located in an estuarine channel, with berths on both banks and distance between margins of approximately 400m. Today, there are many incidents of mooring lines breaking and fender damaging due to the passing ship problem, caused by the hydrodynamic interaction between the moored

ships and the vessel navigating along the channel. The increase in ship size could further aggravate this problem. Therefore, the interaction caused by the 366m long containership was evaluated before to the maneuvering simulations, using a numerical code based on potential flow (Ruggeri et al., 2016). The result was the definition of zones around berths where the vessel should maintain a controlled speed (Figure 5a).



(b)



(c)

Figure 5 (a) Operational limits for three passing distances printed in nautical chart of Port of Santos; (b) Pilot in the TPN-USP real-time simulator bridge ; (c) Real-time containership trajectory for an inbound maneuver

The next step was to execute of real-time simulations commanded by local and experienced pilots of the Port of Santos (Figure 5b). This is a very important step of the present work since it becomes possible to evaluate whether the ship can be indeed controlled and kept distant enough to the moored ships with relatively low speed. Several manoeuvring simulations were carried out, which comprised combinations of draft, outbound/inbound manoeuvres, flood/ebb tides, wind and wave conditions. In each simulation, the pilot commands aim to avoid the ship to pass under the colored areas above the pre-specified velocities. On the other hand, several factors make this task very difficult to be managed, such as for example the

intense traffic of small boats on the navigation channel, wind gusts and also a helmsman delay on complying the pilot command. In many cases, the pilot has to increase the ship speed in order to increase the ship controllability (rudder efficiency), which may expose more the moored ships to the passing ship forces.

The trajectory of the ship in an illustrative inbound maneuver is presented in the Figure 5c. Here, the pilot could keep the vessel in the center of the channel, outside the colored areas.

The final conclusion of the analysis, that combined a potential flow model and a real-time maneuvering simulator is for the feasibility of the 366m long containership in Port of Santos, under environmental and operational limits. 4 tugboats with total 270TON must be used in the maneuver, the port authority must interrupt the ferryboat operation and must guarantee no ship crossing the channel during the transit of the larger vessel. The visibility must be larger than 1nm, winds limited to 15knots and the maneuver must occur in the high tide with very low current. It was also recommended to the port authority to strictly control the mooring lines pre-tension in the vessels alongside the critical berths.

Maneuvering simulations can also be used to verify the necessary changes in the existing infrastructure to accommodate a larger vessel. The changes may be the construction of new berths, expansion of existing berths, dredging of the channel or turning basin. As an example, the Port of Sepetiba is going to expand the existing berth, as well as to dredge a new channel with direct access to the new berths. The Figure 6 (left) shows the modifications proposed by the designer. An extensive maneuvering simulation campaign has been carried out, and the new layout was approved by the pilots, with minor modifications in the bifurcation and in the inner berth approaching, as indicated in the Figure 6 (right).

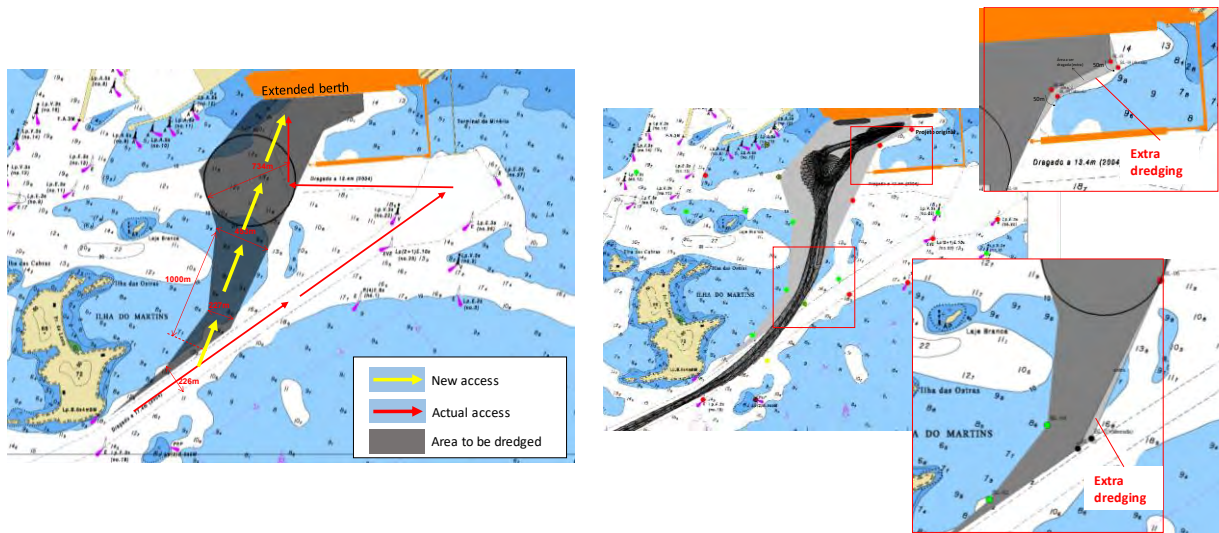


Figure 6 (left) Port of Sepetiba nautical chart showing the new changes; (right) Trajectory of inbound maneuvers of 366m long containership and proposed modifications in the original layout

4.3 Case Study 2: Evaluation of Ship-to-Ship operations

Ship-to-ship (STS) operations have been applied worldwide from military operations to oil/LNG cargo transfer, to improve operational efficiency. In the last years, the increasing oil production in the new pre-salt fields and the lack of available berths/terminals in Brazil has increased transfers in STS. This operation allows the transfer of the oil from the specialized DP shuttle tanker (that brings the oil from the offshore platform) directly to conventional tankers, ready to export, optimizing the occupation of the terminals and on-shore tanks.

The oil companies with operation in Brazil are searching for new areas to perform the STS operation, that can be offshore (STS underway), in sheltered bays (anchored STS) or at berths that can hold the forces generated by two moored vessels (STS alongside the berth). The main challenge is to transfer oil from the Suezmax DP to conventional VLCC tankers.

TPN-USP executed a large number of simulations to verify the manoeuvring feasibility of the STS Operation, as Figure 3 indicated. Figure 7 shows the ports in which the STS feasibility was studied, and the number of tankers simulations carried out by TPN-USP. The largest number of Suezmax tankers reflects that most DP shuttle tankers are Suezmax class vessels.

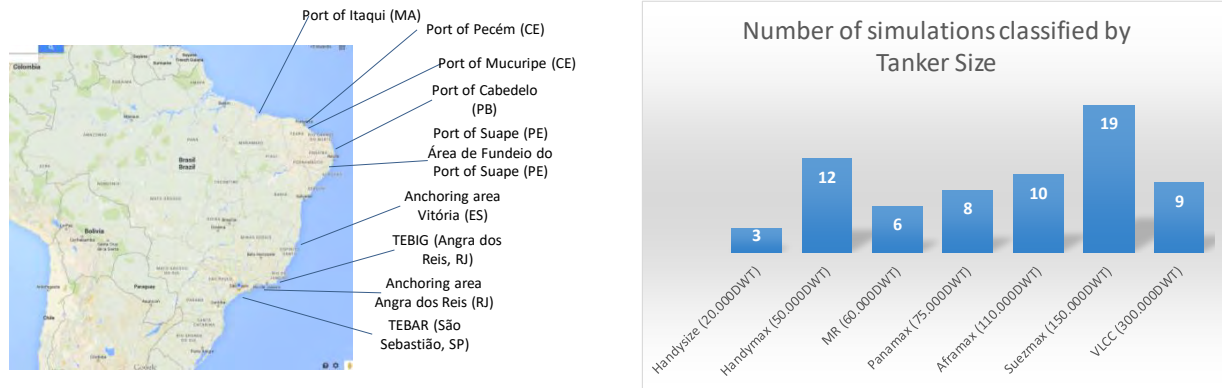


Figure 7 (left) Ports that executed studies with TPN-USP to evaluate the STS feasibility (right) number of simulations classified by tanker size

The analysis and planning of a STS operation require the utilization of state of the art engineering tools. A careful review of different aspects of the operation must be done since it is a new operation in an existing port facility, which was not predicted when the port was originally designed and built. All the procedures are based on the PIANC (2014) detailed design phase. The operations were evaluated in several aspects:

- Calculation of tide, current, wind and waves in the area using in-loco measurements and mathematical models.
- Detailed calculation of the environmental loads acting on the vessels when in ship-to-ship configuration.
- Verification of the as-built layout of the terminal, including the mooring and berthing equipment.
- Mooring analysis; Verification of the loads on the bollards and fenders.
- Berthing and unberthing maneuver and nautical area.
- Bollard pull requirements for tugboats.

A full description of all phases of the analysis for three case-studies may be found in Tannuri et al. (2016a) – Mucuripe Port; Tannuri et al. (2016b) – anchoring area of Vitoria and Ruggeri et al. (2016) – São Sebastião TEBAR Terminal. The maneuverability aspects, which are the target of this paper, should be evaluated through real-time simulation campaigns, with the participation of pilots and tug captains.

Maneuvering simulations should verify, for example, if the approach area to the berth is compatible with the transit of 2 ships. For cases where this area is natural (without dredging), we draw a line delimiting the safe depth in the ECDIS (*Electronic Chart Display and Information System*) or PPU (*Portable Pilot Unit*), and we check the distance along the simulation runs. In cases where the berth approach area is artificial (dredged), it was originally designed for only one ship. Thus, the simulations will allow verifying if with proper use of tugboats and maneuvering techniques it is possible to guarantee the safe approach of the second ship.

As an example of a natural depth approach area, Figure 8 shows the maneuver to the Pier 101 of the Port of Pecém. The STS vessel should turn in the outbound maneuver and may approach “forbidden” area indicated by the black dots. Although the depth is almost constant in the approaching area, waves can penetrate by the SW part of the breakwater, inducing vertical motions on the ship if it moves out of the sheltered region. After several simulations runs, this maneuver was considered safe and feasible. The STS maneuver was also evaluated in the internal berth of the São Sebastião Terminal (PP2). The 16.6m depth line is 106 m from the ship’s side. Figure 3 (left) shows one of the simulated maneuvers, and it was found

that the ship reaches the border of the demarcated area. Thus, the STS maneuver with Aframax vessel was considered unsafe.

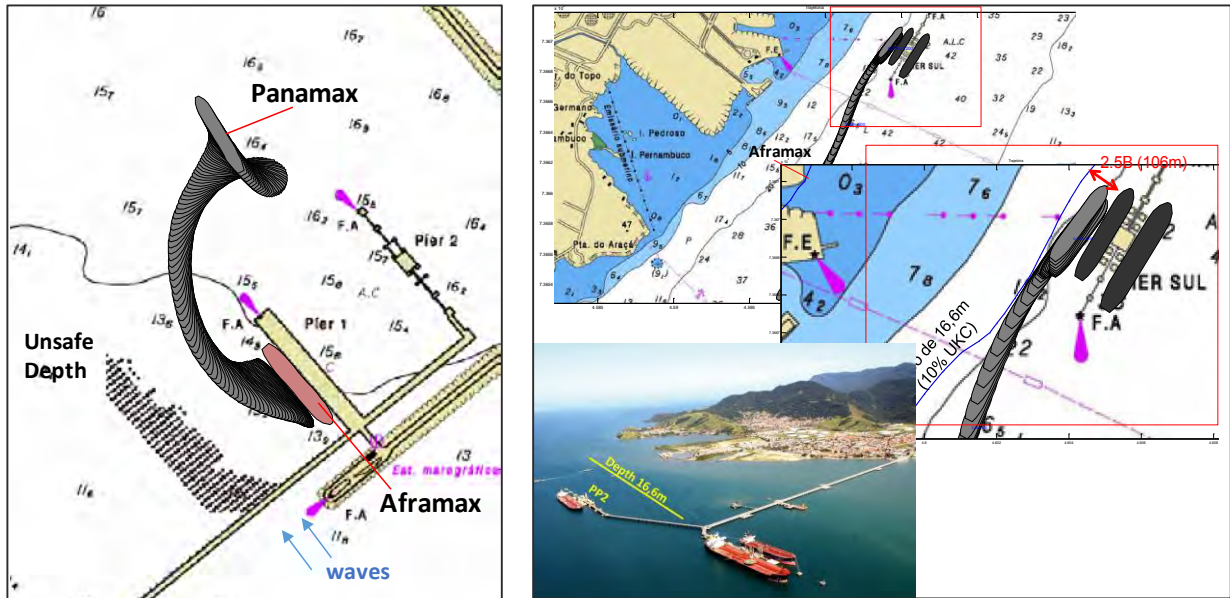


Figure 8 (left) Outbound maneuver at the Pier 101 – Port of Pecém; (right) STS maneuver at the internal berth of the São Sebastião Terminal (PP2).

The Mucuripe Oil Terminal has a dredged access area. The STS operation with Panamax vessels was evaluated by means of maneuver simulations, and it was verified that the STS operation is safe if an extra tug with at least 40TON is used. The distance between the red buoys and the ship in the pier allows approaching or turning safely, even considering the space required for the tugs operation. Figure 9 presents berthing and unberthing maneuvers, which demonstrate this finding.



Figure 9 Inbound and outbound STS maneuvers at Mucuripe Oil Terminal

Maneuvering simulation should also verify the influence of the STS operation in neighboring berths. In the Port of Itaquí, for example, it was found that the two vessels alongside berth 106 would reduce the width of the approach channel to the berth 105, that is used by another company, to 175m (Figure 10 – left). Due to the strong currents and tidal variations in this Port, the maneuver to/from the berth 105 was considered unsafe by the pilots if the berth 106 is occupied by two vessels. This information must be used by the authorities to estimate the economic benefits of the operation, as well as to reconcile the interests of the various operators. On the other hand, the STS operation in the Port of Cabedelo does not prevent the maneuver in the neighboring berths, as shown in Figure 10 (right). Although the width of the approach channel reduces to 180m, the fact that ships are smaller and the currents weaker, allowed the inbound/outbound maneuvers to neighboring berths to be considered safe. Therefore, these two examples

demonstrate the importance of the participation of the local pilots so that the risk assessment considers all the particularities and previous experience of the area.

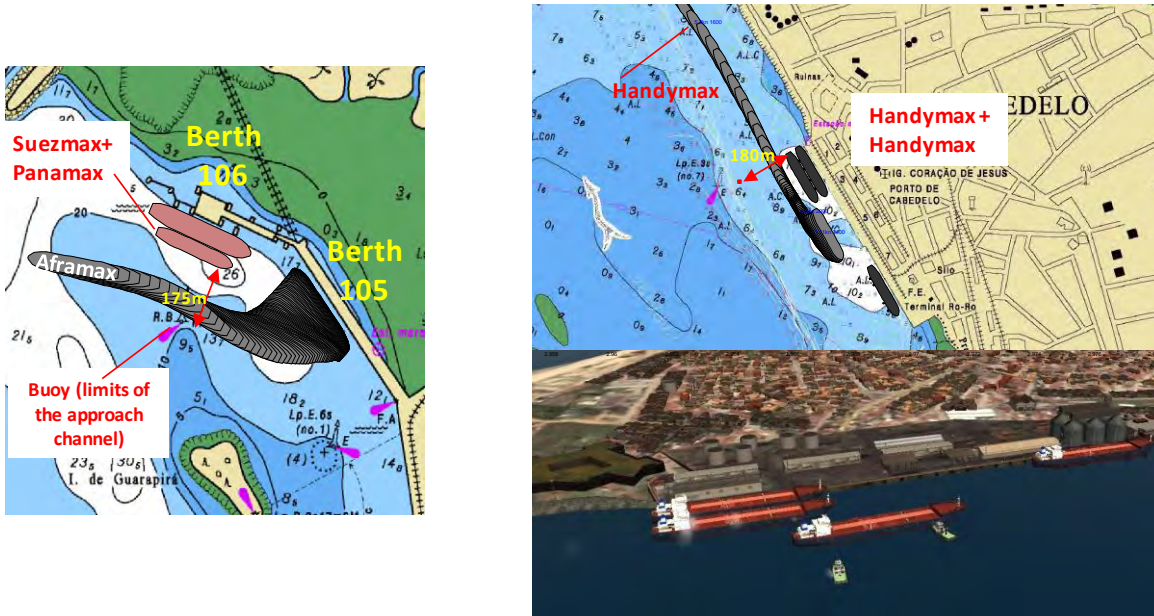


Figure 10 (left) STS operation in the Port of Itaquí; (right) STS operation in the Porto of Cabedelo

The position and heading control of the vessels should also be evaluated in the maneuvering simulation. Particularly in the anchored STS, techniques should be tested to keep the anchored ship stationary when the second ship approaches. Multiplayer simulation campaigns are suggested to test various solutions. Figure 11, for example, presents the actual maneuver executed in the sheltered anchoring area of Angra dos Reis. A tugboat in push-pull mode on the port-quarter of the anchored vessel is used to keep its position. In the case of unsheltered areas, the waves impose restriction on the operation of tugboats on the side. Thus, other solutions of controlling vessel position are being evaluated. One technique under study is the use of an offshore tugboat on a long-line made fast at the stern of the anchored ship, trying to keep its heading during the maneuver. This technique was tested in the simulator and in an experimental operation in the anchoring area of Vitória (Figure 11).



Figure 11 Anchored STS operation in: (left) Angra dos Reis (Sheltered bay); (right) unsheltered anchoring area of Vitória.

4.4 Case Study 3: Evaluation of new port designs

The joint work between the simulator team and pilots with expertise in the area can give important support for engineers during the design of new facilities. The TPN-USP in cooperation with the Brazilian pilots have participated on 30 studies of this category, that can be classified according to the Figure 12.

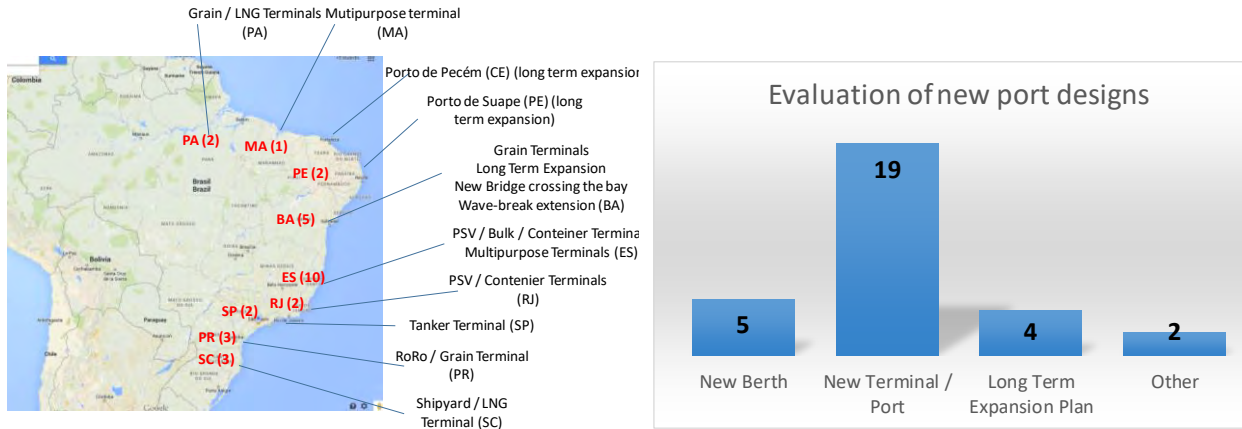


Figure 12 (left) New port facilities that were studied by TPN-USP (right) number of simulations classified by type

As indicated in the PIANC (2014), the maneuvering simulation can be used in the Conceptual Design stage, and is mandatory in the Detailed Design. The following points can be addressed during the simulations of a port in the design stage:

- Dredging optimization of the channel, turning basin and stopping areas
- Verification of localized channel problems for which the recommended width or alignment requirements cannot be satisfied.
- Verification of the influence of the new terminal in the berths or existing ports in the surrounding area
- Assessment of levels of risk during the navigation
- Estimation of the maximum environmental conditions for safe maneuver
- Definition of tug requirements

The long-term expansion plans (up to 30 years) are based on expected port demand, and nautical-port engineering concepts are applied to define the layout for access and position of the berths. The various phases of construction are simulated, and the objective is to evaluate the feasibility of the conceptual proposals, to choose between different proposals, to identify possible design errors and to confirm the defined type ships.

Figure 13 shows two alternatives for expansion of the Port of Suape that were evaluated during maneuver simulations. It is planned to build a new breakwater and new berths for Suezmax tankers. During the simulations, it was verified that Layout 1, even guaranteeing a safe maneuver, would make it impossible to carry out STS operations. Although not originally foreseen by the expansion plan, these operations are carried out frequently by the port in the inner breakwater berths, and the pilots, maritime and port authorities have reached consensus that it would be better to foresee this possibility also for the new cradles. Another advantage point of Layout 2 is that it allows the future construction of new berths, using the structure of the breakwater, as it is already done in the inner berths. So, the Layout 2 was chosen.

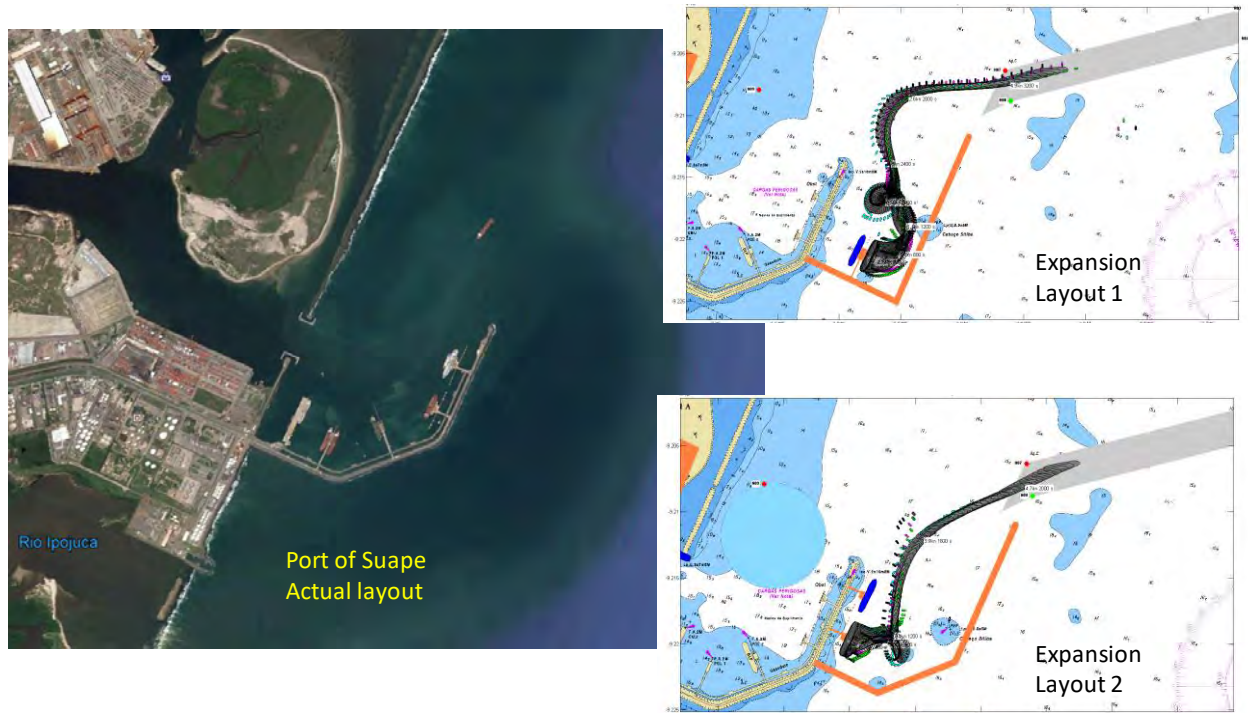


Figure 13 Proposals for the expansion of the Port of Suape

The evaluation of the design of the Porto Central project, a large port facility in the state of Espírito Santo, required several simulation campaigns. The larger ships were simulated in the critical berths, and the maneuver spaces were evaluated, at an initial and final stage of the port construction. Some suggestions for improvement and optimization of the internal arrangement were proposed. A relevant point was the verification of the need for the use of escort tugs for the manoeuvre of the large containerships (LOA greater than 366m), since the unsheltered access channel demands high speed navigation, imposing difficulty for stopping and turning in the sheltered area. With this, it was concluded that tug companies should already be prepared, making the escort tugs available and to start training the tug masters operating in the region.



Figure 14 Porto Central: (left) Maneuvering simulations ; (right) Layout of the port final stage

5 CONCLUSIONS

This paper presented the Maneuvering Simulation Center developed at the University of São Paulo, Brazil, and the benefits arose from a technical partnership established with Brazilian Maritime Pilots Association (CONAPRA) since 2012. We showed, by the description of several case-studies, the importance of the inputs from the experienced pilots since the early phases of the study of a new port or operation and during the maneuvering simulations. It is the only way to ensure that technical ship handling, the important human factors and local particularities are incorporated in the analysis.

6 ACKNOWLEDGMENTS

The authors thank Petrobras for supporting the development of the maneuvering simulation center, and all pilots that participated on the simulation campaigns. The first author thanks the CNPq (process 304784/2017-6) for the research grant and the students and researchers of the TPN-USP Maneuvering Simulation Center.

7 REFERENCES

- ANKUDINOV, V.K. ; MILLER, E.R. ; JAKOBSEN, B.K. ; DAGGETT, L.L. (1990). Manoeuvring performance of tug/barge assemblies in restricted waterways, Proceedings MARSIM & ICMS 90, Japan, pp. 515-525.
- FOSSEN, T.I. ; SMODELI, O. N. (2004) Nonlinear Time-Domain Strip Theory Formulation for Low-Speed Manoeuvring and Station-Keeping, Modeling Identification and Control, Vol. 25, No. 4, 201-221.
- HWANG, W-Y. (2004), Guideline for Ship Model Documentation – Draft 1.1, In 31st IMSF Annual General Meeting, Antwerp, Belgium.
- KOH, K.K. ; YASUKAWA, H. ; HIRATA, N. ; KOSE, K. (2008) Maneuvering simulations of pusher–barge systems. J. Mar. Sci. Technol. 13, 117–126.
- NISHIMOTO, K.; FUCATU, C.H.; MASETTI, I.Q. (2002). Dynasim - a Time Domain Simulator of Anchored FPSO. Journal of Offshore Mechanics Arctic Engineering ASME, v. 124, n. 4, p. 203-211.
- OBOOKATA, J.(1987), On the basic design of single point mooring systems (1st report), Journal of the Society of Naval Architects of Japan, vol161, June.
- QUEIROZ FILHO, A. N. , ZIMBRES, M. , TANNURI, E. A. (2014). Development and Validation of a Customizable DP System for a Full Bridge Real Time Simulator. In: ASME 33th International Conference on Ocean, Offshore and Arctic Engineering, OMAE 2014, San Francisco, USA.
- RUGGERI, F. ; WATAI, R.A. ; TANNURI, E. A. (2016). Passing Ships Interaction in the Oil Terminal of São Sebastião (Brazil): An Applied Study to Define the Operational Limits. In: 4th MASHCON International Conference on Ship Manoeuvring in Shallow and Confined Water, Hamburg, Germany.
- TANNURI, E. A. , RATEIRO, F. , FUCATU, C. H. , FERREIRA, M. D. , MASETTI, I. Q. , NISHIMOTO, K. (2014). Modular Mathematical Model for a Low-Speed Maneuvering Simulator. In: ASME 33th International Conference on Ocean, Offshore and Arctic Engineering OMAE 2014, San Francisco, USA.
- TANNURI, E.A.; CAMARA, J. G. A. ; SILVA, D. S. ; RUGGERI, F. ; LAVIERI, R.S. ; RATEIRO, F. ; MASETTI, F. R. ; HARANAKA, F. ; CLAUZET, G. (2016) . Assessment of new port operations using integrated analysis: a case study in Port of Mucuripe (CE, Brazil). In: Conference on Coastal and Port Engineering in Developing Countries (PIANC COPEDEC IX), Rio de Janeiro, Brazil.
- TANNURI, E.A.; PEREIRA JUNIOR, J. C. ; RUGGERI, F. ; LAVIERI, R. S. ; RATEIRO, F. ; IANAGUI, A.S.S. ; HARANAKA, F. ; WATAI, R.A. (2016). Anchored vessel ship-to-ship operations: environmental limits considering mooring equipments and ship maneuver. In: Conference on Coastal and Port Engineering in Developing Countries (PIANC COPEDEC IX), Rio de Janeiro, Brazil.
- WEBSTER, W.C.(1992). Shiphandling Simulation: Application to Waterway Design", National Academies Press.

"Maritime Port Planning and Operations: An analysis of available ports masterplan guidelines, identification of challenges, and a proposal of evaluation method to measure success factors in the development and implementation of a port masterplan"

by

Paulo Cardoso de Campos ¹, Katrina Dodd ²

Abstract

Ports masterplan is an essential document that defines a ports long term development. The aim of a masterplan is to strategically frame the direction in which port infrastructure and operations will develop in order to meeting future demand, local regulations, as well as environmental and social obligations. Maritime ssociations have attempted to develop boilerplate orientation framework for port masterplan preparation. However, limited progress has been made to incorporate mechanisms within the port masterplan to evaluate success factors in the development and implementation. This paper aims to investigate gaps in the existing models and apply a theoretical framework that draws on theories of planning evaluation to provide guidance for ports planners to use in various stages of the evaluation of the ports masterplan process.

1. Introduction

In globalised trade, goods and commodities are required to travel longer distances for delivery to places that were previously inaccessible. Ports act as main gateways to a country for the import and export of goods providing the infrastructure interface between sea and land logistics transportation network (Herz and Flamig, 2014), allocating facilities to accommodate vessels and handle cargos.

Ports belong to the logistics transportation system (Robinson, 2002). They are recognised as part of logistics centres (Bichou and Gray, 2004), in a port context logistics transportation network such as railway, and roads are infrastructure responsible for moving cargo in and out of ports (Agerschou, 2004). They can be "closed" and have a dedicated function as in some mining operations with their own railway system linking mine to port, or "open" as part of a macro network that connects to a port, including as an example city roads and railways.

With markets becoming increasingly globalised, ports and the associated logistics network play an ever-greater role in the development of a country, emphasizing the importance of a holistic plan to ensure ports and logistics network are designed to cope with this increased demand. This plan, known generally as a ports masterplan, is not just a blueprint for brick-and-mortar facilities, it comprises a long-term horizon plan (Dooms and Verbeke, 2006) in a strategic document that enables ports and associated logistics network to handle future demand, thus facilitating or impeding the growth of a country in the global marketplace.

Ports masterplan is a document that defines how ports will be developed in the future (PIANC, 2014). It is built upon fundamental themes including engineering and construction, community and environment, government regulations, type of services provided, and business focus (PortsAustralia, 2013). It is a living document that looks to the future, and therefore must be dynamic and responsive during its lifetime (Taneja et al., 2010). The preparation of a port

¹ Senior Study Manager Transportation & Logistics at Ausenco Engineering, PhD candidate– Australia, - Paulo.cardoso@ausenco.com - orcid.org/0000-0002-5731-4188

² Vice President Transportation & Logistics at Ausenco Engineering, Katrina.doo@ausenco.com - Australia

masterplan is a complex puzzle. It involves a multi-disciplinary spectrum of stakeholders that require seamlessly interaction when preparing, implementing, and monitoring across all levels.
Communication tool

The process of a port masterplans' development commences well before the port development starts, evolves over time, and expands as the facility grows and changes to meet demand. With most of the world's port infrastructure being in highly populated areas, and with an increase in the number and complexity of stakeholders, ports master planning in all its forms is going to become a more specialised and valued skill.

Whilst there is an attraction to follow industry standards and tailor the port masterplan to conform with local regulations and business needs, this does not always guarantee success of the ports masterplan objectives. Many ports masterplan approach, however, are creating static document (Taneja et al., 2010). The development of a port project, from design to construction, can take several years before is fully operational. Consequently, there are risks that a port masterplan can become obsolete document even before implementation.

Although there are a variety of techniques, standards, and guidelines available to produce a port masterplan, there is little or conflicting guidance that sufficiently covers the evaluation process involved in the ports masterplan, the process of developing the ports masterplan exercise quickly becomes a tangled web of stakeholders with widely different interests and objectives. Given the above backdrop, there is a tendency to develop and adopt various guidelines or none, generating a patchwork of confusing documentation with endless revisions and vague outcomes.

Fundamentally, the lack of an effective planning evaluation framework to be used during the development, implementation, and monitoring stages compromises the ability of the port masterplan to achieve its objectives.

It is of paramount importance organizations realise that a ports masterplan is not just a rigid blueprint document to guide the future development and be kept in bookshelves. The port masterplan must be the skeleton framework for distinct stages of the port operation, enabling the operational processes to be hung from this framework. These processes should be agile and be encouraging evaluation to react to market, environmental and innovative technologies changing conditions, both as risks and opportunities. As the individual processes adapt and grow, the port masterplan framework should be focused enough to enable evaluation against the long term horizon goals.

The aim of this paper is to review the most common guidelines and standards for ports masterplan preparation in the context of improvement of the evaluation process. It is argued in this paper that there is a need to introduce a detailed plan evaluation framework in the port masterplan preparation to support an unbiased evaluation process of port masterplan during development, implementation, and monitoring stages.

This paper is elaborated in five sections. Section 2 provides an analysis of available standards and guidelines in the evaluation process context. Section 3 explore the challenges port masterplan faces during development, implementation, and monitoring stages. Section 4 describes the evaluation framework that can be introduced in the port masterplan development process. Section 5 compile results and propose further research.

2. Port masterplan, guidelines, and standards

A port masterplan is a comprehensive document that involves contribution of many specialists of different disciplines, (Memos and Tsinker, 2004). It provides the development strategy for future years including the relationship between external stakeholders i.e. the port and the city, the financial and economic aspects, and the environmental impacts, Moglia and Sanguineri (2003). A summary of major elements of a port masterplan are described in Figure 1: Port Masterplan Topics



Figure 1: Port Masterplan Topics

As the port masterplan looks to the future, it must be able to be dynamic and responsive (Taneja and Ligteringen, 2010). However, plans in general are notorious for being vague during the preparation stage and are often written to address conflicting requirements. Even if it can achieve its goals, therefore, plans should be evaluated and a conclusion be able to be drawn as to what level of success the plan has achieved (Alexander, 2011).

Port authorities and operators demand a port masterplanning guideline is supplied by international maritime associations. The Permanent International Association of Navigation Congresses (PIANC) defines the port masterplan as a set of policies and guidelines to lead future development of ports within an overall development plan, PIANC (2014).

The PIANC Master Planning of Existing Ports Report (PIANC, 2014) provides a succinct guideline emphasizing different levels of ports masterplan from multinational to local level incorporating the main objectives to fully integrate into cities transportation planning strategies, environmental, urban, physical and eco-social constraints. Whilst the PIANC report covers port masterplan for existing ports, the same document is also applicable for existing and new port development.

Ports Australia, a body that represents Australia’s ports community, highlights in the Leading Practice: Ports Master Planning study published in 2013 that the most relevant elements to be included in a ports masterplan are economic drivers, environmental and social condition, supply chain, and interface planning considerations as well as government regulations, (PortsAustralia, 2013). Although the Ports Australia study focused on Australia ports, the document suggested a detailed guideline to support Australia’s ports in preparation of their ports masterplan, and in some cases it can be recommended as a guideline for other countries.

The American Association of Port Authorities published a framework to assist U.S. ports during the port planning and investment stages, the Port Planning and Investment Toolkit ((AAPA), 2017). The AAPA document does not constitute a regulatory framework, standard, or specification, but aims to provide guidelines for U.S. Ports obtain capital for their projects. Although the document focuses on the funding and financial aspects, it does emphasize essential elements of the planning process common on port masterplan and highlights the importance to provide a clear vision, goals, and objectives of proposed projects.

Despite international associations effort to produce standards and guidelines to support ports masterplan, many port authorities and operators have taken they own path and custom-made a port masterplan framework. Although these custom-made documents incorporate international standards and guidelines principles, they are tailored to reflect specific conditions associated to each terminal.

An interested example is the ports masterplan prepared by NSW Ports (NSW-Ports, 2015). They operate two intermodal logistics terminals and the Port Botany and Port Kembla. The “Navigation the Future – NSW Ports’s 30 Year Masterplan” published in 2015 presents NSW Ports approach to prepare their asset to sustainably operate for the next years. The ports masterplan is built upon four pillars: the logistics intermodal system, use of land and infrastructure, improve productivity and capacity, and the environmental and social aspects. It details a series of construction of capital projects and improvement in each asset recognizing the importance of stakeholder engagement along the process.

Pilbara Ports Authorities (PPA) that operates and manages major ports in the Pilbara region of Western Australia, and the proposed Ports of Anketell, Cape Preston East and Balla Balla published The Port Development Guideline – PDG (Pilbara-Ports-Authority, 2017) that provides an overarching port planning framework establishing objectives and strategies for each port. The

PDG introduces a 5 stages approval process to facilitate proponents along their development phase.

Even though port authorities and operators have developed frameworks to assist the development of a port masterplan, a proper mechanism to subsequently evaluate these port masterplans during development, implementation, and monitoring stages would promote an unbiased process during distinct stages of the port masterplan development reducing the risks of the document become obsolete.

3. Challenges ports masterplan faces

Ports are vulnerable infrastructure systems exposed to numerous potential disruptive events along the years. These events could originate from internal or external influences, trade, war or “acts of god” and the extent, duration and magnitude of such are not able to be forecast during the planning phase with any great accuracy. They are factors with the potential to cause profound consequences in a port operation resulting in direct or indirect losses (Mansouri et al., 2010). Kleindorfer and Saad (2005) categorise disruptive events as risks to interrupt ports operation and it can be defined as natural hazards, terrorism and political instability.

A port masterplan is developed based on specific parameters that direct define how ports infrastructure will operate and develop in the future. Some parameters including future demand, shipping traffic and innovative technologies are considered key drivers because disruption on these parameters completely change the proposed port infrastructure defined during the preparation of the ports masterplan. These key drivers are exposed to constant change and if incorrectly established can result in a non-functional port operation.

After completion and implementation, a port masterplan can become a static document unable to manage uncertainties including future demand, shipping traffic and innovative technologies which consequently result in failure of the port masterplan to act as a planning document or failure of the port to adapt to change if strictly adhering to the plan. (Taneja et al., 2014).

Forecasting the demand involves the use of potentially complex and sophisticated methods. However, estimating future demand is essential to determine potential ports expansion development scenarios (Patil and Sahu, 2015). The forecast of future demand suggests optimistic and pessimistic projections to demonstrate ways to ports handle different demand capacities (Suryani et al., 2012).

Innovative technologies are emerging and the pace of change is increasing, exposing ports to a dynamic environment that is perpetually reshaping, and regularly demanding continuous preparation of ports systems to adapt for changes. Lee and Lam (2016) observe that one of the key drivers that directly impacts infrastructure development is innovative technologies.

However, most of the port masterplans do not adhere to what they have planned and are infrequently updated. This leads to ad hoc and often momentary or last-minute actions which are knee-jerk corrective adjustments in some cases entirely distinct from the port masterplan (Taneja et al., 2010). A case study presented by Taneja et al. (2010) describes the example of Nhava Sheva port in Mumbai, India. The plan was initially conceived involving two containers terminals and one bulk cargo terminal, but the demand of containers was wrongly forecasted. This required the port to convert the bulk cargo into a container terminal to accommodate for a substantial increased demand in containerised cargo. This is an example of how a ports masterplan falsely assumes the accuracy of its forecasts.

It is important to emphasize the importance of understanding the key drivers in a port masterplan, and demonstrate the vulnerability of port development to disruptive events. These parameters in most of the cases are difficult to conjure up during the port masterplan development stage. Therefore, it is imperative that a strategic data collection phase to identify the key drivers and the potential disruptive events should be completed in advance and clearly articulated throughout the port masterplan.

4. The need for a plan evaluation framework for ports masterplan

Plan evaluation has to be a rigorous method to assess plans and process results against a predetermined set of criteria (Laurian et al., 2010). It fosters accountability in planners and institutions presenting results, and effectiveness of the plan including expected and unexpected results (Leeuw and Furubo, 2008). Plan evaluation encourages improvement of plans, promotes transparency, and identifies efficiency and success; however, plan evaluation is not frequently adopted (Guyadeen and Seasons, 2015).

Evaluation is the key to turn the plan from a blue sky image to one which identifies the levers to be pulled to enable the best operation, and provides a framework on how and when to activate them. therefore an evaluation criteria should be implemented to evaluate plans during preparation, implementation, and after implementation

Plan evaluation is divided into three theoretical general methods: (i) rational; that concentrates on the connection between plans and current developments, (ii) communicative; that considers plans a guideline for future planning not restricting to original plan objectives., and (iii) pragmatic integrative; that considers a combination of rational or communicative approaches depending on the circumstances (Laurian et al., 2010).

Traditionally, plan evaluation comprises distinct stages including (a) Elaboration that occurs during preparation of the plan, (b) Implementation takes place during the application of the plan, and (c) Verification occurs after the plan is implemented to identify if the plan accomplished its goals, (Oliveira and Pinho, 2010).

Despite these different evaluation methods, ports masterplan should be evaluated during distinct stages of the planning making process by different type of evaluators, and It should have distinct criteria of what is being evaluated.

Plan evaluation can be defined in two important concepts, the conformance and performance based processes (Baer, 1997). The conformance or input based process follows plans as a blueprint document to meet the intend objectives by controlling the plan execution, whereas the performance or output based process the plan is used as a guideline and variations of the plan are if deemed necessary to meet a performance objective. Due to the complexity of port masterplan involving multiple disciplines, a distinct plan evaluation method is necessary to be adopted because the lack of a specific method to evaluate ports masterplan can compromise the efficacy of plans achieve its objectives.

The methodology selected to address the objectives of the ports masterplan evaluation framework involves the use of plan evaluation theory. The aim is to adapt the concepts of planning process model and the list of general criteria for plan assessment described by Baer (1997) and tailor to the evaluation of ports masterplans.

Baer illustrates distinct evaluation stages described for the plan evaluation process. Several types of evaluation can be applied during the development of a plan, thus a plan can be evaluated in any or all stages of the planning process. The types of evaluation include:

1. Plan assessment: It occurs in any stage of the process from the Problem Diagnosis to Evaluation stage.
2. Plan testing: It comprises of the testing of alternative plans and comparison of these to the base plan. The team that prepared the base plan conducts the comparison to alternatives.
3. Plan critique: It is conducted after the plan being published, but before the plan is implemented. The evaluation is executed by a team of people not involved in the planning preparation process.
4. Comparative research and professional evaluation: It is conducted after the plan being implemented. The evaluation is executed by a representative that was involved in the planning preparation process and a researcher.

5. Evaluation post hoc of plan outcomes: It is conducted after the plan is concluded and implemented. The objective is to confirm whether the plan was indeed implemented, how the plan performed, and how effective the plan was.

5. Results and recommendation

Port masterplan contents come in different forms and shapes in order to function in a range of diverse types of operations. However, most port masterplans lack a structured evaluation framework to assess ports masterplan effectiveness. In particular, it fails to recognize the potential change to key drivers and impact of disruptive events that critically affect the core premises of the port masterplan. Therefore, It is important to allocate a specific set of criteria in order to determine how the port masterplan should be evaluated during development, implementation, and outcome.

A specific port masterplan framework should be developed to do more than just categorize the level of success or failure of a proposed ports masterplan (Figure 2 - Ports Masterplan Framework) . The port masterplan evaluation framework should identify areas of the port masterplans that require corrective actions to refocus the ports masterplan in case disruptions in the key drivers occur.

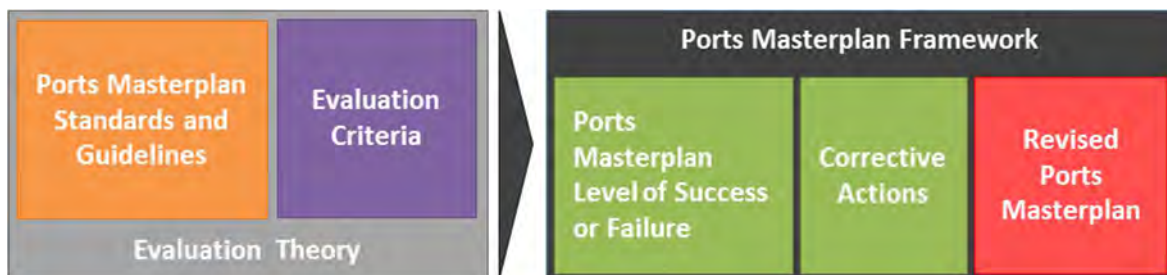


Figure 2 - Ports Masterplan Framework

The proposed port masterplan framework intends to be used by port engineers, operators, and other stakeholders to evaluate their plans. They are responsible to integrate a variety of stakeholders during the preparation stage of ports masterplan namely community representatives, government bodies, investors, and future potential clients.

6. Reference List

- (AAPA), T. A. A. O. P. A. 2017. Port Planning and Investment Toolkit.
- AGERSCHOU, H. 2004. Planning and design of ports and marine terminals, London, Thomas Telford.
- ALEXANDER, E. R. 2011. Evaluating planning: What is successful planning and (how) can we measure it?, Abingdon, Oxon, Routledge.
- BAER, W. C. 1997. General plan evaluation criteria- An approach to making better plans. *Journal of the American Planning Association*, 63, 3, pg 329, 16.
- BICHOU, K. & GRAY, R. 2004. A logistics and supply chain management approach to port performance measurement. *Maritime Policy & Management*, 31, 47-67.
- DOOMS, M. & VERBEKE, M. 2006. Integrating the Extended Gateway Concept in Long-Term Strategic Seaport Planning A European Case Study. 42.
- GUYADEEN, D. & SEASONS, M. 2015. Plan Evaluation: Challenges and Directions for Future Research. *Planning Practice & Research*, 31, 215-228.
- HERZ, N. & FLAMIG, H. 2014. Understanding supply chain management concepts in the context of port logistics: An explanatory framework. *Transport*, 29, 376-385.
- KLEINDORFER, P. R. & SAAD, G. H. 2005. Managing Disruption Risks in Supply Chains. *Production and Operations Management*, 14, 53-68.
- LAURIAN, L., CRAWFORD, J., DAY, M., KOUWENHOVEN, P., MASON, G., ERICKSEN, N. & BEATTIE, L. 2010. Evaluating the Outcomes of Plans: Theory, Practice, and Methodology. *Environment and Planning B: Planning and Design*, 37, 740-757.
- LEE, P. T.-W. & LAM, J. S. L. 2016. Developing the Fifth Generation Port Model. *Dynamic Shipping and Port Development in the Globalized Economy, Volume 1: Applying Theory to Practice in Maritime Logistics*, 25.

- LEEUW, F. L. & FURUBO, J. E. 2008. Evaluation Systems: What Are They and Why Study Them? *Evaluation*, 14, 157-169.
- MANSOURI, M., NILCHIANI, R. & MOSTASHARI, A. 2010. A policy making framework for resilient port infrastructure systems. *Marine Policy*, 34, 1125-1134.
- MEMOS, C. D. & TSINKER, G. P. 2004. *Port engineering: planning, construction, maintenance, and security*, Hoboken, N.J, Wiley.
- MOGLIA, F. & SANGUINERI, M. 2003. Port Planning: the Need for a New Approach? *Maritime Economics & Logistics*, 5, 413-425.
- NSW-PORTS 2015. *Navigating the future*.
- OLIVEIRA, V. & PINHO, P. 2010. Evaluation in Urban Planning: Advances and Prospects. *Journal of Planning Literature*, 24, 343-361.
- PATIL, G. R. & SAHU, P. K. 2015. Estimation of freight demand at Mumbai Port using regression and time series models. *KSCE Journal of Civil Engineering*, 20, 2022-2032.
- PIANC 2014. *PIANC - Master Planning of existing Ports*. 230.
- PILBARA-PORTS-AUTHORITY 2017. *Port Development Guidelines*.
- PORTSAUSTRALIA 2013. *Leading Practice: Port Master Planning - Approaches and Future Opportunities*. 38.
- ROBINSON, R. 2002. Ports as elements in value-driven chain systems: the new paradigm. *Maritime Policy & Management*, 29, 241-255.
- SURYANI, E., CHOU, S.-Y. & CHEN, C.-H. 2012. Dynamic simulation model of air cargo demand forecast and terminal capacity planning. *Simulation Modelling Practice and Theory*, 28, 27-41.
- TANEJA, P. & LIGTERINGEN, H. 2010. Dealing with uncertainty in design of port infrastructure systems. *J. Design Research*, Vol. 8, 18.
- TANEJA, P., VELLINGA, T. & SOL, S. R. 2014. *planning and Management of Port Infrastructure Projects under Uncertainty*. 10.
- TANEJA, P., WALKER, W. E., LIGTERINGEN, H., VAN SCHUYLENBURG, M. & VAN DER PLAS, R. 2010. Implications of an uncertain future for port planning. *Maritime Policy & Management*, 37, 221-245.

PHYSICAL MODELLING OF PROPELLER SCOUR ON AN ARMoured SLOPE

by

Neville Berard¹, Sundar Prasad¹, Brett Miller² and Mathieu Deiber²

ABSTRACT

CITIC Pacific Mining (CPM) is proposing to increase throughput at their existing terminal in Western Australia, using self-propelled Handysize transshipment shuttle vessels (TSV) instead of dumb barges. An initial assessment indicated that the armoured rock slope adjacent to the berth face would incur damage due to propeller wash from the vessel side thrusters and the main propeller. Large scale (13.5:1) physical model tests were undertaken at the University of New South Wales (UNSW) to measure wash velocity and armour stability. Empirical equations for propeller velocity along the axis well reproduced the bow and stern thruster velocities but could not match the profile of the larger main propeller measurements. Measurements made along the axis of the vessel bow thrusters were not affected by the operation of the second thruster, indicating that traditional equations for side by side propellers may overpredict velocities. Additionally, the physical modelling demonstrated that the rock slope was more stable than predicted, but still incurred the mobilization of a small amount of armour stone. Additional tests were then completed to investigate the efficacy of Articulated Concrete Block Mattresses (ACMs) to protect the rock slope from propeller wash. These tests showed that the mats performed well as additional protection on the armour slope but only if tied together to stop the edges from becoming dislodged and overturning.

1. INTRODUCTION

The CITIC Pacific Mining Sino Iron Magnetite project is located 100 km southwest of Karratha, in Western Australia and initiated commercial operation in 2013.



Figure 1: Aerial view of the Cape Preston facility showing a transshipment barge prior to the facility modifications. (Subcon, 2018)

¹ Ausenco, Canada, neville.berard@ausenco.com

² UNSW Sydney, Water Research Laboratory, Australia

The facility, shown in Figure 1, was originally designed to berth transshipment barges with no propulsion capability. The berth was recently modified to enable berthing of larger self-propelled Transshipment Shuttle Vessels (TSV). Canada Steamship Lines (CSL) was engaged to modify and provide the TSV Donnacona to be fit for these operations. The vessel is equipped with a combination of bow and stern thrusters in addition to the main propeller for unassisted berthing and de-berthing. The propulsion arrangement for the Donnacona is shown in Figure 2, Figure 3 and summarized in Table 1.

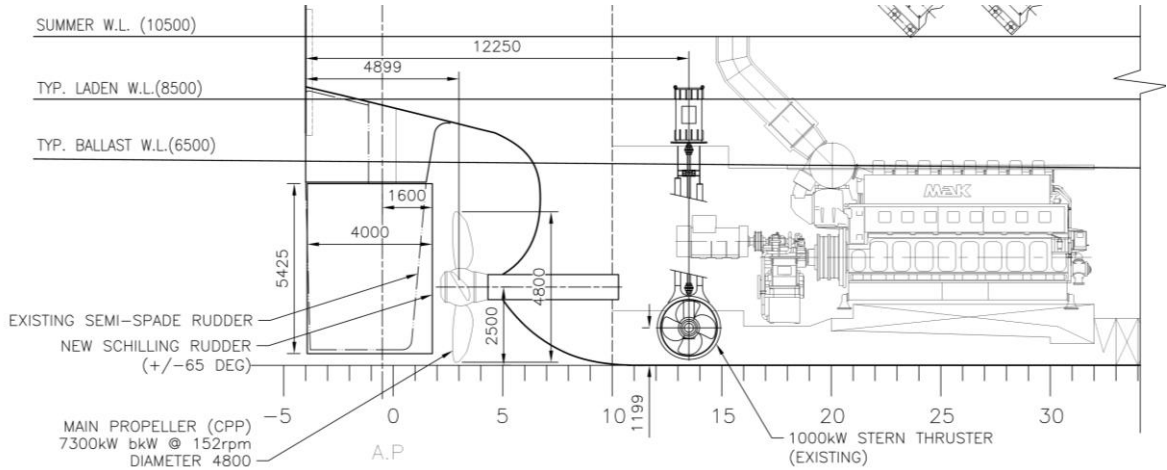


Figure 2: Donnacona stern propulsion arrangement

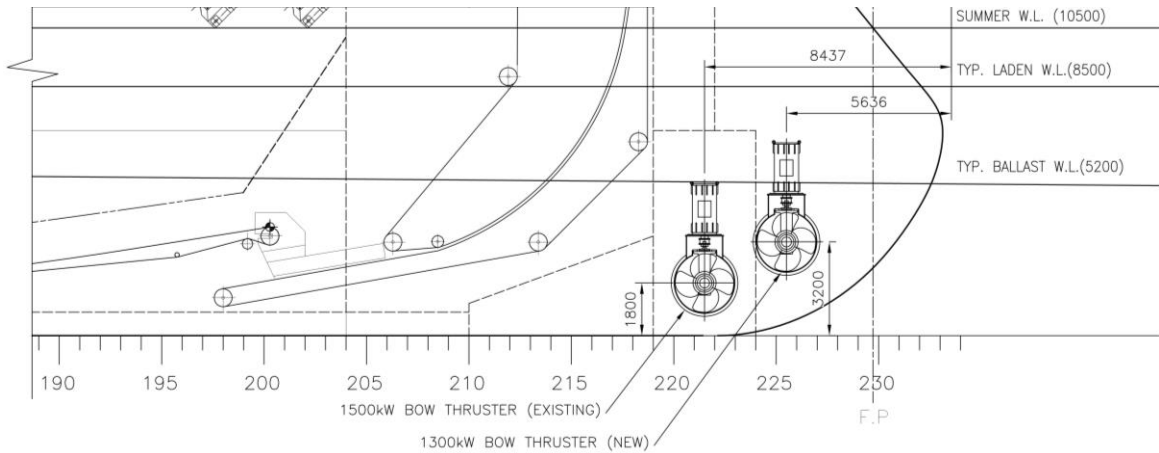


Figure 3: Donnacona bow propulsion arrangement

Table 1: Donnacona propulsions

| Propeller | Diameter (m) | Power (kW) | Shaft Height above Keel (m) | Revolution (rpm) |
|----------------|--------------|------------|-----------------------------|------------------|
| Main Propeller | 4.8 | 7300 | 2.5 | 152 |
| Stern Thruster | 1.75 | 1000 | 1.2 | 378 |
| Bowthruster 1 | 2.0 | 1500 | 1.8 | 324 |
| Bowthruster 2 | 2.0 | 1300 | 3.2 | 324 |

A desktop study was initiated because of concerns that the propulsion systems of the Donnacona could compromise the integrity of the armoured slope. Numerical calculations were performed following the latest guidance for slope stability by PIANC (2015) which includes three methods for the calculation of minimum rock weights for stability. All methods indicated that bow thrusters were likely to cause slope stability issues, but the three methodologies did not agree on whether the slope at the facility would be stable for the stern thruster and the main propeller.

A physical model study was determined to be the best method of reconciliation to confirm the findings of the numerical assessment and provide guidance on the stability of the armour stone at the terminal.

2. THEORETICAL BACKGROUND

The study of propeller velocities on slopes has gained more attention in recent years due to the increase in ship size and their respective propulsion systems. To determine the minimum diameter for stable armour, PIANC (2015) recommends two methods: the Dutch and the German formulations. Both methods involve two steps: the calculation of flow velocities produced by the propeller and then the subsequent calculation of armour stone to withstand those velocities. PIANC (2015) provides a warning that the two sets of equations for flow can vary significantly and therefore the corresponding equations (Dutch or German) for minimum diameter for stable armour stone should be used.

Recent physical model scale testing programs conducted by Dykstra et al. (2010) and van Doorn (2012) have contributed to the ongoing effort to better understand the velocities produced by propellers and their effect on the stability of armoured slopes.

2.1 Jet Velocity

Efflux velocity, the velocity of a jet along the central axis right at the propeller, was calculated according to Blaauw and Van de Kaa (1978):

$$V_0 = C_3 \left(\frac{f_p P_D}{\rho_w D_p^2} \right)^{0.33} \quad (1)$$

where C_3 is 1.17 for ducted propellers or 1.48 for free propellers, f_p is the percent of total engine power, P_D is total installed power, ρ_w is the density of water and D_p is the propeller diameter.

The Dutch equation for flow distribution along the main propeller axis is determined according to:

$$V_x = (2.0 \text{ to } 2.8) V_0 \left(\frac{D_p}{x} \right) n \quad (2)$$

where x is the distance along the central axis from the propeller and n is the square root of the number of propellers. This equation is valid for $x > 2.6 * D_p$, called the zone of free propagation. When $x < 2.6 * D_p$, $V_x = V_0$ which is referred to as the zone of flow establishment.

The German equation is similar but instead of a range of values (2.0 – 2.8) as shown in (2), the equation applies a constant of 2.6.

$$V_x = (2.6) V_0 \left(\frac{D_p}{x} \right) n \quad (3)$$

For the velocity decay of the bow thruster jets (as opposed to main propeller jets) over a slope there is a German equation presented in PIANC (2015) method which was derived from physical model tests with a slope of 1V:3H.

$$V_x = V_0 \text{ for } \frac{x}{D_p} < 1 \quad (4)$$

$$V_x = V_0 \left(\frac{x}{D_p} \right)^{-0.33} \quad \text{for } 1 < \frac{x}{D_p} < 5.375 \quad (5)$$

$$V_x = 2.3V_0 \left(\frac{x}{D_p} \right)^{-0.825} \quad \text{for } \frac{x}{D_p} > 5.375 \quad (6)$$

2.2 Armour Stability

PIANC (2015) includes three separate methods for the determination of stable armour rock on slopes to withstand propeller velocities: The German method, the Dutch/Izbash method and the Dutch/Pilarczyk method. The German methodology is based on research and equations specifically for propeller jets while the Dutch methods use basic stability formulas developed by Izbash and Pilarczyk.

The German stability approach as it is shown in PIANC (2015) is

$$V_{crit} = B_{crit} \sqrt{D_{85} g \Delta} \quad (7)$$

where $B_{crit} = 0.9-1.25$, g is acceleration due to gravity and Δ is the relationship between stone density and the density of water ($\rho_s - \rho_w / \rho_w$). V_{crit} is the critical velocity that mobilizes the armour stone and D_{85} is the diameter that 85% would pass through on a sieve test.

The Dutch/Izbash method uses the following equation:

$$\Delta D_{50} = \frac{1}{B_{crit}^2} \frac{V_{bottom}^2}{2g} \quad (8)$$

where, in this case, $B_{crit} = 0.8$, V_{bottom} is described as the flow velocity near the bed and D_{50} is 50% passing diameter for armour stone.

Finally, the Dutch/Pilarczyk method from CIRIA, CUR, & CETMEF (2007) is:

$$\Delta D_{50} = \phi \frac{0.035 k_h k_t^2 V^2}{\psi_{cr} k_{sl} 2g} \quad (9)$$

where:

Φ = stability parameter (taken as 0.75 for riprap)
 ψ_{cr} = critical Shield's parameter (0.035 for riprap)
 k_h = depth parameter, 1.0
 k_t^2 = turbulence factor, 3.0 from Pilarczyk (1990)
 α = angle of internal friction (40° for riprap)
 θ = revetment slope
 $k_{sl} = \sqrt{1 - \left(\frac{\sin \alpha}{\sin \theta} \right)^2}$

All three of these equations were used during the initial desktop study and yielded significantly different results. For this reason it was unknown which of these methods provided the most realistic results and thus physical model testing was determined to be a more reliable method of determining the stability of the existing armour rock at the facility.

3. PHYSICAL MODEL SET-UP & TESTING

The physical model was constructed in a 4 m x 7 m x 1.4 m deep basin at the University of New South Wales' (UNSW) Water Research Laboratory. Both mobile and fixed bed tests were completed to understand if any observed instabilities were caused by undermining or armour rock instability.

Articulated concrete mattresses (ACMs) had previously been suggested as a solution should the armour stability not be sufficient. These mattresses were also tested in the lab to establish whether the selected mattresses could withstand the propeller velocities.

3.1 Physical Model Layout

The features of the model (shown in Figure 4) were:

- A plywood slope upon which the breakwater was built with a slope of 2V:3H.
- A section of moveable bed with could be covered during fixed bed testing
- A propeller drive and motor for the different configurations
- A beam for supporting and moving the Acoustic Doppler Velocimeter (ADV).

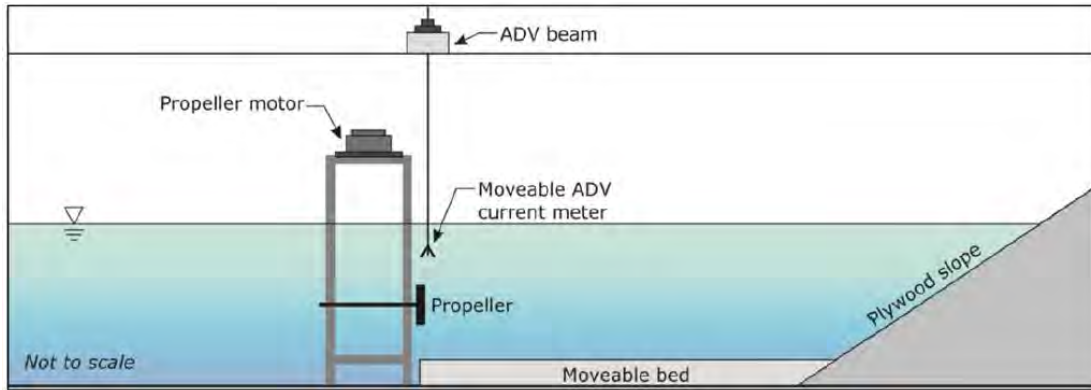


Figure 4: Model features – side view.

The modeling was undertaken at a Froude scale of 1:13.5. This scale was determined so as to:

- Maintain adequate turbulence for the rock stability testing;
- Provide adequate resolution and accuracy for model measurements
- Ensure the basin had enough space for water circulations and jet dispersion;

Propellers were affixed assuming a minimum underkeel clearance of 1.2 m to represent a worst case scenario. Testing set-up of the bow thrusters is shown in Figure 5.



Figure 5: Bow thrusters installation with ADV probe (left) and view of a propeller used for a bow thruster (right)

Prototype armour rock had a median weight of 500 kg and was overlaid on a filter layer which sat directly on the plywood. The seabed at the site is composed of 10 mm rocks. For the mobile bed tests, this was modeled using a scaled mix of sand with diameters between 0.3 mm to 2 mm.

ACMs were modelled after mattresses produced by the manufacturer Subcon. The design for the laboratory prototypes was determined in consultation with them. ACMs were constructed with a density of 2600 kg/m^3 and with an area density of 521 kg/m^2 . Blocks were manufactured by injection mold in two interlocking sections. Model ACMs (shown in Figure 6) were assembled by aligning the blocks over string-lines and clicking the blocks into place.

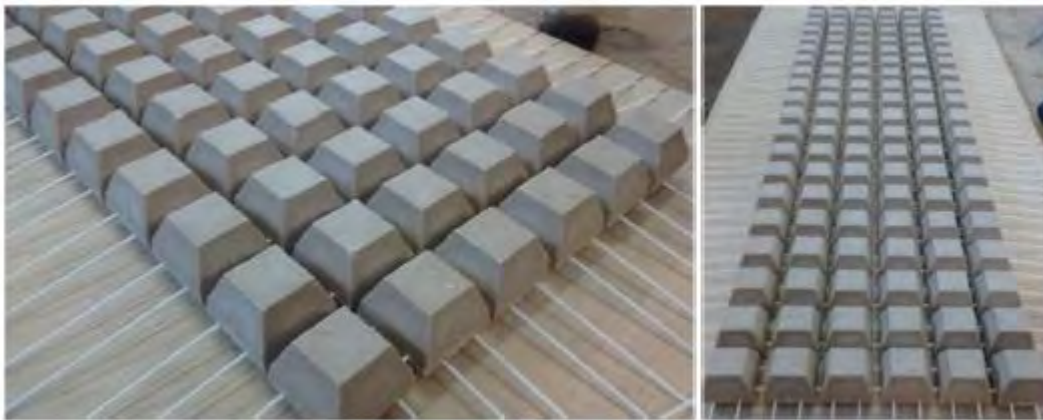


Figure 6: Articulated concrete mattresses (as modelled)

A Nortek Acoustic Doppler Velocimeter (ADV) was used to measure velocities at the propellers during testing. A 3D FARO laser scanner was used to scan the breakwater and mobile bed (if applicable) before and after each test to assess any differences (see Figure 7). At the conclusion of each test the before and after images were compared using 3D point cloud software to determine if rock movement occurred. Rock movement was defined as when a rock moved more than the median rock dimension.

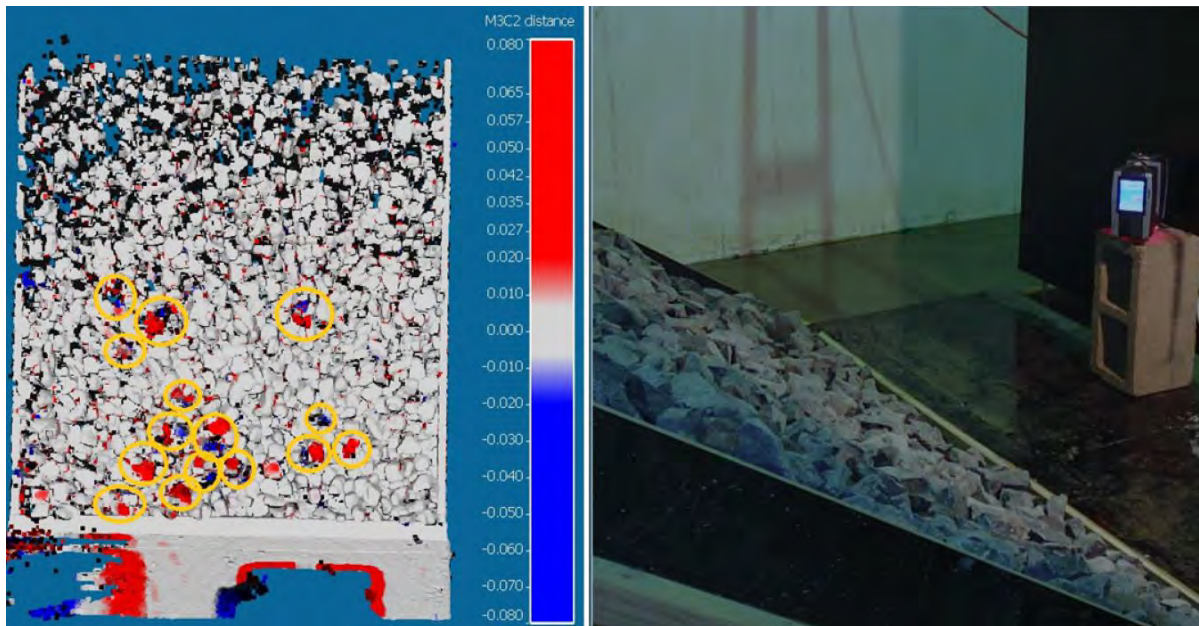


Figure 7: Example of a FARO Scan (left) and the FARO scanner in action in the laboratory

3.2 Testing Program

A description of all tests performed during these experiments is shown in Table 2. Engine power percentages were determined through discussions with the terminal operators, a simulation completed during a maneuvering study by the Australian Maritime College (2016) and using industry recommendations from PIANC (2015).

Mobile bed tests were designed to represent realistic operating conditions at the site. Fixed bed tests allowed the effect of the velocities on the armour rock slope to be isolated for the worst case scenario (minimum underkeel clearance) without any undermining of the slope occurring.

Tests were re-set (slope rebuilt, sand re-flattened or both) at the beginning of each major test series (numbered items in Table 2).

Each test was run for a period of 30 minutes prototype, which translated to approximately 8.5 minutes at the lab scale. This was selected to represent a number of ships calling at the facility and repeated velocities on the slope.

ACMs were used in the final test rounds as a proposed solution to erosion at the toe of the structure and instability of the armoured slope.

Table 2: Test program

| Test # | Propulsion Type | Propeller Power (%) | Fixed or Mobile Seabed | Articulated Concrete Mattress |
|--------|---------------------------------|---------------------|------------------------|-------------------------------|
| 1a | Bow Thrusters | 40 | Fixed | No |
| 1b | Bow Thrusters | 70 | Fixed | No |
| 1c | Bow Thrusters | 100 | Fixed | No |
| 2a | Bow Thrusters | 40 | Mobile | No |
| 2b | Bow Thrusters | 100 | Mobile | No |
| 3a | Main Propeller | 30 | Fixed | No |
| 3b | Main Propeller | 70 | Fixed | No |
| 4a | Main Propeller | 30 | Mobile | No |
| 4b | Main Propeller | 70 | Mobile | No |
| 5a | Main Propeller + Stern Thruster | 30/100 | Fixed | No |
| 5b | Main Propeller + Stern Thruster | 70/100 | Fixed | No |
| 6a | Main Propeller + Stern Thruster | 30/100 | Fixed | Yes |
| 6b | Main Propeller + Stern Thruster | 70/100 | Fixed | Yes |
| 7a | Bow Thrusters | 40 | Fixed | Yes |
| 7b | Bow Thrusters | 70 | Fixed | Yes |
| 7c | Bow Thrusters | 100 | Fixed | Yes |

4. DISCUSSION & ANALYSIS

4.1 Jet Velocity

Data on efflux velocities for the Donnaconna propulsion system was not available so (1) was used to convert engine power and propeller diameter to efflux velocities. The calculated velocities for various engine powers are shown in Figure 8. From this plot, the laboratory model propellers were calibrated to produce the desired velocity output for the simulated engine percentages required for the test program (see Table 2).

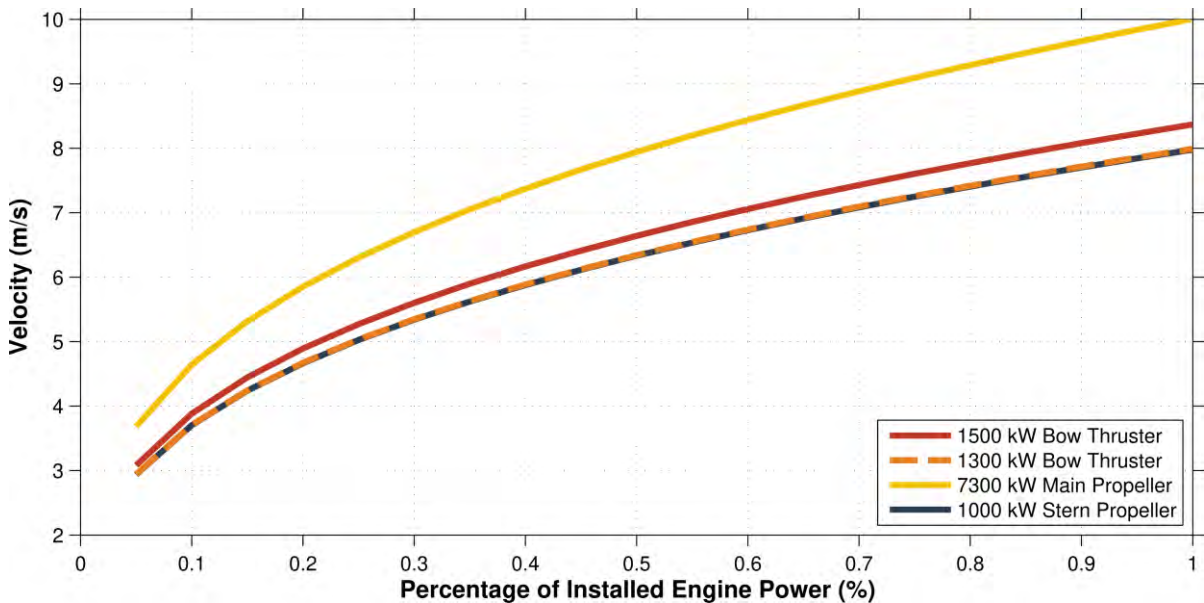


Figure 8: Calculated theoretical efflux velocities for the Donnaconna propulsion systems

Once efflux velocities had been calibrated, the decay of the velocity along the propeller axis was measured for the main propeller, bow thrusters and the stern thruster. The ADV measured velocities were post processed by the program WinADV (Wahl, 2000) by applying the “Phase-space threshold despiking” method from Goring & Nikora (2002). An error value for each velocity measurement was calculated on the post-processed time series as per:

$$x_{rms} = \sqrt{\frac{1}{n}(x_1^2 + x_2^2 + \dots + x_n^2)} \quad (10)$$

where x_{rms} is the root mean square of the data (shown as the error bars in the plots below), n is the total number of values in the time series and x_n is each value in the time series.

These decay measurements were then able to be compared to the available empirical equations from PIANC (2015).

In the case of the main propeller (see Figure 9) the measured velocities were compared to the Dutch Equation (2) and the German Equation (3). The minimum value of the Dutch equation (coefficient from (2) equal to 2.0) is taken to get the best agreement with the data. No guidance is provided in PIANC (2015) on how values between 2.0 to 2.8 for equation (2) should be selected when using this equation. In both cases, the measurements decreased significantly quicker than what was predicted by the equations. The length of the zone of flow establishment, where the efflux velocity is constant, appears to be significantly overpredicted by both methods.

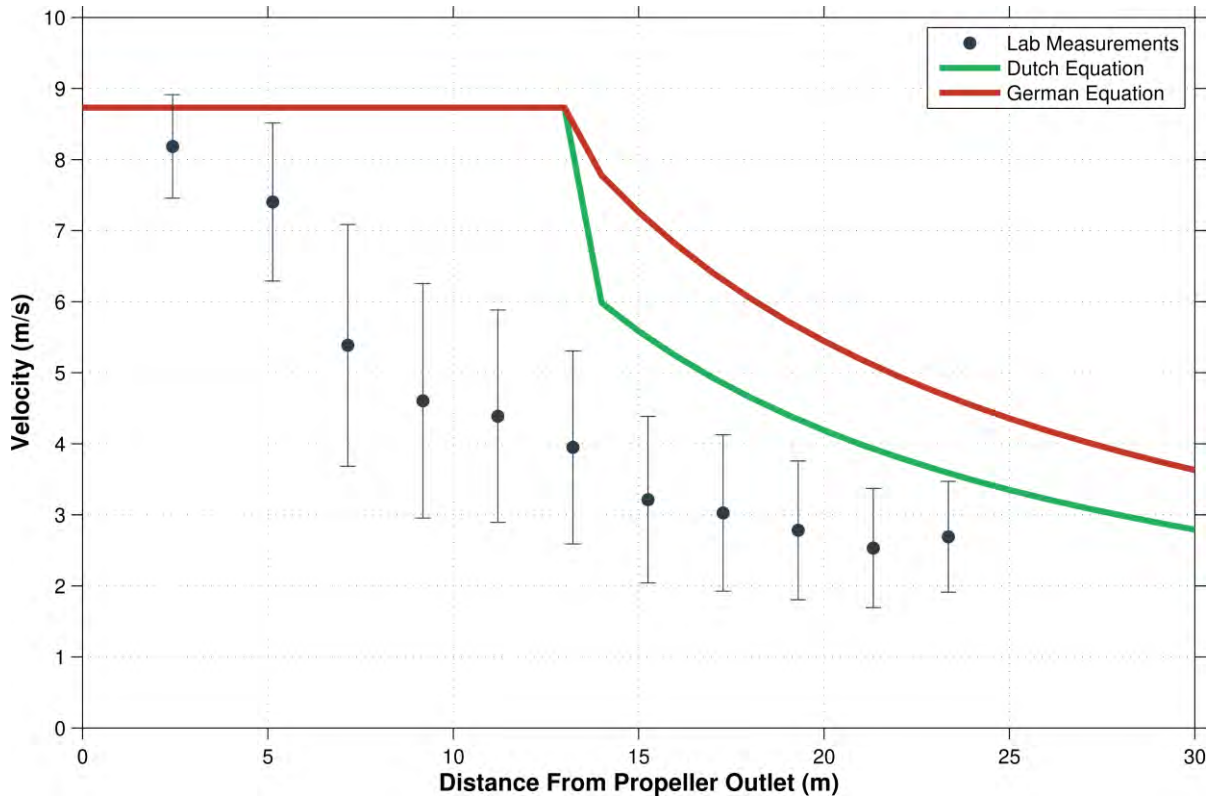


Figure 9: Main Propeller velocity decay profile compared with empirical equations

For the bow thrusters (Figure 10), tests were performed with a single thruster operating and with both thrusters operating. All measurements were taken along the centerline of the lower bow thruster. It is important to note that predicted flow velocities for the case with 2 propellers running would apply between the two axes. In the physical model tests velocities along the centerline of the lower bow

thruster were not influenced by the operation of the second thruster (shown as very little change in the two measurement cases in Figure 10). It is suggested that the equation for two bow thrusters is not relevant and would likely not be representative of many scenarios, especially as it considers that flows increase by the square root of the number of propellers. In this scenario that factor is 1.4 which does not appear to be realistic. More tests would be required to confirm this. The single thruster Dutch equation provides a better approximation but slightly under predicts the velocities at a distance of approximately $4 \cdot D_p$.

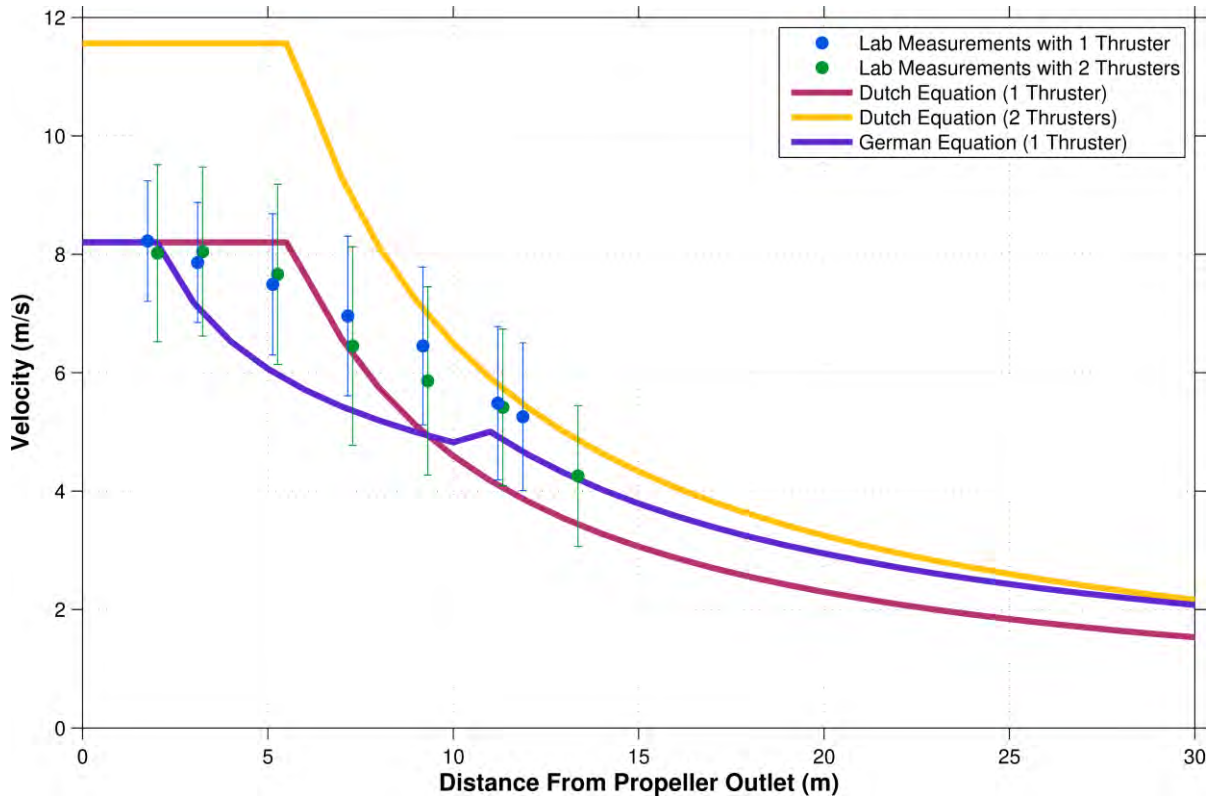


Figure 10: Bow thrusters velocity decay profiles compared with empirical equations

For the stern thruster model tests, a non-ducted propeller was implemented instead of a ducted propeller in order to achieve the desired velocities during the calibration phase. The velocity decay curve is shown in Figure 11 and compares well with both the Dutch and the German equations assuming ducted propellers ($C_3 = 1.17$ in equation (1)). The Dutch equation appears to provide the overall best representation of the flow in this instance.

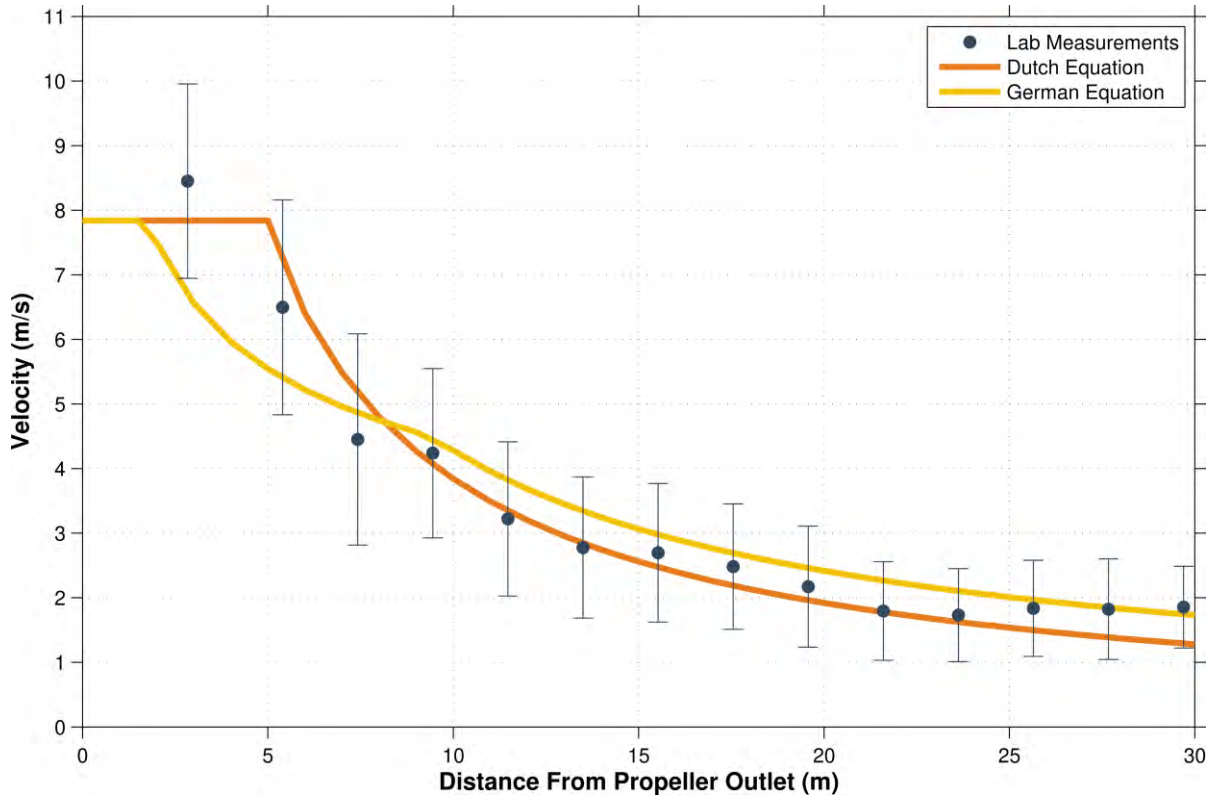


Figure 11: Stern Thruster velocity decay profiles compared with empirical equations

4.1 Armour Stability

Stability was determined mainly using the results of the FARO scan system described above in Section 3.1.

4.1.1 Mobile Bed Tests

Due to the low underkeel clearances considered for this study and the fine sediment native to the berth area, scouring of sediment from underneath the armour slope was the primary failure method throughout all mobile bed tests. During the mobile bed tests significant movement was observed for sediment in front of both bow thrusters (Test 2) and the main propeller (Test 4) during all test scenarios. In all cases this resulted in localized failure of the armour rock slope. An example of the results from Test 2b (bow thrusters in extreme conditions with 100% power) is shown in Figure 12 and Figure 13.

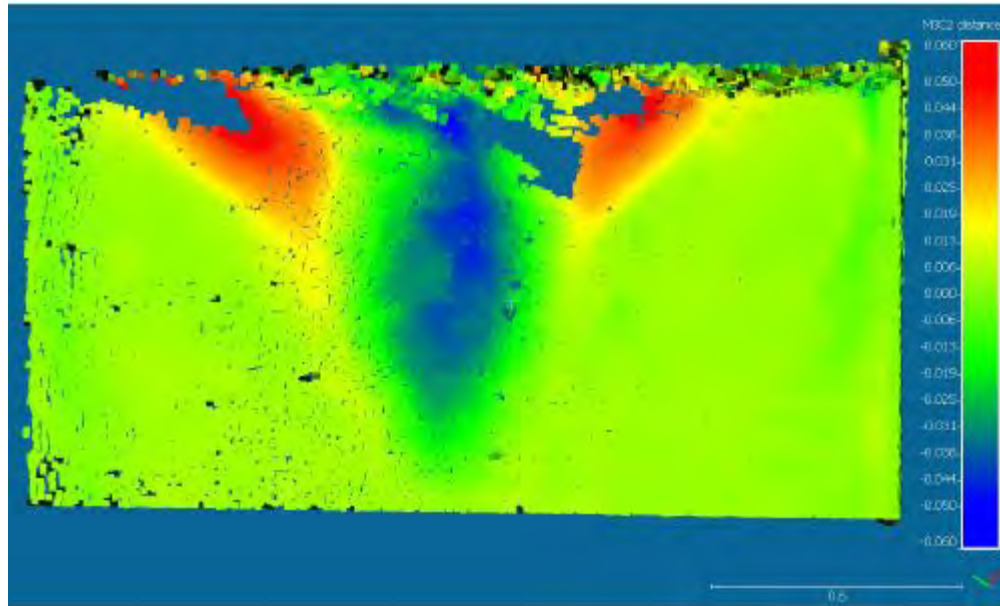


Figure 12: FARO scan results of Test 2b showing show scour hole formation.



Figure 13: Photo of Test 2b scour hole formation

4.1.1 Fixed Bed Tests

Rock movement was observed in all fixed bed tests performed without ACMs. A summary of rock movement is provided in Table 3.

Table 3: Rock movement observed during fixed bed tests

| Test series | Test | Rocks Moved |
|-------------|------|-------------|
| 1 | a | 5 |
| | b | 18 |
| | c | 23 |
| 3 | a | 2 |
| | b | 6 |
| 5 | a | 3 |
| | b | 13 |

Examples of the FARO post-processed scans with rock movement identified are shown in Figure 14 and Figure 15.

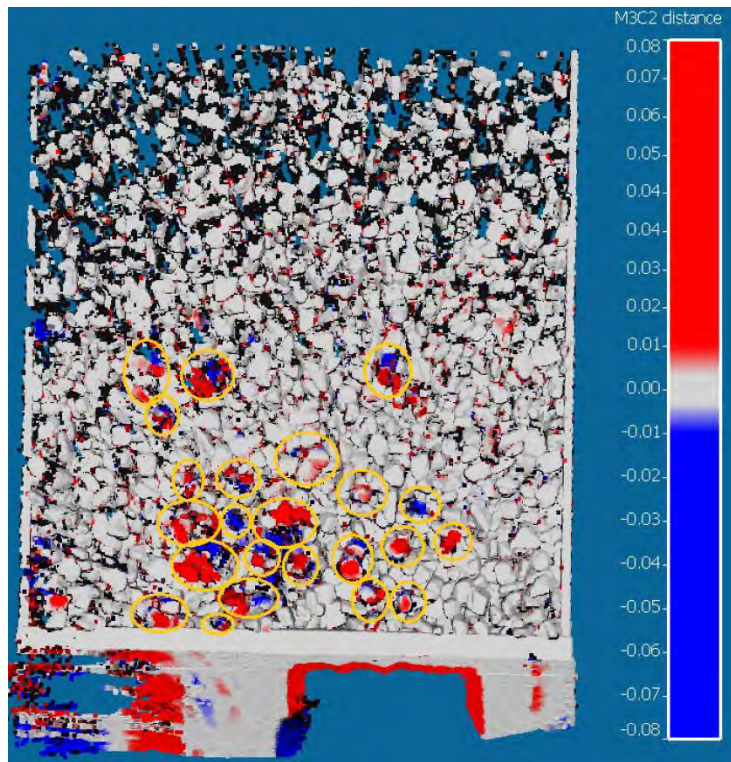


Figure 14: FARO scan at the conclusion of Test 1c. A total of 23 rocks (circled in yellow) moved.

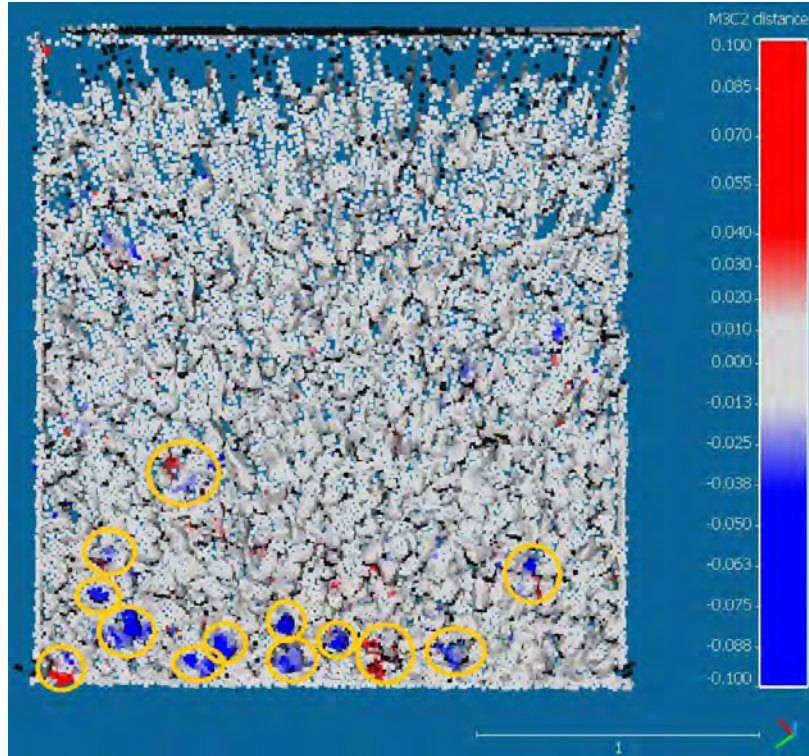


Figure 15: FARO scan at the conclusion of Text 5b. A total of 13 rocks (circled in yellow) moved.

Test results for the bow thrusters during the fixed bed tests showed rock movement outside of the expected wash zone of influence (assuming a 10 degree spread nominally associated with the wash plume). It was assumed that this was due to the rock slope effects, but could also be attributed to the impermeable core (plywood board) used in this model. More testing is required to determine if this pattern is consistent in similar tests. This was important when considering the design limits for additional slope protection such as ACMs.

Using the decay measurements conducted for the propellers (see Figure 9 and Figure 10) an approximate value of the velocity at the slope along the propeller axis was determined. This resulted in $V = 2.5 \text{ m/s}$ @ 25 m from the main propeller outlet and $V = 4.0 \text{ m/s}$ at 14.5 m from the bow thruster propeller outlet. These velocities were used in Equations 7, 8 and 9 to determine what stable rock weights would have been calculated. A stone density of 2700 kg/m^3 was used to replicate the laboratory conditions. For equation 7, a ratio of $D_{50} = D_{85}/1.25$ was used to allow the comparison between all three equations.

Resulting rock weights (shown in Table 4) were then compared with the physical model test results (Table 3). Test 1c was the extreme case for the bow thruster scenario which is assumed to be representative of unstable armour slope conditions (23 total rocks moved). Test 3b was the extreme scenario for the main propeller testing which saw limited rock movement and was marginally unstable.

Table 4: Predicted stable rock weights for each stability equation

| Wash Source | Required Rock Weight, W_{50} (kg) | | |
|----------------|-------------------------------------|--------------|-----------------|
| | German | Dutch/Izbash | Dutch/Pilarczyk |
| Main Propeller | 21 - 155 | 75 | 1,770 |
| Bow Thrusters | 360 – 2,585 | 1,280 | 29,700 |

The German methodology provided a wide range of values when using the recommended B_{crit} (0.9-1.25) values. With $B_{crit} = 1.25$, rock sizes are clearly under predicted ($W_{50} = 21$ and 360 for main propeller and bow thrusters respectively). Using $B_{crit} = 0.9$ resulted in the stable rock weight for the main propeller being too small (155 kg) but the bow thruster recommended weight of 2,585 kg is likely a realistic value.

Similarly, the Dutch/Izbash equations underpredict the rock sizes for the lower main propeller velocity but propose a reasonable 1,280 kg for bow thruster protection. Both of these methods (German and Dutch/Izbash) require more research into why reasonable values for protection are only produced at higher velocities. More guidance is also needed on the wide range of values proposed in PIANC (2015) for the B_{crit} constant in the German equation.

Finally, the Dutch/Pilarczyk method has significantly higher values for both propulsion methods. In this case the main propeller stable armour weight is of a reasonable scale (~1.8t) while the bow thruster armour weight is not. This equation has a significant amount of parameters and the guidance provided in PIANC (2015) could be further refined to improve its predictive ability

Overall, all three equations predict a significant increase in weight for a velocity increase of 1.5 m/s. More testing is required to determine if there is an optimal velocity range that some of these equations work well for or if the equations require modification when being used with actual velocity values, as opposed to predicted velocities output by equations 1 – 6.

4.1.2 Articulated Concrete Mattresses

For Test 6 and Test 7 ACMs were placed on the slope and secured at the top using their cables. They extended 2.7 m from the toe of the armour slope (approximately 6 square units)

For Test 6 the ACMs were secured only from the top of the slope in order to see if the weight of the mattresses alone was sufficient to add protection to the slope. After both of the tests in the series, progressive flipping of the mats was observed which made them ineffective. An extreme example of the flipping that occurred from Test 6b is displayed in Figure 16 .

For the final test, the mats were tied together at the toe and mid way up the slope to see if this would remove the flapping and subsequent flipping of mattresses observed during Test 6. During Test 7, some flapping was observed during the actual testing but no movement was documented by the scan at the ending of the test as seen in Figure 17.

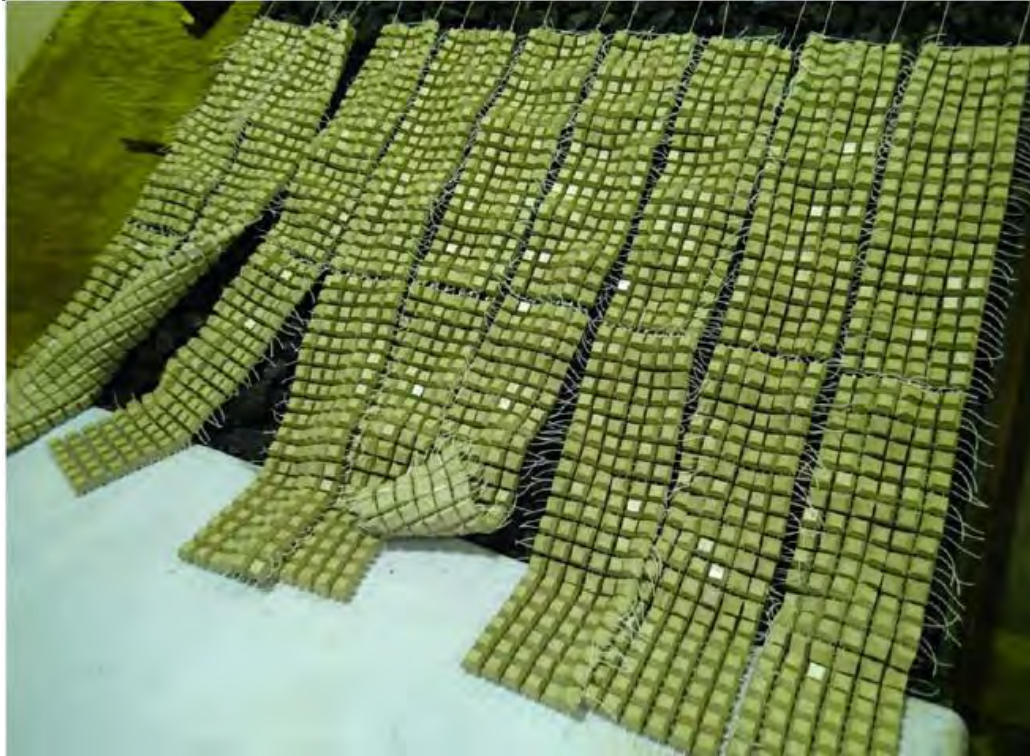


Figure 16: Armoured slope with ACMs after the conclusion of Test 6b.

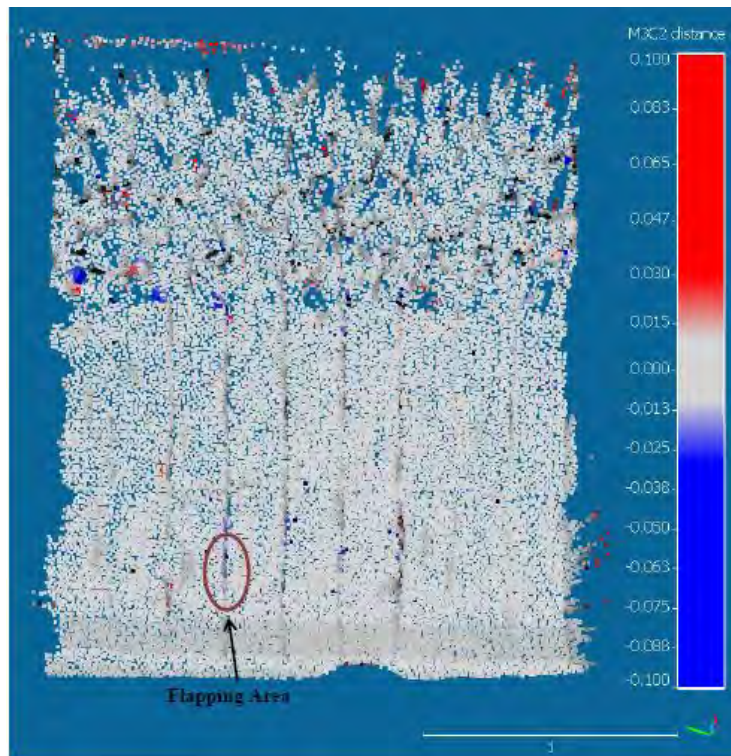


Figure 17: FARO scan at the conclusion of Test 7b.

5. CONCLUSION

A series of physical model tests were performed to better understand the effects of the TSV Donnaconna's propulsion system on an armour slope during the berthing process. Over the course of these tests, measurements of the decay of velocities as a function of distance from the propeller provided the following conclusions:

- For all three propeller type tests, velocities were seen to drop sharply with distance from the propeller. This leads to the conclusion that the zone of flow establishment which is typically valid for $2.6 \cdot D_p$ may not be representative for large propellers;
- In addition to the over prediction of the zone of flow establishment, both the Dutch and German equations significantly over predicted the velocities with increasing distance from the main propeller jet;
- When measuring along the centerline of a one bow thruster jet there was no increase in velocity along the propeller axis when the second jet was operational. The modification of equation (2) for two jets is likely conservative, especially in the zone closest to the propeller outlet. This supports the findings of Dykstra et al. (2010) who came to similar conclusions; however, more tests are needed to determine if the results are the same for different bow thruster arrangements.
- The Dutch equation (2) provided the best approximation of flow decay for all three test cases in these physical model experiments.

Measurement of armour rock stability during fixed bed tests provided the following conclusions:

- During the operation of the bow thrusters, rock movement was witnessed outside of the expected zone of influence (assuming a 10% spread of the jet). This is likely due to the effects of the rock slope and should be considered when providing additional protection to slopes in the zones of influences of thrusters;
- Articulated Concrete Mattresses were found to be effective at stabilizing the velocities produced by the propulsion system only if tied together at the toe and top of the slope. For real world applications it is recommended that the ACMs should be connected along their full length to neighbouring mats;
- More testing is required to understand and refine the equations from PIANC (2015) sizing rock for armour stability. Calculations for measured velocities show that the German and the Dutch/Izbash equations provide reasonable estimates of stable rock sizes at higher velocities produced by bow thrusters but under predicted rock sizes for a propeller velocity of 2.5 m/s. The Dutch/Pilarczyk predicted significantly higher velocities than the other equations but also had a significant discrepancy between the two velocities tested. More research is needed to refine and understand the use of these equations with measured velocity values.

Based on the results presented herein, equations used to predict propeller wash velocities and subsequent stable armour rock are highly variable and require further research. For these reasons scale physical models are recommended to determine and test suitable armour protection for vulnerable slopes at port facilities.

ACKNOWLEDGMENTS

Generous thanks to Nathan Fuller from CITIC Pacific Mining for enabling this contribution.

REFERENCES

Australian Maritime College (2016). CSL Shipping: Cape Preston Donnacona Simulations.

Blaauw, H.G., and van de Kaa, E.J. (1978). Erosion of bottom and sloping banks caused by the screw race of manoeuvring ships. Delft Hydraulics Laboratory, publication no. 202.

CIRIA, CUR, CETMEF (2007). "The Rock Manual. The use of rock in hydraulic engineering". 2nd Edition.

Dykstra, D., Tschirky, P., Shelden, J., & Cornett, A. (2010) Physical Model Tests of Bowthruster Impacts on Armored Slopes. Ports 2010.

Goring, D.G., and Nikora, V.I. (2002). Despiking Acoustic Doppler Velocimeter Data. Journal of Hydraulic Engineering, 128(1), 117-126.

PIANC (2015). Report No 180, Guidelines for Protecting Berthing Structures from Scour Caused by Ships, PIANC, Brussels.

Pilarczyk, K. (1990). "Coastal Protection". Proc. of a short course, published by A.A. Balkema, Rotterdam.

Subcon (2017). Subcon awarded sino iron project for manufacture & supply of concrete scour mattresses. November 3, 2017. www.subcon.com.

van Doorn, R. (2012). Bow thruster currents at open quay constructions on piles. Master's Thesis from Delft University of Technology, Delft, The Netherlands.

Wahl, T. (2000). Analyzing ADV Data Using WinADV. 2000 Joint Conference on Water Resources Engineering and Water Resources Planning & Management. Minneapolis, Minnesota.

PRESSURE DISTRIBUTION ACTING ON BREAKWATER CAISSON UNDER TSUNAMI OVERFLOW

by

Kojiro Suzuki¹ and Kenichiro Shimosako²

ABSTRACT

Many caissons of breakwaters were slid or overturned due to tsunami overflow pressure caused by 2011 Tohoku earthquake. To prevent this sliding failure, the pressure estimation method under tsunami overflow was introduced in the new Tsunami-Resistant Design Guideline for Breakwater in 2015. In this guideline, the uplift and the overburden pressure are not considered, instead only static buoyancy acting on the caisson is considered. However, under tsunami overflow, the pressure difference between the bottom and the top of breakwater caisson, especially the caisson having a large parapet, can be extremely larger than the buoyancy force. In order to examine this excess uplift force, a series of hydraulic experiments and numerical simulations were conducted. The experiment was conducted in an experimental flume in which the large pump was installed to produce tsunami overflow. Through the experiments and numerical simulations, it was clarified that the large uplift pressure and the small overburden pressure cause the dynamic buoyancy larger than the quasi-static buoyancy estimated by the design guideline. This upward force reduces the stability of caisson, especially the caisson having the large parapet.

1. INTRODUCTION

The caissons of many breakwaters either slid or overturned due to overflow pressure of the tsunami triggered by the 2011 Tohoku earthquake. For example, the offshore tsunami breakwater of Kamaishi Port, constructed to protect Kamaishi City, was destroyed by the huge tsunami overflowing the breakwater. Up until the 2011 disaster, tsunami overflow had not been considered in breakwater design; rather, it had been estimated by Tanimoto's tsunami force formula (1)-(4) (Tanimoto et al., 1984). However, Tanimoto's formula cannot express the force of tsunami overflow.

$$\eta^* = 3.0a_I \quad (1)$$

$$p_1 = 2.2\rho_0 g a_I \quad (2)$$

$$p_u = p_1 \quad (3)$$

$$p_L = p_2 \quad (4)$$

Since the widespread damage engendered by the Tohoku tsunami overflow, the pressure formula under tsunami overflow has been studied using hydraulic experiments, and, in 2015, the experimental results were introduced in the Tsunami-Resistant Design Guideline for Breakwater (MLIT, 2015). In the guideline, the new tsunami pressure formula is expressed by the quasi-hydrostatic pressure due to the tsunami water level. The front and the rear pressure are expressed as modified hydrostatic pressures (5)-(7). The modification factor is 1.05 at the front (α_f) and 0.9 at the rear (α_r).

$$p_1 = \alpha_f \rho_0 g (\eta_f + h') \quad (5)$$

$$p_3 = \alpha_r \rho_0 g (\eta_r + h') \quad (6)$$

¹ Maritime Structures Group, Port and Airport Research Institute, suzuki_k@pari.go.jp

² Senior Director for International Affairs, Port and Airport Research Institute

$$p_2 = (\eta_f - h_c) / (\eta_f + h') p_1 \quad (7)$$

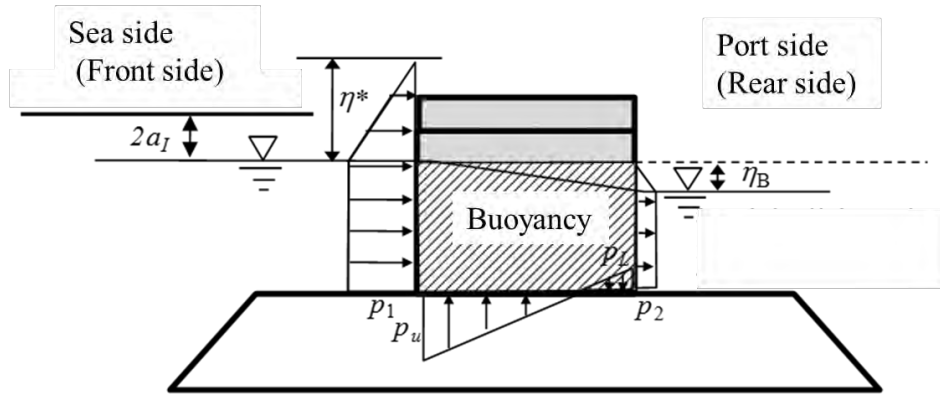


Figure 1: Tanimoto's tsunami pressure distribution (expressed as hydrodynamic pressure)

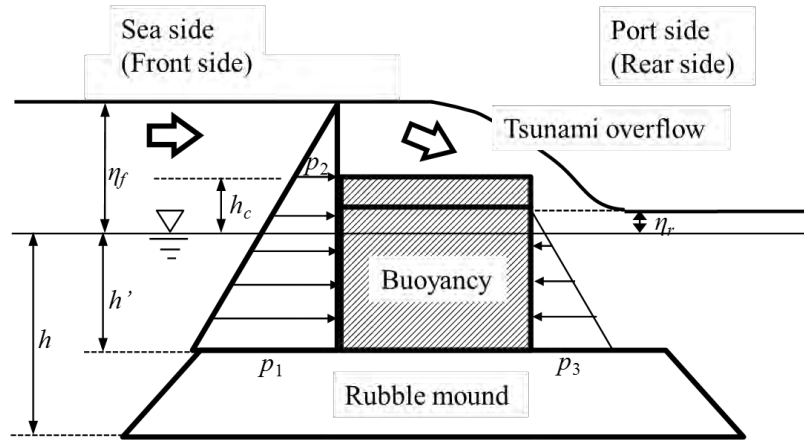


Figure 2: Pressure distribution and buoyancy defined by the Tsunami-Resistant Design Guideline for Breakwater (2015) (expressed as quasi-hydrostatic pressure)

Many breakwaters in Japan have been inspected and redesigned using the new design formula. However, some design problems remain. Because the new design formula is intended for simple rectangular caisson-type breakwaters, the uplift and overburden pressure are not considered; instead, only the buoyancy acting on the caisson is considered in the guideline. However, the buoyancy under hydrostatic condition can be different from the buoyancy under hydrodynamic tsunami condition as shown in the schematic figure (Fig. 3).

In the hydrostatic condition, the buoyancy is equivalent to the weight of the fluid that would otherwise occupy the volume of the object, i.e. the displaced fluid (Fig. 3 (a), (c)). The buoyancy is equivalent to the pressure difference between the bottom and the top of the immersed object. However, under tsunami overflow condition, the pressure difference between the bottom and the top of the breakwater caisson, especially a caisson having a large parapet, can be extremely larger than the buoyancy under hydrostatic condition (Fig. 3 (b), (d)). Here, we define the buoyancy under static condition (tsunami dynamic condition) as static buoyancy, B_{static} (dynamic buoyancy, $B_{dynamic}$).

Sato et al. (2016) estimated the overburden pressure p_o as a trapezoidal pressure distribution. However, the shape of the water surface elevation at the top of caisson isn't a trapezoidal shape while the flow changes from subcritical flow to supercritical flow. Moreover, if the parapet is high and thin and overflow depth is small, mass of displaced fluid can be extremely less than the uplift pressure.

In order to examine this buoyancy, a series of hydraulic experiments and numerical simulations were conducted in this study.

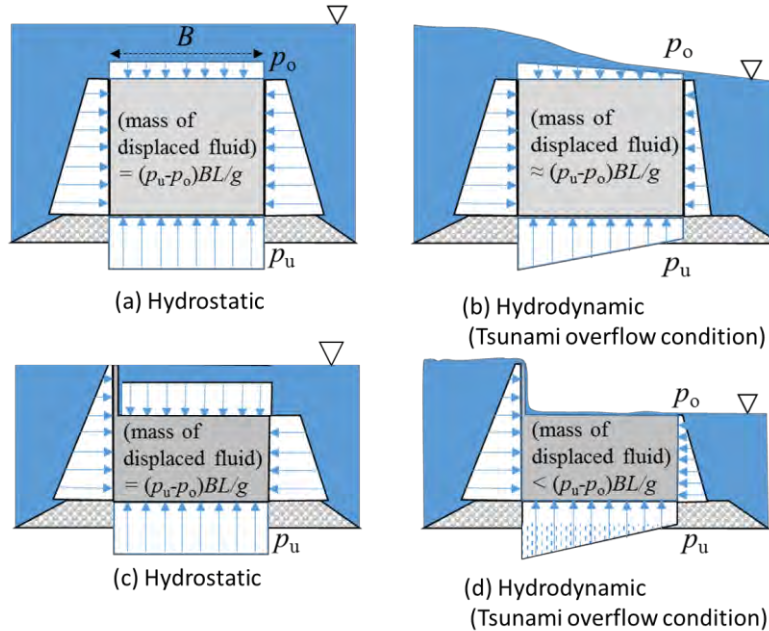


Figure 3: Schematics of buoyancy and pressure distribution under static and dynamic overflow condition. B (L) is the width (length) of the caisson.

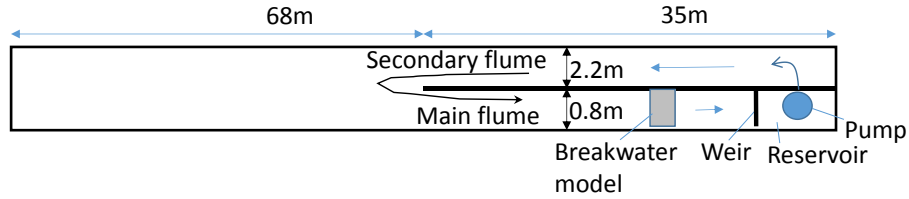
2. HYDRAULIC EXPERIMENT

2.1 Experimental Setup and Condition

The experiments were performed using a flume with the length of 105m. As shown in Fig. 4, the flume was separated by the vertical wall and the width of the main flume and the sub-flume, for circulation of the water, were set to 0.8m and 2.2m, respectively. As shown in Fig. 4, tsunami overflowing on a breakwater model was reproduced under uniform flow, which was generated by a pump installed behind a weir in the main flume, and circulated through the main and secondary flumes. Pressure gauges, water elevation gauges and propeller-type current profilers were installed around breakwater model.

Initial water depth h_f (inundation depth η_f) was changed from 0.42 to 0.52m (from 0.044 to 0.144m). The height of weir was changed from 0.14 to 0.35m.

(a) Plan view



(b) Sectional view

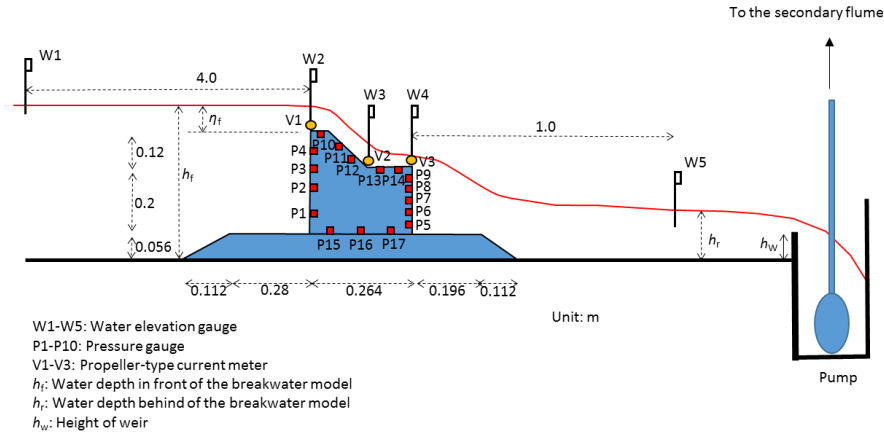


Figure 4: Details of the experimental flume and the model

2.2 Experimental Results

Fig. 5 shows the pressure distribution around the caisson under overflow condition. The pressure distribution in front and behind the caisson is almost static and triangle shape. In contrast, the pressure on the caisson is different from the pressure distribution estimated from the water surface elevation. The pressure at the front part (rear part) of the top of caisson measured by the pressure gauges is smaller (larger) than the pressure estimated from the water surface elevation. Decrease of pressure at the front part is supposed to be caused by the increase of velocity, the significant downward acceleration of the water particle around the curving flow and the occurrence of eddy. On the other hand, increase of pressure at the rear part is supposed to be caused by the collision of water on the caisson.

Fig. 6 shows the relationship between the velocity (V1) and the pressure decrease, Δp (P10) at the top of the caisson. The pressure is nondimensionalized by the water depth, η at P10. Pressure decreases as the velocity increases. The pressure decrease is supposed to be caused by the increase of velocity and the significant downward acceleration of the water particle around the curving flow

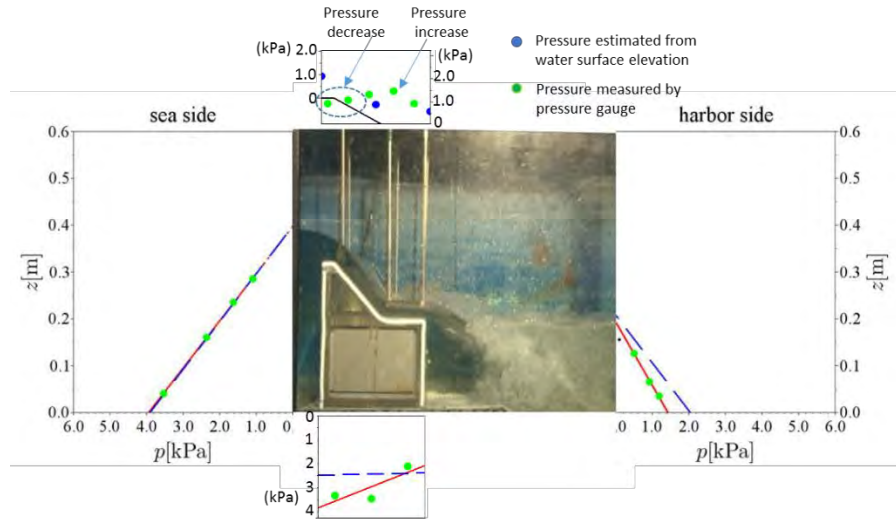


Figure 5: Pressure distribution on top of the caisson

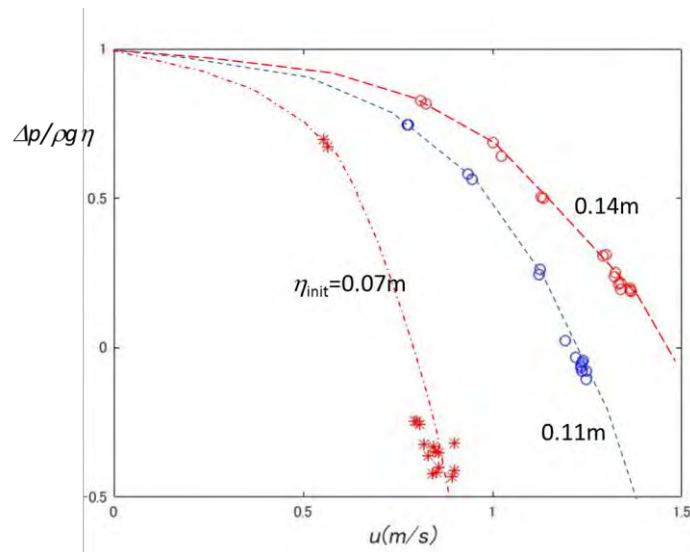


Figure 6: Relationship between velocity and pressure decrease at the top of the caisson

3. NUMERICAL ANALYSIS

3.1 Computation method

Tsunami overflow reproduced in the hydraulic experiment was simulated by the VOF method implemented in the CADMAS-SURF-2D CFD model (CDIT, 2001). Fig.7 shows the schematic of the computation domain and boundary condition. Inflow (Outflow) velocity is set as 0.02-0.1m/s (0.3m/s) at the offshore (onshore) boundary. The horizontal and vertical grid size is 0.01m. The initial water depth was set at 0.39-0.45m. The weir set the water level behind the caisson and the height was 0.14 and 0.2m.

Four caisson models were examined as shown in Fig. 8. Cross section 1 (CS1) corresponds to the caisson model of the experiment.

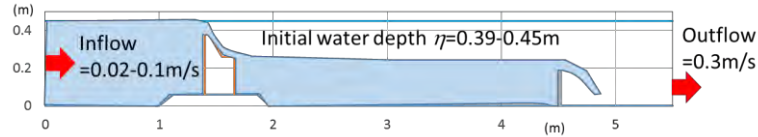


Figure 7: shows the cross section of numerical

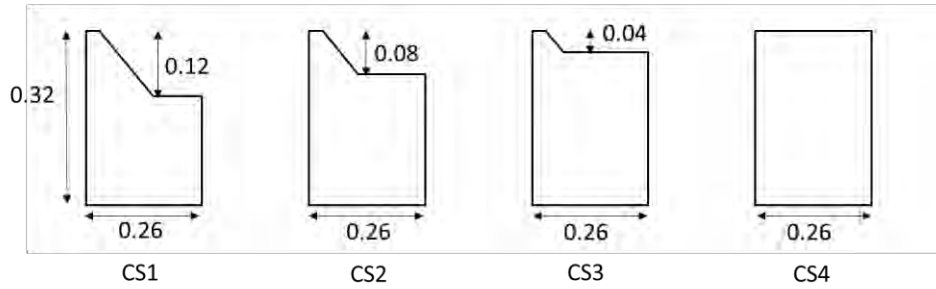


Figure 8: Cross sections of caisson model

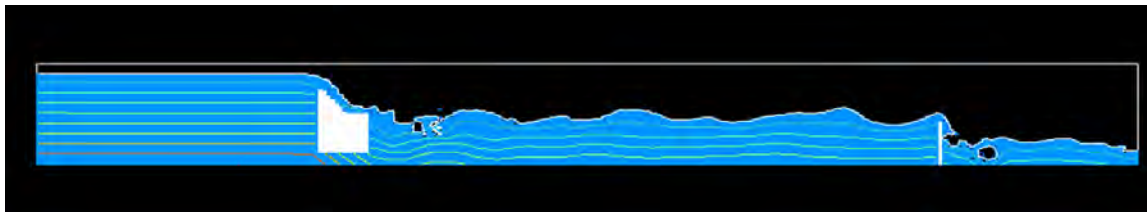
3.2 Computation Result

Fig.9 shows the snapshot of the CS1. The water surface elevation in front of caisson is 0.45m and the height of the weir behind the caisson is 0.2m.

Fig.10 shows the pressure at the top and bottom of the caisson (p_{bottom} , p_{top}) with water surface elevation ($h_{surface}$). Pressure head ($p_{top}/\rho g$) at the front part of the top of caisson is smaller than the water surface elevation ($h_{surface}$) as shown in the experimental result (Fig.5).

Fig.11 shows the ratio of dynamic buoyancy ($B_{dynamic}$) and static buoyancy (B_{static}) with different water surface elevation ($\eta_{front}/h_{caisson}$) when the height of weir (h_{weir}) is 0.14m. Here, η_{front} is defined as water surface elevation in front of caisson during tsunami overflow and $h_{caisson}$ is the caisson height. Since the water depth behind the caisson is shallow, the pressure at the bottom of the caisson is small, resulting the dynamic buoyancy ($B_{dynamic}$) is smaller than the static buoyancy (B_{static}).

In contrast, the ratio of Fig.12 is much larger than the ratio of Fig.11 when the height of weir (h_{weir}) is 0.2m. In the case of CS1 and CS2 (Caisson with large parapet), the dynamic buoyancy ($B_{dynamic}$) is 5% larger than the static buoyancy (B_{static}).



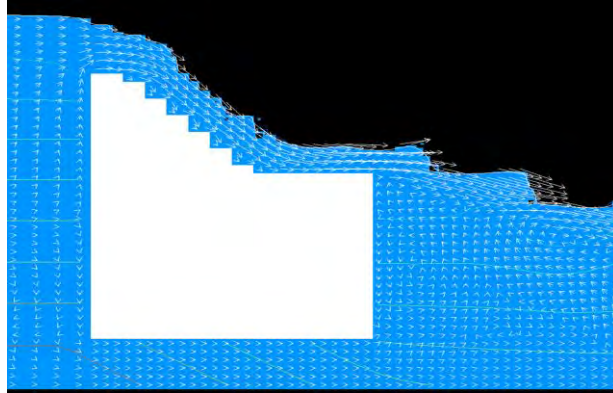


Figure 9: Snapshot of CS1 ($h_{\text{front}}=0.45\text{m}$, $h_{\text{weir}}=0.2\text{m}$)

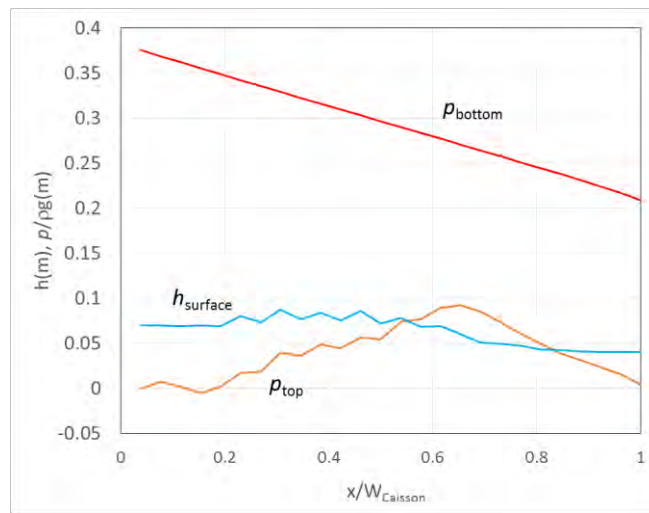


Figure 10: Pressure at bottom and top of the caisson (p_{bottom} , p_{top}) with water surface elevation (h_{surface}) (CS1, $h_{\text{front}}=0.45\text{m}$, $h_{\text{weir}}=0.2\text{m}$)

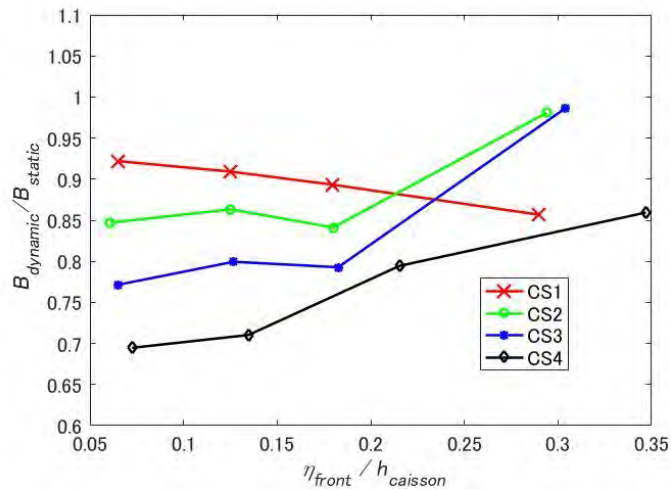


Figure 11: Ratio of dynamic and static buoyancy ($h_{\text{weir}}=0.14\text{m}$)

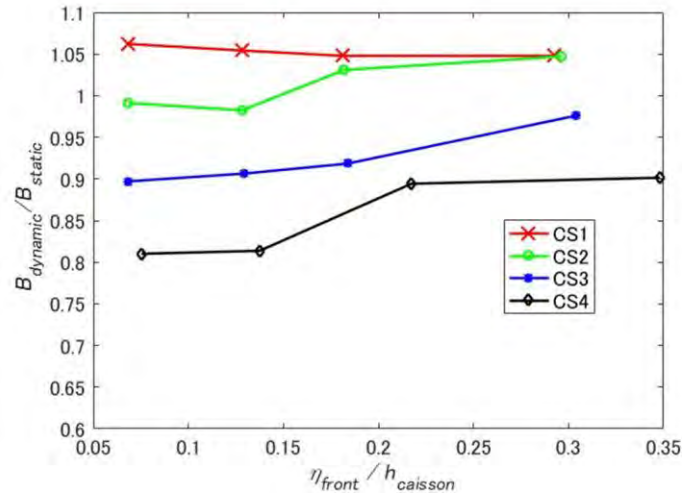


Figure 12: Ratio of dynamic and static buoyancy ($h_{weir}=0.2m$)

4. CONCLUSIONS

A hydraulic experiment and a numerical simulation of tsunami overflowing on the caisson type breakwater was conducted and the following clarified.

- 1) The pressure on the caisson under tsunami overflow condition is smaller than the static water pressure corresponding to the water level. The significant downward acceleration of the water particle around the curving flow appears to be the main reasons of the observed pressure drop at the front end of the caisson.
- 2) The large uplift pressure and the small overburden pressure during tsunami overflow cause the large dynamic buoyancy. The dynamic buoyancy acting on the caisson with large parapet is 5% larger than the static buoyancy estimated by the design guideline (2015).

References

- Coastal development institute of technology (CDIT) (2001). CADMAS-SURF, CDIT library No. 12, 68p.
- Ministry of Land, Infrastructre, Transport and Tourism (MLIT) (2015). Tsunami-Resistant Design Guideline for Breakwater, website; http://www.mlit.go.jp/kowan/kowan_tk5_000018.html. (in Japanese).
- Sato, M., Omura, A., Shibata, D., Uehara, K., Oikawa, T., & Aoki, N. (2016). Analysis on the Effect of Widening Works of Breakwaters against Tsunami-induced Seepage Flow in the Rubble Mound, Journal of Japan Society of Civil Engineers, Ser. B3 (Ocean Engineering), Vol.72, No.2, pp.I_533-I_538. (in Japanese).
- Tanimoto, K., Tsuruya, H. and Nakano, S. (1984). Experimental Study of Tsunami Force and Investigation of the Cause of Sea Wall Damage During 1983 Nihonkai Chubu Earthquake, Proc.31st Japanese Conf. Coastal Eng., pp.257-261. (in Japanese)

DESIGN VALUES FOR BERTHING VELOCITY OF LARGE SEAGOING VESSELS by

A.A. Roubos¹, L.Groenewegen², J. Ollero³, C. Hein⁴ and E. van der Wa⁵

ABSTRACT

While ships evolve constantly, berthing velocity curves developed during the 1970s are still embedded in the design of marine structures. Associated safety factors for the design of fender systems have not been verified and validated by measurement campaigns. In this study, field observations of modern large seagoing vessels during berthing manoeuvres in Bremerhaven, Rotterdam and Wilhelmshaven were used to evaluate safety factors for berthing energy and berthing impact loads in line with the Eurocode design philosophy. Berthing velocities were examined for several types and categories of vessels at various berths and under different operational conditions, resulting in an increased understanding of the factors influencing berthing energy. Navigation conditions were accounted for by differentiating factors such as vessel characteristics, environmental conditions and berthing policy. The results show that characteristic values of berthing velocity with a return period of 50 years are in line with design recommendations in the relevant literature. Design values of berthing velocity are quite sensitive to the number of berthing operations during the service life of a marine structure. The measured berthing velocities largely depend on the general berthing regulations and local experience of pilots and navigational aids. Due to newly acquired insights, some historically embedded hypotheses will need to be reconsidered. For instance, the assumption that berthing velocities are correlated to the size of large seagoing vessels could not be confirmed based on the measurements for ships larger than 30,000 DWT. The key findings of this study are useful for the design of new berthing facilities and for the assessment of existing marine structures. It is highly recommended to update the PIANC 2002 guideline titled 'Berthing velocities and fender design' in the upcoming years.

1. INTRODUCTION

Marine structures, such as quay walls, jetties and flexible dolphins, are required all over the world to accommodate ships' berthing, mooring and loading operations. During the service life of a marine structure, functional requirements may change. These changes often result in uncertainty regarding the actual berthing energy of vessels and structural integrity of marine structures, especially if the size of the design vessels due to modified operational requirements increases at existing berthing facilities [15]. The current design guidelines for assessing berthing energy, such as PIANC [17], British Standards [4], EAU [6] and Spanish ROM [13], propose to use safety factors for abnormal berthing. These recommendations are not based on a semi-probabilistic design method and do not include partial factor analyses of individual parameters. Hence, it is not clear how resultant fender forces derived from such analyses should be applied in accordance with the design philosophy of the Eurocode Standards [10].

¹ Port of Rotterdam, Port Development, aa.roubos@portofrotterdam.com; TU Delft, Department of Hydraulic Engineering.

² Delta Marine Consultants, Maritime Structures, l.groenewegen@dmc.nl.

³ INROS LACKNER SE, Juan.Ollero@inros-lackner.de.

⁴ Port of Bremerhaven, Port Development, christian.hein@bremenports.de.

⁵ Port of Rotterdam, Port Development, e.wal@portofrotterdam.com.

Metzger et al. [9] stated that load demands on berthing structures are not well understood due to a lack of information about berthing parameters. Therefore, there is a strong need to determine corresponding design values for these parameters and partial safety factors by using field observations. Although design guidelines recommend to collect comprehensive berthing records, data are mostly not available. Ueda et al. [19] showed that berthing velocity is the crucial design parameter in defining berthing energy. The port authorities of Bremerhaven [7] and Rotterdam [14] therefore decided to start a measurement campaign on berthing velocity in order to evaluate and validate the performance of existing berthing facilities and the design guidance of EAU and PIANC. The objective of this campaign was to validate the berthing velocity curves given by the EAU and PIANC, presented in Figure 1, for modern vessels.

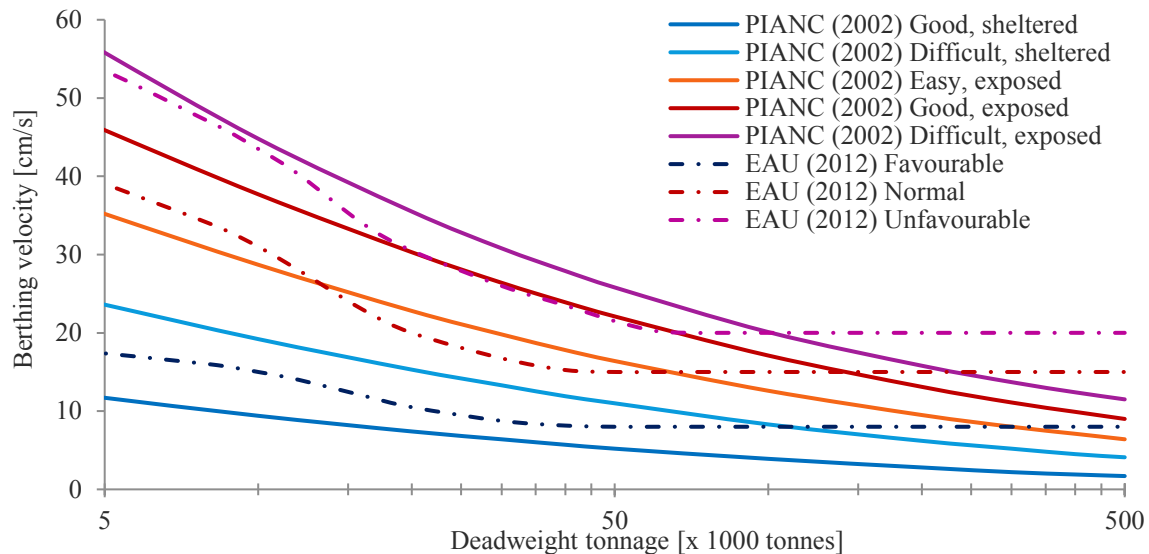


Figure 1: Berthing velocity curves of PIANC 2002 (Brolsma curves [2]) and EAU 2012 as a function of navigation conditions and vessel size [14]

The berthing velocities given by the PIANC and the EAU – EAU values are based on the ROM recommendations – represent berthing velocities with a return period of 30 and 50 years, respectively [1], [15]. Since the development of the Brolsma curves in the 1970s, new measurements of berthing velocities have become available [7], [14], [20]. These studies resulted in a better understanding of various factors influencing berthing velocity. The most important conclusion was that the collected data do not confirm the historical assumption that berthing velocities are strongly related to ship dimensions of large seagoing vessels. Where berthing records are available, existing design guidelines do not provide explicit recommendations with regard to the statistical examination of berthing velocities. It is therefore mostly unclear how the results of field observations could be incorporated in the design process.

This paper aims to provide guidance on the use of field observations in the assessments of marine structures. It should be noted that ship collision impact is not taken into consideration in this study [18]. During the study, recently recorded field observations of berthing velocity in the ports of Bremerhaven, Rotterdam and Wilhelmshaven were used to determine theoretical design berthing velocities and corresponding partial safety factors in accordance with the Eurocode Standard [10].

2. GENERAL PRINCIPLES OF BERTHING ENERGY AND IMPACT

The objective of this section is to elucidate the definition of berthing energy E and the associated resulting berthing impact load F . The berthing energy is generally calculated using the following equation:

$$E_{kin} = \frac{1}{2} M v^2 C_m C_s C_c C_E \quad (1)$$

in which:

| | |
|-----------|---|
| E_{kin} | Kinetic energy [kJm] |
| M | Mass of vessel/water displacement [tonnes] |
| v | Total translation velocity of centre of mass at time of first contact [m/s] |
| C_m | Virtual mass factor [-] |
| C_s | Ship flexibility factor [-] |
| C_c | Waterfront structure attenuation factor [-] |
| C_E | Eccentricity factor [-] |

PIANC berthing velocity curves are widely used by the industry to determine the 'normal' berthing energy. Given a normal berthing energy, a berthing impact factor C_{ab} is applied to derive an abnormal berthing energy. An overview of abnormal berthing factors in literature is given in Table 1.

$$E_{abnormal} = C_{ab} E_{normal} \quad (2)$$

in which:

| | |
|----------------|--------------------------------|
| $E_{abnormal}$ | Abnormal berthing energy [kJm] |
| C_{ab} | Abnormal berthing factor [-] |
| E_{normal} | Normal berthing energy [kJm] |

Table 1: Abnormal berthing factor C_{ab} [-] in literature.

| Ship type | Size | PIANC [17] | EAU [6] | BS 6349-4 [4] | ROM [13] | OCDI [16] | EN 1990 [10] |
|-----------------|------------------|------------|------------------------|-------------------|----------|-----------|--------------|
| Tankers | Largest-Smallest | 1.25-2.00 | 1.25-2.00 ¹ | - | 2.00 | - | - |
| Bulkers | Largest-Smallest | 1.25-2.00 | 1.25-2.00 ¹ | - | 2.00 | - | - |
| Container | Largest-Smallest | 1.50-2.00 | 1.50-2.00 ¹ | - | 2.00 | - | - |
| General Cargo | - | 1.75 | 1.75 ¹ | 1.50 ² | 2.00 | - | - |
| RoRo, ferries | - | ≥ 2.00 | ≥ 2.00 ¹ | - | 2.00 | - | - |
| Tugs, workboats | - | 2.00 | 2.00 ¹ | - | 2.00 | - | - |
| LNG, LPG | - | - | - | 2.00 | 2.00 | - | - |
| Island berth | - | - | - | 2.00 | 2.00 | - | - |

¹) Based on PIANC 2002 [17]

²) Continuous quay handling conventional cargo vessels

The berthing impact load F to which a marine structure is subjected is a function of the kinetic energy absorbed by the berthing system and of its deformation characteristics δ [13], [15]. Given a certain berthing velocity, the resulting berthing impact load largely depends on the stiffness of the marine structure and the soil conditions [13]. When significant softening occurs between a characteristic berthing impact load (service limit state) and a design berthing impact load (ultimate limit state), a reduction of the partial factor γ_Q could be considered, for instance in the design of flexible dolphins equipped with cone fenders. The effect of softening on energy absorption due to linear and non-linear behaviour is illustrated in Figure 2. When the hatched areas below the linear (left) and non-linear (right) load-deflection curve are equal, the design berthing impact load F_d is lower in the case of softening.

$$E_{kin} = \int_0^{\delta_{max}} F(\delta) d\delta \quad (3)$$

in which:

- F Berthing impact load [kN]
- δ Deflection of berthing structure [m]

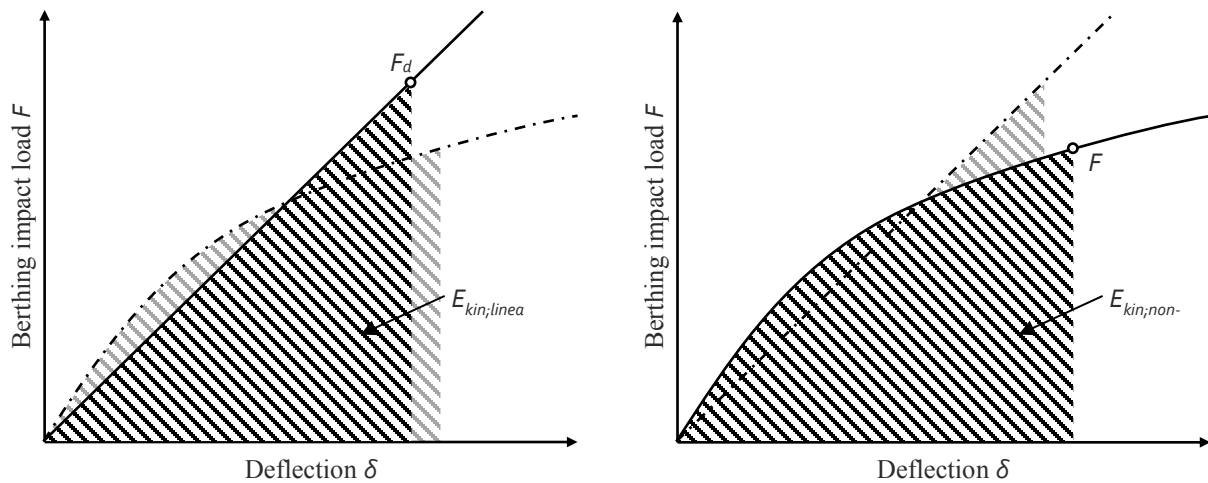


Figure 2: Linear system (left) and non-linear system with significant softening (right)

3. MATERIAL & METHODS

3.1 Data collection

Approximately 1950 records of berthing operations were collected in Germany (#1393) [7] and the Netherlands (#555) [14]. Various types of vessels, berths and navigation conditions were represented in the datasets. All berthing records were collected in well-organised port environments, namely Bremerhaven (1235), Rotterdam (555) and Wilhelmshaven (158). An overview of the collected data is given in **Table 2**. The berths in Bremerhaven were classified as exposed and berthing operations seemed to be influenced by strong tidal currents; the tidal range is typically about 3.8 m with tidal currents of 2.5–3.5 knots. All other berths were classified as sheltered.

Table 2: Overview of field observations of berthing velocity [15]

| Ship type [-] | n [-] | v_{μ} [cm/s] | v_{max} [cm/s] | Berth type [-] | Berthing aids [-] | Wind [-] | Waves [-] | Current [-] |
|------------------|------------|---------------------|---------------------|-------------------|----------------------|-------------|--------------|----------------|
| Container □ | 177 | 4.0 | 10 | Closed quay | None | High | Sheltered | Low |
| Tankers ○ | 329 | 4.3 | 12 | Jetty / dolphin | PPU/ docking system | High | Sheltered | Low |
| Bulkers ◇ | 144 | 4.4 | 13 | Closed quay | Portable pilot units | High | Sheltered | Low |
| Container □ | 1235 | 6.6 | 26 | Closed quay | None | High | Exposed | High |

3.2 Partial factors

A probabilistic study by Ueda et al. [19] showed that the contribution of berthing velocity to the uncertainty in kinetic berthing energy was approximately 85%, indicating that safety factors should be applied predominantly to berthing velocity. When defining kinetic berthing energy, berthing velocity is assumed to be the only stochastic variable in Equation (1). The partial factors derived in the present research were therefore applied to a characteristic value of berthing velocity. The partial factor γ_v was defined as the ratio between a design berthing velocity v_d and a characteristic berthing velocity v_k [15]:

$$\gamma_v = \frac{v_d}{v_k} \quad (4)$$

in which:

- γ_v Partial factor for berthing velocity [-]
- v_d Design value of berthing velocity [cm/s]
- v_k Characteristic value of berthing velocity [cm/s]

OCDI [16] and Roubos et al. [14] statistically examined field observations of single berthing velocities. Both studies showed that a distribution fit of the low-probability tail was closer to a Weibull distribution $F(x;\lambda,k)$ than to a normal or lognormal distribution. In the present study, the characteristic and design values of berthing velocities were therefore described using a Weibull distribution fit on the basis of maximum likelihood estimation. Assuming that the number of berthings per year n and the required target reliability β_d during a certain reference period t_{ref} are known, characteristic v_k and design berthing velocities v_d were established by extrapolating the Weibull distribution fit.

$$v_k = \lambda (\ln(T_R n))^{\frac{1}{k}} \quad (5)$$

$$v_d = \lambda \left(\ln \left(\frac{n}{1 - (1 - \Phi(-\alpha_s \beta_d))^{\frac{1}{t_{ref}}}} \right) \right)^{\frac{1}{k}} \quad (6)$$

in which:

- λ Scale parameter Weibull distribution [cm/s]
- k Shape parameter Weibull distribution [-]
- T_R Return period [years]
- n Number of berthings per year [-]
- α_s Sensitivity factor for dominating load/solicitation [-]
- β_d Target reliability index [-]
- Φ^{-1} Inverse of standard normal distribution function [-]
- t_{ref} Reference period [years]

In the present study, characteristic berthing velocities had a return period of 50 years representing a time-variant berthing velocity with a 2% probability of being exceeded during a reference period of one year. This is in accordance with the recommendations of the ROM [13] and EAU [6], whereas the Brosema curves [2] in PIANC 2002 [17] and the BS2394 [4] represents a reference period of 30 years. For comparison, the number of berthings was set at approximately 100 berthings of a design vessel per year. This is similar to the underlying assumption of the berthing velocity curves derived by Brosema et al. [2].

A design value for berthing velocity is typically selected such that a marine structure has sufficient reliability (or a sufficiently low probability of failure). Target reliability indices β_d and importance factors α_s are generally prescribed in design codes, such as Eurocode Standards [10] and ISO 2394 [8]. The target reliability indices for the different Reliability Classes RC1, RC2 and RC3 are 3.3, 3.8 and 4.2, respectively. For non-dominant and dominant loads α_s are typically 0.4 and 0.7, respectively [5], [8].

When establishing extreme berthing velocities from field observations, the size of the datasets was of significant importance, because extreme berthing velocities are influenced by the fit of the low probability tail of an extreme value distribution to field observations. In the present study, three large datasets were developed, namely 'All tankers', 'All sheltered' and 'All exposed'. The dataset of all tankers is a subset of the dataset all sheltered and represents the use of berthing aid systems, such as portable pilot units (PPU) and fixed shore-based laser docking systems. The use of berthing aid systems could reduce the probability of extreme/ uncontrolled berthing events. Further, the available data were subdivided into sheltered and exposed navigation conditions. An overview of the datasets is given in Table 3. The reader is referred to the studies of Hein [7] and Roubos et al. [15] for further details.

Table 3: Large datasets

| Large datasets [-] | n [-] | v_{μ} [cm/s] | λ [cm/s] | k [-] | Berth type [-] | Berthing aids [-] | Wind [-] | Waves [-] | Current [-] |
|------------------------|------------|---------------------|---------------------|------------|-------------------|----------------------|-------------|--------------|----------------|
| All tankers \circ^1 | 392 | 4.6 | 5.2 | 2.69 | Open | PPU/dock. system | High | Sheltered | Low |
| All sheltered Δ | 713 | 4.4 | 4.9 | 2.28 | Mixture | Mixture | High | Sheltered | Low |
| All exposed \square | 1235 | 7.1 | 7.4 | 1.61 | Closed | None | High | Exposed | High |
| All data | 1948 | 6.6 | 6.4 | 1.57 | Mixture | Mixture | High | Mixture | Mixture |

¹⁾ Dataset is a subset of all sheltered

4. RESULTS

4.1 Extreme berthing velocities

In this study the characteristic and design berthing velocities were derived by direct interpolation of a Weibull distribution fit to large datasets of Table 3, and hence the associated partial factors were determined. The results are given in Table 4.

Table 4: Extreme berthing velocities individual vessel classes and partial factors in accordance with reliability classes of EN1990 [15]

| Reliability class T_R [Years] | $kDWT$ | n^1 | max^2 | Extreme berthing velocities [cm/s] | | | | | | | Partial factors [-] | | |
|------------------------------------|--------|-------|---------|------------------------------------|------|------|------|------|--------|--------|---------------------|-------|-------|
| | | | | v_k | | | | | | | $RC1$ | $RC2$ | $RC3$ |
| | | | | 50 | 100 | 475 | 1000 | 4750 | 12,500 | 38,250 | | | |
| All tankers \circ | 60-319 | 932 | 12 | 11.5 | 11.8 | 12.6 | 12.9 | 13.5 | 13.9 | 14.3 | 1.17 | 1.20 | 1.24 |
| All sheltered Δ | 7-365 | 713 | 13 | 12.6 | 13.1 | 14.0 | 14.4 | 15.2 | 15.7 | 16.3 | 1.21 | 1.25 | 1.29 |
| All exposed \square | 7-195 | 1235 | 26 | 26.4 | 27.7 | 30.4 | 31.6 | 34.1 | 35.6 | 37.2 | 1.29 | 1.34 | 1.41 |
| All data | 60-319 | 1948 | 26 | 25.0 | 26.3 | 29.1 | 30.4 | 32.9 | 34.4 | 36.2 | 1.31 | 1.38 | 1.44 |

¹⁾ Number of field observations

²⁾ Maximum measured berthing velocity

Figure 3 shows that the Weibull distribution fits to the datasets of 'all tankers' and 'all sheltered' navigation conditions slightly underestimate low probability berthing velocities. This was considered acceptable, because the highest measured berthing velocities were caused by fairly conservative measurements, for example small seagoing tankers and large seagoing bulkers [14]. The dataset 'All exposed' contains numerous berthing velocities just below 20 cm/s [7], as well as two higher berthing velocities of 25 and 26 cm/s (Figure 3) [15].

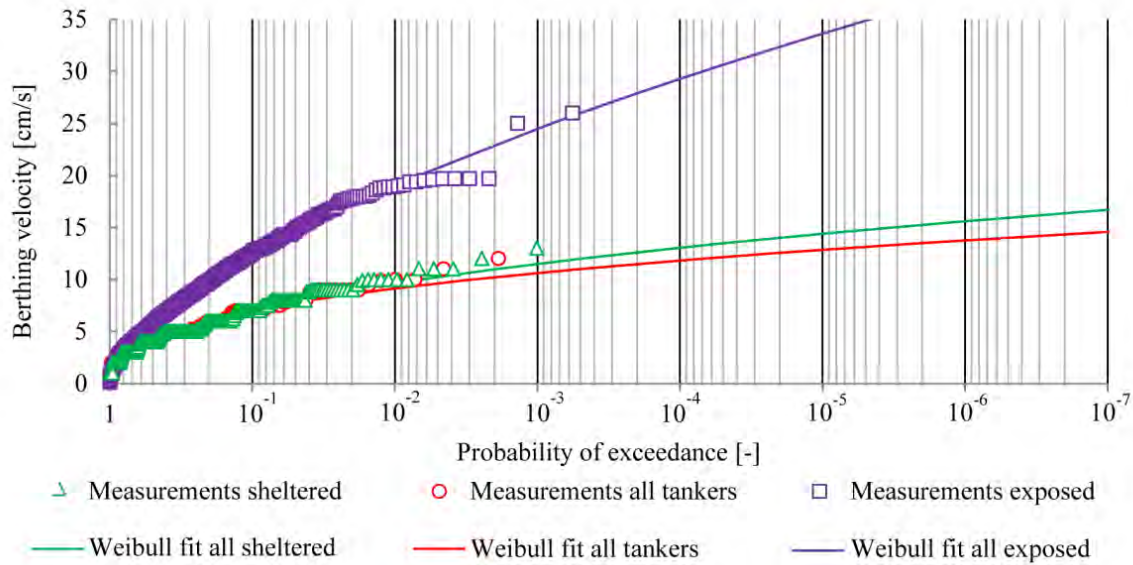


Figure 3: Probability of exceedance plot large datasets [15]

4.2 Sensitivity analysis

When assessing design values for berthing velocity in accordance with equation (6), the effect of alternative target reliability indices, reference periods and berthing frequency could be taken into consideration. In this section the influence of these aspects on the design value for berthing velocity is presented in the next figures. Figure 4 shows the influence of the number of berthings n . When the number of berthings per years is equal to 10 instead of earlier assumed 100 a reduction of 7-12% in the design value was found. In accordance with NEN8700 [11] the assessment of existing structures is generally performed using an alternative reference period and target reliability index. For the reliability level for disapproval in accordance with reliability class RC1 an alternative reference period of 15 years is suggested for variable loads in combination with a target reliability index of 2.5. Figure 5 shows that a change in reference period from 50 to 15 years leads to a 5-7% decrease in the design value for berthing velocity and a change in target reliability index from 3.3 to 2.5 leads to a 4-7% decrease (Figure 6).

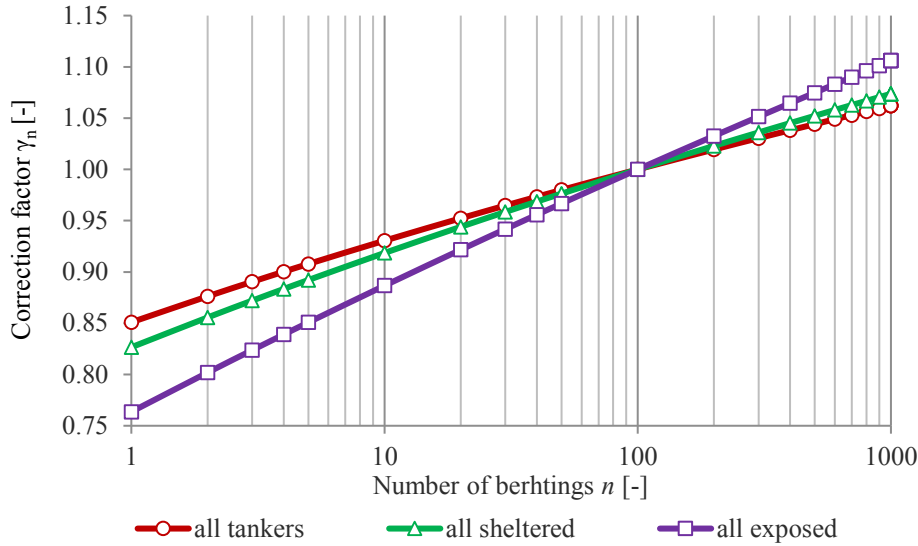


Figure 4: Influence of number of berthing's per year n compared to $n=100$, $t_{ref}=50$ years and $\beta_d=3.3$

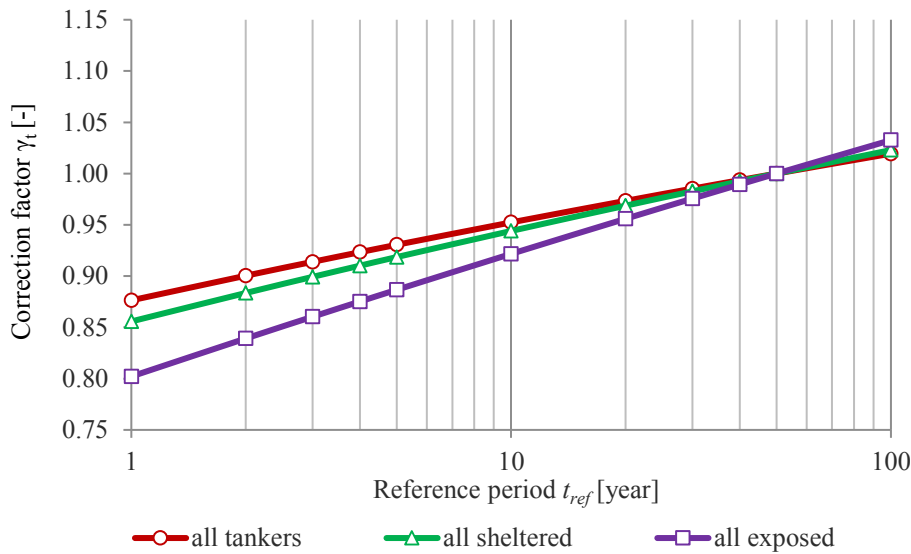


Figure 5: Influence alternative reference periods t_{ref} compared to $n=100$, $t_{ref}=50$ years and $\beta_d=3.3$

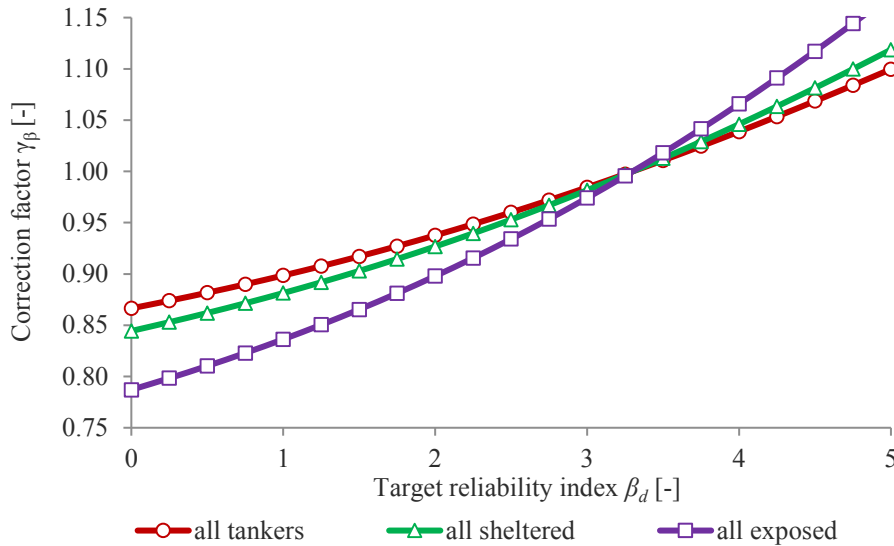


Figure 6: Influence alternative target reliability indices β_d compared to $n=100$, $t_{ref}=50$ years and $\beta_d=3.3$

Example: Suppose that the original design of a marine structure in sheltered navigation conditions is based on a berthing frequency of $n=100$, a reference period $t_{ref}=50$ years and a target reliability index of $\beta_d=3.3$. During the service life the actual berthing frequency of the design vessels appeared to be $n=10$. If a reference period of 15 years is considered in combination with a reliability index of 2.5, the design value for the berthing velocity is approximately 20% lower compared to the original design ($t_{ref}=50$ years and $\beta_d=3.3$). In case of exposed navigation conditions the same analysis leads to a decrease of approximately 30%.

5. DISCUSSION

5.1 How to use berthing velocity records and partial factors in the design

This section discusses how to implement field observations of berthing velocity and partial factors in structural assessments of marine structures subject to berthing impact loads. The process to derive a design berthing impact load is illustrated in Figure 7. On the left side the partial factor γ_v is applied to the characteristic berthing velocity v_k and on the right side to characteristic berthing impact load using the suggested partial factor γ_Q by design codes and standards, such as EN 1990. The flowchart starts with the determination of a characteristic berthing velocity v_k by using field observations.

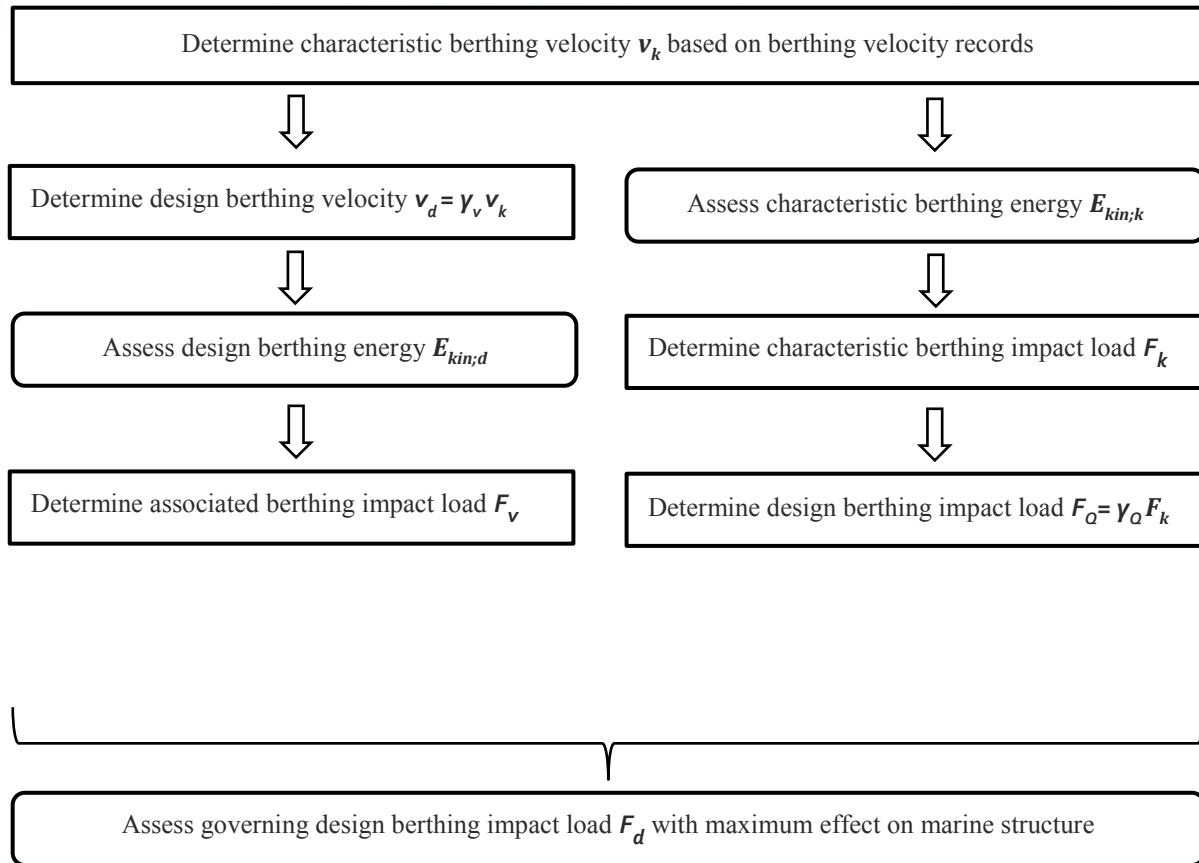


Figure 7: Global flowchart assessing berthing impact on a marine structure [15]

The derivation of partial factor γ_v was based on a statistical examination of comprehensive datasets of representative field observations. However, γ_v does not take uncertainty in modelling the effects of loads into account, while γ_Q complies with design codes and standards - such as EN 1990 [10], ROM [12] or BS2394 [3] - and already includes model uncertainty. In analogy with the Eurocode Standard, equation 6.2 of EN1990, an additional partial factor $\gamma_{sd} \approx 1.05$ for berthing impact load F_v needs to be applied. It should be noted that the governing berthing impact load F_d depends on the type of berthing structure [15] and the values of partial factors γ_v , γ_{sd} and γ_Q . Typical values for γ_Q are 1.35, 1.5 and 1.65 for RC1, RC2 and RC3, respectively.

Table 5 presents generalised partial factors for berthing velocities γ_v as concluded in this study for large seagoing vessels. It should be noted that γ_v is proportional to $\sqrt{C_{ab}}$. For the dataset of sheltered navigation conditions, lower partial factors were found compared to the dataset of exposed navigation conditions (strong tidal currents). The use of berthing aid systems resulted in even lower design velocities and lower partial factors.

Table 5: Partial factor γ_v for berthing velocity (v_k) and abnormal berthing factor C_{ab} for berthing energy (E_k) given well-organised navigation conditions

| Navigation conditions | Pilot assistance | Symbol | Reliability class EN 1990 | | |
|--------------------------------------|------------------|------------|---------------------------|------|------|
| | | | RC1 | RC2 | RC3 |
| Sheltered and monitored ¹ | Yes | γ_v | 1.15 | 1.20 | 1.25 |
| | | C_{ab} | 1.35 | 1.45 | 1.55 |
| Sheltered | Yes | γ_v | 1.20 | 1.25 | 1.30 |
| | | C_{ab} | 1.45 | 1.55 | 1.70 |
| Exposed ² | Yes | γ_v | 1.30 | 1.35 | 1.40 |
| | | C_{ab} | 1.70 | 1.80 | 2.00 |

¹) Pilots are aware of the allowable berthing velocity and use berthing aid systems, such as portable pilot units.

²) Strong tidal currents.

It should be noted that Table 5 assumes the berthing impact load to be a dominate design variable ($\alpha_s=0.7$), and hence can be used in the design of quay walls, jetties and flexible dolphins. However, if berthing loads are not dominant a lower importance factor ($\alpha_s=0.4$) could be taken into consideration or for instance combinations factors in case of multiple design loads.

Another finding is that higher extreme berthing velocities were observed for manoeuvres subject to high tidal currents. However the associated berthing angles at the moment of impact were very low [7], and hence the amount of energy transferred was lower compared to the original design.

5.2 Evaluation of partial factors

Although existing design guidelines do not differentiate between sheltered and exposed navigation conditions, the partial factors listed in Table 5 are in the range of the recommended values in literature (see Table 6). BS 6394-4 [4] recommends using $C_{ab}=1.5$ for situations with a low risk profile, such as berths facilitating general cargo vessels, and $C_{ab}=2.0$ for situations with a high risk profile, such as marine structures for LNG, LPG and ferry terminals.

PIANC [17] and EAU 2012 [6] recommend applying lower abnormal berthing factors, approximately $C_{ab}=1.25$, for large seagoing tankers and bulkers. In this study, higher abnormal berthing factors were found. PIANC seems to be aware of this fairly low reliability level and recommends using a higher confidence level for normal berthing (section 4.2.8.4 of PIANC 2002 [17]) for berths with very low approach velocities. The higher abnormal berthing factors could be explained by an increase in target reliability index, a longer reference period and the use of shore-based docking systems in all the measurement data used by Brotsma [2]. However, the results of this study show that one should be very careful using $C_{ab}<1.5$ for flexible dolphins equipped with buckling fender systems, because almost all berthing manoeuvres result in the maximum reaction force.

PIANC 2002 and EAU 2012 suggest that there is a correlation between vessel size and abnormal safety factor C_{ab} . Although berthing policy (e.g. use of berthing aid systems, pilot and tug assistance) was to some extent related to vessel size, in this study no correlation between type and size of vessel and partial factor γ_v was found.

BS 6349 [4] also recommends applying an additional partial factor to the resulting berthing impact load. The partial factors representing normal (characteristic) and design situations given in the code are 1.35 for persistent and 1.2 for transient situations. The values found were quite similar to the partial factor of exposed and sheltered navigation conditions. Although without accounting for non-linear softening, a design following BS 6349 could result in a conservative design.

6. CONCLUSION

This paper provided guidance on the use of field observations and partial factors for berthing velocity and loads on marine structures. However, it should be noted that the results of this study are based on observations at different ports having typical navigation conditions, i.e. Rotterdam being fully sheltered from waves and currents and Bremerhaven exposed to strong currents and slightly by waves. Fully exposed berths – high swells, strong currents and winds – have not been considered. The results of the research were used to evaluate existing design guidance for similar navigation conditions. The most important conclusions are:

- Partial factors for berthing velocity are not fixed values, as they are influenced by the prescribed probability of failure during a reference period and variation of the berthing velocity.
- The partial factors found did not show a correlation with vessel size. Higher partial factors were found for exposed navigation conditions (strong tidal currents) and lower partial factors when berthing aids were applied.
- The existing design guidelines were considered to be safe for most situations. Applying the British Standards [4] could result in a conservative design. When using the recommendations of PIANC [17] and EAU [6], applying an abnormal berthing factor C_{ab} lower than 1.5 should be done with great care.

The presented methods for deriving characteristic and design values for berthing velocity are easy to apply and could be beneficial for assessing new and existing marine structures. It is recommended to use a characteristic value of berthing velocity with a return period of 50 years. This return period in combination with a berthing frequency of 100 berthings of the design vessel per year resulted in a close correlation with existing recommendations for the design of new marine structures. However, when assessing existing marine structures, the effect of lower target reliabilities, alternative reference periods and berthing frequency could be taken into consideration. This will generally result in lower design berthing velocities up to 10%-30%.

It is highly recommended to further study the risk of the fairly high berthing velocities found for navigation conditions subject to strong tidal currents. In particular, the effect of a second berthing impact could reduce the amount of energy transferred if berthing angles are quite low. Sophisticated datasets and partial factors for berthing velocity of inland barges and smaller seagoing coasters are still lacking. It is recommended to collect field observations of smaller vessels in order to better account for the human influence, which is believed to be stronger when berthings are not assisted by well-trained pilots.

7. ACKNOWLEDGEMENTS

On behalf of Port of Bremerhaven, Port of Rotterdam, Delta Marine Consultants and Inros Lackner the authors would like to thank all companies involved for their support, funding and hospitality. Special thanks Mr M. Gaal, who, on behalf of Trelleborg, was really one of the main driving forces in accomplishing this research by providing the SmartDock® portable laser during the field measurements. Prof. dr. S.N. Jonkman, Prof. dr. R.D.J.M Steenbergen and Dr. D.J. Peters are gratefully acknowledged their contribution on behalf of the TU-Delft, TNO and RH-DHV. Finally, the cooperation with PIANC WG 145 was of great importance in sharing and developing knowledge. Also the support of Prof. S. Ueda contributed to the interpretation of the collected data. The port authorities of Bremerhaven and Rotterdam express their appreciation of the partnership with all the companies involved.

8. REFERENCES

- [1] Beckett Rankine (2010). *Berthing velocities and Brotsma Curves*. London. United Kingdom.
- [2] Brotsma, J.U., Hirs J.A., & Langeveld J.M. (1977). *Paper on Fender Design and Berthing Velocities*. Leningrad, Russia. PIANC World Congress.
- [3] BS 6349-1-2 (2016). *Maritime works: General – Code of practice for assessment of actions*. London, United Kingdom. ISBN 978-0-580-76229-1
- [4] BS 6349-4 (2014). *Maritime Works: Code of practice for design of fendering and mooring systems*. London, United Kingdom. ISBN 978-0-580-66969-9
- [5] Leonardo da Vinci Pilot Project (2005). *Implementation of Eurocodes - Handbook 2 - Reliability backgrounds*. Prague, Czech Republic. CZ/02/B/F/PP-134007
- [6] Grabe, J. (2012). *Recommendations of the Committee for Waterfront Structures Harbours and Waterways EAU 2012*, 9th edition. Hamburg, Germany. ISBN 978-3-433-03110-0
- [7] Hein, C. (2014). *Berthing velocity of large container ships*. San Francisco, USA. PIANC World Congress.
- [8] ISO 2394 (2015). *General principles on reliability for structures*. International organization for standardization. Geneva, Switzerland.
- [9] Metzger., A.T., Hutchinson, J., & Kwiatkowski, J. (2014). Measurement of marine vessel berthing parameters. *Marines Structures*. 39. 350-372
- [10] NEN-EN 1990 (2011). *Eurocode – Basis of structural design*. European Committee for standardization. Brussels, Belgium.
- [11] NEN-EN 8700 (2011). *Basis of structural assessment of existing structures – Buildings – The minimum safety level*. Delft, the Netherlands. Normalisatie Instituut NEN.
- [12] ROM 0.0 (2002). *General procedure and requirements in the design of harbor and maritime structures*. Madrid, Spain. Puertos del Estado. ISBN 84-888975-30-9
- [13] ROM 0.2-90 (1990). *Maritime works recommendations: Actions in the design of maritime and harbour works*. Madrid, Spain. Puertos del Estado. ISBN 978-8-488-97500-3
- [14] Roubos, A.A., Groenewegen, L., & Peters, D.J. (2017). Berthing velocity of large seagoing vessels in the port of Rotterdam. *Marines Structures*. 51. pp. 202-219
- [15] Roubos, A.A., Peters, D.J., Groenewegen, L. & Steenbergen, R.D.J.M. (2018). Partial safety factors for berthing velocity and loads on marine structures. *Marines Structures*. 58. pp.73-91
- [16] OCDI (2009). *Technical Standards and Commentaries for Port and Harbour Facilities in Japan*. Tokyo, Japan. The Overseas Coastal Area Development Institute. pp. 16-27
- [17] PIANC (2002). *Guideline for design of fender Systems*. Brussels, Belgium. ISBN-2-87223-125-0
- [18] PIANC (2014). *Design of Lock Gates for Ship Collision*. Brussels, Belgium. ISBN 978-2- 87223-215-4

[19] Ueda, S., Yamase, S., & Okada, T. (2010). *Reliability Design of Fender Systems for Berthing Ship*. Proc. Of Intl'l. Navig. Congr. No. 79

[20] Yamase, S., Ueada, S., Okada, T., Arai, A., & Shimizu, K. (2014). *Characteristics of measured berthing velocity and the application for fender design of berthing ship*. San Francisco, USA. PIANC World Congress.

A MODERN CYCLONE HARBOUR FOR ESCORT CLASS TUGS IN NORTH-WEST AUSTRALIA

by

Lars Peter Madsen¹, Dr. Douglas Treloar², Justin McPherson³, Dr. Winnie S Wen⁴, and Duncan Ward⁵

ABSTRACT

This paper describes the design and layout of the marine facilities associated with the recently constructed Hunt Point Tug Harbour in Port Hedland. Port Hedland is located 1,322km north of Perth in Western Australia. The DMS latitude:longitude coordinates for the harbour are 20°18'14"S, 118°34'11"E. It is Australia's highest tonnage port and one of the largest iron ore loading ports in the world. Port Hedland is situated on one of the most cyclone affected stretches of coastline of the southern hemisphere with a tidal range of 7.5m.

The key design challenges addressed in the design were:

1. A requirement for post-cyclone operability up to and including a 500 years ARI cyclone event.
2. Safe egress from the tugs following completion of the cyclone mooring procedure in up to gale force winds (35 knots).
3. A design storm tide (including an allowance for 0.4m sea level rise) of 9.2m above LAT.
4. Cyclone berths catering for *RAstar 85* Escort Tugs with maximum displacement 1175t.
5. Minimise the environmental footprint and any regret capital expenditure associated with the potential future expansion of the harbour.

The resulting harbour design has met with approval from all stakeholders including the operations personnel.

1. INTRODUCTION

BHP identified a requirement to increase their towage services in Port Hedland. The strategic aims achieved through the recently completed harbour include:

- Mitigate the significant risk associated with the potential grounding of a vessel blocking the shipping channel which is 42km in length, tidally constrained and uni-directional.
- Provide new state-of-the-art tug berths to support the increased towage requirements associated with the planned future expansion of the iron-ore export operations at the port.
- Reduce the cyclone related disruption to port operations.

The new facility at Hunt Point has been designed to accommodate eight (8) new escort class tugs. Located behind an existing seawall, the environmental footprint, impact on recreation at the adjacent public beach and the requirement for marine based construction plant have been minimised. Four (4)

¹ BEng (Hons) FIEAust Managing Director, Madsen Giersing, peter_madsen@madsengiersing.com.au

² BE (Hons) ME PhD Senior Principal - Coastal Engineering, Cardno, doug.treloar@cardno.com.au

³ BE (Hons) ME MRINA Managing Director, International Maritime Consultants, justin.mcpherson@imcau.com.au

⁴ BE (Hons) ME PhD Design Engineer, International Maritime Consultants, winnie.wen@imcau.com.au

⁵ BE (Hons)/BSc MIEAust Senior Design Engineer, Madsen Giersing, duncan@madsengiersing.com.au

berthing pontoons are located within the harbour catering for two (2) tugs at each berth. To provide for improved operability of the berths, the following features have been included on each pontoon:

- Fixed rotating access brows at two locations to allow bow-in and bow-out operational mooring of the tugs.
- Cyclone mooring line reels.
- Mooring line hangers.
- 1.8m wide gangways (of maximum 1:4 slope at LAT) providing a zero-step access to each pontoon through the full 7.49m tide range.
- Along-side cyclone mooring arrangement capable of surviving cyclones up to 500 years ARI (compared with a four-point cyclone mooring arrangement used elsewhere within Port Hedland).
- Mooring line snap-back guards for safe egress after mooring the tugs in pre-cyclonic conditions.
- Shore power, compressed air, drinking water and fire-water provided via the gangway.

In addition to the eight (8) tug berths, a pontoon for small boats is provided in the south-west corner of the harbour, as are navigation aids (including day-night lead marks designed in accordance with IALA specifications), revetments and other associated shoreside facilities.

2. TUG HARBOUR LOCATION AND LAYOUT

The Hunt Point Tug Harbour location was selected as the preferred location as it provides a number of benefits including:

- No increase in environmental footprint.
- Least energetic conditions within the lease boundary enabling a safer, less complex cyclone mooring design.
- Located within an existing seawall allows for shelter to be achieved with minimum effort.

The general arrangement of the harbour can be seen in Figure 1.

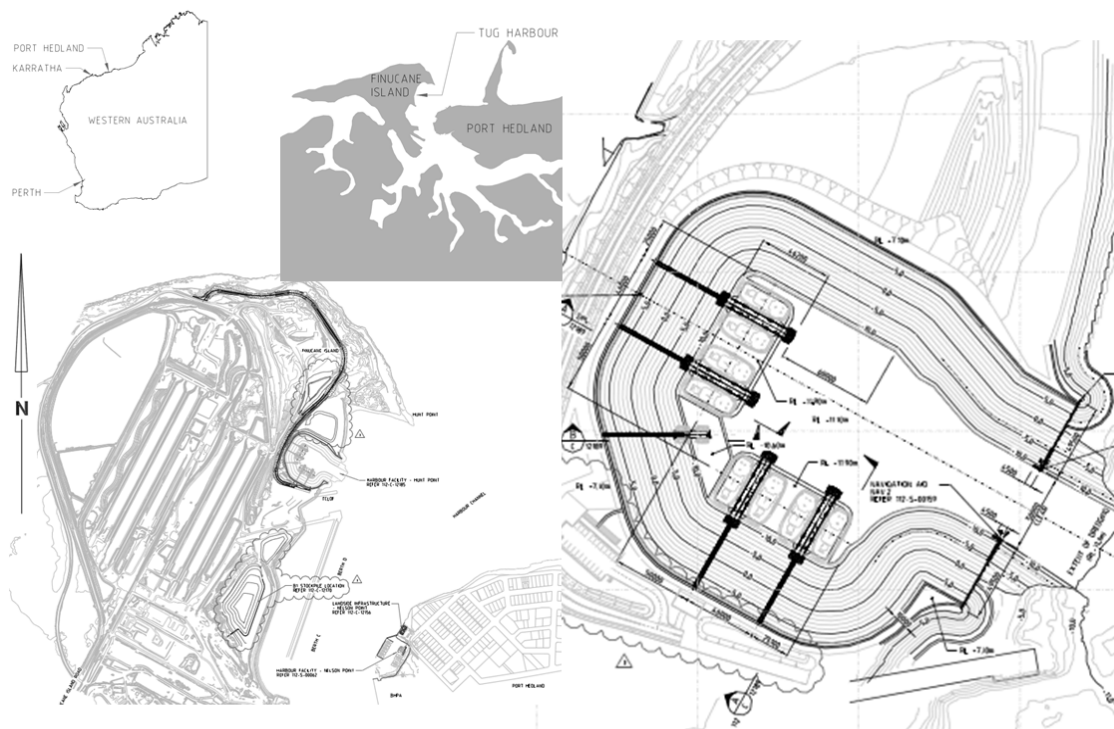


Figure 1: General arrangement and locality of the harbour

Part of an existing sea wall was removed to create the 50m wide (at the toe of the entrance channel) entrance to the facility. Two 45m long piled sea-walls are located either side of the entrance to the harbour to protect the heads of the revetments in severe weather conditions and minimise wave penetration into the harbour.

2.1 Operational and Cyclone Berthing Arrangement

A cyclone mooring arrangement alongside a pontoon has been adopted in lieu of the four-point arrangement used elsewhere in the port. This provides the following benefits:

- Reduced per-berth footprint.
- Safe for access to shore following completion of cyclone mooring procedure.
- Reduced cyclone mooring procedural complexity.
- Simpler tide-following mooring point details integrated into the pontoons.

The facilities provided within the Hunt Point Tug Harbour satisfy the requirements of operational and cyclone berths for eight (8) escort tugs. This is provided via four (4) 52m long, 5.85m wide pontoons. The pontoons are arranged so that two are parallel to the adjacent coastline (NNE-SSW) behind the causeway to the south of the entrance and two lie WNW-ESE on the far side of the harbour. Each of the four pontoons has been designed to be capable of berthing two (2) of the escort tugs. The operational mooring berths for four (4) crew transfer vessels are provided by a 21.6m long by 4.5m wide pontoon running E-W.

Each tug pontoon has been designed to allow the tugs to moor either bow-in or bow-out during non-cyclonic periods. For cyclone mooring, the tugs are required to moor bow-out. The crew transfer pontoon is for operational use only and is not required to moor boats during cyclonic conditions.

The mooring of the vessels alongside the pontoon prior to the onset of gale force winds (pre-cyclonic conditions) enables landside access via the pontoon and access gangways for the crew to go ashore after completing the cyclone mooring procedure.

The fendering system comprises two twin air-block fenders per tug (four per pontoon). Low friction facing is used on a 2.4m wide fender panel to increase the contact width on the tug sponson. The air-block fenders provide a low reaction at small deflections making them ideal for use on the pontoons and with the tug hull geometry. The size of the air-block fenders is governed by the design cyclonic conditions. The energy absorption requirements during normal and abnormal berthing are significantly lower than those for peak cyclone events.

3. DESIGN INPUT AND DECISIONS

The following are key inputs affecting the tug harbour design. The final design was the result of carefully balancing the requirements for safety, operability, navigability and minimising the environmental footprint on one hand, while ensuring cyclone survivability, durability, and constructability at the same time.

3.1 Geometric considerations

To keep the footprint of the tug harbour substantially within the existing sea-wall, all critical dimensions needed to be kept to safe minimums; in part due to the presence of a site boundary to the west of the harbour limiting the space available to construct the harbour. The dimensions minimised included:

- Berth pocket width and length
- Berth spacing
- Proximity of the tugs to the revetment
- Swing basin geometry
- Length of the gangways

- Size of the pontoons

The slope of the batters was also maximised, however, due to the dredged material fill in the upper layers, this could not be made steeper than 1:2.75.

3.2 Operability

For operability, the following minimum clearances were provided:

- 50m wide entrance
- 100m x 100m swing basin for manoeuvring
- 5m clearance to the revetment at LAT
- 2m clearance either side of vessels on final approach to berth when a tug is moored at the adjacent pontoon.

3.3 Geotechnical

The geotechnical investigations indicated five (5) general layers. They were:

- Fill (dredge spoil) – cohesive and granular from (0m to +11m Australian Height Datum – hereafter AHD)
- Holocene deposits – beach sands and estuarine sediments (between -5m and 0m AHD)
- Coastal deposits – uncemented (1m layer around -5m AHD)
- Upper red beds – stiff clay (below -5m AHD)
- Lower red beds – very stiff clay (below -15m AHD)
- Calcareous conglomerate – high strength rock (below -25m AHD)

Note that the levels indicated are only approximate and significant variation occurs across the site. The excavation of the harbour extended through the top layers down to the red beds – ‘in the dry.’ The piles which restrained the pontoons were subject to lateral loads and they founded in the lower red beds, which is a stiff clay. Initial soil springs used in the dynamic simulation were determined in accordance with ISO 19902 methods for stiff clay with and without the effects of scour.

Cyclic loading was of concern following the work of Reese et al. (1975)⁶ This is because under cyclic lateral loads, the strength of stiff clays once loaded past a threshold diminishes rapidly. This work was based on loading a pile to the same peak load 100 times. It showed:

1. Deterioration in stiffness of the upper levels once loaded past a peak (up to which reasonably elastic behaviour was observed).
2. If subject to a load which exceeded the peak load it had been previously subject to, no significant reduction in stiffness or load carrying capacity was observed. I.e. a large once-off load should not be treated as a representative cyclic load.

A representative cyclic load was generated by reviewing the bending moment occurring at sea bed level in the dynamic simulation for the largest 100 pile load events. Further details are presented at the end of Section 4.

3.4 Meteorological / oceanographic data

The most significant challenge to the design of cyclone moorings in Port Hedland is the significant tidal range and related peak storm wave conditions. Two distinct sets of waves affect the site. Within the harbour, these are:

⁶ L.C. Reese, W.R. Cox and F.D. Koop, ‘Field Testing and Analysis of Laterally Loaded Piles in Stiff Clay’, *Proc. 5th Annual Offshore Technology Conf.*, OTC 2312, Houston, Texas, April 1975

- Waves that enter Port Hedland through the shipping channel and which are caused by tropical cyclones that pass the north-west shelf area ($H_s = 2\text{m}$, $T_p = 7\text{s}$ to 11.5s).
- Waves that are caused by cyclonic winds blowing from the southerly sector across the relatively short fetch within the harbour ($H_s = 1.4\text{m}$, $T_p = 4.5\text{s}$)

There is a strong correlation between the wave heights entering the harbour and the water level. Several ambient extreme wave conditions and pre-cyclonic conditions affecting the site were also investigated to confirm operability of the pontoons.

Table 1 gives the tidal planes at the site.

| Tidal plane | | Level (mCD) |
|---------------------------|------|-------------|
| Highest astronomical tide | HAT | +7.49m |
| Mean high water springs | MHWS | +6.66m |
| Mean high water neap tide | MHWN | +4.60m |
| Mean sea level | MSL | +3.93m |
| Australian height datum | AHD | +3.902m |
| Mean low water neap tide | MLWN | +3.26m |
| Mean low water springs | MLWS | +1.19m |
| Lowest astronomical tide | LAT | 0.00m |

Table 1: Tidal planes at the Hunt Point tug harbour

The 500 years Average Recurrence Interval (ARI) was adopted for the design. Design wave conditions in the harbour were developed based on previous work associated with the Port Hedland Outer Harbour Project which included the development of a synthetic Monte Carlo based 10,000 years cyclone track database.

3.5 Design vessel description

The berths were designed to accommodate the following RAstar 85 Class escort tugs designed by Robert Allan Ltd. The tugs provide an 85t bollard pull for escort operations via two azimuthing stern drives (3m diameter props) powered by two 2,550kW (@1800rpm) engines. A cyclone mooring post with a 306t SWL is provided aft for fixing the stern lines and the 400HP main winch of the vessel has a braking capacity of 250t.

The design vessel has the following particulars.

| | | |
|------------------------|-------|--------|
| Length | L | 34.94m |
| Beam (width) | B | 14.75m |
| Maximum displaced mass | M_d | 1175t |
| Maximum draft | D | 6.18m |

Table 2: Particulars of the RAstar 85 tugs

4. SIMULATION AND MODELLING APPROACH

4.1 Wave penetration modelling

Wave penetration investigations were undertaken using the MIKE-21 Boussinesq Wave (BW) model system developed by the Danish Hydraulics Institute (DHI). In addition to forming the basis for the design of the combi walls, internal and external revetments, and rock armour, the modelling was required to provide input to the dynamic mooring simulation. The wave data extracted for each berth included the H_{m0} (spectral definition), T_p (spectral peak period), as well as the direction spread and peakedness of the JONSWAP spectral form. A fitting function was used to extract up to four distinct wave components (frequency-direction bands), at each berth as input to the dynamic mooring simulations.

Examples of the directional spectra extracted from the model and the associated fitting are presented in Figure 2.

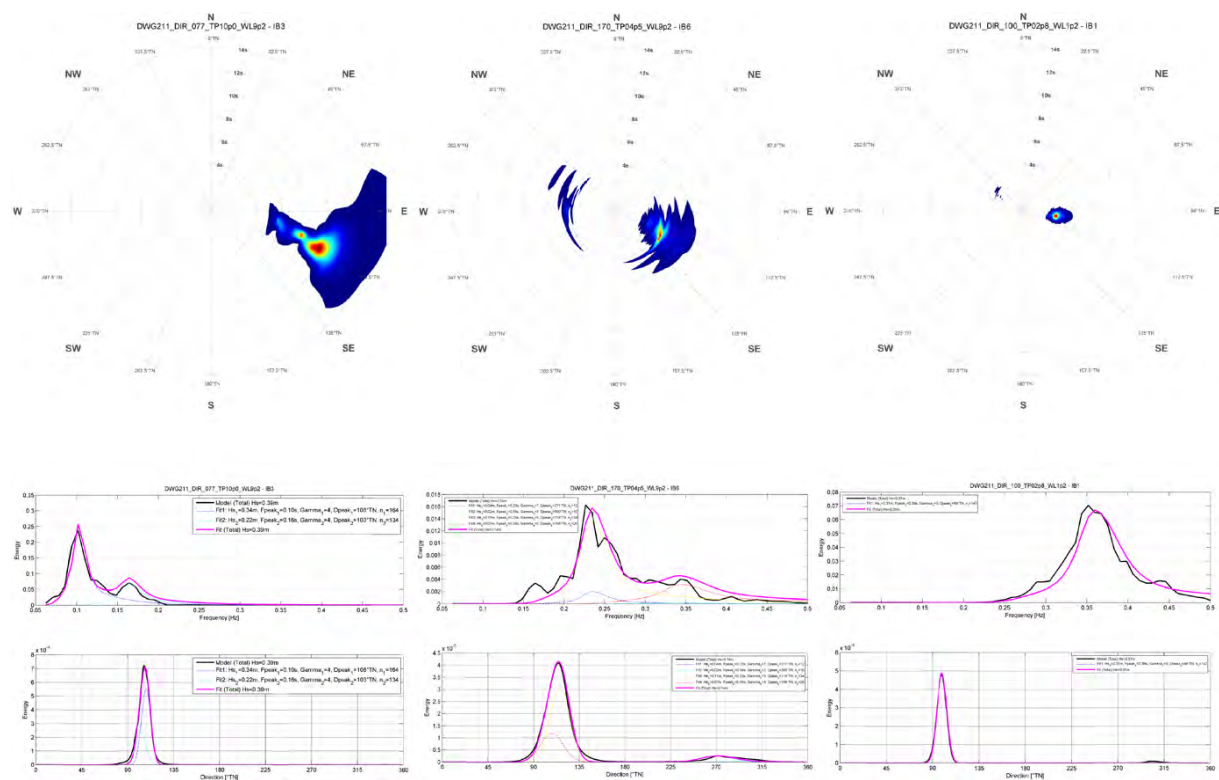


Figure 2: Directional spectra (top) for three scenarios, the associated wave spectra (black) and fit (pink) for the frequency domain (middle) and directional spread (bottom)

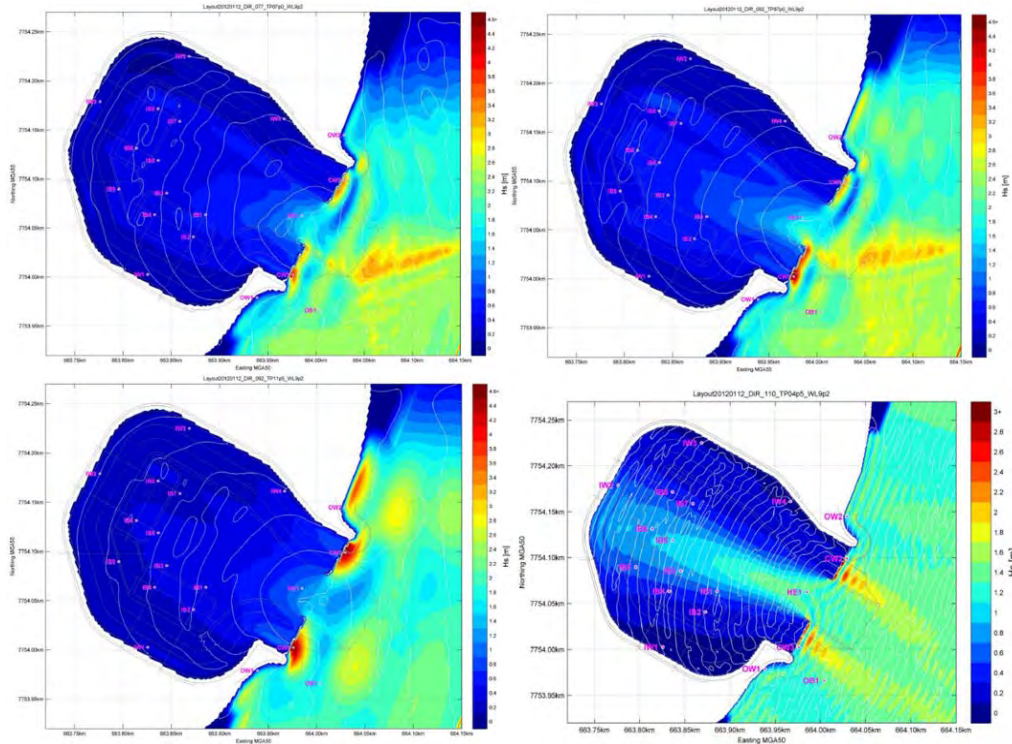


Figure 3: Example wave penetration modelling results for a 500 years ARI storm tide of 9.2m. Model boundary waves as follows: (top left) $T_p = 7s$, $h_{sig} = 2m$, $dir = 77^\circ TN$, (top right) $T_p = 7s$, $h_{sig} = 2m$, $dir = 92^\circ TN$, (btm left) $T_p = 11.5s$, $h_{sig} = 2m$, $dir = 92^\circ TN$, (btm right) $T_p = 4.5s$, $h_{sig} = 1.4m$, $dir = 110^\circ TN$

Figure 3 indicates significant attenuation of the longer period waves with the use of vertical piled seawalls at the entrance. The walls are integrated with the existing seawall by way of roundheads comprising rock infill and an external layer of 3t rock. Wave run-up and overtopping rates were also calculated for the revetment design in accordance with EurOtop.

4.2 Dynamic mooring simulation

A hydrodynamic analysis using ANSYS AQWA-Line was conducted to calculate the response of the tugs and the pontoon with interaction effects between the multi-bodies taken into account. Response amplitude operators (RAO's), quadratic transfer functions (QTF's), added mass, damping and hydrostatic stiffness were then input to the time domain software OrcaFlex. This was used to generate the 6 degree of freedom (DOF) motions of the tugs and the pontoon subject to the various incident design wind and wave conditions, mooring line and fender reactions. Due to the large tides, and high correlation between tide level and wave heights, a 1-hour simulation time frame (the maximum duration of peak tide at which the design waves can penetrate into the harbour) was completed for each of the four berths subject to a total of 20 design incident wave conditions. The resultant 80 cases were run through nine iterations of the design.

Yokohama pneumatic ship-ship type fenders were adopted initially based on initial simulations using monochromatic design waves. However, upon completion of the full set of simulations, some peaks exceeding various design limits resulted in several iterations trying to balance the control of vessel motions with the peak line loads and fender reactions on the vessel. The design of the tugs had been completed prior to the harbour design and so there was limited scope for the modification of the tugs.

At the end of the design, a significant amount of data had been generated:

- 90 core variables were extracted from each simulation including fender reactions, line loads, vessel motions, pontoon motions, pile loads, brace loads etc.
- 20 design wave scenarios (applied to each iteration of the design)
- 4 twin-tug berths with distinct wave climates at each berth

- 360,000 time-steps (0.01s) per simulation
- 2.6Billion data points generated per design iteration
- >23Billion data points generated throughout the design

Significant effort was employed to reduce the amount of analysis using intuition. At the end of each set of simulations, the worst cases for key design criteria would be chosen for re-analysis with adjustments made to pre-tensions, fender, and line arrangements. The worst five or so cases were reasonably consistent from iteration to iteration in a general sense, i.e. cases causing generally more dynamic responses from the berth would be consistent. However, as peak loads were often caused by short periods of resonance within the system, they would often occur sporadically in a case which was not in the set of worst cases analysed at the previous design iteration.

It became apparent after the first few iterations, that while general trends could be observed and predicted with reasonable accuracy, individual peaks occurring for $\ll 1s$ were very difficult to predict with certainty before all 80 combination cases had been analysed. A compounding factor was that different berths would govern for different fender properties and line geometries at each iteration as the design developed.

In the end running all 80 test cases at each design iteration progressed the design in the shortest possible time.

It is noted that, while the detailed simulation approach is becoming the state of the practice, the design approaches of yesteryear, in the vast majority of cases, continue to provide acceptable outcomes. With the dawn of the automation of the design process upon us, there will be some important questions regarding the cost-benefit of adopting complex analysis approaches. For now, the application of intuition, sound judgement and efficient operation of modern design tools remains paramount to the efficacy of the design process.

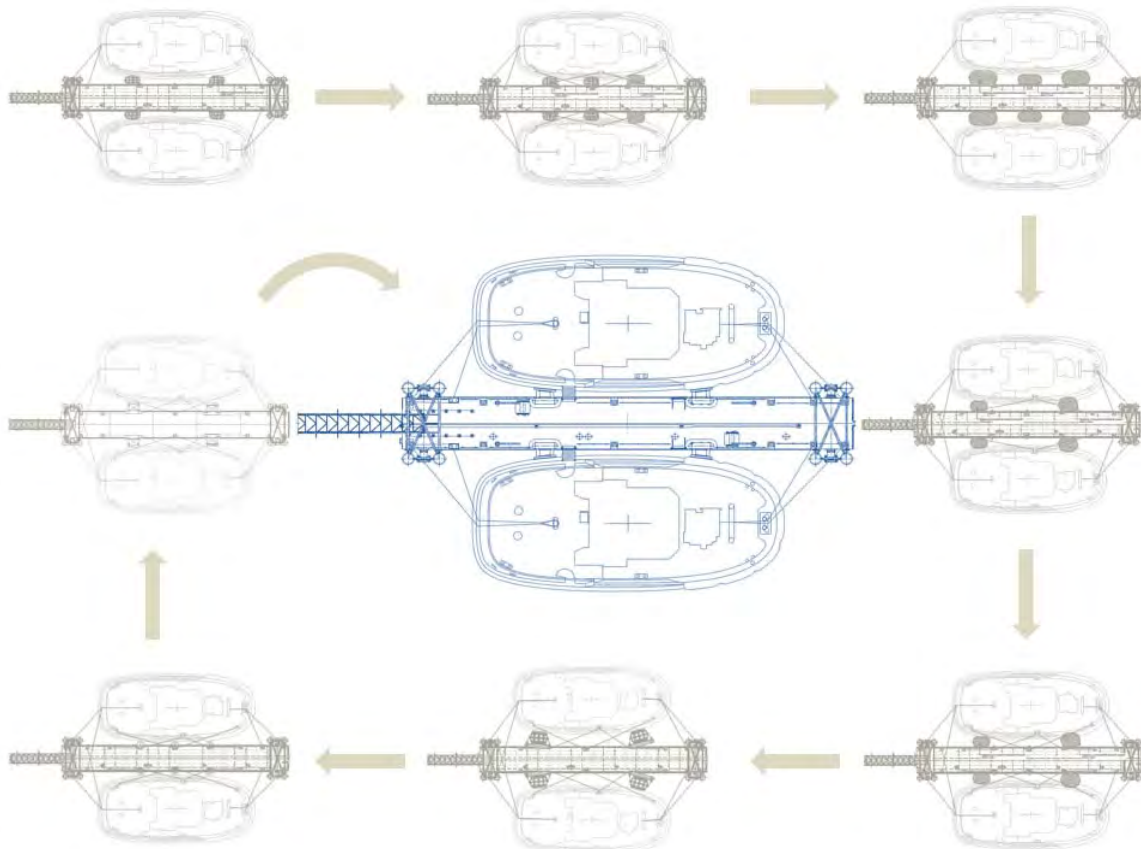


Figure 4: Design iterations leading to the final design with twin Yokohama ABF-P fenders and two head and two stern lines with 18t pretension in each line

4.3 Determining a representative cyclic load for pile design

Typically wind loads would result in cyclic loads about some non-zero average and so it is not possible to define a *load event* as a maximum load occurring between two *zero load* points. Instead, recursive maximisation was used to find significant load fluctuations that could be considered peak individual load events filtering out higher frequency fluctuations near the maximum. Upon review of the data, the best result for the simulation data was achieved with three recursive maximisations. An example is indicated in Figure 5.

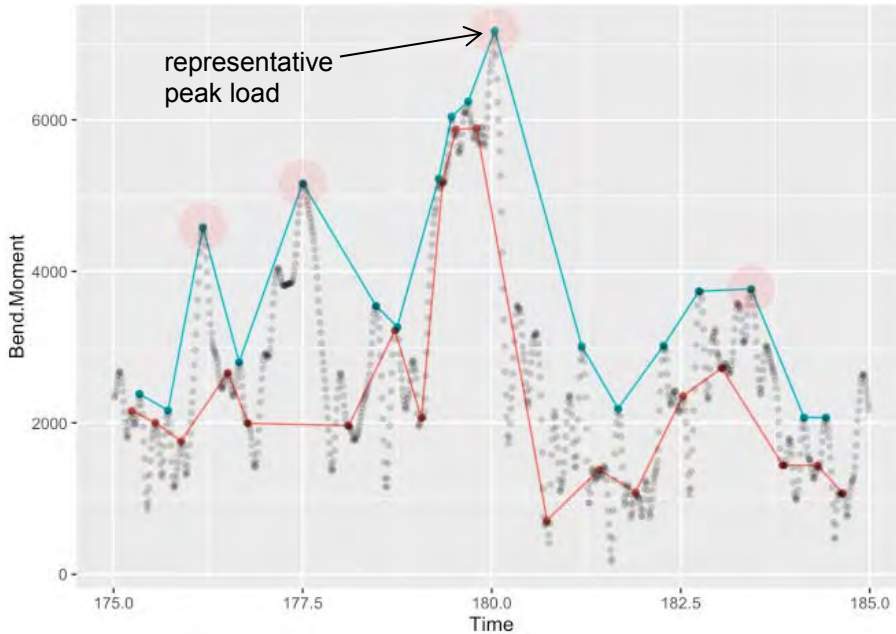


Figure 5: Cyclic load assessment – finding representative peak pile loads showing raw data (black translucent dots), and the result of three passes of recursive local maxima finding (large red translucent dots). The blue line indicates local maxima included in the second and used for the final pass and the red line represents local maxima which were reclassified as local minima in the second pass.

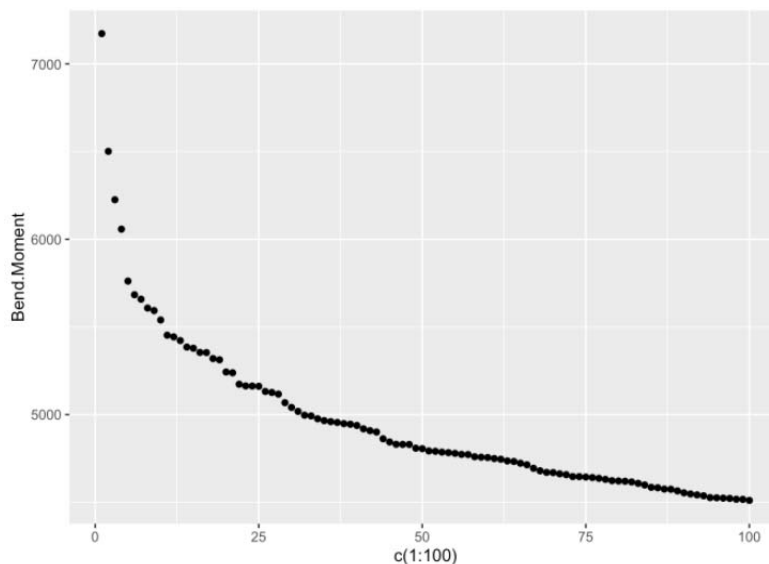


Figure 6: Top 100 *peak load* events for a pile (showing pile bending moment at sea bed level)

Upon review, for the given site and cyclic load levels, only the very upper-most embedded section of pile (~1-2m below ground level) was loaded past the peak and so the effect on the lateral capacity and deformation of the piles was negligible.

5. FENDER AND LINE SELECTION

The major innovation in respect to the mooring design came with the adoption of dual Yokohama air-block fenders. These fenders provided several benefits. The location of the load on the tug hull, which is highly contoured, could be controlled so that it was applied to the sponson on the tug (also the strongest part of the hull) and there was a significant variation in the level over which contact could occur due to the relative roll and heave of the pontoons and the tugs in a design conditions. The added benefit of this was that at low deflections, a low reaction was provided, while at large deflections, large loads were applied. This resulted in a good balance between allowing small oscillations to occur without excessive loads developing in the system on the one hand, while on the other hand effectively arresting the largest motions and preventing tugs from colliding with tugs at adjacent berths, or the revetments in extreme conditions.

While loads extracted from the simulation represent ultimate fender reactions, fenders are generally specified for operational loads with a factor on the energy for an abnormal berthing. The supports for the fenders are then designed with a load factor on the rated reaction at the rated energy to account for (among other variabilities), potential overloading of the fender. Yokohama were most helpful in providing for specific impact speeds and events extracted from the model, what the recommended maximum reactions were for the air-block fenders (beyond the rated capacity).

Similarly, the nylon double braid mooring lines provided a flexibility and associated energy absorption capacity providing the dissipation necessary for an along-side mooring.

To size the fender panel, the height of the relative position of the tugs and pontoon were extracted from the dynamic simulation and analysed to determine the range of relative heights. The following is an example of the peak load occurring at each level relative to the centre of the twin ABF fenders.

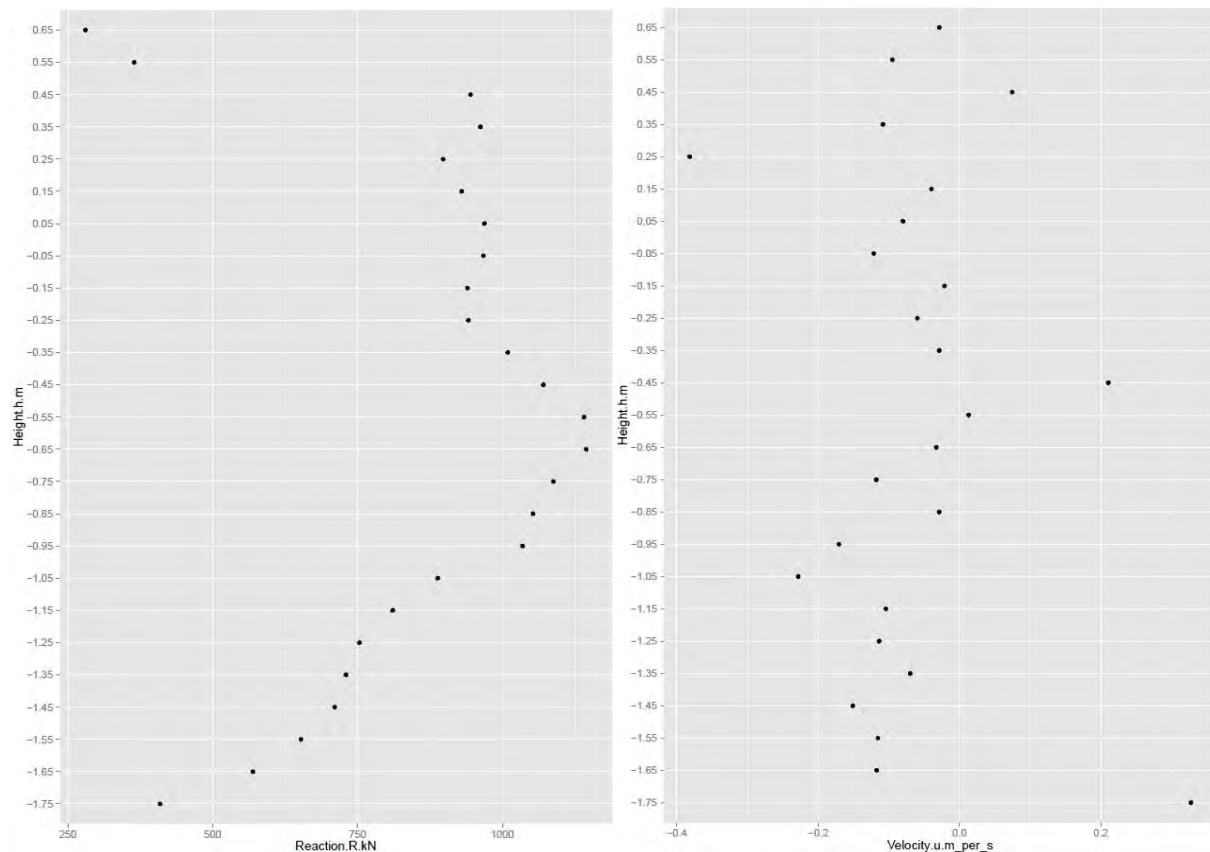


Figure 7: Peak design load varying with distance from the centre of the Yokohama twin ABF-P fenders (*left*) and associated velocity at impact (*right*)

Extracting and summarising the data in this way allows both the effects of low and high impacts to be assessed against the capacity of an individual fender, which will be taken by a single fender, as well

as ensuring that the panel extends sufficiently to ensure the tug does not ride up over the fender panel nor get caught underneath. More than 115 million data points were used to create each graph.

6. OPERABILITY FEATURES

The key benefit of the adopted design is the alongside mooring in preparation for a cyclone, which allows crew to disembark safely following completion of the cyclone mooring procedure via rotating access brows provided on the pontoons. Mooring line hangers are used to minimise manual handling and maximise efficiency setting the operational mooring lines and mooring line reels are used to store and protect from UV and salt spray the cyclone mooring lines when not in use. The access brows are 1.5m wide and manually operable (<15kg load) from both the tug (using a boat hook) and the pontoon side. Snap-back guards have been provided at the end of the gangway where the tug crew must pass lines under pre-tension as they leave the pontoon after completing the cyclone mooring procedure. The features described above are shown in Figure 8.

Tugs enter the harbour and align in a swing basin within the harbour prior to entering the berths. A full-bridge simulation was completed for the facility and found that berthing was possible at all berths in pre-cyclonic conditions with tug operator training.



Figure 8: Operability features (clockwise from top left): access brow lowered, access brow raised, snapback guards, mooring line hangers, cyclone mooring line reels

6.1 Operational mooring

The following operational mooring design arrangement comprises two lines connected to bits on the tug. The typical operational mooring is a bow-in arrangement, this maximises the distance between

the main operating plant of the tug and the adjacent revetment slope. Access is provided via rotating access platforms aligned with the access at the aft of the tug. These are self-latching and manually operable by boat hook or hand so that it is possible to lower and raise the brow from either the tug side or the pontoon side.

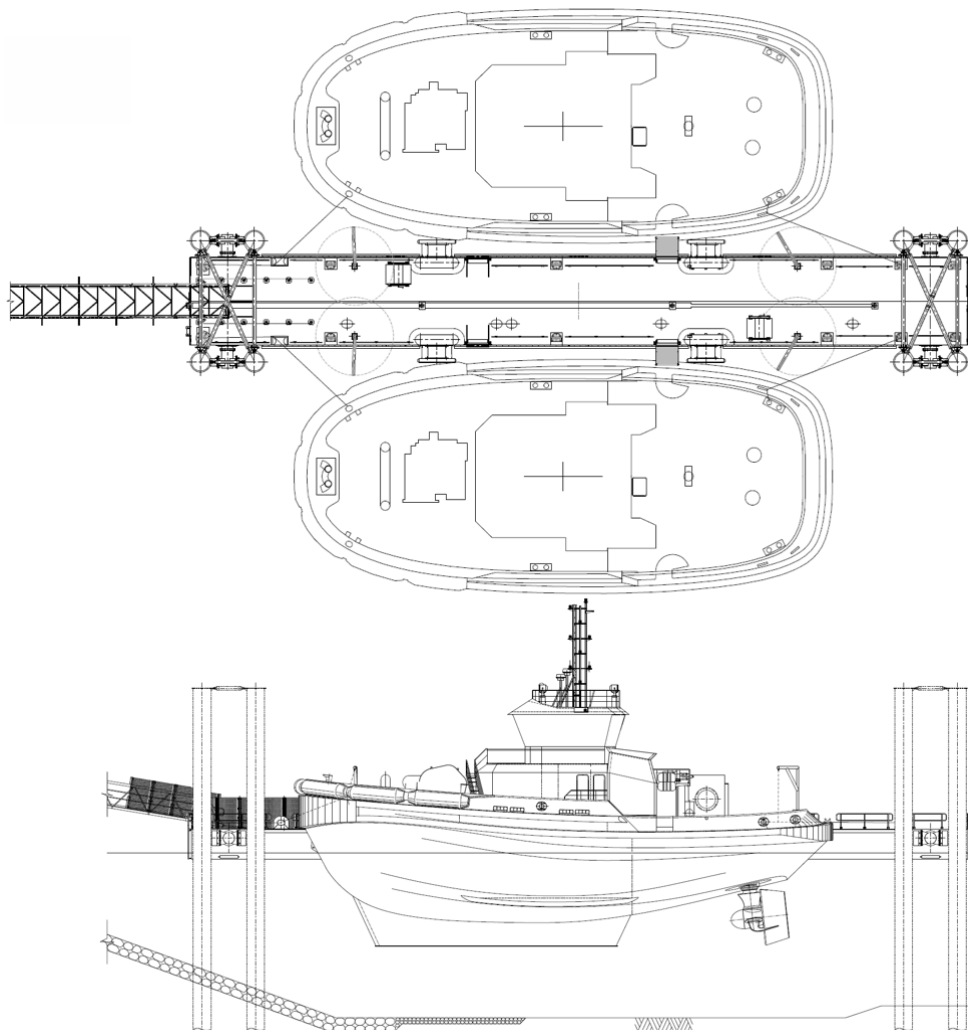


Figure 9: Operational mooring arrangement

6.2 Cyclone mooring arrangement

The cyclone mooring arrangement has the tug in the bow-out position. Each of the four (4) 88mm diameter Samson Super Strong double braid nylon mooring lines are tensioned to 180kN using the main winch on the tug. The bow-out mooring of the tug minimises the response of the vessels to waves entering through the harbour entrance in cyclone conditions. While the tension in the aft lines is relatively low (<15% MBL), it was a client requirement that snap-back guards be provided to protect the crew leaving the vessel. Access is provided by rotating access brows aligned with the aft access on the vessels. Part of the cyclone mooring procedure requires that the mooring line hangers (used for operational mooring) are locked and the brows returned to a vertical position upon disembarkation to prevent impact between these and the tug.

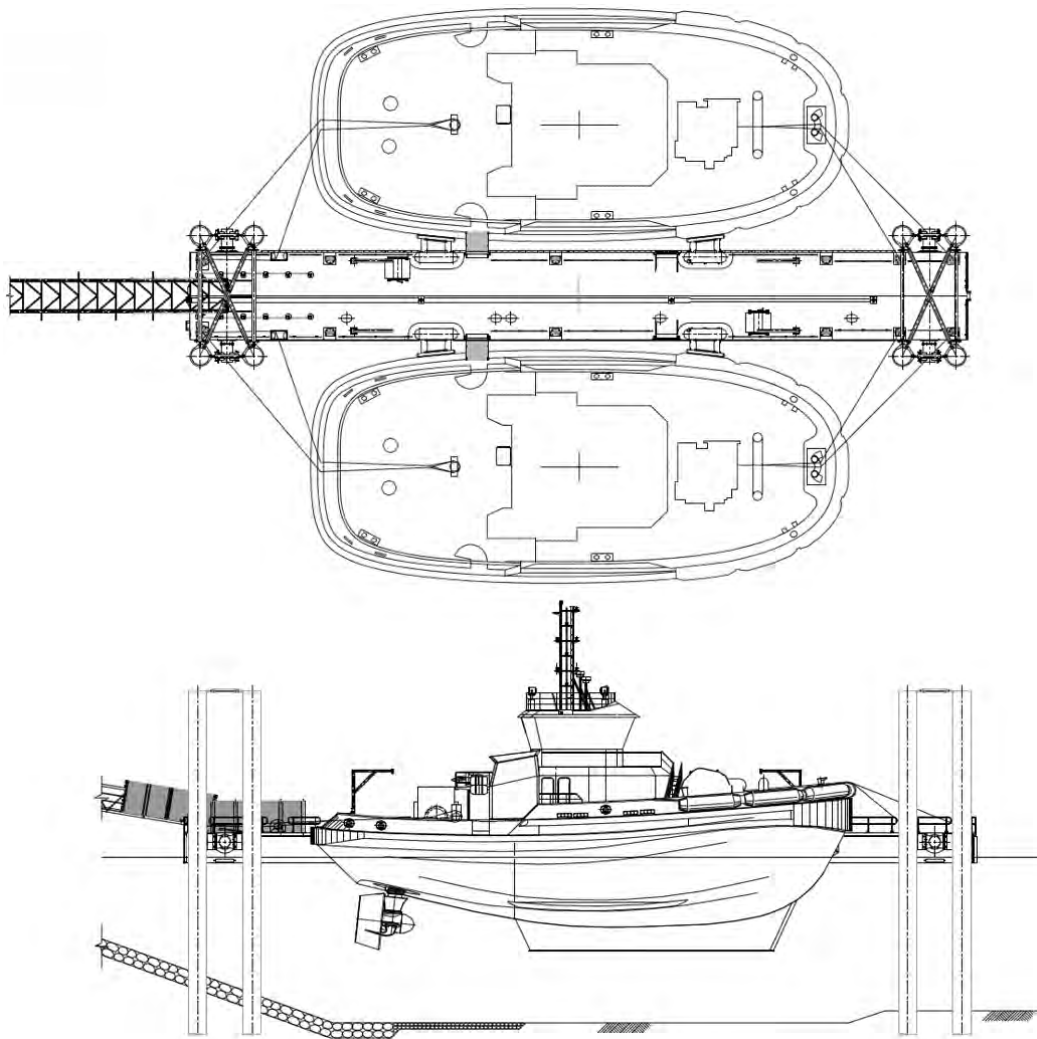


Figure 10: Cyclone mooring arrangement

6.3 Value through simplicity

The pontoon restraints and construction tolerance for the piles is achieved through pinned brace connections at the top of the piles and through extruded rubber SC and arch fenders providing contact between the MDPE coated piles and the pontoons. The MDPE coating provides superior wearing characteristics compared with steel, and the fendering units are easily accessed and simple to maintain.

A key objective of the mooring design was to avoid the use of spring lines. The use of dual head and stern lines provides redundancy in the mooring arrangement, while at the same time avoiding the operational complexity that would be introduced if crew needed to walk across spring lines when leaving the tug following completion of the cyclone mooring.

7. COMMISSIONING

One of the essential components of the cyclone mooring line – to which peak loads were determined to be quite sensitive – was the initial pretension. In the model, the pre-tension was applied in the absence of environments, and with the tug located in a neutral position, aligned centrally between the fenders.

The design initially called for the tug winch reading to be used to confirm that the correct pretension had been achieved in the system (~36t force in the winch). However, the combination of fixed-length

stern lines and friction between the tug and the fendering panels resulted in significant variation with the tension in the head lines far exceeding the tension in the stern lines. This behaviour was replicated in the model and sensitivity tests were carried out to see if this would affect the behaviour of the tug. The results of the analyses showed that provided the lengths of all four lines were correct, the initial pretensions were not so important.

The challenge at this point was to get accurate measurements of all four (4) line lengths under the specified tension with the tug in the correct position alongside the pontoon. This was achieved by using four long-stroke rams which were able to tension each line to the required pretension. The test arrangement is indicated in Figure 11.



Figure 11: Making template lines

Upon completion of the measurements, lines were made up to a tight tolerance ($\pm 0.2\text{m}$) and the two head lines were marked where they should sit over the level wind on the winch. This allowed the repeatability in cyclone mooring procedure to be assured. This also removes the reliance on instrumentation, and a dependence on the assessment of tension in variable wind and wave conditions, changes in the initial position of the vessel or instrumentation failure.

7.1 Feedback from operations

The comments received from operations have been most positive. The tug crews indicated that they very much like the fendering and that the harbour has been *“built to last”*. And it has.

Acknowledgements

The authors would like to thank BHP and Lendlease for giving us the opportunity to be involved in the project and allowing this technical paper to be presented.

References

L.C. Reese, W.R. Cox and F.D. Koop, 'Field Testing and Analysis of Laterally Loaded Piles in Stiff Clay', *Proc. 5th Annual Offshore Technology Conf.*, OTC 2312, Houston, Texas, April 1975

OPTIPORT: AN INNOVATIVE HARBOUR DECISION-MAKING TOOL

by

M^a Izaskun Benedicto¹, Rafael M. García¹, Javier Marino² and Francisco de los Santos³

Abstract

The planning and management of a port and its resources have become a difficult task because of the increasing number of elements involved in port operations, their nature and the relations between them. Traditional methods, like empirical formulas or queuing theory are useful to simple cases. However, in the case of complex systems, the problem needs to be tackled from a holistic point of view, and more advanced methodologies should be considered. In these cases, simulation may turn out to be an appropriate solution, especially nowadays, when computation and data management are increasingly more efficient.

In this work, OptiPort, a reliable, robust, user friendly and agile software tool, to be used by port managers as a decision support tool for the management and planning of the port and its resources, is presented.

OptiPort is based on a probabilistic methodology. For a given port management strategy, OptiPort uses simulation techniques to obtain realizations of the time series that characterize climate and ship-related variables. With these variables, it reproduces port operations and obtains a series of indicators that measure the performance of the port regarding operationality, waiting times, occupancy and use of harbour services. The port performance is characterized from a statistical point of view. The tool also implements a multicriteria decision method that considers the uncertainty of the results, compares different port strategies and ranks them according to their performance.

1 INTRODUCTION

International shipping trade, and therefore, port activity, has increased dramatically in the recent decades. Harbours have become dynamic places where many operations are performed simultaneously and with many interrelated elements. Thus, dealing the port management and planning in a holistic way, considering all the port elements and their relationships, has turned into a difficult task, not only because of the high number of elements but also because of the random nature of the agents involved in port operations. And, in this context, efficiency has become an important issue in port management and planning, where delays are not easily assumed.

Simultaneously, the advances in information technologies and the increasing computing power have allowed the generalisation of certain tools or routines, like simulation.

In the recent years, simulation tools have been evolved deeply, so that they have become in useful tools to predict the performance of ports and terminals. However, they usually focus on a particular aspect of the port operations, such as a specific terminal, navigation channel dimensions, etc.

In this work, a simulation software tool based on a probabilistic and holistic methodology of port operations is presented. For a given port management strategy, the software uses simulation techniques to obtain realizations of the time series that characterize random variables -climate and ship variables-. With these variables, it reproduces port operations and obtains a series of indicators that measure the performance of the alternative in regards to operationality, waiting times, occupancy and use of harbour services. The software also compares different strategies or alternatives, which are ranked taking into

¹ PROES Consultores, S.A., Spain. ibenedicto@proes.engineering, rgarcia@proes.engineering

² FCC Industrial, Spain. jmarinor@fcc.es

³ Algeciras Port Authority, Spain. fsantos@apba.es

account uncertain multiple criteria according to the Stochastic Multicriteria Decision Method SMAA-2, Lahdelma, R. and P. Salminen (2001).

The paper is organised as follows. First, section 2 describes the methodology in which the software is based. Then, the main utilities and functionalities of the software are shown in section 3. In section 4, the case study used to validate the software is shown, as well as the results of the validation process. Finally, some potential applications of the software are presented in section 5.

2 METHODOLOGY

A holistic methodology to evaluate port performance through a simulation model and taking into account the uncertainty of the random variables involved in the process has been developed. The bases of the methodology were established in Benedicto et al., (2013). Garcia Morales et al., (2015) and CIT-460000-2009-021 (2011).

The methodology is based on probabilistic methods and Monte Carlo simulations, and it allows obtaining the statistical characterisation of the port performance under some circumstances or situations at the port (future extensions, future traffic growth, alternative models of port services provision, etc.).

The application of the methodology has four basic steps: (1) define the case study, (2) reproduce port operations, (3) analyse the results and (4) compare different alternatives or scenarios.

In the following sub-sections, the main bases of the methodology are described: the procedure to reproduce port operations, the simulation of the input random variables, and the multicriteria decision method.

2.1 Reproducing port operations

To reproduce port operations, a discrete-event simulation model is used:

- A time axis is established, with an accuracy of one second, and the year as the time interval to be analysed.
- As the year progresses, ships make demands (e.g., when a ship arrives at the port and needs to operate at a certain quay or when a ship finishes its operations at a certain berth and desires to leave).
- The process involves analysing –as they arise– if ships' demands can be satisfied.
- To achieve this, each time a demand arises:
 - a. All information related to the ship and its demand is read: ship's characteristics, the specific demand, the port services needed to satisfy that demand (pilot, tugs, etc.), climate thresholds that determine that ship operation and the port management criteria and rules that can influence the operation.
 - b. A flowchart verification process begins. Step by step, availability of ship's needs to satisfy the specific demand is checked: destination (berth, anchorage, etc.), navigation channels and port services, as well as values of climate variables, and port management criteria and rules.
 - c. If results obtained are positive, all the resources needed are reserved for the ship and the demand is satisfied. If any of the steps cannot be carried out, the ship will have to wait.
 - d. Either way, all the information is stored accordingly.

- One by one, the demands that take place throughout the year are analysed, and all information related to occupancy of port destinations and services, delays and operability¹ is recorded.
- At the end of the year, the information recorded is processed to obtain a set of indicators that describe the performance of the port in that iteration² (e.g. mean waiting time due to different reasons, occupancy rate of berths or occupancy rates of port services).

The port system is outlined in Figure 1 while a general diagram of the methodology used to reproduce port operations is given in Figure 2.

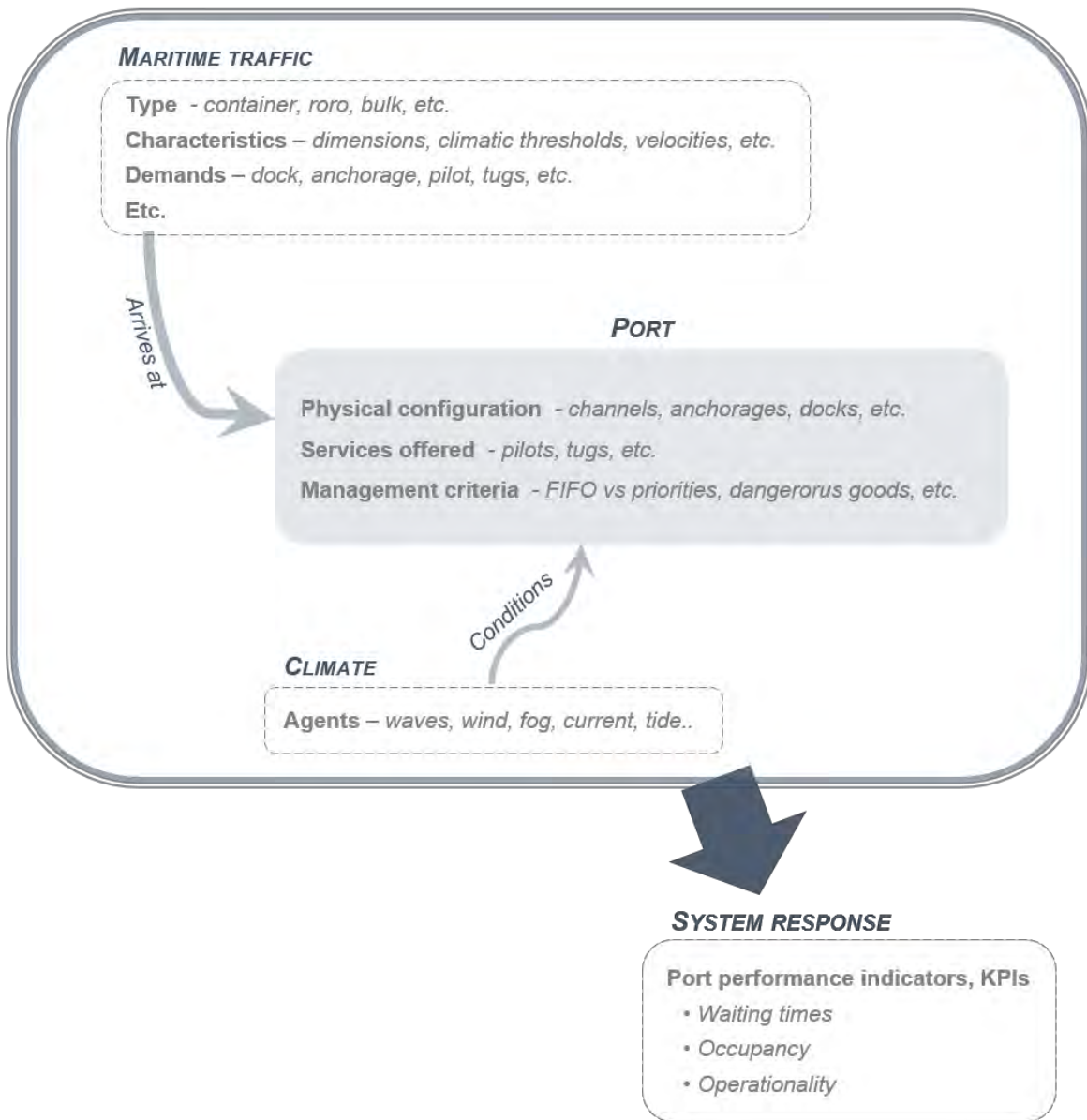


Figure 1. Port system

¹ Operability represents the percentage of times something that is asked for is available the moment it is requested (without delay).

² Iteration stands for one the reproduction of the year port operations

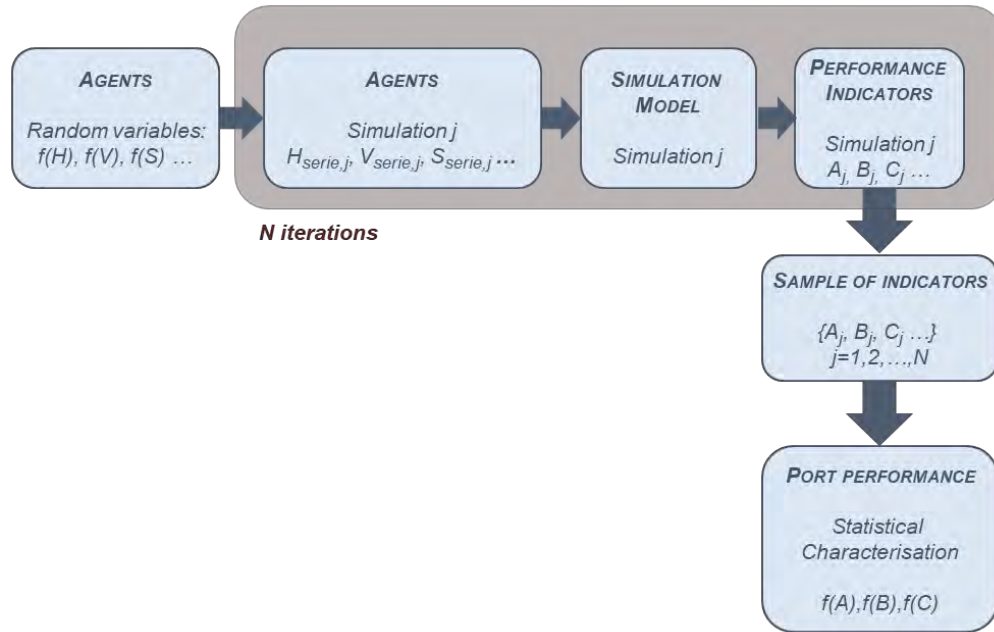


Figure 2. General diagram of the methodology

2.2 Simulation

Upon considering interrelation between elements that determine port operations, the methodology enables obtaining the result from a holistic point of view.

However, due to the random nature of some of the elements (climate agents and maritime traffic), one reproduction of the year operations does not give a representative result of the real operations at the port.

In order to have a real picture of the port operations, simulations need to be carried out. Port operations along the year need to be reproduced a high number of times (N), so that each time (iteration) a set of inputs is generated and therefore, a set of results is obtained. At the end of the simulation (N iterations) a sample of results is recorded and a statistical analysis is carried out to obtain the probabilistic characterization of the port performance.

Climate agents

Climate agents, such as waves, wind, currents, tide or fog, determine port performance.

Operations are subjected to safety procedures related to the intensity of agents such as waves or wind. For example, containers handling is not allowed when the wind speed exceeds certain thresholds. Thus, characterizing the climate agents along the year is essential to reproduce port operations.

In order to obtain series of the climate agents at the port location, the methodology proposed by Solari et al. (2011) and Solari and Losada (2012) is implemented in the software. This methodology considers an autoregressive model that uses non-stationary mixture distributions for climate variables. From climate data -wind and wave- in a point outside the port, the model analyses and generates random series that have the same characteristics as the real data.

For fog simulation, a specific probabilistic model that takes into account monthly probability of fog events, their intensity, duration of the event and event starting time has been developed.

Ship traffic

Ship traffic is simulated assuming different distribution functions for their random variables (arrivals at port, ship sizes, etc.). The inference of these distributions can be made through traffic forecasts and data analysis, as well as distribution functions defined in bibliography. For example, for some type of traffic, ships arrival can be assumed to follow a Poisson process, and the time between two consecutive ship arrivals can be modelled with an exponential distribution. However, this is not always the case, and Gamma or Erlang distributions may be more appropriate to reproduce ships arrivals. The methodology allows choosing the distribution in order to reproduce ships arrival process in the best way. It allows also taking into account that ships arrivals are made on a regular timely schedule. Vessel service times, namely, the time in which a ship stays berthed, can be modelled with continuous distributions (normal, lognormal, gamma, etc.). Bernoulli distributions are used for other random variables, like the dimension of the ships.

2.3 Decision making - Multicriteria decision method

Besides the evaluation of the port performance of a certain alternative, the software includes a module with a multicriteria decision method to compare different alternatives. This module gives the best alternative among a set of them, according to a set of defined criteria and decision maker preferences. A classic multicriteria method uses deterministic values of the criteria and weights that are combined to obtain the evaluation of each alternative. In this case, there are two aspects to take into account:

- The values of the criteria are not deterministic but uncertain. As seen in previous paragraphs, the software gives a statistical characterisation of the port performance through distribution functions of a set of indicators.
- The preferences of the decision makers about the criteria are not known, so it is not possible to define a deterministic weight.

In order to deal with these two aspects, a SMAA-2 method (Lahdelma and Salminen, 2001) was included in the multicriteria decision method module. This analysis ranks alternatives and calculates the relative importance of each criterion in the decision-making process.

3 THE SOFTWARE

The software presented in this work follows a methodology to evaluate the performance of a port through a simulation model taking into account the uncertainty associated with the random variables involved (climate agents, traffic characteristics).

The software comprises several modules to (1) define the case study, (2) reproduce port operations, (3) analyse the results and (4) compare different alternatives or scenarios.

3.1 Case study - Scenario definition module

To define a case study or scenario the following need to be addressed: port configuration, climate data, ship traffic, port services and management and operational criteria.

Port configuration

The configuration of the port (docks, anchorages, channels, etc.) is defined by the user drawing the different elements in a GIS-based map of the port area. The elements that can be defined within the software are those that are used by the ships during their operations at the port:

- Entrance of the port
- Navigation channels
- Manoeuvring areas
- Docks

- Jetties and berths
- Single-buoys

Anchorage

Figure 3 shows a screenshot of the configuration of the port of Algeciras defined within the software.

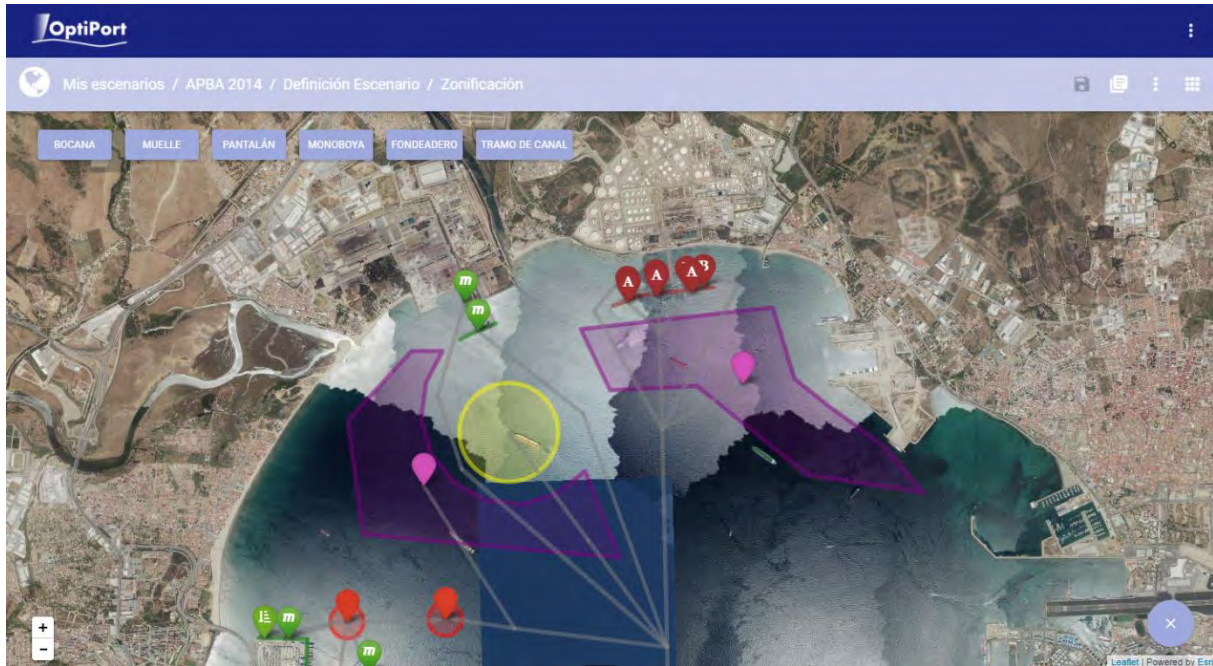


Figure 3: Screenshot of harbour configuration module

Once an element is drawn, its properties can be defined. The properties depend on the type of the element, for example, a berth is defined by – besides its location–, the depth and the maximum length of ships allowed in it.

Climate data

Port operations are subjected to the action of climate agents. Operational and safety procedures are based on the values that some agent variables reach during a certain ship operation. For example, some operations, like ship berthing, must be delayed if the wave height or the wind speed during the manoeuvre exceeds an operational threshold.

The climate agents considered in the software are waves, wind, current, visibility and sea level. The user provides the information that is necessary to generate random series of the agents in different points of the harbour:

- Wind and wave historical data (SIMAR or GOW data or similar).
- Wave propagation coefficients and port areas related to those points, so that the climate in each port destination can be computed.
- Tidal harmonic constituents.
- Probabilistic characterisation of fog events to simulate the visibility at the port.

The software gives the user the option to simulate the current generated by wind.

Ship traffic

The ship traffic module allows the user to define all the variables related to ships that arrive to the port and how they behave during their operations. This module has three parts.

Ship routes. Once the navigation channels are defined (*Port configuration*), the paths that ships follow between two points in the port are defined in this module. The routes can be defined by the user or computed automatically by the software, in which case a minimum distance criterion is used.

Ship velocities. Ship’s navigation velocity is defined in this module through a set of reference points in which the entrance and exit velocity is set.

Fleets. A fleet is defined like a group of ships of a certain type (container, tanker, etc.), that share some characteristics or patterns. In this module, the user can define as many fleets as the port under study has. For each fleet, the software allows defining:

- Arrival patterns, defined by distribution functions and their related parameters or by a regular schedule.
- Dimensions, defined by a histogram. Figure 4 shows a screenshot of the definition of the dimensions of a group.
- Climate thresholds for certain operations, like berthing or loading/unloading.
- Destinations or group of destinations in which ships can operate within the port.
- Schedule of the ships at the port, like the number of destinations they go to in the same call.
- Harbour services demand, like the number of tugs that they demand depending on their size, type of operation, etc.
- Service time, namely, the time that they spend at a certain destination (dock, berth, anchorage, etc.), defined by a distribution function and their related parameters.



Figure 4. Screenshot of ship dimensions definition

Port services

The harbour services that are considered in the software are pilot assistance, tug assistance and mooring/unmooring. In this module, the variables to define how these services are provided by the port are defined. Some of those variables are the following:

- Areas of provision depending on the destination or the place where the resources are based.

- Season variations of the number of available resources.
- Working shifts times and number of available resources per shift.

Management and operational criteria

The software includes general operational criteria, such as FIFO method to allocate port spaces and resources and a safety clearance between two consecutive ships navigating along the same navigation channel. Besides, the software allows to define exceptions to general criteria or to create new ones, such as:

- Giving priority to some type of ships, like big containerships.
- Allowing ships pass other ships when they have different speed.
- Creating special procedures for fog events.
- Creating zones in which ships cannot navigate simultaneously because, for example, they carry dangerous goods.
- Closing the port when the climate agents exceed certain thresholds.

3.2 Simulation module: Reproducing port operations

Once the scenario is complete and correctly defined, the software simulates the scenario according to the information introduced in the previous module. For each iteration, the software:

- Generates the information for the simulation: series for climate agents, ship arrivals, etc.
- Simulates port operations for every ship and registers the information related to ship movements.
- Aggregates the registered information in order to obtain indicators that measure the port performance for that iteration.

The number of iterations is chosen by the user, and it should be enough to characterise in a correct way the performance of the port.

After the simulations, the software uses the results obtained in all the iterations to statistically characterise the performance of the scenario through distribution functions or mean values of the indicators of the port performance.

3.3 Results module: Assessing port performance

The results module shows the results obtained in the simulations in a user-friendly way. This module shows different kind of results, like mean values, distribution functions or values per iterations of the indicators. The indicators that are computed and shown are:

- Operationality, defined as the percentage of times in which a ship demanded a space at any dock or berth or a resource of any port service and the call was attended without waiting times.
- Occupancy rate of port destinations, either mean values or time distributions.
- Occupancy rate of port services and other indicators related to the use of those services, like the number of resources working simultaneously. Like destinations, the module provides mean values and time distributions.
- Waiting times caused by climate, unavailability of docks or unavailability of port services.

Figure 5 shows a figure created by the software. This figure represents the percentage of time in which a certain number of resources are providing a service at the same time under a certain situation or configuration.

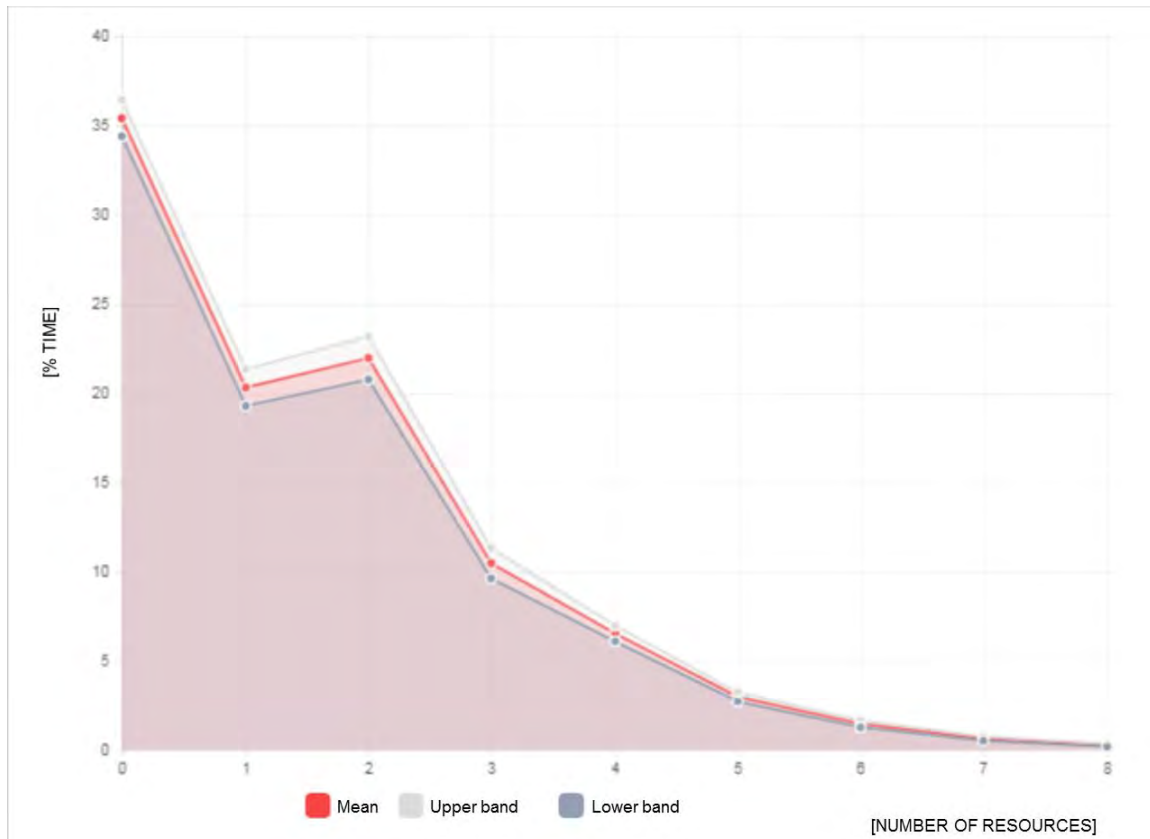


Figure 5: Number of tug boats operating simultaneously

The amount of different variables and values that are obtained with the simulations, and the flexibility and usability of the module that shows the results make this software a powerful tool to analyse the behaviour of a certain port configuration. The results can be observed and classified according to destinations, ship groups or cause of waiting, among many other criteria.

3.4 Optimization module: Comparing different alternatives

The software includes a tool to compare different alternatives through a multi-criteria decision method that takes into account the randomness of the port performance indicators. In the optimization module, the alternatives to be compared are selected, as well as the performance indicators to be used as criteria in the decision making process.

The results of the optimization module are the following:

- A ranking of the selected scenarios as alternatives.
- Acceptability index of each alternative, namely, the probability to be the best (optimal) alternative of the analysis.
- Central weight vector of each alternative, which gives an idea of how important is a criterion to select that alternative.

3.5 Technical characteristics of the software

The application has two different parts: a web application for user interface and a desktop application to compute and simulate.

Web application. The user introduces the information to define the scenarios using the web application. This application also allows the user launch the simulations and multicriteria analysis. This part has two modules:

- Front-end module, related to the visual aspect of the user interface. It has been developed using HTML5+CSS3+Javascript technologies.
- Back-end module, related to business and data layers. It has been developed using JAVA technology.

Desktop application. The second part includes the modules and engines to simulate, aggregate results, multicriteria analysis and auxiliary computations. All modules have been coded using C++ language.

4 VALIDATION CASE

4.1 The port of Algeciras: pilot port of the software

The software has been validated with a real case study at the port of Algeciras, which also took part at the software development as the port pilot.

The port of Algeciras is located at the south of Spain, next to the strait of Gibraltar. With this strategic location, at the entrance of the Mediterranean Sea and in the way of many of the main interoceanic shipping routes, the port is an important logistic hub in maritime shipping. The port is the Spanish busiest port and the fourth in Europe, with more than 100 millions of tons handled in 2016 and 2017.



Figure 6. General view of Algeciras port.

The port of Algeciras is suitable to validate the methodology and the software because of some of its characteristics:

- The port of Algeciras handles different kinds of cargo, such as container, solid and liquid bulk, ro-ro traffic or passenger traffic.
- There are different types of berthing elements, like docks, docks with ro-ro ramps, jetties, single-buoys and anchorages.
- The port receives a high number of ship calls every year, of the order of 22 thousand in the year 2014.

4.2 Modelling the pilot port

The port has been modelled within the software after collecting the input information of each module. The information has been provided by the Algeciras Port Authority, and it includes, for example, the following:

- Inventory of elements (docks, berths, anchorages, etc.) and their characteristics, like length, depth or largest vessel dimensions allowed.

- Historic climate data, like wave and wind registers.
- Navigation routes and procedures.
- Traffic information: ship arrivals, ship dimensions, service times at berths, port services demand, AIS data, etc.
- Provision of port services: shifts, number of resources, provision areas, etc.
- Other rules, like ship priorities or safety procedures for dangerous cargo.

This information was analysed and processed to obtain the models and needed inputs that were introduced in the harbour configuration module of the software. This is an important step, since obtaining accurate results will depend on the quality of input information and how the defined models reproduce that information.

Furthermore, the information provided by the port was analysed to obtain the real performance of the port through a set of indicators that measure occupancy rates of port elements and services. The main obtained indicators are:

- Occupancy rates of docks, berths and anchorages.
- Occupancy rate of tug boats.
- Utilisation of tug boats indicators, like the number of tug boats working simultaneously.

These indicators were used to compare with the results obtained from the simulations.

4.3 Results

Once the definition of the scenario that models the port of Algeciras is finished, the performance of the port is simulated. As said above, the optimal number of iterations depends on the variability and randomness of the data and defined models. In the validation case, it was observed that, after 20 iterations, steady mean values for most variables were obtained.

The simulated values obtained by the software and the real calculated values were compared to validate the models and the methodology. In the following paragraphs, the comparison of those indicators is described.

First, the real and simulated occupancy rates are compared. This rate depends on many variables, like the schedule of the ship at the port or the expected time to be spent by the ships at docks or berths and their dimensions. The average occupancy rate of each terminal has been calculated. Table 1 shows the difference between real and simulated values (unfortunately real occupancy values cannot be shown because of their confidentiality).

It can be seen that the simulated results were close to the real ones in most cases. The lowest observed difference is 0,03% (CLH) and the highest observed difference is 5,6% (Acerinox). The mean difference is lower than 0.7%. In general, the simulated values are similar to real values.

| Terminal/Area | Type of traffic | Difference between real and simulated occupancy rates |
|-----------------|-----------------|---|
| APM Terminal | Container | -1,1 |
| Hanjin Terminal | Container | 2,6 |
| Cepsa | Oil products | 0,7 |
| Single-buoy | Oil | 1,2 |
| Acerinox | Solid bulk | 5,6 |
| Endesa Descarga | Solid bulk | 1,6 |
| Vopak | Oil products | -0,4 |
| Galera | Ro-Pax | -0,1 |
| Ro-Ro ramps | Ro-Ro | -0,2 |
| CLH | Oil Products | 0,0 |
| Anchorage areas | - | -2,2 |

Table 1. Terminals average occupancy rate - difference between real and simulated values.

Figure 7 shows the distribution of the occupancy at a certain dock, namely, the percentage of time in which the dock has a certain percentage of occupancy. It can be seen how the simulated values reproduces in an accurate way the trend of the curve related to real values.

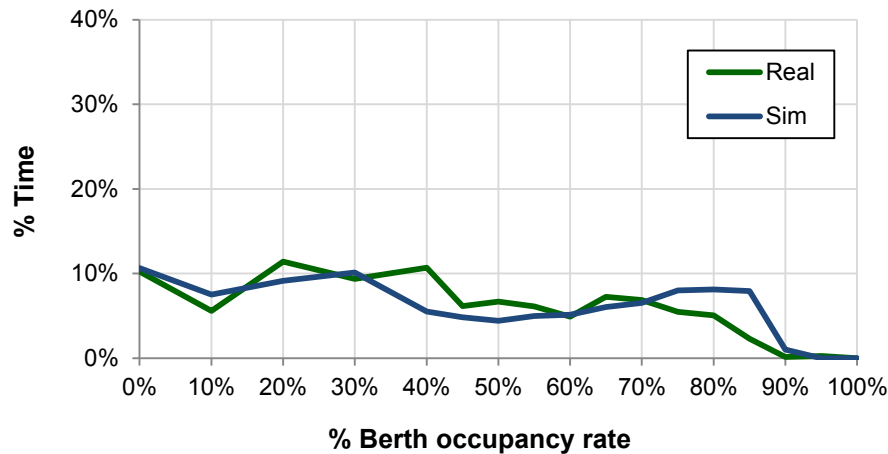


Figure 7. Time distribution of the occupancy rate.

Regarding harbour services, the information available about the provision of tugs service allows the calculation of many indicators about the performance of this port service. For example, the occupancy rate of the tugs and the distribution of time in which a certain number of tugs are working simultaneously were obtained based on the data.

The difference between the real and simulated occupancy rate of tug service is about 1%. The difference between the real and simulated time distributions of simultaneous working tugboats fluctuates between 0,0% and 2,9%. These results show that the software reproduces accurately the use and occupancy of tug boats at the port of Algeciras.

In conclusion, it has been proven that the software reproduces precisely the port performance. That allows its use to many applications to port management and planning. In the next section, examples of some of those applications are described.

5 APPLICATIONS

OptiPort is a tool to be used by port managers as a decision support tool in decision making processes related to the management and planning of the port and its resources. In this section, a set of planning and management situations or problems in which OptiPort can be applied is described. Some of these planning and management problems can be dealt with traditional tools or methodologies. Even in those cases, OptiPort gives the user additional information and a different approach, which makes the decision making process more transparent.

The evaluation of the port performance made by OptiPort allows a wide range of applications. The first and most simple one is to make a diagnosis of the operational performance of the port and its resources. Regarding the port services (pilot assistance, tug assistance and mooring/unmooring), OptiPort can detect if there are excessive delays due to the unavailability of port services resources, by analysing the waiting times causes. The occupancy rate and utilisation indicators are also good indicators of the operational performance of the port services. It is possible to detect if the occupancy rate is over a reasonable value or if there are underused resources.

The influence of climate agents on the performance of the harbour can also be measured by OptiPort, analysing the waiting times caused by the climate variables (wave, wind and currents) and by the operational procedures related to visibility. It is not possible to change the climate agents in a port, but it does enable to modify the operational procedures or thresholds related to climate agents, as well as to plan a new facility taking climate influence in port operations into account.

The utilization of berths, docks and other berthing or flotation areas is also obtained with OptiPort. Indicators, like occupancy rate and number of simultaneous ships at docks, give important information about how overused/underused are berths and docks. This information and the delays caused by the unavailability of destinations can be used to detect bottlenecks and ways to improve the management of the port.

Once the diagnosis of the port has been made, port managers can use OptiPort to evaluate different management strategies to improve the performance of the port. The strategies can be long-term ones or short-term. The first ones need appropriate traffic forecast, not only the number of expected ship calls in a certain year in the future, but also the characteristics of the those ships, for example, ship dimensions.

If inefficient performance is detected related to port services provision, OptiPort allows port managers to evaluate the efficiency of an increase of the number of resources (medium to long term, depending on the service) or another short term solutions, such as modify the location of the base of the port resources or the areas in which the services start or are provided.

Related to port infrastructures (docks, berths, anchorage areas, etc.), OptiPort can be used to detect how traffic evolution will affect the occupancy rates and waiting times, and to evaluate future port extensions. For example, OptiPort gives decision-makers more information to select the best alternative in a harbour Master Plan.

As well as port services and port infrastructures, OptiPort allows evaluating changes in port operations procedures and how they affect the harbour performance. For example, prioritizing certain traffics (large containerhips) will improve the performance of those ships, but maybe other are seriously penalized. Safety procedures are also evaluated by OptiPort, related to climate agents or to dangerous goods. For example, ships carrying dangerous goods need special clearance procedures during their navigation, like areas of exclusive navigation, which will cause delays that can be evaluated by OptiPort.

OptiPort is a useful tool that helps port managers at the decision making process, having the possibility to evaluate the performance of different strategies related to port services, port infrastructures and port operations procedures.

6 CONCLUSIONS

This paper presents OptiPort, an innovative software tool, to be used by port managers as a decision support tool for the management and planning of the port and its resources.

Optiport has been developed in Spain by the companies Proes Consultores and FCC Industrial, and the Port of Algeciras as pilot port.

The software, that evaluates the performance of a port based on simulation and probabilistic techniques, is reliable, robust, agile and user friendly, to be used by port managers.

For a given port management strategy, OptiPort uses simulation techniques to obtain realizations of the time series that characterize climate and ships-related variables. With these variables, it reproduces port operations and obtains a series of indicators that measure the performance of the port regarding operationality, waiting times, occupancy and use of harbour services. The port performance is characterized from a statistical point of view. The tool also implements a multicriteria decision method that considers the uncertainty of the results, compares different port strategies and ranks them according to their performance.

7 REFERENCES

Benedicto, I., A. Baquerizo, F. Santos, I. Sanchidrián and M. A. Losada (2013). Software de optimización de la operatividad portuaria mediante técnicas de simulación. XII Jornadas Españolas de Ingeniería de Costas y Puertos.

García Morales, R., A. Baquerizo and M.A. Losada (2015). Port management and multiple-criteria decision making under uncertainty. *Ocean Engineering*, Vol. 104, 31-39 doi: 10.1016/j.oceaneng.2015.05.007.

Lahdelma, R. and P. Salminen (2001). SMAA-2: Stochastic multicriteria acceptability analysis for group decision making. *Operations Research*, 49, 444-454.

CIT-460000-2009-021 (2011). Final Project Report. Optimizing harbor operations through simulations techniques, 2009-2012. Spain.

Solari, S., Losada, M.A. (2011). Non-stationary wave height climate modeling and simulation. *J. Geophys. Res.* 116, 1–18. doi:10.1029/2011JC007101.

Solari, S., Losada, M.A., 2012, "Unified distribution models for met-ocean variables: Application to series of significant wave height", *Coastal Engineering*, vol. 68, pp. 67–77.

Ways & Rails for Slipways for Dry Docking Ships

by

Keith Mackie¹

1. ABSTRACT

The slipway is the oldest method of dry docking ships. However, at least for more remote sites without heavy demand, even at the present levels of development, they are the most practical and economic system. With proper development of the technology, they can exceed other systems in these aspects.

The slipway, however is the most technically complex of all forms of dry docking and this complexity is not well understood – if it is recognised at all. As a result, it has remained the ‘Cinderella’ of the industry.

The discussions in this paper are intended to remedy this situation – to expose and illuminate this complexity, provide a basic design guide and show the way to further investigations.

2. BACKGROUND

2.1. Origins of the Slipway

There are two basic types of dry docks in use: the hydraulic systems of graving docks and floating docks and the mechanical systems, of which the slipway forms part together with shiplifts and straddles. It is based on the use of the inclined plane and is the oldest form of dry docking. In the 20th century, the development of the slipway has lagged behind developments in other forms of dry docking. However, when modern technology is brought to bear, the slipway can be the safest and most efficient method of dry docking. In areas of lower demand, for vessels under 1000 tons docking displacement but even up to 5000 tons the slipway can be the most economical system

In the beginning, when vessels were small, they were just hauled up and down the beach – **Fig 1** and **Fig 2** and from this the slipway developed – **Fig 3** and **Fig 4**.



Fig 1: Beaching, Soalara, Madagascar 2012 **Fig 2: Beaching, Vilanculos, Mozambique, 2009**

The formal slipway probably first came into use in the Mediterranean and for thousands of years² the slipway consisted of a sled of heavy timber runners over timber sleepers laid on the beach. Some of these are still in use.

¹ Keith Mackie Consulting Coastal & Harbour Engineer, keith@mackie.co.za

² At least as far back as the Late Bronze Age



Fig 3: Shipsled, Bosphorus, 2010



Fig 4: Shipsled, Chania, Crete, 1986

2.2. Types of Slipway

The slipway in its modern form of a cradle on wheels on rails can be precisely dated to the patent awarded to Thomas Morton of Leith in 1819 (Prosser R.B.1894) and his system came to be known as a 'patent slipway'. The cradles were built of timber baulks with small cast iron wheels set in wheel boxes under the longitudinal baulks. These facilities were always built to the three-way system so that the whole weight of the vessel was carried on the centre, keel way. The outrigger ways were for lateral stability.



Fig 5: Patent Slip Cape Town c 1920



Fig 6: Crandall Railway Dry Dock

In the mid-19th century the Crandall family of Boston, Massachusetts (Crandall 1967) developed their own peculiar system commonly referred to as a 'marine railway' or 'railway dry dock'. They use live rollers instead of wheels and cradles built up aft to a wedge shape so that the line of the keel blocks is level.

During the 20th century steel cradles began to replace timber although in general, the three-way system was retained. The modern trend, however, is to exploit the strength of steel and move to a two-way system where the keel block loads are suspended between the two ways by transverse steel cradle beams.



Fig 7: Modern Slipway, Lamberts Bay, South Africa, 1990

3. WAYS GEOMETRY

Slipways can be laid out as either end haul or side haul. End haul systems have a greater extent into the water area but a much smaller extent along the shoreline. Side haul systems have a relatively short extent into the water – and a concomitant steeper grade – but a much greater extent along the shoreline.

Side haul slipways have a series of parallel ways, normal to the shore, spaced along the length of the cradle, transverse to the cradle.

With end haul slipways the ways are again normal to the shore but parallel to the cradle. They commonly use either two or three ways although more can be used. In the case of a four-way system, the central, keel way is split into two parallel ways a short distance apart. Rails are fixed to the ways, usually a single rail to the outriggers but, on larger systems two rails to the keel way.

Given that the ways profile is never perfect, there is a better load distribution to the ways on a two-way system than on a three-way system and, to a lesser extent, on four-way systems. Given that slipway cradles are unsprung, accuracy in vertical alignment of the ways is paramount and the spreading of the keel load to ways set apart does assist in the load distribution.

Gradient of the ways usually varies from about 1:10 for very small units to about 1:25 for very large units. At the very flat grades some form of downhaul will usually be necessary. The usual grades lie between 1:15 to 1:20.

3.1. Straight Grade Ways

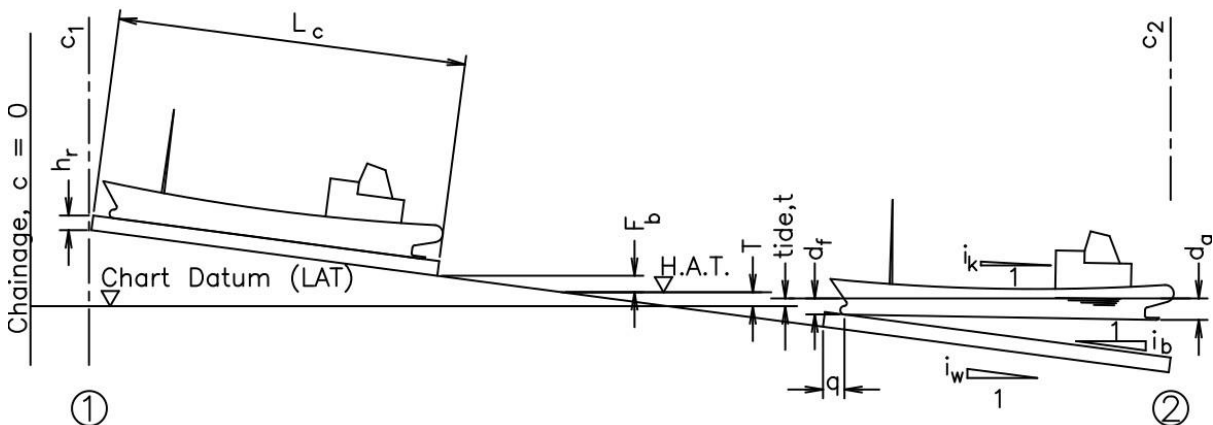


Fig 8: Straight Grade Ways Geometry

The geometry of the straight grade ways as shown in figure 8 is pretty intuitive and is given for completeness. Given:

- | | |
|--|---|
| c = chainage measured horizontally | h_r = vertical height of reference block above ways |
| c_1 = chainage at landward end of ways | L_c = length of cradle over blocks |
| c_2 = chainage at seaward end of ways | i_w = grade of ways as tangent of slope |
| h_c = level of ways at chainage c | i_b = tan of angle between line of blocks and ways |
| h_1 = level at landward end of ways | F_b = freeboard above tide |
| h_2 = level at seaward end of ways | T = max tide range from LAT to HAT |
| d_f = draft fore | t = stage of tide |
| d_a = draft aft | |

Note: the 'reference block' refers to the foremost keel block on the front of the cradle

Level, h_c at any chainage c :
$$h_c = h_1 + i_w(c_1 - c_2) \quad (1)$$

Chainage c at any level h_c :
$$c = c_1 + \frac{h_1 - h_2}{i_w} \quad (2)$$

Horizontal extent of the ways:

$$c_2 - c_1 = \frac{1}{i_w} (F_b + T + h_r + d_f - q \cdot i_b) + 2 \cdot L_c \cdot \cos \tan^{-1} i_b \quad (3)$$

Total slope length of the ways:
$$L_w = \frac{c_2 - c_1}{\cos \tan^{-1} i_w} \quad (4)$$

Remember: longitudinal dimensions on the cradle are slope dimensions and do not correlate directly with the horizontal chainage dimensions on the ways!

3.2. Vertically Curved Ways

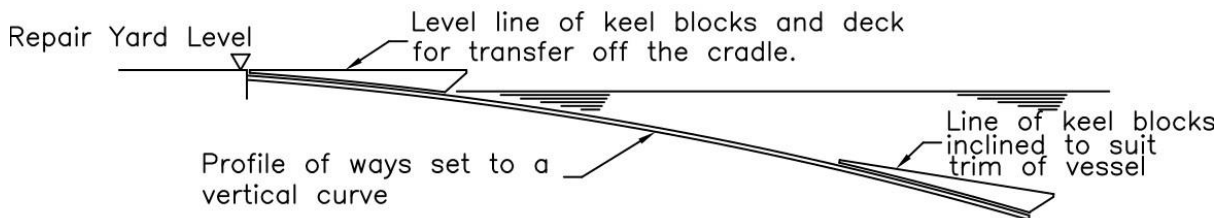


Fig 9: Vertically Curved Ways

Vertically curved ways as shown in **Fig 9**, can make a significant cost saving on the construction of a slipway and improve the operation of the facility. The curve shortens the total length of the ways, reduce the grade of the ways at the landward end and reduces the amount of any rock excavation by bending the ways over the rock.

The computation of the circular curve is complicated by the need to compute the versines (1-cosine) of small angles. It is only with the advent of modern computers that this has become practical.

To determine a suitable ways profile - position and curvature - by trial and error – first establish a site co-ordinate system. Use Chart Datum as the vertical datum, the orientation of the ways as the longitudinal datum and a transverse datum some distance inshore of the proposed ways. The crown of the curve is unlikely to be near the origin of the co-ordinate system. The site will generally suggest initial values. The geometry is shown in **Fig 10**.

For each trial, choose:

| | | | |
|--------------------------|---------------------|--|----------|
| Chainage at landward end | c_1 | Gradient at landward end | i_1 |
| Chainage at seaward end, | c_2 | Chord length between ref block and end of cradle | L_c |
| Level at landward end, | h_1 (usually +ve) | Angle of build-up of keel blocks | ϕ_b |
| Level at seaward end, | h_2 (usually -ve) | | |

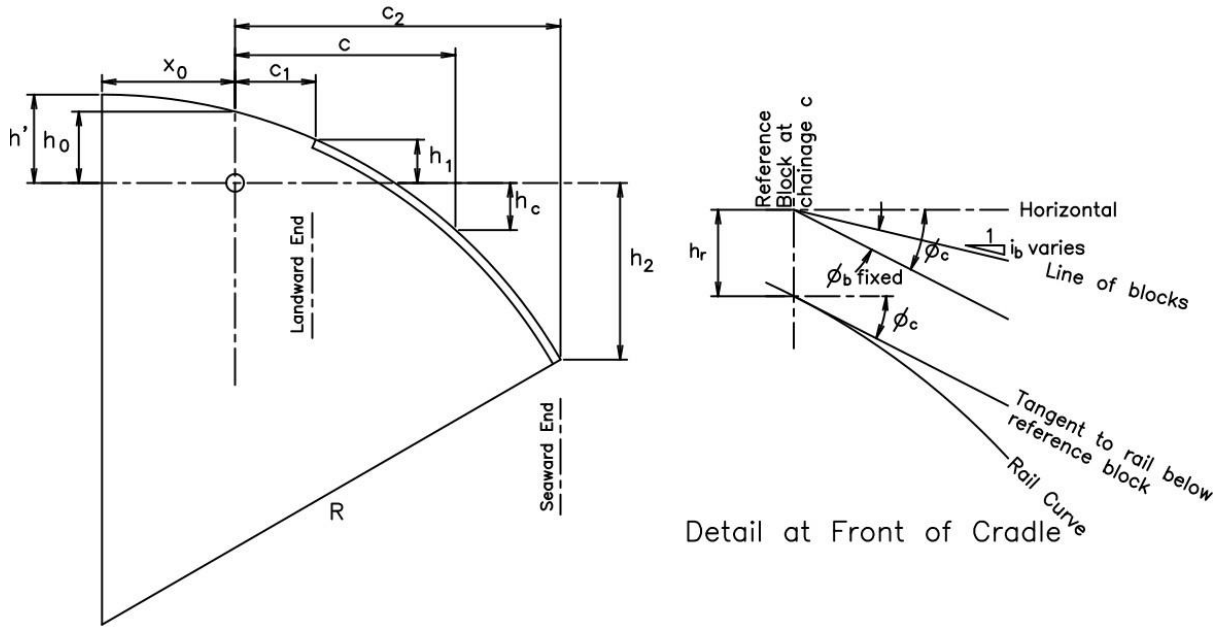


Fig 10: Geometry of Vertically Curved Ways

Now compute the following:

$$\alpha_1 = \tan^{-1} i_1 \quad (5)$$

$$\alpha_2 = 2. \tan^{-1} \frac{h_1 - h_2}{c_1 - c_2} - \alpha_1 \quad (6)$$

Grade of seaward end: $i_2 = \tan \alpha_2 \quad (7)$

Curve radius: $R = \frac{h_1 - h_2}{\cos \alpha_1 - \cos \alpha_2} \quad (8)$

Crown to origin: $x_0 = R. \sin \alpha_1 - c_1 \quad (9)$

Height of crown: $h' = h_1 + R. (1 - \cos \alpha_1) \quad (10)$

For construction, compute:

Level at ch c: $h_c = h' - R(1 - \cos \sin^{-1} \frac{x_0 + c}{R}) \quad (11)$

Arc length ch c_1 to ch c: $A_c = R \left(\sin^{-1} \frac{x_0 + c}{R} - \alpha_1 \right) \quad (12)$

Gradient at ch c: $i_c = \tan \sin^{-1} \frac{x_0 + c}{R} \quad (13)$

Chainage at h_c : $c = R. \sin \cos^{-1} \left(1 - \frac{h' - h_c}{R} \right) - x_0 \quad (14)$

Chainage at i_c : $c = (R. \sin \cos^{-1} i_c) - x_0 \quad (15)$

These equations apply to a reference surface - normally the rolling surface of the rail head. For any other surface, e.g. the underside of the rail flange or, in effect, the surfaces supporting the rail, increase or decrease, as appropriate, the curve radius, R by the offset between the two surfaces, normal to the surfaces at any point, and use this revised value, R' in (9) to (15).

In the case of rails or prefabricated beams supporting the rails, the applicable lengths are the arc lengths given in (12) and the relevant surface is the neutral axis of the rail or beam. The radius of curvature of

the ways is usually large enough, compared to the section depths that it is unnecessary to pre-form the sections. They will take up the curvature with a minimum of strain.

The trial profiles must be checked against a series of different vessels and of different stages of the tide to ensure that the target vessels can all be got onto the blocks at acceptable stages of the tide.

3.3. Other Curvature

Other vertical curves can be used, notably transitions from a straight grade to a vertical curve but they are only practical on two-point support which, depending on the capacity may involve articulated multi-wheel carriages. This system is particularly applicable to side haul systems where the ways transition from inclined to level.

4. SUING A VESSEL

4.1. The Process of the Sue

The action of suing a vessel is the critical activity in dry docking a ship. It is the action of setting the ship down on the keel blocks. On a slipway it is the action of drawing the vessel up the ways on the cradle as she settles onto the blocks. (The word has the same origin as its legal usage being derived from the Latin meaning *to follow*).

The sue of a vessel begins with the first touch of one or other end of the keel on the keel blocks. The process of the sue is the process of lifting the vessel at this point of first touch, to rotate the vessel longitudinally, to change the apparent trim of the vessel until it is the same as the line of the keel blocks. The keel will then be in contact with the blocks along its full length. In principle, at this instant, the whole reaction between keel and blocks is still at the point of first touch and reaches a maximum value. But immediately, as the vessel continues to be lifted out, the increasing total load is spread out over all the blocks and the point sue load begins to diminish. Once the vessel is high and dry, the sue load disappears and the first touch or sue block only carries its fair share of the total load.

At first touch the marks at the sue end of the vessel will begin to rise out of the water. At the other end of the vessel the marks will, in general, sink into the water by about a third of the amount they rise at the sue end. When the keel touches fore and aft, the marks at the other end will cease to sink and begin to rise out of the water. It is just before and during this period that the vessel must be held in position to locate her correctly on the blocks.

4.2. Sue Loads

The significance of sue loading depends very much on the match between the vessel and the dry docking system.

Where the keel and keel blocks are very nearly parallel the sue loads will be very small and can be ignored. Where there is a large angle between the keel and the line of the keel blocks there will be a heavy sue and the docking of the vessel will be difficult.

4.3. Determination of Sue Load on Straight Grade Ways

Determining the magnitude of the sue load amounts to establishing the upwards force at one end of the keel needed to rotate the vessel longitudinally to change the trim of the vessel to match the slope of the keel blocks. Minikin (Minikin, R.R. 1963) suggests an allowance of between one eighth to one third of the displacement of the vessel. This gives excessive results and better values are needed.

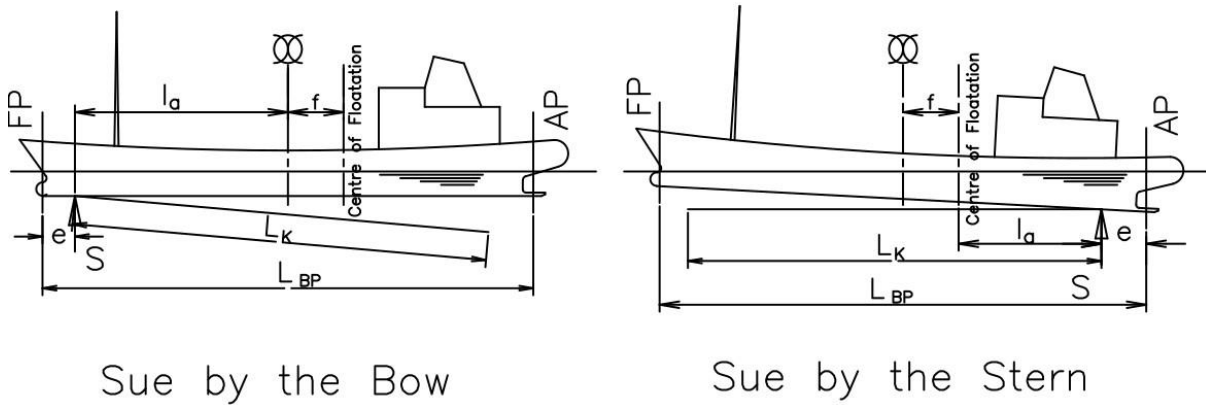


Fig 11: The Sue of a Vessel

The traditional analysis of sue load is given in texts on naval architecture as launching or grounding calculations. To do this, the hydrostatic curves for the vessel are needed. In dry docking design work, these are not normally available.

A first approximation can be obtained by treating the vessel as a rectangular box (ignoring small angle effects at the vertical ends) and analysing the forces involved.

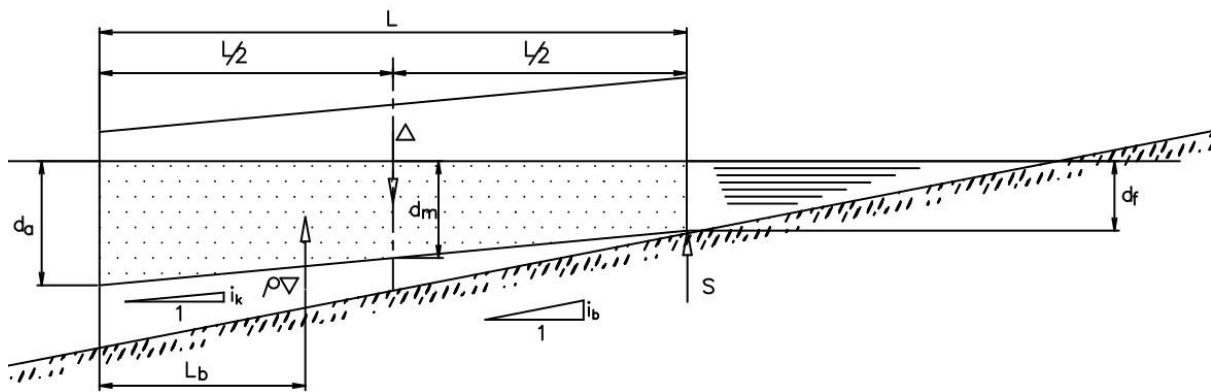


Fig 12: Sue of a Rectangular Box

This analysis of the sue load of the box in **fig 12** gives:

$$S = \frac{1}{6} \Delta \frac{L_{BP}}{d} (i_b - i_k) \quad (16)$$

Although modern ship hull form is approximating more closely to that of a box – i.e. the block coefficient is increasing – a more detailed analysis is needed to take into account the fining of the lines of a real ship. This can be done by approximating all the hydrostatic curves by power functions. Using well-known approximations to typical ship form, the constants to the equations can be approximated by various combinations of block and water plane coefficients.

When the results are evaluated, they are very close to (16) and the sue load can be expressed as:

$$S = k \cdot \Delta \cdot \frac{\delta T}{d_m} \quad (17)$$

Where change in trim during the sue, δT is given by:

$$\delta T = L_{BP} (i_b - i_k) \quad (18)$$

and values of k are given in **Table 1: Values of k**.

| Block Coefficient C_b | Z – Ratio of Distance of Sue Point to Near Perpendicular to L_{BP} | | | | | | |
|-------------------------|--|------|------|------|------|------|------|
| | 0 | 0.05 | 0.10 | 0.15 | 0.20 | 0.25 | 0.30 |
| 0.3 | 0.18 | 0.19 | 0.21 | 0.23 | 0.26 | 0.29 | 0.33 |
| 0.4 | 0.107 | 0.19 | 0.21 | 0.23 | 0.26 | 0.30 | 0.35 |
| 0.5 | 0.17 | 0.19 | 0.21 | 0.23 | 0.26 | 0.31 | 0.37 |
| 0.6 | 0.17 | 0.18 | 0.21 | 0.23 | 0.27 | 0.31 | 0.38 |
| 0.7 | 0.17 | 0.18 | 0.20 | 0.23 | 0.27 | 0.32 | 0.39 |
| 0.8 | 0.17 | 0.18 | 0.20 | 0.23 | 0.27 | 0.32 | 0.4 |
| 1.0 | 0.17 | 0.19 | 0.21 | 0.24 | 0.28 | 0.33 | 0.42 |

Table 1: Values of k

and
$$Z = \frac{e \pm f}{L_{BP}} \quad (19)$$

The remaining symbols are as shown in **Fig 8**, **Fig 10** and **Fig 11**

Draft at Sue Point at Full Sue:

Sue by the bow
$$d_s = \frac{\Delta - S}{C_b \cdot L_{BP} \cdot B} - \left(\frac{L_{BP}}{2} - e + f \right) i_b \quad (20)$$

Sue by the stern
$$d_s = \frac{\Delta - S}{C_b \cdot L_{BP} \cdot B} + \left(\frac{L_{BP}}{2} - e - f \right) i_b \quad (21)$$

The critical points for the sue load are given by:

First touch:
$$h_t = t - d_s - h_r \quad (22)$$

Chainage of first touch:
$$c_t = c_1 + \frac{h_1 - h_t}{i_w} \quad (23)$$

Chainage at full sue
$$c_s = c_1 + \frac{h_1 - t + d_s + h_r}{i_w} \quad (24)$$

Keel Dries when the stern is at:

$$c_d = c_1 + \frac{t - h_r}{i_w} \quad (25)$$

4.4. Sue on Vertically Curved ways

On vertically curved ways, the grade of the ways is constantly changing during the sue and the analysis becomes much more complex.

Using the same approach of approximating the hydrostatic curves by power functions, the following formulae have been established to compute the magnitude and position of the peak sue load:

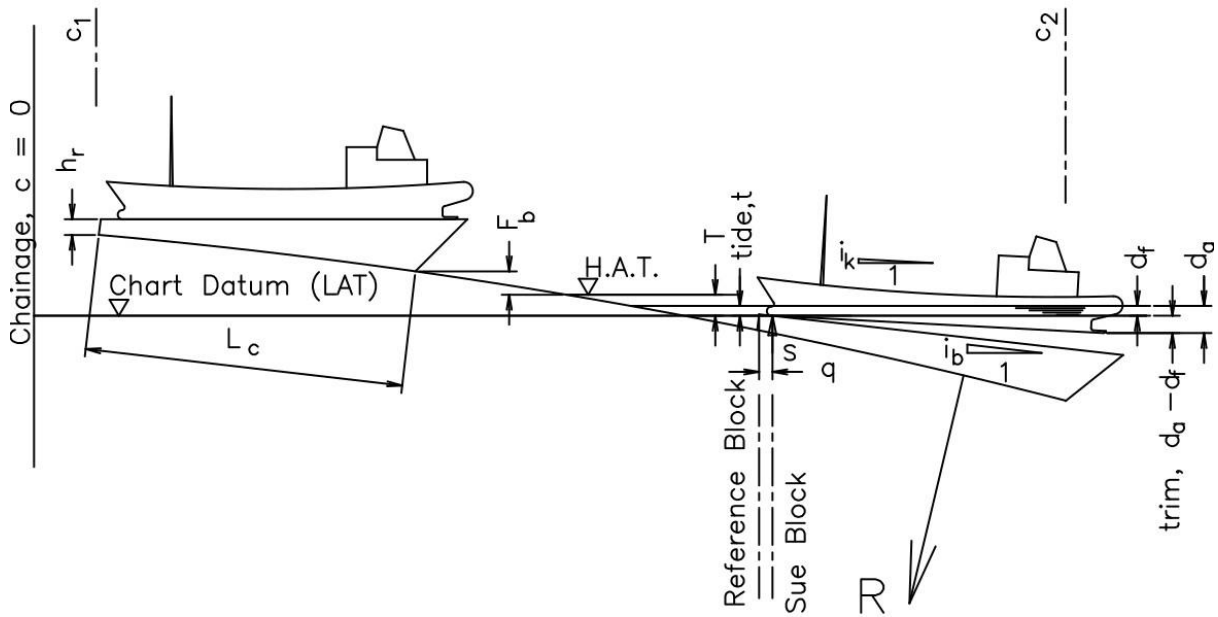


Fig 13: Sue on Vertically Curved Ways

$$\text{Slope of the keel at full sue} \quad i_s = i_{bs} = \frac{|\sqrt{A^2+B}| - A}{R} \quad (26)$$

$$\text{Sue by the bow} \quad A = R \cdot \varphi_b + q + K \cdot \frac{d_f + d_a}{2} + \frac{1-2.z}{2} \cdot L_{BP} \quad (27)$$

$$\text{Sue by the stern} \quad A = R \cdot \varphi_b + q + K \cdot \frac{d_f + d_a}{2} - \frac{1-2.z}{2} \cdot L_{BP} \quad (28)$$

$$\text{and} \quad B = 2 \cdot R \left[h_1 + h_r - t + \frac{d_f + d_a}{2} \left(1 + K \cdot \frac{d_a - d_f}{L_{BP}} \right) \right] \quad (29)$$

| Block Coefficient C _b | Z – Ratio of Distance of Sue Point to Near Perpendicular to L _{BP} (19) | | | | | | |
|----------------------------------|--|------|------|------|------|------|------|
| | 0.00 | 0.05 | 0.10 | 0.15 | 0.20 | 0.25 | 0.30 |
| 0.3 | 0.10 | 0.11 | 0.12 | 0.13 | 0.15 | 0.18 | 0.22 |
| 0.4 | 0.10 | 0.12 | 0.13 | 0.15 | 0.16 | 0.20 | 0.24 |
| 0.5 | 0.11 | 0.13 | 0.14 | 0.16 | 0.18 | 0.22 | 0.23 |
| 0.6 | 0.12 | 0.14 | 0.15 | 0.18 | 0.20 | 0.24 | 0.29 |
| 0.7 | 0.13 | 0.15 | 0.16 | 0.19 | 0.22 | 0.26 | 0.32 |
| 0.8 | 0.14 | 0.16 | 0.18 | 0.20 | 0.24 | 0.28 | 0.35 |
| 0.9 | 0.15 | 0.18 | 0.19 | 0.22 | 0.26 | 0.31 | 0.38 |
| 1.0 | 0.16 | 0.19 | 0.21 | 0.24 | 0.28 | 0.33 | 0.42 |

Table 2: Values of K

5. KEEL BLOCK LOADING

Although the quality of the docking plans that are being provided with ships are improving, appropriate docking plans are commonly not available at a slipway design stage. The following procedures will provide an adequate assessment of the loading estimates needed for the structural design of the ways.

5.1. Average Keel Block Loading

Start the process with an assessment of the average keel block loading.

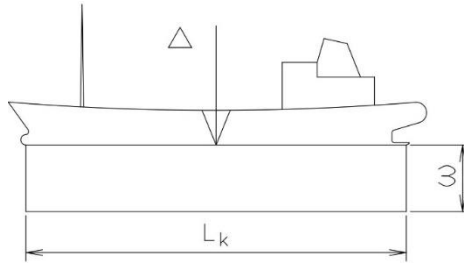


Fig 14: Average Keel Block Loading

$$\omega = \frac{\Delta}{L_k} \tag{30}$$

5.2. Parabolic Loading

In practice the load distribution on the keel is non-uniform and in general tends to an asymmetrical parabolic shape. (McSporran 2000) The position of the peak load will be off centre and its position must be made by estimation.

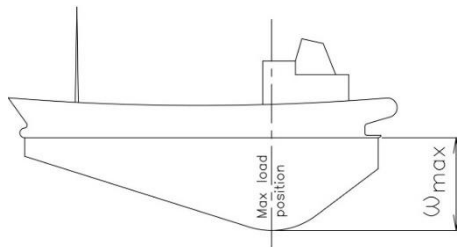


Fig 15: Parabolic Load distribution

The maximum load distribution is given by:

$$\omega_{max} = c \cdot \omega \tag{31}$$

Unless better suggestions are available, use values of c as given in **Table 3: Keel Block Load Factors**

| Type of Vessel | Constant c |
|--|------------|
| Very stiff vessels, e.g. submarines | 1.5 |
| Stiff vessels e.g. tugs and trawlers | 1.6 |
| Medium stiff vessels e.g. freighters and container ships | 1.75 |
| Flexible vessels e.g. 'all aft' VLCC's and Cape Bulkers | 1.8 – 1.9 |

Table 3: Keel Block Load Factors

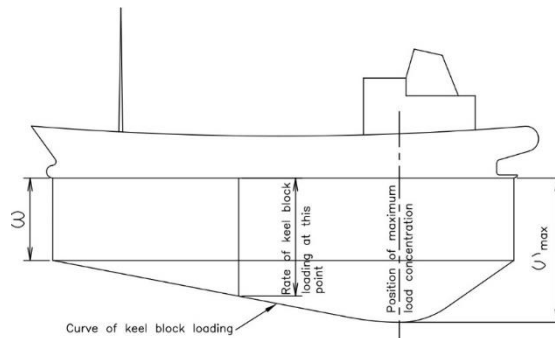


Fig 16: Practical Load Assumption

5.3. Trapezoidal Loading

In general, the substructure of the ways is relatively stiff. With the usual flat, unsprung, cradle the combination will be quite rigid compared to even relatively stiff vessels and the parabolic load distribution as proposed here gives a reasonable load estimate. However, in some cases, particularly when the cradle is built up aft, the system substratum becomes much more flexible relative to stiff vessels. Under these conditions, the asymmetry of the loading becomes pronounced and the load distribution begins to approximate a trapezoidal form (McSporran 2000).

With a trapezoidal load distribution, estimating the position of the peak load intensity is no longer relevant. The key input is the position of the centre of weight of the vessel and whether it is within or without the middle third of the keel (Crandall 1967).

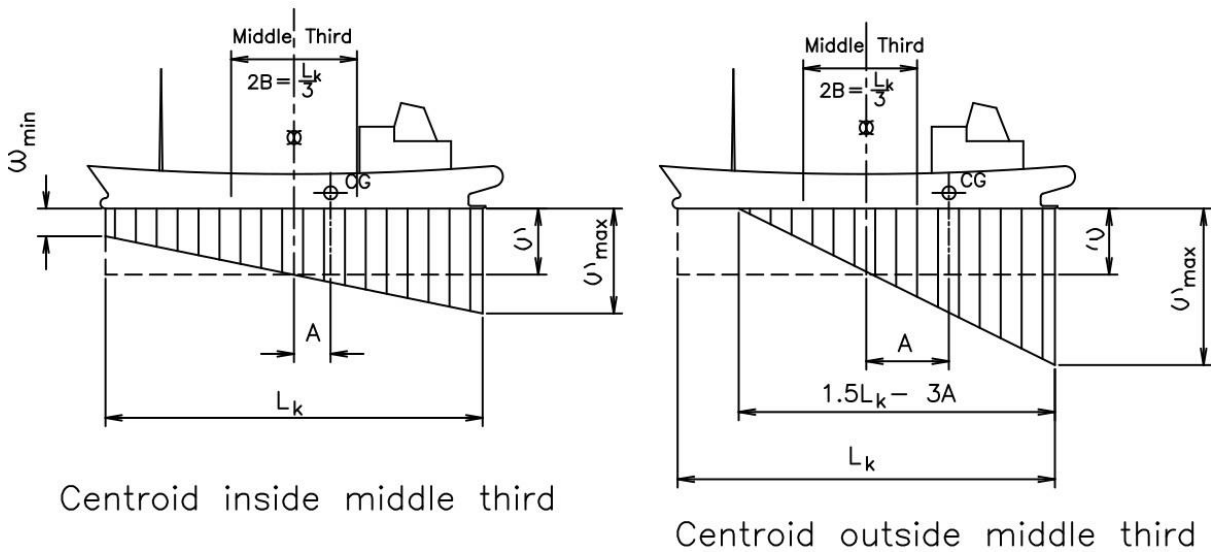


Fig 17: Trapezoidal Keel Block Load Distribution

Where the CG falls within the middle third, the minimum and maximum rates of loading are given by:

$$\omega_{min} = \omega \left(1 - \frac{A}{B}\right) \quad (32)$$

$$\omega_{max} = \omega \left(1 + \frac{A}{B}\right) \quad (33)$$

Where the CG falls outside the middle third, the effective length of keel blocks carrying load is given by:

$$L_{keff} = 1.5L_k - 3.A \quad (34)$$

and the maximum rate of keel block loading is given by:

$$\omega_{max} = 2. \omega \quad (35)$$

5.4. Lloyds Rules

Lloyds Rules (Lloyds Register 1981) have been developed for shiplifts but are applicable to slipways. Their load assessments are based on the parabolic method and they define two concepts:

Maximum Distributed Load (**MDL**): this is the maximum safe rate of loading on the keel blocks

Nominal Lifting Capacity (**NLC**): this is the maximum safe total lifting capacity of the cradle/ways system and is given by:

$$NLC = MDL \times L_k \times \text{Distribution factor} \quad (36)$$

Lloyds allow a maximum distribution factor of 0.83 but normally they will not accept this higher value and limit the distribution factor to a maximum value of 0.67. This is equivalent a minimum value of *c* of 1.5 in **Table 3**.

6. WAYS LOADING – MINIKIN DIAGRAM

Minikin (Minikin R.R. 1963) described a method of plotting the variation of expected peak loading on the ways over the lifetime of the slipway. This is shown in **Fig 15: Minikin's Original Diagram**

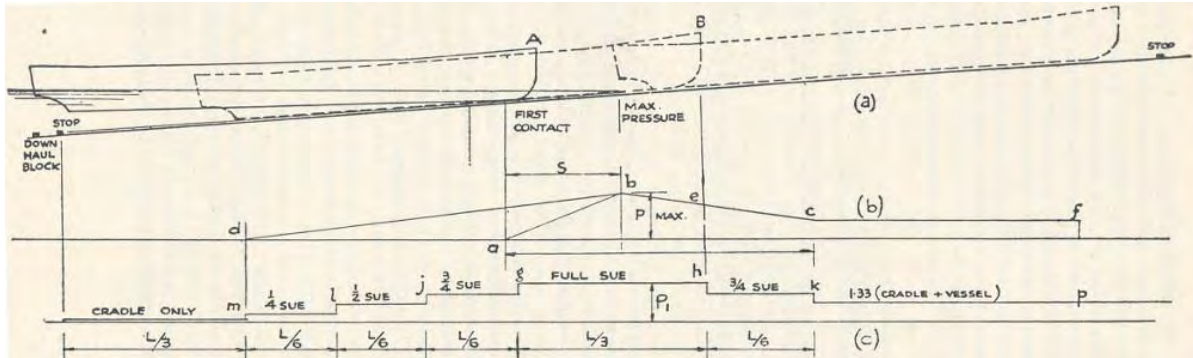


Fig 18: Minikin's Original Diagram

Given the procedures set out above, this diagram must be constructed from a montage of values for different vessels and different stages of the tide.

7. LATERAL SUPPORT FORCES

Ships are normally built symmetrical and balanced about the centreline. In the water they are normally trimmed to float on an even keel without any list to either side. In principle such a ship, dry docked, should balance on its keel without the need of any lateral support. Quite obviously, this would be a most dangerous practice but since the ship is balanced it is not at all clear what forces will be generated in the lateral support system.

Whatever the cause of overturning forces acting on a dry docked ship, they should be treated as overturning moments in order to calculate the forces acting on the support structures.

7.1. Transverse, (Wind) Forces

These occur when the vessel is high and dry and the normal procedures for wind loading on buildings apply. Lloyds (Lloyds Register 1981) propose a horizontal force of 2.5 kN/m² or a vertical loading at the outrigger ways or at the bilge supports equal to 20% of the keel loading.

7.2. Vessels with List or Loll

If a vessel is docked on the blocks heeled over at some small angle then it will topple over as it sues unless it is restrained by the lateral support structures – forces that will then be transmitted to the ways structures. As shown in **Fig 16**, the analysis depends on a knowledge of the lever arm l_a and this is difficult to determine. This condition is normally only found in smaller fishing vessels without adequate trimming tanks to bring the vessel back to upright. In general, an allowance of 5° of heel should be sufficient for design purposes.

In practice, vessels liable to cause such problems, will arrive heeled over at some small angle that it is not possible to correct before docking. This situation can be analysed by the principles of hydrostatics irrespective of whether it is the result of list or loll to yield the value of the overturning moment.

The overturning moment is given by:

$$M_t = [(c_1 \cdot L_{BP} \cdot B^3) + (c_2 \cdot d_m \cdot \Delta)] \tan \phi \quad (37)$$

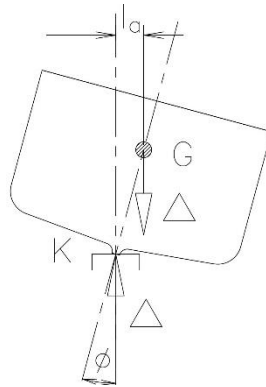


Fig: 19 Overturning Moment

The values of the constants, c_1 and c_2 given in **Table 4: Overturning Moment Factors** have been given in terms of block coefficient although they are actually functions of the waterplane area coefficient, not the block coefficient. However, the block coefficient is usually much easier to obtain than the waterplane area coefficient and appropriate corrections have been made.

| Cb | C1 | C2 |
|-----------|-----------|-----------|
| 0.4 | 0.031 | 0.759 |
| 0.5 | 0.038 | 0.750 |
| 0.6 | 0.046 | 0.742 |
| 0.7 | 0.055 | 0.736 |
| 0.8 | 0.064 | 0.731 |
| 0.9 | 0.073 | 0.726 |
| 1.0 | 0.083 | 0.722 |

Table 4: Overturning Moment Factors

Equation (37) above gives an approximate, not an exact value but one which should be quite adequate for dry docking purposes. ϕ is the angle of heel.

8. WAYS CONSTRUCTION

It is usual and economical to build slipway cradles without any suspension. In this respect they are akin to container cranes. Both require track that is set to extremely accurate levels. For container cranes, on the quayside, in the dry, this is not a difficult matter. Slipway rails underwater are a completely different matter. Extreme accuracy is required from the trade of marine construction underwater that is perhaps the roughest in the construction industry. Some ingenious engineering is required to marry these two.

Generally, a target accuracy better than ± 1.5 mm in level and ± 3.0 mm in line is adequate. To achieve this, very high accuracy levelling is needed. Where there is a reinforced concrete quay wall or jetty adjacent to the ways, parallax plate and invar staff levelling can be used. A chain of benchmarks will be needed and the highest level of accuracy is needed in surveying these. At this level of accuracy there will be some inconsistency in repeat measurements due to the tidal distortions of the earth's crust. Where suitable structures are not available some form of water tube levelling will be needed.

A 20 second construction theodolite will generally be sufficient to control the line of the ways.

8.1. Construction in the dry

Construction in the dry reverts to the sort of conventional construction used for container crane rails where it is relatively easy to achieve the required tolerances.

There are parts of the world with extreme tide ranges so that the ways can be constructed in the dry by working at low tide and only taking the ways down to spring low water. This is only really practical for smaller units and dry docking must take place as the tide rises.

Alternatively, the ways can be coffered so that work takes place in the dry. With proper geotechnical design, this is a very effective method but probably not the most economic.



Fig 20: 1200 ton Slipway Construction in the Dry, Port Elizabeth 1945 – Military Specs!

8.2. Prefabricated Construction

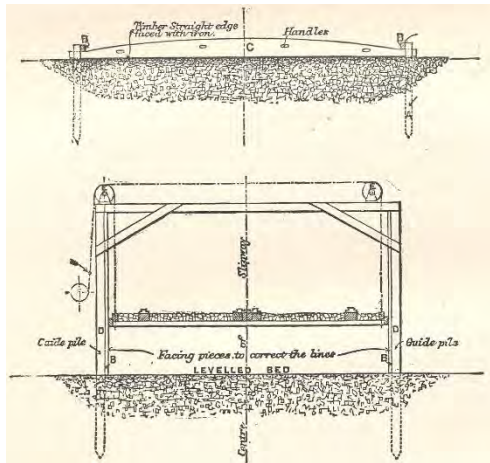


Fig 21: Construction Method for Slipway Ways ca 1895

Brysson Cunningham (Cunningham 1922) describes a method of construction used in 1895 to construct the 1500 ton slipway in East London, South Africa. The ways were still in good condition 100 years later although the facility had been decommissioned some years earlier. In this method, a crushed stone bed was levelled by trammel off prelevelled screed rails. The ways were assembled on pallets of timber and lowered on to the stone bed. See **Fig: 21** (Cunningham 1922).

For the construction of the 1200 ton slipway in Hobart, Tasmania, John Tubb (Tubb J.R. 1970) used load-bearing, prefabricated steel beams in 13 m long sections spanning between piled supports as the ways structure. See **Fig 22** and **Fig 23** (Tubb J.R. 1970) Each section, complete with rail and shuttering for encasing concrete, was template matched on land to the preceding section by means of ϕ 76 mm (3 inch) pins in 0.8 mm (1/32 inch) clearance holes. The sections fitted precisely without any

discontinuity in the top surface between sections. Levelling for this project was done to an accuracy ± 1.5 mm. Accuracy of the final construction was probably somewhat coarser.

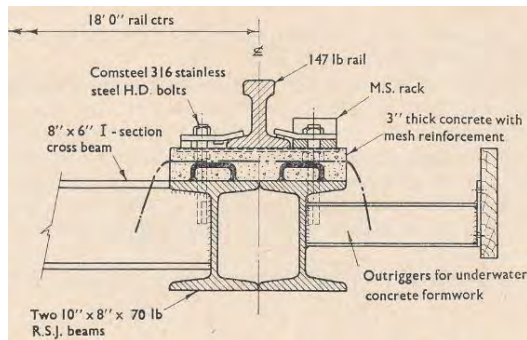


Fig 22: Prefabricated Steel Beam Ways

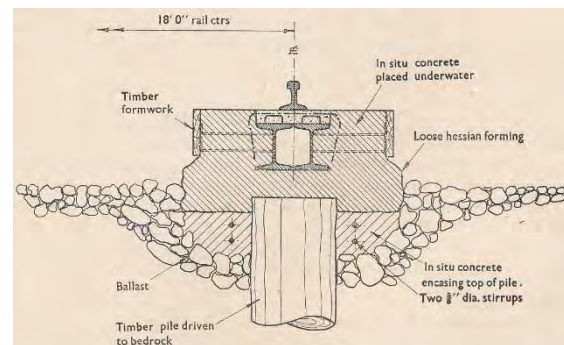


Fig 23: Installation of Steel Ways

Similar methods have been used with precast concrete elements for the ways structure. In general, these are not nearly as effective in meeting the tolerances. In the Saldanha Bay case, there were a number of discontinuities in the order of 25 mm (Mackie, K.P. 1970).

8.3. Incremental Launching

The use of incremental launching of continuously cast concrete ways avoids the problem with joints. This is best done with precast concrete pedestals set to the required level, accuracy and head slope to receive the ways. Rollers can be attached to these pedestals to convey the ways with a 6 mm clearance and then removed when the launching is complete so that the ways settle onto the pedestals. The top of the ways provides the accurate surface for fixing the rails.

For small slipways, ways beams sufficient to carry the load will be light enough to launch over the pedestal rollers and be supported by the pedestals so that no further support is necessary. The only foundation needed is the foundation for the pedestals. For larger slipways a much more substantial structural support must be provided at rough tolerances by conventional construction. The control pedestals can then be set into these supports. The ways beam can be launched over this and encased off it to the required tolerances. In this case the ways beam is fairly insubstantial and serves only to provide an accurate surface for fixing the rails and transferring the loads to the more substantial substructure.

9. ANTI-FRICTION SYSTEMS

9.1. Greased Timber

When ship sleds are used over greased timber the friction is in the order of 10%. Appropriate grease is a heavily graphited No 2 calcium grease i.e. bulldozer track grease.

9.2. Wheels

Very small wheels, generally about $\phi 200$ mm were used on the old patent slipways and they tended to crack like nuts (Tubb J.R. 1970). Friction, particularly with inaccurate track is in the order of 5% to 10%. More recently larger wheels of $\phi 300$ mm to $\phi 350$ mm have been used with the longitudinal members of the cradle steelwork resting on top of the axles. Friction is generally from 2% to 5%. With this arrangement the keel blocks are quite high above the rails necessitating longer ways.

An alternative is to use very large wheels, ϕ 600 or larger, and hang the longitudinal steelwork below the axles. With this arrangement, there is a significant reduction of the height of the keel blocks above the rails. With these large wheels, friction is $< 1\%$.

It is normal practice to use plain bearings on slipway wheels. Appropriate grease is a No 2 lithium automotive grease or a heavily graphited No 2 calcium grease.

On a 200 ton slipway using the 3-way system, 100 no ϕ 300 wheels rated at 20 tons would have been needed. Using ϕ 600 underslung wheels rated at 32 tons on a 2-way system, only 16 no wheels were needed.



Fig 24: ϕ 600 Underslung Wheel

9.3. Live Rollers

Common practice on railway dry docks is to use live roller trains instead of wheels but they can be used equally on slipways. Friction is commonly $< 1\%$.

Like the wheel, these systems are basically very simple and robust but like the wheel there is a body of specialist knowledge needed to design and maintain them

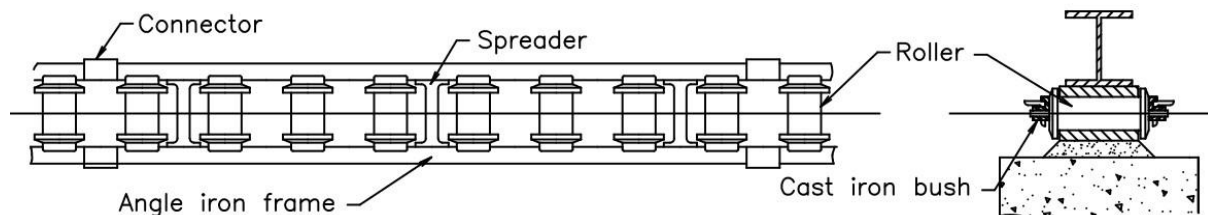


Fig 25: Typical Live Roller Frame

10. Rails

Rails are characterised by the Hertz contact stresses between wheel and rail or between roller and plate. These reach their peak values below the contact surfaces where, even at a safe level, they can exceed the yield stress of the steel and are only safe to the extent that they are contained by the surrounding metal. Steel sections intended for rolling surfaces must have a minimum of section depth – hence the blocky design of a rail head. Provided adequate depth of section is maintained, design of rolling surfaces reverts to the structural issues of support of the load either by shear and bending where the rail spans between supports or by beam on elastic foundation theory where it has continuous support on the ways beam. The former only applies to flat bottom rails with sufficient I value to carry load in bending; the latter to either flat bottomed rails or to roller plates.

10.1. Fastening

Ideally no part of the fastenings should be cast into the concrete. All should be removable and replaceable to simplify rail maintenance. While various standardised, often patented rail clip systems are available, the attachment component is not. Inevitably this involves purpose designed attachments. After the corrosion effects on the rail itself, these are the most maintenance intensive component of system. Unfortunately, the class of person who commonly gets involved in this work, long after the construction has been completed, generally has no concept of the issues involved and lacks the nous

to have replicas of the relevant parts fabricated. By and large they all have one knee-jerk reaction: “drill baby drill” and use grouted-in bolts.

The answer is to join them and use properly designed, permanently fixed bolts. For durability these should be of stainless steel. However, the usual grades of 304 or 316 are not adequate. There are a number of more recent alloys that are much more appropriate and a competent stainless steel specialist should be consulted on the alloy selection.

With stainless steel bolts, they may not be allowed to come into contact with the reinforcement. Hence the bolts must be accurately placed. Cast-in bolts are not recommended. The upper surface of the ways beam needs to be steel floated to a fair flat surface and the templates needed to locate the bolts will interfere with the surface finishing. The bolts holes should be drilled into the concrete once it has set using a template to control the drilling. An appropriate proprietary bolt fixing system should be used to set the bolts into the holes in the concrete. The bolts must be set in to the correct depth so that heads of the bolts are at the correct level. Depending on the rail selection and cradle design, high bolts will foul the cradle. This is a common problem with bolts replaced underwater. The heads of the bolts are often set too high and are damaged by the cradle.

With stainless steel bolts it is vital that there is no electrical contact between the bolt and the rail. **Fig 26** is a suggest method of fixing the rails using UHMWPE as spacers and washers to isolate the stainless steel.

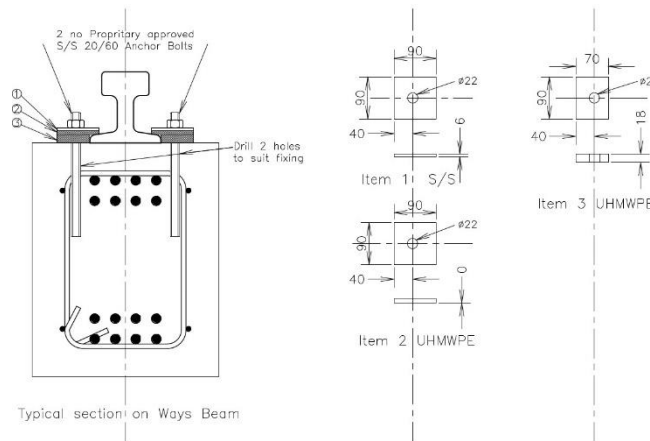


Fig: 26 Suggested Rail Fixing

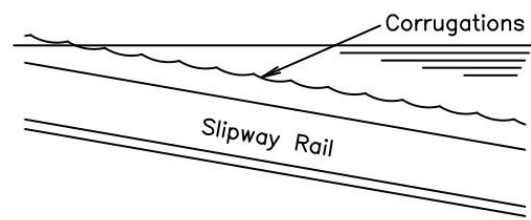
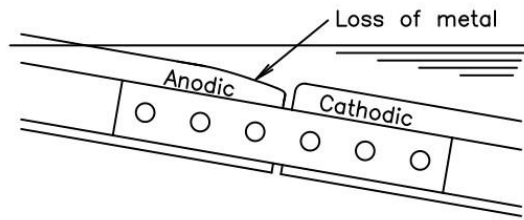
10.2. Corrosion

Slipway rails exhibit pronounced Accelerated Low Water Corrosion (ALWC) although in the case of these rails, Microbially Induced Corrosion (MIC) does not appear to play any role. Rail corrosion is most intense just below low water springs. On flat bottom rails the weakest part is the thinnest, the web of the rail. With cathodic protection, this corrosion is suppressed below mid tide but becomes severe between mid and high tide. Generally, rails with thickened webs – in the order of 30 mm – should be used and all rails should be given a heavy duty anti corrosion coating.

Flat bottomed rails suffer from two other forms of corrosion, differential aeration cell corrosion and corrugation corrosion both focussed on the tidal zone particularly the lower tidal zone.

The differential aeration cell corrosion occurs in the lower tidal zone and only occurs on the lower end of the upper rail of a pair of rails joined by fishplates and is limited to a short length from the join. There seems to be an electro-chemical couple between the two ends and the head of the upper end of the lower rail is protected and shows no loss of metal. The simple cure is to use full penetration butt welded joints – either copper block welded or thermite welded.

The corrugation corrosion seems to be initiated by pitting corrosion in the rail head. Rolling work hardens the surface of the head outside the pits, changes its electro-chemical potential to more cathodic and sets up a couple between the work hardened metal and the metal in the pit. The effect is exacerbated by the natural frequency of the cradle. Cathodic protection will help.



Differential Aeration Cell Corrosion



Fig: 27 Differential Aeration Cell Corrosion

Corrugation Corrosion



Fig 28 Corrugation Corrosion

The plate rolling surfaces needed for live roller trains seem to exhibit far less corrosion problems than flat bottomed rails.

11. CONCLUSION

The above information, albeit abbreviated, gives a good overview of the complexity of slipway design and should provide a good companion to the design of a slipway and point the way to further investigations.

12. REFERENCES

- Crandall Dry Dock Engineers Inc (1967) Railway Dry Docks
- Cunningham, B. (1922) Principles and Practice of Dock Engineering (3rd ed) Charles Griffin London
- Lloyds Register (1981) Code for Lifting Appliances in a Marine Environment – Mechanical Lift Docks
- Mackie, K.P. (1970) Diagram of precise survey of the ways to the 1200 ton Saldanha Bay Slipway
- Mackie, K.P. (1979) Mechanical Systems of Dry Docking, University of Cape Town
- Mackie, K.P (2012) Manual of Basic Coastal & Harbour Engineering
- Mackie, K.P. (2016) Dry Dock Manual
- McSporran, R (2000) Analysis of Ships in Dry Docks, Thesis no 21, Dept of Civ. Eng., UCT
- Minikin, R.R. (1963) Winds, Waves and Maritime Structures, Charles Griffin London
- Munro-Smith, R (1967) Merchant Ship Design, Hutchinson
- Prosser, R.B. (1894) on Thomas Morton, Dictionary of National Biography, vol 39, Smith Elder, London
- Tubb, J.R. (1970) Some Aspects of the Design of Large Slipways, Proc ICE vol 46, May 1970

APENDIX: Vertically Curved Ways Calculator - Formulae
SHEET 1

| Ways Curve Input | | | | | Ways Curve Output | | | | |
|---|-----------------|------|--|---|---|-----------------|------|--|--|
| Cell | Label | Cell | Input | Description | Cell | Label | Cell | Input | Description |
| G2 | c ₁ | H2 | Input | Chainage at landward end (m) | P2 | x' | Q2 | =G4-\$F\$3 | Distance from landward to seaward end (m) |
| G3 | c ₂ | H3 | Input | Chainage at seaward end (m) | P3 | y' | Q3 | =G\$5-\$G\$6 | Height landward end above seaward end (m) |
| G4 | h ₁ | H4 | Input | Level at landward end (m) | P4 | α ₁ | Q4 | =ATAN(G\$7) | Slope Angle at land end (rad) |
| G5 | h ₂ | H5 | Input | Level at seaward end (m) | P5 | α ₂ | Q5 | =2*(ATAN(\$X\$4/\$X\$3))-X\$5 | Slope Angle at sea end (rad) |
| G6 | l ₁ | H6 | Input | Gradient at landward end (i in 1) | P6 | l ₂ | Q6 | =TAN(X\$6) | Gradient at seaward end (i in 1) |
| G7 | L _c | H7 | Input | Chord, ref block to cradle end (m) | P7 | R | Q7 | =X\$4/((COS(X\$5))-COS(X\$6))) | Radius of vertical curve (m) |
| G8 | l _{bb} | H8 | Input | Build-up of blocks (i in 1) | P8 | x ₀ | Q8 | =(X\$8*(SIN(X\$5)))-F\$3 | Distance from crown to coord origin (m) |
| G9 | δR | H9 | Input | Height above or below ref surface (± m) | P9 | h' | Q9 | =G\$5+X\$8*(1-(COS(X\$5))) | Height of crown above datum (m) |
| G10 | T | H10 | Input | Maximum tide range (m) | P10 | h _r | Q10 | =G\$12+G\$13 | Block height above rail at reference point (m) |
| G11 | w | H11 | Input | Height of shim base above ref surface (m) | P11 | R' | Q11 | =X\$8+G\$10 | Revised radius of vertical curve (m) |
| G12 | b | H12 | Input | Height of block above shim base (m) | P12 | x' ₀ | Q12 | =(X\$12*(SIN(X\$5)))-F\$3 | Revised distance from crown to coord origin (m) |
| G13 | L _w | H13 | Input | Length over keel blocks between block centres (m) | P13 | h'' | Q13 | =G\$5+X\$12*(1-(COS(X\$5))) | Revised height of block above rail height at ref (m) |
| Ways Profile by Arc Length | | | | | Ways Profile by Chainage | | | | |
| Repeat row 19 for further stations at other arc lengths from c ₁ | | | | | Repeat row 19 for further stations at other chainages | | | | |
| Cell | Label | Cell | Input | | Cell | Label | Cell | Input | |
| B18 | A | B19 | Input arc length from c ₁ | | J18 | c | J19 | Input chainage from c ₁ | |
| C18 | c _a | C19 | =X\$8*(SIN((A19/X\$8)+X\$5))-X\$9 | | K18 | A _c | K19 | =Y\$8*((ASIN((\$Y\$9+#REF!)/Y\$8))-Y\$5) | |
| D18 | h _a | D19 | =X\$10-X\$8*(1-COS(ASIN((\$X\$9+B19)/X\$8))) | | L18 | h _c | L19 | =Y\$10-Y\$8*(1-COS(ASIN((\$Y\$9+#REF!)/Y\$8))) | |
| E18 | l _A | E19 | =TAN(ASIN((\$X\$9+B19)/X\$8)) | | M18 | l _c | M19 | =TAN(ASIN((\$Y\$9+#REF!)/Y\$8)) | |
| Vessel Data | | | | | | | | | |
| Cell | Input | Cell | Label | Description | Input Vessel Data | | | | |
| Data | | | | Description | Cell | Input | Cell | Input | etc |
| D34 | 1 | E34 | 2 | | F34 | 3 | G34 | 4 | H34=5, I34=6 etc as needed |
| D35 | 2 | E35 | Item | | Label cases - selected design vessels - as needed | | | | |
| D36 | 3 | E36 | L _{o/a} | Length overall (m) | Input Cols F, G, H etc as needed | | | | |
| D37 | 4 | E37 | L _{B/P} | Length between perpendiculars (m) | do | | | | |
| D38 | 5 | E38 | L _k | Docking length of keel (m) | do | | | | |
| D39 | 6 | E39 | c _b | Block coefficient | do | | | | |
| D40 | 7 | E40 | c _w | Waterplane coefficient | do | | | | |
| D41 | 8 | E41 | Δ | Docking displacement (tons weight) | do | | | | |
| D42 | 9 | E42 | d _f | Draft fore (m) | do | | | | |
| D43 | 10 | E43 | d _a | Draft aft (m) | do | | | | |
| D44 | 11 | E44 | e | Offset of sue point from near perp, fore or aft (m) | do | | | | |
| D45 | 12 | E45 | q | Offse of sue point from cradle reference point | do | | | | |
| D46 | 13 | E46 | h _r | Block height above rail at reference point (m) | All=P10 | | | | |
| D47 | 14 | E47 | T | Maximum tide range (m) | All=H10 | | | | |

PIANC – World Congress Panama City, Panama 2018

| APENDIX: Vertically Curved Ways Calculator - Formulae | | | | | | | | |
|---|------------------|------|---|------|-----------------|------|--|--|
| Sheet 2 | | | | | | | | |
| Cell | Label | Cell | Input Data | Cell | Label | Cell | Computed Data | |
| | | B2 | 3 | C4 | R | C5 | =Sheet1!\$Q\$7 | |
| C2 | L _{o/a} | C3 | =VLOOKUP(3,Sheet1!\$D\$34:Sheet1!\$N\$47,\$O\$5) | D4 | x _o | D5 | =Sheet1!\$Q\$8 | |
| D2 | L _{B/P} | D3 | =VLOOKUP(4,Sheet1!\$D\$34:Sheet1!\$N\$47,\$O\$5) | E4 | h' | E5 | =Sheet1!\$Q\$9 | |
| E2 | L _k | E3 | =VLOOKUP(5,Sheet1!\$D\$34:Sheet1!\$N\$47,\$O\$5) | F4 | α ₁ | F5 | =Sheet1!\$Q\$4 | |
| F2 | L _c | F3 | =Sheet1!\$H\$7 | G4 | α ₂ | G5 | =Sheet1!\$Q\$5 | |
| G2 | C _b | G3 | =VLOOKUP(6,Sheet1!\$D\$34:Sheet1!\$N\$47,\$O\$5) | H4 | c ₁ | H5 | =Sheet1!\$H\$2 | |
| H2 | Δ | H3 | =VLOOKUP(8,Sheet1!\$D\$34:Sheet1!\$N\$47,\$O\$5) | I4 | d _m | I5 | =(J3+I3)/2 | |
| I2 | d _r | I3 | =VLOOKUP(9,Sheet1!\$D\$34:Sheet1!\$N\$47,\$O\$5) | J4 | i _{hb} | J5 | =Sheet1!\$H\$8 | |
| J2 | d _a | J3 | =VLOOKUP(10,Sheet1!\$D\$34:Sheet1!\$N\$47,\$O\$5) | K4 | h _r | K5 | =Sheet1!\$Q\$10 | |
| K2 | i _k | K3 | =(J3-I3)/D3 | L4 | A _b | L5 | =2*\$C\$5*(ATAN((F\$3)/(2*(C\$5+L\$3)))) | |
| L2 | w | L3 | =Sheet1!\$H\$11 | M4 | i _r | M5 | =ATAN(J\$5-ASIN((F\$3)/(2*(C\$5+L\$3)))) | |
| M2 | b | M3 | =Sheet1!\$H\$12 | N4 | i _a | N5 | =TAN(J\$5+ASIN((F\$3)/(2*(C\$5+L\$3)))) | |
| N2 | T | N3 | =Sheet1!\$H\$10 | | | O5 | 3 | |

| Intermediate Parameters | | | | Sue Load Parameters | | | |
|-------------------------|------------------|------|--|---------------------|------------------|------|---|
| Cell | Label | Cell | Output | Cell | Label | Cell | Output |
| C7 | δt | C8 | Repeat input fraction of tide e.g. 0 to 1 x 0.1 in C8 to C18 | C20 | δt | C21 | Repeat input fraction of tide e.g. 0 to 1 x 0.1 in C21 to C31 |
| D7 | t | D8 | =C8*\$N\$3 | D20 | t | D21 | =D8 |
| E7 | h _{r1f} | E8 | =D8-\$I\$3-\$K\$5 | E20 | i _{sf} | E21 | =ABS(SQRT((O8^2)-4*\$M8*\$O8)))/(2*\$M8) |
| F7 | h _{r1a} | F8 | =D8-\$J\$3-\$K\$5-\$J\$5*\$F\$3 | F20 | i _{sa} | F21 | =ABS(SQRT((O8^2)-4*\$M8*\$P8)))/(2*\$M8) |
| G7 | C _{r1f} | G8 | =(C\$5*(SIN(ACOS(1-((E\$5-E8)/C\$5)))))-D\$5 | G20 | n | G21 | =G\$3^(0.67) |
| H7 | C _{r1a} | H8 | =(C\$5*(SIN(ACOS(1-((E\$5-F8)/C\$5)))))-D\$5 | H20 | h _{da} | H21 | =D21-\$K\$5-\$J\$5*\$F\$3 |
| I7 | A _f | I8 | =C\$5*(ASIN((D\$5+G8)/C\$5)) | I20 | C _{da} | I21 | =(C\$5*(SIN(ACOS(1-((E\$5-H21)/C\$5)))))-D\$5 |
| J7 | A _a | J8 | =C\$5*(ASIN((D\$5+H8)/C\$5)) | J20 | S _f | J21 | =((1+\$K8)/2)*(\$Q8*\$H\$3*\$E\$3*(E21-\$M\$5-\$K\$3)/\$I\$5) |
| K7 | v | K8 | =(L\$5-\$J8+\$I8)/ABS(L\$5-\$J8+\$I8) | K20 | S _a | K21 | =((1-\$K8)/2)*(\$Q8*\$H\$3*\$E\$3*(F21-\$N\$5-\$K\$3)/\$I\$5) |
| L7 | K' | L8 | =1/((12*(3-2*(G\$3^(0.33))))+((G\$3^(0.67))-1)) | L20 | A _{r1f} | L21 | =C\$5*((ASIN((D\$5+G8)/C\$5))-F\$5) |
| M7 | A | M8 | =C\$5/2 | M20 | A _{r1a} | M21 | =C\$5*((ASIN((D\$5+H8)/C\$5))-F\$5) |
| N7 | B | N8 | =C\$5*\$M\$5/2+\$L\$8*\$E\$3 | N20 | A _{sf} | N21 | =((1+\$K8)/2)*C\$5*((ATAN(E21))-F\$5)-L\$5/2 |
| O7 | C _f | O8 | =C\$5*(M\$5/2)-E\$5-\$K\$5-\$I\$5+\$D8-(L8-0.5)*K\$3*\$E\$3 | O20 | A _{sa} | O21 | =((1-\$K8)/2)*C\$5*((ATAN(F21))-F\$5)-L\$5/2 |
| P7 | C _a | P8 | =C\$5*(N\$5/2)-E\$5-\$K\$5-\$I\$5+\$D8+(L8-0.5)*K\$3*\$E\$3 | P20 | A _{da} | P21 | =C\$5*(ASIN((D\$5+I21)/C\$5))-F\$5 |
| Q7 | K | Q8 | =L8*G\$3^(0.67) | Q20 | A _{max} | Q21 | =P21-L\$5/3 |

t = tide (m) i_{sf} = Grade of rail fore at full sue i_{sa} = Grade of rail aft at full sue A_{max} = Arc distance from datum of max load
h_{da} = Height of rail at aft end of cradle when keel dries (m) C_{da} = Chainage of rail at aft end of cradle when keel dries (m)
A_{r1f} = Arc distance from datum to ref point at 1st touch fore (m) A_{r1a} = Arc distance from datum to aft end of cradle at 1st touch aft (m)
A_{sf} = Arc distance from datum to point of full sue fore (m) A_{sa} = Arc distance from datum to point of full sue aft (m)
A_{da} = Arc distance from datum to end of cradle S_f = Full sue fore(t) S_a = Full sue aft (t)

BELGIAN ROYAL DECREE FOR SEA-GOING INLAND VESSELS: A REVIEW FOR CONTAINER AND BULK CARGO VESSELS

L. Donatini¹, T. Van Zwijnsvoorde², Y. Meersschaut³, W. Hassan⁴, M. Vantorre⁵

ABSTRACT

The Belgian Royal Decree of 2007 allows inland vessels meeting certain requirements to perform a limited, non-international sea journey. After ten years of practice, the need to evaluate the performance of the Royal Decree arose, in particular with respect to inland container and bulk cargo vessels. In the present work, four reference vessels are selected as representative examples of existing container/bulk cargo vessels. For each of the four reference vessels, three significant loading conditions are selected. The Royal Decree requirements regarding stability and vertical relative motions are analyzed in detail for each vessel and loading condition. Based on the results of this analysis, a possible update of the requirements of the Royal Decree is proposed.

1 INTRODUCTION

Inland vessels are indispensable in the transportation of cargo, as an alternative to road and rail transport. The possibilities of a port to grow depend, among other things, on the availability of a stable connection with the inland waterways. In some cases, however, this connection can be unavailable for inland vessels above a certain size due to the limited dimensions of the waterways in the proximity of the port. Even when the connection is available, it could be affected by long travelling times due to the presence of locks and bridges.

When inland waterways can be reached via a limited sea-journey, it is interesting to explore the possibility of allowing inland vessels at sea, provided that strict safety conditions are met. Inland vessels are not compliant with IMO/SOLAS conventions, and as such they cannot perform an international sea-journey. Nevertheless, for a journey between two ports located in the same country, the state authority can grant permission to a specific type of inland vessel to navigate at sea. This strategy is particularly appealing in Belgium, where the connection between coastal ports and the main European inland waterway network is limited. From the coastal port of Zeebrugge, in fact, vessels larger than CEMT-IV can only travel inland as far as Brugge, since the following connection to Ghent is precluded to larger vessels. If allowed on a national sea-journey between the coastal ports and the mouth of the River Scheldt, on the other hand, large inland vessels are able to reach Antwerp and consequently the wider European network from there.

Currently, the possibility for an inland vessel to sail at sea is regulated by the Belgian Royal Decree of 8 March 2007, which stipulates an extensive list of requirements the vessel needs to comply with. Concerning the behaviour of the vessel in waves, the Royal Decree prescribes a full risk analysis aimed to evaluate, among other things, the probability that the ship faces excessive relative vertical motions which can lead to shipping of water. According to the Belgian Royal Decree, tankers and closed hatch vessels wanting to sail the estuary trajectory up to a maximum significant wave height of 1.2 m can be exempted from the need to perform a full risk analysis, provided that certain deterministic requirements on the minimum freeboard are met. Such an exemption is not present for container and open hatch bulk cargo vessels. However, a simpler way to allow these vessels on the estuary trajectory in controlled wave conditions could attract more traffic.

This study is focused on an assessment of the performance of open hatch inland dry cargo vessels along the estuary trajectory between the port of Zeebrugge and the mouth of the Scheldt estuary, with respect to the requirements of the Belgian Royal Decree. The aim of the study is to verify whether it is feasible to introduce new deterministic exemptions from the risk analysis, valid also for container and open hatch dry cargo inland vessels. Moreover, a review of the current stability regulations enforced

¹ PhD student, Ghent University, Maritime Technology Division, luca.donatini@ugent.be

² PhD student, Ghent University, Maritime Technology Division, thibaut.vanzwijnsvoorde@ugent.be

³ Head of unit environment and ICT, Flemish Authorities, Department of Mobility and Public Works, Maritime Access, youri.meersschaut@mow.vlaanderen.be

⁴ Expert researcher at Flanders Hydraulics Research, Antwerp, wael.hassan@mow.vlaanderen.be

⁵ Professor, Ghent University, Maritime Technology Division, marc.vantorre@ugent.be

by the Royal Decree is proposed. The study is based on four design vessels, which represent the entire European fleet of inland vessels with open hatches (container/bulk cargo) of CEMT class Va and larger. The study is part of a larger project entitled “Nautical-hydrodynamic investigation of the possibilities of an inland navigation connection over sea for the port of Zeebrugge” performed by the Maritime Technology Division of Ghent University and commissioned by the Flemish Government (Department of Mobility and Public Works, Maritime Access).

2 ESTUARY TRAFFIC IN FLANDERS/BELGIUM

2.1 History

Estuary traffic originated even before the seaward expansion of Zeebrugge (1972-1985). Bunker companies located in Antwerp needed to reach Zeebrugge in order to fuel sea-going vessels. For these vessels, a service rule was developed in 1962 by the Belgian Shipping Inspectorate. The vessels were only allowed to perform the journey in favourable conditions, up to 1.2 m significant wave height (average of the 33% highest waves, denoted as H_s); in practice, these trips were allowed in wind conditions up to 5 Beaufort. Freeboard requirements were given as deterministic rules, as a function of the length of the vessel. These tankers, with length of around 70 m, could easily fulfil strength requirements.

Along the trajectory waves exceed 1.2 m H_s 13% of the time (Vantorre & Van Zwijnsvoorde, 2016), based on wave recordings at the Bol van Heist (BVH) measuring buoy (see paragraph 3.1). In order to establish a more reliable connection, skippers started to request an extension of the limiting conditions up to 1.6 m and even 1.9 m H_s , which would grant them almost permanent access to the sea-trajectory. Not only tankers, but also car carriers and container vessels were interested to get involved in this promising market. Initially, these requests were taken into consideration on an individual basis. Three tankers (Tanzanite, Breitling and Texas) and three RoRos (Waterways 1/2/3) were granted permission based on individual assessments in the period 2003-2007. Two of these ships are shown in Figure 2-1.



Figure 2-1 : Estuary tanker Tanzanite⁶ and Roro vessel Waterways I⁶.

This ad-hoc approach ended in March 2007 with the publication of the Royal Decree (RD2007) of *inland vessels performing non-international sea-journeys* (Federale Overheidsdienst Mobiliteit en Vervoer, 2007). The Royal Decree enforces a set of general regulations to allow an inland vessel at sea. Such regulations were designed based on a feasibility study executed by Ghent University and Lloyd's Register (Vantorre, et al., 2006). A more detailed description is given in paragraph 2.3.

Up to this day, inland vessels which want to navigate at sea must be certified based on this regulatory document. An example of a vessel certified according to RD2007 is the container vessel Deseo (Figure 2-2). All vessels certified according to the regulation will be called *estuary vessels* in the following text.

⁶ Rights belong to Teun De Wilt (Tanzanite), Christian Westerink (Waterways I) and Patrick Hermans (Deseo).



Figure 2-2 : Estuary container vessel Deseo⁶.

2.2 Port of Zeebrugge

Europe's biggest ports are all located in Western Europe. The biggest European ports are found in the stretch between Le Havre and Hamburg: Le Havre, Antwerp, Rotterdam, Amsterdam, Bremerhaven and Hamburg (Figure 2-3). The port of Zeebrugge needs to compete with these harbours, when it comes to attracting cargo and passenger lines. A major aspect in the competitiveness of a port is the availability of a developed hinterland connection, to improve the speed and cost effectiveness at which goods reach their end destination. Since the Belgian road network is congested and rail transport always faces limitations due to influence of the passenger train schedule, there is a need of sufficient inland vessel transport capacity in the modal split. For the ports of Antwerp and Ghent (Ghent is part of 'North Sea Port'), 38% (Port of Antwerp, 2017) and 50% (Port of Ghent, 2016) of the cargo is transported by inland vessels. For Zeebrugge, this share is negligible, at 0.3% (Port of Zeebrugge, 2016) of the total cargo.



Figure 2-3 : Location of largest European ports in the Hamburg – Le Havre range.⁷

This can be explained by looking at the inland waterways surrounding the port of Zeebrugge, shown in Figure 2-4. CEMT-VI vessels are able to reach Brugge using the Boudewijnkanaal. However, only CEMT IV vessels are able to pass Brugge and continue their journey towards Ghent, from where a connection with Antwerp is possible through the Ghent-Terneuzen canal and the River Scheldt. Therefore, large travel times (Truijens, Vantorre, & Vanderwerff, 2006) and/or limited cargo capacity explain the small share of inland transport in the port's modal split. An upgrade of the present inland waterways has been explored (new canal, enlarging existing waterway), but never executed because of political, environmental and social reasons. A project for an upgrade of the nautical infrastructure near Brugge is currently going on⁸, focusing on the main bottlenecks represented by bridges and locks (Steenbrugge bridge and Dampoort lock).

⁷ © OpenStreetMap-authors

⁸ <http://stadsvaart.be/waar/> (in Dutch)

The port of Zeebrugge thus really depends on estuary traffic to increase the amount of cargo transported by inland vessels. Nowadays, the estuary traffic forms 5.8% (Port of Zeebrugge, 2016) of the harbour's modal split. A simplification of the requirements in RD2007 to allow inland vessels at sea could attract more parties to invest in sea-going inland vessels. Naturally, a review of the current regulations must be preceded by a thorough study of the impact on safety of any planned simplification to the rules.



Figure 2-4 : Inland waterways connecting Zeebrugge to the hinterland.⁹

2.3 Royal Decree 2007

The Belgian legislation introduced in 2007 focuses on the role of the flag state in the safety of the vessel: ensuring the safety of the crew and protecting the marine environment. As the vessels need to be certified by a classification society, these class rules ensure the safety of the ship itself and the cargo it carries (Truijens, Vantorre, & Vanderwerff, 2006). An estuary vessel is conceived as an inland vessel with increased strength, and as such it needs to comply with the rules for inland vessels described in the European standard ES-TRIN (CESNI, 2017).

The strength of the vessel falls under the responsibilities of the classification society, and is not explicitly regulated in RD2007. The legislation RD2007 stipulates all the other requirements that the inland vessel needs to comply with in order to navigate at sea between Belgian coastal ports. Inland vessels are conceived to perform journeys on rivers and canals, which means that little to no wave action is present and that the crew is always at a relatively short distance to shore. As the flag state is responsible for the wellbeing of the crew, there are strict demands regarding, among other matters, fire safety (A60 doors), rescue equipment (FRC) and navigational equipment (sea radar). Since the inland vessel is performing a sea journey, it needs to comply with MARPOL (prevention of pollution of ships), without certificate, and COLREG (preventing collisions at sea).

A substantial part of the decree deals with the stability and behaviour in waves of the vessel. These two aspects will be briefly described in the following.

2.3.1 Stability requirements

The stability requirements imposed by the decree closely mirror the criteria prescribed by the IMO International Code on Intact Stability (IMO, 2008). The requirements for the righting lever curve and the weather criterion are the same ones valid also for ocean going ships, despite the fact that the estuary route is short and very close to the coast, where calmer met-ocean conditions can be expected. Moreover, inland vessels are only allowed to start a sea voyage when the wave height does not exceed a certain value.

Due to the very low flooding angles of inland vessels, it is almost impossible for such vessels to comply with the IMO requirements on stability. A modification of the stability requirements for inland vessels at sea, which takes into account both the typical structure of such vessels and the much more controlled environmental conditions, is proposed in section 5.

⁹ Taken from <https://www.binnenvaart.be/waterwegen-en-havens/waterwegenkaarten>

2.3.2 *Behaviour in waves*

Assuming that the stability (see above) and the strength of the vessel (responsibility of the class) are sufficient, shipping of water and slamming are the prime concerns for the safety of an inland vessel. Slamming causes high peak loads at the bow and vibrations of the vessel, load cases which are not considered when building an inland vessel. Shipping of water (green water) can lead to heavy loading of the deck, but also to flooding of cargo holds and deckhouse.

The behaviour of the vessel in waves is evaluated according to a risk analysis, which is described in an attachment of the decree. Tankers and closed hatch vessels which want to sail in favourable conditions (up to 1.2 m H_s), are exempted from the risk analysis, and they can be authorized to sail at sea provided that they comply with deterministic requirements on the freeboard, aimed at limiting the risk of shipping of water. The deterministic requirements are a copy of the demands mentioned in the service rule of 1962 (see 2.1). These rules prescribe a minimum freeboard as a function of the vessel length: $F_{min} = 0.5m + (L_{pp} - 50) * 0.005m$. Moreover, a minimum hatch height of 0.9m is prescribed for closed hatch vessels.

2.4 Worldwide estuary traffic

The access to maritime ports by adapted inland vessels has already been the subject of PIANC report 118 (PIANC, 2013). Apart from the Belgian situation described in this paper, there are several other cases where this topic is of great interest. In Europe the following cases are well known:

- France (1): Connection between *Port 2000* and the river Seine, using a northern (2 nm) and southern (20 nm) trajectory.
- France (2): Connection between Port of Marseille terminals (Golfe de Fos) and the river Rhone.
- France (3): Connection between Port of Sète and river Rhône (using various canals), two paths: 1.24 nm and 4.44 nm, depending on size of the vessel. A breakwater has been constructed to shelter the trajectory from the incoming waves.
- Italy: Coastal journey between (A) Venice and Porto Levante (33 nm) and (B) Ravenna and Porto Levante (55 nm). Additional connection between Porto Levante and Porto Mantova Valdarò (Mantova-Adriatic sea canal, 70 nm). The weather conditions are denoted as 'good' all year around (Adriatic Sea).

Outside of Europe, an application is the connection between the Beilun district and the Yongjiang river. (6 nm) in China. For an elaborate overview of the applications and specific regulations worldwide, the reader can refer to (PIANC, 2013).

3 WAVE CLIMATE

The Belgian Royal Decree states that the response of the ship must be calculated based on directional wave spectra measured during one year. This requirement imposes the use of wave data measured by buoys and precludes the use of hindcast data. However, hindcast wave data have some advantages over the measured ones, as explained below, and were used in this study. A change in RD2007 to allow the use of hindcast data is one of the proposed reviews to the regulation.

Buoy data are based on physical measurements, which do not require a validation process apart from the removal of erroneous measurements (spikes). However, despite the dense network of measuring buoys in the coastal zone between Zeebrugge and the Western Scheldt estuary, the measured data are only representative of the wave climate in the immediate surroundings of the buoy. This issue becomes more relevant as the areas of interest shift more towards coastal areas, where the influence of bathymetry on wave propagation induces a higher spatial variability of wave climate. When assuming the measured data to be representative of a large coastal area, some inaccuracies are unavoidably introduced. At least a broad estimation of the magnitude of such inaccuracies should always be performed and considered in the interpretation of the results of further calculations.

On the other hand, wave hindcast simulations can be designed to produce results at high spatial resolutions, allowing to describe in higher detail the wave climate in the area of interest. In this case, the shortcoming is the validation process which must be performed to ensure the accuracy of the simulated results. On top of that, taking into account the geographical variability of the wave climate complicates the risk analysis calculations.

3.1 Bol van Heist buoy measurements

In previous studies performed by the UGent Maritime Technology Division to assess the seaworthiness of estuary vessels, the readings of the Bol van Heist measuring buoy (BVH, +051.400 N +003.217 E) were used as a reference, according to the requirements of RD2007. The wave climate measured by the buoy was considered to be representative for the estuary trajectory between Zeebrugge and the mouth of the Western Scheldt. The assumed trajectory is 16 nm long with a direction almost parallel to the coastline ($70^\circ/250^\circ$, relative to the North direction, positive clockwise).

As the measuring buoy BVH is located more offshore than the trajectory of interest, the measured wave climate is more severe than the one which could be encountered by vessels along the trajectory (Figure 3-1). This approach, in line with the requirements formulated in the Royal Decree, yields conservative results.

3.2 SWAN hindcast simulations

An analysis based on hindcast simulations performed in (Verelst, 2006) clearly shows that the wave heights in the area of interest decrease when approaching the coast as well as when moving towards the mouth of the river. As an example, in Figure 3-2 the significant wave height simulated at a specific time frame is plotted for 14 points along the trajectory (line connected). The wave height measured by BVH is plotted as a separate point (star). The 14 points considered are the points along the trajectory shown in Figure 3-1.

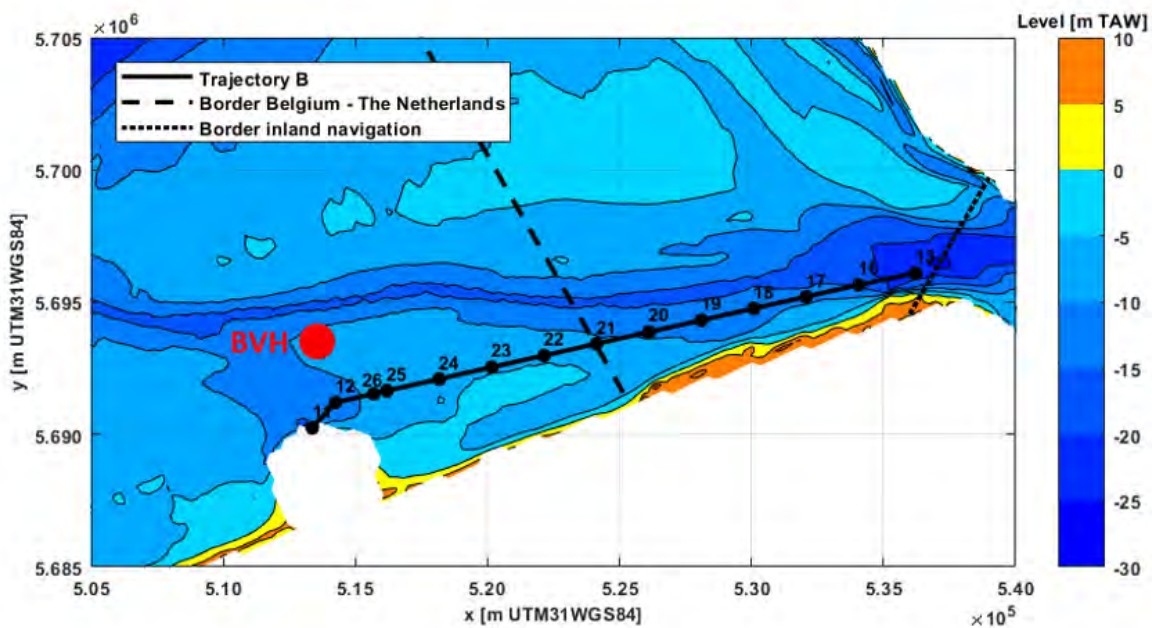


Figure 3-1: Bol Van Heist buoy and sea trajectory.

In this case, calculations of the ship responses based on simulated wave spectra along the trajectory are expected to deliver less conservative and more realistic results with respect to the ones obtained using the buoy data as a reference. This also means that a safety factor, which was introduced by the use of BVH wave data, is no longer present in the calculations.

For all the calculations shown in this paper, hindcast wave data were used as an input. The simulated data were produced by Flanders Hydraulics Research (FHR) with the spectral wave model SWAN, and validated using the BVH buoy measurements from the year 2013 (Suzuki, Hassan, Kolokythas, Verwaest, & Mostaert, 2016). The data provided cover an entire year, for all the two hourly timeframes where a valid measurement by BVH is available. Wave data are provided for each of the 14 points shown in Figure 3-1. In Figure 3-3 the cumulative distribution of H_s along the different points of the trajectory is outlined.

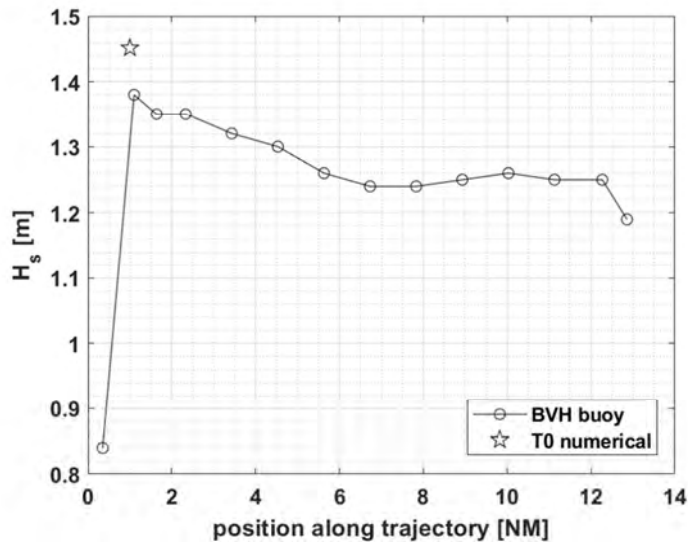


Figure 3-2: Wave climate variations along the trajectory.

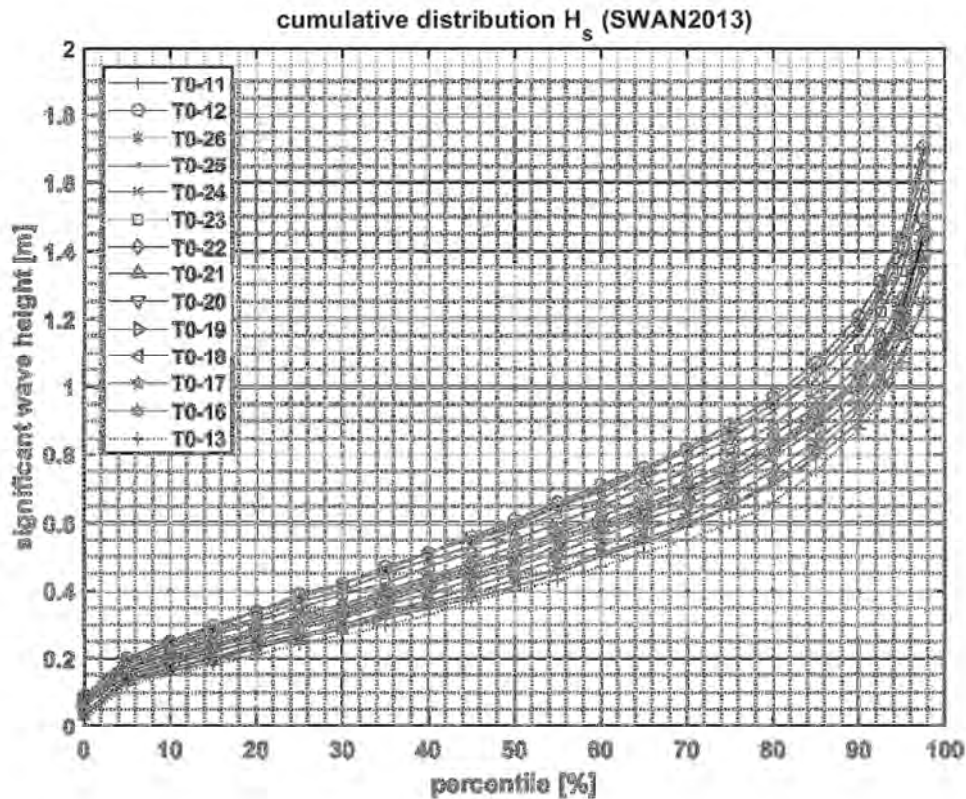


Figure 3-3: Cumulative distribution significant wave heights, based on SWAN output (validated using BVH 2013 measurements).

4 DESIGN VESSELS

To assess the feasibility of an extension to inland vessels with open hatches of the deterministic rules in RD2007, a comprehensive campaign of calculations was performed. The navigating fleet was studied and a limited number of recurring vessel designs was outlined. Four “*design vessels*” were selected to represent the entire fleet of open hatch inland vessels with lengths of 110 m and above, which are of prime interest due to their large loading capacity and their inability to reach the inland waterway network in another way.

4.1 Belgian and European inland fleet

The design vessels were selected based on an extensive research on two different databases: the W&Z (Waterwegen en Zeekanaal NV, now merged to De Vlaamse Waterweg NV) database, representing the Belgian inland vessel fleet, as well as an online database of European inland vessels¹⁰. The analysis of the databases was complemented by the pre-existing knowledge of the UGent Maritime Technology Division in performing studies for estuary vessels on the sea-trajectory. The database of W&Z contains extensive information on the main ship dimensions (length, width, draft and available freeboard) for 40 vessels. In the European online database, 518 vessels with the required characteristics can be found, including the vessels present in the W&Z database. A disadvantage of this database is that the depth of the vessels is not available. The number of vessels in the database is plotted in Figure 4-1 against the overall length and breadth of the vessels. Four main clusters of vessels sharing the same main dimensions are clearly visible.

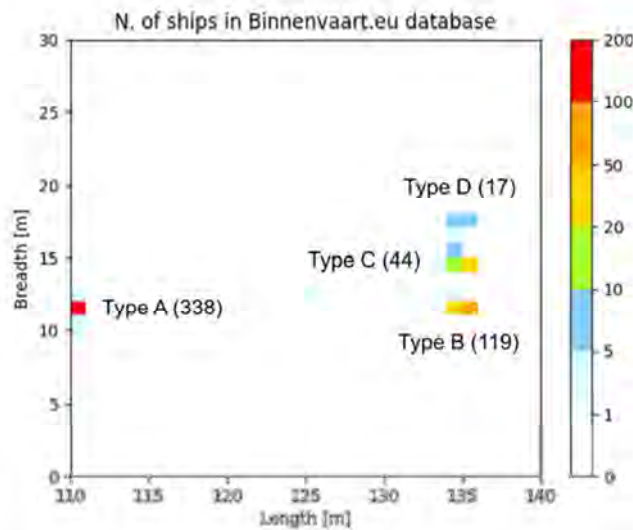


Figure 4-1: Number of vessels in the binnenvaart.eu database.

4.2 Main dimensions

The vessels found in the databases can be subdivided based on their main dimensions, as shown in Figure 4-1. The overall length of the vessels is well defined, with hardly any deviation from standard reference values. The breadth is mostly based on the number of container rows which the dry cargo vessel can accommodate. Slight differences are present, which can be explained by the fact that some vessels are primarily built for transporting bulk cargo instead of containers, allowing the breadth to differ from a multiple of the container width. The dimensions selected for the design vessels are summarized in Table 4-1. It is relevant to point out that the design draft is the one for inland service. The table shows also Rijkswaterstaat 'RW' classes (Rijkswaterstaat, 2011). The types A to D considered in this study coincide with the RW classes M8, M9, M11 and M12. M10 is a motor vessel with a length of 110 m and a breadth of 13.20 m, which is a typical value for tankers. No dry cargo vessel with such dimensions was found in the database.

| Type | RW class | L _{OA} | B _{OA} | T _{design} | D |
|----------|------------|-----------------|-----------------|---------------------|------|
| | | [m] | [m] | [m] | [m] |
| A | M8 | 110.00 | 11.45 | 3.55 | 3.65 |
| B | M9 | 135.00 | 11.45 | 3.60 | 4.25 |
| C | M11 | 135.00 | 14.20 | 4.00 | 4.80 |
| D | M12 | 135.00 | 17.10 | 4.00 | 5.50 |

Table 4-1: Design dry cargo vessels.

¹⁰ <https://www.binnenvaart.eu>

4.3 Loading conditions

The behaviour of a ship in waves is strongly influenced by the vessel's loading conditions. Both the mass distribution and the coordinates of the centre of gravity play a significant role in defining the ship responses. When calculating the performance of a ship in waves it is thus very important to make a good estimation of the loading conditions in order to get accurate results.

The focus of this study was not on a specific ship, but rather on a wide class of similar ships, represented by the four design vessels. Therefore, a precise estimation of the loading conditions was not possible. However, some simplifying assumptions were introduced in order to outline a range for the possible loading conditions.

A reduced draft was taken as the reference draft for each vessel, assuming that the vessels would not be able to sail the estuary route when loaded up to their inland design draft:

$$T_{red} = 0.8 \cdot T_{design}$$

This draft reduction was estimated based on preliminary calculations described in (Vantorre & Van Zwijnsvoorde, 2016). The mass distribution of the cargo was modelled in a simplified manner by assuming standard values for the roll, pitch and yaw radii of gyration:

$$k_{xx} = 0.37 \cdot B_{OA}$$

$$k_{yy} = k_{zz} = 0.25 \cdot L_{OA}$$

Concerning the vertical position of the centre of gravity, \overline{KG} , a range of possible values for this parameter was calculated for each type of ship. Since the inland vessels under investigation are used as both container vessels and bulk carriers, the lowest and highest position of the centre of gravity were calculated for both bulk and container loading conditions. This calculation was based on simplified assumptions about the cargo distribution.

For container loading conditions the cargo arrangements for the four design vessels was deduced from the database information, as shown in Figure 4-2. The lowest possible \overline{KG} was calculated considering 20 ft High Cube containers loaded at the maximum of their mass capacity, namely 30 t, placed as low as possible in the number needed to reach the defined reduced draft. On the other hand, the highest \overline{KG} was calculated considering the vessels loaded with the maximum number of containers, each assumed to have the same uniform weight. The uniform weight was calculated as the one needed to reach the defined draft.

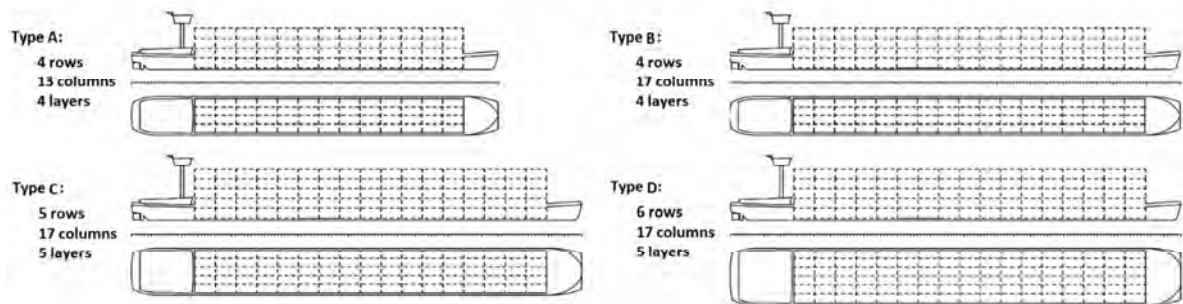


Figure 4-2: Container arrangement of the four design vessels.

Similar considerations were applied for bulk cargo. Since the higher \overline{KG} value obtained for bulk cargo conditions was very close to the lower \overline{KG} value for container cargo, the distinction between bulk and container cargo was dismissed. At the end, three loading conditions were considered for each design vessel, corresponding to three vertical positions of the centre of gravity:

- *LC1* corresponds to the highest \overline{KG} obtained for container cargo (see Figure 4-3).
- *LC3* corresponds to the lowest \overline{KG} obtained for bulk cargo (see Figure 4-3).
- *LC2* was chosen between the other two conditions based on the natural roll period, as described below.

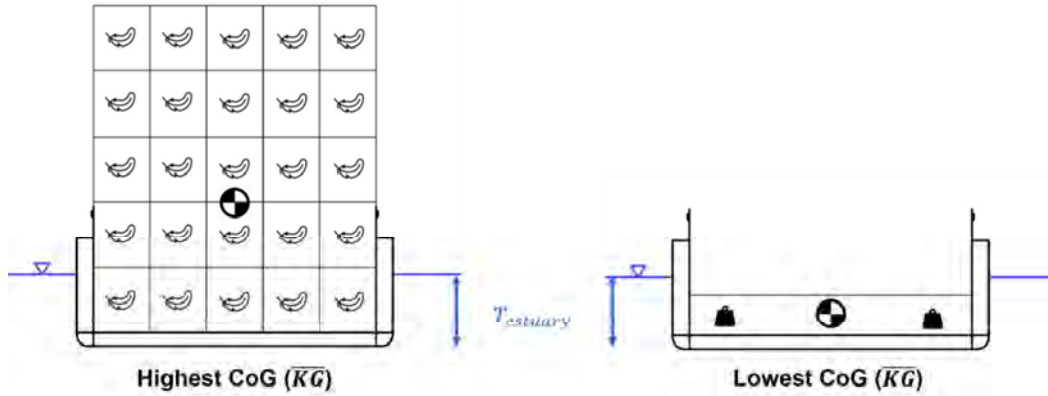


Figure 4-3: Highest and lowest \overline{KG} configurations.

The roll natural periods, T_φ , corresponding to the two extreme loading conditions were calculated and the loading condition *LC2* was chosen as the one leading to a roll natural period which is halfway between the two extreme values. The three loading conditions adopted for each type of ship are summarized in Table 4-2.

| Type | LC1 | | | LC2 | | | LC3 | | |
|------|-----------------|-----------------|-------------|-----------------|-----------------|-------------|-----------------|-----------------|-------------|
| | \overline{KG} | \overline{GM} | T_φ | \overline{KG} | \overline{GM} | T_φ | \overline{KG} | \overline{GM} | T_φ |
| | [m] | [m] | [s] | [m] | [m] | [s] | [m] | [m] | [s] |
| A | 4.52 | 0.94 | 10.33 | 3.79 | 1.67 | 7.69 | 1.31 | 4.15 | 5.03 |
| B | 4.66 | 0.73 | 11.77 | 4.00 | 1.39 | 8.44 | 1.38 | 4.01 | 5.09 |
| C | 6.34 | 0.62 | 16.22 | 5.61 | 1.35 | 10.82 | 1.47 | 5.49 | 5.45 |
| D | 6.78 | 2.68 | 9.38 | 5.31 | 4.15 | 7.53 | 1.77 | 7.69 | 5.70 |

Table 4-2: Loading conditions of the four design vessels, expressed as \overline{KG} and corresponding \overline{GM} and T_φ .

4.4 Speed

A constant cruise speed along the trajectory of 10 knots was considered in this study for all design vessels.

4.5 Reference points and levels

Concerning shipping of water, RD2007 prescribes that the relative vertical motion at different control points along the vessel should not exceed a threshold value more than once in a lifetime (20 years, 300 round trips per year). The threshold value not to be exceeded by the relative motion is defined in the RD2007 as a distance between a reference level and the calm water free surface.

RD2007 prescribes the following control points and reference levels (see Figure 4-4):

- Foremost point of the bow (*F5C*). The reference level is the top of watertight bulwark. The relative motion to be considered needs to be increased due to the dynamic effect of the bow wave, according to the formula:

$$\delta z = 0.2 \cdot z + 0.6 \cdot V^2 / (2 \cdot g)$$

where δz is the increase in the relative motion, z is the calculated relative motion, V is the speed of the vessel in m/s and g is the gravitational acceleration.

- Aftmost points of the fore deck, at both sides (*F4S*, *F4P*). The reference level is the top of watertight bulwarks.
- Aftmost, foremost and central points of the cargo deck, at both sides (*F2S*, *F2P*, *F3S*, *F3P*, *F4S*, *F4P*). The reference levels are:
 - 0.9 m above the main deck (1.35 m above for tankers).
 - the top of the coamings for closed hatch dry cargo ships and tankers.

- $0.8 \times$ the distance between the top of the coamings and the still water free surface below the previous value for open hatch dry cargo ships.
- Aftmost and foremost points of the aft deck, at both sides ($F1S$, $F1P$, $F2S$, $F2P$). The reference level is the top of watertight bulwarks.

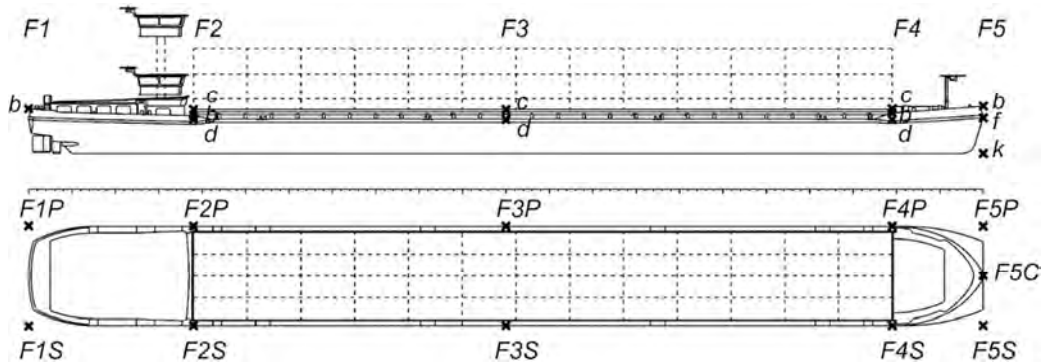


Figure 4-4: Position of selected points for vessel type A.

As for slamming, RD2007 requires to check the vertical relative motion at the intersection between the vertical line passing through the foremost point of the ship and the keel line. A slamming event is considered to happen when this relative motion exceeds the forward draft and the keel emerges from the water. A maximum of one slamming event per year is prescribed by RD2007. Point $F5C$ needs therefore to be checked, considering the forward draft of the vessel as the reference level.

Several inland vessels in the database, especially the larger ones, show considerably flared bow sections, with flare angles lower than 20° . These shapes allow to achieve a wider fore deck, but on the other hand could cause dangerous impact phenomena when the ship is sailing in waves. The Royal Decree does not require to assess a risk of bow flare impacts since the probabilistic study was originally developed for vessels explicitly designed for the estuary service, which do not have flared bows. In the present study, which focuses on an analysis of existing inland vessels, the risk of bow flare impact was also assessed. Bow flare impacts are assumed to happen when the vertical relative motion exceeds the distance between the lowest point of the flared bow and the free surface. In accordance with the requirements of RD2007 for slamming, one exceedance per year was considered as the maximum allowed value. The lateral points of the flared bow at both sides, $F5S$ and $F5P$, were selected as control points, with a reference level given by the height of the lowest point in the foremost section where the flare angle is smaller than 20° .

5 MODIFIED STABILITY REQUIREMENTS

5.1 Flooding angle

RD2007 does not explicitly request a minimum flooding angle, but the requirements for the righting lever curve set an implicit lower limit of 30° . Inland vessels, however, because of their own peculiar geometry, show very low flooding angles, often far below 30° . In the proposed modification of the stability requirements the minimum flooding angle is lowered to 17° , as prescribed in the French Decree for the navigation of inland vessels between the container terminal Port 2000 and the historic harbour of Le Havre (Legifrance, 2014).

5.2 Righting lever curve

RD2007, reflecting (IMO, 2008) paragraph 2.2, prescribes that the area under the righting lever curve should be:

- not less than $0.055 \text{ m}\cdot\text{rad}$ up to an angle of 30° .
- not less than $0.090 \text{ m}\cdot\text{rad}$ up to 40° or the flooding angle, whichever the lowest.
- not less than $0.030 \text{ m}\cdot\text{rad}$ between 30° and the lowest among 40° and the flooding angle.

The last two requirements are impossible to be met for inland vessels with a flooding angle lower than 30°. To account for low flooding angle vessels, an exception is proposed in the proposed renewal for the decree:

- If the flooding angle is less than 30°, the area under the righting lever curve up to the flooding angle should not be less than 0.055 m·rad. This replaces the other three requirements.

Therefore, ships are allowed to have flooding angles as low as 17° provided that they possess a dynamic stability up to the flooding angle which is at least equal to the one required by (IMO, 2008) up to an angle of 30°.

5.3 Weather criterion

RD2007 prescribes a weather criterion equal to the one described in (IMO, 2008). According to (IMO, 2008), the wind pressure which needs to be taken into account for the weather criterion is 504 Pa (which corresponds with Beaufort 10 wind conditions), while the initial heel angle due to the wave action needs to be calculated with simplified formulas as a function of the ship's dimensions and natural roll period.

A different way to calculate both the wind pressure and the initial roll angle is proposed, accounting for the calmer met-ocean conditions expected on the estuary route with respect to the open ocean. Concerning the wind pressure to take into account, its proposed value is given as a function of the maximum H_s for which the certificate is requested, according to Table 5-1. The values in the table are derived from the indications of Bureau Veritas (Bureau Veritas, 2014). Such indications were found to be close to the correlation between H_s measured in Zeebrugge and the associated maximum wind speed measured at Bol van Heist.

| | | | | | | | | | | | | | | | | |
|-------|------|-----|-----|-----|-----|-----|-----|-----|-----|-----|-----|-----|-----|-----|-----|-----|
| H_s | [m] | 0.6 | 0.7 | 0.8 | 0.9 | 1.0 | 1.1 | 1.2 | 1.3 | 1.4 | 1.5 | 1.6 | 1.7 | 1.8 | 1.9 | 2.0 |
| P | [Pa] | 214 | 231 | 247 | 262 | 277 | 290 | 303 | 315 | 327 | 339 | 350 | 361 | 371 | 381 | 391 |

Table 5-1: Proposed wind pressures for the weather criterion.

As for the initial heel angle θ_1 , it is prescribed to be equal to the roll angle expected to occur once in a lifetime according to the risk analysis. For those ships exempted from the risk analysis (up to $H_s=1.2$ m), deterministic values based on the probability analysis performed for the four design vessels are proposed (Table 5-2).

| | | | | | | | | |
|------------|-----|-----|-----|-----|-----|-----|------|------|
| H_s | [m] | 0.6 | 0.7 | 0.8 | 0.9 | 1.0 | 1.1 | 1.2 |
| θ_1 | [°] | 7.0 | 7.7 | 8.3 | 9.0 | 9.7 | 10.3 | 11.0 |

Table 5-2: Proposed initial heel angles for the weather criterion in the new decree.

6 RISK ANALYSIS FOR DESIGN VESSELS

In order to assess the feasibility of new deterministic freeboard requirements for open hatch vessels, the performances of the four design vessels described in section 4 with respect to the probabilistic requirements of RD2007 were analysed. For each of the vessels, a full risk analysis was performed for all three loading conditions outlined in paragraph 4.3. The possibility for the vessels to sail up to H_s of 1.2 m was investigated according to the requirements of RD2007. The calculations showed that this is possible for all the four vessels, with reasonable drafts between 80% and 100% of the inland design draft.

6.1 Methodology

A vertical relative motion RAO (response amplitude operator) was obtained with the code *Seaway* (Journée & Adegeest, 2003) for each ship, loading condition and selected point. *Seaway*, originally developed by J.M.J. Journée¹¹ and currently part of ABB's software *Octopus*, is a frequency-domain

¹¹ The Knowledge Centre Manoeuvring in Shallow and Confined Water (Flanders Hydraulics Research – Ghent University) wishes to pay tribute to prof. ir. Johan Journée who passed away on December 15th, 2017, at the age of 76. We remember a very nice co-operation in validating the *Seaway* code for (very) shallow water conditions by model test results performed at FHR in Antwerp.

seakeeping code based on linear strip theory. As for the wave data, the simulated directional spectra described in paragraph 3.2 were used.

By combining the wave data with the calculated RAOs, the number of times that a threshold value is exceeded during one round trip along the trajectory can be calculated for each of the available wave spectra, as described in (Vantorre, Eloit, & Delefortrie, 2010). The number of exceedances per round trip will be referred to as NER in the following. The calculated NER values can be grouped in wave height classes, but to do so, a single source of time dependent wave data should be chosen as representative of the wave conditions along the whole trajectory. In this study, the simulated wave data along the trajectory were used to calculate space and time dependent NER values, as pointed out in paragraph 3.2, while the H_s measurements from BVH were used as a common reference to split the NER values into wave height classes.

By averaging the grouped exceedance numbers, a *cumulative average number of exceedances* per round trip, NER_{AVG}^{cum} , can be calculated for each H_s class. The H_s leading to a number of exceedances per round trip equal to the maximum one prescribed by RD2007 (see paragraph 6.2) can be subsequently derived. A comprehensive explanation of the procedure can be found in (Vantorre, Eloit, & Delefortrie, 2010).

The following calculations were repeated for each design vessel, loading condition and control point. An array of threshold relative vertical motions (z_{rel}^{thr}) was introduced, with values ranging from 0.6 m to 1.8 m. For each of these values, the H_s leading to a number of exceedances of the threshold value equal to the maximum prescribed by RD2007, $NER_{AVG}^{cum}(z_{rel}^{thr}) = NER_{MAX}$, was calculated. These values of $H_s = f(z_{rel}^{thr})$ were interpolated through a second degree polynomial fit, and the threshold relative motions corresponding to discrete values of H_s (between 0.6 and 1.2 m with a step of 0.1 m) were calculated. Therefore, relations of the type $z_{rel}^{thr} = f(H_s)$ were derived. Finally, an available margin for the relative motion was calculated as a function of H_s by subtracting z_{rel}^{thr} from the distance between the free surface and the reference level associated with the considered control point (see paragraph 4.5).

6.2 Number of journeys per year

The Royal Decree does not explicitly impose a NER_{MAX} value. It defines a minimum return time for exceeding a threshold value of a ship response. For example, these return periods are the lifetime of the ship (20 years) for the vertical relative motions related to the risk of water overtake, and 1 year for the relative motions related to slamming phenomena.

In order to calculate a NER_{MAX} , a number of round trip journeys along the estuary trajectory in one year must be assumed. RD2007 assumes that an estuary vessel performs 300 journeys per year. This means that the ship sails the trajectory almost on a daily basis. This number is proposed to be lowered to a minimum of 100 journeys per year, like in the French legislation (Legifrance, 2014), which seems a much more realistic value when assuming that the vessels will sail in inland waters for a good share of their operational cycle. If a vessel wants to perform more estuary trips, this should be mentioned in the certificate, which could be handed over only after performing a full risk analysis.

Based on the reduction of the number of trips per year described above, the following maximum numbers of exceedances per round trip were assumed in this study:

- $NER_{MAX} = 0.0005$ for the risk assessment of water intake.
- $NER_{MAX} = 0.01$ for the risk assessment of slamming and bow flare impact.

6.3 Results

The results of probabilistic calculations indicate that the four design vessels can obtain a certificate to sail the estuary trajectory in H_s up to 1.2 m according to RD2007. Compliance with requirements for shipping of water can be achieved, for all plausible vertical positions of centre of gravity, with a reasonable reduction of the design draft for inland service, in line with the one assumed in paragraph 4.3.

Based on the results of the probabilistic calculations a maximum allowable draft was calculated as a function of H_s for each of the vessel types and loading conditions. To do so, available margins for the relative motions were calculated for each of the control points along the vessel, as described in paragraph 6.1. The lowest amongst the available margins was added to the reduced draft used in the

probabilistic calculations to yield the maximum allowable draft. The results of this approach are summarized in Figure 6-1a.

For ship types B, C and D the draft assumed in the calculations, equal to 0.8 times the inland design draft, is always sufficient to ensure compliance with RD2007 requirements, while for ship type A it is found to be acceptable only up to $H_s = 1.1$. Higher values of H_s can be reached if a limitation to the metacentric height (loading condition) is imposed. Concerning ship type D, the relative motion margins are sufficiently high to allow the compliance with RD2007 even with the design draft for inland service (4.0 m), up to $H_s = 1.2$ m for the lowest \overline{GM} loading condition and up to 1.0 m for the other two loading conditions.

When flared bow sections are considered, the study outlines some criticalities: apart from type D, all the considered design vessels are expected to face severe limitations on the draft or the allowed H_s in order to prevent excessive occurrences of bow flare impacts. This is clearly outlined by the minimum drafts (Figure 6-1 - right), which for ship types A, B and C are significantly lower than the ones obtained for conventional bow shapes (Figure 6-1 - left).

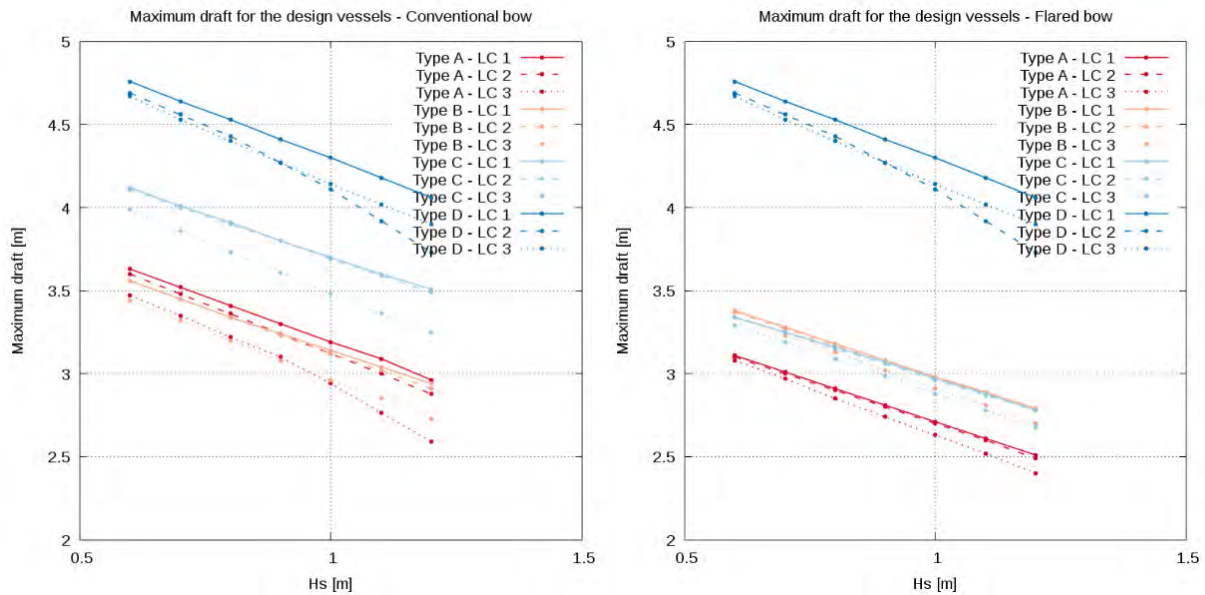


Figure 6-1: Maximum allowable draft for the design vessels.

7 NEW DETERMINISTIC REQUIREMENTS

The information collected through the probabilistic analysis of design vessels was used as a base to develop new deterministic freeboard criteria which could extend the deterministic rules for tankers and closed hatch vessels in RD2007. The new criteria are designed to exempt from the risk analysis all inland vessels with a length between 110 m and 135 m which request to sail the estuary trajectory between the port of Zeebrugge and the Western Scheldt up to a significant wave height of 1.2 m (measured at Bol van Heist).

In order to generalize the results of the probabilistic calculations described in section 6, the threshold vertical relative motions of control points for each of the considered ships and loading conditions were thoroughly analysed. A simplified relation between the threshold relative motion and H_s was derived for each of the control points, as described in paragraph 7.1.

The simplified formulas for the calculation of threshold relative motions were combined with the reference levels prescribed by RD2007. Minimum values for the height of specific points along the topsides of a vessel were finally determined as a function of H_s . The minimum values for the freeboard of inland vessels prescribed by a resolution from (UNECE, 2011) were also considered.

7.1 Threshold values for the vertical relative motions

The threshold vertical relative motions calculated for the design vessels at four of the control points are reported in Figure 7-1. The results related to water intake at foremost point (point *F5C*, $NER_{MAX} = 0.0005$) were increased for the dynamic effect due to the presence of the bow wave.

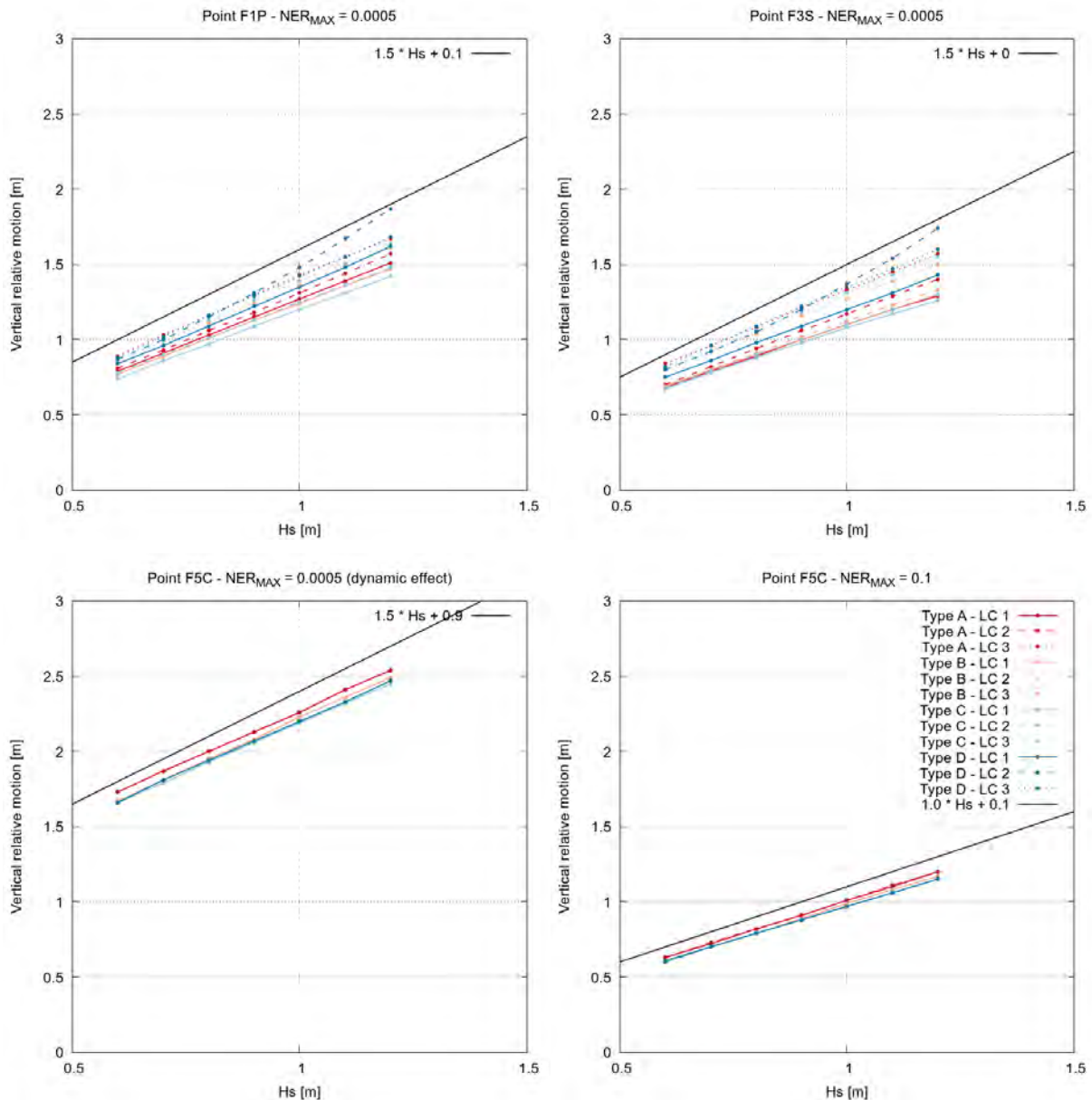


Figure 7-1: Threshold vertical relative motions at four control points.

Each of the plots in Figure 7-1 describes one control point, illustrating the results obtained for the 12 combinations of ship type and loading condition (see paragraphs 4.2 and 4.3). The complete series of plots which include all the control points is not shown here for space reasons. In any case, the plots not included in this paper show the same trends outlined by the plots in Figure 7-1.

In order to simplify the development of simplified equations for the threshold relative motions, the envelope of the highest relative motion curves was considered for each point. Therefore, simple relations were derived for an estimation of the threshold vertical relative motion (z_{rel}^{thr}) as a function of H_s only. These functions are summarized in Table 7-1 and, graphically, as a black curve on each of the plots in Figure 7-1.

The probabilistic requirements of the Royal Decree also prescribe to assess the risk of water reaching the level of two specific additional points: the lowest non watertight opening in the hull and the lowest point of the aft deck, if such point is lower than the main deck. The position of these points along the vessel can be very different from ship to ship, leading to different relative motions.

In order to keep the formulation simple, a generic equation was derived for the two additional points, independently from their specific position. Following a conservative approach, the equation leading to the highest motions among the ones derived for the other control points (excluding the one influenced by the dynamic factor) was chosen.

| Point | NER_{MAX} | z_{rel}^{thr} |
|-------------------|-------------|-----------------------|
| | [-] | [m] |
| <i>F1 (S/P)</i> | 0.0005 | $1.5 \cdot H_S + 0.1$ |
| <i>F2 (S/P)</i> | 0.0005 | $1.5 \cdot H_S$ |
| <i>F3 (S/P)</i> | 0.0005 | $1.5 \cdot H_S$ |
| <i>F4 (S/P)</i> | 0.0005 | $1.5 \cdot H_S + 0.1$ |
| <i>F5 (C+dyn)</i> | 0.0005 | $1.5 \cdot H_S + 0.9$ |
| <i>F5 (C)</i> | 0.01 | $1.0 \cdot H_S + 0.1$ |
| <i>F5 (S/P)</i> | 0.01 | $1.2 \cdot H_S$ |
| <i>Opening</i> | 0.0005 | $1.5 \cdot H_S + 0.1$ |
| <i>Aft deck</i> | 0.0005 | $1.5 \cdot H_S + 0.1$ |

Table 7-1: Simplified functions for the calculation of the threshold vertical relative motion at control points.

7.2 Minimum distances above free surface

By combining the simplified equations for the calculation of threshold vertical relative motions (Table 7-1) with the prescriptions of RD2007 about the control points and reference levels (see paragraph 4.5), minimum vertical distances between the considered reference level and the still water free surface were derived for each of the different control points.

According to the different reference levels to be considered, different equations were derived for ships with a watertight closed deck (*tankers*), dry cargo ships with closed hatches and dry cargo ships with open hatches.

The final equations for the minimum vertical distance above the free surface, $VDAFS$, for each of the control points and reference levels are summarized in Table 7-2. Most of the reference levels in the table were already described in paragraph 4.5. The exceptions are the keel level at the longitudinal foremost point of the ship (k) and the vertical position of a specific opening (o).

As a matter of fact, the deterministic rules can be considered as a simplified version of the risk analysis, where the threshold vertical relative motions are approximated by simplified equations (see Table 7-1) instead of being calculated by means of a full probabilistic sea-keeping study. Since the simplified equations were designed to be conservative with respect to the actual calculations, the satisfaction of the deterministic requirements guarantees that the vessel is able to comply with the risk analysis prescribed by RD2007.

| Response | Point | Level | NER_{MAX} | $VDAFS_{min}$ | | |
|----------------------------------|---------------------|-------|-------------|---------------------------|-----------------------|------------------------|
| | | | | <i>open hatches</i> | <i>closed hatches</i> | <i>tankers</i> |
| | | | [-] | [m] | [m] | [m] |
| Aft deck water intake | <i>F1 (S/P)</i> | b | 0.0005 | $1.5 \cdot H_S + 0.1$ | $1.5 \cdot H_S + 0.1$ | $1.5 \cdot H_S + 0.1$ |
| | <i>F2 (S/P)</i> | b | 0.0005 | $1.5 \cdot H_S$ | $1.5 \cdot H_S$ | $1.5 \cdot H_S$ |
| Loading compartment water intake | <i>F2 (S/P)</i> | d | 0.0005 | $1.5 \cdot H_S - 0.9$ | $1.5 \cdot H_S - 0.9$ | $1.5 \cdot H_S - 1.35$ |
| | <i>F2 (S/P)</i> | c | 0.0005 | $1.875 \cdot H_S$ | $1.5 \cdot H_S$ | - |
| | <i>F3 (S/P)</i> | d | 0.0005 | $1.5 \cdot H_S - 0.9$ | $1.5 \cdot H_S - 0.9$ | $1.5 \cdot H_S - 0.9$ |
| | <i>F3 (S/P)</i> | c | 0.0005 | $1.875 \cdot H_S$ | $1.5 \cdot H_S$ | - |
| | <i>F4 (S/P)</i> | d | 0.0005 | $1.5 \cdot H_S - 0.8$ | $1.5 \cdot H_S - 0.8$ | $1.5 \cdot H_S - 1.25$ |
| | <i>F4 (S/P)</i> | c | 0.0005 | $1.875 \cdot H_S + 0.125$ | $1.5 \cdot H_S + 0.1$ | - |
| Fore deck water intake | <i>F4 (S/P)</i> | b | 0.0005 | $1.5 \cdot H_S + 0.1$ | $1.5 \cdot H_S + 0.1$ | $1.5 \cdot H_S + 0.1$ |
| | <i>F5 (C+dyn)</i> | b | 0.0005 | $1.5 \cdot H_S + 0.9$ | $1.5 \cdot H_S + 0.9$ | $1.5 \cdot H_S + 0.9$ |
| Bow impact | <i>F5 (S/P)</i> | f | 0.01 | $1.2 \cdot H_S$ | $1.2 \cdot H_S$ | $1.2 \cdot H_S$ |
| Slamming | <i>F5 (C)</i> | k | 0.01 | $1.0 \cdot H_S + 0.1$ | $1.0 \cdot H_S + 0.1$ | $1.0 \cdot H_S + 0.1$ |
| Opening | <i>Open point</i> | o | 0.0005 | $1.5 \cdot H_S + 0.1$ | $1.5 \cdot H_S + 0.1$ | $1.5 \cdot H_S + 0.1$ |
| Aft deck | <i>Lowest point</i> | d | 0.0005 | $1.5 \cdot H_S + 0.1$ | $1.5 \cdot H_S + 0.1$ | $1.5 \cdot H_S - 1.25$ |

Table 7-2: Deterministic $VDAFS$ requirements.

7.3 Range of application and minimum freeboard values

In agreement with the existing exemptions of the current Royal Decree, the new deterministic rules are designed to be applied up to $H_S = 1.2$ m. Moreover, a lower limit of $H_S = 0.6$ m is introduced: if the requested sailable H_S is below this threshold, the requirements for $H_S = 0.6$ m must be applied.

When an H_S of 0.6 m is considered, null or even negative values for the vertical distance between the main deck and the free surface are obtained from the equations in Table 7-2. This means that a null freeboard would be sufficient for the vessel to comply with the risk analysis. Such peculiar result follows from the definition in RD2007 of the reference level not to be reached by water more than once in a lifetime, which is set between 0.90 m and 1.35 m above the deck level. Nevertheless, a null freeboard should obviously never be allowed. Therefore, additional requirements for the minimum freeboard are introduced in the deterministic rules.

For this purpose, the minimum freeboards recommended by the harmonized Europe-wide technical requirements for inland vessels published in (UNECE, 2011), are used as a reference. In these recommendations the minimum freeboard is expressed as a function of the ship type and length. Moreover, different minimum freeboards are recommended for three inland navigation zones, each characterized by a maximum wave height ($H_{1/10}$). Assuming a Rayleigh distribution for the wave heights, the $H_{1/10}$ wave height can be converted to the significant wave height through the relation:

$$H_S = 0.787 \cdot H_{1/10}$$

Focusing on ships with a length between 110 m and 135 m sailing in wave conditions below $H_S = 0.6$ m, the lowest allowed wave height, the minimum freeboards prescribed by (UNECE, 2011) are:

- In Zone 3 ($H_{1/10} < 0.6$ m; $H_S < 0.47$ m): 0.15 m.
- In Zone 2 ($H_{1/10} < 1.2$ m; $H_S < 0.94$ m): 0.60 m for open hatches vessels, 0.34 for vessels with closed watertight hatches and 0.22 m for tankers.

These values were linearly interpolated to obtain freeboard requirements for $H_S = 0.6$ m:

- For tankers: 0.17 m
- For closed hatch dry cargo vessels: 0.20 m
- For open hatches dry cargo vessels: 0.27 m

In the final proposed deterministic rules, the equations in Table 7-2 are considered, together with an explicitly enforced minimum value for the distance between a reference level and the free surface. For all the reference levels except the deck level, the minimum allowed distance is the result of the

equations for $H_s = 0.6$ m. When the deck level is considered, on the other hand, the three values described above are introduced as the minimum freeboard instead of the null or negative values resulting from the corresponding equation.

8 CONCLUSION

The connection between the Flemish coastal ports and the main European inland waterway network is limited for large inland vessels. In order to increase the amount of cargo transported through waterways, some inland vessels were allowed on the estuary trajectory between Belgian ports and the mouth of the River Scheldt by the Belgian Shipping Inspectorate since the '60s. Certificates to sail at sea, in controlled met-ocean conditions, were given to inland vessels based on individual assessments.

A more structured approach was introduced with the Belgian Royal Decree of 2007, which enforces general rules to allow inland vessels on the estuary trajectory. Together with other requirements, the IMO stability regulations must be respected and a full probabilistic study must be performed to assess the risk of water overtake. An exemption from the last point is granted to tankers and closed hatch vessels which want to sail up to significant wave heights of 1.2 m.

For container and bulk cargo vessels the strict requirements of RD2007 mean in practice that only vessels which are specifically designed for the estuary service can be allowed on the trajectory. As of today, only a very restricted number of such vessels are allowed at sea. The aim of this paper was to study the behaviour at sea of standard inland vessels with respect to the requirements of RD2007, and check the feasibility of new deterministic rules to exempt also open hatch vessels from the risk analysis.

An update to the stability requirements of RD2007, deemed as too strict for the coastal nature of the sea trajectory, was proposed. From the stability point of view, this would allow inland vessels with low values of the flooding angle to sail the trajectory provided that they show a sufficient dynamic stability up to the flooding angle.

Moreover, four design vessels were outlined based on the information contained in two databases. Plausible loading conditions were derived as well. The compliance with the probabilistic requirements about the risk of water overtake contained in RD2007 was positively ascertained for all the design vessels and loading conditions, requiring only reasonable reductions of the design draft for inland service. New deterministic exemptions were designed based on the results of the probabilistic calculations on the design vessels. These new rules could allow existing inland vessels on the trajectory, in controlled met-ocean conditions, without the need of a risk analysis.

The approach described in this paper could help to increase the waterborne transport share in the modal split of the Flemish ports, and to tackle lacks in the inland waterways network with temporal and economic scales orders of magnitude lower than the ones associated with a renewal of the waterways infrastructure. While the study is specifically focused on the Belgian coastal situations, the general concepts described in the paper can be applied to any other area of interest where an extension of the operational range of inland vessels could benefit the total efficiency of waterborne transport.

9 REFERENCES

- Bureau Veritas. (2014). *Rules for the Classification of Inland Navigation Vessels*.
- CESNI. (2017). *European Standard laying down Technical Requirements for Inland Navigation vessels*.
- Federale Overheidsdienst Mobiliteit en Vervoer. (2007). *Koninklijk besluit betreffende binnenschepen die ook voor niet-internationale zeereizen worden gebruikt (RD2007)*.
- IMO. (2008). *Adoption of the International Code on Intact Stability (2008 IS Code). Resolution MSC.267(85)*.
- Journée, J., & Adegeest, L. (2003). *Theoretical manual of strip theory program "Seaway for Windows". Report 1370*. TU Delft & Amarcon.
- Legifrance. (2014). *Arrêté du 15 décembre relatif à la navigation de bateaux porte-conteneurs fluviaux en mer pour la desserte de Port 2000 et des quais en Seine à Honfleur*.
- PIANC. (2013). *Report n. 118: Direct Access to Maritime Ports by Adapted Inland Waterway Vessels*.
- Port of Antwerp. (2017). *2017 Facts and Figures*. Antwerp.
- Port of Ghent. (2016). *Feiten en cijfers 2016*. Ghent.
- Port of Zeebrugge. (2016). *Jaarverslag 2016*. Zeebrugge.
- Rijkswaterstaat. (2011). *Richtlijnen Vaarwegen 2011*.
- Suzuki, T., Hassan, W., Kolokythas, G. K., Verwaest, T., & Mostaert, F. (2016). *Wave climate for inland vessels between Zeebrugge and the mouth of the Western Scheldt: estimation by the Belgian coast model in SWAN. Version 4.0. FHR reports, 15_026*. Antwerp: Flanders Hydraulic Research.
- Truijens, P., Vantorre, M., & Vanderwerff, T. (2006). On the design of ships for estuary service. *Trans. R. Inst. Nav. Archit. Int. J. Marit. Eng.*, 148(A2).
- UNECE. (2011). *Reccomendations on Harmonized Europe-wide Technical Requirements for Inland Navigation Vessels - Resolution No.61 (ECE/TRANS/SC.3/172/Rev.1)*. United Nations Publication.
- Vantorre, M., & Van Zwijnsvoorde, T. (2016). *Zeewaartse binnenvaartverbinding voor Zeebrugge : Berekening van de scheepsresponsies voor scenario T0, E1 en F1 : Vaarroute doorheen de opening in de oostelijke dam en aanleg golfwerende constructies*. Universiteit Gent.
- Vantorre, M., Eloot, K., & Delefortrie, G. (2010). *Estuary Traffic: an alternative hinterland connection for coastal ports. Port infrastructure seminar*. Delft.
- Vantorre, M., Vandevoorde, B., De Schrijver, M., Smits, H., Laforce, E., Mesuere, M., et al. (2006). Risk analysis for inland vessels in estuary service. Estoril Congress Centre, Portugal: 31st PIANC congress.
- Verelst, K. (2006). *Bepaling van een directionele correlatie voor golfhoogte en golfrichting t.b.v. estuaire vaart*. Antwerp: Ministerie van de Vlaamse Gemeenschap – Afdeling Waterbouwkundig Laboratorium en Hydrologisch Onderzoek.

EARLY WARNING SYSTEM TO SUPPORT CONSTRUCTION & MANAGEMENT OF PORT INFRASTRUCTURES: THE CASE OF TX-1 AÇU PORT CONSTRUCTION

by

Antonio Tomás¹, Manuel Simancas², Gabriel Díaz-Hernández¹, Javier L. Lara¹, Inigo J. Losada¹ and Francisco Esteban²

¹ Environmental Hydraulics Institute (IHCantabria), Universidad de Cantabria, Spain. antonio.tomas@unican.es

² FCC Citizen Services, Spain.

ABSTRACT

This study presents an integrated early-warning system to support construction and manage the harbor infrastructures exposed at different construction stages. The system is designed as a flexible tool, with a user-friendly interface, to be relocatable in any location. It is oriented to obtain the short and mid-term (within 180-hour prediction) characteristics of met-ocean conditions (waves, water level and wind) at the harbor surroundings in the site, as well as, wave-structure interaction characteristics for any construction phase. The system goes beyond the classical met-ocean alert system, because integrates the use and coupling of different numerical models, downscaling techniques, met-ocean databases and validation and/or calibration procedures with in-situ measurements. It is fully coupled with construction protocols related with any specific activities at any location along the harbor. One of the main objectives is to help the construction managers to improve and establish human safety threshold, related with the different tasks along the harbor, exposed to the met-ocean variables, and interacting with the unfinished harbor structures. On the other hand, the system also allow to optimize exploitation and construction costs and to achieve the individual deadlines of every task or activity.

1. INTRODUCTION

Harbors construction and management in highly exposed locations (i.e. severe met-ocean conditions) is a challenging issue. Met-ocean conditions highly affect the normal development of construction activities, seriously jeopardizing every task at the surroundings of the water-land threshold. Construction managers demand, not only the information about wave and wind conditions during construction, but also their influence and interference with daily construction activities, first, to reduce accidents, and second, to improve the management of the construction agenda along different stages. It is necessary to optimize construction costs and to achieve the individual deadlines of every task or activity. Note that some construction operations are very expensive, because use resources very specialized, and they could be used only during specific met-ocean time-windows.

Once the construction of the port has been completed, it is necessary to manage the exploitation and planning of port activities through a reliable met-ocean forecasts, in order to optimize the available resources.

Aware of this problem, in the last few years IHCantabria has been working on the development of a new methodology to solve these problems and to generate a new set of tools to aid the constructors and managers of ports infrastructures. The new methodology has been applied to several ports around the world, improving and optimizing the tools.

The first IHCantabria implementations of early warning system to support port constructions were in Sancti-Petri in Spain and Langosteira harbor in Spain (Díaz-Hernández et al., 2010 and Díaz-Hernández et al., 2017). Then, new developments of these tools were implemented in the TX-1 Açú port construction in Brazil (the example explained in this study) and the ongoing Aberdeen port construction (United Kingdom). These systems were developed thanks to the support and confidence

of companies such as DRAGADOS and FCC Citizen Services, and the methodological principles came from Spanish R&D&i projects (SAYOM and CLIOMAR).

On the other hand, a lot of examples of IHCantabria early warning systems to support the management of ports are now operating in Spain. Eleven systems (Gijón, Málaga, Almería, Carboneras, Santa Cruz de La Palma, Santa Cruz de La Gomera, Santa Cruz de Tenerife, Las Palmas, Arrecife, Puerto del Rosario and Barcelona) are installed in the framework of SAMOA Project (Rodríguez et al., 2017). And new developments are implemented in the Port of Algeciras in the framework of SAFEPOR Project (De los Santos et al., 2016). All these systems are installed in “Puertos del Estado” (Spanish Ministry of Civil Works) and accessible via <http://www.puertos.es> and <https://cma.puertos.es>. Other IHCantabria operational systems for port management are in operation at the ports of Langosteira and Santander; and Huelva, Tenerife and Algeciras in the framework of ATHENEA Project (Castanedo et al., 2012).

The new early warning system methodology contains different modules, and it is design as a flexible tool that can be adapted according to the harbor location, the construction procedures and the met-ocean complexity. The system is oriented to obtain the short and mid-term (within 180-hour prediction) characteristics of met-ocean conditions (waves, water level and wind) at the harbor surroundings in the site, as well as, wave-structure interaction characteristics for any construction phase. The system goes beyond the classical met-ocean alert system, because it use the best “solution” for each “problem”. Each module integrate and couple the best numerical models, downscaling techniques, met-ocean databases, and/or calibration procedures with in-situ measurements. The modules are fully coupled with construction protocols related with any specific activities at any location along the harbor.

One of the main objectives is to help the construction managers to improve and establish human safety threshold, related with the different tasks along the harbor, exposed to the met-ocean variables, and interacting with the unfinished harbor structures. On the other hand, the tools allow to optimize exploitation and construction costs and to achieve the individual deadlines of every task or activity.

2. METHODOLOGY

The new early warning system methodology contains different modules, and is design as a flexible tool that can be adapted according to the harbor location, the construction procedures and the met-ocean complexity.

First, deep water a met-ocean module (as the main core of the system) should be defined, covering two main tasks: a) the wind, wave and sea-level hindcast analysis, based on high-accurate and validated global datasets; and b) the 7-days hourly prediction for wind, wave and sea-level forecasting system, such as NOMADS system (provided by NOAA).

Second, the downscaling module designed to propagate the met-ocean variables from deep to coastal zone and to any location near, in front and/or inside the harbor.

Third, the met-ocean-structure interaction module that contains high-resolution analysis for one or more of the following processes: harbor agitation and resonance due infragravity waves (mild slope and Boussinesq modelling); wave run-up and overtopping (laboratory data, analytical formulations and CFD modelling); scour and silting (analytical approximations and CDF modelling); moored ship response (CFD, Boussinesq and potential theory approximation); dredging (measurements and dredge protocols); and wake waves (Boussinesq modelling), considering any construction stage for any bathymetric characteristics and any unfinished harbor structure geometries.

It is important to note that the information provided by this third module is relevant because is combined with the construction activities, recommendations and protocols along the breakwaters, basins, and berthing zones, as well as, the crucial importance in the use of CFD numerical modelling to cover the

lack of semi-empirical formulations in literature for unfinished breakwater cross-sections. In particular wave overtopping information (i.e.: mean discharge, maximum volume) is considered as a crucial product to be crossed with secure thresholds related with the different construction works to determine its viability and safety.

Finally, the system can include a fourth module dedicated for the assimilation of real-time measurements provided by met-ocean data (nowcast), as a quick quality control module for each variable predicted.

The robustness of the early warning system makes it suitable for the construction stages, as well as for the optimization of the operation of these infrastructures once the works are finished.

3. APPLICATION & RESULTS

3.1 Introduction

To illustrate the application of the new early warning system, and to better understand the methodology, the tools and the results, one example is presented: the early warning system for the construction of Açú TX-1 terminal in Brazil.

In 2013, the company FCC Citizen Services within the Joint Venture FCC Tarrío TX-1 Construção LTDA started the construction of the TX-1 terminal of Açú Superport in São João da Barra, 315 kilometers north of Rio de Janeiro (Brazil). The works include the construction of a breakwater, composed by a 600 m long rubble-mound breakwater 600 m long (Core-loc 10T) and a 2.100 m long vertical breakwater (47 reinforced concrete caissons), with a crest at +10 m elevation.

To support the construction of Açú Port, a high-resolution operational system in the port was developed, ad-hoc for the FCC constructive resources and techniques.

This operational system allows planning the operations in advance (more than a week forecast) and realistic (assimilating in-situ instrumental information), from the numerical prediction of wind, sea level, waves, long-waves, agitation and overtopping, taking into account the geometric evolution of the works in each construction stage. The system produces daily safe working conditions

- (1) to transport the caissons from Ríó de Janeiro to the port of Açú,
- (2) to construct the caissons,
- (3) to anchor the caissons and
- (4) to construct the crest.

All the modules are integrated in a friendly web-based interface, available 24/7 service for the managers. The web gives a quick understanding about the daily activities at the different areas of the port. Information is daily updated and sent also by e-mail to the managers.

3.2 Methodology

In figure 1, it is presented the general methodology and the modules used in the early warning system application for the construction of the Port of Açú and the general methodology:

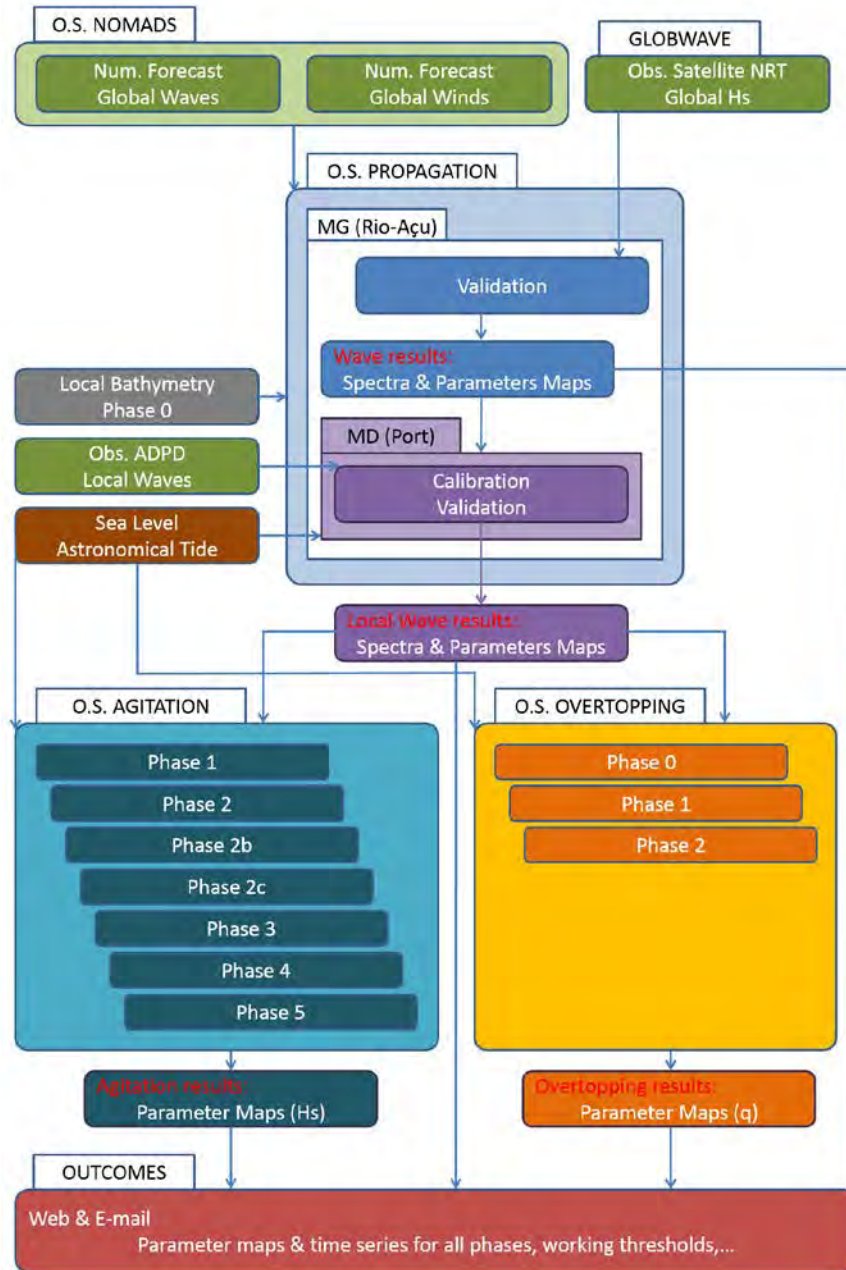


Figure 1: Overall methodology of the early warning system for the construction of Açu TX-1 terminal in Brazil

The operational system of propagation (O.S. PROPAGATION), based on the global wave and wind conditions of the NOMADS operational system, performs dynamic downscaling or propagation to determine the local wave conditions in the surroundings of the port. The system solves the processes of coastal propagation (refraction, diffraction, shoaling, bottom friction, wind generation and wave breaking) with the SWAN (Booij et al., 1999) numerical model based on the energy balance equation. As a result, all wave results have hourly temporal resolution with a prediction horizon of 7.5 days and are updated several times a day.

The SWAN model is carried out by means of several nested meshes that increase the spatial resolution as it gets closer to the port of Açú. The General Mesh (MG Rio-Açú) covers the entire study area from Rio de Janeiro to the port of Açú with a spatial resolution between 1 and 5 km. The results of this General Mesh are validated with the data measured by the Jason-2 satellite in real time (Near Real Time), see figure 2. MG results are wave spectra and parameters, providing the wave and wind conditions on the navigation route from Rio de Janeiro to the Port of Açú and also the forcings for its different nested meshes.

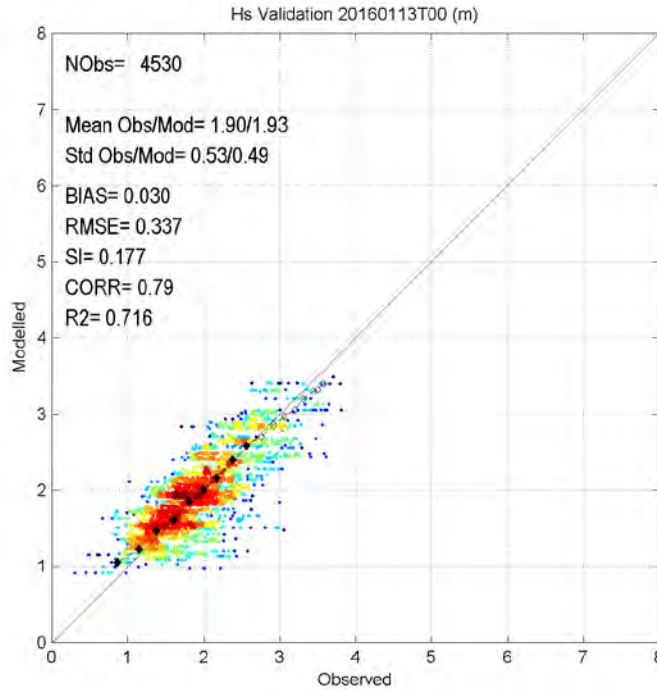


Figure 2: Example of validation of the OS PROPAGATION, General Mesh, with the significant wave height data observed by Jason-2 satellite up to January 13, 2016.

The Detail Mesh (MD Port) reaches a spatial resolution of about 50 meters and uses the detailed bathymetry of the study area and the local sea level to propagate the waves to the port. As a result, the incident waves in the port are obtained, without taking into account their interaction with the breakwaters, which is why it is called construction Phase 0 (without port). These results are validated, every month, with measurements taken in-situ by an ADCP located outside the area of influence of the breakwaters under construction. The biases or systematic errors obtained from these comparisons are assimilated by the system, so the results finally obtained by the system in the following predictions are corrected or calibrated, improving their quality (see figure 3). Finally, the results in the Detail Mesh provide incident wave conditions (wave spectra and parameters) at the port of Açú (Phase 0, without breakwaters) and also the forcings for the operational systems of agitation and overtopping over the vertical breakwater.

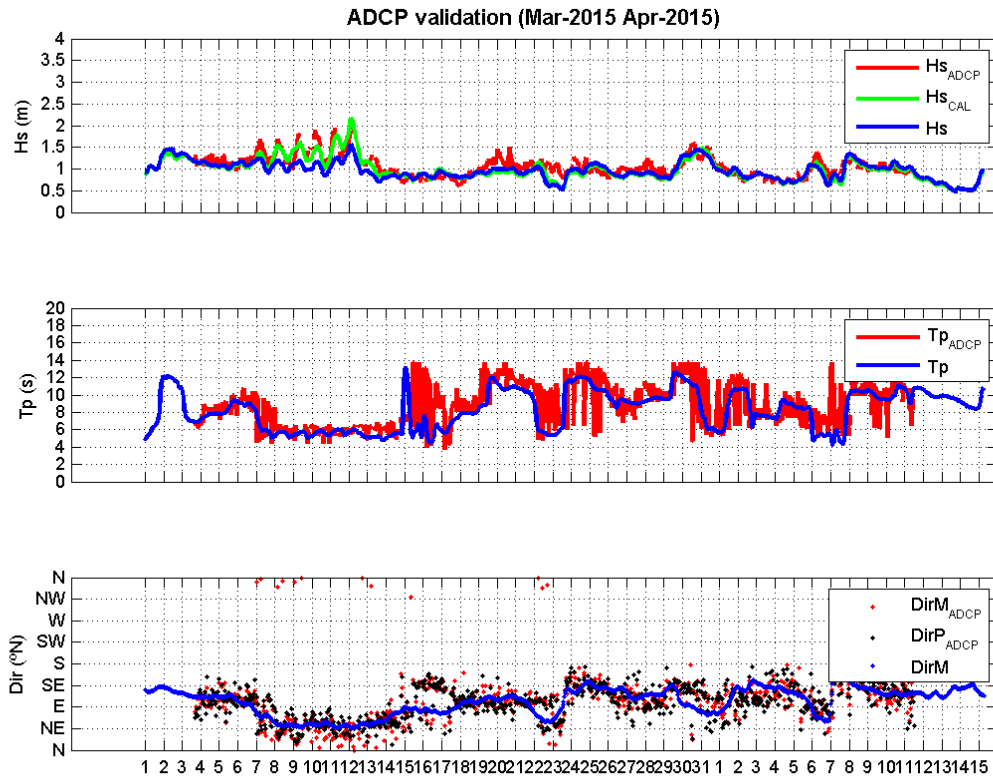


Figure 3: Example of time series validation of the significant wave height (Hs), peak period (Tp), and mean wave direction (DirM) of the original Operational System (blue), the Calibrated Operational System (green) and ADCP measurements in the Port of Açú (red), from March 3, 2015 to April 11, 2015.

The operational system of agitation or internal disturbance (O.S. AGITATION) takes into account the interaction of waves with the contours, breakwaters or quays in the port of Açú (both vertical and rubble mount breakwaters). The MSP model (based on the elliptic Mild SloPe equations) is used to solve the agitation (the linear processes of refraction, diffraction, shoaling, total or partial reflection, bottom friction and wave breaking). For this reason, the computational grids of this model are specifically defined for each construction phases of the port. Each construction phase (1, 2, 2b, 2c, 3, 4 & 5) take into account the time-variation in its layout, either by advancing the rubble mounds layers or by the anchoring of the caissons for the vertical breakwater (see example of 4 different phases in figure 4). Note that wave results change drastically for each phase construction.

The MSP model uses, as a forcing, for each construction phase, the sea level and wave spectra of Phase 0 (SWAN model Detail Mesh) and generates the significant wave height maps with a spatial resolution in the order of 10 m; taking into account the geometric and reflection characteristics of the different elements of the port phase construction. The results are updated several times a day and have 7.5 day prediction horizons with hourly time resolution.

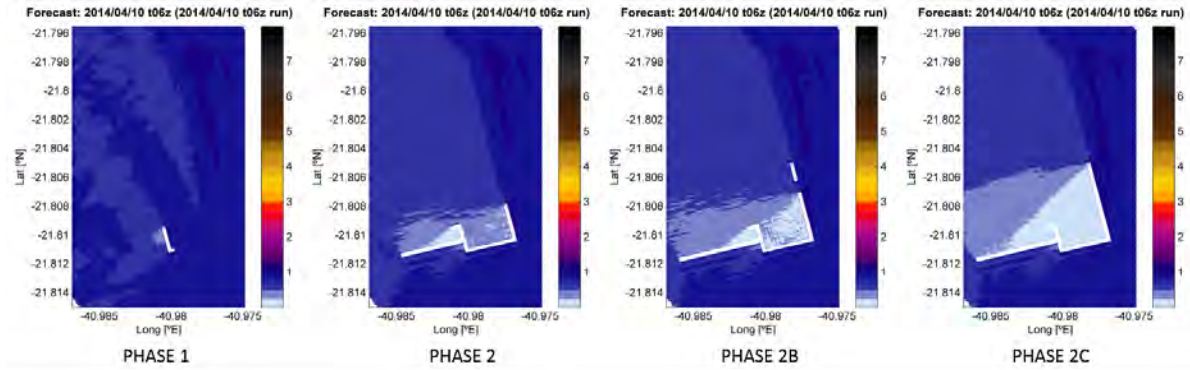


Figure 4: Example of significant wave height (H_s) prediction inside the Port of Açú for four different agitation phases (1, 2, 2B and 2C). White areas indicate the progress of works.

The operational system of overtopping (O.S. OVERTOPPING) also uses the sea level and wave spectra predictions from Phase 0 (SWAN Model Detail Mesh) as forcing. Based on these predictions, it calculates the hourly mean overtopping rate (q) over the 7.5 day forecast horizon, for each of the three construction phases of the crest (see figure 5), taking into account the different caisson typologies used in the Port of Açú.

The overtopping calculation is carried out using formulae previously adjusted for each type of section and construction phase of the crest, using the sea level and wave values specific to each caisson of the port of Açú. These formulae have been determined from a catalogue of numerical simulations carried out ad-hoc, with the numerical model IH2VOF, for the specific characteristics of the vertical breakwater of the port of Açú; covering its complete range of geometries, waves and sea levels. The model called IH2VOF (Losada et al. 2008, Lara et al. 2008) is an advanced numerical tool that solves the two-dimensional RANS (Reynolds Average Navier-Stokes) equations and includes small-scale physical processes such it solves the flow in porous media, the realistic wave breaking and the consequent phenomenon of run-up, the overtopping on the structure, forces on monolithic parts of the structure (ie caissons); taking into account non-linear and turbulent effects resulting from the temporal interaction between individual waves and the structural elements of the port.

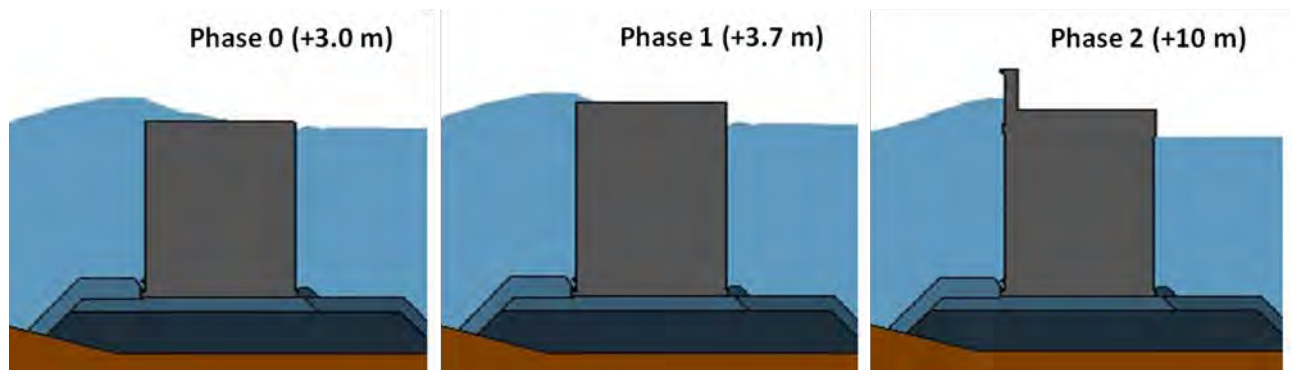


Figure 5: Example of overtopping results simulated by IH2VOF for three different crest construction phases (0, 1 and 2) in the caisson vertical breakwater.

Finally, all the results obtained (OUTCOMES) are displayed in a web page, which represents in a friendly way, the maps and time series of the last forecast of the operational system. Results for the following 7.5 days, of the different parameters of wind, waves, sea level, agitation and overtopping on the vertical breakwater, for each of the constructive phases of the port, are shown. Also, the different results are interpreted and crossed with different work thresholds defined by FCC for the transport and anchoring of caissons and the construction of the crest. Excel® sheets with the most relevant results of each operational system update are also automatically sent by e-mail to the managers of the works, for the construction phase that is currently in progress.

3.3 Results

In figure 6 is shown the initial view of the web page where all results are displayed. There are 12 panels to access the different modules results:

RIO-AÇU: O.S PROPAGATION, General Mesh (Operational System to the transport of caissons from Río de Janeiro to the port of Açú).

PHASE 0: O.S PROPAGATION, Detailed Mesh (Operational System to anchor the caissons)

PHASE 1: O.S AGITATION (Operational System to construct and anchor the caissons).

PHASE 2: O.S AGITATION (Operational System to construct and anchor the caissons).

PHASE 2B: O.S AGITATION (Operational System to construct and anchor the caissons).

PHASE 2C: O.S AGITATION (Operational System to construct and anchor the caissons).

PHASE 3: O.S AGITATION (Operational System to construct and anchor the caissons).

PHASE 4: O.S AGITATION (Operational System to construct and anchor the caissons).

PHASE 5: O.S AGITATION (Operational System to construct and anchor the caissons).

PHASE 0 OVERTOPPING (Operational System to construct the crest of the caissons).

PHASE 1 OVERTOPPING (Operational System to construct the crest of the caissons).

PHASE 2 OVERTOPPING (Operational System to construct the crest of the caissons).

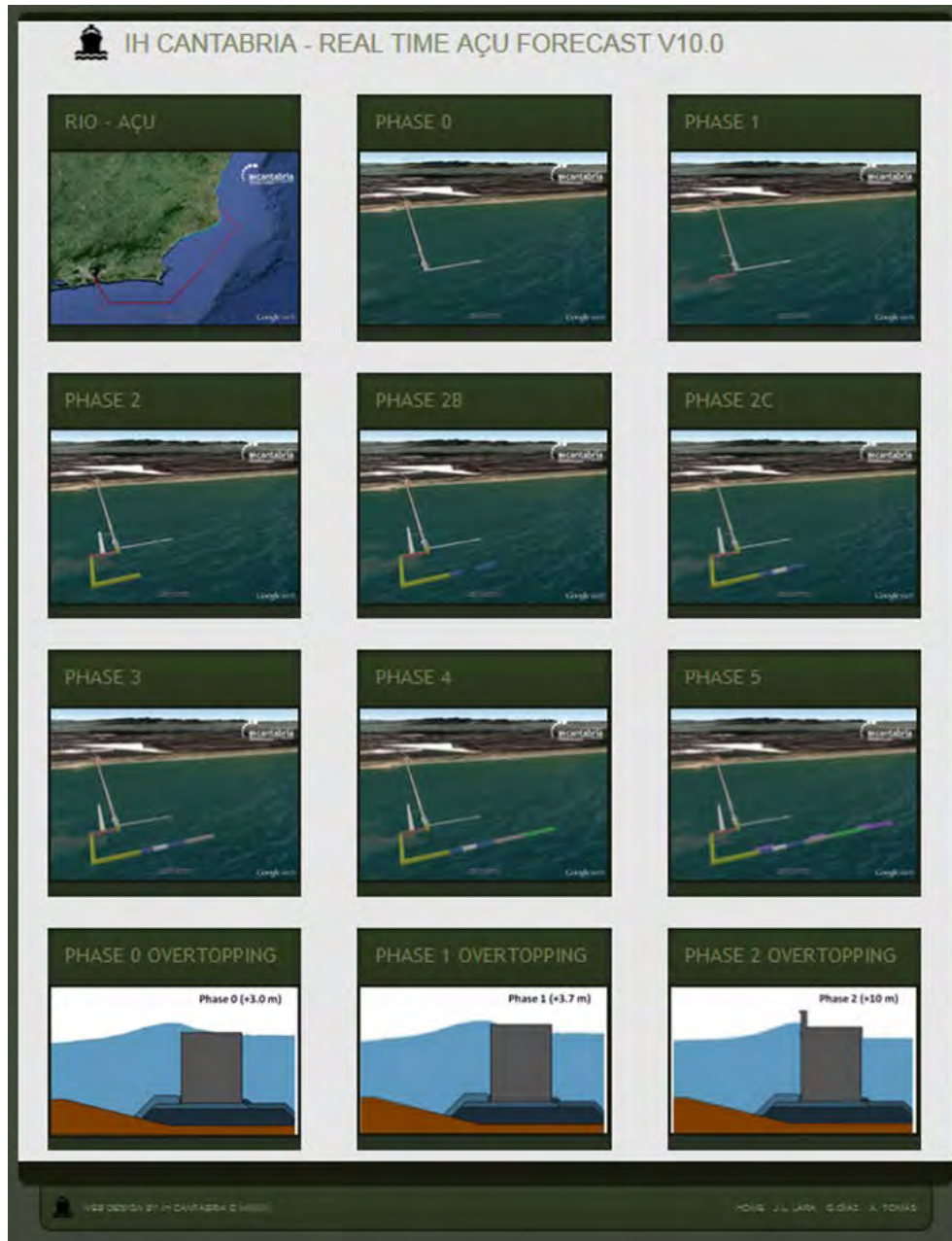


Figure 6: Initial view of the web page of the early warning system for the construction of Açú TX-1 terminal in Brazil

Figure 7 shows an example of the results that can be obtained from the system (RIO-AÇU) for a safety development of the marine transportation of the caissons from Rio de Janeiro to Port of Açú. In the upper part (1), several options are available: i) downloading an excel with the numerical information of the last prediction; ii) downloading png images with the hourly spatial fields of the significant wave height, peak period and wind; iii) downloading the validation of operational system with satellite data. Next in (2) there is an animation with the 180 hours of wave and wind predictions. Hs is represented in a color scale, with black arrows representing wave direction and grey arrows representing wind direction. The navigation route from Ríó Janeiro to Açú port is represented in grey. Next in (3), access to the Hs and W predictions and navigation thresholds (green, red) in the prediction horizon (X axis)

along the location of the navigation route (Y axis) are included. Finally, at the bottom (4), for the selected prediction instant, locations where the navigation threshold is exceeded are represented in red, and represented in green when navigation is permitted.

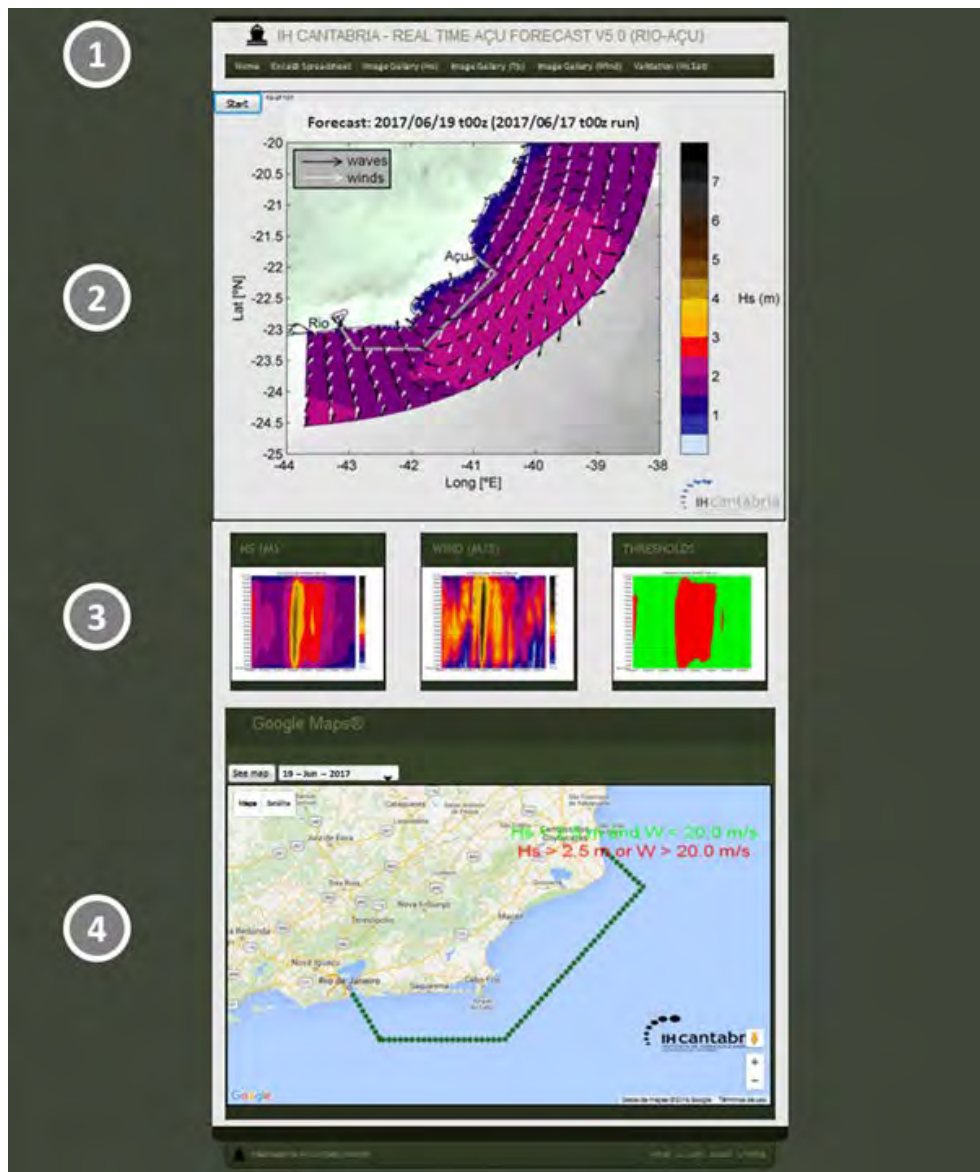


Figure 7. General view of the web page of the RIO-AÇU module. (1) Access to the Excel sheet with all the data from the last prediction. (2) Animation with 180-hourly the spatial Hs prediction. (3) Time series of the Hs and W prediction and the thresholds in all the locations of the navigation route. (4) Geo-spatial representation of the threshold along the navigation route (Hs and W) for each prediction horizon.

Figures 8 and 9 shows, similar to figure 6, examples of the results that can be obtained from the O. S. AGITATIONS module to construct and anchor the caissons (PHASE 4 in figure 8) and O.S. OVERTOPPING to construct the crest of the caissons (PHASE 1 OVERTOPPING in figure 9).

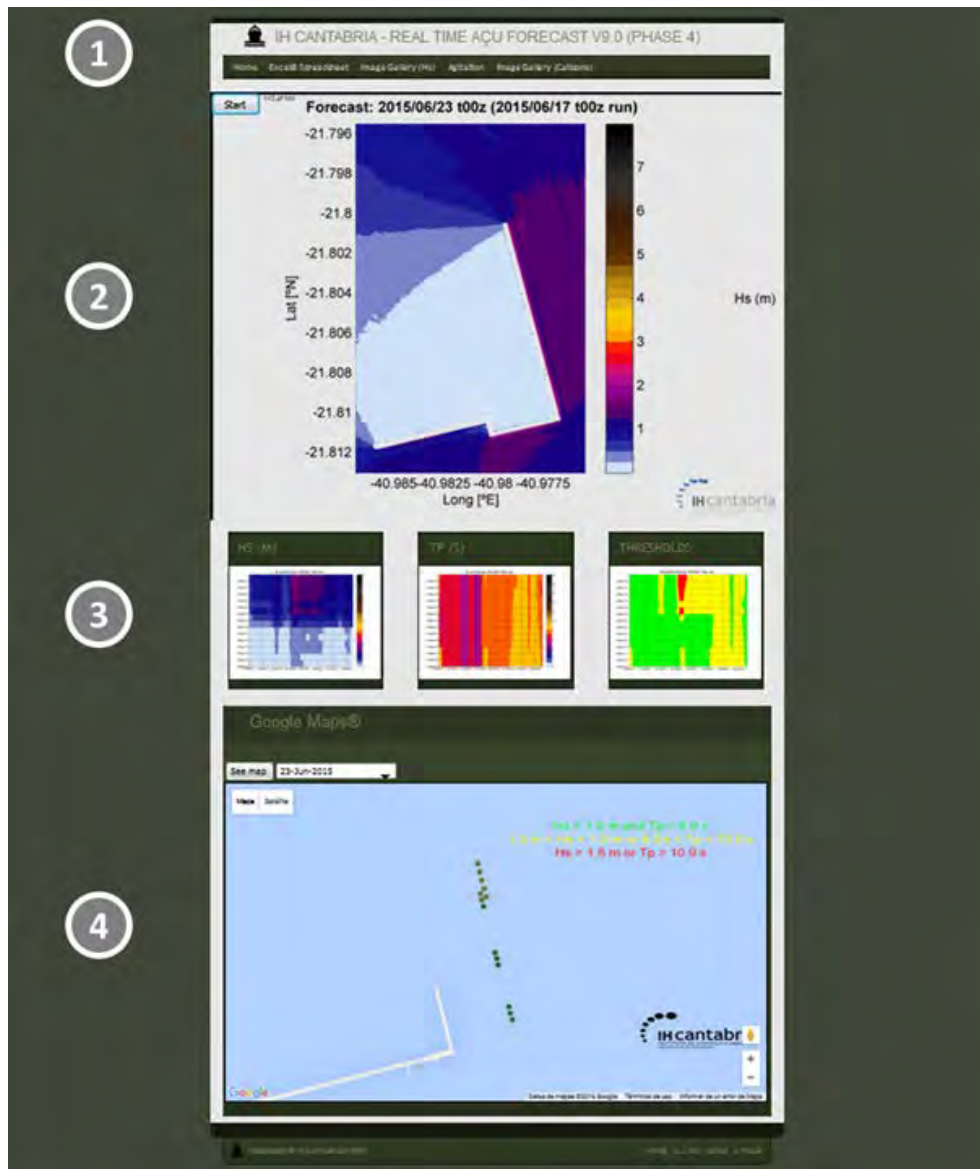


Figure 8. General view of the web page of the PHASE 4 module. (1) Access to the Excel sheet with all the data from the last prediction. (2) Animation with 180-hourly the spatial Hs prediction. (3) Time series of the Hs and Tp prediction and the thresholds in all the locations of caissons for anchoring. (4) Geo-spatial representation of the threshold for each caisson for anchoring (Hs and Tp) for each prediction horizon.

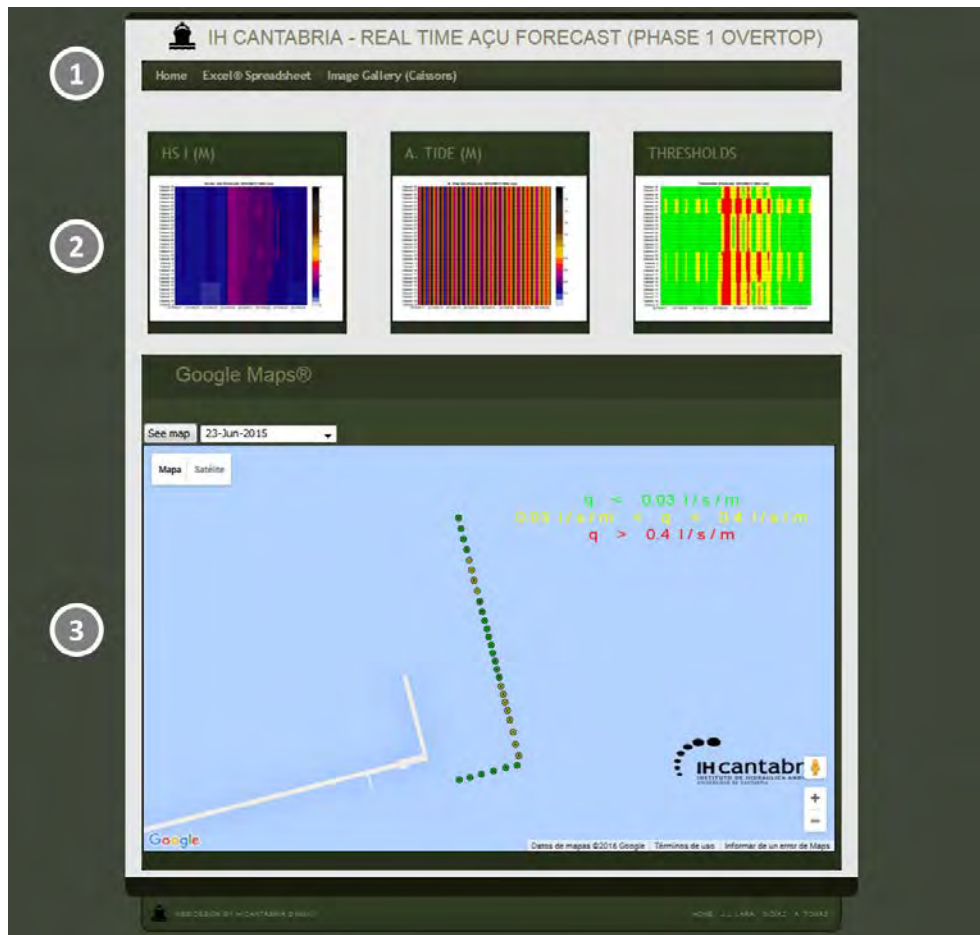


Figure 9. General view of the web page of the PHASE 1 OVERTOPPING module. (1) Access to the Excel sheet with all the data from the last prediction. (2) Time series of the Hs and Sea Level prediction and the thresholds in all the locations of caissons for working on the crest. (3) Geo-spatial representation of the threshold for each caisson for working on the crest (q) for each prediction horizon.

4. CONCLUSIONS

This study presents an integrated methodology of early-warning system to support construction and manage the harbor infrastructures exposed at different construction stages. The system is designed as a flexible tool, with a user-friendly interface, to be relocatable in any location. Results of the early warning system for the construction of Açú TX-1 terminal in Brazil, are presented.

An operational system of very high spatial resolution and specific for the construction processes of the Port of Açú has been implemented. This system offers results with a prediction horizon of one week (180 hours), hourly time resolution and is updated at least 3 times a day.

The prediction of all the climatic information in open waters (waves, sea level and wind) provided by the NOMADS system has been integrated, confirming the need to increase the spatial-temporal resolution of the dynamics and, at the same time, to adequately resolve the processes that condition the safety of the different works in the Port of Açú:

Maritime transport from Rio de Janeiro

Construction of caissons

Anchoring of caissons

Construction of the crest

The operational system has been successfully structured in several modules that numerically model, with the latest generation tools, the different processes at the most appropriate scale: operational system of propagation (SWAN model), operational system of agitation (MSP model) and operational system of overtopping (IH2VOF model).

The numerical runs have been carried out for each configuration and phase of works, updating the results according to the constructive and realistic progress of the works.

The system is validated and verified the benefits of the forecasts by comparing the expected values with the real ones measured by the in-situ ADCP. Results of the system were improving by assimilation of real data measured by the ADCP.

Specific working thresholds have been defined and validated on site (for transporting the caissons, anchoring the caissons and work on the crest) which are automatically crossed with weather forecasts. With this procedure, working parts (red, yellow and green) are generated daily and distributed via web and e-mail. This make possible to plan the different working conditions on site quickly, truthfully, reliably and safely.

A friendly and easily accessible web page has been implemented to distribute all results of the latest update of the predictions (geo-spatial representation, animations, figures, numerical data...). Results can be shows by different users. The system allows to the end user to trace the flow of all the information generated.

The robustness of Açu's operational system allows it to be adapted for the construction of other maritime works, as well as for the optimization of the operation of these infrastructures once the works are completed.

The close collaboration between IHCantabria-FCC has improved the quality of the results obtained by the operational system.

The system help the construction managers to improve and establish human safety threshold, related with the different tasks along the harbor, exposed to the met-ocean variables, and interacting with the unfinished harbor structures. And the system results also allow to optimize exploitation and construction costs and to achieve the individual deadlines of every task or activity.

5. REFERENCES

Booij, N.; Ris, R.C.; Holthuijsen, L.H. (1999). A third-generation wave model for coastal regions, Part I: Model description and validation. *Journal of Geophysical Research*, 104(C4). pp 7649-7666. doi: 10.1029/98JC026222.

Castanedo, S., Abascal, A.J., Camus, P., Tomás, A., Cárdenas, M., Medina, R., (2012) High resolution oil spill forecasting using hybrid downscaling techniques. 33th International Conference on Coastal Engineering. Santander (Spain).

De los Santos, F.J.; Rodriguez-Rubio, P.; Terrés, J.M.; Mans, C.; Molina, R.; Díaz-Hernández, G.; Tomás, A.; Lara, J.L.; Álvarez, E. (2016) Proyecto Algeciras-Safeport para la gestión de riesgos

océano-meteorológicos en entornos portuarios: oleaje, viento, agitación, rebase y oleaje generado por el paso de embarcaciones. VI Congreso Nacional de la Asociación Técnica de Puertos y Costas. (ATPYC) Palma de Mallorca (Spain). pp 257-269. ISBN 978-84-88975-91-1 (in spanish)

Díaz-Hernández, G., Losada, I.J., Mendez, F.J., Guanche, R., Reguero, B., Camus, P. (2010). An early-alert system to support construction of port infrastructures. 32th International Conference on Coastal Engineering. Shangai, (China)

Díaz-Hernández, G., Losada, I.J., Mendez, F.J (2017). Improving construction management of port infrastructures using an advanced computer-based system. Automation in Construction, 81, pp 122-133. doi: 10.1016/j.autcon.2017.06.020

Lara, J.L.; Losada, I.J.; Guanche, R. (2008). Wave interaction with low mound breakwaters using a RANS model. Ocean Engineering, ELSEVIER. Vol. 35(13), pp. 1388-1400

Losada, I.J.; Lara, J.L.; Guanche, R.; Gonzalez-Ondina, J.M (2008). Numerical analysis of wave overtopping of rubble mound breakwaters. Coastal Engineering, ELSEVIER. Vol. 55(1), pp. 47-62

Rodríguez, B., Díaz-Hernández, G., García-Valdecasas, J. M., Álvarez-Fanjul, E., Lara, J. L., Medina, R., Tomás, A. (2017) Validación pre-operativa y puesta en marcha del sistema operacional de agitación portuaria del proyecto SAMOA. XIV Jornadas Españolas de Ingeniería de Costas y Puertos. Alicante (Spain). pp. 85-86. (in spanish)

SEIZING OPPORTUNITIES FROM PANAMA CANAL EXPANSION THROUGH ADAPTIVE PORT PLANNING

O. Soto Reyes¹, P. Taneja², B.A. Pielage³, M. van Schuylenburg⁴

ABSTRACT

The third set of locks of the Panama Canal opened to traffic on June 26th, 2016 enabling the transit of Neo-Panamax⁵ (NPX) vessels through the 100-year old maritime route. This historic milestone will impact the business cases of port- and transport infrastructure within its region of influence which includes Caribbean countries such as Bahamas, Trinidad and Tobago, Venezuela, Colombia, Jamaica, Panamá, Puerto Rico and Dominican Republic. This paper presents a study carried out to first assess the impact of the Panama Canal Expansion (PCE) on selected Caribbean ports, and thereafter, to examine how the ports can adapt in order to seize new opportunities created by the expansion. An applied case of long-term planning and flexibility in engineering design under uncertainty by using Adaptive Port Planning (APP) framework is presented for a new port terminal in Barranquilla, Colombia. Further, a method for quantifying opportunities from containerized traffic using dynamic forecasting, Real Options Analysis and Monte Carlo Simulation is presented.

Keywords: Port planning, adaptive, uncertainty, opportunities, flexibility, Panama Canal expansion, Caribbean, dynamic forecasting, Real Options.

1. INTRODUCTION

1.1. Background

The third set of locks of the Panama Canal opened to traffic on June 26th, 2016 enabling the transit of Neo-Panamax (NPX) vessels through the 100-year old maritime route. This historic milestone will impact the business cases of port- and transport infrastructure within its region of influence which includes Caribbean countries such as Bahamas, Trinidad and Tobago, Venezuela, Colombia, Jamaica, Panamá, Puerto Rico and Dominican Republic.

1.2. Objective

This paper presents the results of a study related to the impact of the Panama Canal Expansion (PCE) on selected Caribbean ports. Having examined the vulnerabilities and opportunities created by the PCE for Caribbean ports in general, it focusses on a case study, i.e. a port in Barranquilla, Colombia. It further proposes an approach for adaptive planning of a port whereby ports can deal with the vulnerabilities and seize new opportunities. This approach is applied for the case study and the results are presented in the paper. Further, a method for quantifying opportunities from containerized traffic using dynamic forecasting, Real Options Analysis and Monte Carlo Simulation is presented.

2. IMPACTS OF PANAMA CANAL EXPANSION

2.1. Major impacts

A detailed study of Panama Canal Expansion (PCE) on Caribbean ports (Soto Reyes, 2017) was carried out. The study concluded that the major short-term impact for Caribbean ports would be a decrease in transshipment container volumes, lost to new direct services deploying NPX vessels calling to the newly adapted ports of the United States (US) East Coast and the Gulf of Mexico. However, due to their

¹ Panama Canal Authority, Panama, soto.oscar@gmail.com

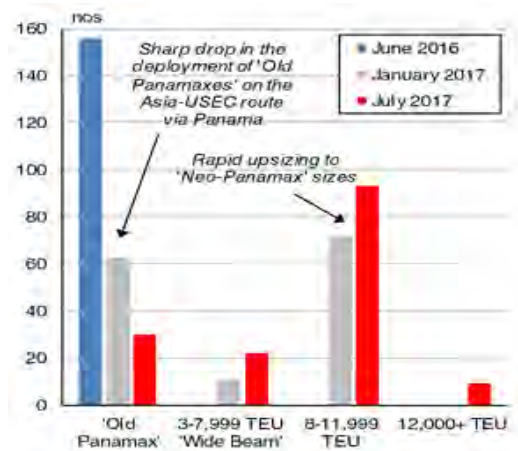
² Delft University of Technology, The Netherlands

³ Witteveen + Bos Consulting Engineers, The Netherlands

⁴ Port of Rotterdam Authority and IHE Delft, The Netherlands

⁵ Neo-Panamax (NPX) vessels: Vessels with the following maximum dimensions 366 meters Length over All (LOA), 49 meters beam, and 15.2 meters draught in Tropical Fresh Water (TFW).

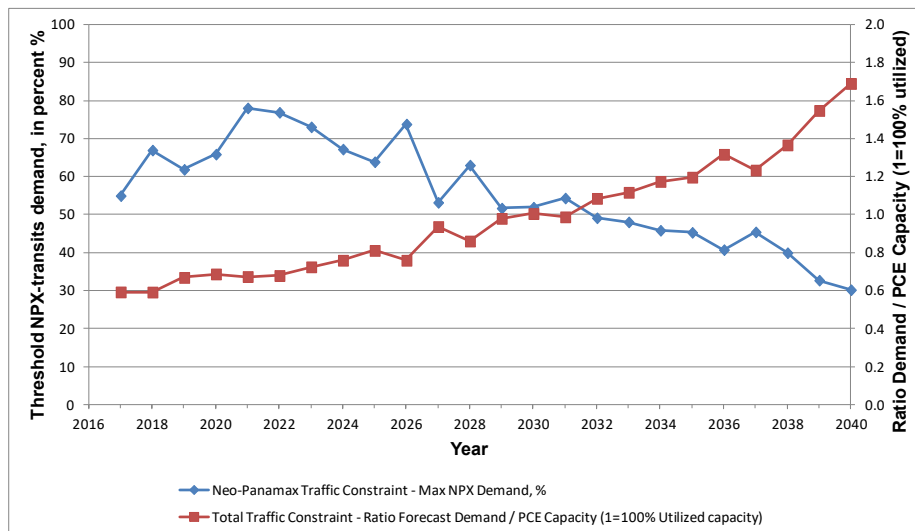
privileged geographical location in the crossroad of important maritime routes their development will continue to be intrinsically linked to the Panama Canal beat.



Source: Excerpted from (Clarksons Research, 2017)

Figure 1. Deployment shift of Panamax (PX) vessel in Trans-Pacific Panama Canal services, after PCE

Contemporaneously, a sharp drop in deployment of Panamax (PX) vessels in Panama Canal services, and a surge in the scrapping of such “old” Panamax take place; thus the substitute fleet of NPX vessels being deployed in services via Panama Canal is expected to continue growing steadily, as shown in Figure 1. Accordingly, it has been also estimated in this research that expanded Panama Canal, may reach its full capacity around year 2030 (Soto Reyes, 2017), as shown in Figure 2.



Source: Excerpted from (Soto Reyes, 2017)

Figure 2. Expanded Panama Canal capacity, 1-run dynamic forecasting

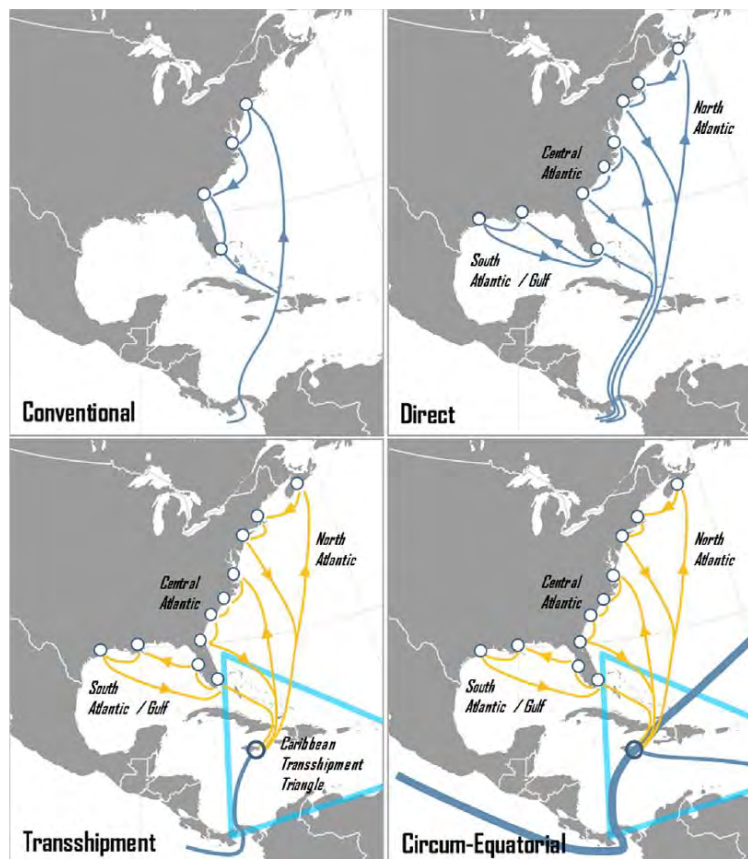
Since the construction of a fourth set of locks remains uncertain, such future bottlenecks in the expanded Panama Canal, in its current configuration, may result in new opportunities for the Caribbean ports. Hence, the study concludes that the expanded Panama Canal may eventually attract more Caribbean port traffic and thus container transshipment may regain business, in the mid- and long term.

In addition to the intrinsic uncertain developments discussed above, the Caribbean Ports are beset with other future uncertainties related to technology, market and economy, politics and legislation as well as society and environment and yet must ensure functionality, capacity and service quality during their design life time in a sustainable manner (PIANC, 2014a, 2014b; Taneja, 2013). We advocate an adaptive planning approach in the next sections.

2.2. Uncertainties in the aftermath

As previously noted, it may be expected a certain extent of decreased container transshipment traffic in the Caribbean region just after the completion of PCE, mostly due to the migration towards direct calls to the ports in the US East Coast and the Gulf of Mexico (Rodrigue & Ashar, 2016). However, such new sailing patterns, as the shown in Figure 3, may evolve themselves into diverse configurations –e.g., “conventional or traditional single rotation”, “direct regional specialized service”, “transshipment hub-and-spoke”, “equatorial round-the-world”, “fourth-revolution global grid” (Knight, 2008; Rodrigue & Ashar, 2016) – depending on a variety of uncertain developments, including but not limited to such related to:

- Development options of individual Caribbean port terminals (Notteboom, Ducruet, & Langen, 2010), and with regard to their respective level of transshipment incidence, namely gateway/feeder ports, regional gateway ports, hub ports, pure transshipment ports (Rodrigue & Ashar, 2016).
- Trans-Pacific trade development, congestion issues at US West Coast and Land Bridge, the emergence of new US East Coast gateways (Notteboom et al., 2010)
- Inter-range evolution of different transshipment patterns involving the Caribbean port system namely, direct services, “by-passing” services, “tail-cutting” services, “hub-and-spoke” services, “intersection” services, “relay” services (Rodrigue & Ashar, 2016).
- Competition and collaboration schemes amongst Caribbean ports (Notteboom et al., 2010)
- Intra-range transshipment structures of Caribbean ports, e.g., the development and evolution of a “transshipment funnel”, “transshipment triangle”, “transshipment corridors” or individual “transshipment clusters” (Rodrigue & Ashar, 2016).
- Dynamics of LNG⁶ trade patterns or game-changers such a Valemax-class very large ore carriers.
- Global impacts of One Belt One Road long-term project (China Britain Business Council, 2017).
- Increased navigability of seasonal Arctic routes (Snyder, Doyle, & Toor, 2013).
- The construction of a new Interoceanic Canal in Nicaragua (HKND Group, 2018).
- Global maritime industry trends, e.g., mergers, acquisitions, and bankruptcy of shipping lines.



Source: Excerpted from (Notteboom et al., 2010)

Figure 3. Potential sailing patterns in Caribbean basin, after PCE

⁶ Liquefied Natural Gas (LNG)

In Section 5, a method for quantifying opportunities from containerized traffic using dynamic forecasting, Real Options Analysis and Monte Carlo Simulation is presented.

3. ADAPTIVE PORT PLANNING: THEORETICAL FRAMEWORK

APP aims at developing plans that take uncertainties explicitly into account, allowing for change, learning, and adaptation over time based on new knowledge and changing circumstances. Such flexible or adaptable plans will allow the port to be functional under new, different, or changing requirements in a cost-effective manner, and seize opportunities.

Figure 4 portrays the basic steps of the Adaptive Port Planning methodology that were followed during the development of the real case study in Barranquilla, Colombia, as defined and thoroughly depicted by (Taneja, 2013).

3.1. Step 1: Definition of the project objectives and success criteria

This stage includes the definition of both success and, consequently the objectives of the project. With such input, preliminary forecasting and planning are performed as well as the initial set of alternatives and/or strategies, for the expected useful time horizon of the project.

Definition of Success: Compiled specification or desired project outcomes *vis-à-vis* the previously stated mission, vision, objectives and constraints which the stakeholders would find as of an acceptable satisfaction level (Taneja, 2013; Walker, Rahman, & Cave, 2001). Consequently, failure may be defined as any set of possible project results which would be deemed as unacceptable by the stakeholders (Walker et al., 2001).

3.2. Step 2: Definition of the basic plan and assumptions

For the initial set of alternatives/strategies, a SWOT⁷ analysis should be performed for each alternative or strategy, in order to rank the most prominent opportunities and vulnerabilities for the project.

Assumption: Is an assertive statement about relevant and specific features of the future that underlies the existing operations or plans of an enterprise. Vulnerable assumptions are those which, if impacted by vulnerabilities within the planning time horizon, will certainly fail (Dewar, Builder, Hix, & Levin, 1993; Taneja, Walker, Ligteringen, Schuylenburg, & Plas, 2008).

Critical assumption: Assumption whose failure would mean the failure of the plan (Taneja et al., 2008). Not all the vulnerable assumptions are critical, but all the critical assumptions are vulnerable.

Development or element of change: Is a future world event or condition that means a change to status quo, it is credible within the planning time horizon and is relevant to the existing operations or plans of an organization (Dewar et al., 1993; Taneja, 2013).

3.3. Step 3: Proactive incorporation of flexibility and robustness

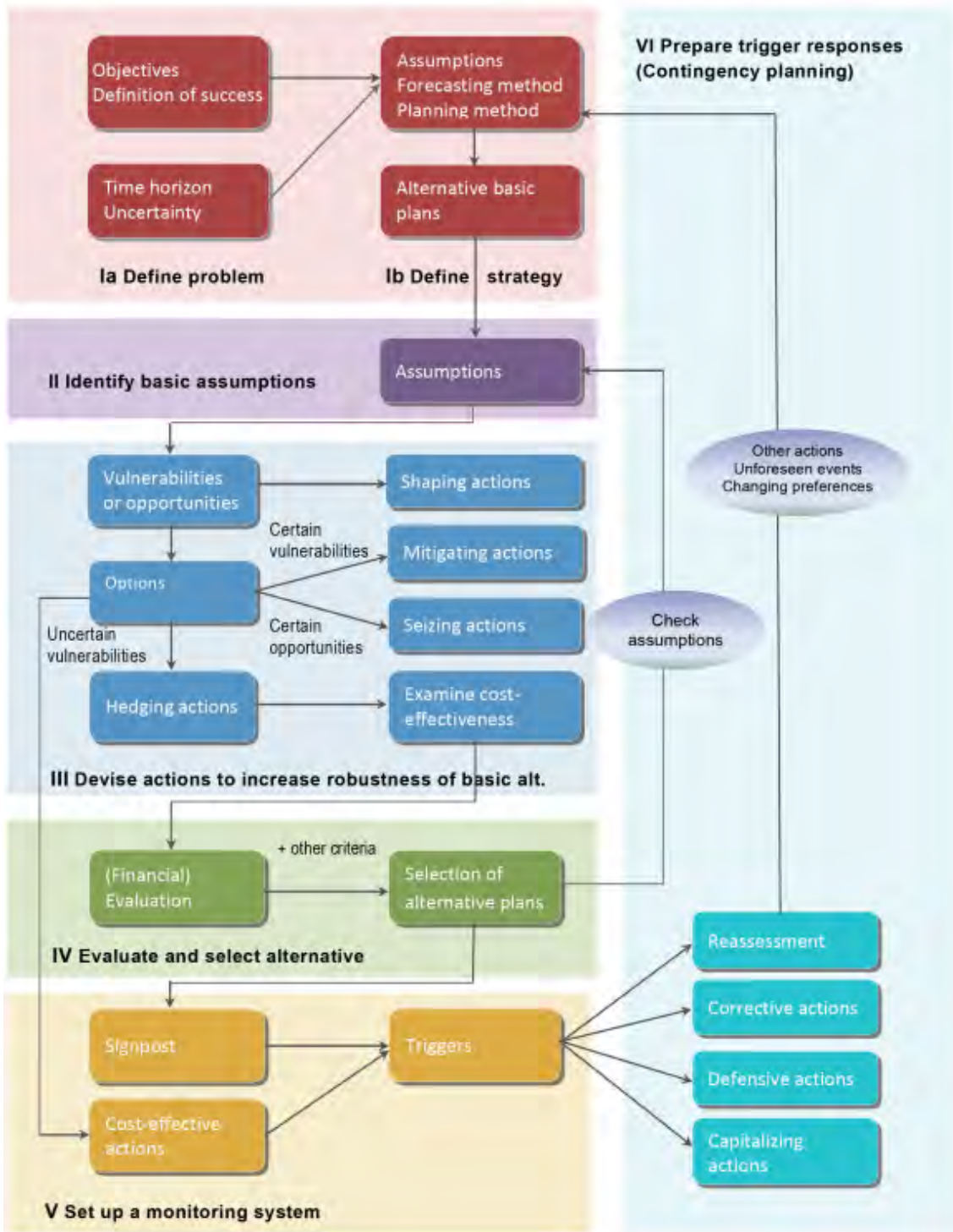
This stage, along with Step 4 may be deemed as the core stages in APP methodology. At this point, efforts should be focused on enhancing “certain and uncertain” opportunities and, more importantly on, planning actions to be taken for the mitigation of “certain” threats and to turn “uncertain” vulnerabilities into new opportunities in the future.

Vulnerabilities: Any possible development or element of change that may be a hindrance to the success of the plan (Taneja et al., 2008).

Opportunities: Any possible development of element of change that may enhance the success of the plan (Taneja et al., 2008).

Mitigating actions: Organizational actions to be taken *in advance* to reduce the negative effects of reasonably *certain* vulnerabilities of the plan, i.e., seeking the *robustness* of the plan (Kwakkel, Walker, & Marchau, 2010; Walker et al., 2001).

⁷ SWOT: Strengths, Weaknesses, Opportunities and Threats



Source: Excerpted from (Taneja, 2013)

Figure 4. Adaptive Port Planning (APP) methodology

Hedging actions: Organizational actions to be taken *in advance* to reduce the potential negative effects of *uncertain* vulnerabilities of the plan, i.e., seeking the *robustness* of the plan (Kwakkel et al., 2010; Walker et al., 2001).

Shaping actions: Organizational *pro-active* actions precisely intended ‘to shape’ future *certain and uncertain* externalities to either weaken vulnerabilities or enhance opportunities (Dewar et al., 1993; Kwakkel et al., 2010), or turning vulnerabilities into opportunities or a combination thereof.

Seizing actions: Organizational actions planned *in advance* to be executed in the future to grab at reasonably *certain* available opportunities (Kwakkel et al., 2010).

3.4. Step 4: Evaluation and selection of alternatives (strategies)

At this stage the most challenging tasks are expected to be the valuation, or quantitative assessment, of the “flexibilities” incorporated in the previous stage, and the internalization of the associated additional costs into the final project appraisal.

3.5. Step 5: Contingency planning (incorporation of adaptive elements)

Since the proposed APP methodology should be proactive and dynamic, then monitoring the specific external factors affecting the maritime industry in the studied region becomes of a paramount importance. Accordingly, to close the loop on the adaptive and flexible nature of the planning, it is necessary also to draft the lines of action for the cases when residual vulnerabilities become reasonably evident to occur, or to seize any new opportunities as they may appear on the lifetime horizon of the project.

Signposts: Originally defined as an event or threshold indicative of the future development of any given uncertainty, signposts may be also depicted as mechanisms implemented for specifying, collecting, and monitoring information deemed as an indicators of whether the plan is on track for success, or not. Such indicators should be *unambiguous* and, should be duly paired with their respective vulnerabilities or opportunities (Dewar et al., 1993; Kwakkel et al., 2010).

Triggers: Threshold values of signpost indicators which, when surpassed, should spark the implementation of either defensive, corrective or capitalizing mechanisms, as established in the contingency plan (Taneja et al., 2008; Walker et al., 2001).

Defensive actions: Organizational *after-the-fact* actions to either clarify the plan, respond to external challenges or to preserve its benefits; while the basic plan remains substantially unchanged (Kwakkel et al., 2010; Taneja et al., 2008).

Corrective actions: Signpost-triggered organizational adjustments leading to a better enforcement of the plan in response to dynamic external conditions (Kwakkel et al., 2010; Taneja et al., 2008).

Capitalizing actions: Organizational *after-the-fact* actions to leverage future opportunities and thus enhancing plan’s performance (Kwakkel et al., 2010; Taneja et al., 2008).

Reassessment: It is the *re-examination and revision* of the plan to be triggered whenever neither defensive, nor corrective actions would suffice to reroute the plan towards success or whenever the plan’s critical assumptions have, undoubtedly and irreversibly, lost their validity (Dewar et al., 1993; Kwakkel et al., 2010; Walker et al., 2001).

3.6. Step 6: Implementation and monitoring

Finally, after duly setting up the signposts, triggers and contingency responses, the adaptive port planning process should then transition to the implementation phase, e.g. design, construction, operations and maintenance, while the managerial team should continue proactively monitoring the signposts-and-trigger indicators (Taneja et al., 2008). Hence, an adaptive planning approach enables policy-makers and decision-takers to take advantage of the benefits from both a proactive present-to-future outlook and, future-to-present retrospective analysis (Walker et al., 2001).

4. CASE STUDY: BARRANQUILLA NEW PORT TERMINAL

4.1. Project description and objectives

The new port terminal is projected to be constructed on the East bank of Magdalena River, two (2) kilometres upstream from the mouth of the river at Bocas de Ceniza, as shown in Figure 5, and would become part of the port complex of Barranquilla, Colombia.

The core business of the new port terminal will be the imports of liquid bulk, e.g., diesel and other oil and petroleum derivatives. A single-buoy mooring system for super-tankers is also projected to be installed as part of the project. Nevertheless, the three main cargoes to be handled will be liquid bulk, grain dry bulk and containers. Aboveground storage tank farms will be built for the liquid bulk whereas

the grain dry bulk will be shifted by conveyor belt to storage silos. The container stacking yard has been originally conceived for a declared capacity of 6,000 TEU/year.⁸

The initial project will consist of 4.2-Hectare land reclamation, with two (2) berths, loading/unloading platform and trestle for the liquid bulk terminal, and one (1) multi-purpose 300-meter berth for the dry bulk and container terminal, as shown in Figure 5.

The design vessel dimensions are 200 meters Length Over-All, beam of 32.2 meters and, a draught of 10.0 meters, i.e., slightly smaller than Panamax dimensions. The terminal only hinterland connection should be via river barges sailing the Magdalena River, in diverse push boat-barge convoy configurations.

The conceptual design provides for a 300-meter length multi-purpose quay wall. The quay area devoted for ship-to-shore operations is 30-meter width, but such an area is not taken into account for container handling capacity calculations. The container handling yard, as conceptually designed, is 1.5 hectares, i.e., a rectangular-shaped yard with dimensions 300x50m. The throughput capacity for the fixed base case has been estimated to be 30,000 TEUs/year.⁹

The contractual dredging design level for the base case has been set to elevation -12,20m CD, hence, allowing only for a maximum draught of 10m. Such restriction will make this terminal unable to handle the Neo-Panamax (NPX) vessels, with a 15.2m draught, now transiting the Panama Canal Expansion (PCE), and hence will render the terminal unable to profit from the PCE-generated traffic.



Source: Adapted from (Soto Reyes, 2017)

Figure 5. General layout and regional location of the case study port terminal

4.2. Identification of project uncertainties

Adaptive Port Planning (APP) methodology makes use of the multi-stakeholder brainstorming as an out-of-the-box process to identify and categorize project uncertainties, as well as to perform a qualitative assessment of their drivers and impacts on the development of the project. Moreover, the so called “wildcards” or “black-swans” developments are also brought into consideration (Taneja, 2013).

⁸ The reader may find a difference between the declared capacity of 6,000 TEU/year as indicated in the conceptual design (confidential) documentation and, the estimated handling capacity of 30,000 TEU/year used in this paper as the fixed base case design. Nevertheless, it is necessary to explain that, for the purpose of this paper and real case study, the latter capacity has been calculated following the best practice and benchmarking on terminal capacity calculations and, under the paramount assumption of installing one (1) Ship-To-Shore (STS) crane per each 100-meter length of quay wall, with a capacity of 100,000 TEU/year/STS crane and, a standard 500-meter wide container handling yard all along the quay wall length.

⁹ Ibid.

Table 1 presents the different sources of intrinsic uncertainties identified for the case study project, grouped under four (4) major categories, namely Technology, Market and Economy, Politics and Legislation and, Society and Environment.

Table 1. Categorized credible developments and their impacts

| Category | Credible development | Impact |
|-----------------------------------|--|--|
| Technology | Development of new and more environmentally-friendly technologies. | Environmental dredging may facilitate the permits for deeper capital and maintenance dredging of ports along Magdalena river, especially nearby protected areas. |
| | Supply of utilities across Magdalena river. | Since the project will be basically an island in the middle of an environmentally protected area, logistics for utilities supply from the West bank to the terminal would represent a logistics issue for the construction of the terminal. |
| Market & Economy | Construction of offshore Single Buoy Mooring (SBM) for bigger LNG vessels. | The project may raise opposition from the public and stakeholders on grounds of the environmental issues of laying a pipeline across a protected area. |
| | Development of inland waterway terminals (infrastructure and operators). | The case study terminal is being projected to serve the hinterland by means of river barge convoys; hence, for the business case to remain valid, a proper network of inland intermodal terminals should be developed and maintained by externals. |
| | Less Panamax ships deployed on Panama Canal routes. | Since both the case study terminal and Magdalena river navigability plan only provide for 10-meter draught Panamax vessels, the fact that such vessels may incrementally be scrapped would severely impact the business plan of the port terminal. |
| Politics & Legislation | Peace process implementation. | Should the peace process be implemented, opportunities for a bigger economic growth of the country could also foster new port developments, e.g., greenfield port of Antioquia-Urabá (Puerto Antioquia Website, 2017), that would be competitors to the case study terminal. |
| | Trade with Venezuela. | A large share of Colombian trade is conducted with Venezuela. A highly unstable political turmoil in the neighboring country may have repercussions on maritime trade. |
| | Granting of concession by CORMAGDALENA. ¹⁰ | The whole project execution is subject to the approval of the full package of studies required by CORMAGDALENA. |
| Society & Environment | Upstream river basin development plans by regulatory entity CORMAGDALENA. | The planning and design process for future port terminals. |
| | Climate change / Sea Level Rise (SLR). | Port infrastructures should duly take into account climate change and sea level rise issues; otherwise, such costly projects may become vulnerable to such impacts. |
| | Society's opposition (wetlands, erosion). | Should the project promoters fail to effectively engage stakeholders of the overall benefits of the new port, societal and environmental opposition may be able to put the project on hold for an uncertain period of time. |

Source: Excerpted from (Soto Reyes, 2017)

¹⁰ Corporación Autónoma Regional del Río Grande de la Magdalena (CORMAGDALENA)

Table 2 concisely shows some sources of uncertainty, either vulnerabilities or opportunities, which may be deemed as external to the case study project.

Table 2. External sources of uncertainties for the project

| Vulnerability / Opportunity | Specific drivers |
|---|---|
| Vulnerability: Scrapping of Panamax vessels. | The opening of the expanded Panama Canal. Economies of scale from Neo-Panamax and other Post-Panamax categories of vessels. |
| Vulnerability: Decay of transshipment on Caribbean ports. | Deepening of US East Coast and Gulf ports and improvement of their hinterland connections. |
| Vulnerability: Global economics. | Slowdown of China’s economy. |
| Opportunity: LNG import / storage / bunkering business. | LNG becomes the generalized “cleaner” fuel of the future. |

Source: Excerpted from (Soto Reyes, 2017)

Table 3 summarizes some of the so called “wildcards” or “Black Swans” (Taneja, 2013) identified for the specific case study project.

Table 3. Major external wildcards and their impacts

| Wildcards (or “Black Swans”) | Impacts |
|--|--|
| One Belt One Road (OBOR). | It may be deemed as the Chinese response strategy to USA protectionism. Europe and Asia linked by land and maritime bridges with six (6) economic corridors over 60 countries may negatively impact Asia-US East Coast/Gulf trade, from which both the Panama Canal and Caribbean ports benefit. |
| USA Protectionism policies. | Colombian and other Latin American exports to the United States of America may decrease substantially. Consequently, port activity may be affected negatively. |
| EU (partial) disintegration. | Trade agreements would have to be negotiated separately with different European countries and most likely under diverse conditions, which may render trade more difficult. |
| China’s decline and India’s surge. | The two competitive advantages of Colombian port system are: Shorelines in both the Pacific and Atlantic/Caribbean basin and its proximity to the Panama Canal. The latter one would be negatively impacted if the manufacturing pole shifts from Northeast/Southeast Asia to Western India, because the Suez canal route would gain market from the Panama Canal route. |
| Global economic collapse (and reset). | All business cases for port terminals would have to be extensively revised. Only the adaptable or resilient ones may prevail and become stronger after the reset. |
| Latin American integration and upsurge, e.g. “Chile-con Valley” (The Economist, 2012). | Colombia and other Latin American countries unite to conform a strong economic conglomerate, exporting value-added products and services, thus fostering port activity. |

Source: Adapted from (Soto Reyes, 2017)

4.3. Action plan

After the preliminary scanning of the project’s uncertainties, a flexible action plan is drafted, from which the planners will pick their specific flexibilities and formulate the diverse strategies to be further quantified (Taneja, 2013), as it will be performed in the following sections.

Table 4 summarizes the “known” uncertainties for the project and the conceptual responsive actions to either mitigate vulnerabilities, shape the future or seize opportunities in the future, respectively.

Table 4. Certain developments and responsive actions

| Vulnerabilities/Opportunities | Actions: Mitigation (MI): reduce negative effects; Shaping (SH) the future: proactive; Seizing (SZ): grab opportunities |
|---|---|
| Opportunity: Panama Canal Expansion and traffic enhanced by Neo-Panamax container vessels. | Seizing: Design and build port infrastructures enabled to handle Neo-Panamax container ships to attract a share of the new demand. |
| Opportunity: Panama Canal Expansion and new transits of (Neo-Panamax) LNG/LPG vessels. | Seizing: To design and build LNG/LPG importing/storage/bunkering terminals, also enabled for Neo-Panamax carriers. |
| Opportunity/Vulnerability: Panama Canal Expansion and change in sailing patterns by shipping lines. | Shaping: Foster and establish cooperation agreements with Panama Canal and/or with Caribbean transshipment hub ports to manage their overflow in the long-term. Shaping: To broker agreements with shipping lines wanting to offer “greener” hinterland transport by means of inland waterways system of Magdalena river. |
| Vulnerability: Expansion of existing (and competitor) dedicated container terminal in Barranquilla. | Mitigation: Design and built multi-purpose terminals. To sign cooperation agreements with other terminal operators within Barranquilla port complex, perhaps focusing more on the hinterland import/export niche market rather than transshipment. Shaping: Investing in inland waterway terminals and/or “dry port” (Woxenius, Roso, & Lumsden, 2004) facilities. |

Source: Adapted from (Soto Reyes, 2017)

Table 5 summarizes the “unknown” uncertainties for the project and the conceptual responsive actions to either hedge vulnerabilities or shape the future, accordingly.

Table 5. Uncertain developments and responsive actions

| Vulnerabilities/Opportunities | Actions: Hedging (HE): reduce negative effects of vulnerabilities; Shaping (SH): proactive, shape future |
|---|---|
| Vulnerability: Drastic scrapping and eventual disappearing of Panamax vessels from the fleet. | Hedging: Design and build port infrastructures enabled to handle Neo-Panamax vessels. Shaping: Negotiate with minor shipping lines to continue deploying Panamax vessels in their feeder services. |
| Vulnerability: Development of new container terminal at Urabá-Antioquia, Colombia. | Shaping: Join efforts with other Barranquilla port complex terminals to establish cooperation agreements with other Colombian Caribbean ports, to focus in different but complementary niche markets. |
| Vulnerability: Construction of super- deep water port at Bocas de Ceniza, Barranquilla. | Shaping: Establish cooperation agreements with other terminal operators within Barranquilla port complex, to focus in different but complementary niche markets. |
| Opportunity: Regulation enforcing LNG/LPG-powered river vessels. | Shaping: To design and build LNG/LPG importing/storage/bunkering terminals, which are also enabled for Neo-Panamax carriers. |

Source: Adapted from (Soto Reyes, 2017)

4.4. Monitoring, contingency and implementation plans

Table 6 concisely summarizes the opportunities and vulnerabilities to be monitored, as well as their respective threshold values and timing to trigger the implementation of contingency actions, as per APP approach.

Table 6. Monitoring thresholds and triggers

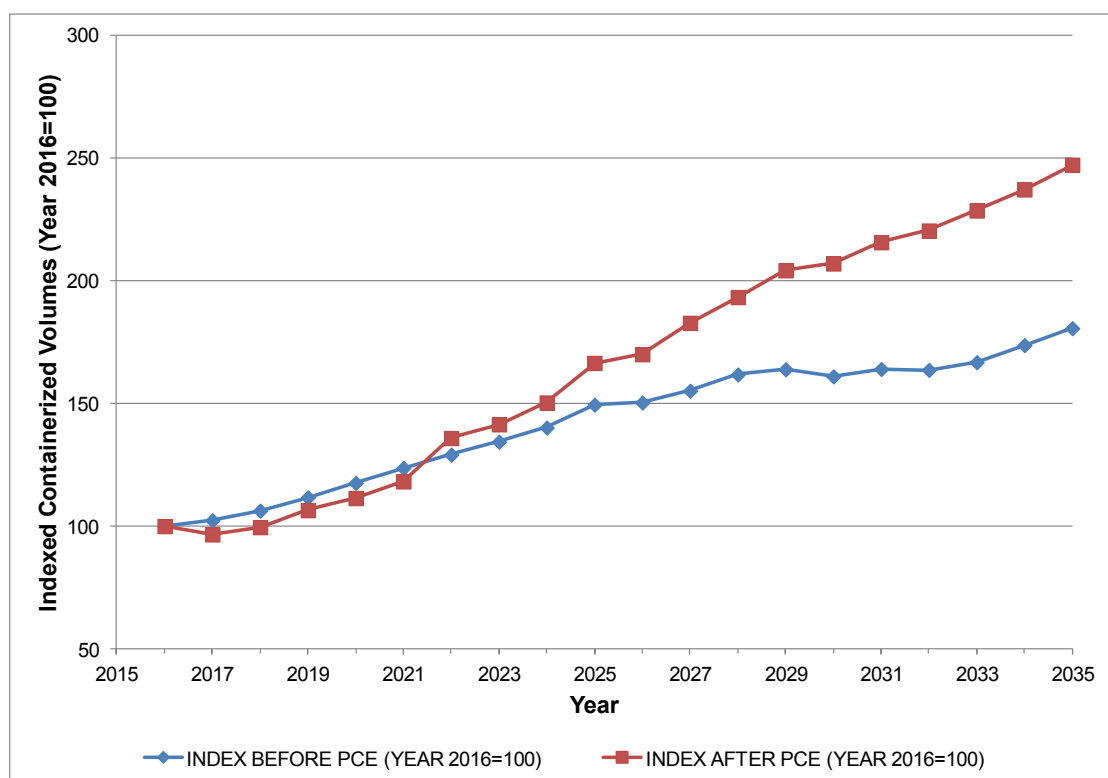
| Vulnerabilities / Opportunities | Monitoring & Thresholds | Actions: Reassessment (RE) or Corrective (CR) or Defensive (DE) or Capitalizing (CP) |
|--|--|--|
| Opportunity: To gain share in existing demand that would otherwise go to another port. | Demand / Capacity ratio equal or greater than 0.95 for two (2) consecutive years. | Capitalizing: Triggers the addition of (modular) handling capacity, i.e., sequential incorporation of flexibilities 1, 2 and 3, as applicable [See Section 5]. |
| Opportunity: To gain share in existing demand that would otherwise go to another port. | NPX-traffic / Capacity ratio greater or equal to 1.00 for two (2) consecutive years. | Capitalizing: Triggers the execution of additional dredging works, i.e., incorporation of flexibility 5, as applicable [See Section 5]. |
| Vulnerability: Total replacement of Panamax vessels. | Yearly scrapping and new orders reports. | Re-Assessment: Enable the port terminal to handle Neo-Panamax vessels, even if traffic volumes are low (better than none). |

Source: Adapted from (Soto Reyes, 2017)

5. CASE STUDY: QUANTIFYING OPPORTUNITIES FROM PANAMA CANAL EXPANSION

5.1. Dynamic forecasting of containerized traffic

Based on calculated container-traffic indexes after the Panama Canal Expansion, as shown in Figure 6, the new demand was calculated by means of dynamic forecasting, which offers the advantage of taking into account the stochastic nature of uncertainties when estimating future demand of variables which may either go up or go down the next year, without any function attached (De Neufville & Scholtes, 2011).



Source: Excerpted from (Soto Reyes, 2017)

Figure 6. Indexed Caribbean containerized port traffic, before and after PCE (1-run estimation)

Available historic traffic data from years 2008-2016 jointly with World Economic Outlook for years 2017-2021 by the International Monetary Fund (IMF, 2016) were used as starting point for the dynamic forecasting process.

For the sake of consistency with flexibility concepts, it was necessary to generate at least 1,000 “possible futures” by means of spreadsheet-based Monte Carlo Simulation. Such simulated future demands thereafter became the input for the screening models performance calculations.

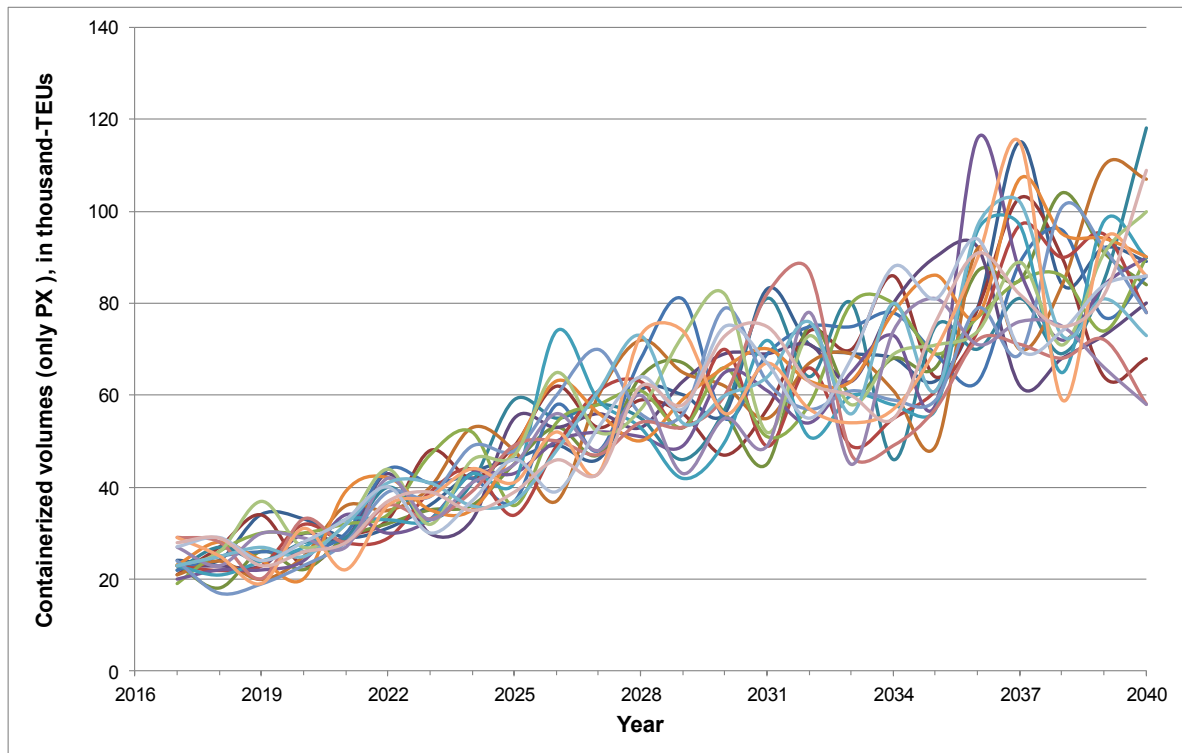
Further assumptions were superimposed on the dynamically forecast Caribbean port traffic to convert it to the demand for the case study port. Accordingly, randomly and gradually-varied market shares were assumed, as shown in Table 7.

After having incorporated such assumptions into the extended dynamic forecasting model, it was possible to obtain both, the dynamic forecasting for only Panamax-borne container traffic, as shown in Figure 7; as well as the dynamic forecast for the total container traffic, i.e. carried in both Panamax and Neo-Panamax vessels, as presented in Figure 8.

Table 7. Market share assumptions for screening models

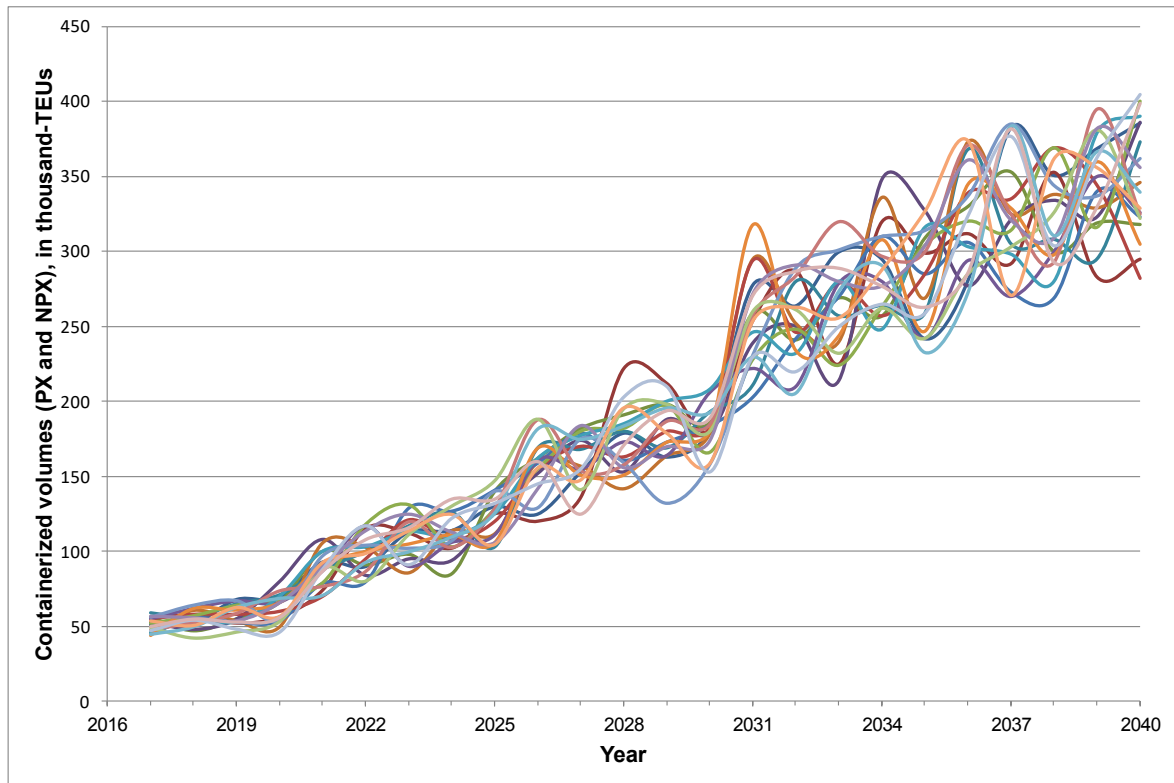
| | Year Range | 2017 | | 2040 | |
|--|------------|-------|-------|-------|-------|
| | | Min | Max | Min | Max |
| PX-borne traffic share, PX | | 40.0% | 50.0% | 20.0% | 30.0% |
| NPX-borne traffic share, NPX | | 50.0% | 60.0% | 70.0% | 80.0% |
| Colombian Caribbean share (of Caribbean Port System) | | 18.0% | | 22.0% | 25.0% |
| Rest of Caribbean System ports | | 82.0% | | 75.0% | 78.0% |
| Barranquilla share (of Colombian Caribbean) | | 5.0% | | 9.0% | 10.0% |
| Santa Marta/Cartagena/Antioquia-Urabá (future) | | 95.0% | | 90.0% | 91.0% |
| Potential Case Study Port share (of Barranquilla) | | 30.0% | 40.0% | 30.0% | 40.0% |
| Calls to other terminals within Barranquilla complex | | 60.0% | 70.0% | 60.0% | 70.0% |

Source: Excerpted from (Soto Reyes, 2017)



Source: Excerpted from (Soto Reyes, 2017)

Figure 7. Dynamic forecasting for case study port: PX-borne only (20-future sample)



Source: Excerpted from (Soto Reyes, 2017)

Figure 8. Dynamic forecasting for case study port: PX- and NPX-borne (20-future sample)

5.2. Evaluation of flexibility by Real Options Analysis

For the sake of conciseness and the purpose of this paper, in the proposed methodology to evaluate flexibilities by means of Real Options Analysis and Monte Carlo Simulation, only uncertainty-flexibility pairs related to containerized market segment will be further assessed throughout the following sections.

5.2.1. Identification and description of specific flexibilities

Base Case (Flexibility 0): It consists of a 300-meter length multi-purpose quay wall. The Ship-to-Shore (STS) operations area is a 30-meter wide strip all. The container handling yard has been originally conceived as a 300-meter length and 50-meter wide, for a total of 1.5 Hectares. This conceptual design, as of today, may be deemed as a fixed (non-flexible) design since, with regard to the container niche market, since it does not provide for either a future quay wall extension nor for additional container handling yards. Assuming the installation of three (3) STS container cranes, the yearly container throughput for this configuration has been estimated in 30,000 TEUs per year, as per standard practice.

Flexibility 1: It consists of an additional container handling area just adjacent to the original yard. Accordingly, additional reclamation works should be performed to allow for such future expansion eastward the original yard. Such expansion may be performed in three phases, by habilitating 1.5Ha in each instance, up to a total of three-fold modular expansion of 4.5Ha, upon market demand. The physical restraint for the implementation of this flexibility will then be the boundaries of the concession polygon. Hence, flexibility in this option stems from its expandable and modular attributes. Flexibility 1 may add a capacity of 90,000 TEUs per year to the system.

Flexibility 2: It consists of the addition of 300-meter of quay wall to the North of the original one. Such quay wall extension may allow for the berthing of more and different combinations of simultaneous vessel calls (e.g., two Panamax ships) in response to potential increase traffic calling to Barranquilla port. The 300-meter quay wall extension should be complemented with the construction of another modular 3x1.5Ha extension of the container handling area, upon market demand. As in Flexibility 1, flexibility in this option stems from its expandable and modular attributes. Flexibility 2 may add a capacity of 90,000 TEUs per year to the system.

Flexibility 3: It consists of the extension of the quay wall 100-meters northward plus a subsequent 3x1.5Ha modular extension of the container handling area, upon market demand. Such additional quay wall length may enable the port to handle two (2) feeder-type vessels simultaneously; however, the handling of two Panamax ships will not be feasible with this layout. As in Flexibilities 1 and 2, flexibility in this option stems from its expandable and modular attributes. Flexibility 3 may add a capacity of 90,000 TEUs per year to the system.

Flexibility 4: Flexibility 4 does not directly add physical capacity but, conversely enables future management to seize new business opportunities, upon market demand. It is a built-in flexibility, consisting of quay wall structures being designed for a dredging design elevation of -16.70m CD, instead of the base case dredging elevation of -12.20m CD. By means of such “over-design” of the quay wall structures, the terminal will be provided with a “dormant capacity” to be enabled in the future to handle Neo-Panamax vessels provided *sine qua non* that:

- Additional dredging works are performed (see Flexibility 5) and,
- Quay wall length is also extended either to a total of 600-meters (Flexibility 2) or 400-meters (Flexibility 3).

Flexibility 5: Flexibility 5 does not directly add physical capacity but, conversely enables future management to activate “dormant built-in” Flexibility 4 and, seize new business opportunities, upon market demand. It consists of additional dredging works down to design level of -16.70m CD, at a later phase, in order to enable the terminal to handle Neo-Panamax vessels provided *sine qua non* that:

- Quay wall structures have been designed and built for a final dredging elevation of -16.70m CD (see Flexibility 4) and,
- Quay wall length is also extended either to a total of 600-meters (Flexibility 2) or 400-meters (Flexibility 3).

Table 8 summarizes the different flexible real options in terms of quay wall infrastructure, container handling yards and, dredging works, as well as the corresponding (non-) capability of the terminal to handle Neo-Panamax vessels.

Table 8. Summary of flexibility real-option structural features

| Flexibility | 0 | 1 | 2 | 3 | 4 | 5 |
|---|---------------|---------------|---------------|---------------|------------|------------|
| Quay wall length, meters | | | | | | |
| 300.00 | ✓ | ✗ | ✗ | ✗ | ✗ | ✗ |
| 100.00 | ✗ | ✗ | ✗ | ✓ | ✗ | ✗ |
| 300.00 | ✗ | ✗ | ✓ | ✗ | ✗ | ✗ |
| Total (flexible) expansion, m | 300.0 | 0.0 | 300.0 | 100.0 | 0.0 | 0.0 |
| Container handling yard, Ha | | | | | | |
| 1.50 | ✓ | ✗ | ✗ | ✗ | ✗ | ✗ |
| 4.50 | ✗ | ✓ | ✗ | ✗ | ✗ | ✗ |
| 4.50 | ✗ | ✗ | ✓ | ✓ | ✗ | ✗ |
| Total (flexible) expansion, Ha | 1.5 | 4.5 | 4.5 | 4.5 | 0.0 | 0.0 |
| Extra-depth at quay wall design | ✗ | ✗ | ✗ | ✗ | ✓ | ✓ |
| Extra-dredging to -16.70m CD | ✗ | ✗ | ✗ | ✗ | ✗ | ✓ |
| Non NPX-capable | ✓ | ✓ | ✓ | ✓ | ✗ | ✗ |
| Dormant NPX-capable | ✗ | ✗ | ✗ | ✗ | ✓ | ✗ |
| NPX-capable | ✗ | ✗ | ✗ | ✗ | ✗ | ✓ |
| ADDED throughput capacity, TEUs/year | 30,000 | 90,000 | 90,000 | 90,000 | 0 | 0 |

Source: Excerpted from (Soto Reyes, 2017)

5.2.2. Definition of real option strategies and screening models

After short-listing the real options for incorporating flexibility, it becomes necessary to define the different strategies for the implementation of such selected flexibilities either as stand-alone or as combined alternative responses to the plausible future developments of global and regional developments in containerized trade. Table 9 summarizes the basic descriptions of strategies in terms of the flexibilities incorporated in each instance.

Table 9. Basic matrix of strategies and flexibilities

| Scenarios | Strategy ID | Base Case | Flexi 1 | Flexi 2 | Flexi 3 | Flexi 4 | Flexi 5 |
|---------------------|-------------|-----------|---------|---------|---------|---------|---------|
| Non NPX-capable | 1 | ✓ | ✗ | ✗ | ✗ | ✗ | ✗ |
| | 2 | ✓ | ✓ | ✗ | ✗ | ✗ | ✗ |
| | 3 | ✓ | ✓ | ✓ | ✗ | ✗ | ✗ |
| | 4 | ✓ | ✓ | ✗ | ✓ | ✗ | ✗ |
| Dormant NPX-capable | 5 | ✓ | ✗ | ✗ | ✗ | ✓ | ✗ |
| | 6 | ✓ | ✓ | ✗ | ✗ | ✓ | ✗ |
| | 7 | ✓ | ✓ | ✓ | ✗ | ✓ | ✗ |
| | 8 | ✓ | ✓ | ✗ | ✓ | ✓ | ✗ |
| NPX-capable | 9 | ✓ | ✓ | ✓ | ✗ | ✓ | ✓ |
| | 10 | ✓ | ✓ | ✗ | ✓ | ✓ | ✓ |

Source: Excerpted from (Soto Reyes, 2017)

Once the strategies have been defined, simple “screening models” (De Neufville & Scholtes, 2011) are required to initiate the process of quantifying the value of the preliminarily proposed flexibilities.

Following recommended practice from (De Neufville & Scholtes, 2011; De Neufville, Scholtes, & Wang, 2006), a particular spreadsheet-based and “adaptive” Discounted Cash Flow (DCF) methodology is then implemented as the backbone of the calculations featuring case-specific threshold-and-trigger mechanisms for the “automated” rules for incorporation of flexibilities (De Neufville & Scholtes, 2011), upon monitoring of external environment and drivers, i.e., relevant expected containerized trade, previously calculated by means of dynamic forecasting (De Neufville & Scholtes, 2011).

For each and every strategy, the following key system parameters were assumed:

Demand: Main input is the expected increased containerized trade derived from the Panama Canal Expansion (PCE).

Thresholds-and-triggers:

- Threshold Demand / Capacity ratio equal or greater than 0.95 for two (2) consecutive years, triggers the addition of (modular) handling capacity, i.e., sequential incorporation of flexibilities 1, 2 and 3, as applicable.
- Threshold NPX-traffic / Capacity ratio greater or equal to 1.00 for two (2) consecutive years, triggers the execution of additional dredging works, i.e., incorporation of flexibility 5, as applicable.

Capacity: Initial and sequentially added flexibility-related capacities are summed up to update a yearly total capacity.

Revenues: Calculated upon a composite average handling tariff estimated as USD 156.0 per TEU.

For the purpose of this paper, it is assumed that the revenues of the system are exclusively originated from the tariffs for handling containerized cargo, either for hinterland or for transshipment markets.¹¹

TEU-factor was assumed as to be 1.50, i.e., 50% of the containers are 20-foot equivalent units (TEUs) and 50% of the containers are 40-foot equivalent units (FEUs)

Analysis period: 23-year horizon, from year 2017 until year 2040, inclusive. Fixed interest rate of eight percent (8.00%). Lead time between trigger and physical implementation was set to one (1) year.

The fixed concession lease and fixed costs have been assumed to be USD 250,000.00 and, the operational expenditures (OPEX) have been estimated to be USD 65.00 per TEU.

Finally, Table 10 summarizes infrastructural features and capabilities for the different analyzed strategies.

¹¹ The case study port may also get revenues from providing a diversity of ancillary services, including but not limited to: Concessions to terminal operators, storing of containers, terminal use fees to river barges operators, value-adding services, among others. Nevertheless, estimation of these additional revenues falls beyond the scope of this paper.

Table 10. Infrastructures and capabilities of strategies

| Strategy | 1 | 2 | 3 | 4 | 5 | 6 | 7 | 8 | 9 | 10 |
|--|---------------|----------------|----------------|----------------|---------------|----------------|----------------|----------------|----------------|----------------|
| Quay wall length, meters | | | | | | | | | | |
| 300.00 | ✓ | ✓ | ✓ | ✓ | ✓ | ✓ | ✓ | ✓ | ✓ | ✓ |
| 100.00 | ✗ | ✗ | ✗ | ✗ | ✗ | ✗ | ✗ | ✗ | ✗ | ✗ |
| 300.00 | ✗ | ✗ | ✗ | ✗ | ✗ | ✗ | ✗ | ✗ | ✗ | ✗ |
| Total (flexible) expansion, m | 300.0 | 300.0 | 600.0 | 400.0 | 300.0 | 300.0 | 600.0 | 400.0 | 600.0 | 400.0 |
| Container handling yard, Ha | | | | | | | | | | |
| 1.50 | ✓ | ✓ | ✓ | ✓ | ✓ | ✓ | ✓ | ✓ | ✓ | ✓ |
| 4.50 | ✗ | ✓ | ✓ | ✓ | ✗ | ✓ | ✓ | ✓ | ✓ | ✓ |
| 4.50 | ✗ | ✗ | ✓ | ✓ | ✗ | ✗ | ✓ | ✓ | ✓ | ✓ |
| Total (flexible) expansion, Ha | 1.5 | 6.0 | 10.5 | 10.5 | 1.5 | 6.0 | 10.5 | 10.5 | 10.5 | 10.5 |
| Extra-depth at quay wall design | ✗ | ✗ | ✗ | ✗ | ✓ | ✓ | ✓ | ✓ | ✓ | ✓ |
| Extra-dredging to -16.70m CD | ✗ | ✗ | ✗ | ✗ | ✗ | ✗ | ✗ | ✗ | ✓ | ✓ |
| Non NPX-capable | ✓ | ✓ | ✓ | ✓ | ✗ | ✗ | ✗ | ✗ | ✗ | ✗ |
| Dormant NPX-capable | ✗ | ✗ | ✗ | ✗ | ✓ | ✓ | ✓ | ✓ | ✗ | ✗ |
| NPX-capable | ✗ | ✗ | ✗ | ✗ | ✗ | ✗ | ✗ | ✗ | ✓ | ✓ |
| Max. TOTAL throughput capacity, TEUs/year | 30,000 | 120,000 | 210,000 | 210,000 | 30,000 | 120,000 | 210,000 | 210,000 | 210,000 | 210,000 |

Source: Excerpted from (Soto Reyes, 2017)

5.2.3. Quantifying flexibilities by Monte Carlo Simulation (MCS)

We have identified the sources of uncertainty and their corresponding flexibilities. Later on, we have put together a set of flexible strategies and their corresponding screening models. Such screening models have been set up as having the expected built-in rules for exercising flexibilities as recommended by (De Neufville & Scholtes, 2011).

The main uncertain variable input for the above depicted screening models is the expected volumes of containerized cargo, previously calculated taking into account uncertainties by means of dynamic forecasting (De Neufville & Scholtes, 2011).

Flexible design and adaptive port planning strive to achieve port infrastructures that are enabled to perform successfully in a wide range of plausible futures. Therefore, in order to quantify the value of flexibility within this framework, it becomes necessary to somehow simulate such wide range of plausible futures. For the purpose of this research, this task was performed by means of a spreadsheet-based Monte Carlo Simulation (De Neufville & Scholtes, 2011; De Neufville et al., 2006).

Accordingly, runs of one thousand futures were generated for each of the ten (10) strategies, calculating their performances in terms of Expected Net Present Values (ENPV). Such ENPV array values were processed by standard statistics methods to generate target curves, i.e. the cumulative distribution function versus the “target” or Expected Net Present Value, for every and each of the analyzed strategies.

(De Neufville & Scholtes, 2011) propose that, given a non-flexible case target curve, the implementation of a flexible design should increase the upsides and reduce the downsides of a project by “pushing” the upper curve to the right positive side and “pushing” the lower curve down, respectively.

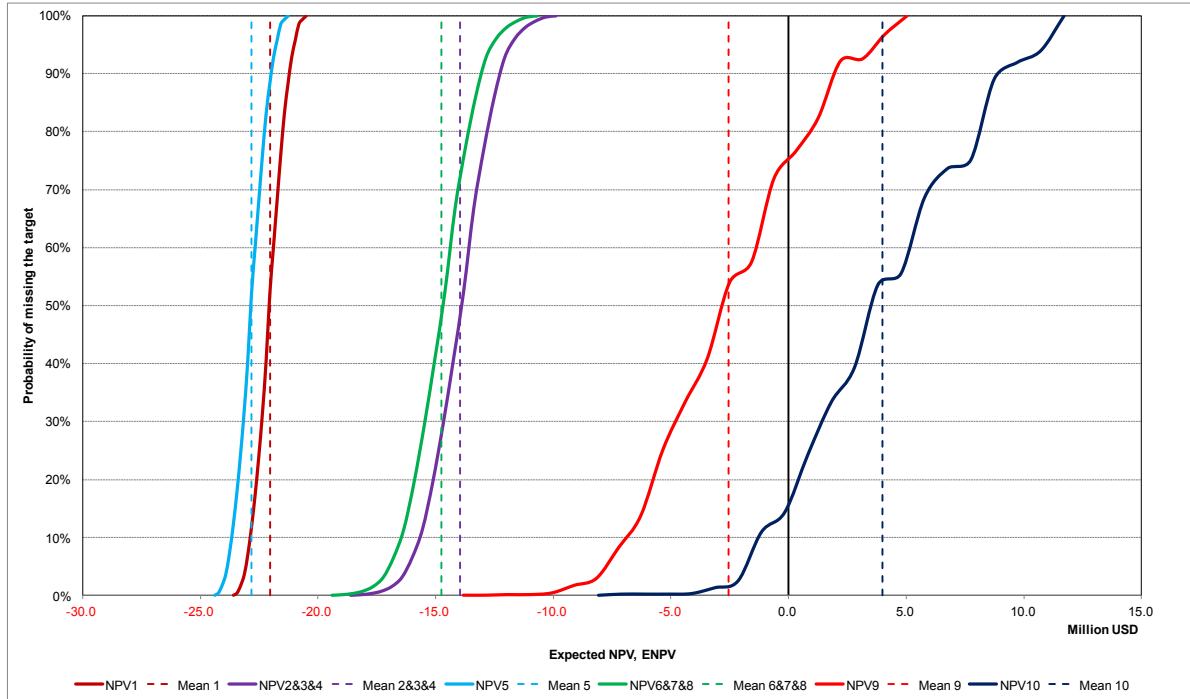
The following sections seek to briefly and concisely explain the processed outputs from Monte Carlo Simulations, to interpret such results and findings in terms of the flexible design theory and, shortlist the most promising alternatives for the case study port in Barranquilla.

Figure 9 showcases simulated target curves for fixed design and flexible strategies, as generated by 1,000-future Monte Carlo Simulation.

5.2.4. Ranking and selection of promising alternatives

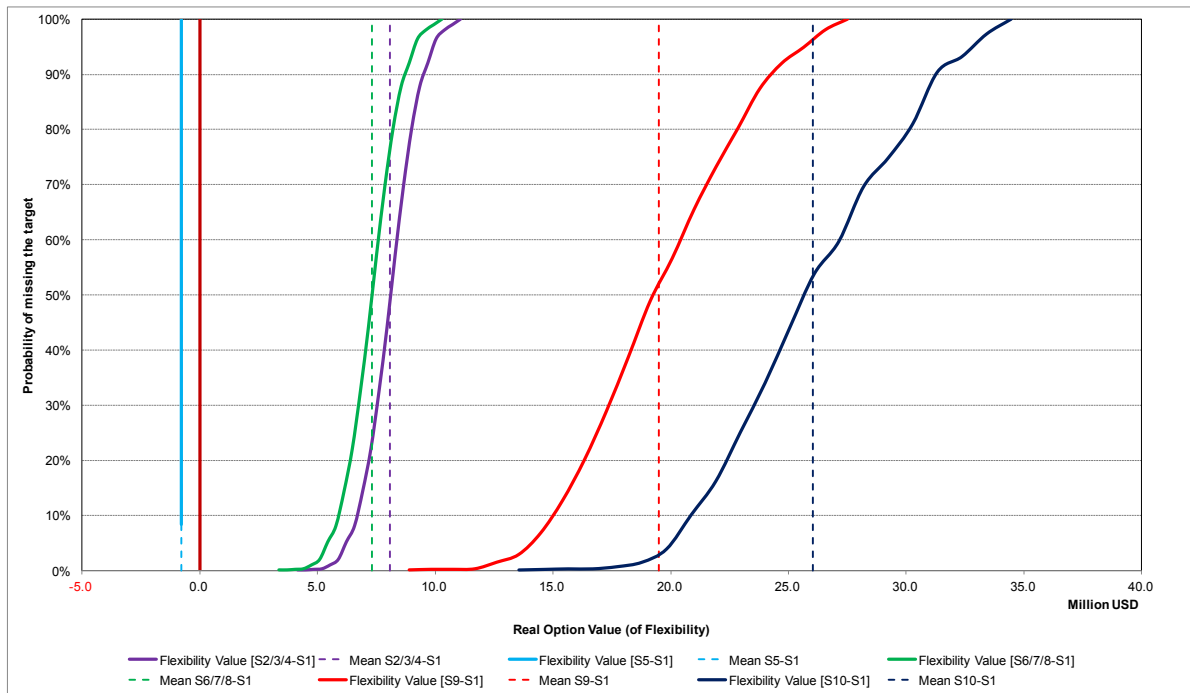
(Rivey, 2007) has concisely defined the term Real Option Value as the difference between the Expected Net Present Value of any given flexibility less the Expected Net Present Value of the traditional fixed base case.

Therefore, after having assessed their individual Expected Net Present Values (ENPV) for each of the ten (10) strategies analyzed, it becomes necessary to assess such Real Option Values as the nine (9) flexible strategies (from 2 to 9) vis-à-vis the non-flexible Strategy 1. Figure 10 compiles the results for such assessments.



Source: Excerpted from (Soto Reyes, 2017)

Figure 9. Simulated target curves for fixed design and flexible strategies



| Flexibility Values | [S2/3/4-S1] | [S5-S1] | [S6/7/8-S1] | [S9-S1] | [S10-S1] |
|------------------------|-------------|----------|-------------|------------|------------|
| Mean, in USD | 8,083,474 | -781,575 | 7,301,898 | 19,502,776 | 26,042,771 |
| Max, in USD | 11,063,946 | -781,575 | 10,282,371 | 27,514,598 | 34,459,608 |
| Min, in USD | 4,138,186 | -781,575 | 3,356,611 | 8,902,564 | 13,562,139 |
| 10% Percentile, in USD | 6,688,408 | -781,575 | 5,906,833 | 15,051,033 | 20,836,378 |
| 90% Percentile, in USD | 9,478,686 | -781,575 | 8,697,111 | 24,282,797 | 31,271,956 |

Source: Excerpted from (Soto Reyes, 2017)

Figure 10. Real Option Values of flexible strategies

To a great extent, Real Options Quantifying reconfirmed the behaviours observed while generating individual simulated target curves for the ten (10) analyzed strategies.

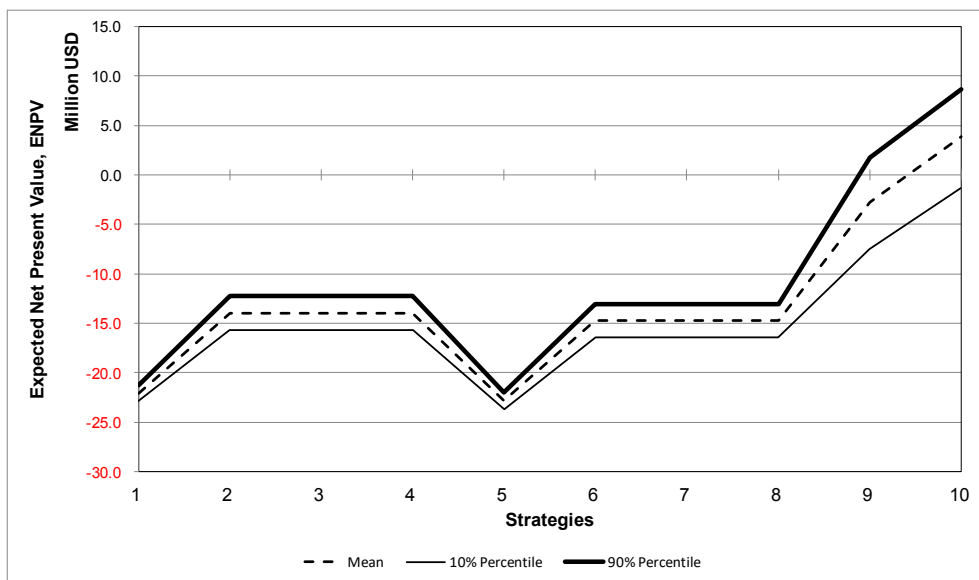
Complementary to the Real Option Quantifying, two useful managerial tools for decision making are the *Upside-Downside curves* and, the so called *Regret Plots* (De Neufville & Scholtes, 2011).

Upside-Downside curves are especially useful to trade off uncertainty, denoted by spread and standard deviation, against Expected Net Present Values (De Neufville & Scholtes, 2011) for the full range of different promising alternatives or strategies.

Regret Plots are useful tools to compare pairs of promising alternatives, upon their reciprocal Real Options Quantifying, i.e., to cross-check how much better –or worse – it is, and in which proportion may a first alternative perform over the second one and vice versa (De Neufville & Scholtes, 2011).

As it can be seen in Figure 11:

- Strategies 1 and 5 show relatively small spreads¹² in the order of USD 1.7 million, with 80% chance of ENPV falling between USD 21.2 million and USD 23.7 million, always negative.
- Strategies 2, 3, 4, 6, 7 and 8, present a moderate spreads of USD 3.4-3.5 million, with 80% chance of ENPV falling between USD 12.3 million and USD 16.5 million, always negative.
- Strategy 9 show a wider spread of USD 8.7 million, with 80% chance of ENPV falling between positive USD 1.8 million and negative USD 7.0 million.
- Strategy 10 has the widest spread of USD 10.1 million, but with 80% chance of ENPV falling between positive USD 8.8 million and negative USD 1.3 million.



Source: Excerpted from (Soto Reyes, 2017)

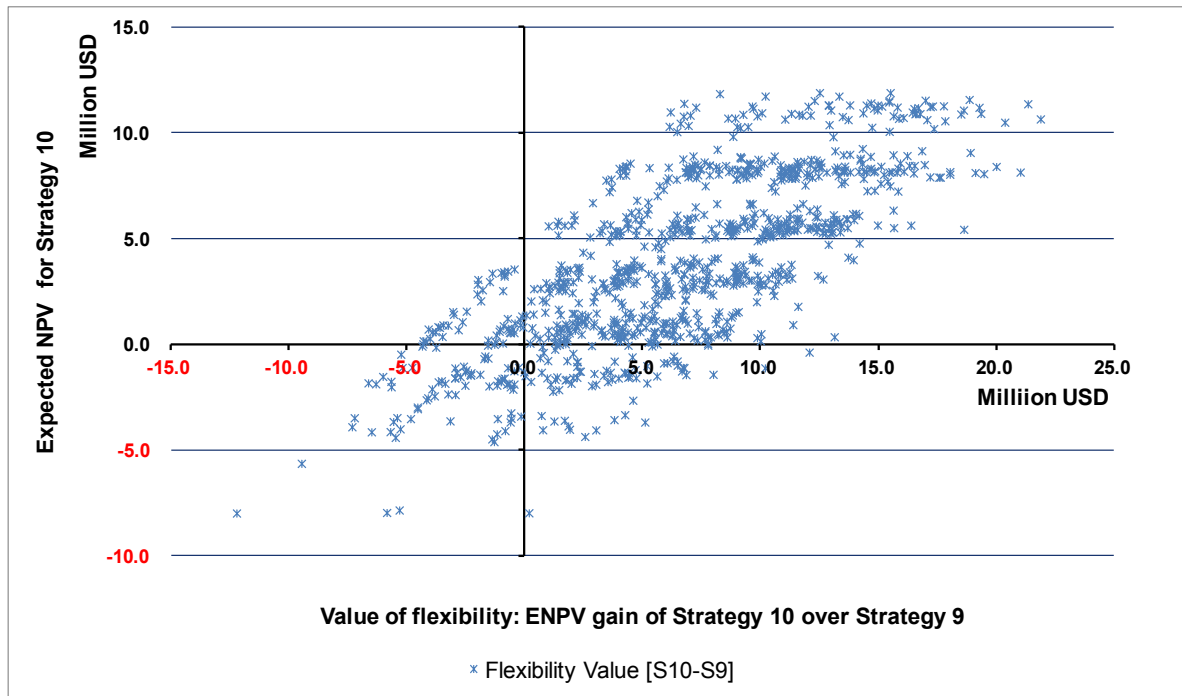
Figure 11. Upside-Downside curves for flexible strategies

At this point, it has been observed that, despite their largest spread and hence larger uncertainties, strategies 9 and 10 appear to be the best performers in terms of Expected Net Present Value, Real Option Value of flexibilities and Upside curves. It may be also observed that both strategies 9 and 10 clearly outperform fixed base case design, i.e., strategy 1.

Therefore, not only strategies 9 and 10 should be shortlisted as the most promising alternatives but, they should also be assessed one against the other in order to provide a rationale and comparative framework for the sake of future decision making.

Thus, the regret plot becomes a useful tool to achieve this objective. More specifically, the plot evaluates the cross-performance of the ENPV for strategy 10 *vis-à-vis* the value of flexibility of strategy 10 over strategy 9.

¹² Spread may be simply defined as the difference between 10-percentile and 90-percentile, for each instance.



Source: Excerpted from (Soto Reyes, 2017)

Figure 12. Regret plot: Strategy 10 versus Strategy 9

Therefore, from Figure 12 the following qualitative analysis items may be pointed out:

- Strategy 10 outperforms strategy 9 in most of the cases, despite some instances where Strategy 10 shows negative ENPV: More than 80 percent of the simulation points are plotted rightward of the Y-axis (1st and 2nd quadrants).
- Strategy 10 yields positive ENPV, even if Strategy 9 would perform better if chosen: Less than 10 percent of simulation points are plotted leftward of the Y-axis and above the X-axis (4th quadrant).
- Strategy 9 performs better than strategy 10 in less than 10 percent of the simulations: Points plotted leftward of the Y-axis and below X-axis (3rd quadrant).

6. CONCLUSION

We should move from risk management to uncertainty management and from static strategic planning to dynamic adaptive planning. Accordingly, uncertainty management and dynamic planning should be deemed as essentially interlinked and contemporaneous. Adaptive port planning is a comprehensive, coherent and integrated methodology to incorporate flexibility into port infrastructure projects.

The Panama Canal expansion will certainly bring cascading impacts on the ports and logistics platforms of the Caribbean region. Initially, this may lead to the decrease of transshipment containers volumes, lost to the new direct services deploying Neo-Panamax vessels. The accelerated scrapping of old Panamax vessels will also have its effects. The eventual capacity constraints of the expanded Panama Canal around year 2030 may however contribute to the recovery of the container transshipment business in the Caribbean port system.

Hence, uncertainty is omnipresent as far as this point, especially when many of the estimations are based on uncertain assumptions of different alternatives for sailing patterns, mergers and alliances, innovative technologies, and global economy's outlooks.

We demonstrated through a specific research case study that incorporating flexible options can result in a more robust project.

Overall, the Adaptive Port Planning methodology, as applied in this research work, proved to be an innovative and yet pragmatic methodology to tackle the somehow tricky task of Quantifying Flexibility, accomplished by means of the simple and transparent tools such as dynamic forecasting, Real Options Analysis and Monte Carlo Simulation.

REFERENCES

- China Britain Business Council. (2017). China Britain Business Council. Retrieved March 27, 2017, from <http://www.cbbc.org/>
- Clarksons Research. (2017). Deployment shifts on the new Locks Transpacific. Retrieved from http://www.clarksons.net/archive/imagelib/2017-07-28_upload_7747907_SIW_1282.png
- De Neufville, R., & Scholtes, S. (2011). *Flexibility in engineering design*. Cambridge: MIT Press.
- De Neufville, R., Scholtes, S., & Wang, T. (2006). Real Options by Spreadsheet: Parking Garage Case Example. *Journal of Infrastructure Systems*, 12(2), 107–111. [https://doi.org/10.1061/\(ASCE\)1076-0342\(2006\)12:2\(107\)](https://doi.org/10.1061/(ASCE)1076-0342(2006)12:2(107))
- Dewar, J. A., Builder, C. H., Hix, W. M., & Levin, M. H. (1993). *Assumption-Based Planning: A planning tool for very uncertain times*. Santa Monica: RAND. Retrieved from http://www.rand.org/pubs/monograph_reports/2005/MR114.pdf
- HKND Group. (2018). Nicaragua Canal Official Website. Retrieved March 23, 2018, from <http://hknd-group.com/>
- IMF. (2016). *World Economic Outlook. International Monetary Fund*. Retrieved from <http://www.imf.org/external/pubs/ft/weo/2016/01/>
- Knight, K. (2008). *The Implications of Panama Canal Expansion to U.S. Ports and Coastal Navigation Economic Analysis*. Retrieved from www.iwr.usace.army.mil
- Kwakkel, J. H., Walker, W. E., & Marchau, V. A. W. J. (2010). Adaptive Airport Strategic Planning. *European Journal of Transport and Infrastructure Research*, 10(3), 249–273. Retrieved from <http://resolver.tudelft.nl/uuid:4de3f8ef-119a-4b2b-bcdf-9a39555577f6>
- Notteboom, T., Ducruet, C., & Langen, P. de. (2010). *Ports in Proximity - Competition and Coordination among Adjacent Seaports. Journal of Transport Geography* (Vol. 18). Burlington, USA: Ashgate Publishing Company. <https://doi.org/10.1016/j.jtrangeo.2009.12.003>
- PIANC. (2014a). *Report n° 158 - 2014 Masterplans for the development of existing ports*.
- PIANC. (2014b). *Report No. 150-2014 "Sustainable ports" A guide for port authorities*. Brussels.
- Puerto Antioquia Website. (2017). Puerto Antioquia - Urabá. Retrieved January 25, 2017, from <http://www.puertoantioquia.com.co/portal/en/>
- Rivey, D. (2007). *A Practical Method for Incorporating Real Options Analysis into US Federal Benefit-Cost Analysis Procedures*. Massachusetts Institute of Technology. Retrieved from http://ardent.mit.edu/real_options/Real_opts_papers/rivey_thesis.pdf
- Rodrigue, J. P., & Ashar, A. (2016). Transshipment hubs in the New Panamax Era: The role of the Caribbean. *Journal of Transport Geography*, 51, 270–279. <https://doi.org/10.1016/j.jtrangeo.2015.10.002>
- Snyder, J. D., Doyle, K., & Toor, P. (2013). The Potential Impacts of the Panama Canal Expansion and Evolving Post-Panamax/Super Post- Panamax Container Ship Routes on Michigan Freight and Hub Logistics.
- Soto Reyes, O. I. (2017). *Adaptive port planning and the impact of Panama Canal expansion on Caribbean ports - A real case study in Barranquilla, Colombia*. UNESCO-IHE.
- Taneja, P. (2013). *The Flexible Port*. Technische Universiteit Delft. Retrieved from <http://repository.tudelft.nl>
- Taneja, P., Walker, W. E., Ligteringen, H., Schuylenburg, M. Van, & Plas, R. Van Der. (2008). Future Scenarios: Implications for Port Planning, 1–21. Retrieved from <http://resolver.tudelft.nl/uuid:c84e0c9c-078c-49ae-91ca-03216bfcaf16>
- The Economist. (2012). The lure of Chilean Valley. *The Economist*. Retrieved from <http://www.economist.com/node/21564589#print>
- Walker, W. E., Rahman, S. A., & Cave, J. (2001). Adaptive policies, policy analysis, and policy-making. *European Journal of Operational Research*, 128(2), 282–289. [https://doi.org/10.1016/S0377-2217\(00\)00071-0](https://doi.org/10.1016/S0377-2217(00)00071-0)
- Woxenius, J., Roso, V., & Lumsden, K. (2004). The Dry Port Concept – Connecting Seaports with their Hinterland by Rail. Retrieved from http://www.pol.gu.se/digitalAssets/1344/1344857_2004_iclsp_dalian_wox-ros-lum.pdf

DESIGN OF THE SCOUR PROTECTION LAYER FOR A BREAKWATER IN AN ESTUARINE ENVIRONMENT

Wim Van Alboom¹, David Martínez¹, Mariana Correa², Mónica Fossati³, Francisco Pedocchi³, Sebastián Solari³

SUMMARY

This paper is a case study covering the hydraulic and geotechnical design of the scour protection of a rubble-mound breakwater designed as a protection of an offshore LNG regasification maritime terminal in the Rio de la Plata, Uruguay.

The paper focuses on the design strategies developed to deal with the challenges raised during the project of this element, due to the high safety standards imposed by the nature of the terminal, and the special hydraulic and geotechnical circumstances involving this marine infrastructure, where different failure modes (of different nature) are definitely interrelated and can be approached from different directions. As a result, a probabilistic approach was proposed to be combined with physical modelling, as well as with the establishment of operational rules related to the inspection and maintenance of the scour protection system.

INTRODUCTION AND PROJECT REQUIREMENTS

A detached rubble mound breakwater of 1,5 km was foreseen as a protection for an offshore LNG regasification terminal in the Rio de la Plata, at two km off the coast of Montevideo, in a fairly uniform water depth of 6 m.



Figure 1: Location of the project (left) and approximate layout of the required scour protection layer (right): breakwater in red; scour protection layer in green.

The project has been developed to assure compliance with high standards for this type of infrastructure. In order to define the general project requirements, the Spanish Recommendations (ROM) have been followed, in particular ROM 1.0-09. In accordance with this recommendation, a maximum joint probability of failure of 1% and a lifetime of 50 years have been considered, both associated with ultimate limit states (ULS). The probability of failure in ULS has been split up between the different failure modes taken into account for the design.

¹ SECO BELGIUM S.A., Belgium

² Gas Sayago S.A., Uruguay

³ Facultad de Ingeniería - Universidad de la República, Uruguay

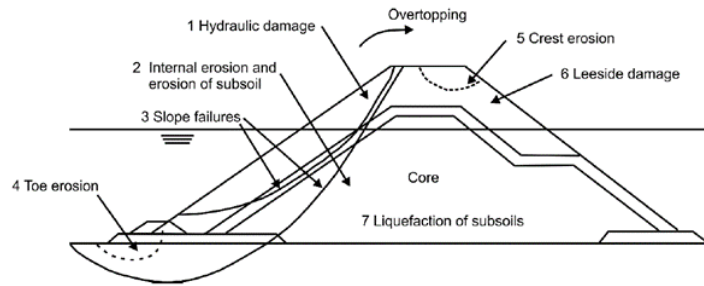


Figure 2: Standard Rubblemound breakwater failure modes (source: The Rock Manual)

The design methodology proposed in the Recommendations for Maritime Works (ROM, Puertos del Estado, Spain) differentiates failure modes between hydraulic and geotechnical on one hand and between principal and non-principal on the other hand. In general, non-principal failure modes can be treated in the design so that negligible failure probabilities can be achieved under moderate costs.

In our case, some of the failure modes shown in Figure 2 were explicitly addressed in the failure analysis of the breakwater as principal failure modes, whereas some others were treated as non-principal failure modes through safe rules of practice (liquefaction, e.g.). The design of the scour protection in front of a breakwater is usually performed assuming a non-principal hydraulic failure mode. However, the special combinations of shallow waters, severe currents and moderate waves, together with very low bearing capacity soils waves presented in the mid Río de la Plata estuary, make that scour protection of this structure should be designed assuming a principal hydraulic failure mode that in turn affects geotechnical failure modes. Additionally, the cost of reducing the failure probability of the scour protection, as a failure mode, to negligible levels is very high.

SITE CONDITIONS

Geotechnical conditions

The Río de la Plata is the confluence of various (and long) South American rivers, full of sediments, that have been deposited all along the estuary during thousands of years. At the location of the project, this sedimentation generates a shallow platform with a few meters of mud, resting over a sequence of alternating very soft cohesive layers and granular deposits, with variable thicknesses but slightly improving in capacity with depth until -20 m to -30 m Local Chart Datum, resting on a very to moderately weathered rock.

In these adverse geotechnical conditions an intensive geotechnical campaign covering the full extents of the project was performed, including several cone penetration tests and boreholes, from which many samples were recovered to allow for an important set of laboratory tests.

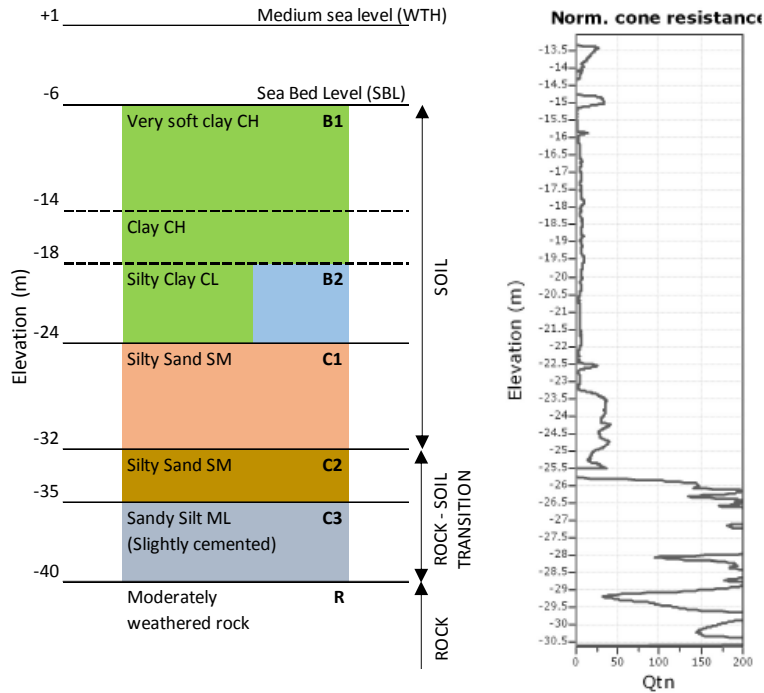


Figure 3: Indicative ground model (left) and typical CPT signal (right)

The results of this campaign allowed for a reliable characterization of the estuary soils and demonstrated the relevance of the very soft cohesive layers (B1 and B2 in figure 3) for the geotechnical design. The extremely low strength properties and the large thicknesses of these layers make them critical in terms of geotechnical stability and confirmed the early stage decision taken for the project to substitute them largely by an extensive backfill of sand (see figure 8 below).

During the detailed interpretation process for the soil properties, care was taken not to mix properties originating from different types of tests. Due consideration was given to use the type of parameter which was judged to be suitable, taking into account the applicable stress state in the actual geotechnical failure mechanism studied, in analogy with the principles below:

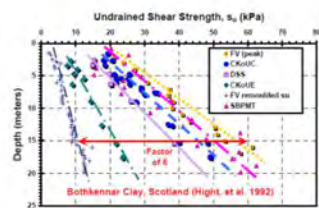


Fig. 7. Various measured undrained shear strengths for well-documented Bothkennar clay, Scotland (data from Nash et. al 1992 and Hight et al. 2003)

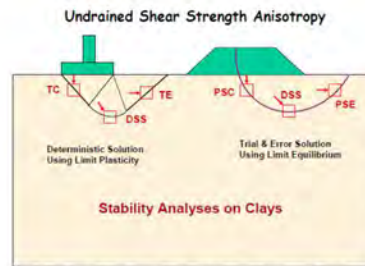


Fig. 8. Applicability of strength modes to foundation and embankment stability

Figure 4: Principles for geotechnical failure mechanism (Source: Paul W. Mayne, 2008)

An increase in the reliability of the soil parameters in this poorly known estuary was achieved by their determination from varied sources (e.g. the execution of SPT's in close proximity to CPT's). In respect of the actual type of parameter to be used for the particular failure mechanism under consideration, due care has been taken to evaluate mechanical properties from laboratory tests as well as from correlations with field testing. In particular, the undrained shear strength of the principal clays, apart from its triaxial determination, has been deduced from correlations with CPTu registration (Mayne, 2008), in an attempt

to find reliable cautious values. The work of Paul W. Mayne, Larsson and Ladd has also been used to incorporate Bayesian knowledge of similar clay materials encountered in other parts of the globe (and their registered coefficients of variation).

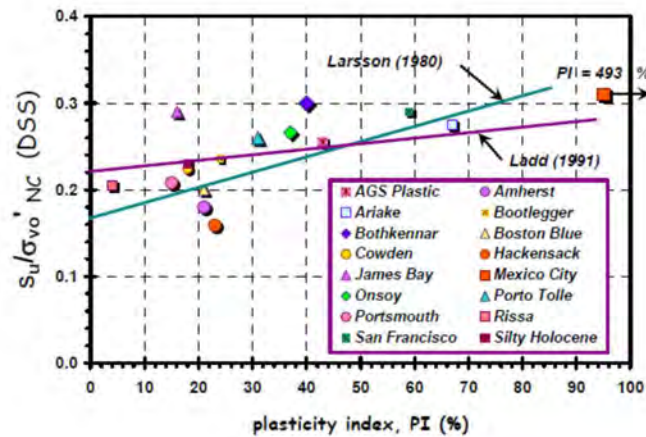


Figure 5: Principles for geotechnical failure mechanism (Source: Paul W. Mayne, 2008)

Maritime climate

The most relevant environmental agents for the design of the breakwater are those related to the maritime climatic: water level, currents and waves. Although the wind is not treated here as an agent acting upon the breakwater, it was indirectly evaluated, as a source of the rest of the agents. In the case of Montevideo in particular, the three mentioned agents have some degree of statistical dependence, as waves depends on local wind conditions (see e.g. Solari et al. 2014) and sea level and currents depends on local and regional wind conditions (see e.g. Santoro et al. 2011). In addition to this, in some cases statistical extrapolation of extreme condition leads to physical unfeasible values; thus it was required to establish physical limits for storm surges and waves taking into account local depth and fetch characteristics.

Water Levels

Total water level in Montevideo is influenced by both astronomical tide and storm surges. While the range of the astronomical tide is fairly small, storm surges are relatively strong due to the shallow, funnel-shaped mouth of the Río de la Plata and the wide and shallow continental shelf (see Santoro et al. 201X), so that in some cases the water level at the moment of high tide can be lower than the mean low water level.

Total water level was analyzed based on local long-term records as well as on a water level hindcast. Despite the limited tidal range usually present in the project location, the statistical analysis performed for large return periods (in agreement with the safety level requirements) led to design water levels ranging from -2.5 m to +6.5 m.

Currents

Storm surges do not only influence the water level significantly, but also affect the currents. The current pattern in the Río de la Plata is quite complex, affected not only by the astronomical tides, storm surges and local wind, but also by rivers discharges and salinity gradient and stratification. Characterization of the design current values in the area of study was obtained through downscaling of a regional hindcast, calibrated and validated with in situ data. Finally, design current values have been calculated from a statistical analysis from modelling data.

The presence of the breakwater results in slight adaptations of the current pattern in the vicinity of the toe, leading to high speeds, up to 4,5 m/s in the seaside for an approx. 1000 years return period, but much lower in the sea side.

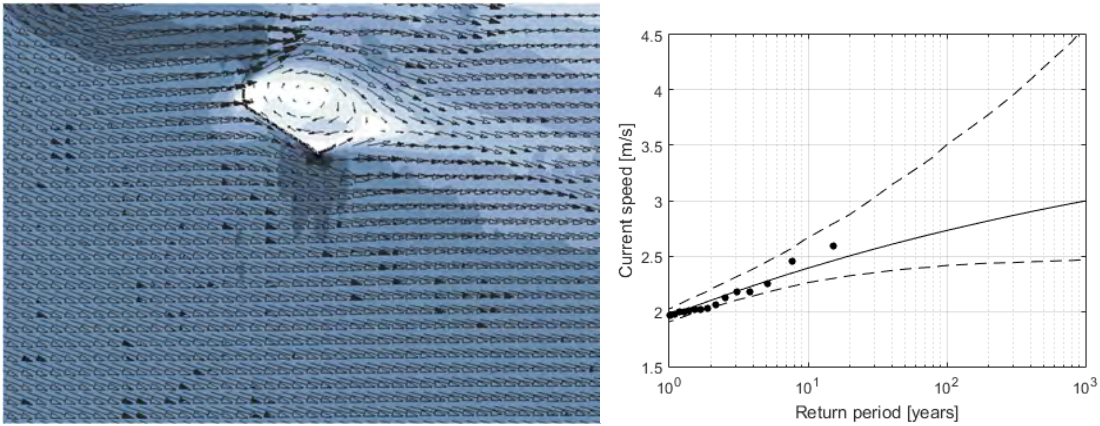


Figure 6: Example of ebb currents field (left) and currents extreme regime near southern elbow.

Waves

The extreme waves that reach the terminal are conditioned by the length of the generation area (fetch), wind intensity and water depth. There is no real fetch limitation for the SE direction, however shallow waters dissipate most of the swell and limits wave growth. Therefore, wave height gradually decreases along the estuary entrance towards the port. On the other hand, the maximum wave heights at the site might be limited by wave breaking by depth.

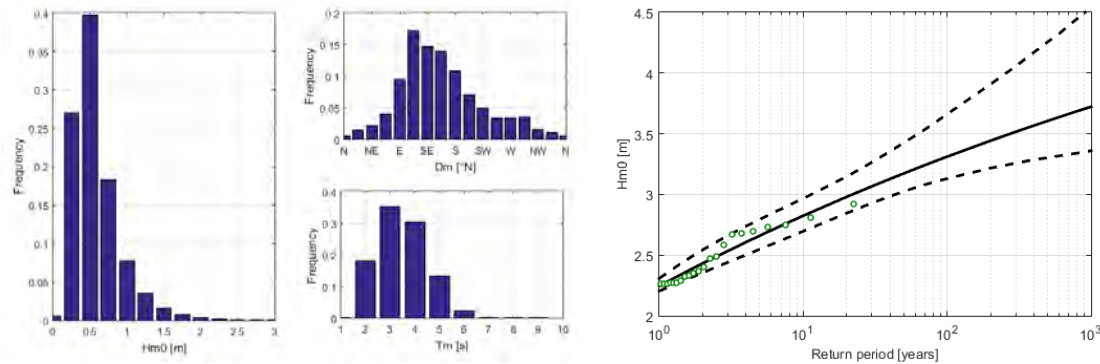


Figure 7: Wave climate: histogram of significant wave height (left), mean wave direction (center top), mean wave period (center bottom) and significant wave height extreme regime (right).

THE PROJECT

Breakwater design. Typical cross section

As expressed above, the project location is subject to very specific geotechnical conditions. The low strength properties of the top layers of the soil have made for a geotechnical design which is very much governed by a global sliding failure mode. In order to improve the geotechnical conditions, it was decided to carry out a global replacement of the soft soil.

The volume of the soil replacement has therefore been a critical parameter in the successful development of the project. From the transverse section presented below (figure 8), the large extent of the sand replacement relative to the section of the breakwater can be appreciated and its economic impact on the project can be understood.

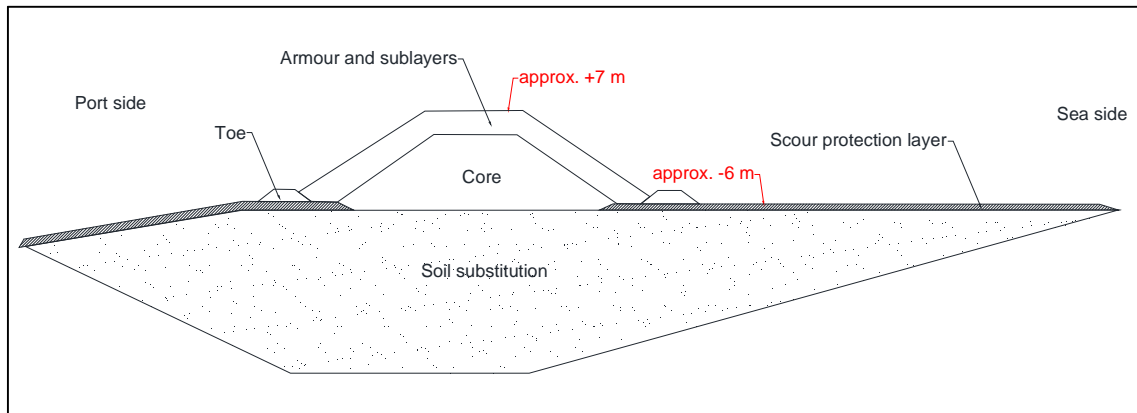


Figure 8: Outline of a typical cross-section of the breakwater

Structurally speaking, the projected breakwater is a conventional rubble mound with an important support function for the toe berm and rock underlayers separating the armour layer from the core. As a main protection against wave action at the sea (river) side, a single armour layer consisting of concrete Accropode units has been design for. The leeside slope of the breakwater is to be protected with quarry units.

Due to the effect of vessel propellers, the back armour and the bottom protection layers have been analyzed thoroughly, as well.

Geotechnical design. Overall stability

The verification of the overall stability was used as a design tool for the dimensioning of the sand replacement. Therefore, the modelling of the global sliding failure modes was carefully assessed.

Overall stability has been verified with the use of different software, such as finite element PLAXIS and GSTABL (rigid body sliding). The impact of using one method over the other has been addressed with parallel calculations for similar design conditions. From a dredging point of view, and due to the permanent sedimentation in the project location, the presence of soft mud remaining in the bottom of the trench, underneath the sand replacement, has been taken into account. It was perceived that the presence of such layers (difficult to exclude completely from the construction process) lead to a significant reduction of the safety factors.

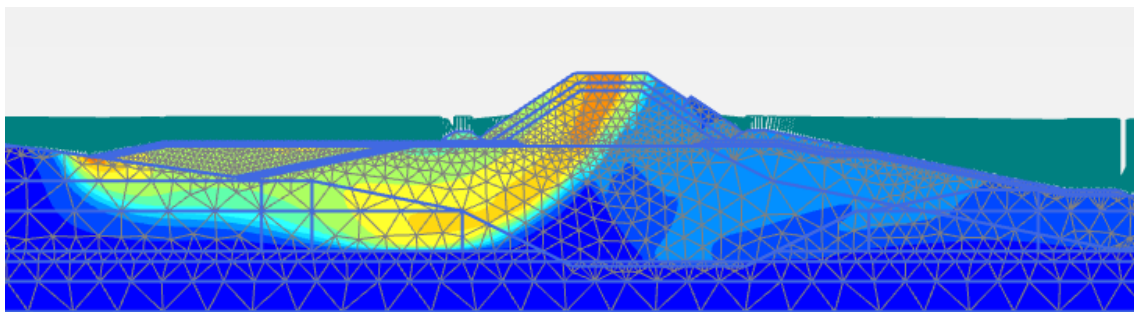


Figure 9: Overall stability Failure Mechanism

As shown in figure 8, the typical failure cross the main body of the breakwater, goes along the sand replacement and the deepest soft clay layers, ending at around 100 m far and more from the axis of the breakwater. This extremely large failure could affect critical structures of the terminal (piping, service platform, main jetty, etc).

Additionally, settlement analyses was carried out with the use of PLAXIS. Settlements in the natural soil and the sand layers occur during the construction and post-construction period, with typical values above 1.5 m.

In the early stages of the project, a semi-probabilistic design was performed for the overall stability (general sliding). As indicated in the 'site conditions' paragraph, attempts were undertaken to reduce the coefficient of variation of the mechanical soil properties. On top of that, the spatial variability of the material properties in the principal clays has been positively affected by the application of normal consolidation laws with depth (physical laws). Finally, the model uncertainty was reduced by testing it to both rigid block sliding algorithms, as well as numerical modelling. Validation of the models was performed for geotechnical problems with analytically known solutions (as described in the Spanish ROM).

Based on all of the above, the geotechnical stability verification was reduced to achieving a standard partial factor on the shear properties of the clays and the sands. Because it was hard to believe that the use of this unique coded factor would result in the target failure probability for the particular problem studied, a variation analysis of the soil properties was performed in accordance with the principle explained in the Spanish ROM. An example of such a variation analysis for a breakwater founded over a sand replacement (with primarily superficial failures) can be found below. Such approach allows to conclude on the importance of the different parameters in the physical problem, hence the importance of the accuracy in their determination.

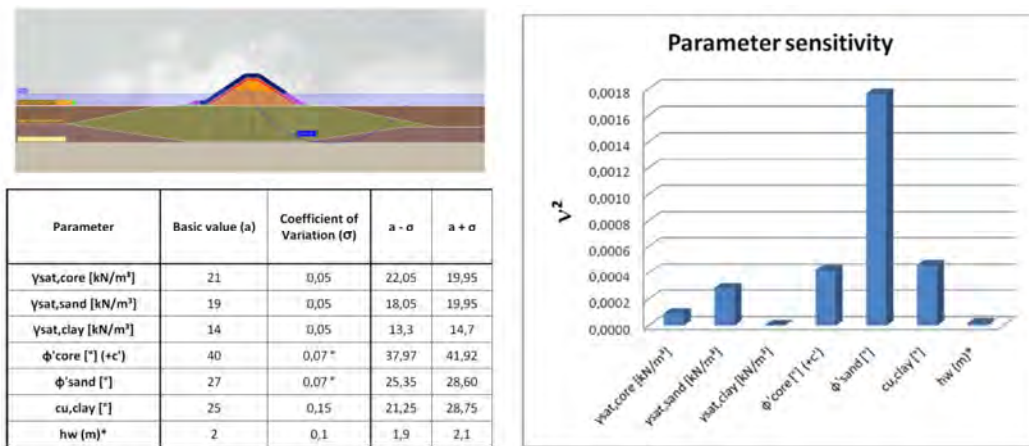


Figure 10: Example sensitivity analysis (ROM05.05 – 3.3.10 Reliability in Geotechnical Engineering)

Hydraulic design

A Preliminary Hydraulic Design of the breakwater was performed in a Level I approach, with the use of standard formulations (Hudson, Van der Meer, etc.) in their deterministic version.

The final hydraulic design has been performed according to the Advanced Design methodology envisaged by the Spanish Recommendations for this kind of structure: 1st) Level I design, 2nd) Level III verification; 3rd) Possible optimization in light of Level I and III results.

Level III verification entails a Monte-Carlo technique to some representative Preliminary Hydraulic Design cross-sections along the breakwater. The verification procedure follows the Spanish Standards (Recommendations for Maritime Works, ROM 1.0-09). In each cross-section, the considered hydraulic failure modes are studied.

The verification equations for each failure mode (the same as used in Level I approach), are implemented now in the probabilistic version (including the random uncertainties of the fit) and the exceedance of the thresholds or the number of failures is evaluated. In view of the low failure probabilities allowed for, special care was taken with the use of the verification or design equations within their limits of application.

Here we have to say that the hydraulic design (Level I plus Level III) involved the design of all elements, including the scour protection, in order to deal with the failure probability assigned to these failure modes. But we will focus on this design in the following sections.

THE SCOUR PROTECTION DESIGN

In order to warrant the lasting presence of the sand replacement in the stability of the breakwater, taking into account the large currents, an extensive scour protection around the breakwater was designed for to exclude that the overall stability of the breakwater would be compromised. The designed strategy ensures that the sand volumes taken into account in the geotechnical stability remain present during the lifetime of the structure. Hence a coupled hydraulic and geotechnical design was proposed as a design solution of the breakwater.

As expressed before, in the context of the design methodology proposed in the Recommendations for Maritime Works (ROM, Puertos del Estado, Spain) the design of the scour protection in front of a breakwater can be performed assuming a non-principal hydraulic failure mode, as it is usually possible to achieve negligible failure probabilities for this element under moderate costs.

Nevertheless, the special conditions of the mid Rio de la Plata estuary make that scour protection of the projected breakwater off the coast of Montevideo, should be designed assuming a principal hydraulic failure mode that in turn affects geotechnical failure modes.

This is a rare situation for which there are few references in the accumulated experience of breakwater design. Perhaps the most relevant precedent is the design and construction of Zeebrugge breakwaters (De Rouck et al. 2008). Moreover, local knowledge on the actual port of Montevideo is of little use given that current breakwaters were built more than 100 years ago (Nieto, 2012).

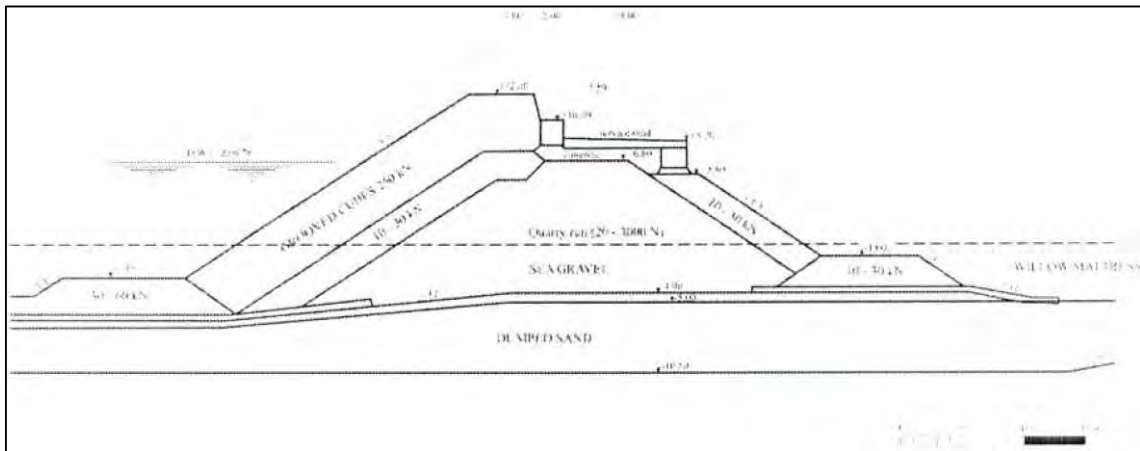


Figure 11. Cross section of the basic design of the breakwater. Zeebrugge Harbour.
Source: Julien De Rouck et al. 2008

Conceptual approach to the design

In the design of the scour protection, the geotechnical and hydraulic challenges come together.

A loss of hydraulic stability of the scour protection layer, due to the combined action of currents and waves, can eventually lead to erosion of the sand replacement in front of the structure. This erosion means a loss of material in a place where is needed to ensure the global geotechnical stability of the breakwater against global sliding failures. Therefore, a clear interaction between the hydraulic failure mode "loss of hydraulic stability of the scour protection layer" and the geotechnical failure mode "global stability of the breakwater", is presented, which cannot be performed decoupled.

The way to deal with this coupled situation is not simple. The methodologies used for hydraulic and geotechnical verifications are fundamentally different, because the temporal scales in which the failures develop, the uncertainties involved in their approach and the analytical and numerical models used in each case are different: on one hand, probabilistic verification techniques are usually an appropriate tool for approaching complex problems of great economic impact and are quite well developed for the verification of hydraulic failure modes; on the other hand, they are not so well developed for the verification of geotechnical failure modes (see e.g. Phoon et al., 2016).

The need of allowing for an unneglectable failure probability of the scour protection (in order to optimize the cost of this element) obliges to make some decisions to lower the failure probability of a geotechnical failure mode (as total failure probability is limited). Therefore, a possible approach to the design is to deal with the hydraulic design calculations according to a certain failure probability, but limiting at the

same time the geotechnical failure induced by the scour by introducing physical limits to the geometry in the geotechnical calculations. This idea will be further explained in the 'Approach to the final design' subsection below.

Calculation and verification of the hydraulic failure modes

From the point of view of calculation and verification of the hydraulic failure modes there are at least three challenges: (1) Multivariate characterization of all the random variables involved in the verification; (2) Determination of a verification equation that relates all these variables at the initiation of damage; and (3) Physical modelling of the problem. These three challenges are described below.

First, the multivariate characterization of all the random variables involved in the verification, namely: wave (incident wave height, direction and period), currents (depth averaged intensity and direction), and sea level. Although usually assumed deterministically, two additional coefficients must be added to this list of random variables: the depth limited wave breaking coefficient and the breakwater reflection coefficient. The intensity of the bottom stresses in front of the structure, responsible for triggering the "loss of hydraulic stability of the scour protection layer", will depend on all these variables. To properly describe statistical dependencies among all these variables, as well as their time evolution during storm events, requires fitting and validating a large set of ad hoc statistical models (see e.g. Li et al. 2014).

Several equations have been derived for the design of protection under wave loads (Hudson, Van del Meer, Pilarczyk). These equations come from the Marine Engineering environment and are quite well developed for rock stability in slopes, toe protection of breakwaters, etc, taking into account some relevant effects related to the interaction water-structure, as braking wave action, reflection or energy dissipation. Other kind of equations are derived for the design of protection against current loads (Pilarczyk et al., 1998), or for sediment transport calculations in a River Engineering environment (du Boys, Van Rijn, Bagnold, Einstein, Parker). As a consequence, these formulations have been developed mainly for the design of revetment and protections in rivers, therefore adapted to the particularities of those conditions (soil material, characteristics of the flow, etc).

Currently there are no accepted equations for the design verification of scour protection layers subjected to the combined action of currents and waves (incident and reflected, possibly depth limited, i.e. highly non-linear). The most similar situation for which there are accepted design equations is the start of the movement of the sand under combined wave-current flow (e.g. Soulsby, 1997). This approach is limited, because it only quantifies whether grains are stable or not. The principle of this method is the calculation of the combined bed shear-stress (τ_m ; τ_{max}) from the values obtained for the bed shear-stresses which would occur due to the current alone (τ_c) and to the wave alone (τ_w), respectively.

$$\tau_{max} = [(\tau_m + \tau_w |\cos \emptyset|)^2 + (\tau_m |\sin \emptyset|)^2]^{1/2} \quad (1)$$

$$\tau_m = \tau_c \left[1 + 1,2 \left(\frac{\tau_w}{\tau_c + \tau_w} \right)^{3,2} \right] \quad (2)$$

This bed shear-stress is then compared to the critical bed shear-stress for start of movement, estimated based on the Shield's parameter and the particle size of the present material.

$$\theta_{cr} = \frac{\tau_{cr}}{g(\rho_s - \rho)d} \quad (3)$$

But all this calculations process are strongly governed by different parameters, as the so-called bed roughness length, which has been derived for sediments as sand or gravel, outside the domain of the size of the usual scour protection in shallow waters.

Obviously the use of these equations in the design of the scour protection involves great uncertainties (on top of the uncertainty already inherent to sand and gravel transport formulations), which must necessarily be taken into account in the final design.

Third, given the uncertainties inherent to the design process, it is common practice to perform reduced scale model test of a breakwater in a hydraulic laboratory prior to its construction. Physically modeling the interaction of waves, currents and a partially reflecting structure, and its effect on the scour protection

layer, presents great challenges for both its implementation in the laboratory and the interpretation of the obtained results, in the latter case mainly due to scale effects.

The implementation of wave and current conditions in a physical model implies the availability of special tank installations, not only to reproduce both agents separately (and accurately), but also to avoid undesirable effects due to their interaction. This interaction leads to difficulties in the determination of the real conditions that are being simulated (when compared with the combined theoretical conditions). Although many tanks exist where water waves can be simulated in 3D conditions, not so many tanks are prepared to combine 3D waves and 3D currents, with the minimum required scale (necessary for the simulation of bed mobility problems), and with the capacity to produce the minimum required current speed.

For the case of the scour protection in front of a breakwater, we are faced with the complexity of simulating (almost) perpendicular water waves and currents, parallel to the breakwater. In this situation, special attention must be given to the generation of the currents, in order to: obtain the right current speed profile at the location of the structure (target zone); avoid reflections in the adjacent structure; and avoid perturbation in the 3D water wave pattern (due to losses of energy in the surrounding area of the target zone). The design of the inlet and outlet structures as well as the splitter walls (both for the current flow and the water wave generation) are certainly crucial for this purpose.

Approach to the final design

In dealing with the above challenges the following approaches were thoroughly discussed during the preparation of the project:

To reduce the probability of failure of both failure modes independently to very low levels, in order to move them away from the failure tree of the principal modes. It was proven that for the circumstances of this project this approach was not feasible, due to: incompatibilities with construction planning, and the high costs involved in the protection. The use of higher caliber material in the scour protection easily creates construction difficulties in view of the respect of the filter rules towards the soil material. In order to accommodate construction constraints, for the design of the filters, the application of open filter layers as well as the installation of geotextiles (e.g. fixed to willow mattresses, a common practice in the Netherlands and Belgium cfr. Verhaeghe et al. 2010) and classical filter layers have been discussed.

To artificially separate geotechnical and hydraulic failure analysis by introducing the concept of a minimum geometry in the geotechnical calculations, based on alarm lines, as was the case for the breakwater in Zeebrugge. Such approach needs to be made consistent with the inspection and maintenance strategy applicable for the project. A first alarm line defines a level at which the operator can start the mobilization process of the equipment that is required to safeguard the situation before the ultimate limit line is exceeded. This second alarm line should correspond with the level of safety that has been required for this geotechnical failure mode. From the operation point of view it is essential that clear alarm line drawings are developed to support the inspection and maintenance strategy for a project.

Even though the second approach requires systematic inspections (and possible also maintenance) during the useful life of the structure, it allows for the economical optimization of the solution. In particular, it allows for setting higher failure probability for the hydraulic failure mode. In return, it requires careful estimation of failure rate as well as failure consequences (as required for the estimation of the time available for intervention after hydraulic failure of the scour protection).

Hydraulic design and verification through Level III methods

Here a simplified version of the Level III verification of the hydraulic failure mode "loss of hydraulic stability of the scour protection layer" is introduced. The objective is to show the most relevant difficulties encountered and to highlight some relevant results.

A Level III Monte Carlo simulation method is based on the simulation of several useful lives of the structure and on the verification of the failure modes for each of the simulated useful lives. Then, the expected failure probability for each failure mode is estimated as the number of useful lives that result in a failure of the given mode over the total number of useful lives simulated. Although conceptually simple, this approach requires:

- (1) A statistical model for the random simulation of extreme multivariate conditions.

- (2) A state equation for the verification of the failure mode.

In both cases uncertainties in models and equations must be taken into account.

In this study case the statistical model developed for the simulation of extreme conditions is as follows:

- (1) Available time series of maritime agents are used to generate a time series of shear stresses. This series is used to identify points in time where the shear stress has local peaks, allowing for the identification of a multivariate time series with the combinations of maritime agents leading to extreme shear stresses (see Mazas et al. 2017 for an approach of identification of events based on one variable that measures the combined effect of several agents).
- (2) A marginal mixture probability distribution is fit to every variable, composed of the empirical distribution function up to a conveniently selected threshold, chosen following Solari et al. (2017), and a generalized Pareto distribution over the threshold. These marginal distributions are used for transforming the original variables to standard normal variables (see e.g. Solari and Van Gelder 2010).
- (3) A mixture of three Multivariate Gaussian distributions is fitted to the standard normal variables.
- (4) A number of extreme events is simulated assuming it follows a Poisson distribution.
- (5) For every extreme event the mixture of Multivariate Gaussians is used for the simulation of a new set of standard normal values.
- (6) Standard normal values are transformed to original variables using the marginal mixture distributions.

By using bootstrapping techniques the uncertainties arising from the statistical model are properly accounted for; i.e. resampling with replacement from the original data for every useful live before performing steps (1) to (6).

Then, for every simulated extreme event, the occurrence of the failure mode is verified. To this end, the maximum wave and current shear stress was estimated following Soulsby (1997). However, how to include uncertainties in this case is not straightforward as no recommendation is given in the references (possibly due to the fact that these formulation were not developed for structural design, possibly due to the great uncertainties involved when dealing with sediment transport formulation, as is the case here). Thus, three approaches are implemented and compared:

- a. To perform a verification using only expected values (i.e. no uncertainty is taken into account in the verification equation).
- b. To use a constant Coefficient of Variation (CV) for the estimated mean diameter of the protection layer required to withstand each storm event.
- c. To use a constant CV for the shear stress estimated at each storm.

In order to implement approaches (b) and (c), CVs are required. Based on Soulsby (1997), where it is stated that typical uncertainty in the estimation of mean grain size is 20% and that differences between results obtained from different methods available for estimation of shear stresses are less than 50%, we assumed that CV is in the range 0.1 to 0.2 in the case of mean grain size, and in the range 0.2 to 0.5 in the case of shear stresses.

Results obtained for one section of the breakwater (other than the change in alignment) are shown below. First, it was verified that the simulation methodology was capable of properly reproducing the observed climate. Figure 12 shows a comparison of the empirical bivariate distributions of significant wave height and total sea level (left) and significant wave height and current speed (right) obtained with the original data (in colors) and with the data simulated for one useful life (black lines). It is noted that in both cases the simulated data reproduces fairly well the behavior of the observed data. Then, mean weight (W50) required for achieving different failure probabilities were calculated, under the three hypotheses listed above. Results are summarized in Table 1. It is noted that the effects of including the uncertainty of the verification equation are significant, almost tripling required rock weight in this particular case.

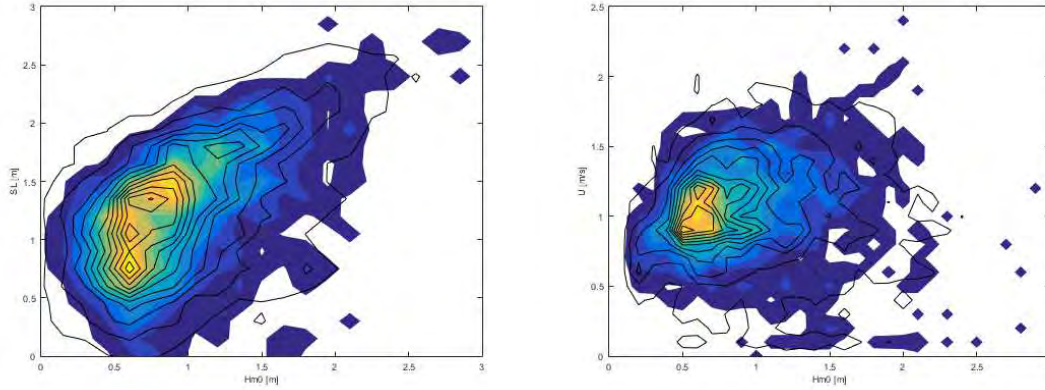


Figure 12 – Empirical bivariate distribution of significant wave height and total sea level (left) and significant wave height and current speed (right). Original data in color and simulated data (one useful life) in black continuous lines.

Table 1 – Mean weight required for assuring different failure probabilities under the different working hypothesis.

| | W50 [kg] | | |
|--------------------------|-----------|-----------|-----------|
| | Pf = 0.5% | Pf = 0.2% | Pf = 0.1% |
| No Uncertainty | 13 | 20 | 29 |
| CV = 0.2 in D50 | 19 | 31 | 46 |
| CV = 0.2 in shear stress | 31 | 53 | 79 |

CONCLUSIONS

At geotechnical level, the preparation of the project has shown some of the possibilities to reduce uncertainty in the design processes and to increase reliability through reliability based design. Deep understanding of the physical failure processes and the geotechnical tests (lab as well as in situ) remain necessary in order to achieve that.

Regarding the verification of the hydraulic failure modes, the lack of a widely accepted verification equation, with properly quantified uncertainty, poses a significant challenge when it comes to the estimation of the failure probability. The different methodologies considered (ad hoc) for the incorporation of some degrees of uncertainty in the verification result in such a spread of results that physical modelling of the work is practically unavoidable. This, however, is not a simple task and can only be performed properly in a limited number of experimental facilities around the world.

From a global point of view, the introduction of the concept of “minimum geometry”, that ensures geotechnical stability while allowing for larger failure probabilities of the scour protection, proved to be useful for tackling the problem. However, this approach open new questions that remain to be addressed; in particular, under this approach it becomes more relevant to know the expected evolution of the scour once the scour protection layer start to mobilize, that is, it becomes particular relevant to know the scour damage evolution, as this evolution conditions the time available for performing surveys and repairing works. Again, to address this issue the available analytical and numerical tools have such big uncertainties that the only feasible solution would be to resort to scale models or take a conservative approach when defining the “minimum geometry”.

References

- CIRIA (2007), The Rock Manual, The use of rock in hydraulic Engineering, 2nd edition
- de Rouck, J., et al. (2008). Zeebrugge outer harbour: the evolution of scouring over the past 20 years. 31st ICCE, International Conference on Coastal Engineering. Hamburg, Germany.
- Li, F., van Gelder, P. H. A. J. M., Ranasinghe, R., Callaghan, D. P., & Jongejan, R. B. (2014). Probabilistic modelling of extreme storms along the Dutch coast. Coastal Engineering, 86, 1–13.
- Mayne P.W. et al. (2008), Piezocone profiling of clays for maritime site investigations, 11th Baltic Sea Geotechnical Conference, Gdansk, Poland.
- Mazas, F., & Hamm, L. (2017). An event-based approach for extreme joint probabilities of waves and sea levels. Coastal Engineering, 122, 44–59.
- Nieto, A. (2012). Montevideo's port breakwaters restoration. 8th PIANC-COPEDEC, Conference on Coastal and Port Engineering in Developing Countries IIT Madras, Chennai, India
- Phoon, K.K. et al. (2016). Some observations on ISO2394:2015 Annex D (Reliability of Geotechnical Structures). 2016 Elsevier Ltd.
- Puertos del Estado. Spanish Recommendations for Maritime Works (Recomendaciones Obras Marítimas, ROM)
- Santoro, P., Fernández, M., Fossati, M., Cazes, G., Terra, R., & Piedra-Cueva, I. (2011). Pre-operational forecasting of sea level height for the Río de la Plata. Applied Mathematical Modelling, 35, 2462–2478.
- Solari, S., Teixeira, L., & Piedra-Cueva, I. (2014). Stochastic extreme waves generator for the mid Rio de la plata estuary northern coasts. In Proceedings of the Coastal Engineering Conference (Vol. 2014).
- Solari, S., Egüen, M., Polo, M. J., & Losada, M. Á. (2017). Peaks Over Threshold (POT): A methodology for automatic threshold estimation using goodness of fit p-value. Water Resources Research, 53, 1–17.
- Soulsby, R. (1997). Dynamics of marine sand. A manual for practical applications. Thomas Telford 1997. ISBN 978-0-7277-2584-X.
- Verhaeghe, H. et al. (2010). CONSTRUCTION OF TWO NEW BREAKWATERS AT OSTEND LEADING TO AN IMPROVED HARBOUR ACCESS, ICCE 2010.

CONTAINER SHIPS MOORED AT THE PORT OF ANTWERP: MODELLING RESPONSE TO PASSING VESSELS.

T. Van Zwijnsvoorde¹, M. Vantorre², S. Ides³

ABSTRACT

Economics of scale act as driving force for the construction of Ultra Large Container Vessels (ULCV). The biggest advantage of container vessels is fast loading and unloading of containers. Large motions of the moored vessel along the quay hamper this process and even cause safety issues. This paper focusses on modelling the behaviour of moored vessels under ship passages, using a two-step approach. The forces acting on the moored vessel are modelled using RoPES (PMH), the behaviour of the moored vessel is modelled using the Ghent University in-house time domain software Vlugmoor. In a first part, four validation cases are presented, based on GPS measurements performed at the North Sea Terminal in the port of Antwerp, where the moored vessel is a Neo-Panamax container vessel. In a second part, the mooring plan of the vessel is discussed in detail. Both on the level of the individual lines, as well as for the mooring plan, efficiency parameters are defined. These parameters express the capability of a mooring plan to deal with longitudinal and transversal forces, based on line angles and line lengths.

1 INTRODUCTION

Economics of scale lead to ever increasing ship sizes. Especially in the container shipping industry, this effect is noticeable, as the container capacity keeps on incrementing. Not only does the beam of the vessels enlarge, in steps of 1 TEU bay/row, also the number of tiers (above deck) is raised. The newest generation of container vessels which are ordered, have 24 container bays, 24 container rows and 24 tiers, which leads to the nickname 'Megamax24' vessels (Port Today, 2018). These bigger vessels are more susceptible to environmental forces. In shallow and confined waters, this has an impact on the manoeuvring capability of the vessel and the behaviour of the moored vessel at the quay. In the Port of Antwerp, channel dimensions are limited and traffic density is increasing year by year. This leads to potential movement of the moored vessel along the quay due to the passing vessel. For container vessels, these motions are highly undesirable, not only because of the impact on the efficiency of loading and unloading operations (PIANC, 2012), but also because it could pose safety issues (Van Zwijnsvoorde and Vantorre, 2017).

The behaviour of the moored vessel is the result of the action of several forces. The passing vessel's pressure field induces forces on the moored vessel, together with currents, wind and wave forces. The movement of the moored ship causes the surrounding water to move, generating hydrodynamic reactions. The mooring lines and fenders create a balance in the force equilibrium, where the characteristics of the lines and their configuration has a major impact on the motions of the vessel.

The Antwerp Port Authority executed a full-scale measurement campaign at the North Sea Terminal in 2015, the terminal in the port of Antwerp which is most exposed to passing ships and which is able to welcome deep drafted container vessels in the range of Neo-Panamax up to Ultra Large Container Vessels (Ides et al., 2018). The goal of these measurements was to find out whether ship-ship interaction effects at this terminal, which was designed and built in the 1990's, do occur and if so which parameters dominate this process at this terminal. This paper uses these measurements to validate the in-house mooring simulation package Vlugmoor, which uses input from the numerical packages Seaway and RoPES. The moored vessel used for the simulations is a 13 000 TEU vessel. The passing traffic is diverse, including a tanker, container vessel and bulk carrier. In a second part of this paper, the mooring configuration is studied, both on the level of individual lines and the mooring configuration as a whole. The efficiency of said lines and configuration is evaluated by defining a set of efficiency parameters.

¹ PhD student, Ghent University, thibaut.vanzwijnsvoorde@ugent.be

² Professor, Ghent University, marc.vantorre@ugent.be

³ Research Engineer, Antwerp Port Authority, stefaan.ides@portofantwerp.com

2 MEASURING CAMPAIGN

As the port of Antwerp is the second largest (container) port in Europe (Port of Antwerp, 2017), multiple container terminals are suited for berthing the largest vessels which are in service up to this point. The port's recent developments also take into account further growth of the container vessel's size. In order to guarantee the safety of these moored vessels, during (un)loading of the containers, the port authority executed measurements of ship motions at these terminals (Ides et al., 2018).

2.1 Location

The measurement campaign at hand is performed at the North Sea Terminal (Figure 2-1), which is the most downstream river terminal of the port. It is subjected to tidal water level changes and currents. Passing vessels sail close to the moored vessels, because of the limited width of the navigational channel; The edge of the navigation channel is indicated as a green dashed line in Figure 2-1. In general, there are three different trajectories: two along the approaches to the locks *Zandvlietsluis* and *Berendrechtssluis* (1a and 1b), and one for vessels approaching to or from terminals located further upstream (2). Due to the presence of certain zones with limited water depth along the Western Scheldt and the approach channels in the North Sea, tidal windows are imposed to vessels with a draft larger than 13.1 m. This means that outbound sailing vessels may attain a considerable speed when passing the North Sea Terminal. Also, vessels need to have sufficient manoeuvrability to change course and combat the current, which demands a certain minimal speed, certainly for vessels with large lateral (wind) surfaces (e.g. RoRo, container vessels). Passing speeds over ground range between 4 and 7 m/s (8 to 14 knots), with passing distances varying between 150 m and 300 m.



**Figure 2-1 : Port Of Antwerp ; Location North Sea Terminal; Three examples of passing trajectories (blue) and edge of navigational channel (green dash).
– image courtesy of Antwerp Port Authority**

2.2 Logged data

On a daily basis, the port authority logs a lot of information regarding the shipping traffic inside the port. At several locations, the coordinates of the vessel, the passing speed and the draft, based on AIS information, are logged. For the dedicated measuring campaign (Ides et al., 2018), moored vessel motions were registered using two GPS devices, installed on port and starboard side on the bridge, in order to monitor roll, lateral and longitudinal motions. As previous studies show (Van Zwijnsvoorde and Vantorre, 2017), the longitudinal motion is always critical for a vessel moored at a quay wall, whereas the lateral motion is rather limited. The focus will thus be on the registration of the longitudinal motion. The port requested information from the ships, concerning the mooring lines used on board.

3 VALIDATION CASES

The aim of this paper is not to present a general discussion on all the data collected during the measuring campaign (Ides et al., 2018), instead there is focussed on a selection of validation cases. For these cases, details regarding moored vessel and passing vessel are presented in chapters 3 and 5.

3.1 Moored vessel

At the North Sea Terminal, container vessels up to Ultra Large Container Vessels berth. However, most measurements were carried out on Neo-Panamax size vessels: these vessels have a length overall (L_{OA}) of 366 m and a beam (B_{OA}) of 48.2 m. They can carry a maximum of around 13 000 TEU. For the present study, two moored vessels of this type have been considered, denoted in this paper as 'C1' and 'C2'. Despite having the same main dimensions, the mooring equipment is different, which is the reason why they are considered as two separate vessels (see section 5).

3.2 Passing vessel

The passing vessel fleet is diverse, as the Port of Antwerp is an important transit port for all kinds of cargo. This means that during the stay of a containership at the terminal (typically around 36 hours), various passage events are registered. The passing events which led to the largest motions along the quay are chosen. For moored vessel C1 a tanker 'T' and an ultra large container vessel 'C3' are considered. For the second moored vessel C2, two passing bulk carriers, 'B1' and 'B2'. The main dimensions of all vessels are summarized in Table 3-1. T_p is the draft of the passing vessel, T_m and h are the draft of the moored vessel and the water depth respectively, at the time of the passing event.

| | C1 (=C2) | C3 | T | B1 | B2 |
|--------------|----------|-------|-------|-------|-------|
| L_{OA} [m] | 366.0 | 399.0 | 182.6 | 190.4 | 190.4 |
| B_{OA} [m] | 48.2 | 53.7 | 32.2 | 32.2 | 32.2 |
| T_p [m] | | 11.0 | 8.9 | 7.0 | 7.6 |
| T_m [m] | | 13.6 | 13.7 | 12.6 | 13.1 |
| h [m] | | 21.1 | 17.6 | 19.7 | 21.0 |

Table 3-1 : Main dimensions moored and passing vessels case study.

3.3 Passing distance and speed

The passing distance and speed are two important parameters, which determine the forces acting on the moored vessel due to the passing ship. Since the forces, assuming potential flow, are proportional to the speed squared, it is important to get a good estimate of this passing speed. For each passing event, the velocity and position are logged at a southern and a northern measuring station, as indicated on Figure 3-1. The input for the numerical simulation is limited to a constant velocity, which is taken as the average of both registered values. This resulting speed over ground needs to be converted to a speed through the water.

As was already shown in Figure 2-1, the passing trajectory is not a straight line. As the numerical package does not allow curved trajectories, the positions measured at both stations are connected, using a straight line (Figure 3-1). In general, outbound sailing vessels pass the moored vessel at closer distances. The vessels approaching from the river upstream will have higher velocities than the ones coming from the locks, which are still accelerating when passing the North Sea Terminal. All cases thus discuss outbound sailing vessels, following the inclined trajectory coming from the river. This means the passing distance varies during the passing event.



Figure 3-1 : Northern and southern measuring section and assumed straight trajectory.
 – image courtesy of Antwerp Port Authority

The average passing distance (d_{pas}) and angle (α_{pas}) relative to the quay wall are given in Table 3-2 and indicated in Figure 3-2. The passing speed is given as $U_{p,g}$ [m/s] and $U_{p,w}$ [m/s], giving the velocity registered by AIS (over ground) and the velocity through the water, taking into account the tidal current. Tanker 'T' passed during turning of the tide, where the current velocity is approximately 0 m/s.

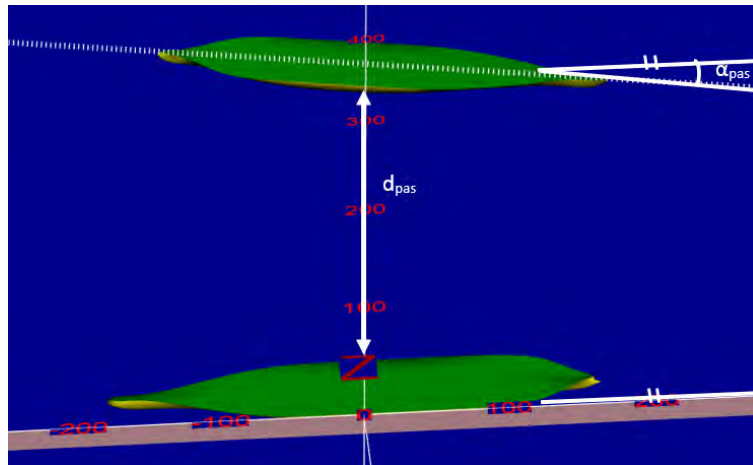


Figure 3-2 : Definition passing distance (d_{pas}) and angle (α_{pas}) for the C1-C3 case.
 Figure generated by RoPES.

| | C3 | T | B1 | B2 |
|--------------------|-------|-------|-------|-------|
| d_{pas} [m] | 292.5 | 205.5 | 241.0 | 205.0 |
| α_{pas} [°] | 10.3 | 10.1 | 11.4 | 9.6 |
| $U_{p,g}$ [m/s] | 4.9 | 5.6 | 6.4 | 5.8 |
| $U_{p,w}$ [m/s] | 4.1 | 5.6 | 6.0 | 5.1 |

Table 3-2 : Average passing distance (d_{pas}) and angle relative to the quay (α_{pas}); Velocity over ground ($U_{p,g}$) and through the water ($U_{p,w}$).

3.4 Time series and definition axis system

The greatest difficulty with modelling the effect of passing vessels is that it concerns a dynamic effect. The passing vessel force (surge, sway, yaw) changes in magnitude and size during the ship passage, which also leads to motions which show a time dependant variation. The relationship between exciting force and resulting motion is a function of several design parameters, as there are (added) mass of the vessel, the hydrodynamic damping and the mooring line and fender characteristics. The chosen mooring configuration and pretension level (or slack !) also influence the behaviour of the moored vessel. For

large vessels, sailing at relatively low speeds, the period of the external force and resulting motion is large. The measured longitudinal motion for the case C1-T is given in Figure 3-3. Throughout this paper, all cases are expressed by the combination of moored and passing vessel (C1-T, C1-C3, C2-B1 and C2-B2). The sign convention and axis system is shown in Figure 3-4. The moored vessel is always moored portside, with an outbound passing vessel.

The forces and motions are given in the axis system (O-x,y,z), where the x-axis is along the longitudinal symmetry plane of the vessel, the y-axis positive to portside and the z-axis positive upwards (Figure 3-4). The origin is located on the water plane, at the midship section, on the symmetry line of the vessel, in its initial position. When the passing vessel approaches the moored ship, the moored ship is attracted in positive x-direction, which means it will move ahead (indicated green in Figure 3-4) . In the second position, the ship is moved astern, according to the negative x-direction (Figure 3-4 – blue). The time (T_r) is expressed relative to the starting point of the motion, which can be seen as the starting point of the passing event. The period of the longitudinal motion (T_x), which is defined as the time between the start of the motion and the equilibrium reached after the passage, is around 160 seconds for the case C1-T. In this paper, measured data is consistently indicated with red colour, modelled results are shown using black lines.

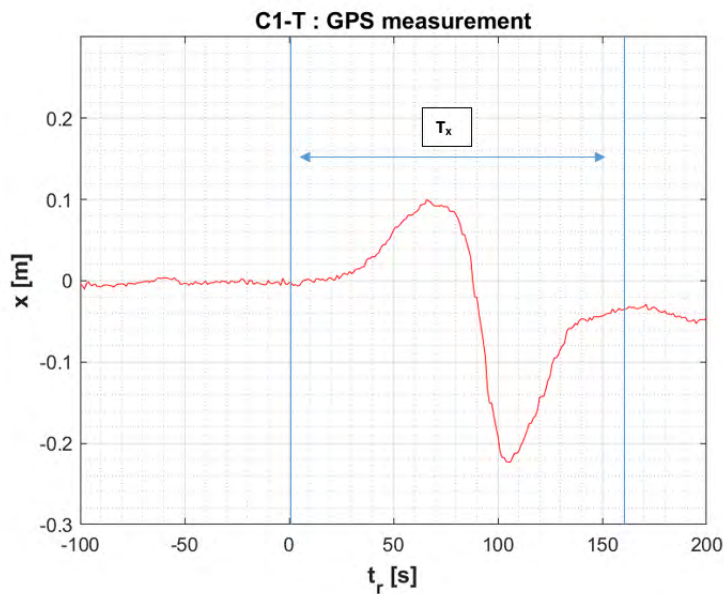


Figure 3-3 : GPS measurement of the longitudinal motion for case C1-T.

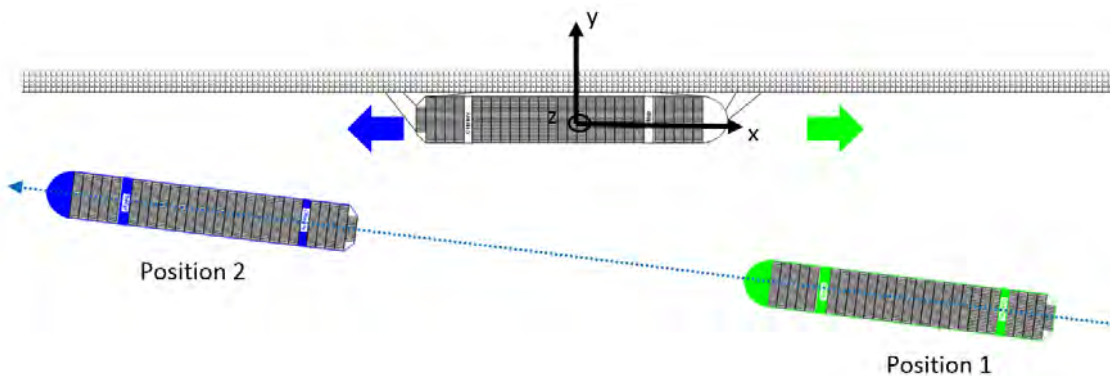


Figure 3-4 : Definition sign convention and axis system O-x,y,z.

4 NUMERICAL MODELS

In order to simulate the behaviour of the moored vessel in the passing event, the effect of several numerical packages needs to be combined, including RoPES (Pinkster Marine Hydrodynamics (PMH)), Octopus Office (ASEA Brown Boveri (ABB) – integration of Seaway, originally developed by J. Journée⁴) and the UGent in-house time domain method Vlugmoor.

4.1 RoPES

The RoPES package has been developed as a joint-industry project (JIP), combining the knowledge of several leading hydrodynamic research institutes. RoPES calculates passing ship forces, using the potential double body flow method (Pinkster, 2014). Figure 3-2 in section 3.3 gives an example of a case generated in RoPES. The theory has its limitations, for example when flow separation zones are present in real life viscous flow. Flow separation typically occurs when ships pass with a non-zero drift angle (van Wijhe and Pinkster, 2008) or in case of entering a narrow channel or lock (Toxopeus and Bhawsinka, 2016). By assuming a rigid water surface, all free surface effects are ignored, including long waves generated by passing vessels (Pinkster, 2004) and their sinkage and trim caused by the water level variations generated by the return flow, known as squat. In order to cope with this last effect, which is a function of the blockage of the wetted section and the passing velocity, the correction factor according to Talstra and Bliet (Talstra and Bliet, 2014), which has been validated using model tests performed at FHR in the framework of RoPES JIP (Delefortrie et al., 2012), is applied on the obtained results from RoPES.

4.2 Octopus office

The reaction of the ship to external forces is largely affected by the hydrodynamic coefficients, which define how much water is moved together with the vessel (added mass) and how the motion damps out. These coefficients are calculated using the 2D strip theory package ‘Seaway’ (Journée and Adegeest, 2003). As the vessel is moored at a quay with restricted water depth, the coefficients need to be generated for shallow water cases. The Seaway code has been validated for shallow water conditions, using tests performed at the towing tank for manoeuvres in confined waters at FHR, in collaboration with Ghent University (Vantorre and Journée, 2003).

4.3 Vlugmoor

Vlugmoor is the in-house package which calculates the behaviour of moored vessels, based on input from RoPES, Octopus Office and the mooring configuration (see chapter 5). The code solves the force equilibrium in 4 degrees of freedom (surge, sway, yaw and roll), with coupling between sway and yaw. Based on the accelerations of the vessel, the new position of the moored vessel is calculated, using trapezoidal integration. In the current software, mooring line forces are calculated as linear springs. As the behaviour of lines is very often non-linear, certainly for very elastic lines, an overhaul of this module is foreseen for the near future, based on full-scale tests. One of the presented cases below, demonstrates the necessity of including non-linear stress-strain behaviour in the simulation software.

5 MOORING CONFIGURATION

The mooring configuration of the vessel has a large influence on the behaviour of the moored vessel. Even for a given number of lines, the differences between configurations can be significant (see chapter 7). The first component is fixed in the design phase of the vessel, being the number of winches and their position, the position of the fairleads and the characteristics of the lines (maximum breaking load (MBL) and elasticity). The quay equipment, bollards and fenders, cannot be changed easily. There are however operational constraints concerning the mooring configuration as well. The most pronounced one is a spatial configuration of the lines, where the aim should be to come up with a well-balanced mooring plan. The second aspect is the pretension in the lines, which plays a huge role in the ship's behaviour and is especially a challenge in a tidal environment. A lack of pretension in some lines already significantly changes the reaction to the passing vessel, leading to large motions and/or large line forces.

⁴ The Knowledge Centre Manoeuvring in Shallow and Confined Water (Flanders Hydraulics Research – Ghent University) wishes to pay tribute to prof. ir. Johan Journée who passed away on December 15th, 2017, at the age of 76.

5.1 Quay equipment

The North Sea Terminal is a dedicated container terminal, with bollards every 21.5 m, combined with high impact fenders at the same positions along the quay wall. Due to the presence of the gantry crane rails, the bollards are positioned close to the vertical quay side. The distance between ship's side and quay, when the ship is held against the fenders due to the pretension in the lines, is equal to the width of the fenders. The distance between the bollards and the ship's hull is taken as 2.0 m.

5.2 Ship equipment

The ship equipment varies highly in between container vessels, which can be explained by the large variety in rope types and sizes. IMO/IACS formulated recommendations in 2005 (IACS, 2005 and IACS, 2014), regarding the MBL of the lines and the number of lines to be used. For newly built container vessels, the more demanding 2016 guidelines (IACS, 2016) has been developed. This new set of guidelines, however, fails at incorporating requirements regarding elasticity of the lines. The mooring lines on board of the vessels C1 and C2 confirm this observation. Table 5-1 gives the number of lines (n_{lines}), the MBL and breaking strain (ϵ_{br}) of the vessels. Whereas the MBL is similar, the breaking strain varies significantly. For the same external force, vessel C2 will move almost twice as much along the quay compared to vessel C1. Note as well that the lines of vessel C2 are expected to show non-linear stress-strain behaviour.

| | C1 | C2 |
|---------------------|-----|-----|
| n_{lines} [-] | 12 | 12 |
| MBL [ton] | 160 | 143 |
| ϵ_{br} [%] | 15 | 28 |

Table 5-1 : Mooring equipment of vessels C1 and C2.

5.3 Lines plan

The mooring lines plan is the end-responsibility of the captain of the vessel, who often receives input from the harbour (in the person of the pilot). At some terminals, there is a fixed mooring plan. This is standard practice at tanker terminals, but not at container terminals. The number of lines however, is imposed by the Antwerp Port Authority. For vessels C1 and C2, a total of 12 lines is demanded (2 fore lines, 2 fore breasts, two fore and two aft springs, 2 aft breasts and 2 aft lines). The exact mooring plan will vary in between vessels and also between two port calls of the same vessel, because of following reasons :

- Conditions (water level, current, wind,...) which were present during the berthing operation.
- Skill of the crew.
- Presence of other vessels at the terminal which limits available bollards at quay.
- Relative position of the vessel with respect to the bollards.

The port of Antwerp delivered some photo material of moored container vessels, as can be seen in Figure 5-1.



Figure 5-1 : Typical mooring configuration of moored 13000 TEU container vessels at North Sea Terminal, using 12 lines. – images courtesy of Antwerp Port Authority

Vessels can be moored portside or starboard side, the latter requiring swinging before berthing. The vessels 'C1' and 'C2' are both moored portside. The lines plan is denoted by the coordinates of the bollards at the quay (x_q, y_q, z_q) and the fairleads of the moored vessel (x_s, y_s, z_s), in the axis system O-x,y,z, which has been defined in Figure 3-4. The top view of the mooring configuration is given in Figure 5-2. The z-coordinates are given with respect to the water surface. They will show slight variations in between the cases, as z_q and z_s depend on the water level and the moored vessel's draft respectively. The levels are given in Table 5-2. Due to the presence of the higher forecastle deck, the fore lines will be steeper than the aft lines, which are located at a lower aft mooring deck. For this validation effort, it is assumed that all lines are pretensioned by default to 10% of the MBL, which is deemed good practice. The fourth passing case shows the importance of the pretension, certainly for highly elastic lines.

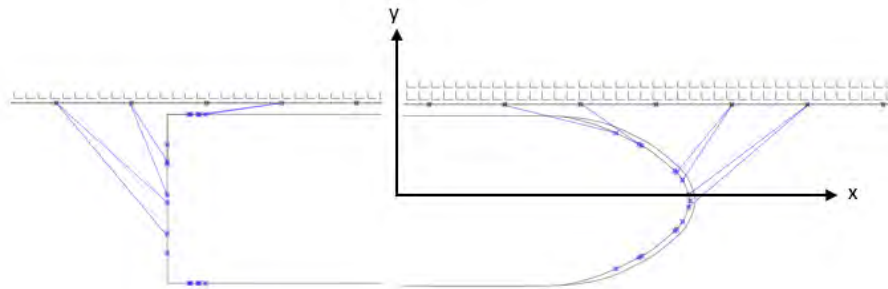


Figure 5-2 : Lines plan C1 and C2, portside mooring.

| | z_q [m] | $z_{s,a}$ [m] | $z_{s,f}$ [m] |
|--------------|-----------|---------------|---------------|
| C1-T | 8.77 | 11.40 | 17.57 |
| C1-C3 | 5.28 | 11.50 | 17.67 |
| C2-B1 | 7.24 | 12.50 | 18.67 |
| C2-B2 | 5.40 | 12.00 | 18.17 |

Table 5-2 : Level of the bollards at the quay (z_q), the aft mooring deck ($z_{s,a}$) and the forecastle mooring deck ($z_{s,f}$), relative to the water surface.

6 COMPARING MEASUREMENTS AND SIMULATIONS : VALIDATION

For the four passing events described in section 3, the registered motions, using GPS, are compared with the numerical results from Vlugmoor. The longitudinal motions, following the definitions from Figure 3-4, are plotted as a function of the relative time t_r [s], which is zero at the moment the moored ship starts to move. Using this definition for both numerical and full-scale data, a comparison of both motion amplitude and period can be made.

6.1 Case C1-T

In the first case, a tanker (T) passes the moored container vessel (C1), which has relatively stiff lines on board. Before comparing the results from the Vlugmoor analyses with the measured GPS result, the longitudinal forces calculated by RoPES are examined. The time series is given in Figure 6-1, including the Talstra and Bliet (T&B) correction factor. The negative force (moving the moored vessel astern) is higher than the positive one (pulling the moored vessel ahead), which is due to the inclined trajectory of the passing vessel (Figure 3-1).

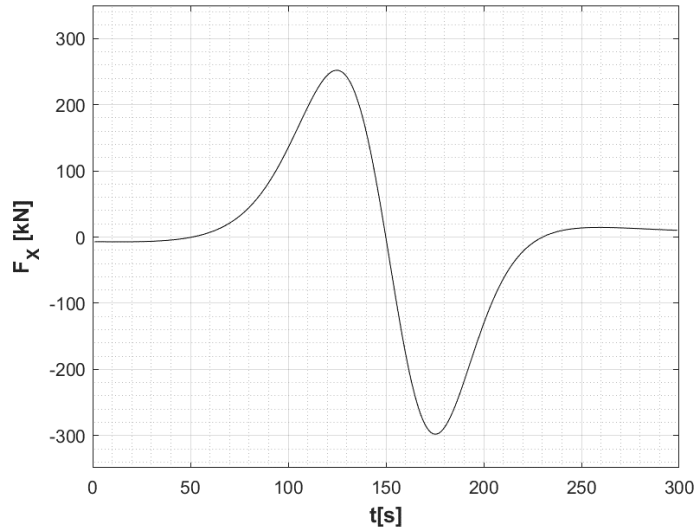


Figure 6-1 : Longitudinal force (F_x) acting on the moored vessel (C1), due to the passing tanker (T). Numerical RoPES results, including T&B correction.

Figure 6-2 compares the measured motion of the moored vessel C1 with the simulation results. It can be observed that the period of the motion is very similar, which means that the calculation of the hydrodynamic masses and the collected AIS data (passing speed and distance) seem correct. The negative motion is significantly larger than the positive motion, which follows from the inclined path of the passing vessel. The motion amplitude is overestimated in the simulation. Both the negative and positive peak are higher than the measured GPS results. This could be allocated to a stiffer reaction of the lines than expected. As the depth-Froude number for this passing event is rather high ($Fr_d = 0.42$), the correction proposed by Talstra and Bliet is significant. The longitudinal force coming from RoPES needs to be multiplied by the factor 1.25 for all time steps. Figure 6-2 also shows the motions of the moored vessel, according to the uncorrected RoPES output. Additional research, using model tests is needed to validate this RoPES correction factor, as it has a significant influence on the results of the mooring analysis in shallow and confined waters. Awaiting these results, the T&B factor is applied for all cases.

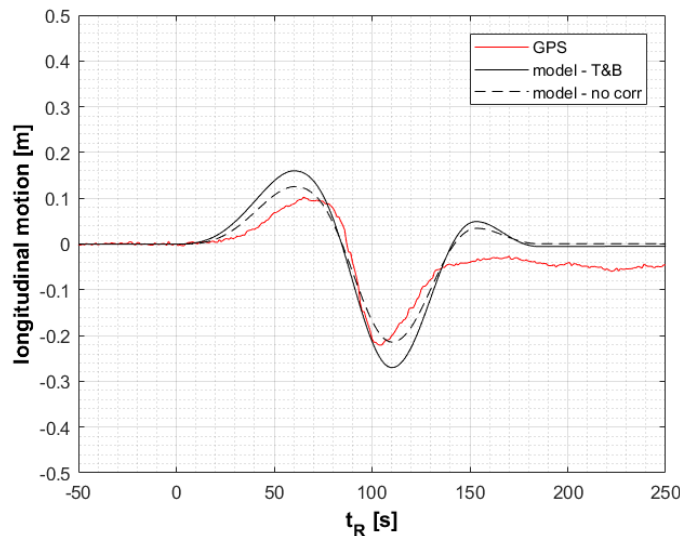


Figure 6-2 : Case C1-T ; Longitudinal motion of the moored vessel : Numerical results with and without T&B correction factor versus GPS measurement.

6.2 Case C1-C3

In this second case, the moored vessel is passed by an Ultra Large Container Vessel, which sails at a lower speed and larger passing distance compared to the tanker. The comparison between GPS

measurements and numerical results is given in Figure 6-3. The total period of the motion is indeed longer, around 250s, with again a good agreement between numerical and measured results. The amplitudes are also very similar in this case. The difference in positive motion might be caused by lower pretension levels in the fore springs and aft lines (see also section 6.4) in reality compared to the simulation assumption (pretension equals 10% MBL).

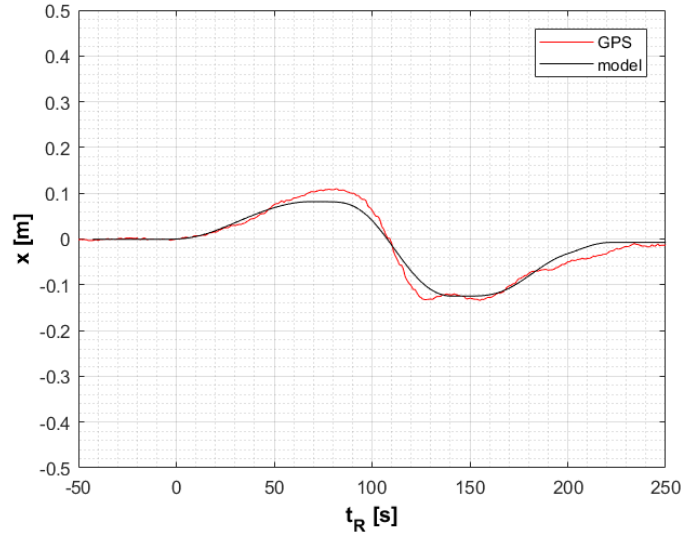


Figure 6-3 : Case C1-C3; Motion of the moored vessel : Comparison GPS and model.

6.3 Case C2-B1

The moored vessel C2 has the same mooring plan, yet the mooring lines have an elongation at break of 28%, compared to the much stiffer lines of the moored C1 vessel. Figure 6-4 shows the comparison between the GPS measurements and the numerical output. The periods of both motions again show good similarity. The GPS measurements, however, show a very large positive motion, which is not expected based on the inclined trajectory of the passing vessel. Here the difference is large with the modelled results, which are more in line with the expectations. The negative amplitude is similar. The difference in positive motion peak might be explained by the non-linear stress-strain behaviour of highly elastic lines. Elastic lines react very elastic at low stress levels, with a gradual stiffness increase with higher line loads. The linearization thus depends on the magnitude of the line forces. If the pretension is low (or absent), the lines show large elongations even at low stress levels. This leads to large ship motions, as displayed in Figure 6-4. The non-linear line behaviour is discussed further in the next section.

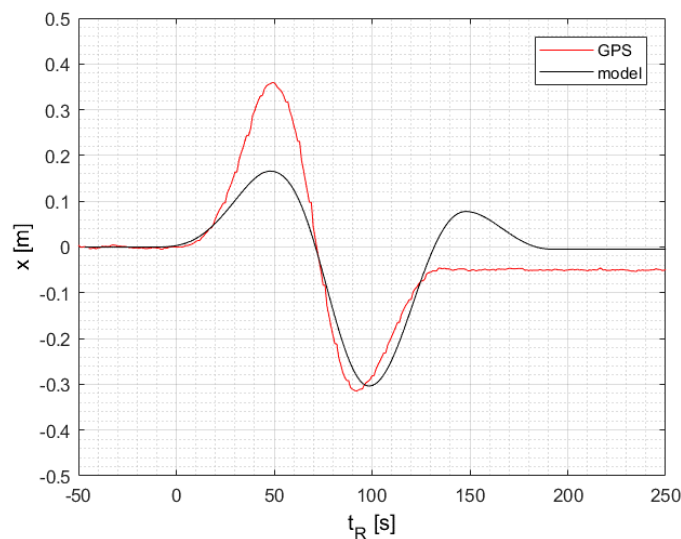


Figure 6-4 : Case C2-B1; Motion of the moored vessel : Comparison GPS and model.

6.4 Case C2-B2

In this last case, the same moored container vessel is passed by a bulk carrier B2, with similar dimensions as the first one (B1). A comparison between the numerical and the measured results is given in Figure 6-5.

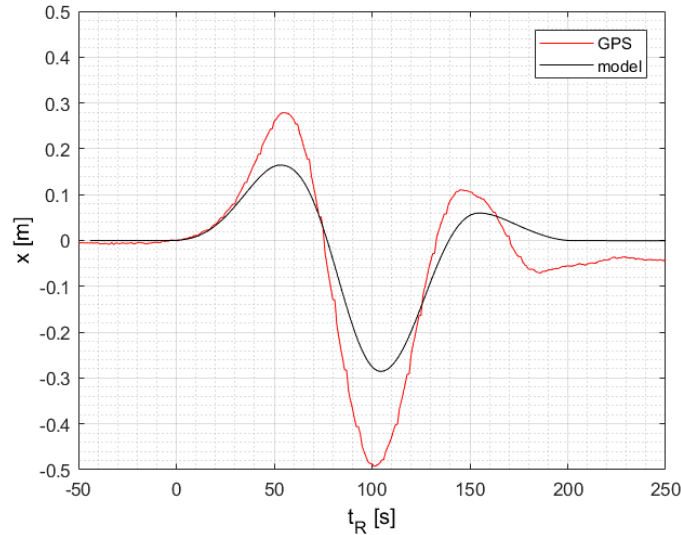


Figure 6-5 : Case C2-B2; Motion of the moored vessel : Comparison GPS and model.

A large discrepancy between GPS measurements and the numerical results is present, when comparing the motion amplitudes. The period of the motion shows decent agreement, which again means that the confidence in the passing vessel’s input data and the moored vessel’s hydrodynamics is high. The motions, however, are underestimated, in both senses. Again, non-linearity of the lines seems to be the cause of these differences. Without knowing the exact stress-strain curve of the mooring lines, the general curve of a highly elastic material is given in Figure 6-6. Three different linear approximations are shown :

- In case sufficient pretension is present ($F_{pr} = 10\%$ MBL), the highly-elastic part of the curve is avoided. If the line loads are high, the green curve is chosen as linear stress-strain factor, which is the average slope of the curve between F_{pr} and MBL.
- In a second case, again pretension level is satisfactory (10% MBL), the forces in the lines during the ship passages remain limited. In this loading zone, the line will react according to the blue line. This approximation is used for case C2-B1 (Figure 6-4) and in Figure 6-5.
- In a third case, the pretension is low (5% F_{br}), which causes the line to react very elastic. The red linearization in Figure 6-6 is used for the simulation shown in Figure 6-7.

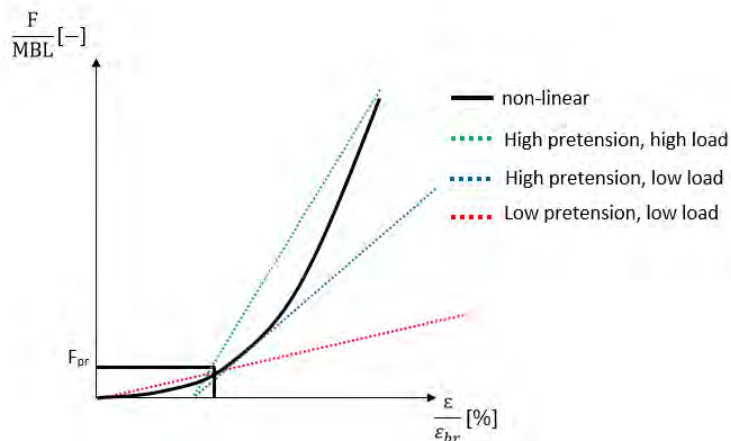


Figure 6-6 : Non-linear stress-strain behaviour highly elastic line : three linear stiffness approximations.

The same passing event is now modelled according to the red stress-strain line in Figure 6-6, which means a 50% stiffness reduction compared to the blue curve. The resulting motions are given in Figure 6-7. The modelled motion amplitude is closer to the measured GPS data. The period becomes larger, due to reduced stiffness of the line, which causes larger motions and consequently a longer period of the motion. Of course, the results shown are again based on a simulation using linear lines, including a lower line stiffness and pretension value. The conclusion here is that a lack of pretension, for non-linearly deforming elastic lines, can lead to high motions, even with relatively low line forces. In order to fully capture this effect, a full non-linear model needs to be implemented in the software.

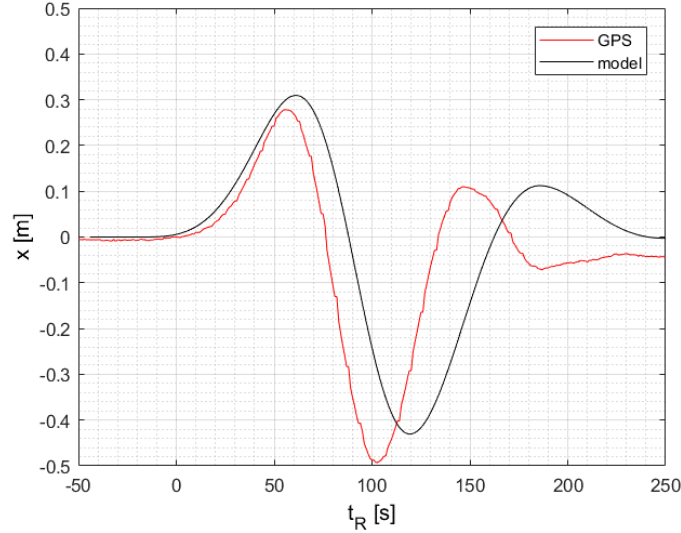


Figure 6-7 : Case C2-B2; Motion of the moored vessel : 5% pretension, reduction of stiffness by 50% compared to the results shown in Figure 6-5.

7 DETAILED STUDY OF THE MOORING PLAN

In this section, the mooring plan of the vessel is examined, from an operational point of view. The starting point of the discussion is the case C1-C3, with the mooring plan given in Figure 5-2 and Table 5-2. The configuration, which consists of 12 lines, is discussed on the level of the individual lines and the configuration as a whole. In a first stage, an efficiency parameter is derived for each line. These are then combined into four parameters, which show the balance and potential of the mooring plan.

7.1 Discussion on the level of the individual lines

The argument is started by looking at the position of the individual lines. The line segment between the bollard on the quay and the fairlead, is given by three coordinates for each point (x,y,z). These six parameters can be expressed as the angles in horizontal and vertical plane (α and β), as well as the length of the line (l), between bollard and fairlead. The total line length (ℓ) is the sum of l and l_{fw} , being the line length between fairlead and winch. By transferring the origin of the axis system to the centre of the bollard, α , β and l are expressed as follows (see Figure 7-1).

$$\beta = \tan^{-1} \frac{z_s - z_q}{\sqrt{(x_s - x_q)^2 + (y_s - y_q)^2}} \quad (1)$$

$$\alpha = \cos^{-1} \frac{x_s - x_q}{\sqrt{(x_s - x_q)^2 + (y_s - y_q)^2}} \quad (2)$$

$$\ell = \sqrt{(x_s - x_q)^2 + (y_s - y_q)^2 + (z_s - z_q)^2} + l_{fw} \quad (3)$$

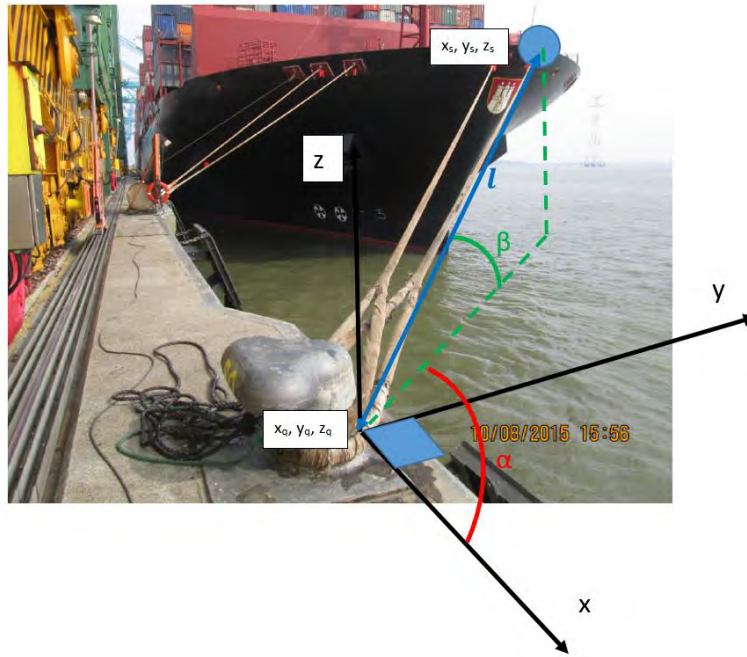


Figure 7-1 : Definition line angles α and β and the length of the line section between bollard and fairlead (l).

The values for α , β and l for each line are summarized in Table 7-1.

| | α [°] | β [°] | l [m] | | α [°] | β [°] | l [m] |
|---------------------|--------------|-------------|---------|--------------------|--------------|-------------|---------|
| Fore lines | 140 | 16 | 52 | Aft lines | 54 | 17 | 32 |
| | 144 | 17 | 49 | | 65 | 13 | 35 |
| | 124 | 27 | 35 | | 39 | 8 | 50 |
| | 130 | 28 | 32 | | 48 | 7 | 61 |
| Fore springs | 28 | 40 | 43 | Aft springs | 174 | 17 | 35 |
| | 20 | 23 | 48 | | 175 | 15 | 37 |

Table 7-1 : Mooring line angles (α , β) and lengths (l); Mooring configuration C1 (case C1-C3).

Table 7-1 shows that due to the height of the forecastle deck, the fore lines and springs show large angles with the horizontal plane, which means that they will show lower efficiency at taking up horizontal forces, which are of interest here. The fore and aft lines show angles in the horizontal plane (α) between 40° and 60° (140° and 120°), which indicates that they will help at taking up both transversal and longitudinal forces. Breast lines (α close to 90°) are not present in the configuration, indicating that in case of heavy (lateral) wind loads, the capacity of the configuration in the transversal direction might be insufficient. Due to the level and shape of the aft mooring deck, the aft springs are very efficient (α close to 180° and $\beta < 20$). The fore springs are hampered by the shape and level of the forecastle, leading to less efficient fore springs. The total of the lines, l , is important when evaluating the efficiency of the lines within the mooring plan. Long lines will react slowly to external forces, whereas short lines will show large strain at smaller deformations, leading to large forces in the lines.

The mooring line angles (α, β) and the line length l are combined in efficiency parameters, expressing the potential for lines to take up longitudinal and transversal loads. In a first step, the lines are presented as force vectors in the 3D space. Based on simple geometrics, the x and y component of the force vector F , which represents the total line force, are given as :

$$F_x = F \cdot \cos \beta \cdot \cos \alpha ; F_y = F \cdot \cos \beta \cdot \sin \alpha \quad (4)$$

In order to build up force, the line needs to elongate. For the longitudinal forces, the potential of the line is expressed as the elongation 'dl', which is present for a longitudinal motion 'dx' (see Figure 7-2). It is assumed that the motion is small compared to the line length. For a line which is located in the x,y-plane, the following is valid, only considering first order terms.

$$l_1^2 - l_0^2 = x_1^2 - x_0^2 \Rightarrow dl \cong \cos \alpha \cdot dx \quad (5)$$

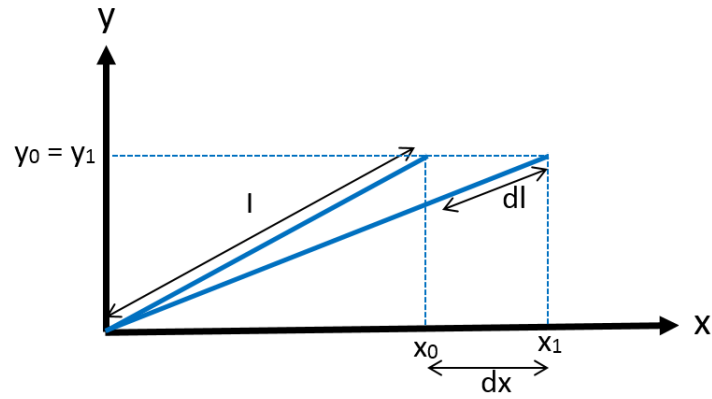


Figure 7-2 : Elongation of the mooring line dl in function of a longitudinal ship motion dx .

Assuming linear behaviour of the line, the force build-up is a linear function of the strain (ε) in the line. Using (eq. 5), this is expressed as :

$$\varepsilon = \frac{dl}{l} \cong \cos \alpha \cdot \frac{dx}{l} \quad (6)$$

Based on the force components (eq. 4) and the relation between strain and motion components (eq. 6), the efficiency of a line with angles α_i , β_i and length l_i , is given as:

$$e_{xi} = \cos^2 \beta_i \cdot \cos^2 \alpha_i \cdot \left(\frac{l_i}{l_{ref}} \right)^{-1} \quad (7)$$

$$e_{yi} = \cos^2 \beta_i \cdot \sin^2 \alpha_i \cdot \left(\frac{l_i}{l_{ref}} \right)^{-1} \quad (8)$$

$$l_{ref} = \frac{1}{n} \cdot \sum_{i=1}^n l_i \quad (9)$$

In (eq. 7) and (eq. 8), l_{ref} , the average line length, is added to non-dimensionalise the efficiency parameters. The resulting efficiency parameters for all lines are given in Table 7-2.

| | e_{xi} [-] | e_{yi} [-] | | e_{xi} [-] | e_{yi} [-] |
|---------------------|--------------|--------------|--------------------|--------------|--------------|
| Fore lines | 0.45 | 0.31 | Aft lines | 0.41 | 0.78 |
| | 0.52 | 0.27 | | 0.20 | 0.96 |
| | 0.30 | 0.67 | | 0.50 | 0.34 |
| | 0.43 | 0.60 | | 0.31 | 0.37 |
| Fore springs | 0.45 | 0.12 | Aft springs | 1.09 | 0.01 |
| | 0.68 | 0.09 | | 1.06 | 0.01 |

Table 7-2 : Efficiency of the lines in mooring configuration C1 (case C1-C3).

The conclusions are similar to the ones made based on the angles α and β (Table 7-1), but the results can be interpreted more easily, as the angles are rewritten as two efficiency parameters, for both longitudinal and transversal directions. The parameters also include the effect of the line length on the reaction of the line to external loads. For the longitudinal direction, the most efficient lines are the aft springs ($e_{xi} = 1.09$ and 1.06), combining favourable line angles and relatively short lines, which leads to an efficiency larger than the unity. The fore springs only show efficiencies of 0.45 and 0.68, due to the large vertical angle and inclination with respect to the quay wall in the horizontal plane. Due to the absence of breast lines, the lateral efficiency of all lines is limited. Only two of the aft lines reach values of 0.78 and 0.96. As can be expected, the fore and aft springs have a negligible contribution towards taking up lateral forces, with e_{yi} values between 0.01 and 0.12.

7.2 Discussion on the level of the mooring plan

The definition of the efficiencies of the singular lines allows to evaluate and compare mooring plans, both for the same vessel and in between different vessels. Focussing on the quality of the mooring plan of a given vessel (design parameters fixed), e_{xi} and e_{yi} are translated in the following efficiency parameters.

$$e_{xp} = \sum_{i=1}^{n_{\alpha < 90}} \cos^2 \beta_i \cdot \cos^2 \alpha_i \cdot \left(\frac{\ell_i}{\ell_{ref}} \right)^{-1} \quad (10)$$

$$e_{xn} = \sum_{i=1}^{n_{\alpha > 90}} \cos^2 \beta_i \cdot \cos^2 \alpha_i \cdot \left(\frac{\ell_i}{\ell_{ref}} \right)^{-1} \quad (11)$$

$$e_{yf} = \sum_{i=1}^{n_f} \cos^2 \beta_i \cdot \sin^2 \alpha_i \cdot \left(\frac{\ell_i}{\ell_{ref}} \right)^{-1} \quad (12)$$

$$e_{ya} = \sum_{i=1}^{n_a} \cos^2 \beta_i \cdot \sin^2 \alpha_i \cdot \left(\frac{\ell_i}{\ell_{ref}} \right)^{-1} \quad (13)$$

e_{xp} and e_{xn} express the capability of the configuration to deal with positive and negative longitudinal forces. For the transversal direction, e_{yf} and e_{ya} are defined, which show the potential to take up lateral forces on the fore and aft of the vessel. For the mooring plan for the C1-C3 case, given in Figure 5-2, these four parameters are given in Table 7-3.

| e_{xp} [-] | e_{xn} [-] | e_{yf} [-] | e_{ya} [-] |
|--------------|--------------|--------------|--------------|
| 2.55 | 3.85 | 2.07 | 2.47 |

Table 7-3 : Efficiency of the mooring plan C1 (case C1-C3, Figure 5-1).

The mooring plan efficiencies as given in (eq. 10) to (eq. 13) and Table 7-3 are only suited to evaluate different mooring plans for the same vessel. In order to make a comparison in between different vessels possible, several additional terms need to be added to the equation, including amongst others:

- The (total) number of lines.
- The breaking strength and elasticity of the lines, relative to a reference value, should be included in a similar way as the line lengths are represented. In case of mooring lines showing non-linear stress-strain curves, this process becomes more complex.
- Linked to the previous bullet, a correction factor for pretension of the lines.

Future research will include further development of the efficiency parameters by comparing different vessels' mooring configurations and simulation results. The next section focusses on the application of the efficiency parameters to evaluate mooring plans for the C1 vessel.

7.3 Study of the mooring plan for case C1-C3

The starting point for this section is the mooring plan which has been used for the validation study, given in Figure 5-2 and repeated below in Figure 7-3, indicated as plan I. The second plan aims at optimising the configuration to cope with longitudinal forces, which is the case for passing ship events. Note that at busy terminals, limited distance in between moored vessels often makes it impossible to achieve this configuration. The fore spring position is also adjusted, to increase its efficiency, as the efficiency parameter e_{xi} for this line is low (0.45, Table 7-2). By adjusting its position, this efficiency increases from 0.45 to 0.59. The fore and aft lines are positioned to limit the angles α and β . The downside of this repositioning is the increase in line lengths, which leads to less reactive lines. This is taken into account by keeping the reference length, ℓ_{ref} , constant for the three cases, as the average length of all lines in plan I. Plan III is very compact, which occurs when multiple vessels, in some cases larger than the design vessel, are moored at the quay, minimising the available bollard space for the fore and aft lines.

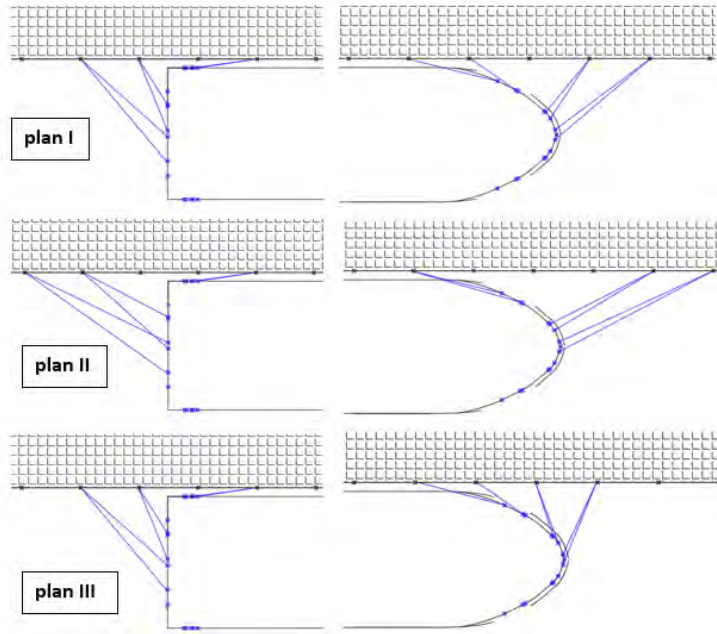


Figure 7-3 : Case study C1-C3 : mooring plan I (validation study, Figure 5-1), plan II and plan III.

The efficiency parameters for the configurations given in Figure 7-3 are given in Table 7-4.

| Plan | e_{xp} | e_{xn} | e_{yf} | e_{ya} |
|------|----------|----------|----------|----------|
| I | 2.55 | 3.85 | 2.07 | 2.47 |
| II | 3.37 | 4.36 | 0.69 | 0.79 |
| III | 2.77 | 2.48 | 3.61 | 2.47 |

Table 7-4 : Efficiency of the mooring plans I,II and III, case C1-C3.

Table 7-4 parameterizes the above description of the mooring plans. In the second plan, the longitudinal efficiency increases, whereas the transversal capacity is lowered significantly. In the passing events at hand however, the transversal forces are small, which limit the impact of said decrease in lateral efficiency. In the third plan, the efficiency in the negative longitudinal sense (e_{xn}) decreases, the lateral efficiency of the fore lines (e_{yf}) on the other hand, is augmented. This configuration is thus not balanced in the lateral direction and will show yaw rotation under large lateral forces. Figure 7-4 compares the longitudinal motions for the three plans, where it can be clearly observed that the efficiency parameters indeed give a good indication for the impact of the change in mooring plan on the longitudinal motions.

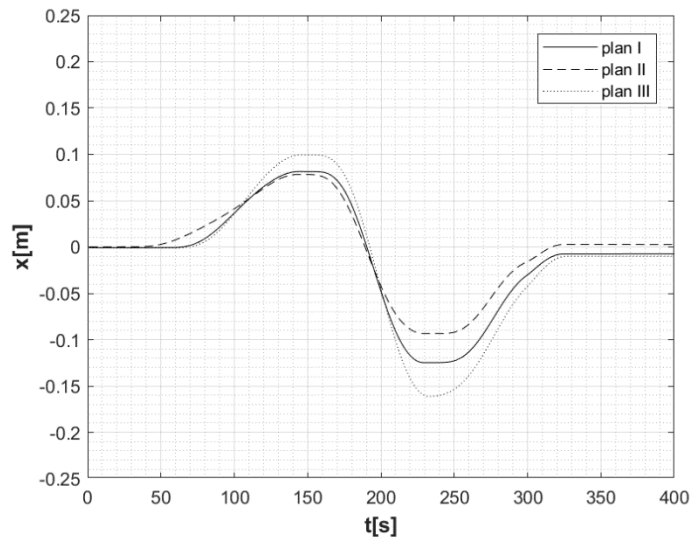


Figure 7-4 : Modelled longitudinal motion C1-C3, mooring plan I,II and III.

8 CONCLUSION

This paper elaborates on the validation of the UGent in-house software package Vlugmoor, which models the behaviour of moored vessels, using motion measurements performed at North Sea Terminal in the Port of Antwerp. Four events are considered, with four different passing vessels, the moored vessel being a 13 000 TEU container vessel in each case. In the first two cases, the moored vessel has relatively stiff mooring lines, which react in a linear way. The period of the motion as well as the motion amplitude show good agreement in between the GPS measurements and numerical results. The largest deviation is observed with the passage of the tanker, where the passing speed is reasonably high. This leads to a large correction factor, according to Talstra and Blik, for the longitudinal forces due to the passing vessel. This factor should be the subject of future validation work, focussing on passing events in sections with rather high blockages and Froude numbers.

In the next two cases, the moored vessel has elastic mooring lines, which are known for showing a highly non-linear stress-strain behaviour. In the first of these two events, a linear approximation of the elasticity seems to predict the motion peak well, but not the entire motion time series. In the second one, the linear formulation falls short to predict the motion peaks, as well as the full time dependent behaviour. This is because in cases with small pretension force and moderate line forces, the stiffness of the lines in this region of the stress-strain curve is limited. Reducing the modelled stiffness by 50% leads to better agreement with the measured motions, however the motion period differs more from the measurements. There must be concluded that in case of highly elastic lines and low pretension force, the current linear model for the elasticity is insufficient to predict the motions accurately. An overhaul of the model is planned, based on the results of full-scale experiments on lines. In general, use of highly elastic lines leads to large motions, certainly when the pretension level is not kept at an adequate level (generally around 10% MBL), during the stay at the berth. In the presence of tidal current and associated water level change, accompanied by draft variation during loading, this requires a continuous effort of the ship's crew.

The paper discusses a first effort to come up with efficiency parameters, which define the potential of a line to take up longitudinal and transversal forces in the horizontal plane. Based on force and strain considerations, the efficiency parameters e_x and e_y are defined as a function of the line angles and the line length. These efficiency parameters are used to identify the most (in) efficient lines, in function of the orientation of the external load, and to perform targeted adjustments to the position of the lines. In reality the practical constraints of the operational container terminal, including the distance between moored vessels, has to be taken into account. The balance and performance of the mooring configuration is summarized using four efficiency parameters, denoting the suitability to take up longitudinal and lateral forces. A simple example is given, where starting from the mooring plan used for validation, a change of the lines' position, influences the performance of the configuration significantly. Further work into the potential of these coefficients is scheduled.

Acknowledgement

The authors would like to thank Cynthia Pauwels of the Antwerp Port Authority, for her help in providing support regarding the GPS measurements and logged passing parameters at the North Sea Terminal.

REFERENCES

- Delefortrie, G., Vantorre, M., Capelle, J., Ides, S.,** (2012) "The Effect of Shipping Traffic on Moored Ships.", in: 10th International Conference on Hydrodynamics October 1-4, St. Petersburg, Russia. pp. 1–6.
- IACS,** (2016) "Anchoring, Mooring, and Towing equipment."
- IACS,** (2014) "IACS : Requirements concerning mooring, anchoring and towing."
- IACS,** (2005) "IACS : Rec. No. 010 : Equipment."
- Ides, S., Pauwels, C., Torfs, P.,** (2018) "Motions of moored vessels due to passing vessels : full-scale measurements at a container terminal in the Port of Antwerp.", in: PIANC World Congress Panama.
- Journée, J.M., Adegeest, L.M.J.,** (2003) "Theoretical Manual of Strip Theory Program "SEAWAY for Windows".", Report 1370.
- PIANC,** (2012) "Report n° 115 - Criteria for the (Un)loading of Container Vessels".
- Pinkster, J.A.,** (2004) "The influence of a free surface on passing ship effects.", Int. Shipbuild. Prog. 61, pp. 313–338.
- Pinkster, J.A., Pinkster, H.J.M.,** (2014) "A fast, user-friendly, 3-D potential flow program for the prediction of passing vessel forces.", in: PIANC World Congress. San Francisco, USA.
- Port of Antwerp,** (2017) "2017 Facts and Figures."
- Port Today,** (2018) "<https://port.today/msc-cma-cgm-open-door-megamax-24-era/>" , accessed 15/03/2018.
- Talstra, H., Bliet, A.J.,** (2014) "Loads on moored ships due to passing ships in a straight harbour channel.", in: PIANC World Congress. San Francisco, USA, pp. 19.
- Toxopeus, S.L., Bhawsinka, K.,** (2016) "Calculation of hydrodynamic interaction forces on a ship entering a lock using CFD.", in: Proceedings of 4th MASHCON (BAW), Karlsruhe, Germany, Hamburg, Germany, pp. 305–314.
- van Wijhe, H.J., Pinkster, J.A.,** (2008) "The effects of ships passing moored container vessels in the Yangtzehaven, Port of Rotterdam.", in: International Conference on Safety and Operations in Canals and Waterways. Glasgow, UK, pp. 117–130.
- Van Zwijnsvoorde, T., Vantorre, M.,** (2017) "Safe Mooring of Large Container Ships at Quay Walls Subject to Passing Ship Effects.", Int. J. Marit. Eng. 159(A4), pp. 467–476.
- Vantorre, M., Journée, J.M.J.,** (2003) "Validatie van het scheepsbewegingenprogramma SEAWAY met behulp van zeeangspoeven in ondiep water.", in: Numerical Modelling Colloquium, Flanders Hydraulics Research, Antwerp, October 2003. pp. 1–22. (Dutch)

Numerical ship-wave generation, propagation and agitation analysis, related with harbor downtime management

Gabriel Diaz-Hernandez^{1,2}, Antonio Tomás Sampedro¹, Beatriz Rodríguez Fernández¹, Javier L. Lara^{1,2}, Francisco J. de los Santos³, Iñigo J. Losada^{1,2}

ABSTRACT

The present study describes the works related with the numerical evaluation of waves generated by passing ships within the harbor. Ship-waves (or wake waves), are generated by the disturbance of the moving vessel, which delivers a set of oscillations that may interrupt or interfere the safe-mooring activities.

Since energy, shape and frequency of ship-waves depends on: speed, accelerations, track and geometry of the vessel; bathymetric contours; and wharf geometries, it is necessary to design a reliable tool that integrates all these characteristics.

Activities such (safe) loading/ unloading of materials/ passengers, navigation and sedimentary dynamics adjacent to harbour infrastructures (silting), are closely related with ship-wave generation and propagation.

Thus, this study presents a numerical alternative to characterize this forcing, to provide a new diagnosis system for any harbour manager. This will provide a decision tool based on a realistic harbour agitation study, forced by a ship travelling inside real basins, for any vessel/ operator/ route/ navigation protocol/ speed, etc.

Harbour managers will be able to evaluate the agitation effects, know and establish the speed limits, change routes, hours, and even the ship geometries and sizes, in order to satisfy the Port Authority safety limits and to improve the downtime records.

1. INTRODUCTION

In the present study, the main methodology for the numerical generation of ship-waves is described. The aim of this research is to obtain a robust and reliable system that predicts, in a realistic approach, the magnitude of the wave generated by the passing ships inside any port and harbour.

Ship-waves are first generated by the moving vessel and then propagated towards the port basin, channel and contours, and finally interacts with the berthing zones, breakwaters, and moored ships.

The numerical tool described here has been validated with several benchmark cases (laboratory) and in-situ measurements, obtaining very good predictions. Furthermore, the tool can be easily adapted/ integrated into any operational strategy designed for port management, as an individual module that allows the predictive knowledge of ship-waves, starting from a predefined selection (catalog) of trajectories, type of vessels and representative speeds taken from the whole vessel database (i.e. Automatic Identification System, AIS) of any port to be analyzed.

With this innovative product, a new predictive knowledge is established within any Port Authority in order to manage better any operation areas, docks and berthing areas to be analyzed, and that may be interpreted according to the operational conditions that each Port Authority considers.

2. METHODOLOGY

The methodology deals with the modification of a wave propagation numerical model, based on the non-linear and dispersive Boussinesq equations, by including the effect of the passing ship and the subsequent flow perturbation, propagation, and interaction with bathymetries docks AND basins.

¹ Environmental Hydraulics Institute "IHCantabria", Spain.

² University of Cantabria, Spain.

³ Algeciras Port Authority (APBA), Spain.

The numerical strategy requires the establishment of a complete working methodology: pre-processing and adaptation of the bathymetric, port and AIS data, in order to provide an easy-to-use, relocable and reliable tool ready to be applied in any real harbor at any stage: pre-design, design, construction, operation and modification (extension, improvement, etc.).

Hence the following tasks were developed:

- i. A state-of-the-art review related with the mathematical and numerical generation of the waves generated by passing ships, in order to identify the best strategy that suits the numerical needs.
- ii. Adaptation of the numerical tool to be used for a good ship-wave generation, taking into account the most relevant physical characteristics of the ship (speeds and geometries), as well as the spatial trajectories physics. This task involves an exhaustive validation process of the numerical tool using benchmark laboratory tests and field data.
- iii. A detailed guideline to numerically assimilate the ship routes, sizes and speeds for an extensive catalogue of ships for any Port Authority is presented, based on realistic AIS databases. This catalogue is used in the following tasks.
- iv. Run of the catalogue of ships with the numerical tool (once modified, adapted and validated), in order to obtain the corresponding characteristics of the shipwaves (individual wave heights and associated oscillation periods), at different pre-established control points and ship maneuvering areas.

Each task is described below.

2.1 Task 1. State-of-the-art review related to ship-waves generation and propagation

This section undertakes an exhaustive review of the state-of-the-art. In particular, a review is made of issues related to the numerical modeling of the phenomenon and the physical characteristics of ship-waves for its future use and assimilation within the research.

When a boat sails produces two types of ship-waves, some divergent and some transverse (see Fig. 1), the form and existence of these depends mainly on the speed at which the boat sails, distinguishing three speed types: sub-critical, trans-critical and super-critical defined by the Froude number (1) according to the ship length (L), the translation speed (u) and the acceleration of gravity (g).

$$F_{RL} = \frac{u}{\sqrt{g \cdot L}} \quad (1)$$

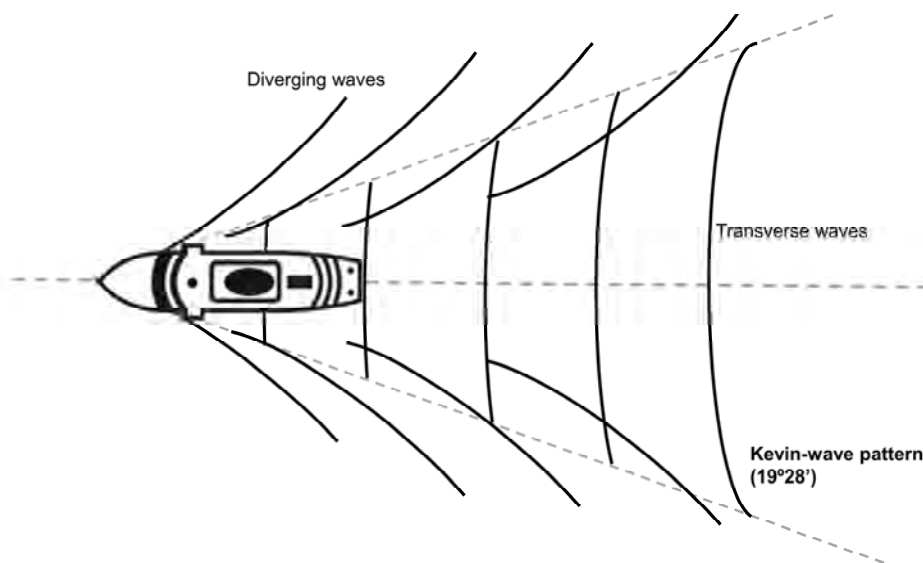


Figure 1: Ship-waves typical pattern and geometry

One of the fundamental documents to understand the generation and general characteristics of ship-waves is presented by McFarlane (2012), where it can be highlighted that the most relevant situation for the creation of ship-waves and therefore, on which the study should focus, is the trans-critical stage, because it is where there is more variation of the four characteristic parameters of the waves: its the period (T), the attenuation coefficient (n), the wave height constant (γ) and the angle between the direction of navigation and the line that intersects the transverse waves with the divergent ones ($\theta=19^{\circ}28'$).

The ship-wave trains (space-time propagated free-surface waves) contain very different types of waves. Within each group of waves, three types can be distinguished: Type A, B and C. In order to understand the whole study, the difference between them must be understood (see Fig. 2).

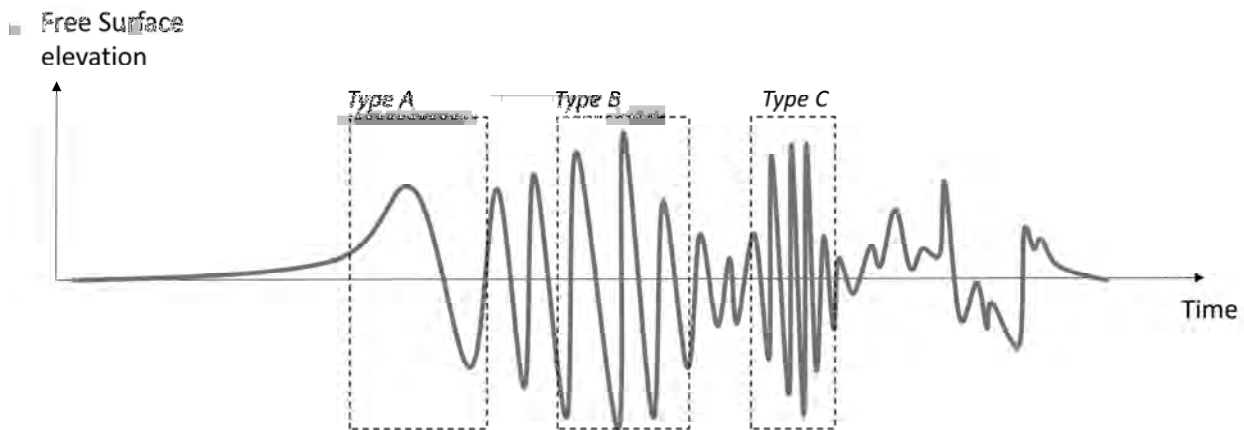


Figure 2: Ship-wave profiles A, B and C

Type A: is the wave with the longest period but the lowest height. Sometimes it can reach more height and with more energy. However, despite being the least high are those that have greater area under the trough since the period is longer, that is, the distance between peaks is larger and, therefore, have much more energy. These waves differ well in supercritical speeds, since the ridges are larger and their footprint is more noticeable.

Type B: they go after the waves A. They have a shorter period than the previous ones, although they are sometimes similar. What differentiates them from the previous ones is the increase in their height. They also have a lot of energy despite not being the wave with the highest height and period.

Type C: they are small divergent waves and reach the maximum height. They always follow waves A and B, and they have the shortest period. If it is in a sub-critical or trans-critical situation, the height is smaller.

Regarding the numerical modeling of the ship-wave generation phenomenon, the literature gathers different mathematical strategies that can be grouped into three large families: a) Analytical approaches, b) modeling with potential approximations, c) codes based on the theory called "thin ship "(TS), d) modeling based on Boussinesq approximations, and e) three-dimensional modeling with CFD (Computational Fluid Dynamics) models.

All the aforementioned approaches try with more or less success the adequate evaluation of the characteristics of the ship-waves for two well differentiated zones: 1. the field near the navigation line of the vessel where the funds can be considered deep and constant, and 2. the far field to the boat where the waves interact with the coastal or port areas with variable bathymetries.

Raven, (2000) and Kofoed-Hansen et al. (2000) indicate that the applied methods usually analyze these two zones individually and uncoupled, performing a post-coupling process to try to couple and give continuity to the process of generation-propagation-interaction of the shiop-waves throughout the domain (from the field near to the distant one).

The Raven analytical approaches (2000) are based on mathematical adjustments of empirical measurements in the field or laboratory, carried out under controlled situations of navigation and vessel geometry, with a limited number of typologies and bathymetries with a constant background. These basic formulations only offer a first outline of the wave heights and periods that can be expected for a standard vessel sailing at speeds with limited speed ranges that do not differentiate between the different subcritical to supercritical translation regimes. Analytics usually focus their range of application only to the near field and constant depths of propagation.

Approaches based on potential models proposed by Raven (2000) and Hughes (2001) often employ models that solve the free surface of the flow considering only the linear interactions within the flow. The surface of the water and the body or volume that defines the three-dimensional shape of the vessel is represented by a three-dimensional mesh of panels. The surface of the fluid is derived from obtaining the collapse and settlement of the fluid due to the pressures of the boat in motion and depending on the speeds of translation, the boat's own geometry and the weight or tonnage of each one of them. The generated subsidence propagates in the rest of the domain, initially at rest, solving the equations of the potential flow based on the initial perturbation, for constant background. This solution is not realized taking into account the temporary or transitory behavior of the propagation phenomenon of the ship-waves, so the results obtained are limited to a static photograph of the equilibrium state of the flow for any instant of time. This approach usually provides information about ship-waves very detailed and realistic in the area near the boat (near field) since it takes into account the detailed and three-dimensional shape of each floating body. However, the stationarity, the constant background limitation and the computational effort, which can be expensive (depending on the geometrical detail of the vessel and its size), make this approach move away from the needs of the current project.

Third, TS-type codes are based on the linear assimilation of Kelvin-type sources and sinks placed along the centerline of the vessel to represent the free surface. This approach is again limited to constant funds, linear behavior of the WW generated and waves with small amplitude compared to their lengths. These codes proposed by Havelock (1908), Mitchell (1898), Eggers et al. (1967), Gadd (1999), Molland et al. (2000), Tuck et al. (2001) and Doctors (1997), which solve the equations based on multiple integrations of each established source and sink, can only be applied at constant (not transient) translation speeds and preferably below the Froude critical regime and shallow depths. Finally, this type of approach usually shows instabilities for the evaluation of ship-waves in the far field, even with a constant background, either by numerical dissipation or by obtaining ship-waves height well above reality.

On the other hand, the codes based on the Boussinesq equations have focused primarily on the evaluation of ship-waves in the far field. That is, once the initial perturbations are generated in the near field, either with a potential model or a TS type. Kofoed-Hansen (1999, 2000) propose the use of models based on the Boussinesq equations for the subsequent solution of the far field. This coupling between models allows solving the wave propagation type WW over variable and complex backgrounds, taking into account the non-linear and transitory effects, interaction with port contours with complex geometries and even the evaluation of the hydrodynamics in the surf zone, currents in beach, break and approximate run-up, all in extensions of the order of kilometers.

This scheme of solution to the problem seems, therefore, the most appropriate for a correct evaluation of the effects of the ship-waves in the wharf or coast, especially if the objective is to evaluate fully and integrated large coastal areas. However, this coupling technique usually involves complex difficulties when trying to integrate the physical effects of the flow related to the propagation of the near field to the far field, and supposes simplifying hypotheses when generating the wave type ship-waves (constant bathymetry, constant velocity of the boat, straight trajectories, etc.). Therefore, if you want to make an easy assessment of ship-wave generation towards realistic boat traffic scenarios, this strategy can be a difficult and tedious numerical challenge.

For this reason, Chen and Sharma (1995) investigated the possibility of integrally solving the generation and subsequent propagation of ship-wave using Boussinesq models, managing, in a single step, the generation in the near field and its subsequent propagation to the field. far. This solution seems the best from the point of view of operational management to evaluate the characteristics of ship-waves in the quay and the coast. This strategy has been developed in depth by Jiang (2000) for vessels in motion, with variable trajectories and changing speeds. However, for this he used the simplified Boussinesq equations (weakly dispersive and non-linear).

This strategy has the disadvantages of having a poor spatial definition of the vessel geometry, because the mesh discretizations of the Boussinesq models for areas of the order of kilometers are usually not smaller than 5 m in general, so the digital boat generated is synthesized to polygonal or prismatic geometric shapes. However, Jiang et al. (2002) have shown that with an adequate validation process, the ship-wave generation in the near field can be calibrated with simplified ship forms.

Finally, there are the CFD-type approaches (eg FLOW models, OpenFoam) that are responsible for solving the near field of the generation of the WW taking into account the completely three-dimensional flow around the vessel in motion, also considering the detailed geometry of the boat (of the order of millimeters). This strategy is analogous in area of influence and conditions to the panel method, with the fundamental difference that the solution of the flow is made using the Navier Stokes averaged equations (RANS) that solve the complete 3D flow, considering all the transitory effects, non-linear, viscous and turbulent. These models, in addition to being highly computationally expensive, are usually focused on the evaluation of the efforts in the structure of the vessel by the wave action generated and projected on it, the evaluation of the geometry for the optimization of the hydrodynamic and turbulent performance, and the optimization of competition prototypes. So, if you want to use this type of modeling in the creation of vessel and trajectory typology scenarios, it does not seem to be a recommendable strategy.

In summary, the state-of-the-art provides information on the characteristics of the ship-waves generated in the near field and the strategies for its evaluation and subsequent propagation to the far field. Once the conditioning factors of each of them have been analyzed, and based on the objectives of the study, the decision has been made to adopt the integral solution technique, using the Boussinesq model proposed by Jiang et al. (2002), extending its scope to a better definition of the numerical domain (a better spatial resolution) and to improve the processes of wave propagation towards the far field through the adaptation of the non-linear and dispersive Boussinesq equations. All this with the final objective of evaluating the general characteristics of the ship-wave type waves and their temporal evolution, including waves type A and type B waves (the highest in energy) previously discussed in different areas within any port, as well as the post-processing of said series in the form of histogram, spectral and general statistics charts of the individual waves of the record.

2.2 Task 2. Numerical model adaptation towards a ship-wave generation strategy

IHCantabria has developed IH-BOUSS model, which solves the temporal patterns of wave propagation, transformation and agitation, within numerical domains of the order of kilometers with complex contours, on real bathymetries, through the use of regular meshes in finite volumes and solving the two-dimensional (2DH) patterns of velocities, pressures, and free surface, considering the processes of asomeration, refraction, diffraction, and run-up in beach and port structures, as well as the reflection and radiation of the waves.

In addition, the numerical model includes in its formulation the processes of energy dissipation by partial or total absorption of the contours, processes associated with wave breakage, bottom friction and turbulent effects.

One of the fundamental advantages of using the IH-BOUSS numerical model is that it is based on advanced capabilities to solve wave patterns on a numerical domain with real complex contours, considering a temporal evolution of these patterns, and how the waves propagate and interact with port contours. This allows the evaluation of the general characteristics of wave trains on foot of the structure, inherently including the non-linear and transitory processes that this has experienced from its point of generation to the structure.

Following the methodology proposed by Jiang et al. (2002), the IHBOUSS model must follow an adaptation protocol in order to generate ship-wave in a simple, repeatable and reliable way, taking into account the following boundary conditions of the problem:

- Consider the different dimensions of the vessels to be analyzed (length, draft and beam).
- Take into account realistic trajectories of vessel movement: turns and accelerations.
- Consider a good spatial definition of the element that represents the digital vessel to be simulated.
- Be able to evaluate an extensive area of the order of 10 to 15 km, with a mesh resolution of the order of 2 m to be able to meet the dimensional needs of the bay of Algeciras and the geometries of the vessels, respectively.

- That the generated numerical domains are executed in competitive computational times in order to simulate at least a N number of reosentative types of vessels / trajectories / speeds within the project (i.e. for the Alceiras study, a $N=40$ ships were selected and simulated).
- That the model adapted for the ship-wave is then tested to a rigorous validation process with instrumental, mathematical or analytical data to guarantee its reliability when generating the aship-waves.

Taking into account the different conditions mentioned above, the effort has been focused on this process of adapting the IH-BOUSS model for the creation of ship-waves. Basically, the adaptation of the numerical model has been based on the inclusion of a mobile "sink" element in the domain of the IH-BOUSS model, similar to the classical source function proposed by Wei et al. (1999) but considering only the state of negative oscillation below the mean sea level, and a prismatic volumetric form that can move freely through the numerical domain $[X, Y]$, taking into account the instantaneous position X and Y for any instant temporal $X_i = f(X_{i-1}, t_i)$; $Y_i = f(Y_{i-1}, t_i)$.

Fig. 3 shows an example of the realistic trajectory for any vessel sailing at variable speed within a 500 x 1000 m domain. The spatio-temporal trajectory known a priori, therefore, can be adjusted to a mathematical function that defines it and that can be included in the model. In this way a faithful numerical representation of the real movement of the vessel and an easy assimilation of this behavior by the model is guaranteed, avoiding in this way tedious adaptations of trajectory reading and post-processing of these (for example, from the Raw Information System (AIS) data).

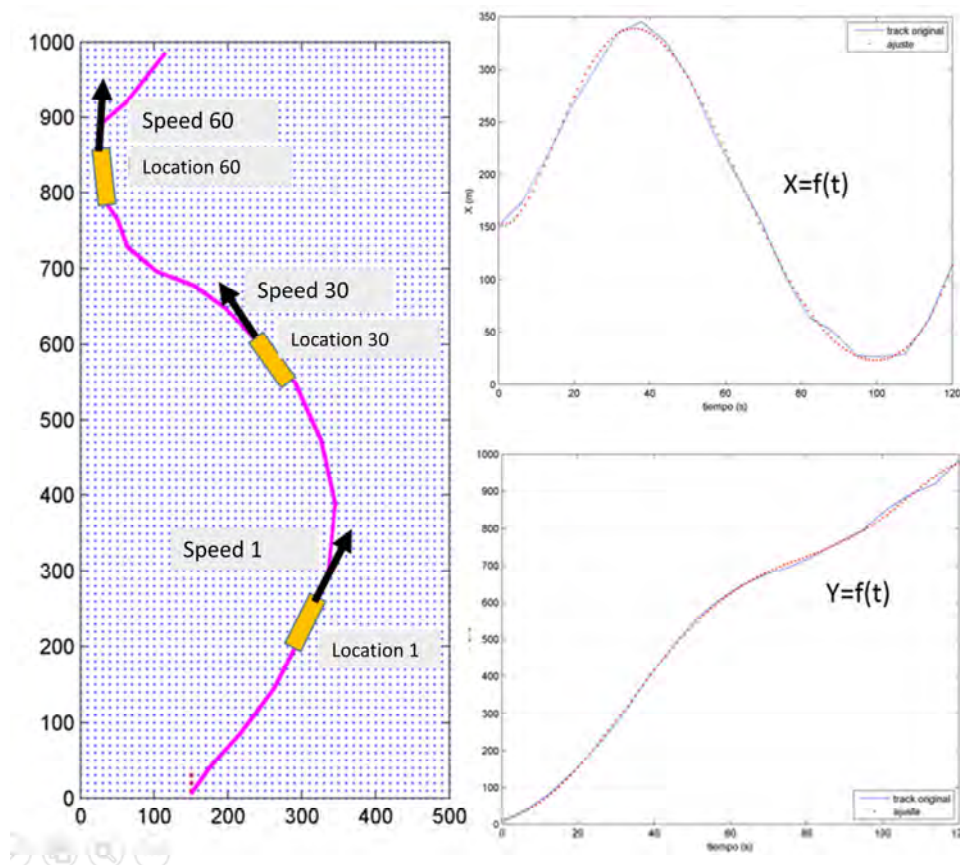


Figure 3: Ship trajectory assimilation within $[X, Y]$, taking into account the ship speed and turns

Regarding the inclusion of the new source function represented by the ship, different tests and approximations have been made, finding that the inclusion of a rectangular prism representing the vessel in motion is more than enough to generate realistic and suitable ship-waves type waves. It is true that the near field (very close to the boat), possibly lacks sufficient detail to be able to consider a flow well represented in this area. However, the results so far found and validated indicate that once the initial disturbance in the flow (originally at rest), the ship-waves manages to adopt realistic forms and speeds consistent with the phenomenology studied. The assimilation of the typical dimensions of a boat (the minimums for its correct definition: beam or beam (W), draft or draft (d) and length (L)) in the rectangular numerical prism that has been included in the model IH-BOUSS.

Fig. 4 to 6 show preliminary results of different validation examples so far carried out, considering container type (general dimensions) and Ferry, sailing under different geometric characteristics.

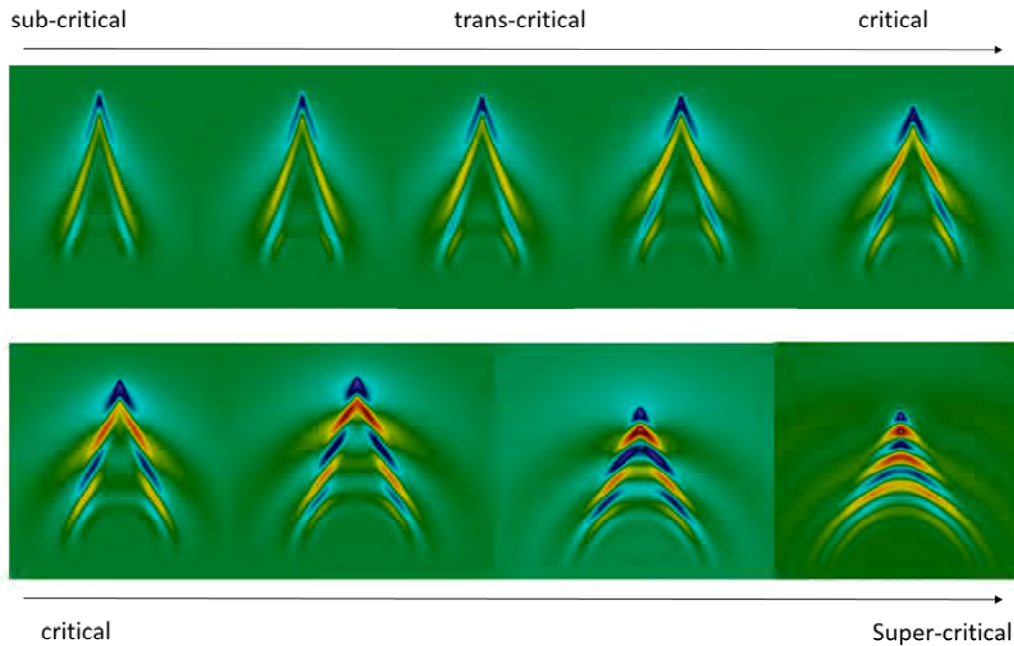


Figure 4: Ship-wave behavior example generated by IH-BOUSS model for different critical regimes (Froude numbers)

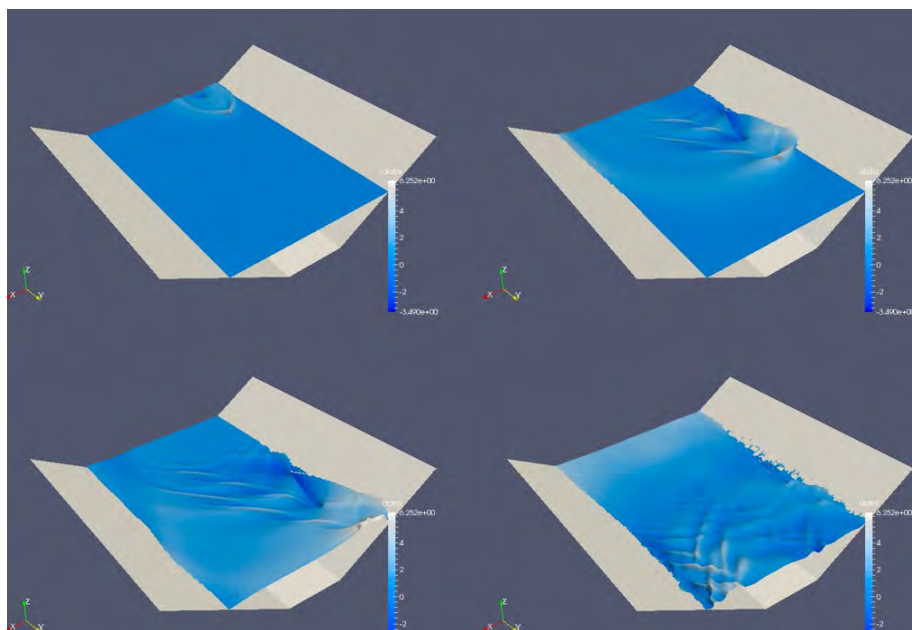


Figure 5: Ship-wave example generated with IH-BOUSS model for a ship travelling along a inner waterway and ship-wave run-up generation

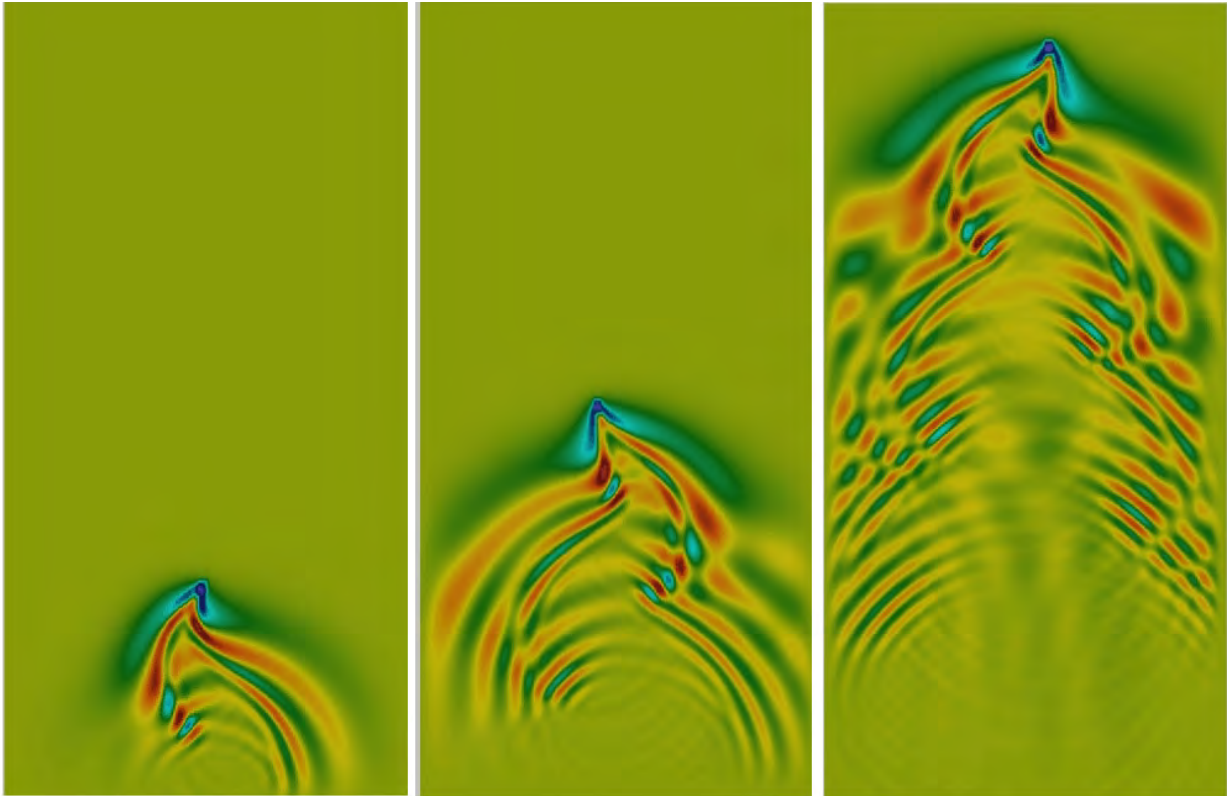


Figure 6: Ship-wave example generated with IH-BOUSS model for a ship travelling along a sinusoidal path with accelerations

2.3 Task 3. Numerical model validation

The prismatic and rectangular shape included in the IH-BOUSS model shows numerically a good numerical stability and fairly qualitatively adequate results according to the previous observations made in the literature. However, during the validation process, it was observed that the wave heights and periods (type B mainly) showed a general tendency to be overpredicted, regardless of the speeds and the type of vessel analyzed.

For this reason and based on the instrumental comparison information used to validate the model, we have chosen to impose some adjustment coefficients for each numerical dimension of the rectangular prism α , β , and γ , which multiply the real dimensions: length (L), draft (d) and sleeve (W) respectively.

Figure 5 shows an example of the validation results for two type vessels (containers and Ferry) and for values of $\alpha = 0.6$, $\beta = 0.25$, and $\gamma = 1.0$. These parameters seem to adequately adjust the measurements of the wave height (type B) and their respective periods. In addition, they remain constant regardless of speeds, types of boat and bathymetric levels. So it seems that the final and final adjustment values will be around the aforementioned values. With this validation and with the calibration coefficients set, a second round of validation is carried out considering instrumental data for different vessels, mainly related to a high-speed ferry typology (see an example of the validation task in Fig. 7).

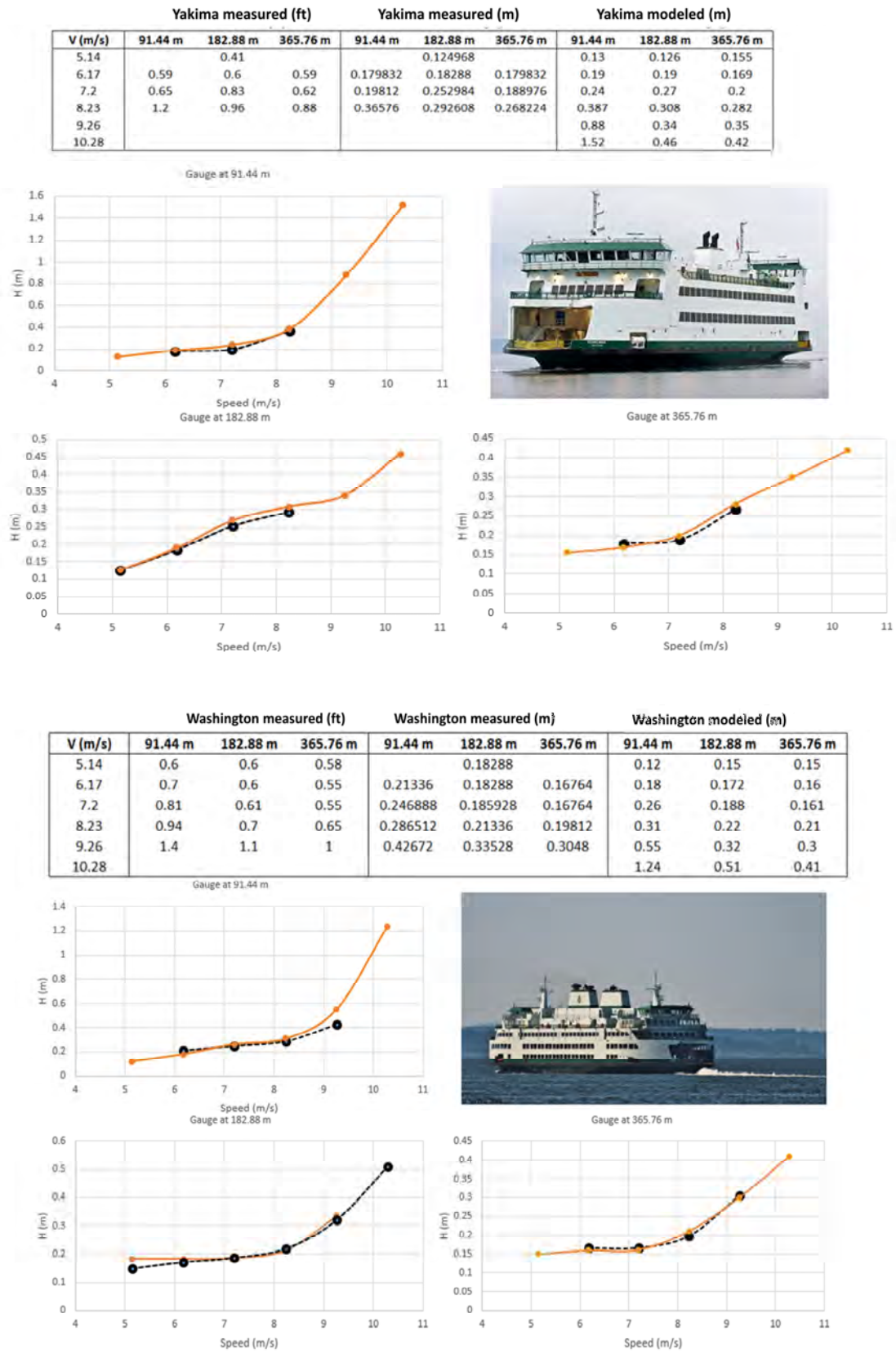


Figure 7: Wave height (type B) validation for a Fast-Ferry ship (Yakima, Washington State Ferries & (Seath, Washington State Ferries).

2.4 Task 4. AIS database pre-process

Regarding the pre and post-process work of the AIS database (provided by any Port Authority), a brief description of the work carried out and final products produced is presented below. From now on, the explanation and description will be based on the Port of Algeciras experience (developed by IHCantabria the Algeciras Bay-Port Authority, APBA).

The APBA provided the AIS information in .CSV (raw comma-separated values) format for two years of measurements, in 2014 and 2015. This information requires an intense process of analysis and pre-processing to be appropriate to the study. Specifically, the numerical model needs to be forced with information about the trajectories, type of vessels (geometry and general dimensions) and translation speeds of these, for a finite catalog of simulations ($N=40$). Thus, it has been necessary to establish an automated reading protocol of the raw AIS series that allows obtaining as a first fundamental product, a disaggregated database for each individual ship that has sailed within the Bay of Algeciras between 2014 and 2015. From this form, by having individual files that describe the boats and their navigation history in a specific way, it will be possible to make an intelligent selection of the catalog of 40 simulations that represent, in the best possible way, the casuistry of generation and propagation of ship-waves within the study area. This task has focused on the pre-processing of AIS information in order to obtain the individualized files for vessels mentioned above. To this end, a series of MATLAB© programs has been carried out that allow the automatic reading of the two large families of CSV files for each year. The ultimate goal is to have information broken into individual files of each type of vessel (see Fig. 8), which will include all data related to them (names, international identifiers, dimensions, spatial and temporal position, etc.).

Once the execution of both programs, 8126 files are obtained corresponding to the same number of individual vessels that have sailed within the Bay of Algeciras in the years 2014 and 2015. The obtaining of these files supposes the completion of the pre-process work and the beginning of the post process, where the representative cases (40) to be simulated by the IHBouss model are obtained and that in turn will be dumped in the operational system of evaluation of the waves type ship-waves according to the typologies or cases that the port manager considers within the finite catalog. Figure 6 shows an example of the graphic representation of the spatiotemporal trajectories of four different vessels, once their data has been separated into individual files. Once the pre-selection has been defined and in line with the APBA after its presentation in project control meetings, the final selection of 40 cases based on the possibility of repeating the type of vessels is made, in order to give more weight to those boats that obtained the most weight in the pre-selection. In this way it is ensured to cover a wider spectrum in the spatial effects of the most important vessels for the APBA.

2.5 Task 5. Numerical run of N selected ships and post-process

This section summarizes the results obtained after the execution of the final catalog of the $N=40$ events, as well as the post-treatment of the wave series type ship-waves obtained in the whole numerical domain. In the first place, the numerical domain is defined where vessels will pass from their entrance through the Bay of Algeciras to their different destinations in docks and anchorage areas. For the design of the numerical domain it is important to point out that the extension of the bay should be considered in the same simulation, in order to capture numerically the ship-waves generated by the passage of a vessel from one end of the Bay to the other. Therefore, it is decided to create a domain with a resolution of 3 x 3 m for the whole Bay considering the following spatial box (in UTM coordinates).

$$X_{min} = 279761.3033; Y_{min} = 3998912.3298; X_{max} = 288598.9463; Y_{max} = 4006805.3941$$

The final numerical mesh has 2946 x 2632 nodes in each of the orthogonal directions. Fig. 9 shows the final bathymetric and numerical domain proposed for the simulations.

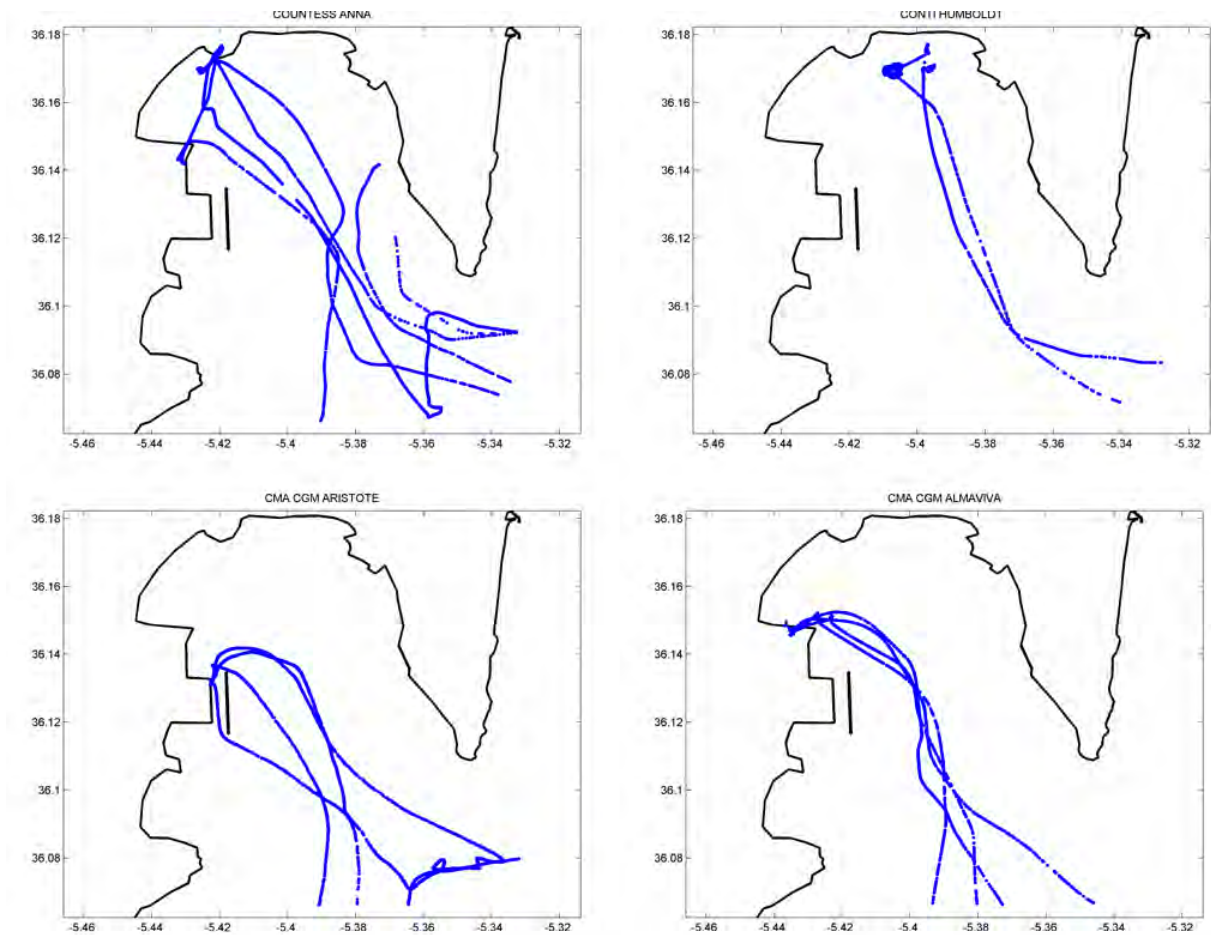


Figure 8: Example of 4 individual ships isolated from the whole 2-year AIS database

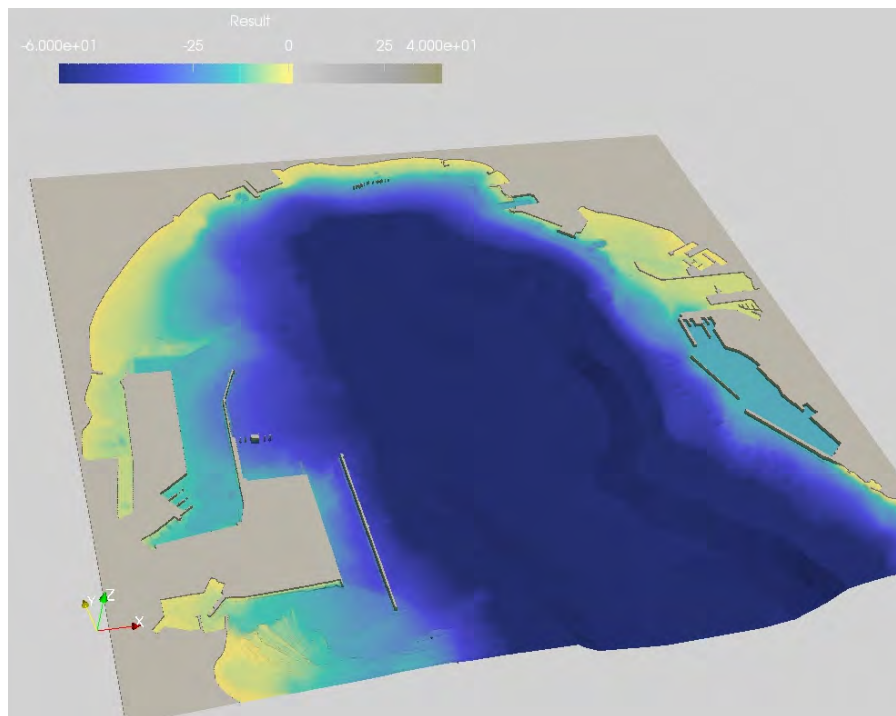


Figure 9: Numerical domain and bathymetry used in the APOBA domain and adapted for IH-BOUSS model

Each of the $N=40$ simulations has been executed in parallel using 16 processors, obtaining satisfactory final results, finding an absolutely stable behavior of the numerical tool, showing wave heights type ship-waves realistic and within the ranges observed in the literature, a propagation of these waves towards the adequate port contours and very competitive computational times (3 to 4 days of simulation as a mean for durations of events of 1 hour of ship trajectories).

Once the simulations are finished (see Fig. 10), two types of numerical results are collected: a) temporary maps of free surface in all the numerical domain, and b) temporary series of free surface in 83 control points arranged in different areas of operational interest.

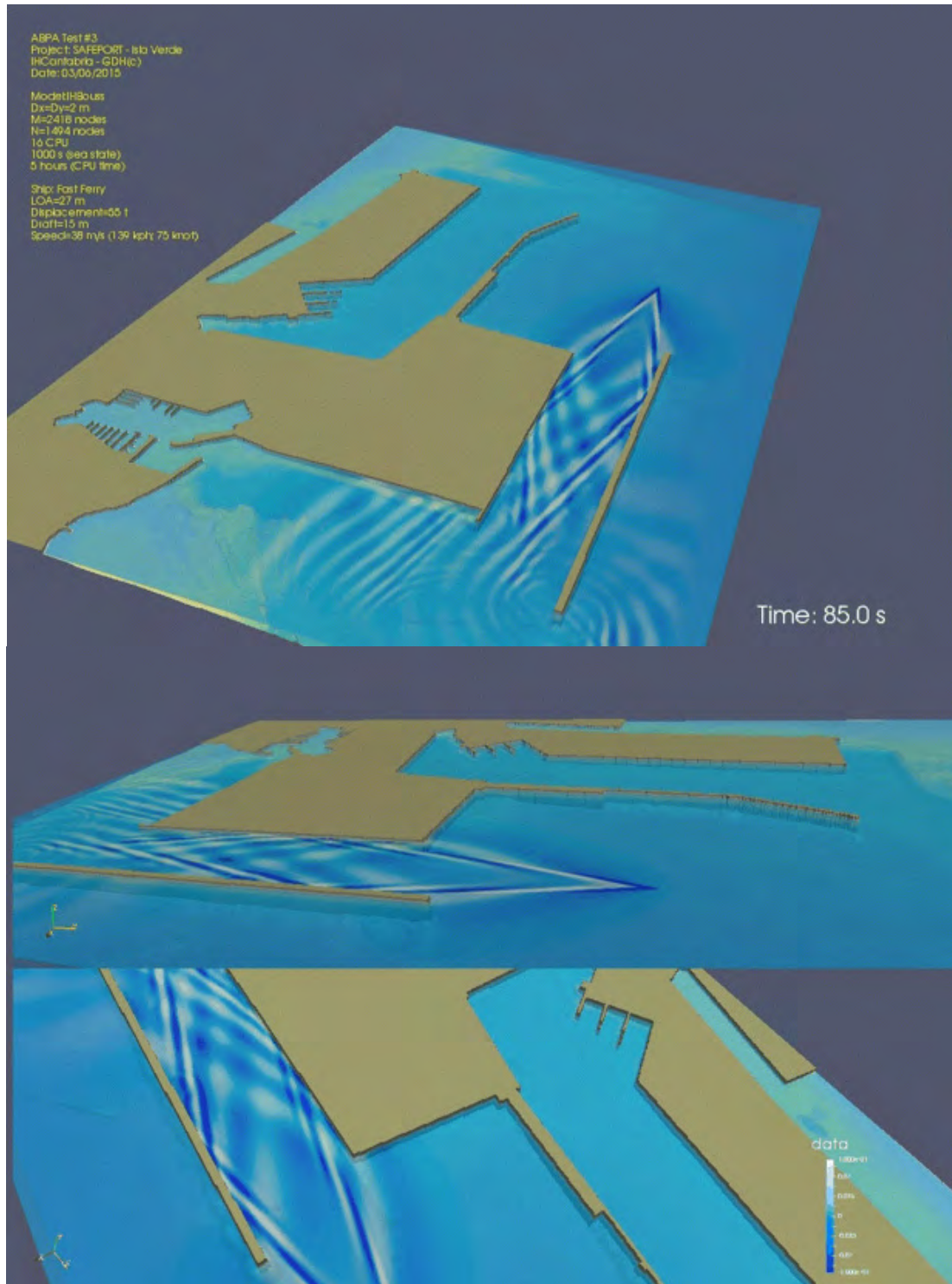
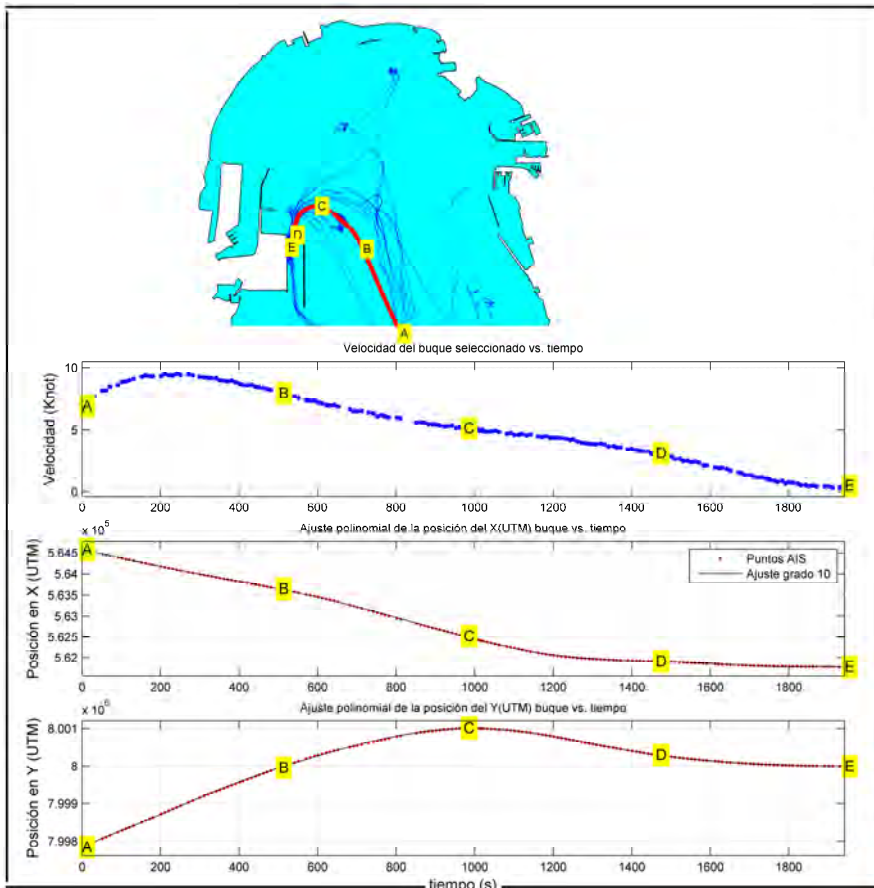


Figure 10: Example of a snapshot for a Fast-Ferry navigating inside APBA's Port (3 different views)

2.6 Task 6. Final results and data sheets obtained for operational port managers

As part of the elaboration of the data-results of each of the 40 simulations carried out, summary-sheets are made that collect and show the general information of each one of the simulations (see Fig. 11), integrating the following data:

- General information on the geometry of the selected vessel, name, identification keys, photograph and start and end dates of the selected path.
- A general map of the Bay of Algeciras that includes all the AIS events recorded for the vessel selected for each of the 40 events (blue dots) and the selected trajectory in the individual event that has been simulated (red dots).
- Instantaneous velocity chart (knots) of the event / vessel selected showing four spatial positions *A*, *B*, *C* and *D* to help its identification on the map of the Bay of Algeciras (see Fig. 11).
- Two graphs that define the time-space evolution of the selected trajectory for each event, showing the time vs. the position *X* (UTM) and *Y* (UTM). Likewise, the adjustment of the 10-degree polynomial used to force the numerical model is included. The 4 guide points *A*, *B*, *C* and *D* are also included.
- A zoom of the general map of the Bay of Algeciras centered on the selected control point, where the trajectory for the event to be analyzed is included, the points closest to the chosen position and the selected trajectory in the individual event that has been simulated (red dots).
- Instantaneous velocity chart (knots) of the selected event / vessel showing four spatial positions *A*, *B*, *C* and *D* to help its identification on the map of the Bay of Algeciras (analogous to that observed in the "A" type sheet).
- Graph of the instantaneous distance of the event / vessel selected according to the analysis point, showing also the four spatial positions *A*, *B*, *C* and *D*.
- Temporary free surface graphic registered numerically at the selected control point.
- Wave height (*H*) and period (*T*) histograms of each individual wave recorded at the selected control point.
- Joint plot of *H* vs. *T* to observe the distribution of wave heights and their relation to periods.
- Two graphs that define the time-space evolution of the selected trajectory for each event, showing the time vs. the position *X* (UTM) and *Y* (UTM). Likewise, it includes the adjustment of the polynomial of degree 10 used to force the numerical model and the 4 orientative points *A*, *B*, *C* and *D*.



Caracterización climática

Oleaje generado por el paso de buques

Nombre: "MARINA"

IMO: 8906743

MMSI: 215210000

Eslora: 236 m

Manga: 32 m

Calado: 8 m

Trayectoria seleccionada

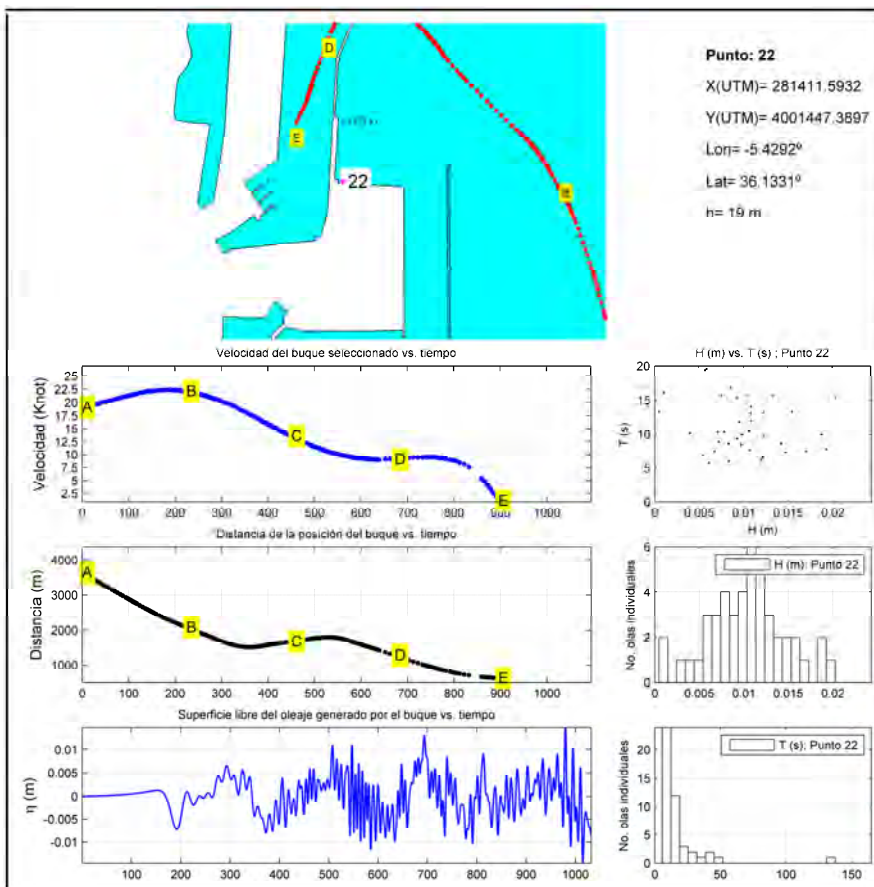
Hora inicial: 17-Oct-2014 17:19:16

Hora final: 17-Oct-2014 17:51:38

Número de eventos AIS: 179

Duración del evento: 1942 s

*Datos AIS proporcionados por la APBA desde enero 2014 a marzo 2015



Caracterización climática

Oleaje generado por el paso de buques

Nombre: "JAUME II"

IMO: 9116113

MMSI: 224195530

Eslora: 81 m

Manga: 26 m

Calado: 3 m

Trayectoria seleccionada

Hora inicial: 05-Aug-2014 21:12:07

Hora final: 05-Aug-2014 21:27:02

Número de eventos AIS: 243

Duración del evento: 895 s

*Datos AIS proporcionados por la APBA desde enero 2014 a marzo 2015



Figure 11. Data-sheet example (in Spanish) for 2 different ships and control point #22.

3. CONCLUSIONS

A complete ship-wave predictor system has been successfully obtained. This system is able to evaluate the waves generated by the passing of the vessels, in a realistic, reliable and computationally agile way. This development allows the generation of products of direct exploitation and exploitation by any power authority that requires to know the response of its facilities to this type of forcing.

This innovative approach opens a new way of study this phenomena considering important improvements compared to the traditional-limited approaches.

As an example, the system is actually integrated into Algeciras Port met-ocean strategy. The APBA has exploited this new knowledge through the adaptation of an innovative operational system for calculating the waves generated by the passage of vessels (ship-waves) in different locations pre-established by the APBA and for a finite number of vessels (catalog of 40 types of boats / speeds / trajectories).

This new information will allow any Port Authority to know, quantify, diagnose and manage its different areas of special operational interest in relation to the existing ship-waves daily in its port environment.

4. REFERENCES

- CHEN, X.-N., SHARMA, S.D., (1995). "A Slender Ship Moving at a Near-critical Speed in a Shallow Channel." *Journal of Fluid Mechanics*, 291: 263-285.
- DANISH MARITIME AUTHORITY, (1997). "Report on the Impact of High-Speed Ferries on the External Environment" (in Danish).
- DEMIRBILEK, Z., VINCENT, L., (2002). "Water waves mechanics." *Coastal Engineering Manual, Part II, Hydrodynamics, Chapter II-1*, L. Vincent, ed., U.S. Army Corps of Engineers, Washington, DC., 1 - 115.
- DOCTORS, L.J., (1997). "Resistance Predictions for Transomstern Vessels." *Fast 2001 The 6th International Conference on Fast Sea Transportation*, Southampton.
- EGGERS, K.W.H., SHARMA, S.D., WARD, L.W. (1967). "An Assessment of Some Experimental Methods for Determining the Wavemaking Characteristics of a Ship Form".
- GADD, G.E. (1999). "Far field waves made by Ferries. *Hydrodynamics of High-Speed Craft*". The Royal Institution of Naval Architects, London, pp. 1-12.
- HAVELOCK, T. H. (1908) "The propagation of Groups of Waves in Dispersive Media, with Application to waves on Water produced by a Travelling Disturbance". *Proceedings of the Royal Society of London, Series A. Vol LXXXI*, pp. 398-430.
- HIGH-SPEED CRAFT CODE, (2000). "International Code of Safety for High-Speed Craft." *International Maritime Organization*, London.
- HUGHES, M (2001) "CFD Prediction of Wake Wash in Finite Water Depth". *HIPER'01 2nd International EuroConference on High Performance Marine Vehicles*, Hamburg, pp. 200-211.
- JIANG T., (2000). "Investigation of Waves Generated by Ships in Shallow Water." In *Twenty-Second Symposium on Naval Hydrodynamics*. The National Academies Press, Washington, D.C., United States.
- JIANG, T., HENN, R., SHARMA, S.D., (2002). "Wash waves generated by ships moving on fairways of varying topography." In *Twenty-Forth Symposium on Naval Hydrodynamics*, Fukuoka Japan 8-13 July 2002.
- KIRKEGAARD, J., KOFOED-HANSEN, H., B. ELFRINK, (1998). "Wake Wash of High-Speed Craft in Coastal Areas." In *Proceedings of the 26th International Coastal Engineering Conference*, 22-26 June 1998, Copenhagen, Denmark.
- KOFOED-HANSEN, H., (1996). "Technical Investigation of Wake Wash from Fast Ferries Summary & Conclusions." 5012, *Danish Hydraulic Institute*, Hørsholm.
- KOFOED-HANSEN, H., JENSEN, T., KIRKEGAARD, J. FUCHS, J., (1999). "Prediction of Wake Wash from High-Speed Craft in Coastal Areas," *Hydrodynamics of High Speed Craft*. The Royal Institution of Naval Architects, London, pp. 1-10.
- KOFOED-HANSEN, H., JENSEN, T., SØRENSEN, O.R. FUCHS, J., (2000). "Wake Wash Risk Assessment of High-Speed Ferry Routes - A Case Study and Suggestions for Model Improvements." *The Royal Institution of Naval Architects*, London.

KOFOED-HANSEN, H. AND MIKKELSEN, A.C., (1997). "Wake Wash from Fast Ferries in Denmark." In Proceedings of the 4th International Conference on Fast Sea Transportation, Sydney, Australia.

MACFARLANE, G.J., BOSE, N. AND DUFFY, J.T., (2012), "Wave Wake: Focus on vessel operations within sheltered waterways", Proceedings of the SNAME Annual Meeting, Providence,, Rhode Island, 24-26th October 2012.

MITCHELL, J. H. (1998). "The Wave Resistance of Ships". Philosophical Magazine, 45 (series 5): 106-123.

MOLLAND, A.F., WILSON, P.A., CHANDRAPRABHA, S. (2000). "The prediction of ship generated Near-Field Wash Waves Using Thin-Ship Theory. Hydrodynamics of High-Speed Craft". The Royal Institution of Naval Architects, London, pp. 1-13.

RAVEN, H.C., (2000). "Numerical Wash Prediction Using a Free-surface Panel Code", Hydrodynamics of High Speed Craft Wake Wash & Motion Control. The Royal Institution of Naval Architects, London, pp. 1-12.

TUCK, E.O., SCHULLEN, D.C., LAZAUSKAS, L. (2001). "Ship Wave PATterns in the Spirit of Michell. IUTAM Conference on Free SURface Flows". The University of Birgmingham, Birmingham.

PORT EXTENSION IN MARTINIQUE, IN THE FRENCH CARIBBEAN: USE OF THE OBSERVATIONAL METHOD IN A HIGHLY SEISMIC AREA

by

Patrick Garcin¹, B. Seidlitz² and G. Casse³

ABSTRACT

Grand Port Maritime de La Martinique (GPMLM), the public authority in charge of the port of Martinique, is rolling out an ambitious action plan to develop its container terminal "La pointe des Grives".

GPMLM has appointed Artelia to provide design and construction supervision services for its container's yard and quay extension in 2013. The project proceedings were decided in two stages: the South extension, realised in 2016, object of the present paper, and the North one, construction bid for tender under launching.

The southeast extension consists in a 2.4-ha increasing of the harbor reclamation area and a 550-meter enclosing berm, which is located in a seismically highly active area, and built on alluvium with very poor characteristics.

According to the French Ministry requirements, the design incorporates a total absence of dredging (no maritime borrow materials, no substitution), in order to preserve the environment in the bay of Fort de France and significant settlement amplitudes are foreseen. Therefore, the method chosen to monitor works implementation is the observational method, involving appropriate complementary geotechnical surveys, a strategy based on granular blending materials, and instrumentation of the reclamation area.

This challenging extension involves an objective of making targeted investments in order to protect the environment in an area with major ecological issues and responding to growth on the Caribbean market (following the Panama Canal expansion project) and the rapid changes taking place in maritime traffic (consolidation of cargo flows).

This paper presents the project constraints and the construction methodology, and sets out the feedback obtained in regard to settlement upon delivery of the reclamation area after 12 months of work.

¹ Project director, Artelia Eau et Environnement, France, Patrick.Garcin@arteliagroup.com

² Engineering & Project department director, Grand Port Maritime de la Martinique, France, b.seidlitz@martinique.port.fr

³ Civil Engineer Project Manager, Artelia Eau et Environnement, France, Geraldine.Casse@arteliagroup.com

1. INTRODUCTION

The French port of Fort de France is currently a major logistical hub serving the Martinique economy: it is the main loading/unloading point for containerized maritime traffic and the only transshipment zone on the island, as shown in figure 1.



Figure 1: Location of Martinique in the Caribbean (photo: Google Maps®)

The Pointe des Grives container terminal was commissioned in 2003.

It includes a 20-hectare reclamation area for container storage and 2 berths capable of accommodating PCRF vessels (CMA-CGM vessels on the North Europe-West Indies line) up to 200 m in length and with capacities of up to 2400 Twenty-foot Equivalent Units (TEU):

- A 460 m long main wharf with a 12.5 m draft,
- A 180 m long secondary berth with a 8.5 m draft (See Figure 2).

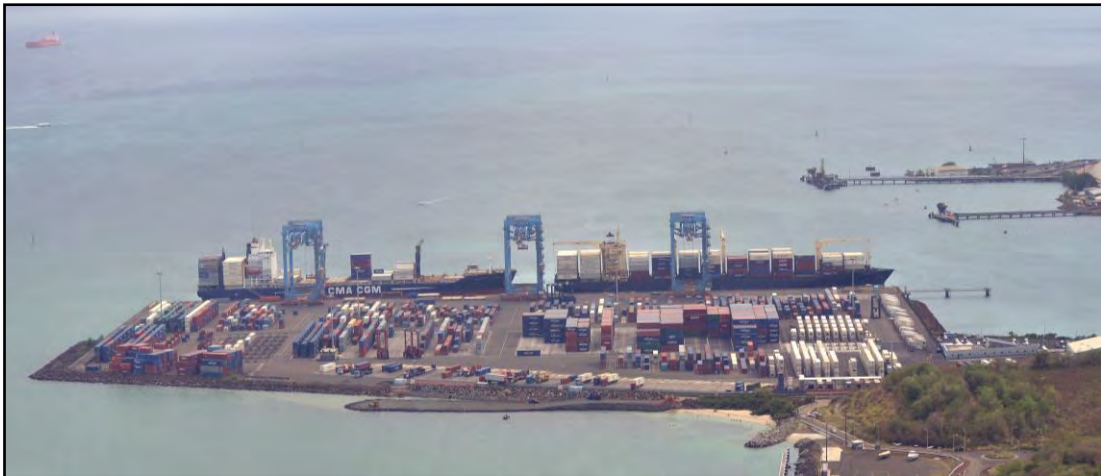


Figure 2: Terminal aerial view in 2016 – 2 vessels berthed (photo: GPMLM)

The commissioning of the third set of locks on the Panama Canal in 2014 portends a significant increase in traffic in the Caribbean area as well as in the size of vessels, container ships in particular.

Given the current and future demand for transshipment of containers in the Caribbean zone, Martinique, which occupies an advantageous position on the major maritime routes of the Eastern Caribbean, wishes to develop its containerized traffic and enhance its geographical position as a transshipment port.

The main challenge of the project lies first and foremost in securing domestic container carriers lines by optimizing vessel filling thanks to the development of transshipment traffic.

Secondly, the optimized service and productivity gains generated by the development of complementary transshipment activity must bring about a more competitive service, as illustrated in figure 3.



Figure 3: Pointe-des-Grives terminal gantry cranes in service (photo: Artelia)

If it is to achieve these objectives, the port must upgrade its facilities in order to accommodate more traffic, more ships and larger vessels than today (figure 4).



Figure 4: Two CMA-CGM vessels berthed at Pointe-des-Grives (photo: Artelia)

That's why Grand Port Maritime de La Martinique (GPMLM), the public authority in charge of the port of Martinique has appointed Artelia to provide design and construction supervision services for its challenging extension.

The ultimate goal is to accommodate the following vessels:

- Over Panamax:
 - From 260 to 294 meters long
 - 12.5 meters draft (up to 13.5 m on certain vessels)
 - 84,500 tons displacement
- Small ship of the Feeder type (for transshipment in the Caribbean zone)
 - From 120 to 150 meters long
 - Between 12,000 and 18,000 tons displacement

Two stages of works are planned to achieve this goal.

The works presented concern the first stage, i.e. the south-eastward expansion of the terminal including a 2.4-ha extension of the harbor reclamation area and a 550-meter enclosing berm (see figure 5).



Figure 5: Overall aerial view of terminal during the works (photo: GPMLM)

The project challenge consists in design the extension in a seismically highly area, and built the reclaimed area on alluvium with very poor characteristics which implies potential significant settlement amplitudes.

Moreover, the French regulations requires a total absence of dredging (no maritime borrow materials, no substitution), in order to preserve the environment in the bay of Fort de France.

Therefore, the design and works construction are based on the observational method involving: appropriate complementary geotechnical surveys, the use of granular blending materials, and implementation of works instrumentation of the reclamation area.

This paper presents the project constraints and the construction methodology, and sets out the feedback obtained of the reclamation area extension after 12 months of work.

2. MAIN PROTAGONISTS

Project Owner:

Grand Port Maritime de La Martinique (GPMLM): Engineering & Project Department

Project manager:

ARTELIA Eau & Environnement (AEE), Maritime business unit, Grenoble

Contractor:

Colas – Balineau La Martinique Joint Venture

3. MAIN QUANTITIES

The south-eastward extension works involve the following main quantities:

- Hub area: 2.4-ha reclamation area,
 - 550 meter-long rockfill enclosing berm,
 - 8,000 m³ of 30/100 kg rock
 - 13,000 m³ of 100/500 kg rock
 - 6,000 m³ of 0.5/1.5 t rock
 - 10,000 m³ of 2/5 t rock
- 140,000 m³ of quarry and andesite granular fill materials, grading: 0 / 300 mm
- Three instrumentation profiles (Water Pore Pressure Cells (CIP in figure 9), electrical and magnetic settlement monitoring).

4. DESIGN

4.1 Geotechnical context

In the context of its assignments, Artelia provided geotechnical design studies at the preliminary (G2-AVP study) and detailed design study stages (G2-PRO study).

The Grives container terminal is located at the mouth of the river Monsieur. The soils consist of alluvium, with organic silty clays and madreporic sands with varying clay contents surmounted by silt. The madreporic sands have a widely varying proportion of coral debris. Large-diameter core samples obtained using suitable drilling techniques are the only means of obtaining a correct representation of the madreporic content. The alluvium thickness varies from 10 m to more than 30 m.

The substratum consists of weathered and then stiff tuffite.

In the southeast extension area, little organic clay is intersected and the madreporic content is higher than in the northwestern area, close to the river Monsieur.

The geotechnical characteristics of the soil layers are given in Table 1.

| Layer no. | Soil type | p_l^* (MPa) | E_m (MPa) | E/PI | α | Q_c (MPa) | R_f (%) | Q_c/p_l^* | C' (kPa) | ϕ' (°) | C_u (KPa) | <80 μ m (%) | <2mm (%) |
|-----------|-----------|---------------|-------------|------|----------|-------------|-----------|-------------|------------|-------------|-------------|-----------------|----------|
|-----------|-----------|---------------|-------------|------|----------|-------------|-----------|-------------|------------|-------------|-------------|-----------------|----------|

| | | | | | | | | | | | | | |
|---|------------------------------|------|-----|----|-----|-----|-----|-----|----|----|-------|----|----|
| 1 | Silty sands | 0.17 | 1.5 | 6 | 1/3 | 0.1 | | | | | | | |
| 2 | Madreporic sands | 0.1 | 1 | 10 | 1/3 | 0.8 | 1.7 | 8 | 3 | 28 | 20/50 | 32 | 67 |
| 3 | Madreporic sands clay facies | | | | | | | | | | | | |
| 4 | Substrate alteration clay | 1.2 | 12 | 10 | 2/3 | 5 | 3.2 | 5.5 | 14 | 26 | 100 | 67 | 88 |
| 5 | Weathered tuffite | 2.3 | 27 | 12 | 2/3 | | | | 16 | 33 | 150 | | |
| 6 | Stiff tuffite | 4.5 | 53 | 12 | 1/2 | | | | 50 | 35 | 250 | | |
| 7 | 0/300 mm granular materials | | | | | | | | 0 | 45 | | | |

Table 1: Geotechnical model parameters

4.2 Consideration of seismic risk - geotechnical stability

The maximum reference acceleration in rocky ground is $a_g = 3 \text{ m/s}^2$.

The importance category for the berms given by the owner is **category I** as per French seismic regulations (of minor importance for public safety), which gives an importance coefficient: $\gamma_I = 0.8$.

The soil parameter for a class D seismic soil (alluvium in place) is **S = 1.35**.

The stability of the enclosing berms is assessed and validated with a **traditional Eurocode 8 approach**, reducing the shear characteristics of the materials in place and the filler materials.

4.3 Hydrodynamic stresses

The bay of Fort-de-France, to the north of which Pointe des Grives container terminal lies, is open to the west on the Caribbean Sea (2,400 km of fetch to Mexico).

The Pointe des Grives site is thus naturally protected from the northeast trade winds, but is less protected from seas raised by cyclones which, on account of their swirling nature, generate waves towards the site irrespective of their trajectory to the west of the site. Two kinds of wind and wave climates must therefore be considered:

- Local wave motion: chop raised by trade winds within the bay itself (100-year return period), water level = 0.94 m NGH, $H_{m0} = 1.2 \text{ m}$, period = 4 s.
- Sea wave motion: offshore swell propagated from the southwest (100-year return period), water level = 1.8 m NGH: $H_{m0} = 2 \text{ m}$, period = 10.5 s.

4.4 Protective berm profiles

The protective berms are composed of:

- Granular material for the core,
- Geotextile between the underlayer and the granular core,
- Rock materials for the underlayer, toe and armor.

The protective berm profiles are illustrated in figures 6 and 7.

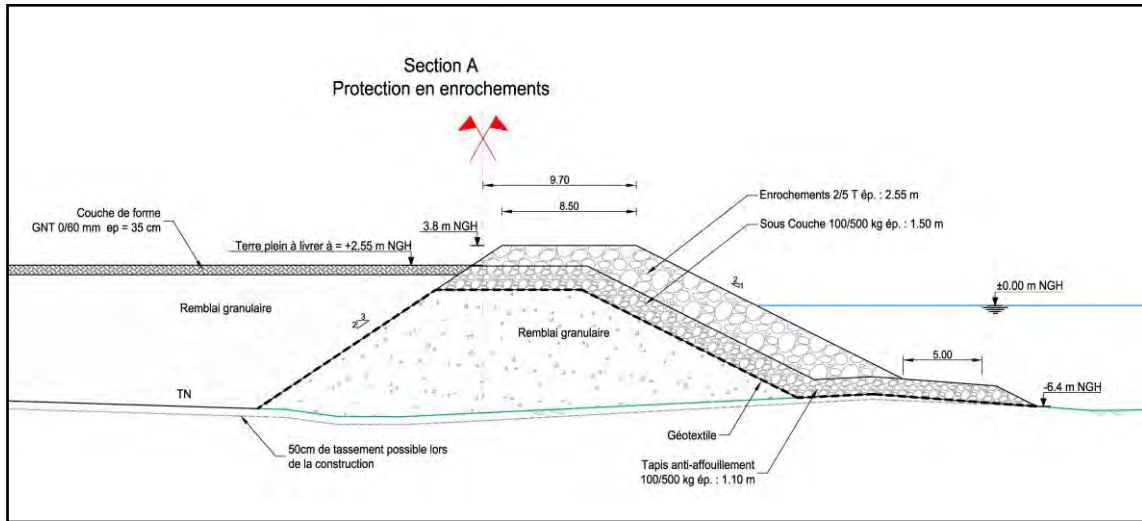


Figure 6: Eastern protective berm – cross section A (Artelia drawing (2015))

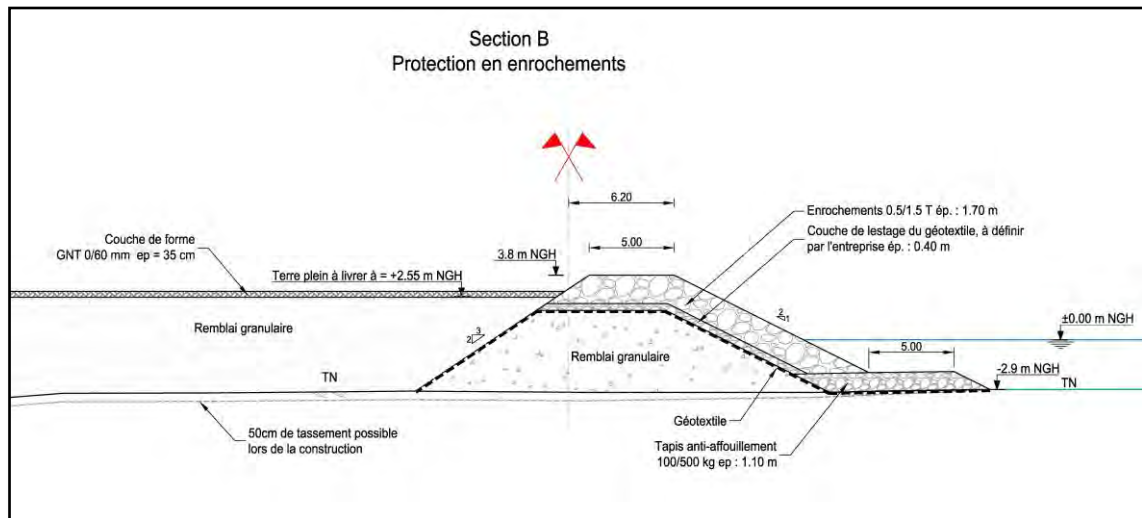


Figure 7: Eastern protective berm – cross section B (Artelia drawing (2015))

4.5 Special features of the design - Observational method

As previously stated, the mechanical characteristics of the soil are poor. However, the representativeness of core samples and pressiometric boreholes is not perfect.

Previous studies found that the soils were compressible, with a metric magnitude settlement.

Since dredging work is prohibited by local regulations, whether for the purpose of obtaining filler materials or purging the most compressible materials, the design solution implemented had to be geotechnical and hydraulic design-based.

In consultation with the client, a strategy of complementary geotechnical surveys suited to the context and the project was implemented. A 20 t heavy static penetrometer was hence transported from mainland France, enabling soil compactness and loose layer thickness to be determined in a continuous manner by crossing the banks of metric madrepores.

The geotechnical and hydraulic design hence take into account the hard, angular and robust quarry materials (quarry materials, Andesite, 0/300 mm, very low fines content).

The calculated settlement amplitude was revised downwards, with values between 30 and 50 cm depending on the fill and madreporic sand heights.

Instrumentation was designed and put in place to monitor settlement, incorporating sensor redundancy to compensate for unavoidable damage during the earthworks:

- Water pore pressure cells (CPI on figure 9) to monitor pore pressure dissipation (verify the consolidation phenomenon),
- Settlement sensors (CT on figure 9; magnetic and electrical) to monitor settlement.

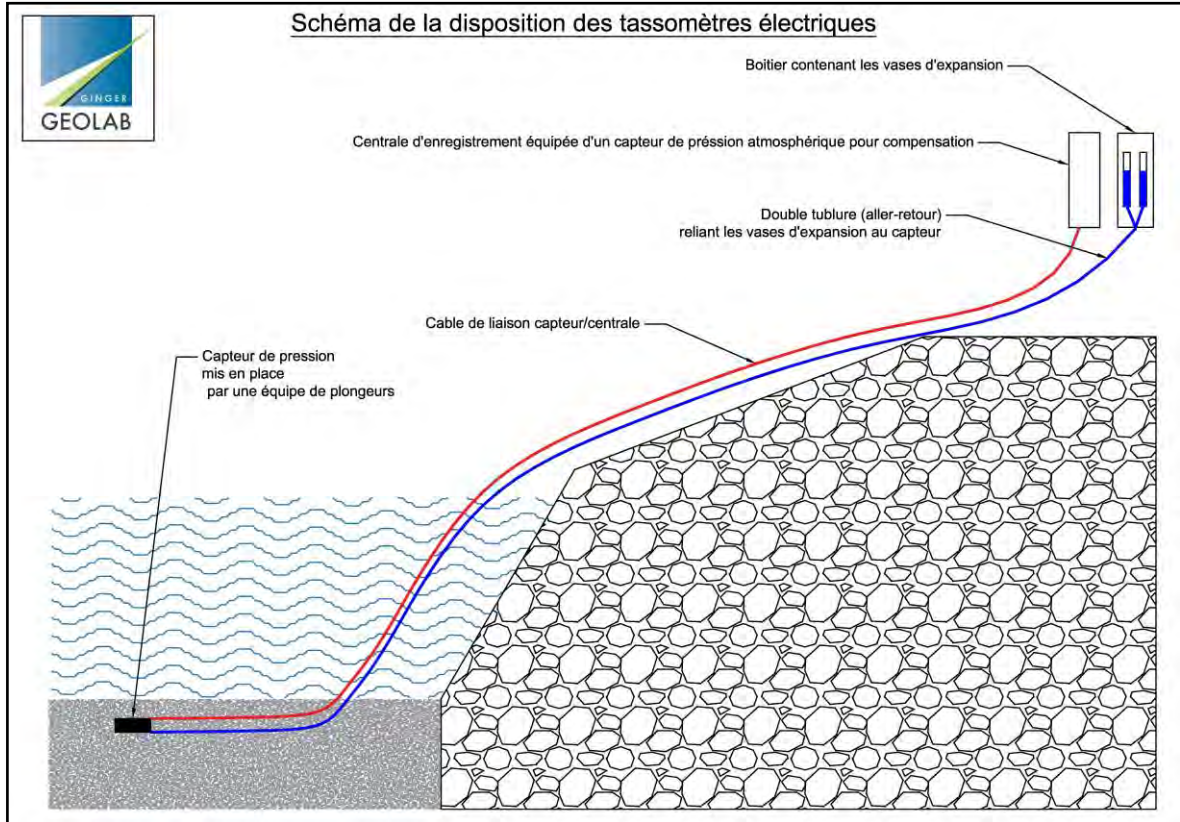


Figure 8: Schematic diagram of automatic data acquisition (Ginger-Geolab sketch, (2015))

Two profiles consisting of 3 IPC + 3 CT were implemented, beneath the water table and the bottom of the rockfill materials (See figure 8), according to the layout presented in figure 9.

The sensors are equipped with automatic acquisition of data and transmission to a control unit placed in an electrical cabinet on the existing reclamation area.

The wiring and ranges of the settlement sensors are geared to an expected elastic settlement amplitude of 20 cm (North) to 50 cm (South).

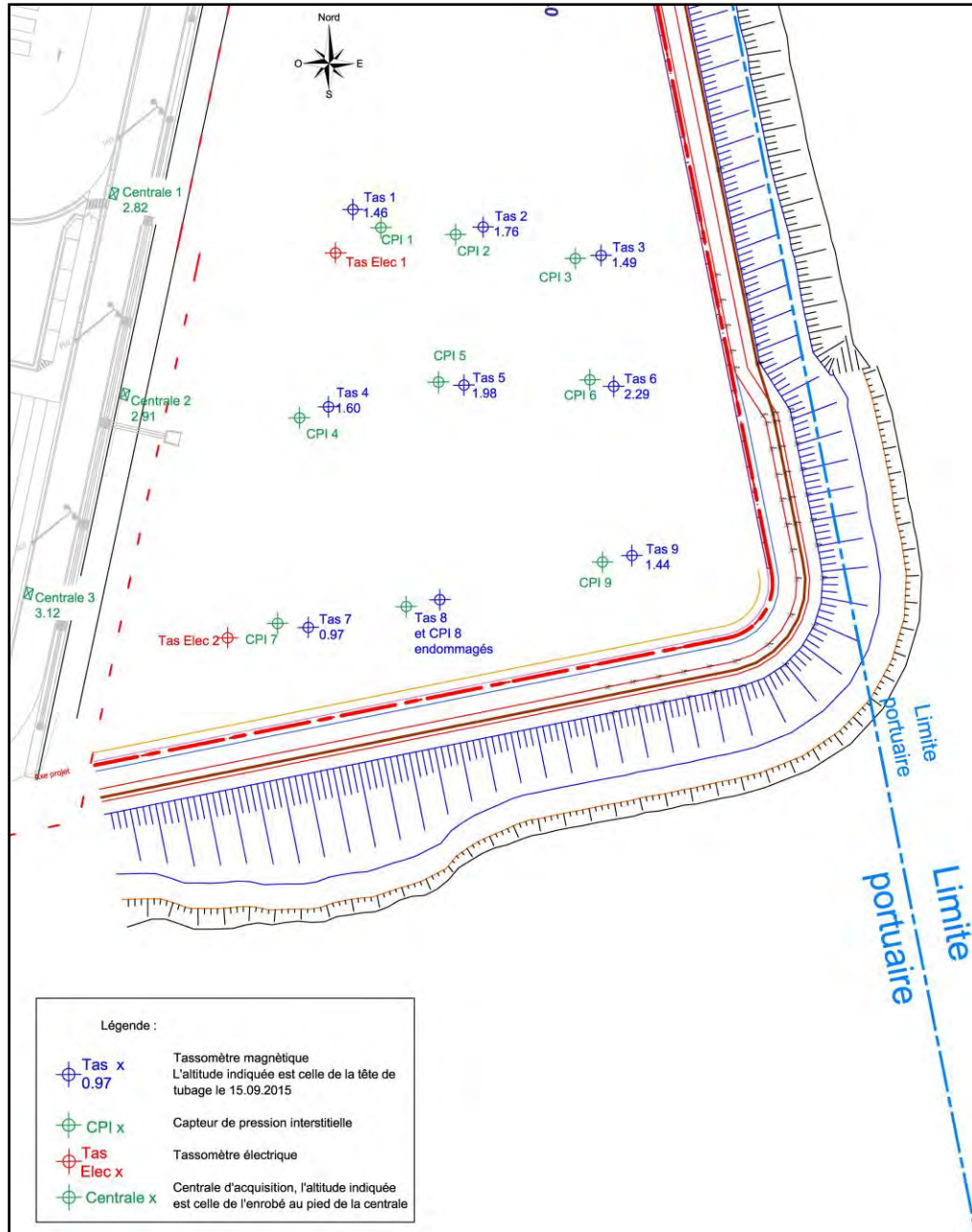


Figure 9: Project instrumentation layout (Ginger-Geolab drawing (2015))

The contractor (a geotechnical and instrumentation subcontractor) carried out measurements with the following frequency:

- Starting point on commissioning the sensors,
- One month after the starting point,
- One month after the reclamation area crest level was reached,
- Then monthly over 6 months.

In the event that settlement exceeds the acceptable design criteria, a soil consolidation solution using ballasted columns can be sized and implemented.

5. CONSTRUCTION WORKS STAGE

The construction works phasing is as follows:

- Dismantling of the berm protecting the existing reclamation area,
- Implementation of new protective berms along about 2/3 of the footprint of the planned reclamation area, in water depths up to 5 m, with a low silt thickness (see figure 10)



Figure 10: Aerial view of the first work phase (photo: Mad'In Drone (2015))

- Backfilling with approximately 40,000 m³ of granular material to create a reclamation area measuring approximately 1 ha, by land (See figure 11)

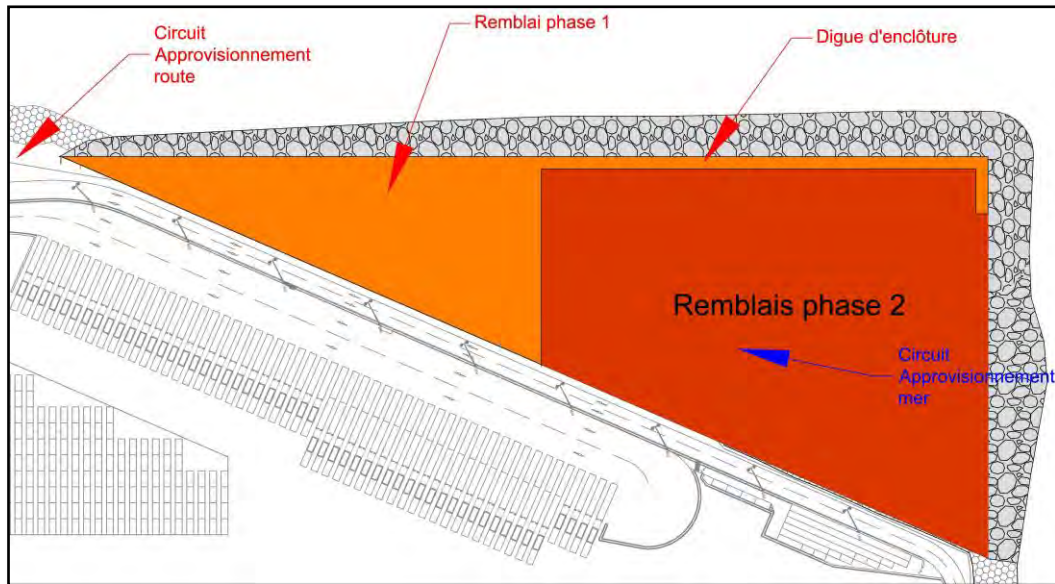


Figure 11: Plan view of stage 1 and stage 2 backfilling (drawing: Artelia (2015))

- Temporary protective rock berm,
- Analysis of the monitoring and of the primary settlement and consolidation kinematics,
- Creation of the reclamation area capping layer using granular materials (see figure 12)



Figure 12: Platform capping and surface dressing layer works (photo: Mad'In Drone (2015))

- Application of a platform surface dressing comprising a two-layer tack coat, to allow use of the newly-created surface for a limited period of time (see figure 12) before creation of the final pavement structure (see figure 13)



Figure 13: Aerial view of final reclamation area pavement (photo: Mad'In Drone (2017))

- Creation of box-outs for the sewerage network outlets and for the fire network.

6. FEEDBACK

6.1 Monitoring results

The instrumentation cables are protected by concrete culverts laid as the project works progressed: first under water, then on land. Despite this protection, approximately 50% of the sensors were damaged. However, thanks to the measurement redundancy, it was still possible to monitor the settlement profiles correctly throughout the construction period.

The maximum settlement amplitudes measured were in the range of 30 cm, occurring mainly during the construction phase. Deferred settlement after one year of works was limited, including in areas where the silty layer is thick.

Monitoring and analyzing settlement therefore provided a means of validating the design, and soil reinforcement measures were not required.

6.2 Environmental protection during reclamation area cell filling

It should be noted that the filling of the reclamation area cell with materials could generate an overflow and thus result in degradation of berms and other structures and the formation of a turbid plume. The contractor implemented the specific measures required to avoid these phenomena: temporary containment of the reclamation area cell, and use of a geotextile curtain.

6.2 A materials strategy to reduce project construction costs

In conclusion, the observational method combined with the management of quarry materials with very good mechanical characteristics provided a means of implementing the works with optimized costs and within the expected deadline.

Moreover, this work had minimal impact on the environment and complied with the requirements of regulations.

7. REFERENCES

Artelia (2015), Report No.1713189_2 R12_V1, Extension du terminal à conteneur de la Pointe des Grives – Programme 2, Projet, Echirolles.

Ginger-Geolab (2015), Report No.C001.F.047D, Instrumentation – Rapport de mesure n°2- Terre-plein Sud – Extension du terminal de la Pointe des Grives, Fort-de-France.

Mad'In Drone (2015 to 2017), Specialist in aerial view in Caribbean, website company: <http://madeindrone.com/Grand-Port-Maritime/Suivi-360.html>, Martinique.